



Prepared for
Lewis Research Center
Under Contract NAS3-21016

December 1991

(NASA-CR-189083) HIGH STRAIN RATE
PROPERTIES OF UNIDIRECTIONAL COMPOSITES,
PART I Final Contractor Report (IIT
Research Inst.) 460 p
CSCL 11D
G3/24 0079761
Unclas
N92-20838

I.M. Daniel
IIT Research Institute
Chicago, Illinois

High Strain Rate Properties of Unidirectional Composites Final Report—Part I

NASA Contractor Report 189083

1N-24
79761

P.460

FOREWORD

This is the Final Report on IIT Research Institute Project No. M06026, "High Strain Rate Properties of Unidirectional Composites," prepared by IITRI for NASA-Lewis Research Center, under Contract No. NAS3-21016. The work described in this report was conducted in the period July 11, 1977 to April 11, 1981. Dr. C. C. Chamis was the NASA-Lewis Project Manager. Dr. I. M. Daniel of IITRI was the Principal Investigator. Additional contributions to the work reported herein were made by Messrs. W. G. Hamilton, G. M. Koller, T. Niro, and S. W. Schramm of IITRI, Dr. T. Liber of Travenol Laboratories, and Mr. R. H. LaBedz of International Harvester.

Respectfully submitted,
IIT RESEARCH INSTITUTE



I. M. Daniel
Science Advisor
Materials and Manufacturing Technology

APPROVED



O. J. Viergutz
Manager
Engineering Mechanics Section



Maurice A. H. Howes, Director
Materials and Manufacturing
Technology Division

HIGH STRAIN RATE PROPERTIES OF UNIDIRECTIONAL COMPOSITES

ABSTRACT

Experimental methods were developed for testing and characterization of composite materials at strain rates ranging from quasi-static to over 500s^{-1} . Three materials were characterized, two graphite/epoxies and a graphite/S-glass/epoxy. Properties were obtained by testing thin rings 10.16 cm (4 in.) in diameter, 2.54 cm (1 in.) wide, and 6 to 8 plies thick under internal pressure. Unidirectional 0-deg, 90-deg, and 10-deg off-axis rings were tested to obtain longitudinal, transverse, and in-plane shear properties. In the dynamic tests internal pressure was applied explosively through a liquid and the pressure was measured with a calibrated steel ring. Strains in the calibration and specimen rings were recorded with a digital processing oscilloscope. The data were processed and the equation of motion solved numerically by the mini-computer attached to the oscilloscope. Results were obtained and plotted in the form of dynamic stress-strain curves. Longitudinal properties which are governed by the fibers do not vary much with strain rate with only a moderate (up to 20%) increase in modulus. Transverse modulus and strength increase sharply with strain rate reaching values up to three times the static value. The in-plane shear modulus and shear strength increase noticeably with strain rate by up to approximately 65%. In all cases ultimate strains do not vary significantly with strain rate.

FOREWORD

This is the Final Report on IIT Research Institute Project No. M06026, "High Strain Rate Properties of Unidirectional Composites," prepared by IITRI for NASA-Lewis Research Center, under Contract No. NAS3-21016. The work described in this report was conducted in the period July 11, 1977 to April 11, 1981. Dr. C. C. Chamis was the NASA-Lewis Project Manager. Dr. I. M. Daniel of IITRI was the Principal Investigator. Additional contributions to the work reported herein were made by Messrs. W. G. Hamilton, G. M. Koller, T. Niro, and S. W. Schramm of IITRI, Dr. T. Liber of Travenol Laboratories, and Mr. R. H. LaBedz of International Harvester.

Respectfully submitted,
IIT RESEARCH INSTITUTE

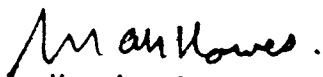


I. M. Daniel
Science Advisor
Materials and Manufacturing Technology

APPROVED:



O. J. Viergutz
Manager
Engineering Mechanics Section



Maurice A. H. Howes, Director
Materials and Manufacturing
Technology Division

HIGH STRAIN RATE PROPERTIES OF UNIDIRECTIONAL COMPOSITES

ABSTRACT

Experimental methods were developed for testing and characterization of composite materials at strain rates ranging from quasi-static to over 500s^{-1} . Three materials were characterized, two graphite/epoxies and a graphite/S-glass/epoxy. Properties were obtained by testing thin rings 10.16 cm (4 in.) in diameter, 2.54 cm (1 in.) wide, and 6 to 8 plies thick under internal pressure. Unidirectional 0-deg, 90-deg, and 10-deg off-axis rings were tested to obtain longitudinal, transverse, and in-plane shear properties. In the dynamic tests internal pressure was applied explosively through a liquid and the pressure was measured with a calibrated steel ring. Strains in the calibration and specimen rings were recorded with a digital processing oscilloscope. The data were processed and the equation of motion solved numerically by the mini-computer attached to the oscilloscope. Results were obtained and plotted in the form of dynamic stress-strain curves. Longitudinal properties which are governed by the fibers do not vary much with strain rate with only a moderate (up to 20%) increase in modulus. Transverse modulus and strength increase sharply with strain rate reaching values up to three times the static value. The in-plane shear modulus and shear strength increase noticeably with strain rate by up to approximately 65%. In all cases ultimate strains do not vary significantly with strain rate.

TABLE OF CONTENTS

	<u>Page</u>
1. INTRODUCTION	1-1
2. TEST PLANNING AND SPECIMEN PREPARATION	2-1
2.1 Material Procurement and Qualification	2-1
2.2 Preliminary Material Characterization	2-5
2.3 Laminate Fabrication	2-6
2.4 Quality Assessment	2-14
2.5 Specimen Preparation	2-16
3. TEST METHOD DEVELOPMENT	3-1
3.1 Preliminary Testing	3-1
3.2 Quasi-Static Testing	3-3
3.3 Dynamic Testing	3-4
3.3.1 Experimental Procedures	3-4
3.3.2 Data Processing	3-7
4. STRAIN RATE CHARACTERIZATION OF UNIDIRECTIONAL COMPOSITES	4-1
4.1 Introduction	4-1
4.2 Longitudinal Tensile Properties	4-1
4.2.1 Graphite/Epoxy (SP288/T300)	4-1
4.2.2 Graphite/Epoxy (SP288/AS)	4-5
4.2.3 Graphite/S-Glass/Epoxy (80AS/20S/PR288)	4-9
4.3 Transverse Tensile Properties	4-18
4.3.1 Graphite/Epoxy (SP288/T300)	4-18
4.3.2 Graphite/Epoxy (SP288/AS)	4-22
4.3.3 Graphite/S-Glass/Epoxy (80AS/20S/PR288)	4-28

TABLE OF CONTENTS (Cont.)

	<u>Page</u>
4.4 In-Plane Shear Properties	4-33
4.4.1 Graphite/Epoxy (SP288/T300)	4-33
4.4.2 Graphite/Epoxy (SP288/AS)	4-36
4.4.3 Graphite/S-Glass/Epoxy (80AS/20S/PR288)	4-41
4.5 Compressive Properties	4-46
4.5.1 Compression Fixture	4-46
4.5.2 Longitudinal Compressive Properties	4-49
4.5.3 Transverse Compressive Properties	4-51
5. SUMMARY AND CONCLUSIONS	5-1
REFERENCES	R-1

LIST OF TABLES

<u>Table</u>	<u>Page</u>
2-1 Qualification Flexure Tests for Graphite/Epoxy SP288/T300	2-2
2-2 Qualification Interlaminar Shear Tests for Graphite/Epoxy SP288/T300	2-2
2-3 Qualification Flexure Tests for Graphite/Epoxy SP288/AS	2-3
2-4 Qualification Interlaminar Shear Tests for Graphite/Epoxy SP288/AS	2-3
2-5 Qualification Flexure Tests for Graphite/S-Glass/Epoxy 80AS/20S/PR288	2-4
2-6 Qualification Interlaminar Shear Tests for Graphite/S-Glass/Epoxy 80AS/20S/PR288	2-4
2-7 Properties of Unidirectional Graphite/Epoxy SP288/T300	2-7
2-8 Properties of Unidirectional Graphite/Epoxy SP288/AS	2-8
2-9 Properties of Unidirectional Graphite/S-Glass/Epoxy 80AS/20S/PR288	2-9
4-1 Quasi-Static Tensile Properties of $[0_6]$ SP288/T300 Graphite/Epoxy	4-2
4-2 Intermediate Strain Rate Tensile Properties of $[0_6]$ SP288/T300 Graphite/Epoxy	4-4
4-3 High Strain Rate Tensile Properties of $[0_6]$ SP288/T300 Graphite/Epoxy	4-6
4-4 Longitudinal Tensile Properties of Unidirectional SP288/T300 Graphite/Epoxy At Various Strain Rates	4-7
4-5 Quasi-Static Tensile Properties of $[0_6]$ SP288/AS Graphite/Epoxy	4-8
4-6 Intermediate Strain Rate Tensile Properties of $[0_6]$ SP288/AS Graphite/Epoxy	4-10
4-7 High Strain Rate Tensile Properties of $[0_6]$ SP288/AS Graphite/Epoxy	4-11
4-8 Longitudinal Tensile Properties of Unidirectional SP288/AS Graphite/Epoxy At Various Strain Rates	4-12

LIST OF TABLES (Cont.)

<u>Table</u>	<u>Page</u>
4-9 Quasi-Static Tensile Properties of $[0_6]$ 80AS/20S/PR288 Graphite/S-Glass/Epoxy	4-13
4-10 Intermediate Strain Rate Tensile Properties of $[0_6]$ 80AS/20S/PR288 Graphite/S-Glass/Epoxy	4-15
4-11 High Strain Rate Tensile Properties of $[0_6]$ 80AS/20S/PR288 Graphite/S-Glass/Epoxy	4-16
4-12 Longitudinal Tensile Properties of Unidirectional 80AS/20S/PR288 Graphite/S-Glass/Epoxy At Various Strain Rates	4-17
4-13 Quasi-Static Tensile Properties of $[90_8]$ SP288/T300 Graphite/Epoxy	4-19
4-14 Intermediate Strain Rate Tensile Properties of $[90_8]$ SP288/T300 Graphite/Epoxy	4-20
4-15 High Strain Rate Tensile Properties of $[90_8]$ SP288/T300 Graphite/Epoxy	4-21
4-16 Transverse Tensile Properties of Unidirectional SP288/T300 Graphite/Epoxy At Various Strain Rates	4-23
4-17 Quasi-Static Tensile Properties of $[90_8]$ SP288/AS Graphite/Epoxy	4-24
4-18 Intermediate Strain Rate Tensile Properties of $[90_8]$ SP288/AS Graphite/Epoxy	4-25
4-19 High Strain Rate Tensile Properties of $[90_8]$ SP288/AS Graphite/Epoxy	4-26
4-20 Transverse Tensile Properties of Unidirectional SP288/AS Graphite/Epoxy At Various Strain Rates	4-27
4-21 Quasi-Static Tensile Properties of $[90_8]$ 80AS/20S/PR288 Graphite/S-Glass/Epoxy	4-29
4-22 Intermediate Strain Rate Tensile Properties of $[90_8]$ 80AS/20S/PR288 Graphite/S-Glass/Epoxy	4-30
4-23 High Strain Rate Tensile Properties of $[90_8]$ 80AS/20S/PR288 Graphite/S-Glass/Epoxy	4-31
4-24 Transverse Tensile Properties of Unidirectional 80AS/20S/PR288 Graphite/S-Glass/Epoxy At Various Strain Rates	4-32

LIST OF TABLES (Cont.)

<u>Table</u>	<u>Page</u>
4-25 Quasi-Static In-Plane Shear Properties of Unidirectional SP288/T300 Graphite/Epoxy	4-34
4-26 Intermediate Strain Rate In-Plane Shear Properties of Unidirectional SP288/T300 Graphite/Epoxy	4-35
4-27 High Strain Rate In-Plane Shear Properties of Unidirectional SP288/T300 Graphite/Epoxy	4-37
4-28 In-Plane Shear Properties of Unidirectional SP288/T300 Graphite/Epoxy At Various Strain Rates	4-38
4-29 Quasi-Static In-Plane Shear Properties of Unidirectional SP288/AS Graphite/Epoxy	4-39
4-30 Intermediate Strain Rate In-Plane Shear Properties of Unidirectional SP288/AS Graphite/Epoxy	4-40
4-31 High Strain Rate In-Plane Shear Properties of Unidirectional SP288/AS Graphite/Epoxy	4-42
4-32 In-Plane Shear Properties of Unidirectional SP288/AS Graphite/Epoxy At Various Strain Rates	4-43
4-33 Quasi-Static In-Plane Shear Properties of Unidirectional 80AS/20S/PR288 Graphite/S-Glass/Epoxy	4-44
4-34 Intermediate Strain Rate In-Plane Shear Properties of Unidirectional 80AS/20S/PR288 Graphite/S-Glass/Epoxy	4-45
4-35 High Strain Rate In-Plane Shear Properties of Unidirectional 80AS/20S/PR288 Graphite/S-Glass/Epoxy	4-47
4-36 In-Plane Shear Properties of Unidirectional 80AS/20S/PR288 Graphite/S-Glass/Epoxy At Various Strain Rates	4-48
4-37 High Strain Rate Compressive Properties of $[0_6]$ SP288/T300 Graphite/Epoxy	4-50
4-38 High Strain Rate Compressive Properties of $[0_6]$ SP288/AS Graphite/Epoxy	4-52
4-39 High Strain Rate Compressive Properties of $[90_8]$ SP288/T300 Graphite/Epoxy	4-54
4-40 High Strain Rate Compressive Properties of $[90_8]$ SP288/AS Graphite/Epoxy	4-55
4-41 High Strain Rate Compressive Properties of $[90_8]$ 80AS/20S/PR288 Graphite/S-Glass/Epoxy	4-57

LIST OF FIGURES

<u>Figure</u>	<u>Page</u>
1-1 Dynamic loading regimes.	1-5
2-1 Strains in 0-deg unidirectional SP288/T300 specimen under uniaxial tensile loading.	2-17
2-2 Strains in 0-deg unidirectional SP288/T300 specimen under uniaxial tensile loading.	2-18
2-3 Strains in 0-deg unidirectional SP288/AS specimen under uniaxial tensile loading.	2-19
2-4 Strains in 0-deg unidirectional SP288/AS specimen under uniaxial tensile loading.	2-20
2-5 Strains in 0-deg unidirectional 80AS/20S/PR288 specimen under uniaxial tensile loading.	2-21
2-6 Strains in 0-deg unidirectional 80AS/20S/PR288 specimen under uniaxial tensile loading.	2-22
2-7 Strains in 90-deg unidirectional SP288/T300 specimen under uniaxial tensile loading.	2-23
2-8 Strains in 90-deg unidirectional SP288/T300 specimen under uniaxial tensile loading.	2-24
2-9 Strains in 90-deg unidirectional SP288/AS specimen under uniaxial tensile loading.	2-25
2-10 Strains in 90-deg unidirectional SP288/AS specimen under uniaxial tensile loading.	2-26
2-11 Strains in 90-deg unidirectional 80AS/20S/PR288 specimen under uniaxial tensile loading.	2-27
2-12 Strains in 90-deg unidirectional 80AS/20S/PR288 specimen under uniaxial tensile loading.	2-28
2-13 Stress-strain curve for unidirectional 0-deg SP288/T300 specimen under compressive loading.	2-29
2-14 Stress-strain curve for unidirectional 0-deg SP288/T300 specimen under compressive loading.	2-30
2-15 Stress-strain curve for unidirectional 0-deg SP288/T300 specimen under compressive loading.	2-31

LIST OF FIGURES (Cont.)

<u>Figure</u>	<u>Page</u>
2-16 Stress-strain curve for unidirectional 0-deg SP288/AS specimen under compressive loading.	2-32
2-17 Stress-strain curve for unidirectional 0-deg SP288/AS specimen under compressive loading.	2-33
2-18 Stress-strain curve for unidirectional 0-deg SP288/AS specimen under compressive loading.	2-34
2-19 Stress-strain curve for unidirectional 0-deg 80AS/20S/PR288 specimen under compressive loading.	2-35
2-20 Stress-strain curve for unidirectional 0-deg 80AS/20S/PR288 specimen under compressive loading.	2-36
2-21 Stress-strain curve for unidirectional 0-deg 80AS/20S/PR288 specimen under compressive loading.	2-37
2-22 Stress-strain curve for unidirectional 90-deg SP288/T300 specimen under compressive loading.	2-38
2-23 Stress-strain curve for unidirectional 90-deg SP288/T300 specimen under compressive loading.	2-39
2-24 Stress-strain curve for unidirectional 90-deg SP288/T300 specimen under compressive loading.	2-40
2-25 Stress-strain curve for unidirectional 90-deg SP288/AS specimen under compressive loading.	2-41
2-26 Stress-strain curve for unidirectional 90-deg SP288/AS specimen under compressive loading.	2-42
2-27 Stress-strain curve for unidirectional 90-deg SP288/AS specimen under compressive loading.	2-43
2-28 Stress-strain curve for unidirectional 90-deg 80AS/20S/PR288 specimen under compressive loading.	2-44
2-29 Stress-strain curve for unidirectional 90-deg 80AS/20S/PR288 specimen under compressive loading.	2-45
2-30 Stress-strain curve for unidirectional 90-deg 80AS/20S/PR288 specimen under compressive loading.	2-46
2-31 Shear stress versus shear strain for unidirectional 10-deg off-axis SP288/T300 specimen.	2-47
2-32 Shear stress versus shear strain for unidirectional 10-deg off-axis SP288/T300 specimen.	2-48

LIST OF FIGURES (Cont.)

<u>Figure</u>		<u>Page</u>
2-33	Shear stress versus shear strain for unidirectional 10-deg off-axis SP288/AS specimen.	2-49
2-34	Shear stress versus shear strain for unidirectional 10-deg off-axis SP288/AS specimen.	2-50
2-35	Shear stress versus shear strain for unidirectional 10-deg off-axis 80AS/20S/PR288 specimen.	2-51
2-36	Shear stress versus shear strain for unidirectional 10-deg off-axis 80AS/20S/PR288 specimen.	2-52
2-37	Components of cavity mold tool for fabricating composite laminate tubes.	2-53
2-38	Sketch showing the center steel mandrel and the sequence of material layers employed in the composite laminate tube fabrication.	2-54
2-39	Roller and carrier template system for wrapping prepreg plies on the tube layup mandrel. (The photograph shows partial layup of a 45-deg fist ply.)	2-55
2-40	Assembled cavity mold tool for composite tube fabrication shown in curing oven with air and vacuum lines attached.	2-56
2-41	Ultrasonic system for scanning tubular specimens.	2-57
2-42	Typical ultrasonic C-scans of acceptable and unacceptable $[0_6]$ graphite/epoxy (SP288/T300) tubes.	2-58
2-43	Fixture for measuring the wall thickness of composite tubes.	2-59
2-44	Composite laminate tube mounted on a rubber-sleeve-covered cutoff mandrel in preparation for cutting ring specimens.	2-60
2-45	Cutting of composite tube on a lathe into rings using a high speed diamond cutoff wheel.	2-61
3-1	Pressure and strain signals for $[90_2/\pm 45]_S$ graphite/epoxy ring loaded by hammer impact on piston of pressure vessel.	3-11
3-2	Fixture for dynamic loading of composite ring specimens.	3-12
3-3	Circumferential strain record in dynamically loaded $[90_2/\pm 45]_S$ graphite/epoxy ring specimen.	3-13
3-4	Circumferential strain records in dynamically loaded $[90_2/\pm 45]_S$ graphite/epoxy ring specimen.	3-14

LIST OF FIGURES (Cont.)

<u>Figure</u>	<u>Page</u>
3-5 Strain records in dynamically loaded aluminum ring (second trace from top is circumferential strain, third trace is axial strain).	3-15
3-6 Failure of dynamically loaded aluminum ring.	3-16
3-7 Fixture for quasi-static loading of composite ring specimens.	3-17
3-8 Photograph of assembled fixture for quasi-static loading of composite ring specimens.	3-18
3-9 Graphite/epoxy ring specimens with strain gages and after failure.	3-19
3-10 Fixture for dynamic loading of composite ring specimens.	3-20
3-11 Photograph of components of fixture for dynamic loading of composite ring specimens.	3-21
3-12 Photograph of assembled fixture for dynamic loading of composite ring specimen.	3-22
3-13 Circumferential strain and pressure records (top trace: strain in $[0_8]$ graphite/epoxy ring; second and third traces: strains in steel ring; bottom trace: pressure transducer).	3-23
3-14 Strain and pressure signals for dynamic loading of steel and $[0_8]$ graphite/epoxy ring specimens.	3-24
3-15 Circumferential strain and pressure records for dynamically loaded $[90_8]$ graphite/epoxy ring.	3-25
3-16 Circumferential strain and pressure records for dynamically loaded $[\pm 45]_{2s}$ graphite/epoxy ring.	3-26
3-17 Circumferential strain and pressure records for dynamically loaded 0.277 cm (0.109 in.) and 0.124 cm (0.049 in.) thick steel rings.	3-27
3-18 Pressure-strain calibration of Vascomax steel rings used as pressure cells.	3-28
3-19 Illustration of smoothing and approximation operations. a) As recorded and smoothed strains, b) strain rate, smoothed strain rate and piecewise linear approximation, and c) stepwise and smoothed strain acceleration.	3-29

LIST OF FIGURES (Cont.)

<u>Figure</u>		<u>Page</u>
4-1	Strains in unidirectional 0-deg SP288/T300 ring specimen under static tensile loading (Specimen No. 19-2).	4-58
4-2	Stress-strain curve in unidirectional 0-deg SP288/T300 ring specimen under static tensile loading (Specimen No. 19-3).	4-59
4-3	Strains in unidirectional 0-deg SP288/T300 ring specimen under static tensile loading (Specimen No. 19-10).	4-60
4-4	Strain records in steel ring and $[0_6]$ SP288/T300 graphite/epoxy ring under dynamic loading for Specimen 40-3 (650 mg pistol powder).	4-61
4-5	Strain records in steel ring and $[0_6]$ SP288/T300 graphite/epoxy ring under dynamic loading for Specimen 40-4 (650 mg pistol powder).	4-62
4-6	Strain records in steel ring and $[0_6]$ SP288/T300 graphite/epoxy ring under dynamic loading for Specimen 40-5 (650 mg pistol powder).	4-63
4-7	Stress-strain curve for dynamically loaded $[0_6]$ SP288/T300 graphite/epoxy ring, Specimen 40-3 (650 mg pistol powder).	4-64
4-8	Stress-strain curve for dynamically loaded $[0_6]$ SP288/T300 graphite/epoxy ring, Specimen 40-4 (650 mg pistol powder).	4-65
4-9	Stress-strain curve for dynamically loaded $[0_6]$ SP288/T300 graphite/epoxy ring, Specimen 40-5 (650 mg pistol powder).	4-66
4-10	Strain records in steel ring and $[0_6]$ SP288/T300 graphite/epoxy ring under dynamic loading for Specimen 19-4 (two 100 mg PETN detonators).	4-67
4-11	Strain and its derivatives in steel ring for Specimen 19-4.	4-68
4-12	Circumferential strain and its derivatives for $[0_6]$ SP288/T300 graphite/epoxy ring under dynamic loading for Specimen 19-4.	4-69
4-13	Strain records in steel ring and $[0_6]$ SP288/T300 graphite/epoxy ring under dynamic loading for Specimen 19-5 (two 100 mg PETN detonators).	4-70
4-14	Strains and its derivatives in steel ring for Specimen 19-5.	4-71
4-15	Circumferential strain and its derivatives for $[0_6]$ SP288/T300 graphite/epoxy ring under dynamic loading for Specimen 19-5.	4-72
4-16	Strain records in steel ring and $[0_6]$ SP288/T300 graphite/epoxy ring under dynamic loading for Specimen 19-6 (two 100 mg PETN detonators).	4-73

LIST OF FIGURES (Cont.)

<u>Figure</u>		<u>Page</u>
4-17	Strain and its derivatives in steel ring for Specimen 19-6.	4-74
4-18	Circumferential strain and its derivatives for $[0_6]$ SP288/T300 graphite/epoxy ring under dynamic loading for Specimen 19-6.	4-75
4-19	Stress-strain curve for dynamically loaded $[0_6]$ SP288/T300 graphite/epoxy ring, Specimen 19-4 (two 100 mg PETN detonators).	4-76
4-20	Stress-strain curve for dynamically loaded $[0_6]$ SP288/T300 graphite/epoxy ring, Specimen 19-5 (two 100 mg PETN detonators).	4-77
4-21	Stress-strain curve for dynamically loaded $[0_6]$ SP288/T300 graphite/epoxy ring, Specimen 19-6 (two 100 mg PETN detonators).	4-78
4-22	Strains in unidirectional 0-deg SP288/AS ring specimen under static tensile loading (Specimen No. 7-1).	4-79
4-23	Strains in unidirectional 0-deg SP288/AS ring specimen under static tensile loading (Specimen No. 7-5).	4-80
4-24	Strains in unidirectional 0-deg SP288/AS ring specimen under static tensile loading (Specimen No. 7-10).	4-81
4-25	Strain records in steel ring and $[0_6]$ SP288/AS graphite/epoxy ring under dynamic loading for Specimen 45-9 (650 mg pistol powder).	4-82
4-26	Strain records in steel ring and $[0_6]$ SP288/AS graphite/epoxy ring under dynamic loading for Specimen 45-10 (650 mg pistol powder).	4-83
4-27	Strain records in steel ring and $[0_6]$ SP288/AS graphite/epoxy ring under dynamic loading for Specimen 45-11 (650 mg pistol powder).	4-84
4-28	Stress-strain curve for dynamically loaded $[0_6]$ SP288/AS graphite/epoxy ring, Specimen 45-9 (650 mg pistol powder).	4-85
4-29	Stress-strain curve for dynamically loaded $[0_6]$ SP288/AS graphite/epoxy ring, Specimen 45-10 (650 mg pistol powder).	4-86
4-30	Stress-strain curve for dynamically loaded $[0_6]$ SP288/AS graphite/epoxy ring, Specimen 45-11 (650 mg pistol powder).	4-87
4-31	Strain records in steel ring and $[0_6]$ SP288/AS graphite/epoxy ring under dynamic loading for Specimen 7-6 (two 100 mg PETN detonators).	4-88
4-32	Strain and its derivatives in steel ring for Specimen 7-6.	4-89

LIST OF FIGURES (Cont.)

<u>Figure</u>		<u>Page</u>
4-33	Circumferential strain and its derivatives for $[0_6]$ SP288/AS graphite/epoxy ring under dynamic loading for Specimen 7-6.	4-90
4-34	Strain records in steel ring and $[0_6]$ SP288/AS graphite/epoxy ring under dynamic loading for Specimen 7-7 (300 mg PETN detonator).	4-91
4-35	Strain and its derivatives in steel ring for Specimen 7-7.	4-92
4-36	Circumferential strain and its derivatives for $[0_6]$ SP288/AS graphite/epoxy ring under dynamic loading for Specimen 7-7.	4-93
4-37	Strain records in steel ring and $[0_6]$ SP288/AS graphite/epoxy ring under dynamic loading for Specimen 7-8 (330 mg PETN detonator).	4-94
4-38	Strain and its derivatives in steel ring for Specimen 7-8.	4-95
4-39	Circumferential strain and its derivatives for $[0_6]$ SP288/AS graphite/epoxy ring under dynamic loading for Specimen 7-8.	4-96
4-40	Strain records in steel ring and $[0_6]$ SP288/AS graphite/epoxy ring under dynamic loading for Specimen 7-9 (100 mg PETN detonator).	4-97
4-41	Strain and its derivatives in steel ring for Specimen 7-9.	4-98
4-42	Circumferential strain and its derivatives for $[0_6]$ SP288/AS graphite/epoxy ring under dynamic loading for Specimen 7-9.	4-99
4-43	Stress-strain curve for dynamically loaded $[0_6]$ SP288/AS graphite/epoxy ring for Specimen 7-6 (two 100 mg PETN detonators).	4-100
4-44	Stress-strain curve for dynamically loaded $[0_6]$ SP288/AS graphite/epoxy ring for Specimen 7-7 (330 mg PETN detonator).	4-101
4-45	Stress-strain curve for dynamically loaded $[0_6]$ SP288/AS graphite/epoxy ring for Specimen 7-8 (330 mg PETN detonator).	4-102
4-46	Stress-strain curve for dynamically loaded $[0_6]$ SP288/AS graphite/epoxy ring for Specimen 7-9 (100 mg PETN detonator).	4-103
4-47	Strains in unidirectional 0-deg 80AS/20S/PR288 specimen under static tensile loading (Specimen No. 10-1).	4-104
4-48	Stress-strain curve in unidirectional 0-deg 80AS/20S/PR288 ring specimen under static tensile loading (Specimen No. 10-5).	4-105

LIST OF FIGURES (Cont.)

<u>Figure</u>	<u>Page</u>
4-49 Strain records in steel ring and [0 ₆] 80AS/20S/PR288 graphite/S-glass/epoxy ring under dynamic loading for Specimen 43-2 (650 mg pistol powder).	4-106
4-50 Strain records in steel ring and [0 ₆] 80AS/20S/PR288 graphite/S-glass/epoxy ring under dynamic loading for Specimen 43-3 (650 mg pistol powder).	4-107
4-51 Strain records in steel ring and [0 ₆] 80AS/20S/PR288 graphite/S-glass/epoxy ring under dynamic loading for Specimen 43-4 (650 mg pistol powder).	4-108
4-52 Stress-strain curve for dynamically loaded [0 ₆] 80AS/20S/PR288 graphite/S-glass/epoxy ring for Specimen 43-2.	4-109
4-53 Stress-strain curve for dynamically loaded [0 ₆] 80AS/20S/PR288 graphite/S-glass/epoxy ring for Specimen 43-3.	4-110
4-54 Stress-strain curve for dynamically loaded [0 ₆] 80AS/20S/PR288 graphite/S-glass/epoxy ring for Specimen 43-4.	4-111
4-55 Strain records in steel ring and [0 ₆] 80AS/20S/PR288 graphite/S-glass/epoxy ring under dynamic loading for Specimen 10-8 (100 mg PETN detonator).	4-112
4-56 Strain and its derivatives in steel ring for Specimen 10-8.	4-113
4-57 Circumferential strain and its derivatives for [0 ₆] 80AS/20S/PR288 graphite/S-glass/epoxy ring under dynamic loading for Specimen 10-8.	4-114
4-58 Strain records in steel ring and [0 ₆] 80AS/20S/PR288 graphite/S-glass/epoxy ring under dynamic loading for Specimen 10-9 (two 100 mg PETN detonators).	4-115
4-59 Strain and its derivatives in steel ring for Specimen 10-9.	4-116
4-60 Circumferential strain and its derivatives for [0 ₆] 80AS/20S/PR288 graphite/S-glass/epoxy ring under dynamic loading for Specimen 10-9.	4-117
4-61 Strain records in steel ring and [0 ₆] 80AS/20S/PR288 graphite/S-glass/epoxy ring under dynamic loading for Specimen 10-10 (330 mg PRTN detonator).	4-118
4-62 Strain and its derivatives in steel ring for Specimen 10-10.	4-119
4-63 Circumferential strain and its derivatives for [0 ₆] 80AS/20S/PR288 graphite/S-glass/epoxy ring under dynamic loading for Specimen 10-10.	4-120

LIST OF FIGURES (Cont.)

<u>Figure</u>	<u>Page</u>
4-64 Stress-strain curve for dynamically loaded [0 ₆] 80AS/20S/PR288 graphite/S-glass/epoxy ring for Specimen 10-8 (100 mg PETN detonator).	4-121
4-65 Stress-strain curve for dynamically loaded [0 ₆] 80AS/20S/PR288 graphite/S-glass/epoxy ring for Specimen 10-9 (two 100 mg PETN detonators).	4-122
4-66 Stress-strain curve for dynamically loaded [0 ₆] 80AS/20S/PR288 graphite/S-glass/epoxy ring for Specimen 10-10 (330 mg PETN detonator).	4-123
4-67 Strains in unidirectional 90-deg SP288/T300 ring specimen under static tensile loading (Specimen No. 3-3).	4-124
4-68 Strains in unidirectional 90-deg SP288/T300 ring specimen under static tensile loading (Specimen No. 3-4).	4-125
4-69 Strains in unidirectional 90-deg SP288/T300 ring specimen under static tensile loading (Specimen No. 3-7).	4-126
4-70 Strains in unidirectional 90-deg SP288/T300 ring specimen under static tensile loading (Specimen No. 3-11).	4-127
4-71 Strain records in steel ring and [90 ₈] graphite/epoxy ring under dynamic loading for Specimen No. 44-5 (650 mg pistol powder).	4-128
4-72 Strain records in steel ring and [90 ₈] SP288/T300 graphite/epoxy ring under dynamic loading for Specimen No. 44-6 (650 mg pistol powder).	4-129
4-73 Strain records in steel ring and [90 ₈] SP288/T300 graphite/epoxy ring under dynamic loading for Specimen No. 44-7 (650 mg pistol powder).	4-130
4-74 Stress-strain curve for dynamically loaded [90 ₈] SP288/T300 graphite/epoxy ring for Specimen No. 44-5 (650 mg pistol powder).	4-131
4-75 Stress-strain curve for dynamically loaded [90 ₈] SP288/T300 graphite/epoxy ring for Specimen No. 44-6 (650 mg pistol powder).	4-132
4-76 Stress-strain curve for dynamically loaded [90 ₈] SP288/T300 graphite/epoxy ring for Specimen No. 44-7 (650 mg pistol powder).	4-133

LIST OF FIGURES (Cont.)

<u>Figure</u>	<u>Page</u>
4-77 Strain records in steel ring and [90 _g] SP288/T300 graphite/epoxy ring under dynamic loading for Specimen No. 3-1 (260 mg pistol powder).	4-134
4-78 Strain and its derivatives in steel ring for Specimen No. 3-1.	4-135
4-79 Circumferential strain and its derivatives in [90 _g] SP288/T300 graphite/epoxy ring under dynamic loading for Specimen No. 3-1 (260 mg pistol powder).	4-136
4-80 Strain records in steel ring and [90 _g] SP288/T300 graphite/epoxy ring under dynamic loading for Specimen No. 3-2 (50 mg PETN detonator).	4-137
4-81 Strain and its derivatives in steel ring for Specimen No. 3-2.	4-138
4-82 Circumferential strain and its derivatives in [90 _g] SP288/T300 graphite/epoxy ring under dynamic loading for Specimen No. 3-2 (50 mg PETN detonator).	4-139
4-83 Strain records in steel ring and [90 _g] SP288/T300 graphite/epoxy ring under dynamic loading for Specimen No. 3-5 (50 mg PETN detonator).	4-140
4-84 Strain and its derivatives in steel ring for Specimen No. 3-5.	4-141
4-85 Circumferential strain and its derivatives in [90 _g] SP288/T300 graphite/epoxy ring under dynamic loading for Specimen No. 3-5 (50 mg PETN detonator).	4-142
4-86 Stress-strain curve for dynamically loaded [90 _g] SP288/T300 graphite/epoxy ring for Specimen No. 3-1 (260 mg pistol powder).	4-143
4-87 Stress-strain curve for dynamically loaded [90 _g] SP288/T300 graphite/epoxy ring for Specimen No. 3-2 (50 mg PETN detonator).	4-144
4-88 Stress-strain curve for dynamically loaded [90 _g] SP288/T300 graphite/epoxy ring for Specimen No. 3-5 (50 mg PETN detonator).	4-145
4-89 Strains in unidirectional 90-deg SP288/AS ring specimen under static tensile loading (Specimen No. 4-3).	4-146
4-90 Strains in unidirectional 90-deg SP288/AS ring specimen under static tensile loading (Specimen No. 5-5).	4-147
4-91 Strains in unidirectional 90-deg SP288/AS ring specimen under static tensile loading (Specimen No. 5-6).	4-148
4-92 Strains in unidirectional 90-deg SP288/AS ring specimen under static tensile loading (Specimen No. 5-10).	4-149

LIST OF FIGURES (Cont.)

<u>Figure</u>	<u>Page</u>
4-93 Strain records in steel ring and [90 _g] SP288/AS graphite/epoxy ring under dynamic loading for Specimen No. 38-7 (650 mg pistol powder).	4-150
4-94 Strain records in steel ring and [90 _g] SP288/AS graphite/epoxy ring under dynamic loading for Specimen No. 38-9 (650 mg pistol powder).	4-151
4-95 Strain records in steel ring and [90 _g] SP288/AS graphite/epoxy ring under dynamic loading for Specimen No. 38-10 (650 mg pistol powder).	4-152
4-96 Stress-strain curve for dynamically loaded [90 _g] SP288/AS graphite/epoxy ring, Specimen No. 38-7 (650 mg pistol powder).	4-153
4-97 Stress-strain curve for dynamically loaded [90 _g] SP288/AS graphite/epoxy ring, Specimen No. 38-9 (650 mg pistol powder).	4-154
4-98 Stress-strain curve for dynamically loaded [90 _g] SP288/AS graphite/epoxy ring, Specimen No. 38-10 (650 mg pistol powder).	4-155
4-99 Strain records in steel ring and [90 _g] SP288/AS graphite/epoxy ring under dynamic loading for Specimen No. 5-9 (260 mg pistol powder).	4-156
4-100 Strain and its derivatives in steel ring for Specimen No. 5-9.	4-157
4-101 Circumferential strain and its derivatives in [90 _g] SP288/AS graphite/epoxy ring under dynamic loading for Specimen No. 5-9 (260 mg pistol powder).	4-158
4-102 Strain records in steel ring and [90 _g] SP288/AS graphite/epoxy ring under dynamic loading for Specimen No. 5-10 (50 mg PETN detonator).	4-159
4-103 Strain and its derivatives in steel ring for Specimen No. 5-10.	4-160
4-104 Circumferential strain and its derivatives in [90 _g] SP288/AS graphite/epoxy ring under dynamic loading for Specimen No. 5-10 (50 mg PETN detonator).	4-161
4-105 Strain records in steel ring and [90 _g] SP288/AS graphite/epoxy ring under dynamic loading for Specimen No. 5-11 (20 mg PETN detonator).	4-162
4-106 Strain and its derivatives in steel ring for Specimen No. 5-11.	4-163
4-107 Circumferential strain and its derivatives in [90 _g] graphite/epoxy ring under dynamic loading for Specimen No. 5-11 (20 mg PETN detonator).	4-164

LIST OF FIGURES (Cont.)

<u>Figure</u>		<u>Page</u>
4-108	Stress-strain curve for dynamically loaded [90 _g] SP288/AS graphite/epoxy ring for Specimen No. 5-9 (260 mg pistol powder).	4-165
4-109	Stress-strain curve for dynamically loaded [90 _g] SP288/AS graphite/epoxy ring for Specimen No. 5-10 (50 mg PETN detonator).	4-166
4-110	Stress-strain curve for dynamically loaded [90 _g] SP288/AS graphite/epoxy ring for Specimen No. 5-11 (20 mg PETN detonator).	4-167
4-111	Strains in unidirectional 90-deg 80AS/20S/PR288 ring specimen under static tensile loading (Specimen No. 1A-4).	4-168
4-112	Strains in unidirectional 90-deg 80AS/20S/PR288 ring specimen under static tensile loading (Specimen No. 1A-5).	4-169
4-113	Strains in unidirectional 90-deg 80AS/20S/PR288 ring specimen under static tensile loading (Specimen No. 1A-6).	4-170
4-114	Strains records in steel ring and 80AS/20S/PR288 [90 _g] graphite/S-glass/epoxy ring under dynamic loading for Specimen No. 39-4 (650 mg pistol powder).	4-171
4-115	Strain records in steel ring and 80AS/20S/PR288 [90 _g] graphite/S-glass/epoxy ring under dynamic loading for Specimen No. 39-5 (650 mg pistol powder).	4-172
4-116	Strain records in steel ring and 80AS/20S/PR288 [90 _g] graphite/S-glass/epoxy ring under dynamic loading for Specimen No. 39-6 (650 mg pistol powder).	4-173
4-117	Stress-strain curve for dynamically loaded [90 _g] 80AS/20S/PR288 graphite/S-glass/epoxy ring for Specimen No. 39-4.	4-174
4-118	Stress-strain curve for dynamically loaded [90 _g] 80AS/20S/PR288 graphite/S-glass/epoxy ring for Specimen No. 39-5.	4-175
4-119	Stress-strain curve for dynamically loaded [90 _g] 80AS/20S/PR288 graphite/S-glass/epoxy ring for Specimen No. 39-6.	4-176
4-120	Strain records in steel ring and [90 _g] 80AS/20S/PR288 graphite/S-glass/epoxy ring under dynamic loading for Specimen No. 1A-1 (130 mg pistol powder).	4-177
4-121	Strain and its derivatives in steel ring for Specimen No. 1A-1.	4-178
4-122	Circumferential strain and its derivatives in [90 _g] 80AS/20S/PR288 graphite/S-glass/epoxy ring under dynamic loading for Specimen NO. 1A-1.	4-179

LIST OF FIGURES (Cont.)

Figure		Page
4-123	Strain records in steel ring and [90 _g] 80AS/20S/PR288 graphite/S-glass/epoxy ring under dynamic loading for Specimen No. 1A-2 (130 mg pistol powder).	4-180
4-124	Strain and its derivatives in steel ring for Specimen No. 1A-2.	4-181
4-125	Circumferential strain and its derivatives in [90 _g] 80AS/20S/PR288 graphite/S-glass/epoxy ring under dynamic loading for Specimen No. 1A-2.	4-182
4-126	Strain records in steel ring and [90 _g] 80AS/20S/PR288 graphite/S-glass/epoxy ring under dynamic loading for Specimen No. 1A-3 (260 mg pistol powder).	4-183
4-127	Strain and its derivatives in steel ring for Specimen No. 1A-3.	4-184
4-128	Circumferential strain and its derivatives in [90 _g] 80AS/20S/PR288 graphite/S-glass/epoxy ring under dynamic loading for Specimen No. 1A-3.	4-185
4-129	Stress-strain curve for dynamically loaded [90 _g] 80AS/20S/PR288 graphite/S-glass/epoxy ring for Specimen No. 1A-1 (130 mg pistol powder).	4-186
4-130	Stress-strain curve for dynamically loaded [90 _g] 80AS/20S/PR288 graphite/S-glass/epoxy ring for Specimen No. 1A-2.	4-187
4-131	Stress-strain curve for dynamically loaded [90 _g] 80AS/20S/PR288 graphite/S-glass/epoxy ring for Specimen No. 1A-3 (260 mg pistol powder).	4-188
4-132	Shear stress versus shear strain for unidirectional 10-deg off-axis SP288/T300 ring specimen (Specimen No. 17-1).	4-189
4-133	Shear stress versus shear strain for unidirectional 10-deg off-axis SP288/T300 ring specimen (Specimen No. 17-2).	4-190
4-134	Shear stress versus shear strain for unidirectional 10-deg off-axis SP288/T300 ring specimen (Specimen No. 17-3).	4-191
4-135	Shear stress versus shear strain for unidirectional 10-deg off-axis SP288/T300 ring specimen (Specimen No. 17-4).	4-192
4-136	Strain records in steel ring and in [10 _g] SP288/T300 graphite/epoxy ring under dynamic loading for Specimen NO. 57-2 (650 mg pistol powder).	4-193
4-137	Strain records in steel ring and in [10 _g] SP288/T300 graphite/epoxy ring under dynamic loading for Specimen No. 57-3 (650 mg pistol powder).	4-194

LIST OF FIGURES (Cont.)

<u>Figure</u>	<u>Page</u>
4-138 Strain records in steel ring and in [10 ₆] SP288/T300 graphite/epoxy ring under dynamic loading for Specimen No. 57-5 (650 mg pistol powder).	4-195
4-139 Shear stress versus shear strain curve for dynamically loaded [10 ₆] SP288/T300 graphite/epoxy ring for Specimen No. 57-2 (650 mg pistol powder).	4-196
4-140 Shear stress versus shear strain curve for dynamically loaded [10 ₆] SP288/T300 graphite/epoxy ring for Specimen No. 57-3 (650 mg pistol powder).	4-197
4-141 Shear stress versus shear strain curve for dynamically loaded [10 ₆] SP288/T300 graphite/epoxy ring for Specimen No. 57-5 (650 mg pistol powder).	4-198
4-142 Strain records in steel ring and [10 ₆] SP288/T300 graphite/epoxy ring under dynamic loading for Specimen No. 17-7 (100 mg PETN detonator).	4-199
4-143 Strain and its derivatives in steel ring for Specimen No. 17-7.	4-200
4-144 Circumferential strain and its derivatives in [10 ₆] SP288/T300 graphite/epoxy ring under dynamic loading for Specimen No. 17-7.	4-201
4-145 Strain records in steel ring and [10 ₆] SP288/T300 graphite/epoxy ring under dynamic loading for Specimen No. 17-8 (100 mg PETN detonator).	4-202
4-146 Strain and its derivatives in steel ring for Specimen No. 17-8.	4-203
4-147 Circumferential strain and its derivatives in [10 ₆] SP288/T300 graphite/epoxy ring under dynamic loading for Specimen No. 17-8.	4-204
4-148 Strain records in steel ring and [10 ₆] SP288/T300 graphite/epoxy ring under dynamic loading for Specimen No. 17-9 (455 mg pistol powder).	4-205
4-149 Strain and its derivatives in steel ring for Specimen No. 17-9.	4-206
4-150 Circumferential strain and its derivatives in [10 ₆] SP288/T300 graphite/epoxy ring under dynamic loading for Specimen No. 17-9.	4-207
4-151 Strain records in steel ring and [10 ₆] SP288/T300 graphite/epoxy ring under dynamic loading for Specimen No. 17-10.	4-208
4-152 Strain and its derivatives in steel ring for Specimen No. 17-10.	4-209
4-153 Circumferential strain and its derivatives in [10 ₆] SP288/T300 graphite/epoxy ring under dynamic loading for Specimen No. 17-10.	4-210

LIST OF FIGURES (Cont.)

<u>Figure</u>		<u>Page</u>
4-154	Stress-strain curve for dynamically loaded [10 ₆] SP288/T300 graphite/epoxy ring for Specimen No. 17-7.	4-211
4-155	Stress-strain curve for dynamically loaded [10 ₆] SP288/T300 graphite/epoxy ring for Specimen No. 17-8 (100 mg PETN detonator).	4-212
4-156	Stress-strain curve for dynamically loaded [10 ₆] SP288/T300 graphite/epoxy ring for Specimen 17-9 (455 mg pistol powder).	4-213
4-157	Stress-strain curve for dynamically loaded [10 ₆] SP288/T300 graphite/epoxy ring for Specimen No. 17-10.	4-214
4-158	Shear stress versus shear strain for unidirectional 10-deg off-axis SP288/AS ring specimen (Specimen No. 15-2).	4-215
4-159	Shear stress versus shear strain for unidirectional 10-deg off-axis SP288/AS ring specimen (Specimen No. 15-3).	4-216
4-160	Shear stress versus shear strain for unidirectional 10-deg off-axis SP288/AS ring specimen (Specimen No. 15-4).	4-217
4-161	Strain records in steel ring and in [10 ₈] SP288/AS graphite/epoxy ring under dynamic loading for Specimen No. 15-9 (650 mg pistol powder).	4-218
4-162	Strain records in steel ring and in [10 ₈] SP288/AS graphite/epoxy ring under dynamic loading for Specimen No. 15-10 (650 mg pistol powder).	4-219
4-163	Strain records in steel ring and in [10 ₈] SP288/AS graphite/epoxy ring under dynamic loading for Specimen No. 15-11 (650 mg pistol powder).	4-220
4-164	Shear stress versus shear strain curve for dynamically loaded [10 ₈] SP288/AS graphite/epoxy ring for Specimen No. 15-9 (650 mg pistol powder).	4-221
4-165	Shear stress versus shear strain curve for dynamically loaded [10 ₈] SP288/AS graphite/epoxy ring for Specimen No. 15-10 (650 mg pistol powder).	4-222
4-166	Shear stress versus shear strain curve for dynamically loaded [10 ₈] SP288/AS graphite/epoxy ring for Specimen No. 15-11 (650 mg pistol powder).	4-223
4-167	Strain records in steel ring and [10 ₈] SP288/AS graphite/epoxy ring under dynamic loading for Specimen No. 15-5 (50 mg PETN detonator).	4-224

LIST OF FIGURES (Cont.)

<u>Figure</u>	<u>Page</u>
4-168 Strain and its derivatives in steel ring for Specimen No. 15-5.	4-225
4-169 Circumferential strain and its derivatives in [10g] SP288/AS graphite/epoxy ring under dynamic loading for Specimen No. 15-5.	4-226
4-170 Strain records in steel ring and [10g] SP288/AS graphite/epoxy ring under dynamic loading for Specimen No. 15-7 (50 mg PETN detonator).	4-227
4-171 Strain and its derivatives in steel ring for Specimen No. 15-7.	4-228
4-172 Circumferential strain and its derivatives in [10g] SP288/AS graphite/epoxy ring under dynamic loading for Specimen No. 15-7.	4-229
4-173 Strain records in steel ring and in [10g] SP288/AS graphite/epoxy ring under dynamic loading for Specimen No. 15-8 (100 mg PETN detonator).	4-230
4-174 Strain and its derivatives in steel ring for Specimen No. 15-8.	4-231
4-175 Circumferential strain and its derivatives in [10g] SP288/AS graphite/epoxy ring under dynamic loading for Specimen No. 15-8.	4-232
4-176 Shear stress versus shear strain curve for dynamically loaded [10g] SP288/AS graphite/epoxy ring for Specimen No. 15-5 (50 mg PETN detonator).	4-233
4-177 Stress-strain curve for dynamically loaded [10g] SP288/AS graphite/epoxy ring for Specimen No. 15-7 (50 mg PETN detonator).	4-234
4-178 Shear stress versus shear strain curve for dynamically loaded [10g] SP288/AS graphite/epoxy ring for Specimen No. 15-8 (100 mg PETN detonator).	4-235
4-179 Shear stress versus shear strain for unidirectional 10-deg off-axis 80AS/20S/PR288 ring specimen (Specimen No. 18-2).	4-236
4-180 Shear stress versus shear strain for unidirectional 10-deg off-axis 80AS/20S/PR288 ring specimen (Specimen No. 18-3).	4-237
4-181 Shear stress versus shear strain for unidirectional 10-deg off-axis 80AS/20S/PR288 ring specimen (Specimen No. 18-4).	4-238
4-182 Strain records in steel ring and 80AS/20S/PR288 graphite/S-glass/epoxy ring under dynamic loading for Specimen No. 18-9 (650 mg pistol powder).	4-239
4-183 Strain records in steel ring and 80AS/20S/PR288 graphite/S-glass/epoxy ring under dynamic loading for Specimen No. 18-10 (650 mg pistol powder).	4-240

LIST OF FIGURES (Cont.)

<u>Figure</u>		<u>Page</u>
4-184	Strain records in steel ring and 80AS/20S/PR288 graphite/S-glass/epoxy ring under dynamic loading for Specimen No. 18-11 (650 mg pistol powder).	4-241
4-185	Shear stress versus shear strain curve for dynamically loaded [10 ₆] 80AS/20S/PR288 graphite/S-glass/epoxy ring for Specimen No. 18-9 (650 mg pistol powder).	4-242
4-186	Shear stress versus shear strain curve for dynamically loaded [10 ₆] 80AS/20S/PR288 graphite/S-glass/epoxy ring for Specimen No. 18-10 (650 mg pistol powder).	4-243
4-187	Shear stress versus shear strain curve for dynamically loaded [10 ₆] 80AS/20S/PR288 graphite/S-glass/epoxy ring for Specimen No. 18-11 (650 mg pistol powder).	4-244
4-188	Strain records in steel ring and [10 ₆] 80AS/20S/PR288 graphite/S-glass/epoxy ring under dynamic loading for Specimen No. 18-5 (100 mg PETN detonator).	4-245
4-189	Strain and its derivatives in steel ring for Specimen No. 18-5.	4-246
4-190	Circumferential strain and its derivatives in [10 ₆] 80AS/20S/PR288 graphite/S-glass/epoxy ring under dynamic loading for Specimen No. 18-5 (100 mg PETN detonator).	4-247
4-191	Strain records in steel ring and [10 ₆] 80AS/20S/PR288 graphite/S-glass/epoxy ring under dynamic loading for Specimen No. 18-6 (455 mg pistol powder).	4-248
4-192	Strain and its derivatives in steel ring for Specimen No. 18-6.	4-249
4-193	Circumferential strain and its derivatives in [10 ₆] 80AS/20S/PR288 graphite/S-glass/epoxy ring under dynamic loading for Specimen No. 18-6 (455 mg pistol powder).	4-250
4-194	Strain records in steel ring and [10 ₆] 80AS/20S/PR288 graphite/S-glass/epoxy ring under dynamic loading for Specimen No. 18-8 (100 mg PETN detonator).	4-251
4-195	Strain and its derivatives in steel ring for Specimen No. 18-8.	4-252
4-196	Circumferential strain and its derivatives in [10 ₆] 80AS/20S/PR288 graphite/S-glass/epoxy ring under dynamic loading for Specimen No. 18-8 (100 mg PETN detonator).	4-253
4-197	Shear stress versus shear strain curve for dynamically loaded [10 ₆] 80AS/20S/PR288 graphite/S-glass/epoxy ring for Specimen No. 18-5 (100 mg PETN detonator).	4-254

LIST OF FIGURES (Cont.)

<u>Figure</u>	<u>Page</u>
4-198 Shear stress versus shear strain curve for dynamically loaded [10 ₆] 80AS/20S/PR288 graphite/S-glass/epoxy ring for Specimen No. 18-6 (455 mg pistol powder).	4-255
4-199 Shear stress versus shear strain curve for dynamically loaded [10 ₆] 80AS/20S/PR288 graphite/S-glass/epoxy ring for Specimen No. 18-8 (100 mg PETN detonator).	4-256
4-200 Arbor for holding test and calibration ring specimens in compression fixture.	4-257
4-201 Specimen holding arbor attached to base plate.	4-258
4-202 Dynamic compression fixture.	4-259
4-203 Fixture for dynamic compressive loading of composite ring specimens.	4-260
4-204 Strain records in steel ring and SP288/T300 [0 ₆] graphite/epoxy ring under dynamic loading for Specimen No. 19-8 (1.56 g pistol powder, KClO ₄ , and aluminum dust).	4-261
4-205 Strain and its derivatives in steel ring for Specimen No. 19-8.	4-262
4-206 Circumferential strain and its derivatives in SP288/T300 [0 ₆] graphite/epoxy ring under dynamic loading for Specimen No. 19-8 (1.56 g pistol powder, KClO ₄ , and aluminum dust).	4-263
4-207 Strain records in steel ring and SP288/T300 [0 ₆] graphite/epoxy ring under dynamic loading for Specimen No. 19-9 (1.56 g pistol powder, KClO ₄ , and aluminum dust).	4-264
4-208 Strain and its derivatives in steel ring for Specimen No. 19-9.	4-265
4-209 Circumferential strain and its derivatives in SP288/T300 [0 ₆] graphite/epoxy ring under dynamic loading for Specimen No. 19-9 (1.56 g pistol powder, KClO ₄ , and aluminum dust).	4-266
4-210 Strain records in steel ring and SP288/T300 [0 ₆] graphite/epoxy ring under dynamic loading for Specimen No. 40-1 (1.56 g pistol powder, KClO ₄ , and aluminum dust).	4-267
4-211 Strain and its derivatives in steel ring for Specimen No. 40-1.	4-268
4-212 Circumferential strain and its derivatives in SP288/T300 [0 ₆] graphite/epoxy ring under dynamic loading for Specimen No. 40-1 (1.56 g pistol powder, KClO ₄ , and aluminum dust).	4-269
4-213 Strain records in steel ring and SP288/T300 [0 ₆] graphite/epoxy ring under dynamic loading for Specimen No. 40-2 (1.56 g pistol powder, KClO ₄ , and aluminum dust).	4-270

LIST OF FIGURES (Cont.)

<u>Figure</u>	<u>Page</u>
4-214 Strain and its derivatives in steel ring for Specimen No. 40-2.	4-271
4-215 Circumferential strain and its derivatives in SP288/T300 [O ₆] graphite/epoxy ring under dynamic loading for Specimen No. 40-2 (1.56 g pistol powder, KClO ₄ , and aluminum dust).	4-272
4-216 Stress-strain curve for SP288/T300 [O ₆] graphite/epoxy ring loaded in dynamic compression, Specimen No. 19-8 (1.56 g pistol powder, KClO ₄ , and aluminum dust).	4-273
4-217 Stress-strain curve for SP288/T300 [O ₆] graphite/epoxy ring loaded in dynamic compression, Specimen No. 19-9 (1.56 g pistol powder, KClO ₄ , and aluminum dust).	4-274
4-218 Stress-strain curve for SP288/T300 [O ₆] graphite/epoxy ring loaded in dynamic compression, Specimen No. 40-1 (1.56 g pistol powder, KClO ₄ , and aluminum dust).	4-275
4-219 Stress-strain curve for SP288/T300 [O ₆] graphite/epoxy ring loaded in dynamic compression, Specimen No. 40-2 (1.56 g pistol powder, KClO ₄ , and aluminum dust).	4-276
4-220 Strain records in steel ring and [O ₆] SP288/AS graphite/epoxy ring under dynamic loading for Specimen No. 45-2 (1.56 g pistol powder, KClO ₄ , and aluminum dust).	4-277
4-221 Strain and its derivatives in steel ring for Specimen No. 45-2.	4-278
4-222 Circumferential strain and its derivatives in [O ₆] SP288/AS graphite/epoxy ring under dynamic loading for Specimen No. 45-2 (1.56 g pistol powder, KClO ₄ , and aluminum dust).	4-279
4-223 Strain records in steel ring and [O ₆] SP288/AS graphite/epoxy ring under dynamic loading for Specimen No. 45-3 (1.56 g pistol powder, KClO ₄ , and aluminum dust).	4-280
4-224 Strain and its derivatives in steel ring for Specimen No. 45-3.	4-281
4-225 Circumferential strain and its derivatives in [O ₆] SP288/AS graphite/epoxy ring under dynamic loading for Specimen No. 45-3 (1.56 g pistol powder, KClO ₄ , and aluminum dust).	4-282
4-226 Strain records in steel ring and [O ₆] SP288/AS graphite/epoxy ring under dynamic loading for Specimen No. 45-4 (1.56 g pistol powder, KClO ₄ , and aluminum dust).	4-283
4-227 Strain and its derivatives in steel ring for Specimen No. 45-4.	4-284
4-228 Circumferential strain and its derivatives in [O ₆] SP288/AS graphite/epoxy ring under dynamic loading for Specimen No. 45-4 (1.56 g pistol powder, KClO ₄ , and aluminum dust).	4-285

LIST OF FIGURES (Cont.)

<u>Figure</u>	<u>Page</u>
4-229 Stress-strain curve for $[0_6]$ SP288/AS graphite/epoxy ring loaded in dynamic compression, Specimen No. 45-2 (1.56 g pistol powder, $KClO_4$, and aluminum dust).	4-286
4-230 Stress-strain curve for $[0_6]$ SP288/AS graphite/epoxy ring loaded in dynamic compression, Specimen No. 45-3 (1.56 g pistol powder, $KClO_4$, and aluminum dust).	4-287
4-231 Stress-strain curve for $[0_6]$ SP288/AS graphite/epoxy ring loaded in dynamic compression, Specimen No. 45-4 (1.56 g pistol powder, $KClO_4$, and aluminum dust).	4-288
4-232 Strain records in steel ring and $[90_8]$ SP288/T300 graphite/epoxy ring under dynamic loading for Specimen No. 44-1 (1.56 g pistol powder, $KClO_4$, and aluminum dust).	4-289
4-233 Strain and its derivatives in steel ring for Specimen No. 44-1.	4-290
4-234 Circumferential strain and its derivatives in $[90_8]$ SP288/T300 graphite/epoxy ring under dynamic loading for Specimen No. 44-1 (1.56 g pistol powder, $KClO_4$, and aluminum dust).	4-291
4-235 Strain records in steel ring and $[90_8]$ SP288/T300 graphite/epoxy ring under dynamic loading for Specimen No. 44-3 (1.56 g pistol powder, $KClO_4$, and aluminum dust).	4-292
4-236 Strain and its derivatives in steel ring for Specimen No. 44-3.	4-293
4-237 Circumferential strain and its derivatives in $[90_8]$ SP288/T300 graphite/epoxy ring under dynamic loading for Specimen No. 44-3 (1.56 g pistol powder, $KClO_4$, and aluminum dust).	4-294
4-238 Strain records in steel ring and $[90_8]$ SP288/T300 graphite/epoxy ring under dynamic loading for Specimen No. 44-4 (1.56 g pistol powder, $KClO_4$, and aluminum dust).	4-295
4-239 Strain and its derivatives in steel ring for Specimen No. 44-4.	4-296
4-240 Circumferential strain and its derivatives in $[90_8]$ SP288/T300 graphite/epoxy ring under dynamic loading for Specimen No. 44-4 (1.56 g pistol powder, $KClO_4$, and aluminum dust).	4-297
4-241 Stress-strain curve for dynamically loaded $[90_8]$ SP288/T300 graphite/epoxy ring, Specimen No. 44-1 (1.56 g pistol powder, $KClO_4$, and aluminum dust).	4-298
4-242 Stress-strain curve for dynamically loaded $[90_8]$ SP288/T300 graphite/epoxy ring, Specimen No. 44-3 (1.56 g pistol powder, $KClO_4$, and aluminum dust).	4-299

LIST OF FIGURES (Cont.)

<u>Figure</u>		<u>Page</u>
4-243	Stress-strain curve for dynamically loaded [90g] SP288/T300 graphite/epoxy ring, Specimen No. 44-4 (1.56 g pistol powder, $KClO_4$, and aluminum dust).	4-300
4-244	Strain records in steel ring and [90g] SP288/AS graphite/epoxy ring under dynamic loading for Specimen No. 38-1 (1.56 g pistol powder, $KClO_4$, and aluminum dust).	4-301
4-245	Strain and its derivatives in steel ring for Specimen No. 38-1.	4-302
4-246	Circumferential strain and its derivatives in [90g] SP288/AS graphite/epoxy ring under dynamic loading for Specimen No. 38-1 (1.56 g pistol powder, $KClO_4$, and aluminum dust).	4-303
4-247	Strain records in steel ring and [90g] SP288/AS graphite/epoxy ring under dynamic loading for Specimen No. 38-2 (1.56 g pistol powder, $KClO_4$, and aluminum dust).	4-304
4-248	Strain and its derivatives in steel ring for Specimen No. 38-2.	4-305
4-249	Circumferential strain and its derivatives in [90g] SP288/AS graphite/epoxy ring under dynamic loading for Specimen No. 38-2 (1.56 g pistol powder, $KClO_4$, and aluminum dust).	4-306
4-250	Strain records in steel ring and [90g] SP288/AS graphite/epoxy ring under dynamic loading for Specimen No. 38-3 (1.56 g pistol powder, $KClO_4$, and aluminum dust).	4-307
4-251	Strain and its derivatives in steel ring for Specimen No. 38-3.	4-308
4-252	Circumferential strain and its derivatives in [90g] SP288/AS graphite/epoxy ring under dynamic loading for Specimen No. 38-3 (1.56 g pistol powder, $KClO_4$, and aluminum dust).	4-309
4-253	Stress-strain curve for dynamically loaded [90g] SP288/AS graphite/epoxy ring, Specimen No. 38-1 (1.56 g pistol powder, $KClO_4$, and aluminum dust).	4-310
4-254	Stress-strain curve for dynamically loaded [90g] SP288/AS graphite/epoxy ring, Specimen No. 38-2 (1.56 g pistol powder, $KClO_4$, and aluminum dust).	4-311
4-255	Stress-strain curve for dynamically loaded [90g] SP288/AS graphite/epoxy ring, Specimen No. 38-3 (1.56 g pistol powder, $KClO_4$, and aluminum dust).	4-312
4-256	Strain records in steel ring and [90g] 80AS/20S/PR288 graphite/S-glass/epoxy ring under dynamic loading for Specimen No. 39-1 (1.56 g pistol powder, $KClO_4$, and aluminum dust).	4-313

LIST OF FIGURES (Cont.)

<u>Figure</u>	<u>Page</u>
4-257 Strain and its derivatives in steel ring for Specimen No. 39-1.	4-314
4-258 Circumferential strain and its derivatives in [90 _g] 80AS/20S/PR288 graphite/S-glass/epoxy ring under dynamic loading for Specimen No. 39-1 (1.56 g pistol powder, KClO ₄ , and aluminum dust).	4-315
4-259 Strain records in steel ring and [90 _g] 80AS/20S/PR288 graphite/S-glass/epoxy ring under dynamic loading for Specimen No. 39-2 (1.56 g pistol powder, KClO ₄ , and aluminum dust).	4-316
4-260 Strain and its derivatives in steel ring for Specimen No. 39-2.	4-317
4-261 Circumferential strain and its derivatives in [90 _g] 80AS/20S/PR288 graphite/S-glass/epoxy ring under dynamic loading for Specimen No. 39-2 (1.56 g pistol powder, KClO ₄ , and aluminum dust).	4-318
4-262 Strain records in steel ring and [90 _g] 80AS/20S/PR288 graphite/S-glass/epoxy ring under dynamic loading for Specimen No. 39-3 (1.56 g pistol powder, KClO ₄ , and aluminum dust).	4-319
4-263 Strain and its derivatives in steel ring for Specimen No. 39-3.	4-320
4-264 Circumferential strain and its derivatives in [90 _g] 80AS/20S/PR288 graphite/S-glass/epoxy ring under dynamic loading for Specimen No. 39-3 (1.56 g pistol powder, KClO ₄ , and aluminum dust).	4-321
4-265 Stress-strain curve for dynamically loaded [90 _g] 80AS/20S/PR288 graphite/S-glass/epoxy ring, Specimen No. 39-1 (1.56 g pistol powder, KClO ₄ , and aluminum dust).	4-322
4-266 Stress-strain curve for dynamically loaded [90 _g] 80AS/20S/PR288 graphite/S-glass/epoxy ring, Specimen No. 39-2 (1.56 g pistol powder, KClO ₄ , and aluminum dust).	4-323
4-267 Stress-strain curve for dynamically loaded [90 _g] 80AS/20S/PR288 graphite/S-glass/epoxy ring, Specimen No. 39-3 (1.56 g pistol powder, KClO ₄ , and aluminum dust).	4-324
5-1 Ratio of dynamic to static longitudinal modulus for three materials as a function of strain rate.	5-4
5-2 Ratio of dynamic to static transverse secant modulus for three materials as a function of strain rate.	5-5
5-3 Ratio of dynamic to static in-plane shear modulus for three materials as a function of strain rate.	5-6

HIGH STRAIN RATE PROPERTIES OF COMPOSITES

1. INTRODUCTION

Some applications of composite materials involve dynamically loaded components and structures. For example, composite jet engine blades are exposed to the hazards of foreign object damage, such as bird impact on rotating blades. Such impacts occur at velocities up to 305 ms^{-1} (1000 ft/sec) and can cause extensive damage to the composite blade. Similarly, in applications to protective armor or other components, composites are subject to high velocity impacts. These impact loadings are of short duration of the order of $100 \mu\text{s}$, and produce stress (strain) wave pulses with strain rates up to a few hundred (m/m) per second. The application of composites to such dynamically loaded structures requires knowledge and understanding of the dynamic loading, induced wave propagation phenomena, and the response of the material to the high strain rates produced. Reliable design of composite components for impact resistance requires characterization of the composite material at high strain rates.

Most composite materials have been amply characterized under quasi-static conditions. Related work under dynamic conditions has been limited. Early attempts were limited to the determination of elastic constants by ultrasonic velocity measurements and vibration testing.¹⁻³ In the few cases investigated it was reported that composite stiffnesses were not greatly affected by strain rate. In the case of complex moduli, the loss modulus was found to be much more sensitive to frequency (strain rate) than the storage modulus.

Testing of composites at high strain rates has been described by Rotem and Lifshitz,^{4,5} Armenakas and Sciammarella,⁶ and Daniel and Liber.^{7,8} The former investigated unidirectional and angle-ply E-glass/epoxy laminates under dynamic tensile loading. They achieved strain rates up to 30s^{-1} using an instrumented falling weight apparatus. In their first study of 0-deg unidirectional E-glass/epoxy they found dynamic strength values of almost three times the static values and a dynamic modulus approximately 50 percent higher than the static.⁴ They also found that the ultimate strain was not affected much by strain rate. In a later study with angle-ply laminates, Lifshitz

found that the initial modulus was unaffected by strain rate and that the dynamic tensile strength was higher than the static, but only by approximately 20 to 30 percent.⁵

Armenakas and Sciammarella⁶ studied the response of 0-deg unidirectional glass/epoxy specimens at strain rates up to 500s^{-1} using an explosively driven testing system. The material they tested was a very low fiber-volume composite prepared in the laboratory. They found a linear variation of the modulus with the logarithm of the strain rate. The ultimate strain, however, decreased with increasing strain rate. The latter is in total contradiction with the results of Rotem and Lifshitz.⁴

Daniel and Liber conducted an experimental investigation to determine the strain rate effects in unidirectional composite specimens of boron/epoxy, graphite/epoxy, S-glass/epoxy, and Kevlar 49/epoxy.^{7,8} Strain rates up to 27s^{-1} were achieved using an electrohydraulic system. Longitudinal, transverse, and in-plane shear properties, including modulus, Poisson's ratio, strength, and ultimate strain, were determined by testing 0-, 90-, and 10-deg unidirectional coupons. The 0-deg properties which are governed by the fibers did not vary much with strain rate except for the Kevlar 49/epoxy material. The strain rate effects on 90-deg properties were also small. The most noticeable effect of strain rate was on in-plane shear properties with shear strength values at high strain rates approximately 15 percent higher than static values.

Compressive properties of composites (steel-wire reinforced epoxy) were studied by Sierakowski et al. at strain rates up to 1000s^{-1} using a split Hopkinson bar.⁹ The failure modes at the high strain rates were significantly different from those at lower rates. The initial modulus remained unaffected by strain rate, but the strength increased by as much as 100 percent at the higher rates. The fact that the failure modes were significantly different at high strain rates may be partly due to the multiaxial states of stress induced in the short cylindrical specimens by the Hopkinson bar.

A variety of testing techniques and procedures have been developed for testing materials at high rates of loading. Different methods are suited for different ranges of strain rate. A diagram illustrating the various basic methods and the corresponding strain rate regimes is shown in Figure 1. The

lowest strain rate region is associated with creep where a constant load is applied and the strain variation with time is recorded. The quasi-static region corresponds to strain rates up to 0.1s^{-1} . Standard hydraulic or screw machines such as the Instron are used to apply loads to coupons at a constant strain rate.

In the intermediate strain-rate region for strain rates up to approximately 50s^{-1} fast-acting hydraulic or pneumatic machines are used. One such machine was the electrohydraulic system used by Daniel and Liber in their recent work on high-rate testing of composites.⁷ An MTS electrohydraulic closed-loop system capable of delivering a wide range of input pulses at velocities up to 5.1 ms^{-1} (12,000 in./min) was used. It was augmented with specially designed fixtures to make its performance conform to the test requirements. In this range of strain rates inertia forces begin to become important and possible mechanical resonances must be taken into account. Similar intermediate strain rates have been applied by falling weight apparatus such as the one used by Rotem and Lifshitz.⁴

In this medium regime wave propagation effects are neglected and uniform stresses and strains are assumed in the test specimen. Load is normally measured with a load cell connected in series with the specimen. Strain gages on the specimen are recorded on oscilloscopes or tape recorders.

Higher strain rates, primarily in compression, can be obtained with mechanical impact from a fast moving mass or by explosively generated pulses. In the highest strain-rate regime wave propagation effects become very dominant and must be accounted for. This fact leads to many difficulties and causes a great deal of uncertainty on the interpretation of results. For this reason the scant data available in this high strain rate region is of doubtful validity.

To overcome the difficulties associated with wave propagation effects a new method for testing composites at high strain rates was developed and has been described recently in the literature.¹¹ The method utilizes a thin ring specimen loaded with a dynamic pressure pulse. The transit time of the stress wave across the thickness of the specimen is very short compared to the duration of the test.

The objective of the present investigation is to characterize unidirectional and angle-ply composite laminates over a wide range of strain rates. The program consists of the following tasks:

Task 1 - Test Planning and Specimen Preparation

The objective of this task is to develop test procedures, procure the material, and prepare the specimens.

Task 2 - Strain Rate Characterization of Unidirectional Composites

The objective of this task is to determine longitudinal, transverse, and in-plane shear properties of three unidirectional composite materials at three different strain rates.

Task 3 - Strain Rate Characterization of Off-Axis Laminates

The objective of this task is to characterize unidirectional composites of two material systems in uniaxial tension at various angles with the fiber direction at three strain rates.

Task 4 - Strain Rate Characterization of Angle-Ply Laminates

The objective of this task is to characterize angle-ply laminates of two material systems in uniaxial tension at three strain rates.

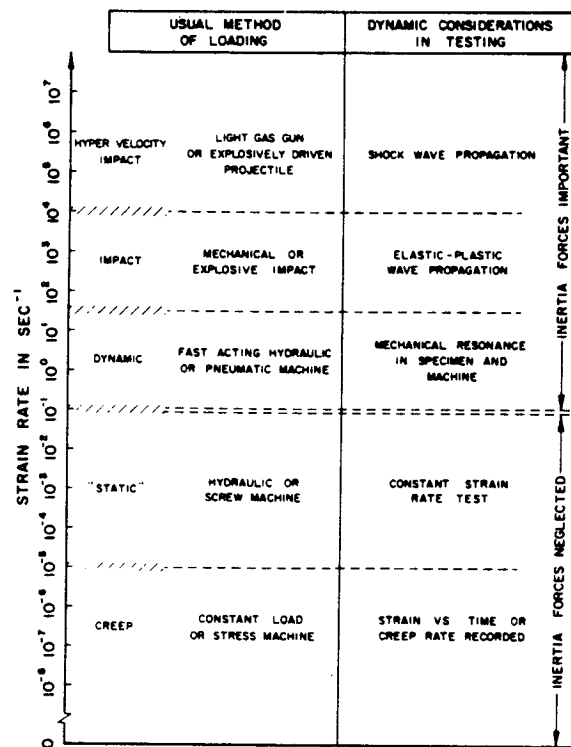


Figure 1-1. Dynamic loading regimes.¹⁰

2. TEST PLANNING AND SPECIMEN PREPARATION

2.1 MATERIAL PROCUREMENT AND QUALIFICATION

The materials selected for characterization are the following:

- (1) SP288T300 graphite/epoxy
- (2) SP288/AS graphite/epoxy
- (3) 80AS/20S/PR288 graphite/S-glass/epoxy
(Intraply hybrid with 80 percent AS fiber
composite and 20 percent S-glass fiber
composite).

These materials consist of Thornell 300 graphite, AS graphite, and S-glass fibers impregnated with PR-288 epoxy resin made by the 3M Company. The material was obtained in the form of 30.5 cm (12 in.) wide and 0.13 mm (0.005 in.) thick prepreg tape. The intraply hybrid prepreg consists of approximately 0.32 cm (0.125 in.) wide strips of S-glass interspersed between the AS graphite prepreg with a spacing of approximately 1.59 cm (0.625 in.).

The prepreg materials above were cured according to the following curing cycle:

- (1) Apply full vacuum to bagged layup
- (2) Pressurize autoclave to 587 kPa (85 psi)
- (3) Heat up to 400°K (260°F) at a rate of 2.8°K (5°F) per minute and hold for 4 hours
- (4) Allow to cool to room temperature, release vacuum and pressure, and remove from autoclave.

Plates 15.2 cm x 15.2 cm (6 in. x 6 in.) and 15-ply thick were fabricated for qualification testing. Flexural strength coupons were 10.2 cm (4 in.) long, 1.3 cm (0.5 in.) wide with a 6.3 cm (2.5 in.) span length. Interlaminar shear strength coupons were 1.5 cm (0.6 in.) long, 0.6 cm (0.25 in.) wide and had a 1 cm (0.4 in.) span length. These specimens were subjected to three-point bending. Results of these qualification tests are tabulated in Tables 2-1 and 2-2.

TABLE 2-1. QUALIFICATION FLEXURE TESTS FOR GRAPHITE/EPOXY SP288/T300

Specimen Number	Thickness, cm (in.)	Width, cm (in.)	Flexural Strength, MPa (ksi)
1	0.188 (0.074)	1.270 (0.500)	1616 (234)
2	0.193 (0.076)	1.265 (0.498)	1610 (233)
3	0.190 (0.075)	1.265 (0.498)	1746 (253)
4	0.193 (0.076)	1.265 (0.498)	1799 (261)
5	0.190 (0.075)	1.267 (0.499)	1770 (257)
		Average:	1708 (248)

TABLE 2-2. QUALIFICATION INTERLAMINAR SHEAR TESTS FOR GRAPHITE/EPOXY SP288/T300

Specimen Number	Thickness, cm (in.)	Width, cm (in.)	Shear Strength, MPa (ksi)
1	0.182 (0.073)	0.635 (0.250)	94.9 (13.8)
2	0.193 (0.076)	0.627 (0.247)	98.9 (14.3)
3	0.191 (0.075)	0.624 (0.246)	100.1 (14.5)
4	0.191 (0.075)	0.622 (0.245)	98.0 (14.2)
5	0.188 (0.074)	0.627 (0.247)	106.9 (15.5)
6	0.191 (0.075)	0.635 (0.250)	105.6 (15.3)
		Average:	100.7 (14.6)

The results above were judged satisfactory since they compare favorably with similar data from the manufacturer.

Qualification test results for the SP288/AS graphite/epoxy are tabulated in Tables 2-3 and 2-4.

TABLE 2-3. QUALIFICATION FLEXURE TESTS FOR GRAPHITE/EPOXY SP288/AS

Specimen Number	Thickness, cm (in.)	Width, cm (in.)	Flexural Strength, MPa (ksi)
1	0.183 (0.072)	1.257 (0.495)	1755 (254)
2	0.191 (0.075)	1.262 (0.497)	1583 (229)
3	0.196 (0.077)	1.267 (0.499)	1592 (231)
4	0.193 (0.076)	1.265 (0.498)	1637 (237)
5	0.196 (0.077)	1.267 (0.499)	1565 (227)
6	0.196 (0.077)	1.257 (0.495)	1613 (234)
Average:			1624 (235)

TABLE 2-4. QUALIFICATION INTERLAMINAR SHEAR TESTS FOR GRAPHITE/EPOXY SP288/AS

Specimen Number	Thickness, cm (in.)	Width, cm (in.)	Shear Strength, MPa (ksi)
1	0.196 (0.077)	0.632 (0.249)	102.6 (14.9)
2	0.191 (0.075)	0.635 (0.250)	95.5 (13.8)
3	0.196 (0.077)	0.635 (0.250)	87.9 (12.7)
4	0.193 (0.076)	0.632 (0.249)	91.1 (13.2)
5	0.196 (0.077)	0.630 (0.248)	108.4 (15.7)
6	0.193 (0.076)	0.635 (0.250)	97.2 (14.1)
Average:			97.1 (14.1)

The results above are very similar to those for the SP288/T300 material.

Qualification test results for the 80AS/20S/PR288 intra-ply hybrid are tabulated in Tables 2-5 and 2-6.

TABLE 2-5. QUALIFICATION FLEXURE TESTS FOR GRAPHITE/S-GLASS/EPOXY 80AS/20S/PR288

Specimen Number	Thickness, cm (in.)	Width, cm (in.)	Flexural Strength, MPa (ksi)
1	0.198 (0.078)	1.265 (0.498)	1255 (182)
2	0.188 (0.074)	1.260 (0.496)	1543 (224)
3	0.188 (0.074)	1.257 (0.495)	1403 (203)
4	0.193 (0.076)	1.265 (0.498)	1268 (184)
5	0.188 (0.074)	1.265 (0.498)	1376 (199)
		Average:	1369 (198)

TABLE 2-6. QUALIFICATION INTERLAMINAR SHEAR TESTS FOR GRAPHITE/S-GLASS/EPOXY 80AS/20S/PR288

Specimen Number	Thickness, cm (in.)	Width, cm (in.)	Shear Strength, MPa (ksi)
1	0.180 (0.071)	0.632 (0.249)	67.3 (9.6)
2	0.183 (0.072)	0.632 (0.249)	68.7 (10.0)
3	0.185 (0.073)	0.632 (0.249)	71.2 (10.3)
4	0.188 (0.074)	0.635 (0.250)	65.7 (9.5)
5	0.183 (0.072)	0.630 (0.248)	69.6 (10.1)
6	0.180 (0.071)	0.635 (0.250)	72.9 (10.6)
		Average:	69.2 (10.0)

No data were available from the manufacturer for comparison with the results above. However, the flexural strength seems to be somewhat lower than expected and the interlaminar shear strength falls between the values obtained for all-graphite and all-glass specimens.

2.2 PRELIMINARY MATERIAL CHARACTERIZATION

The three materials received were fully characterized under static loading conditions. The properties obtained were unidirectional tensile and compressive properties in the fiber and transverse-to-the-fiber directions and intralaminar shear properties. Results of these tests were subsequently compared with those of quasi-static tests using ring specimens to demonstrate the equivalence of coupon and ring specimens under quasi-static conditions.

Unidirectional 0-deg tensile properties were obtained by testing 2.54 cm x 22.9 cm (1 in. x 9 in.) 6-ply coupons. Two specimens of each, instrumented with 2-gage rosettes on each side, were tested. Typical stress-strain curves as well as modulus, Poisson's ratio, strength, and ultimate strain are shown in Figures 2-1 to 2-6. Strains are linear up to approximately 860 MPa (125 ksi); thereafter, an apparent stiffening of the specimen occurs. The graphite/epoxy with T300 fibers is stiffer and stronger than that with AS fibers which in turn is stiffer and stronger than the graphite/S-glass/epoxy hybrid.

Unidirectional 90-deg tensile properties were obtained by testing 2.54 cm x 22.9 cm (1 in. x 9 in.) 8-ply coupons. Two specimens of each, instrumented with 2-gage rosettes on each side, were tested. Typical stress-strain curves as well as modulus, Poisson's ratio, strength, and ultimate strain are shown in Figures 2-7 to 2-12. Strains are linear up to approximately 30 MPa (4.5 ksi) corresponding to axial strains of less than 0.003. The graphite/epoxy with T300 fibers is stiffer and stronger than that with AS fibers which in turn is stronger than the graphite/S-glass/epoxy hybrid.

Compressive properties were obtained using the IITRI-designed compression test fixture which represents an improved modification of the Celanese fixture. The IITRI fixture uses trapezoidal wedges as opposed to the conical grips of the Celanese fixture. The trapezoidal wedges permit surface-to-surface contact at all positions and apply lateral compression to the specimen tabs to prevent slippage. The longitudinal coupons were 13.5 cm x 0.64 cm (5.3 in. x 0.25 in.) and 15-ply thick with a gage length of 9.5 mm (0.375 in.). The transverse coupons were 15-ply thick and had a gage length of 6.4 mm (1/4 in.). The gage sections of these specimens were instrumented with axial gages on both sides, primarily to monitor strains during loading and confirm the axi-ality of

compressive loading up to failure. Three specimens of each type and each material were tested. Stress-strain curves to failure for the unidirectional compressive specimens are shown in Figures 2-13 to 2-30. Also shown in these figures are the modulus, strength, and ultimate strain obtained from these data. Both 0-deg and 90-deg specimens show nonlinear behavior not associated with buckling. The 0-deg graphite/epoxy specimens show a modulus somewhat lower than that obtained from tensile specimens, but this difference may not be significant. The hybrid 0-deg specimens on the other hand show a somewhat higher modulus in compression. The 0-deg compressive strength is lower than the tensile strength, but this difference is smaller in the case of the hybrid specimens. The compressive modulus for the 90-deg specimens is lower than the tensile modulus for the SP288/T300 material, but higher for the SP288/AS and the hybrid materials. The compressive 90-deg strength is much higher than the transverse tensile strength for all three materials. The two graphite/epoxy materials have higher transverse compressive strength than the hybrid material.

In-plane shear properties were determined by testing 10-deg off-axis unidirectional specimens, 1.27 cm (0.50 in.) wide, 6-ply thick, and 25.4 cm (10 in.) long. Four specimens of each material were tested. Two specimens of each material were instrumented with 3-gage rosettes on each side. Shear stress and shear strain computed from the measured data are plotted in Figures 2-31 to 2-36. The in-plane shear modulus, shear strength, and ultimate shear strain are also shown in these figures.

Results from all the characterization tests above for the three materials tested are summarized in Tables 2-7, 2-8, and 2-9.

2.3 LAMINATE FABRICATION

The specimen geometry selected was a ring 10.16 cm (4 in.) in diameter, 2.54 cm (1 in.) wide, and 6 to 8 plies thick. The thin-wall ring specimen under internal pressure is equivalent to a uniaxially loaded flat coupon.¹²⁻¹⁵ The rings are tabless specimens and as such they are free from end constraints. This presents an important advantage over tabbed flat coupons for the determination of off-axis and shear properties of unidirectional composites, because uniform shear deformations can be developed throughout the specimen.

TABLE 2-7. PROPERTIES OF UNIDIRECTIONAL GRAPHITE/EPOXY SP288/T300

Property	Value
Ply Thickness	0.127 mm (0.0050 in.)
Longitudinal Modulus, E_{11}	145 GPa (21.1×10^6 psi)
Transverse Modulus, E_{22}	11.4 GPa (1.66×10^6 psi)
Shear Modulus, G_{12}	6.6 GPa (0.95×10^6 psi)
Major Poisson's Ratio, ν_{12}	0.30
Minor Poisson's Ratio, ν_{21}	0.017
Longitudinal Tensile Strength, S_{11T}	1656 MPa (240 ksi)
Ultimate Longitudinal Tensile Strain, ϵ_{11T}^u	0.01133
Longitudinal Compressive Strength, S_{11C}	1297 MPa (188 ksi)
Ultimate Longitudinal Compressive Strain, ϵ_{11C}^u	0.01142
Transverse Tensile Strength, S_{22T}	71 MPa (10.3 ksi)
Ultimate Transverse Tensile Strain, ϵ_{22T}^u	0.00660
Transverse Compressive Strength, S_{22C}	251 MPa (36 ksi)
Ultimate Transverse Compressive Strain, ϵ_{22C}^u	0.03365
In-plane Shear Strength, S_{12}	73 MPa (10.7 ksi)
Ultimate Shear Strain, ϵ_{12}^u	0.00935

TABLE 2-8. PROPERTIES OF UNIDIRECTIONAL GRAPHITE/EPOXY SP288/AS

Property	Value
Ply Thickness	0.130 mm (0.0051 in.)
Longitudinal Modulus, E_{11}	137 GPa (19.9×10^6 psi)
Transverse Modulus, E_{22}	10.4 GPa (1.51×10^6 psi)
Shear Modulus, G_{12}	6.3 GPa (0.91×10^6 psi)
Major Poisson's Ratio, ν_{12}	0.32
Minor Poisson's Ratio, ν_{21}	0.016
Longitudinal Tensile Strength, S_{11T}	1518 MPa (220 ksi)
Ultimate Longitudinal Tensile Strain, ϵ_{11T}^u	0.01080
Longitudinal Compressive Strength, S_{11C}	1235 MPa (179 ksi)
Ultimate Longitudinal Compressive Strain, ϵ_{11C}^u	0.01080
Transverse Tensile Strength, S_{22T}	64 MPa (9.3 ksi)
Ultimate Transverse Tensile Strain, ϵ_{22T}^u	0.00660
Transverse Compressive Strength, S_{22C}	244 MPa (35 ksi)
Ultimate Transverse Compressive Strain, ϵ_{22C}^u	0.03175
In-plane Shear Strength, S_{12}	79 MPa (11.5 ksi)
Ultimate Shear Strain, ϵ_{12}^u	0.0153

TABLE 2-9. PROPERTIES OF UNIDIRECTIONAL
GRAPHITE/S-GLASS/EPOXY 80AS/20S/PR288

Property	Value
Ply Thickness	0.134 mm (0.0053 in.)
Longitudinal Modulus, E_{11}	107 GPa (15.5×10^6 psi)
Transverse Modulus, E_{22}	11.5 GPa (1.67×10^6 psi)
Shear Modulus, G_{12}	6.2 GPa (0.90×10^6 psi)
Major Poisson's Ratio, ν_{12}	0.30
Minor Poisson's Ratio, ν_{21}	0.027
Longitudinal Tensile Strength, S_{11T}	1290 MPa (187 ksi)
Ultimate Longitudinal Tensile Strain, ϵ_{11T}^u	0.01163
Longitudinal Compressive Strength, S_{11C}	1189 MPa (172 ksi)
Ultimate Longitudinal Compressive Strain, ϵ_{11C}^u	0.01187
Transverse Tensile Strength, S_{22T}	42 MPa (6.2 ksi)
Ultimate Transverse Tensile Strain, ϵ_{22T}^u	0.00394
Transverse Compressive Strength, S_{22C}	166 MPa (24 ksi)
Ultimate Transverse Compressive Strain, ϵ_{22C}^u	0.01567
In-plane Shear Strength, S_{12}	61 MPa (8.9 ksi)
Ultimate Shear Strain, ϵ_{12}^u	0.00940

The same advantage applies to testing off-axis, angle-ply laminates for the determination of biaxial properties and failure envelopes over a limited range of biaxiality.¹³ The ring specimen also has unique advantages in the determination of high strain rate properties of laminates. It needs no grips for internal pressure loading and thus it avoids the dynamic problems associated with tab and grip accelerations in flat coupon tests. Furthermore, it minimizes wave propagation effects as the transit time of the stress wave through the thickness of the ring is much shorter than the duration of the test.

Composite rings are normally cut from longer composite tubes. Composite tubes can be fabricated in any desired ply orientation and stacking sequence.^{12,13,15-17} The method of tube fabrication employed at the IIT Research Institute consists of laying up the various plies around a cylindrical mandrel and then expanding the layup, by means of internal pressure, against the wall of a mold tool.

The tube fabrication mold is shown in Figure 2-37. It consists of a perforated hollow stainless steel mandrel, a silicon rubber sleeve or bladder, two thin aluminum cylinders, two rings, two flanged cylinders, and the two outer valves forming the cylindrical mold cavity. The mold has a 10.16 cm (4 in.) cavity diameter and can be used to make composite tubes of 10.16 cm (4 in.) outer diameter and up to 50.8 cm (20 in.) in length. Tubes of up to 12-ply wall thickness have been fabricated with this tool. The prepreg layup process is quite similar to that used in laying up flat laminates, but is more exacting and requires greater care and close dimensional control.

Figure 2-38 shows a sketch of the consecutive layers of materials around the central steel mandrel required for the layup and fabrication process. The mandrel is hollow and perforated, allowing the rubber bladder that surrounds it to be pressurized by means of air which is fed into the mandrel during the curing stage through an air inlet at one end of the mandrel. Since the bladder is sealed off at both ends by means of O-rings, it forms an expandable pressure envelope which under internal pressure forces the layup toward the cavity wall of the external mold when the fabrication tool is assembled. The steps of the layup and fabrication process are as follows:

- (1) The thickness of all materials used in the layup process is measured, starting with the rubber bladder and ending with the teflon film.
- (2) The silicon rubber bladder (2.5 mm; 0.100 in. thick) is placed over the steel mandrel. The diameter of this assembly is measured and to this value is added twice the sum of the thicknesses of all subsequent material layers. The final diameter of the complete layup should be approximately 0.127 mm (0.005 in.) smaller than the inside diameter of the external mold shown in Figure 2-37. It is important that the total layup be within this tolerance. Otherwise it will have to be forced into the mold causing wrinkling of the prepreg plies.
- (3) A layer of 181 glass vent cloth is wrapped spirally over the silicon rubber sleeve. This layer is usually made of a 7.6 cm to 10.2 cm (3 in. to 4 in.) wide strip. Care must be taken to wrap this layer as tight as possible and to avoid gaps, overlaps, or wrinkles. The vent cloth must extend on the mandrel beyond the location of the vacuum ports in the upper half of the external mold. The ends of the vent cloth are taped to prevent unwinding.
- (4) A 0.025 mm (0.001 in.) thick teflon film separator is wrapped over the vent cloth. This film is cut 7.6 cm to 10.2 cm (3 in. to 4 in.) wider than the length of the tube to be fabricated and is perforated on 5 cm (2 in.) centers with a small needle. The perforations permit transpiration of air and gases into the vent cloth. The separator is wrapped circumferentially around the vent cloth and taped in place.
- (5) A layer of 181 glass bleeder cloth is then wrapped spirally in the same manner as the vent cloth. The bleeder extends only approximately 2.5 cm (1 in.) beyond the length of the tube to be fabricated.
- (6) A layer of TX1040 separator (teflon coated glass scrim cloth) is wrapped over the bleeder cloth and taped in place. This open weave separator should be somewhat longer than the tube to be fabricated. Its function is to facilitate the removal of the bleeder cloth from the tube after

completion of the cure cycle. The open weave permits resin flow into the bleeder, and the teflon coating prevents the bleeder from bonding to the composite tube.

- (7) The individual plies of the prepreg material, precut and layed out on a carrier template of teflon-coated glass cloth, are then wrapped around tightly. Gaps or overlaps are avoided, but if they do occur, care is taken to fill or trim them as required. The one exception is the ply with circumferentially oriented fibers. Here the ply ends should overlap approximately 2.5 cm (1 in.), because, using butting ends would reduce the strength of the composite along the butt line. Consecutive plies with circumferential fiber orientation are wrapped continuously around each other with the end of the final ply overlapping the starting end by approximately 2.5 cm (1 in.).

Figure 2-39 shows the system for wrapping the prepreg plies on the tube layup mandrel. It consists of an assembly of two free rolling rollers which cradle the mandrel, and a carrier template used to align and guide the prepreg ply between the rollers and the mandrel. The carrier has reference marks on it for this purpose.

The carrier template is placed on the flat layup table and the precut prepreg ply placed on the template with the fiber orientation aligned with the appropriate marks on the carrier. The carrier is aligned with the mandrel and its front end is passed between the mandrel and the rollers as shown in Figure 2-39. The carrier is pulled slowly through the roller system while simultaneously the prepreg is peeled off the carrier and wrapped around the mandrel. This should be done very carefully so that the wrapping is tight and does not wrinkle or shift the fibers of the previous ply.

- (8) The separator and bleeder cloth which extends beyond the prepreg is then trimmed to prevent excessive resin flow from the end of the tube.
- (9) The ends of the prepreg tube are taped to the separator layer with high temperature tape. The tape forms a dam, preventing axial fiber wash from the prepreg tube.

- (10) The final layup is then wrapped with a 0.025 mm (0.001 in.) thick layer of teflon film. This aids in assembling the two halves of the external mold over the mandrel and prevents the chance of pinching fibers between the two halves of the mold. Care must be taken to prevent this film from covering the vacuum ports in the upper half of the mold.
- (11) O-rings are inserted over the ends of the mandrel under the rubber sleeve and pushed against the shoulders of the mandrel. The thin aluminum cylinders are inserted over the ends of the mandrel under the rubber sleeve and pushed against the O-rings.
- (12) The mandrel with the layup is inserted in the cavity formed by the two outer halves of the mold which are then bolted together. The end rings and flanged cylinders are inserted at the ends and bolted to the ends of the mold. These flanged cylinders press the rings which press the O-rings to insure complete sealing of the bladder for internal pressurization.
- (13) The whole assembly is finally placed in the oven, and the high pressure air and vacuum lines are attached and the recommended curing cycle is applied (Figure 2-40). The recommended pressurization schedule given for flat laminates should be modified since additional pressure is needed to expand the tube against the walls of the mold cavity. When the ply fibers are oriented axially or at an angle of up to approximately ± 45 -degrees with the axis, a pressure of between 550 to 690 kPa (80 to 100 psi) is sufficient for the radial expansion of the layup. When the fiber directions tend toward the hoop orientation pressures of 1380 to 2070 kPa (200 to 300 psi) may be necessary.

The fabrication of tubes with the fibers in the circumferential direction, $[0_6]$, requires special care. They are normally laid up by wrapping a continuous length of prepreg tape around the mandrel. The end of the tape is extended by a distance of approximately 2.5 cm (1 in.) beyond the beginning of the tape on the inside surface of the tube.

The following curing procedure was adopted for these tubes:

- (1) The temperature was raised to 353°K (175°F) at a rate of 2.8°K (5°F) per minute and held for 3 hours.
- (2) Vacuum was drawn 45 minutes after reaching 353°K (175°F).
- (3) A pressure of 2070 kPa (300 psi) was applied 1 hour after reaching 353°K (175°F).
- (4) The temperature was raised to 408°K (275°F) at a rate of 2.8°K (5°F) per minute and held for 4 hours.
- (5) The mold was allowed to cool to room temperature.
- (6) The laminate was removed and postcured at 408°K (275°F) for 2 hours.

In the case of $[0_6]$ graphite/S-glass/epoxy material, the tube was made by wrapping the prepreg in two staggered segments, so that the glass strips in the prepreg would not be concentrated and stacked on each other. Testing of ring specimens cut from this tube showed that best results could be obtained when the glass strips in the hybrid ring are nearly symmetrically disposed about the transverse plane of symmetry (normal to the axis) of the ring.

In general, ring specimens cut from $[0_6]$ tubes showed a tendency for premature failures near the outer end of the wrap. Subsequently, this area was reinforced with a patch of resin-impregnated glass cloth (No. 181) prior to cutting the tube into rings.

2.4 QUALITY ASSESSMENT

After fabrication the tube quality was assessed in three different ways, by ultrasonic inspection, by measuring the tube thickness at various points along its length and around the circumference, and by measuring the hoop strength of rings cut from the ends and loaded under internal pressure.

The ultrasonic inspection is done to reveal any internal flaws such as delaminations, large voids, and excessive nonuniform fiber distribution. A fixture was designed for holding these tubes and rotating them in an immersion

tank for scanning along closely spaced cylinder generators (Figure 2-41). The ultrasonic scanning system for inspecting composite tubes has been described previously.¹⁸

The method used is immersion ultrasonics where the tube is placed in a water tank and the scanning is done with a single focused transducer in the pulse-echo mode. The tube is positioned in the tank vertically in a ring holder which is driven rotationally about the tube axis by means of a stepper motor. The motor drives the tube in indexed steps, and at each step an ultrasonic line scan is performed axially along the tube wall. By selecting small indexing steps the whole tube wall can be covered with line scans. The series of lines is recorded on a graph using the pen-lift method. In this method the pen draws a line where the material is good and is lifted from the graph where the ultrasonic signal indicates a flaw. Figure 2-42 shows examples of such C-scans of graphite/epoxy tubes. The unacceptable tube shows patches of interrupted lines.

The second method used in assessing tube quality is to measure the variation of the tube wall thickness at various points on the tube wall to check if it is within acceptable tolerances. Figure 2-43 shows the fixture used for this purpose. It consists of a stand with two long parallel feeler arms. The lower one is the feeler arm for the inner surface of the tube. Its front end is equipped with a small steel ball which allows it to make a satisfactory point contact with the inner contour of the tube. The upper arm is equipped with a micrometer dial gage whose measuring stem is positioned over the center of the steel ball of the lower arm. The tube wall thickness at any point on the tube is determined by reading the dial gage while the tube wall is passed between the ball and the measuring stem of the gage.

Tube quality is further assessed by checking the hoop strength of ring specimens cut from the ends of the tube. The procedures for cutting and testing such uninstrumented specimens is the same as for instrumented ring specimens used in determining material strength, stiffness, and ultimate strain. These will be described in following sections.

2.5 SPECIMEN PREPARATION

The specimens selected for quasi-static and dynamic characterization of the composite laminates used in this program were 2.54 cm (1 in.) wide rings cut from the tubes described before. The cutting is done on a lathe. Since the tube is thin walled, it must be supported internally during cutting, and the support must be of a material which permits the cutoff blade to penetrate into it without damage to the blade. Figure 2-44 shows the support fixture used in the ring cutoff operation. The core of the fixture is a circular steel mandrel covered with a rubber sleeve. In this particular case it consists of a spare tube layup mandrel and rubber bladder similar to those shown in Figures 2-37 and 2-38. This arrangement brings the diameter of the cutoff mandrel close to the inner diameter of the tube, and the rubber bladder provides the backup material into which the cutoff blade can penetrate without damage. Foam rubber strips were taped axially to the rubber bladder and the laminate tube was slipped over them on the mandrel. The strips serve to take up the radial space between the rubber bladder and the laminate tube and serve also to center the tube over the cutoff mandrel. The ends of the laminate tube were taped to the bladder with masking tape.

Before a composite laminate tube is cut into ring specimens, its ends are trimmed by cutting off at least 1.27 cm (0.5 in.) wide rings from both ends of the tube. To cut ring specimens the mandrel with the laminate tube was mounted in a lathe as shown in Figure 2-45, and rotated by the lathe at moderate speed on its axis. An independently powered circular diamond cutoff blade spinning at high speed, was guided radially into contact with the rotating tube, at the desired location for the cut, and was fed radially into the tube wall until the wall was cut through. Successive cuts, spaced at specimen width distances, produce the desired ring specimens.

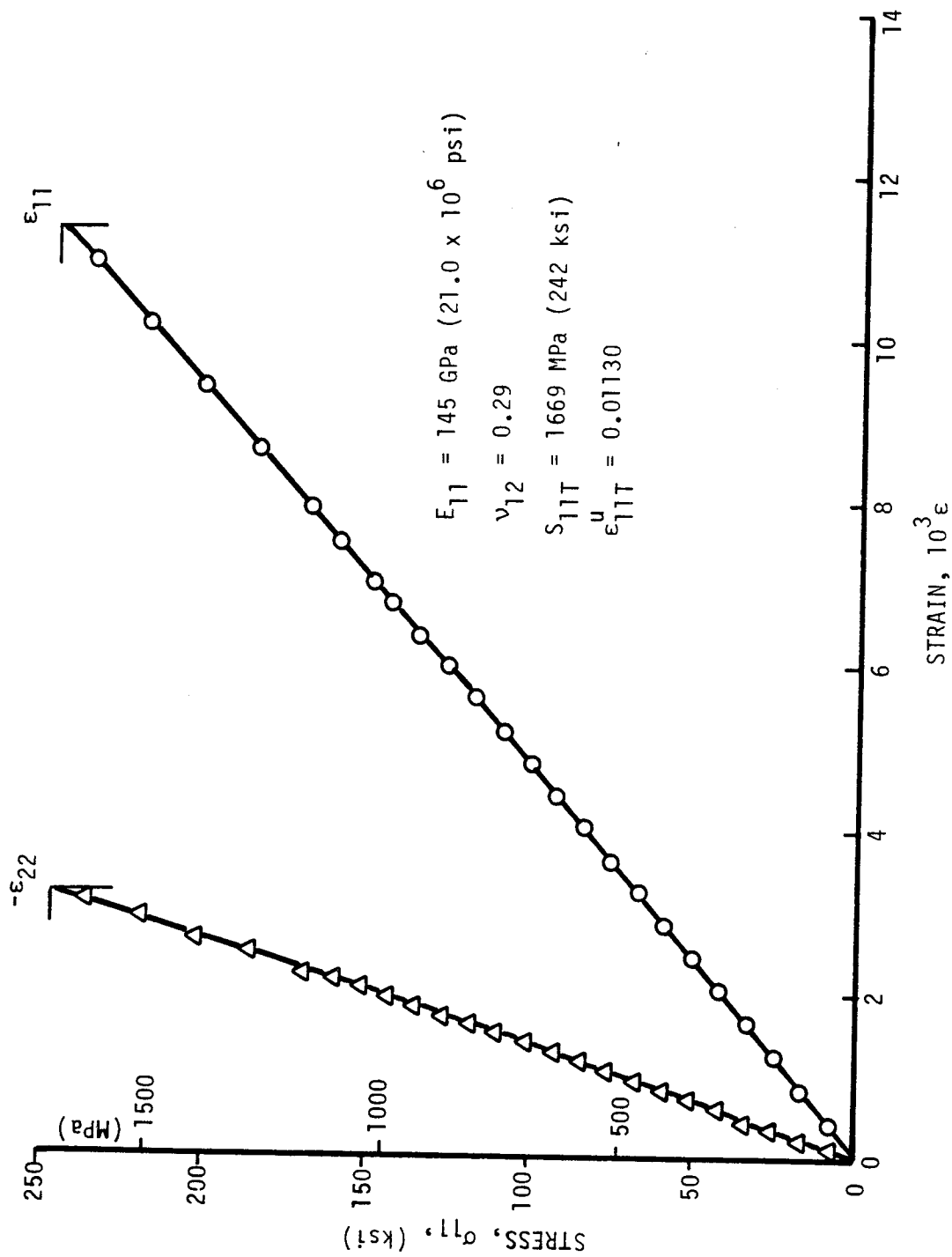


Figure 2-1. Strains in 0-deg unidirectional SP288/T300 specimen under uniaxial tensile loading.

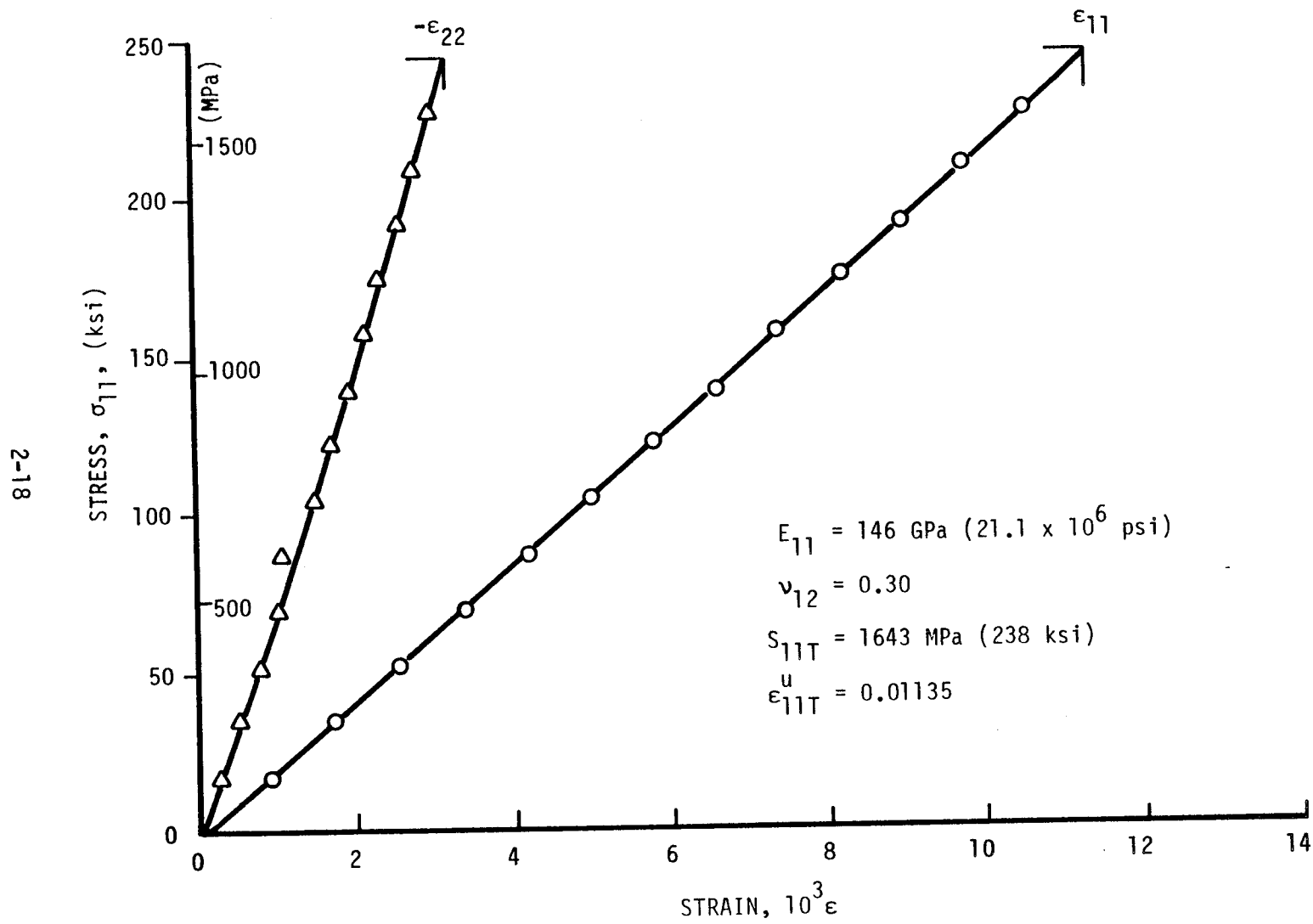


Figure 2-2. Strains in 0-deg unidirectional SP288/T300 specimen under uniaxial tensile loading.

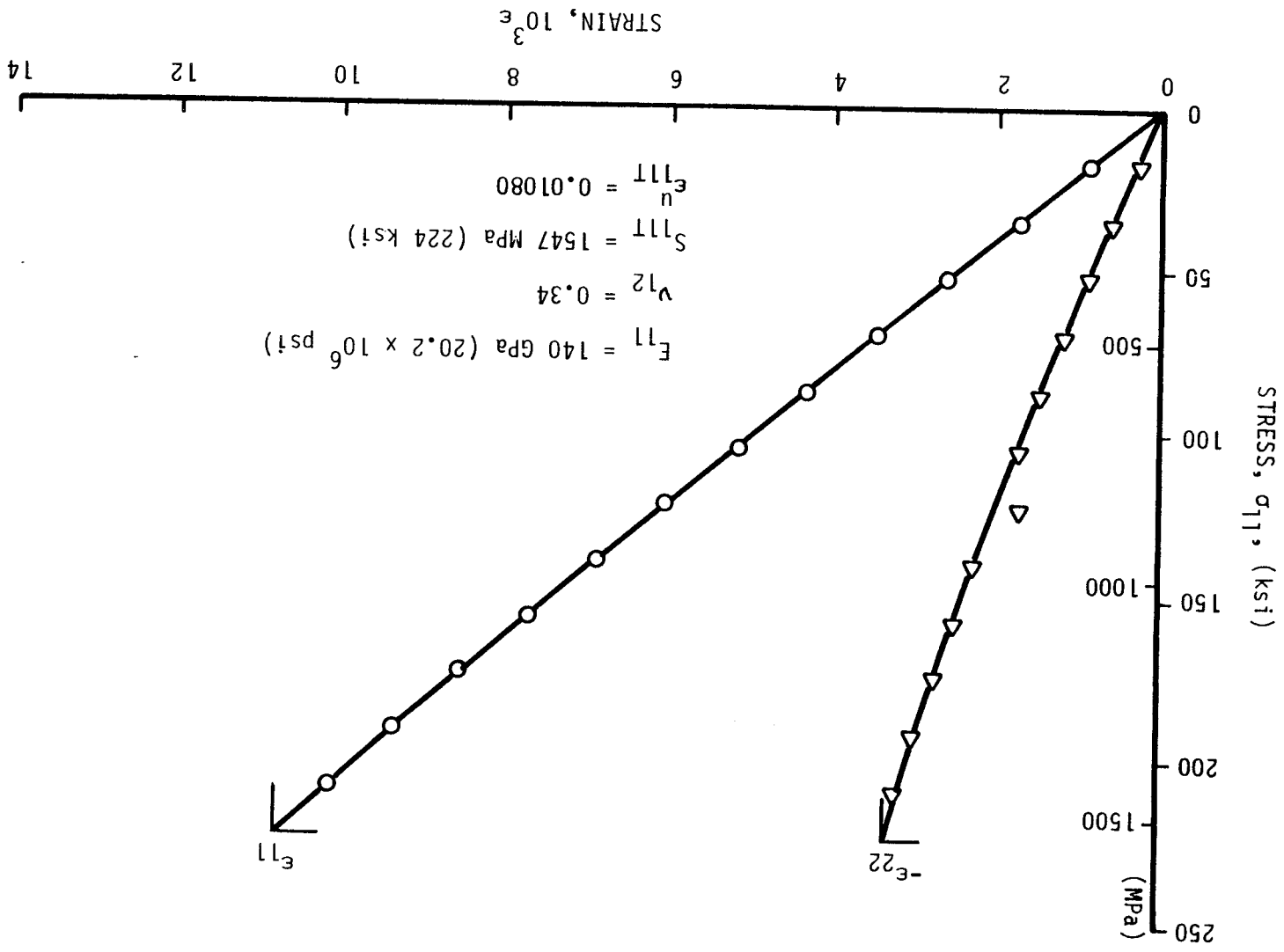


Figure 2-3. Strains in 0-deg unidirectional SP288/AS specimen under uniaxial tensile loading.

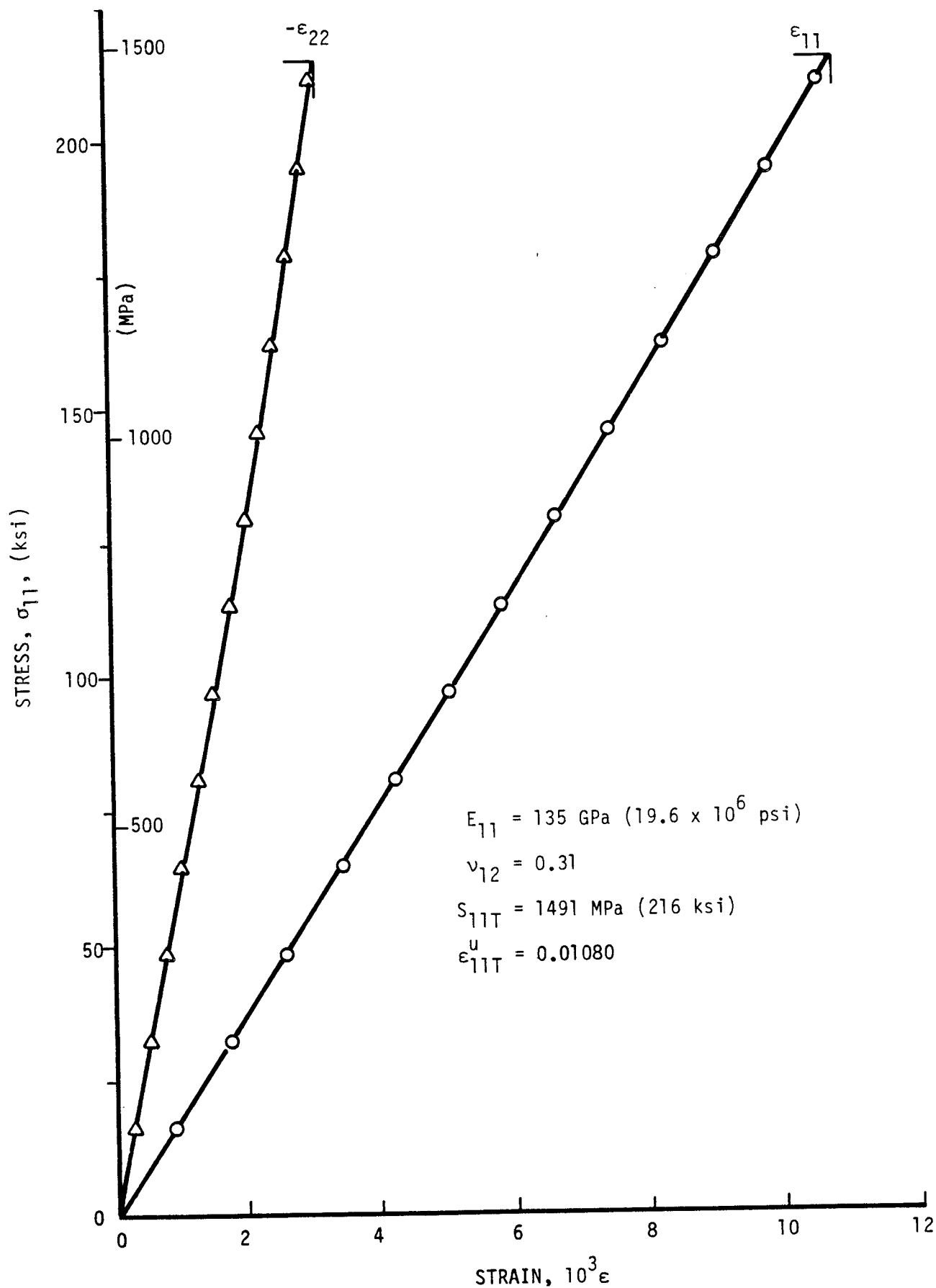


Figure 2-4. Strains in 0-deg unidirectional SP288/AS specimen under uniaxial tensile loading.

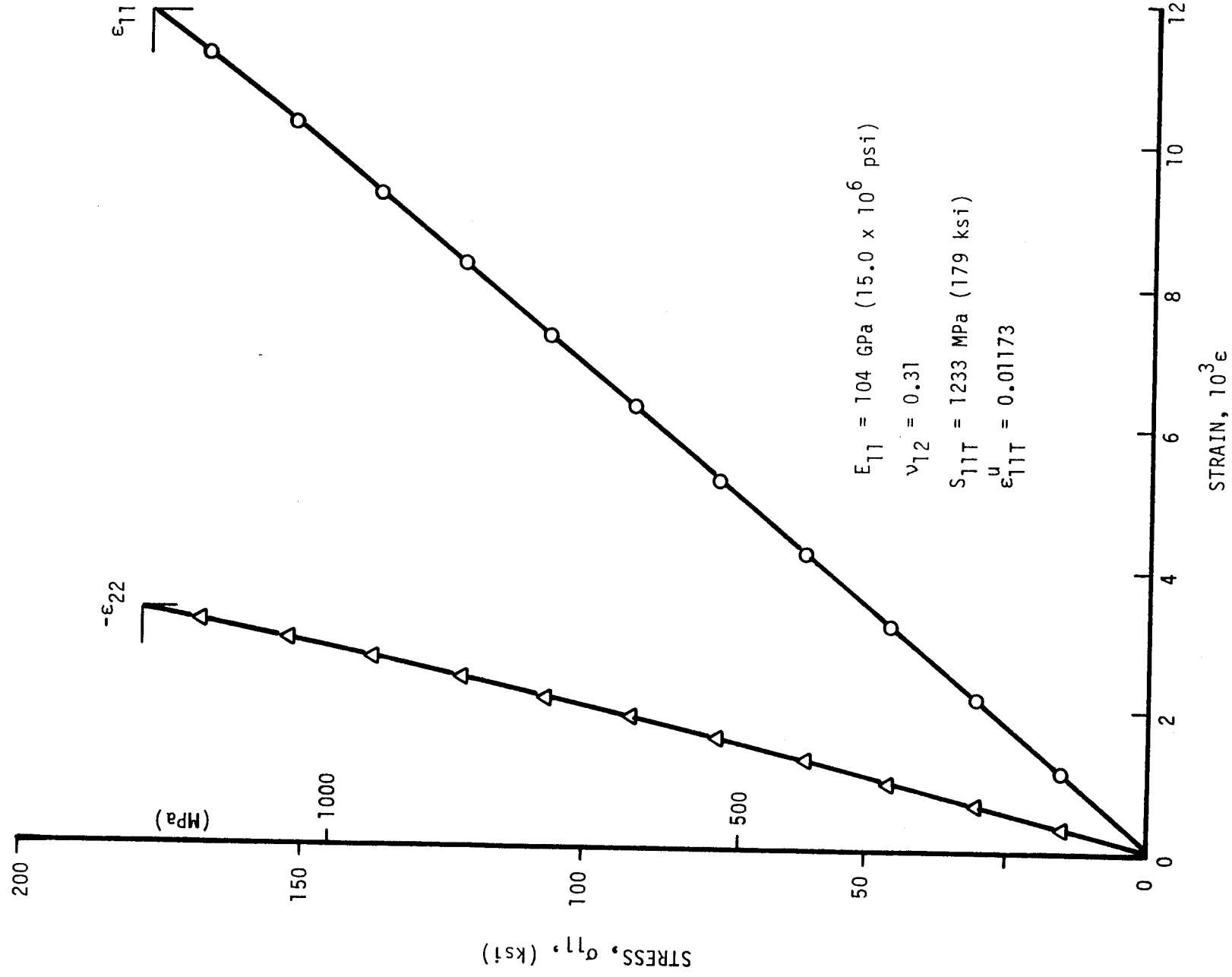


Figure 2-5. Strains in 0-deg unidirectional 80AS/20S/PR288 specimen under uniaxial tensile loading.

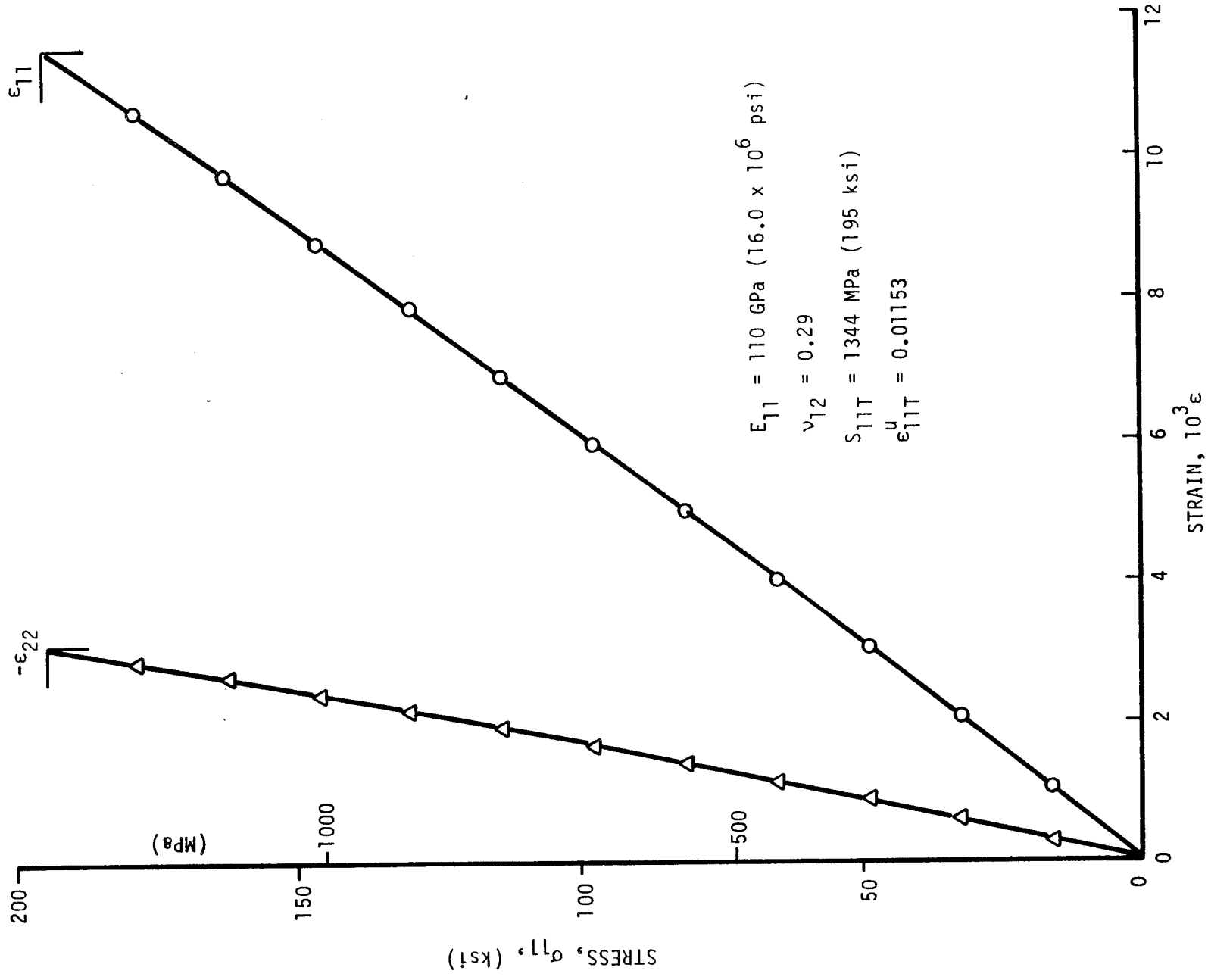


Figure 2-6. Strains in 0-deg unidirectional 80AS/20S/PR288 specimen under uniaxial tensile loading.

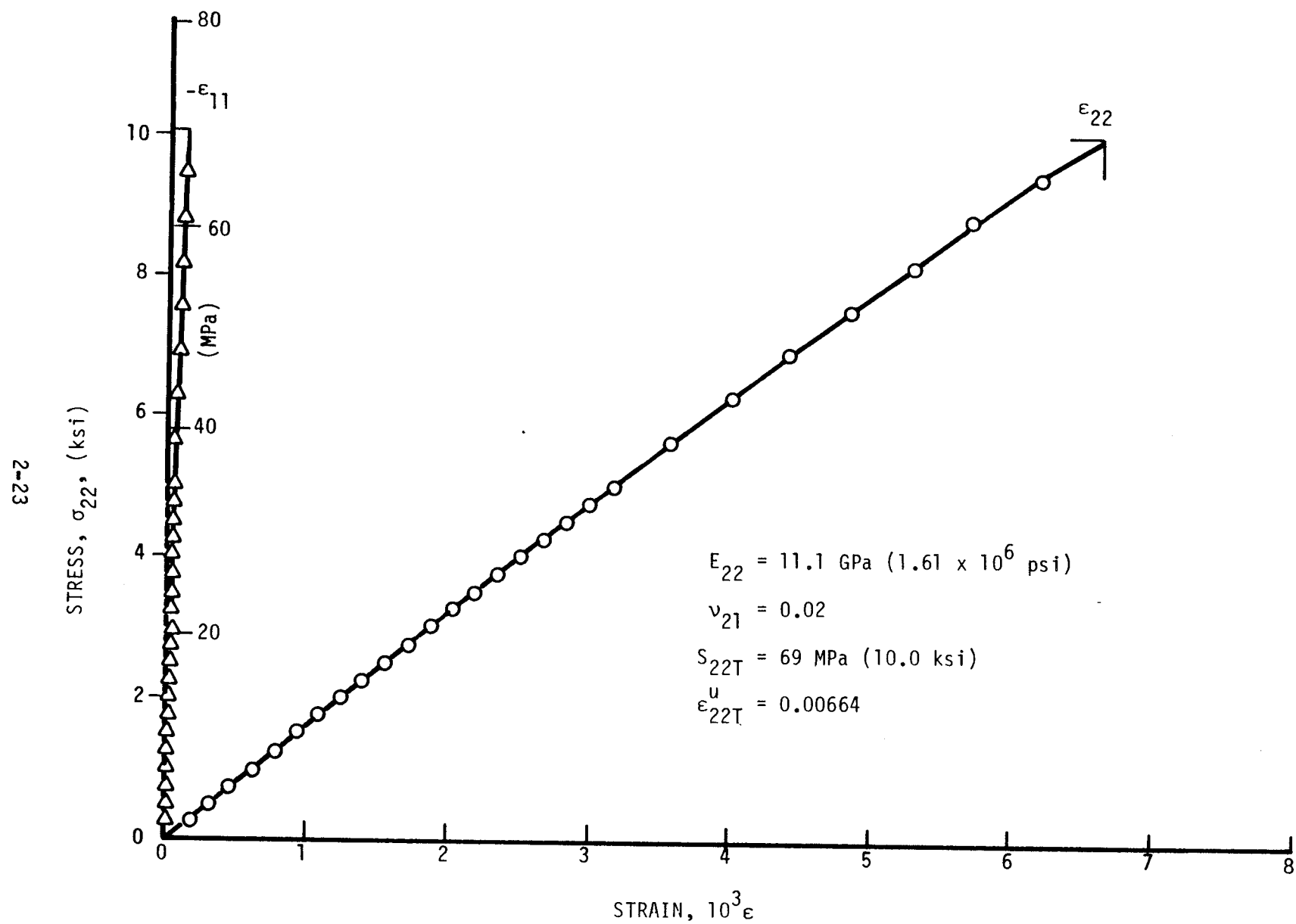


Figure 2-7. Strains in 90-deg unidirectional SP288/T300 specimen under uniaxial tensile loading.

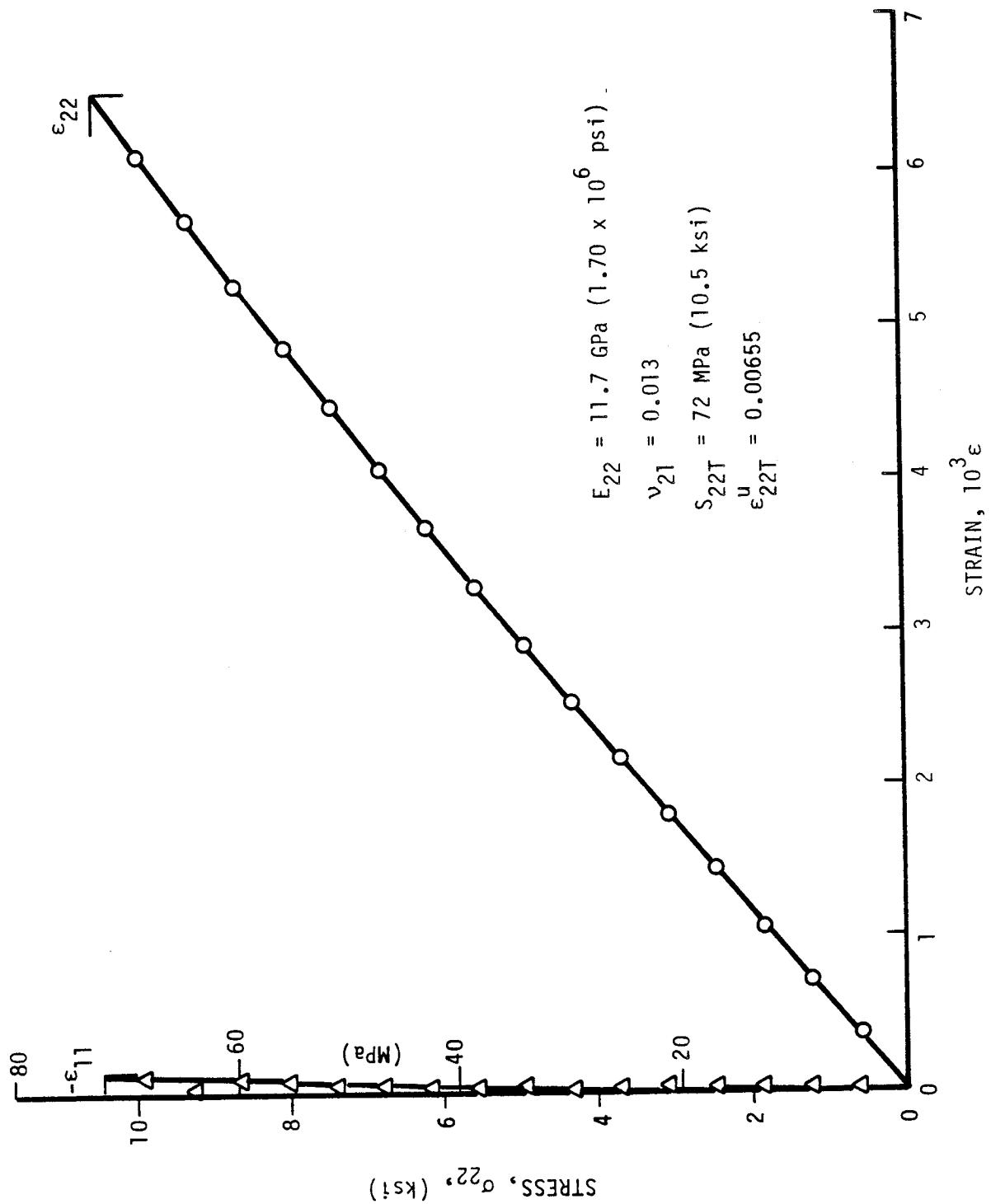


Figure 2-8. Strains in 90-deg unidirectional SP288/T300 specimen under uniaxial tensile loading.

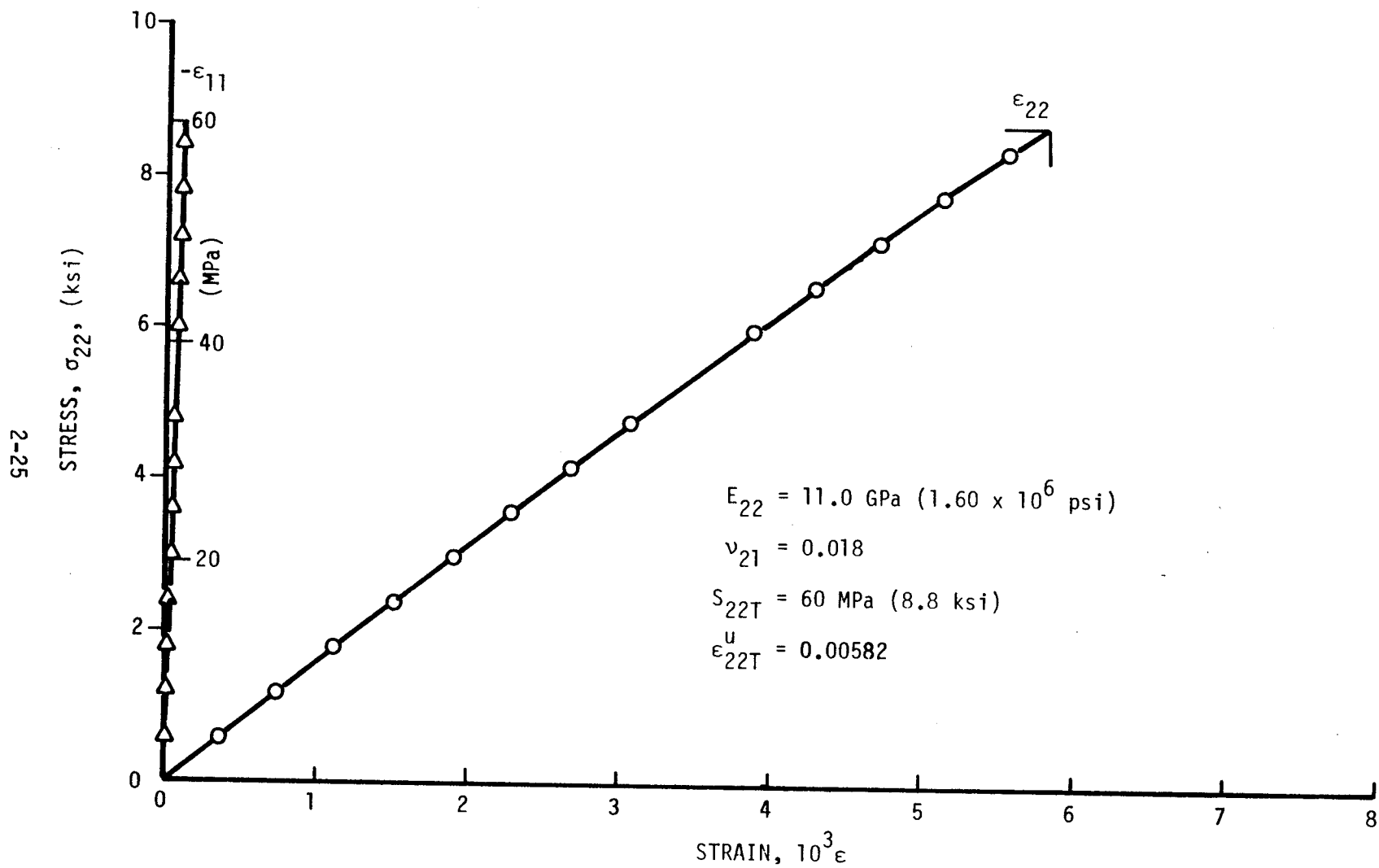


Figure 2-9. Strains in 90-deg unidirectional SP288/AS specimen under uniaxial tensile loading.

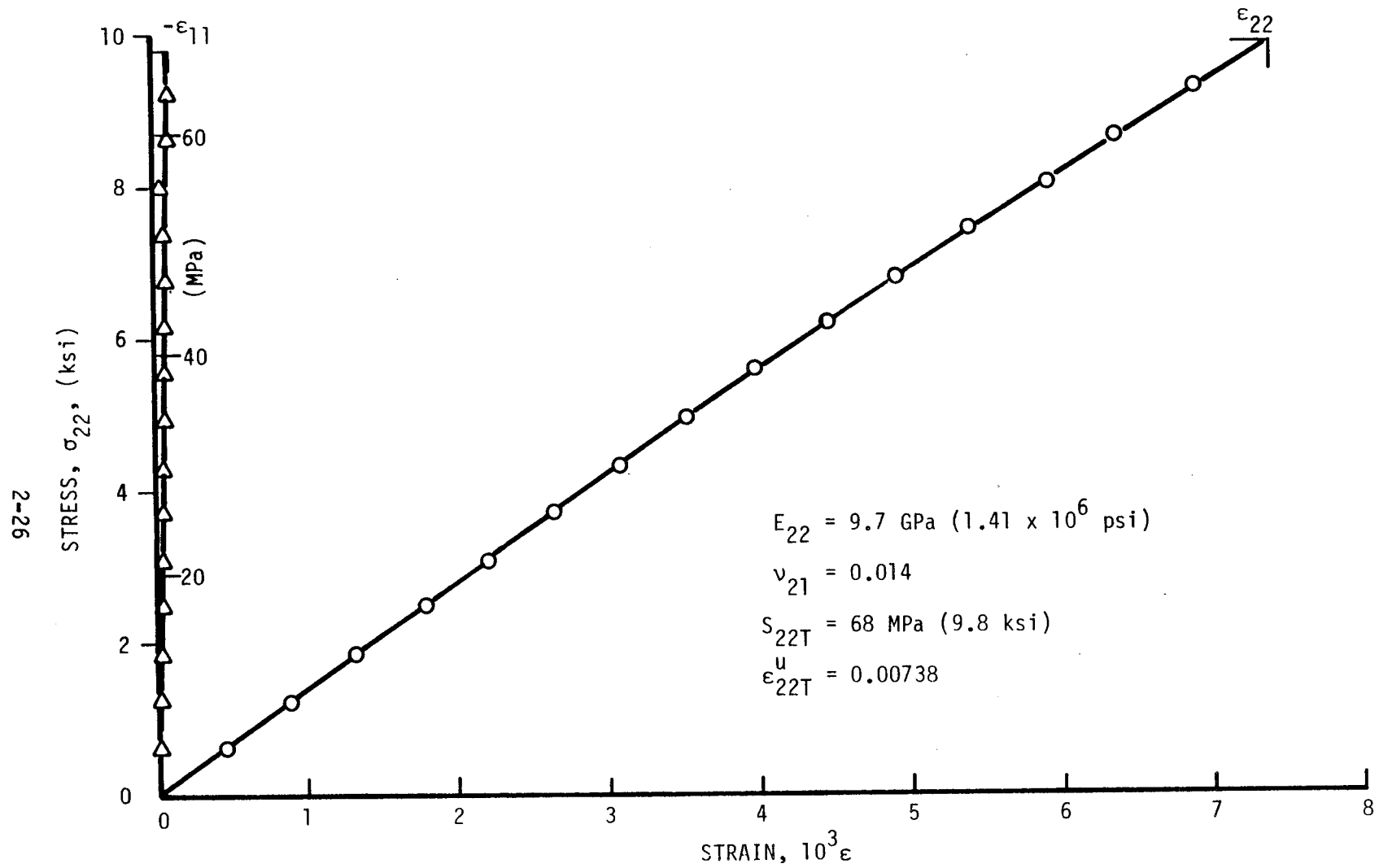


Figure 2-10. Strains in 90-deg unidirectional SP288/AS specimen under uniaxial tensile loading.

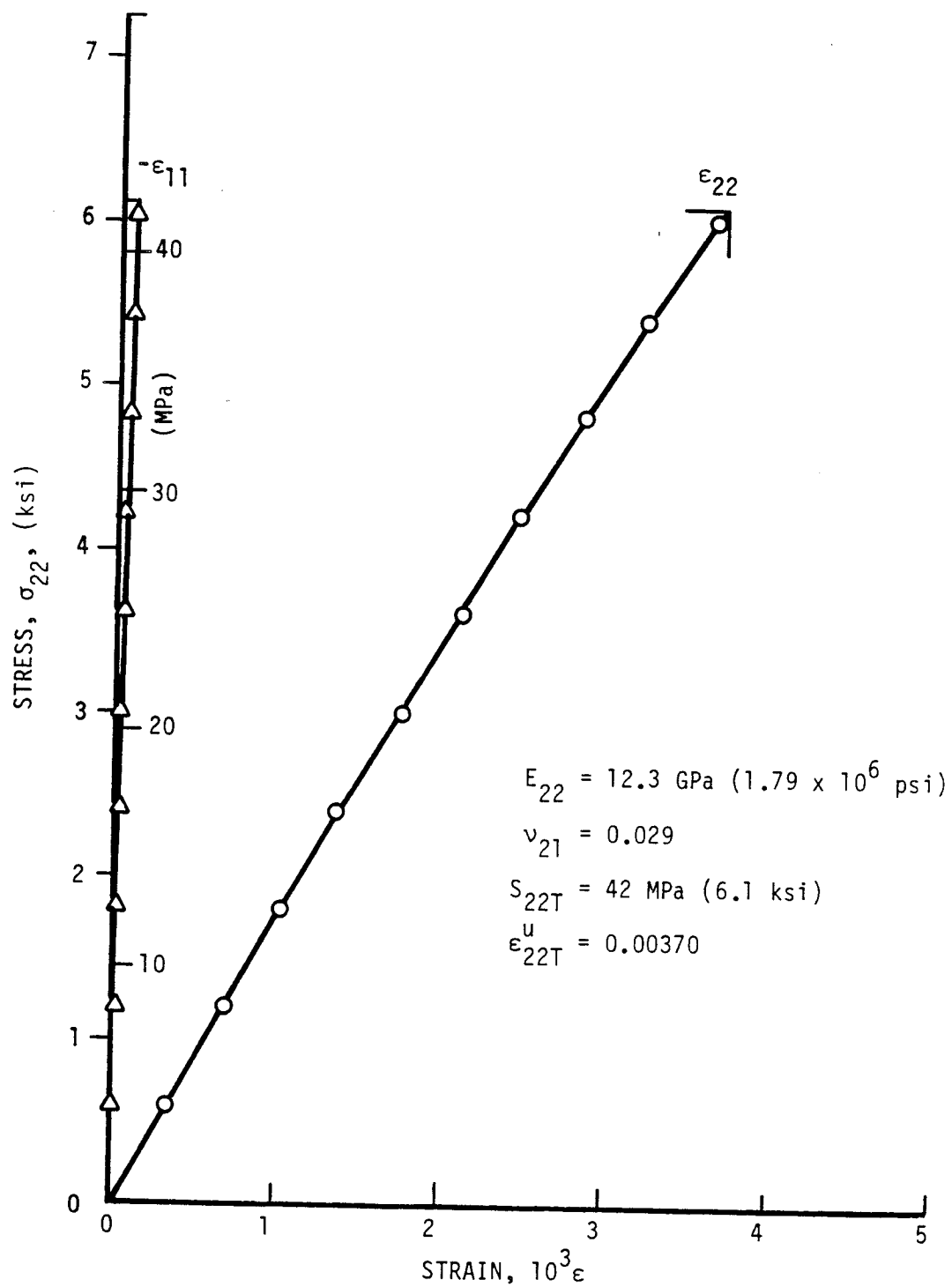


Figure 2-11. Strains in 90-deg unidirectional 80AS/20S/PR288 specimen under uniaxial tensile loading.

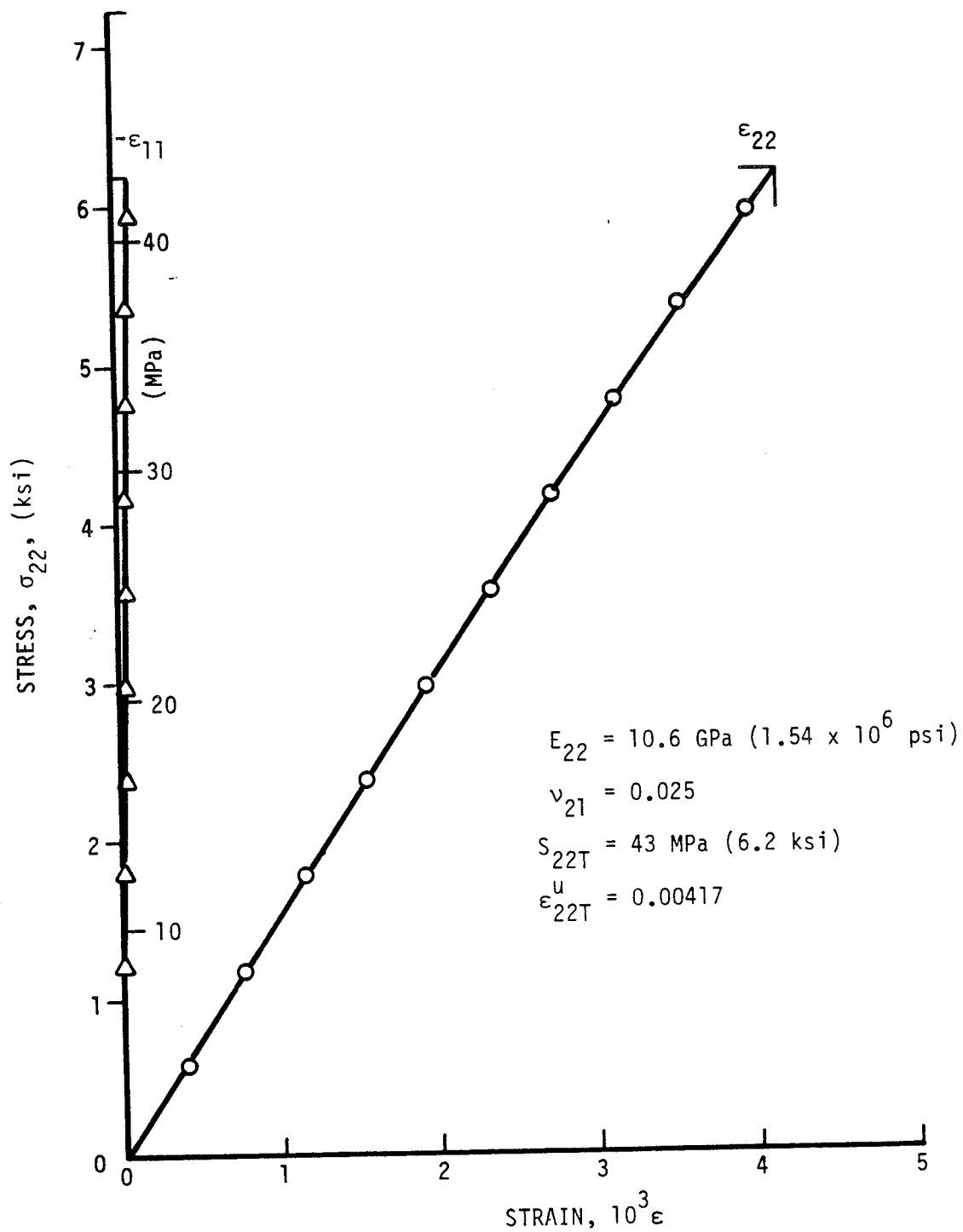


Figure 2-12. Strains in 90-deg unidirectional 80AS/20S/PR288 specimen under uniaxial tensile loading.

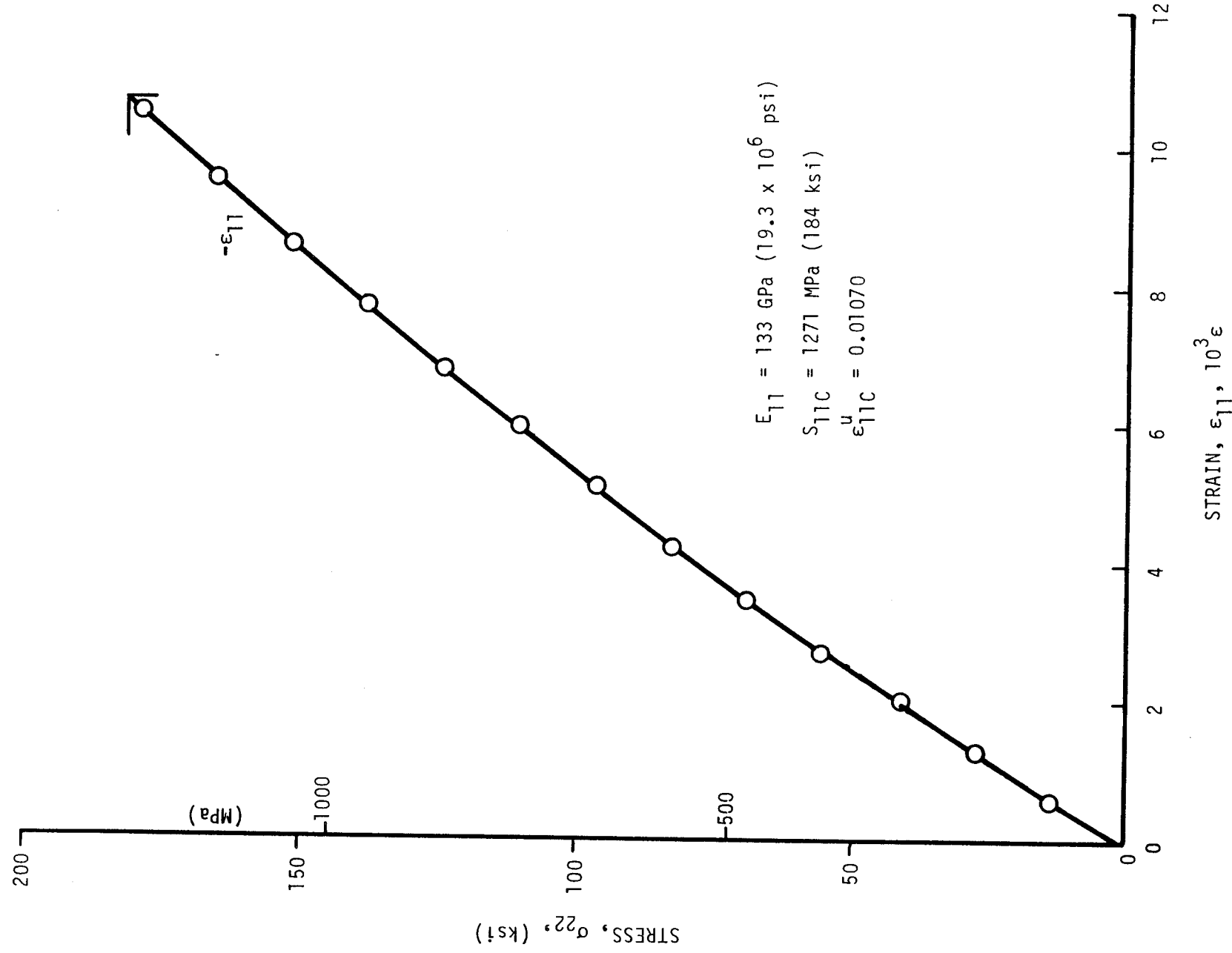


Figure 2-13. Stress-strain curve for unidirectional 0-deg SP288/T300 specimen under compressive loading.

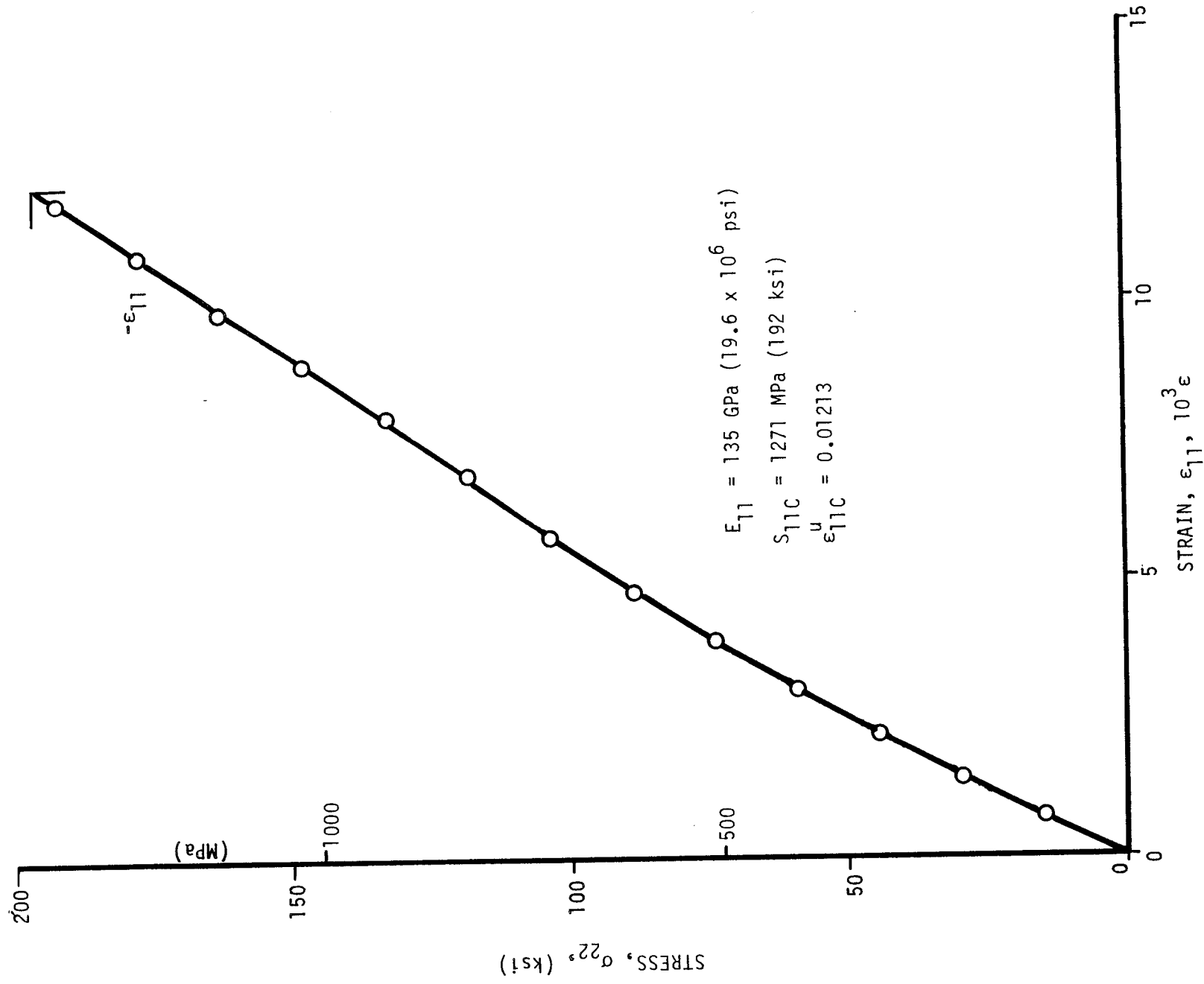


Figure 2-14. Stress-strain curve for unidirectional 0-deg SP288/T300 specimen under compressive loading.

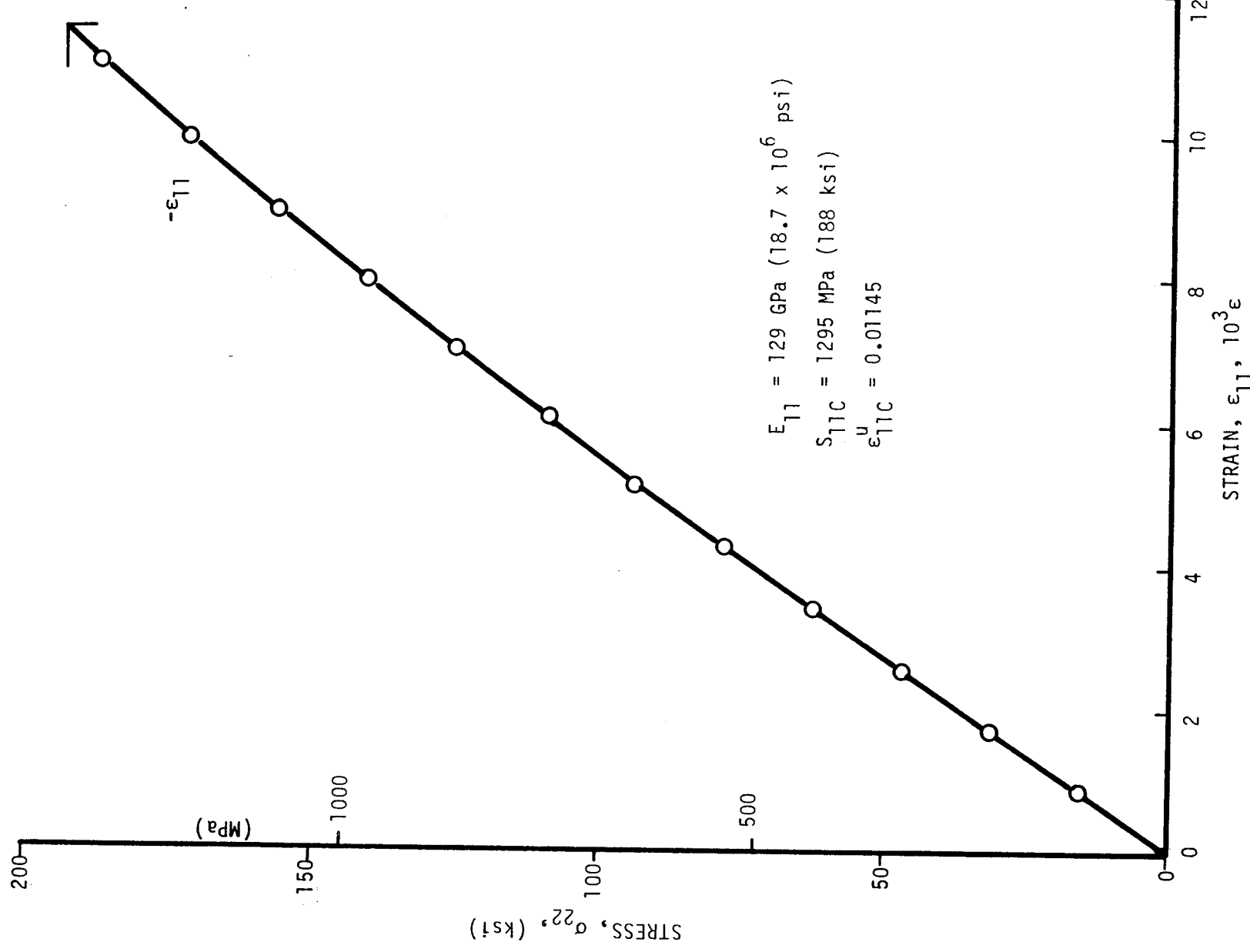


Figure 2-15. Stress-strain curve for unidirectional 0-deg SP288/T300 specimen under compressive loading.

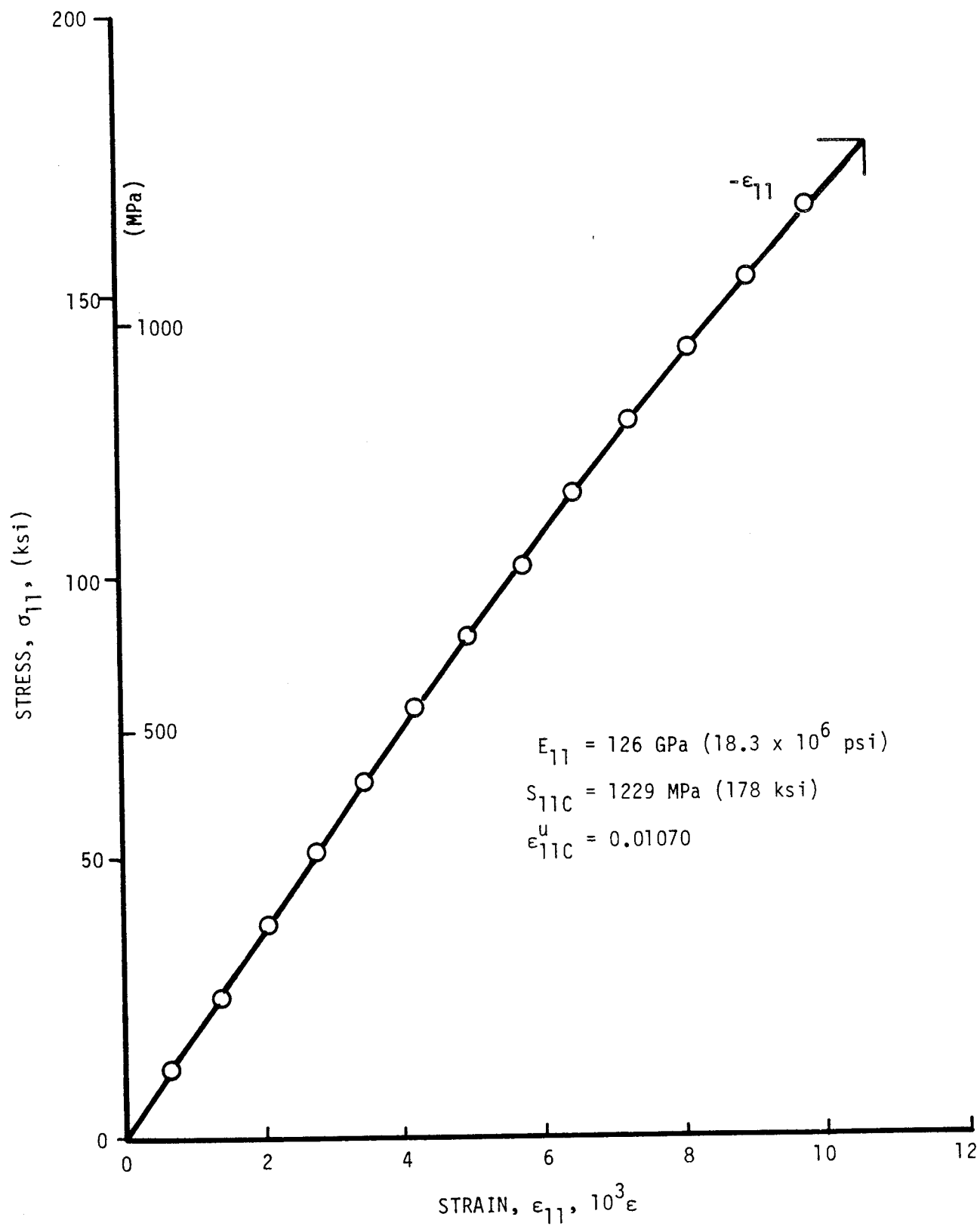


Figure 2-16. Stress-strain curve for unidirectional 0-deg SP288/AS specimen under compressive loading.

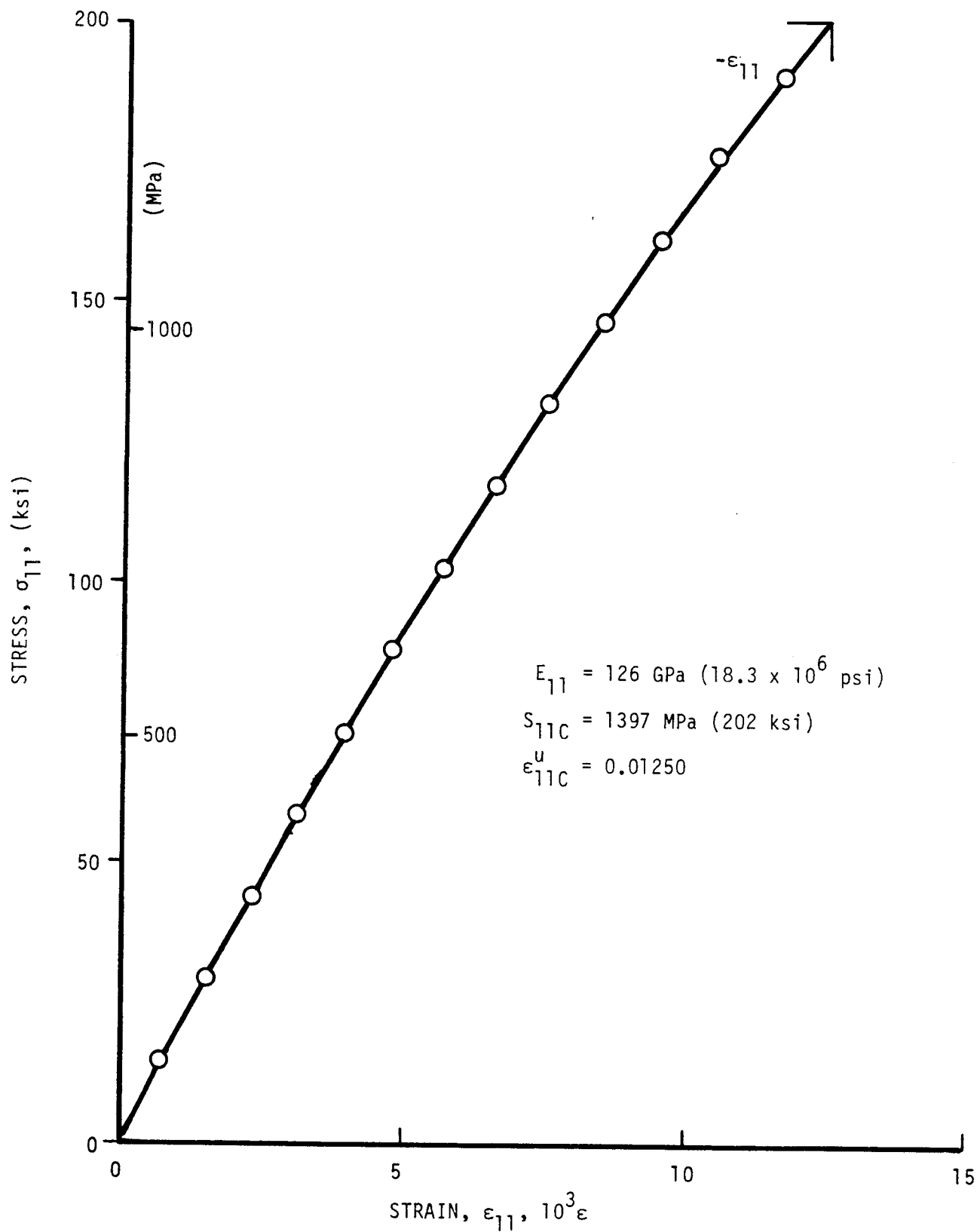


Figure 2-17. Stress-strain curve for unidirectional 0-deg SP288/AS specimen under compressive loading.

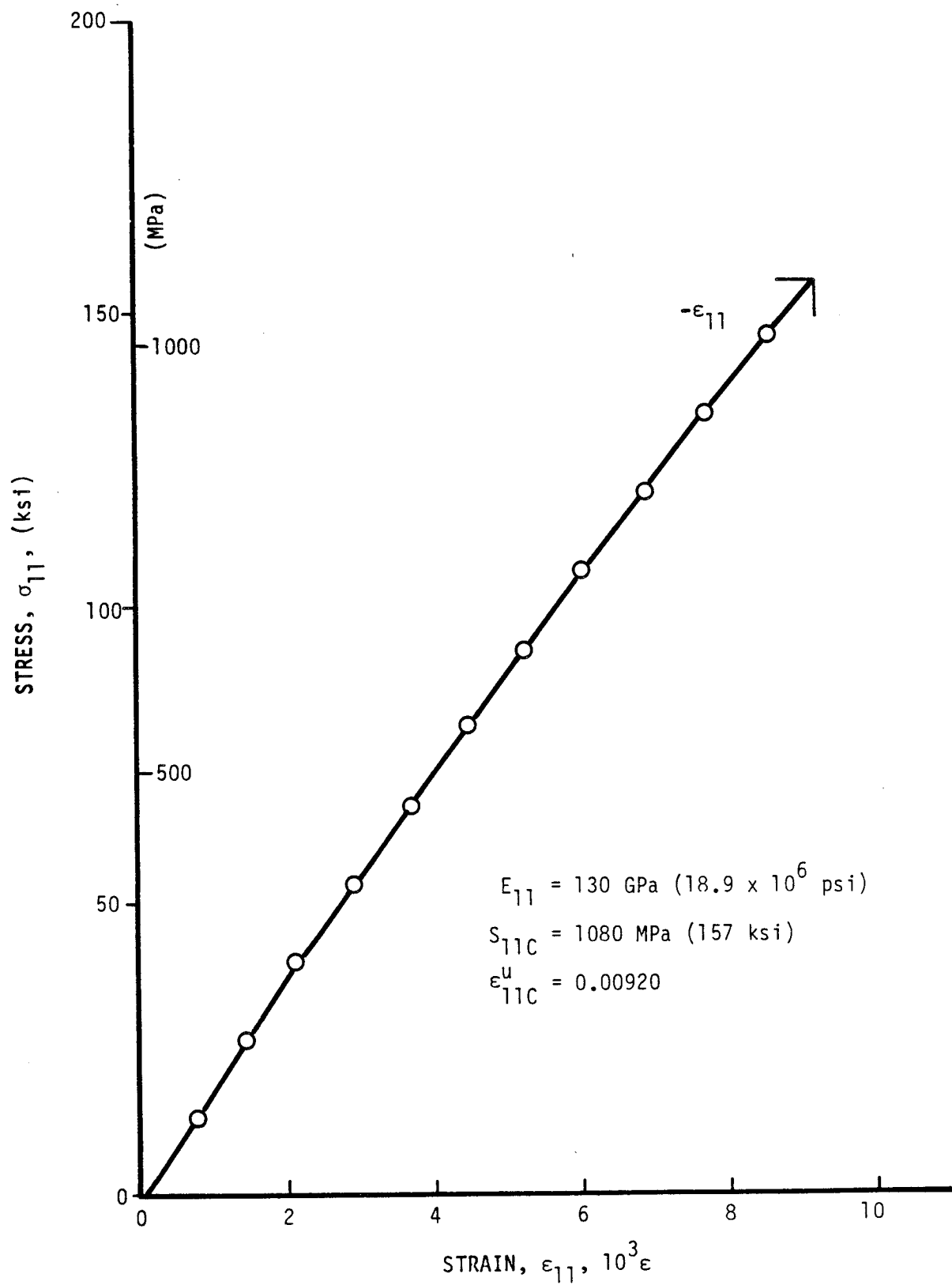


Figure 2-18. Stress-strain curve for unidirectional 0-deg SP288/AS specimen under compressive loading.

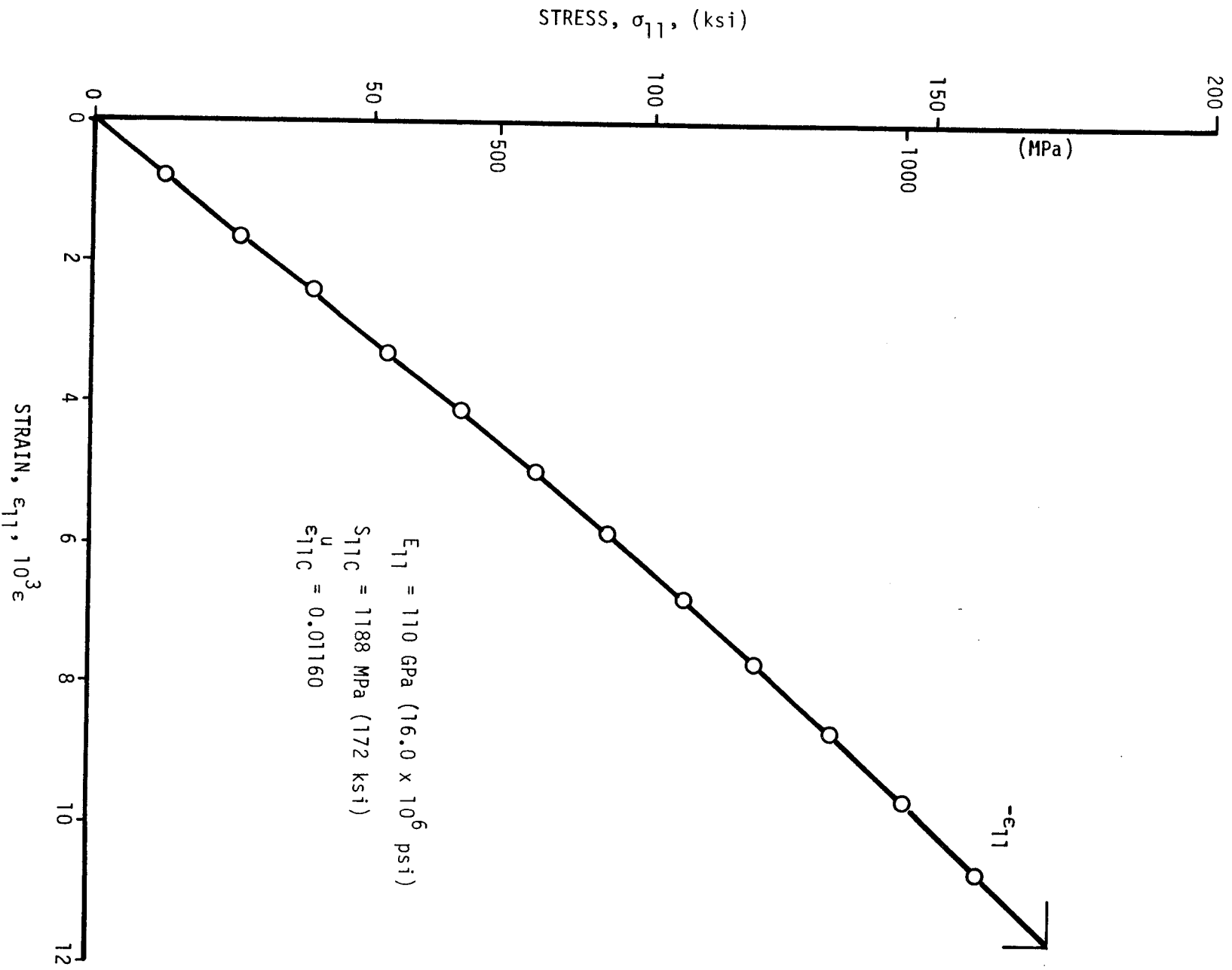


Figure 2-19. Stress-strain curve for unidirectional 0-deg 80AS/20S/PR288 specimen under compressive loading.

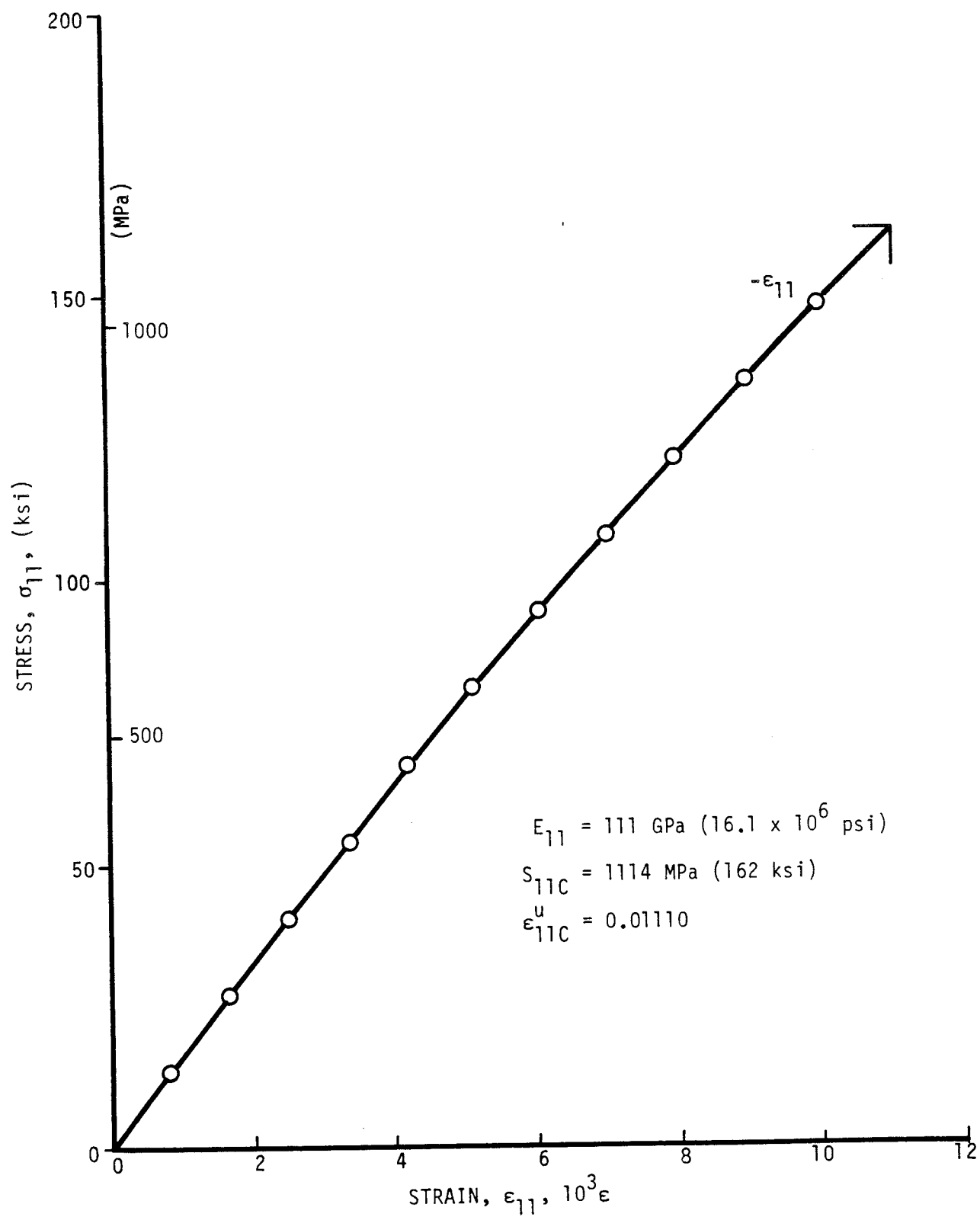


Figure 2-20. Stress-strain curve for unidirectional 0-deg 80AS/20S/PR288 specimen under compressive loading.

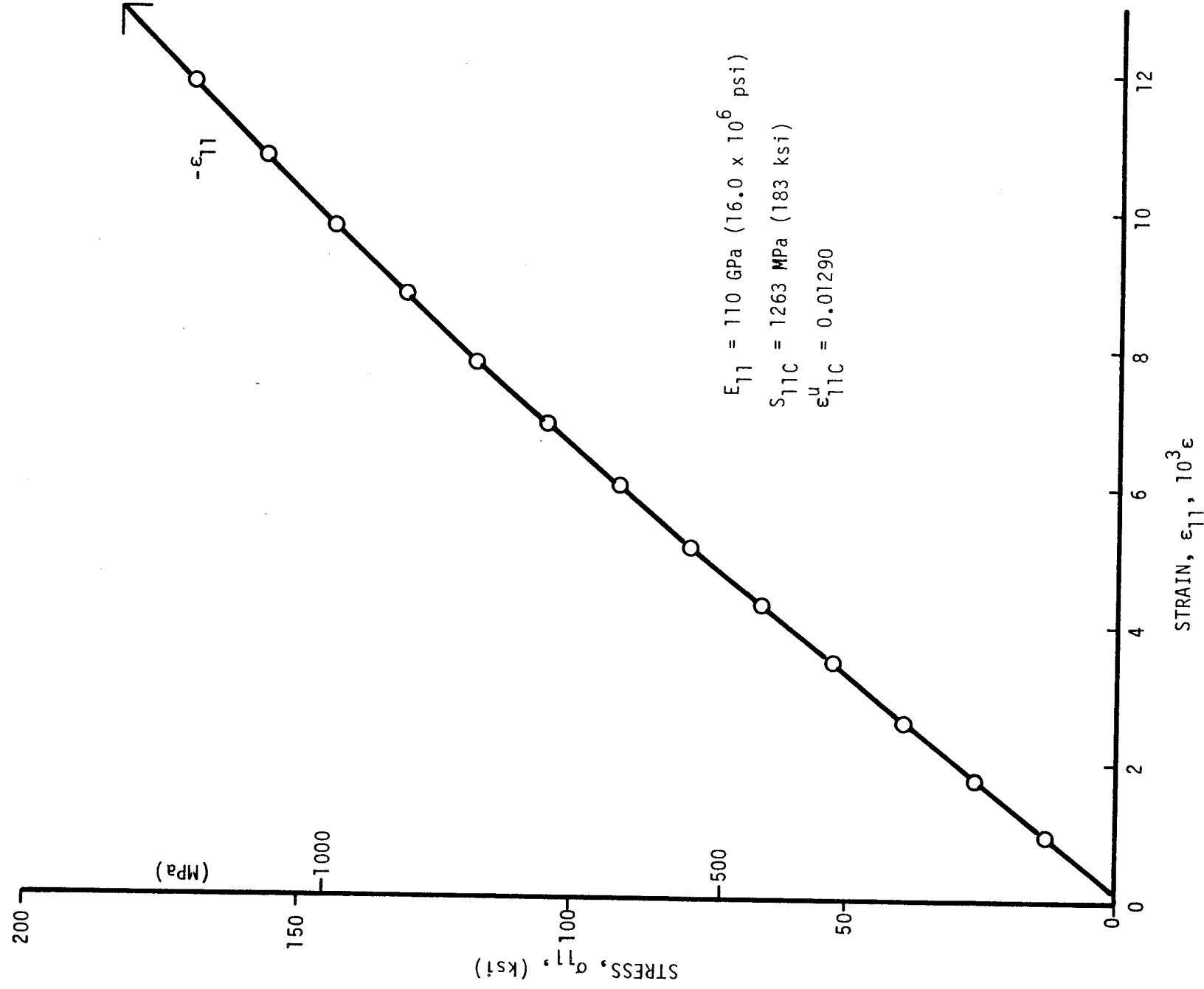


Figure 2-21. Stress-strain curve for unidirectional 0-deg 80AS/20S/PR288 specimen under compressive loading.

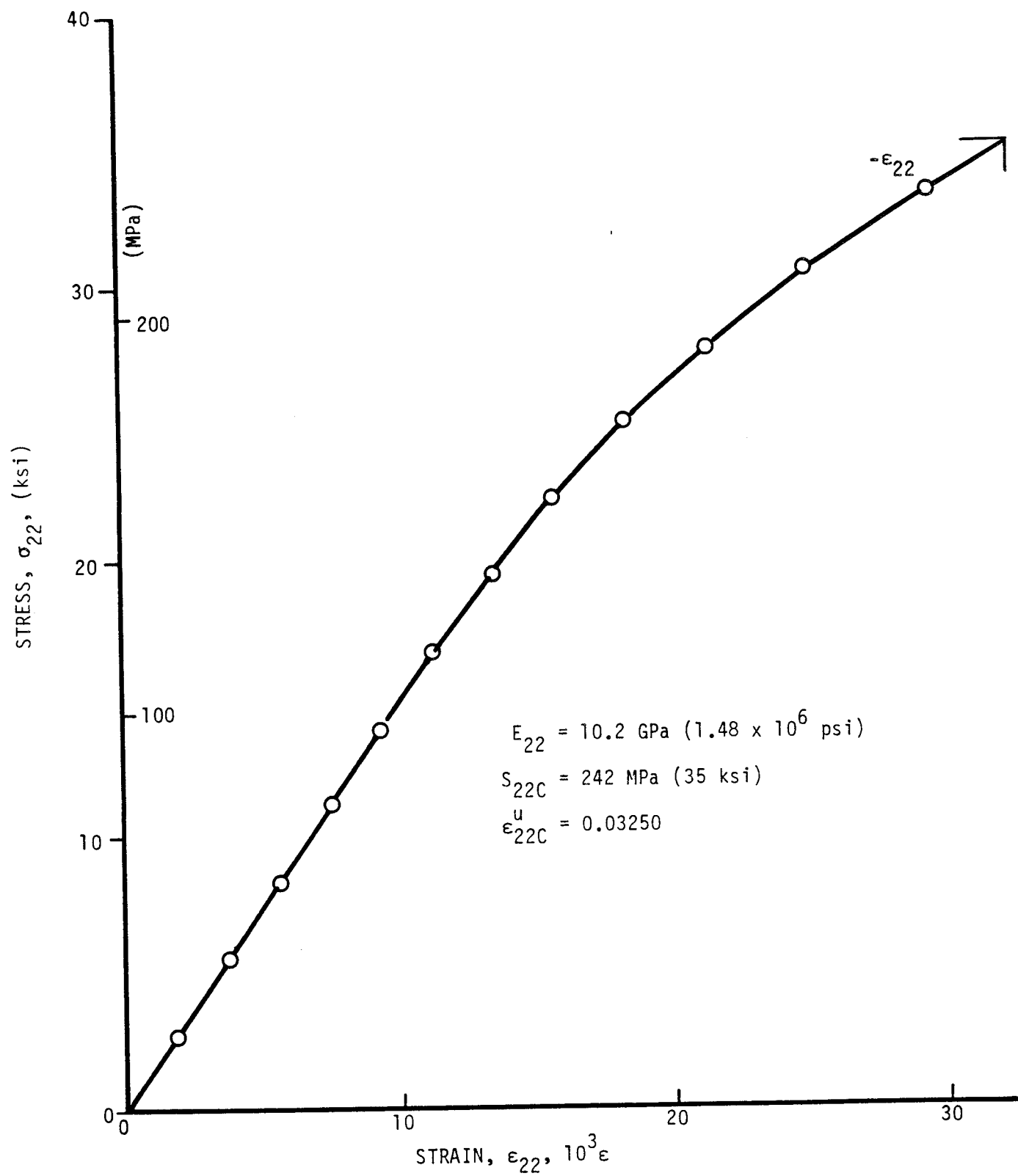


Figure 2-22. Stress-strain curve for unidirectional 90-deg SP288/T300 specimen under compressive loading.

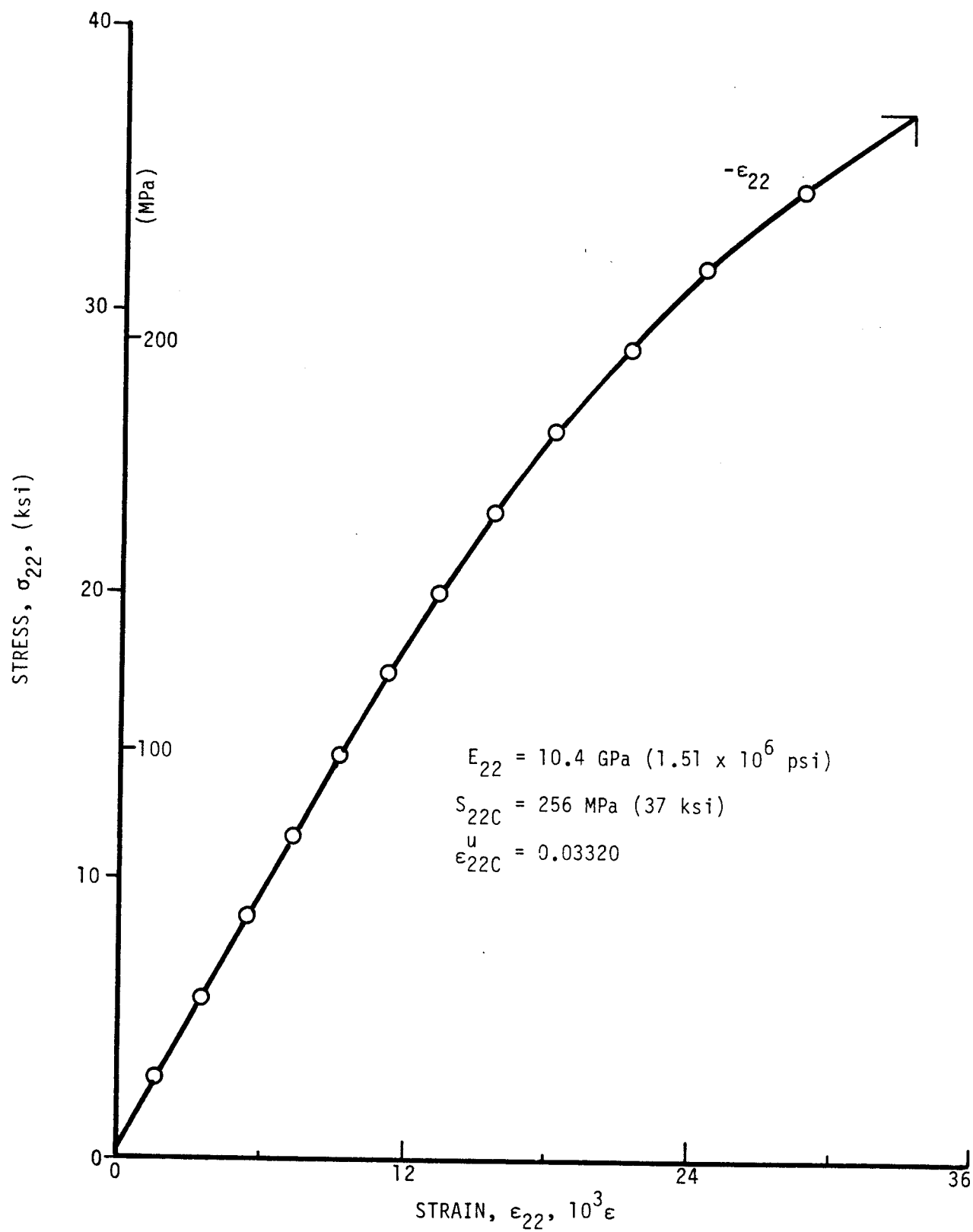


Figure 2-23. Stress-strain curve for unidirectional 90-deg SP288/T300 specimen under compressive loading.

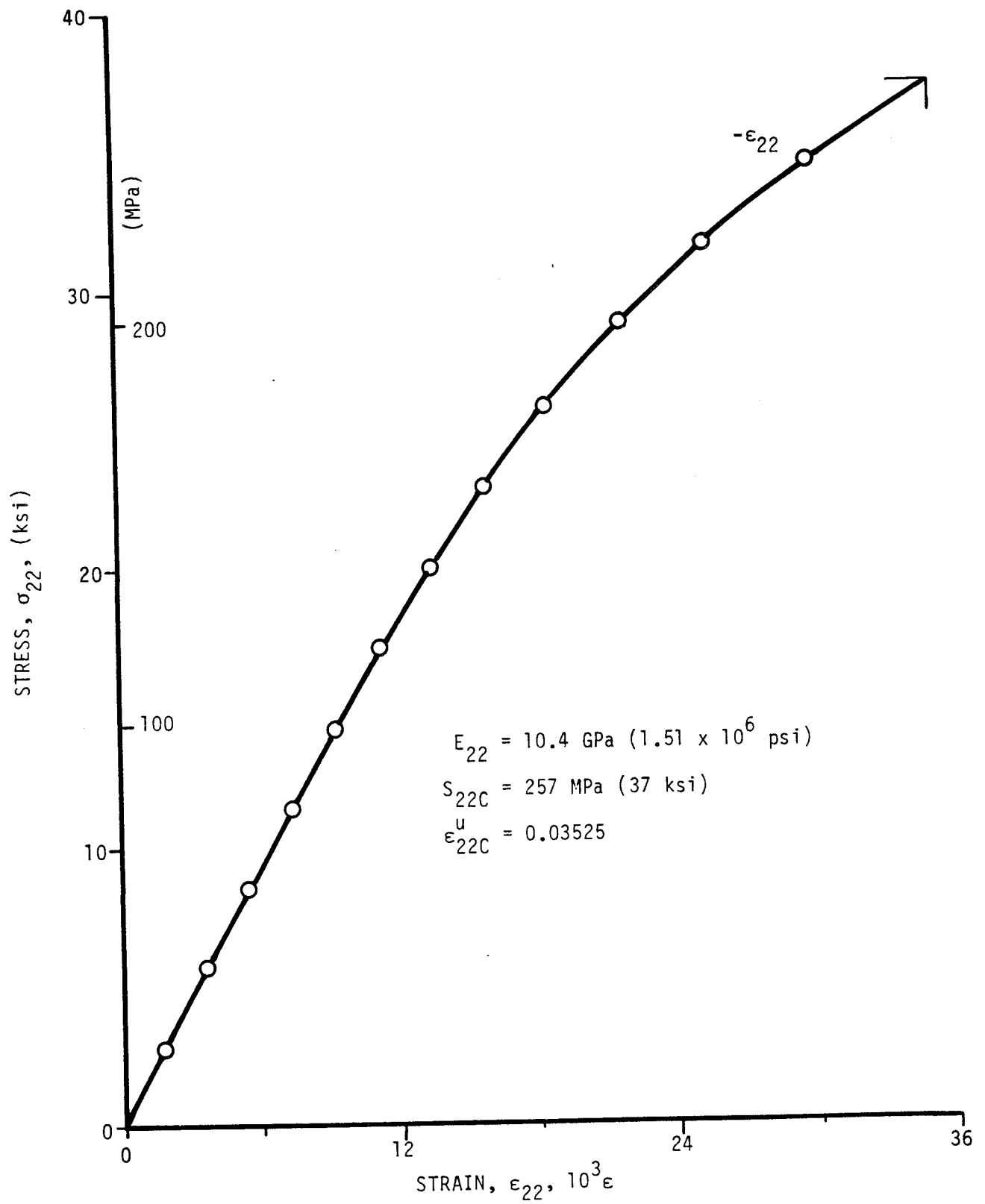


Figure 2-24. Stress-strain curve for unidirectional 90-deg SP288/T300 specimen under compressive loading.

2-47

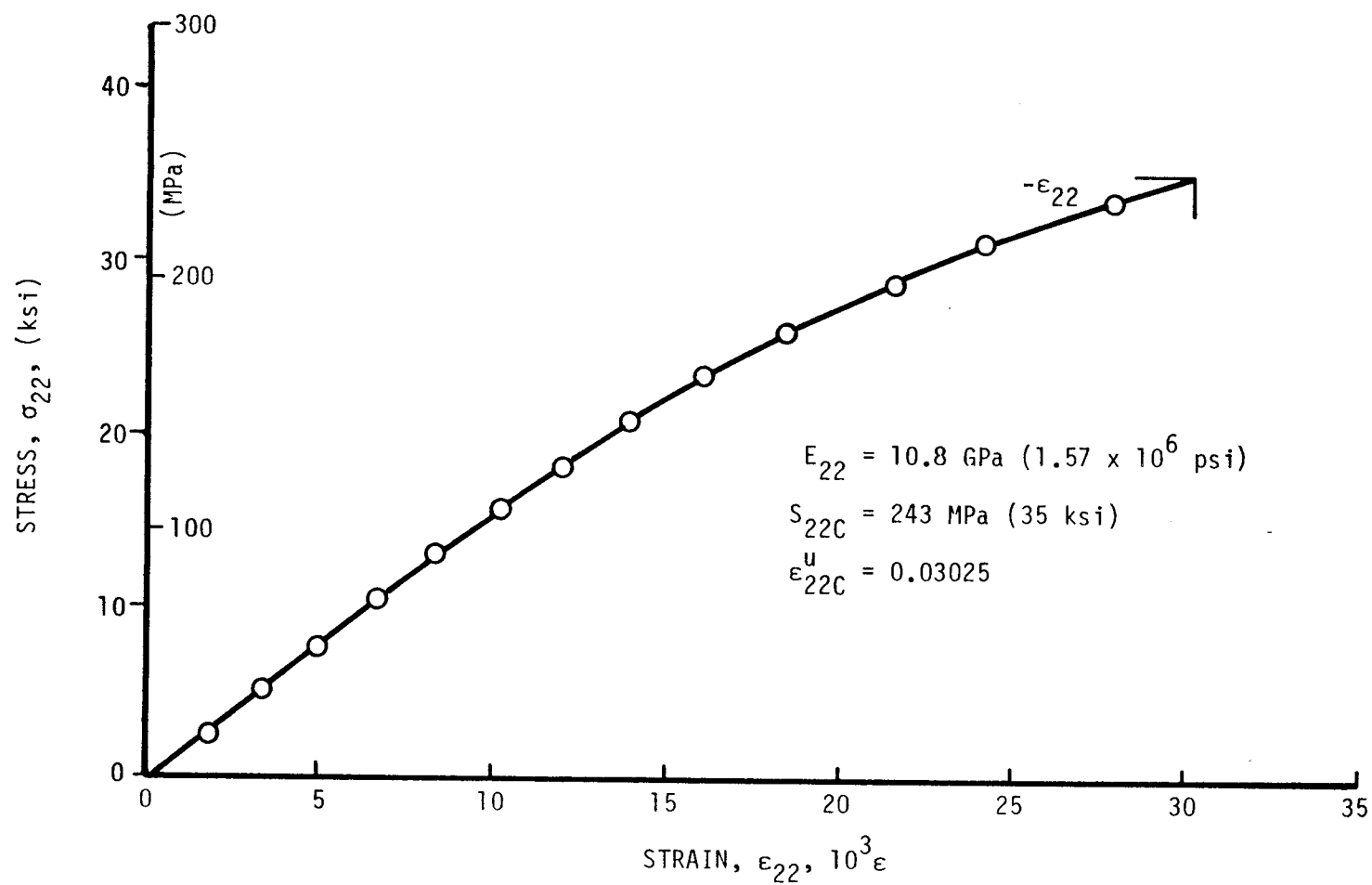


Figure 2-25. Stress-strain curve for unidirectional 90-deg SP288/AS specimen under compressive loading.

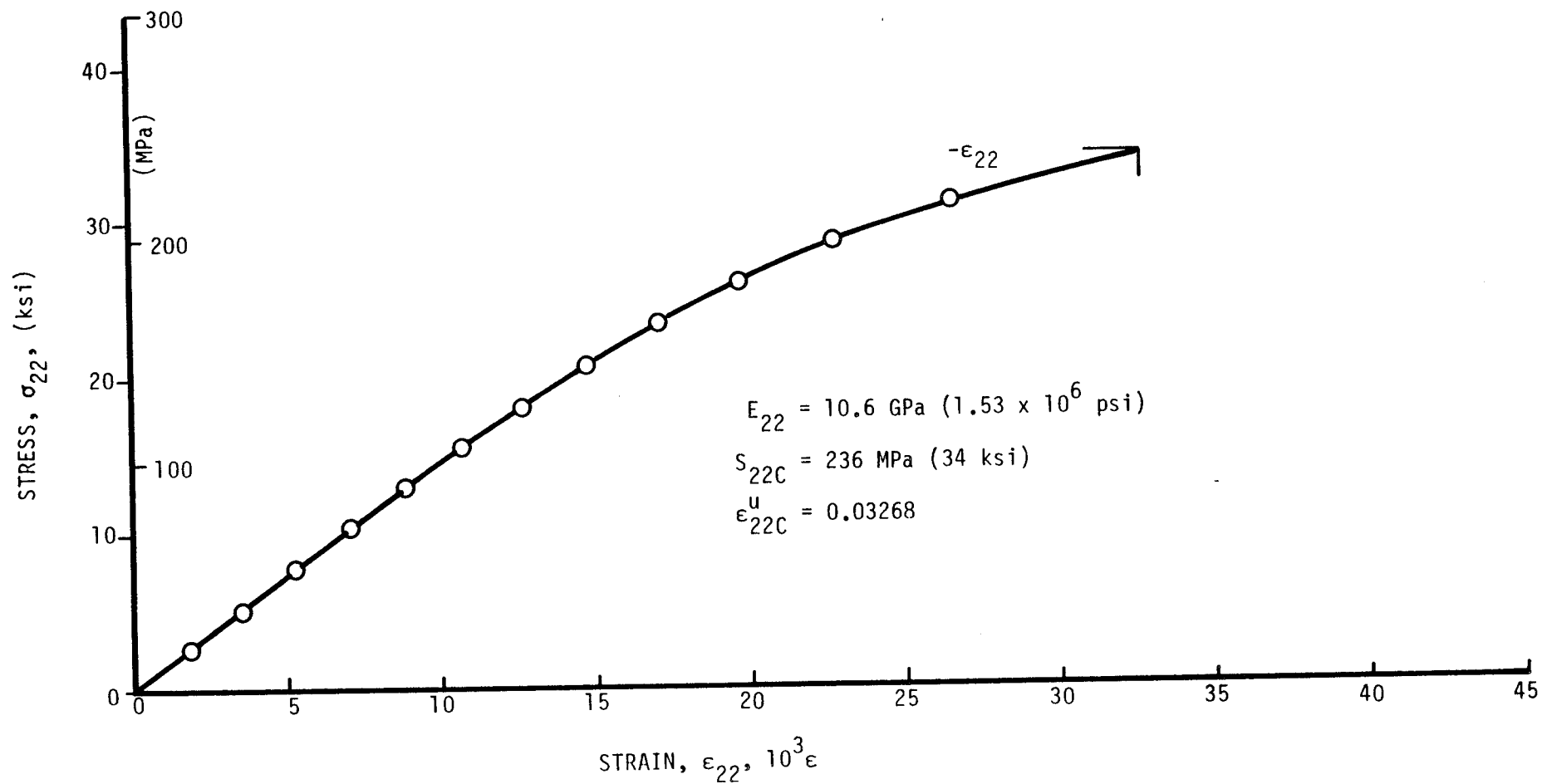


Figure 2-26. Stress-strain curve for unidirectional 90-deg SP288/AS specimen under compressive loading.

2-43

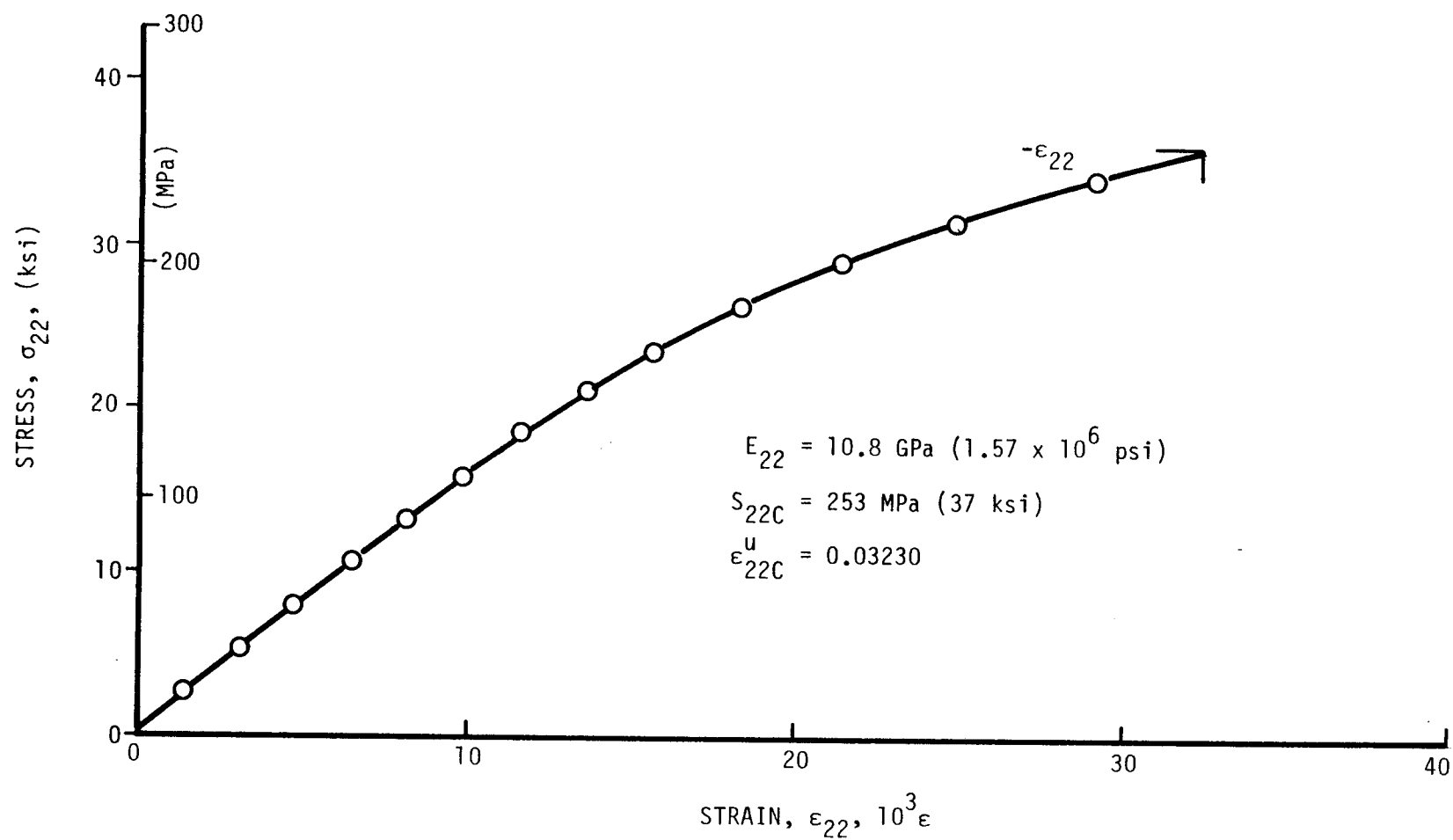


Figure 2-27. Stress-strain curve for unidirectional 90-deg SP288/AS specimen under compressive loading.

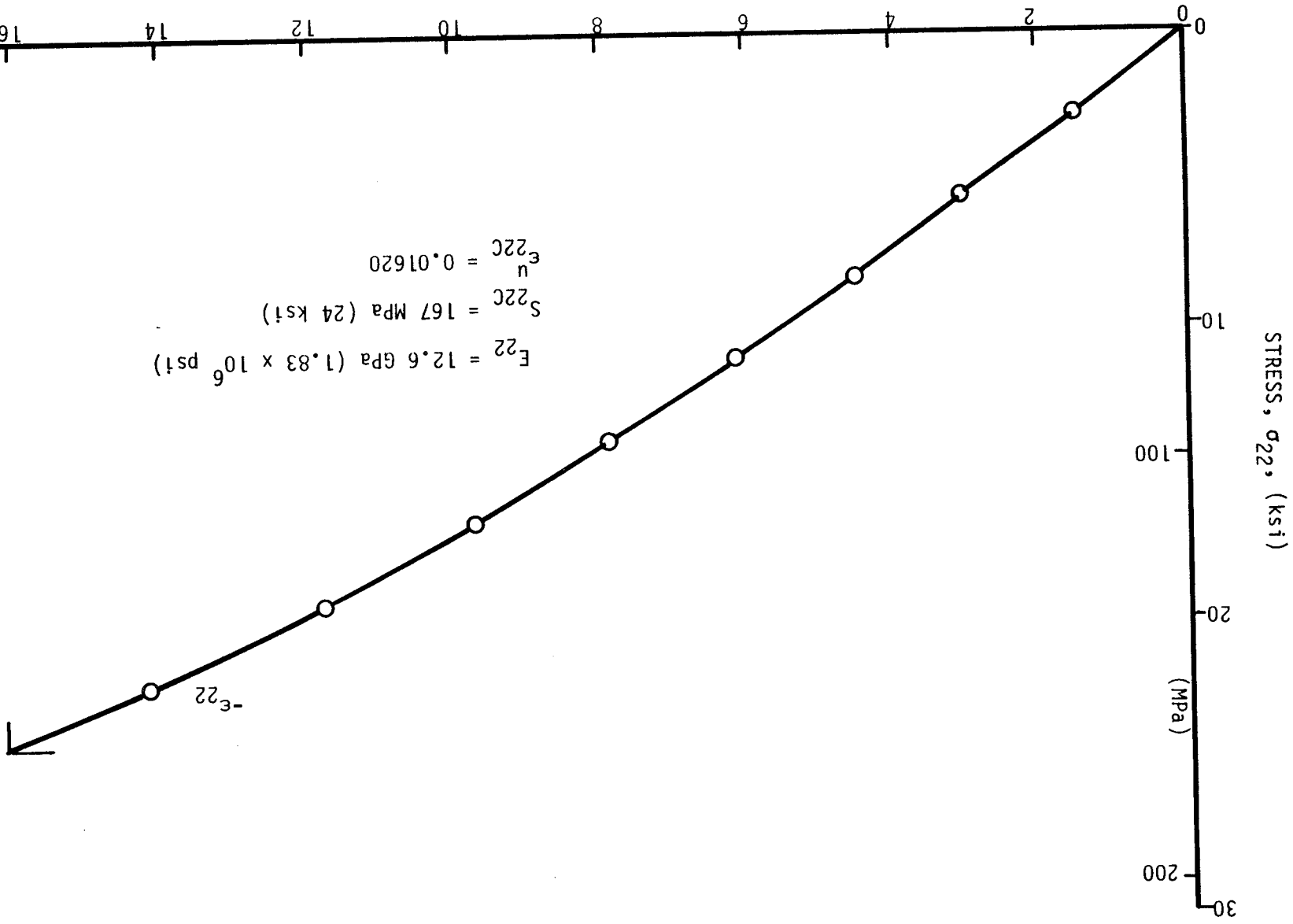


Figure 2-28. Stress-strain curve for unidirectional 90-deg 80AS/20S/PR288 specimen under compressive loading.

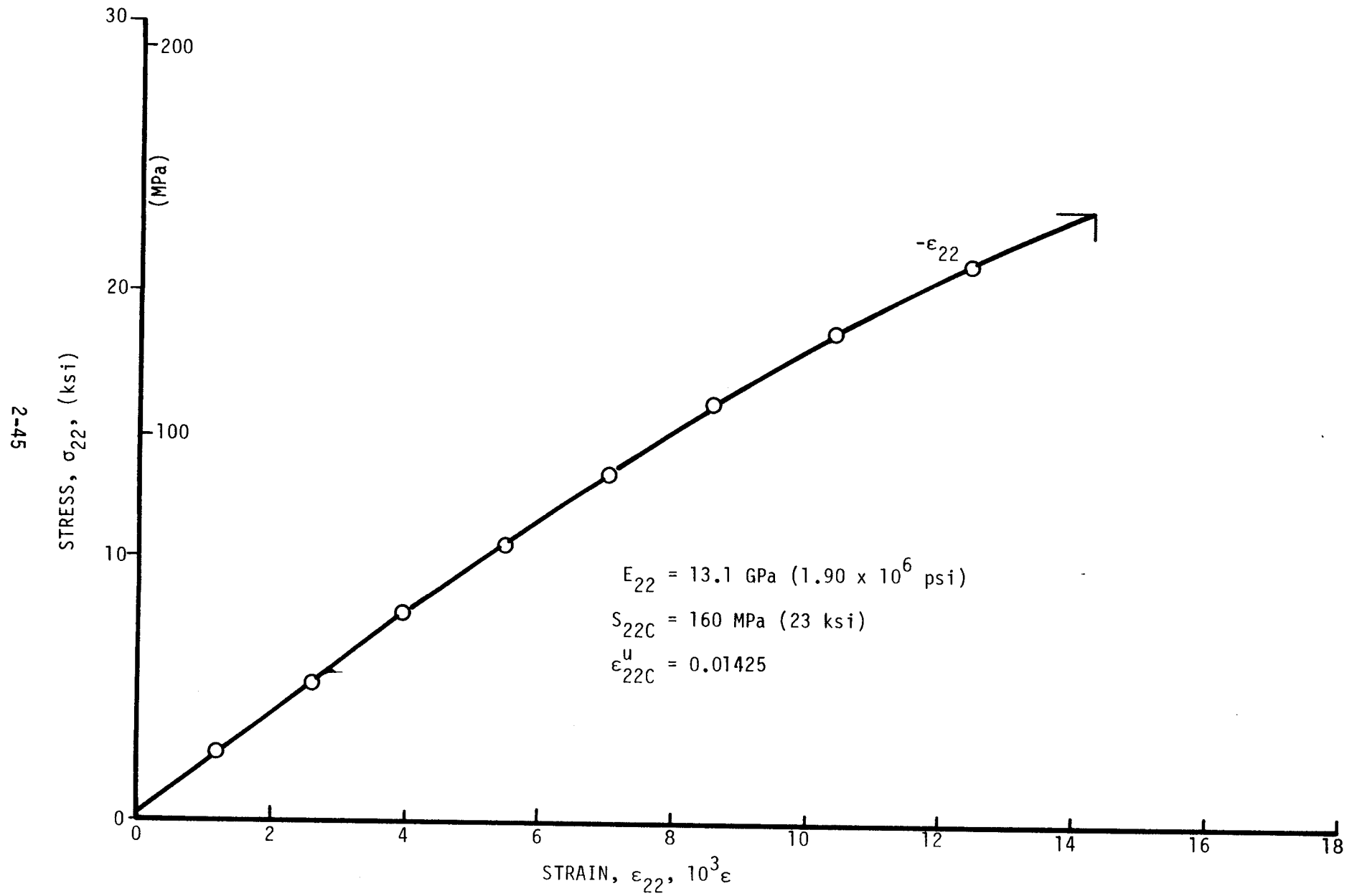


Figure 2-29. Stress-strain curve for unidirectional 90-deg 80AS/20S/PR288 specimen under compressive loading.

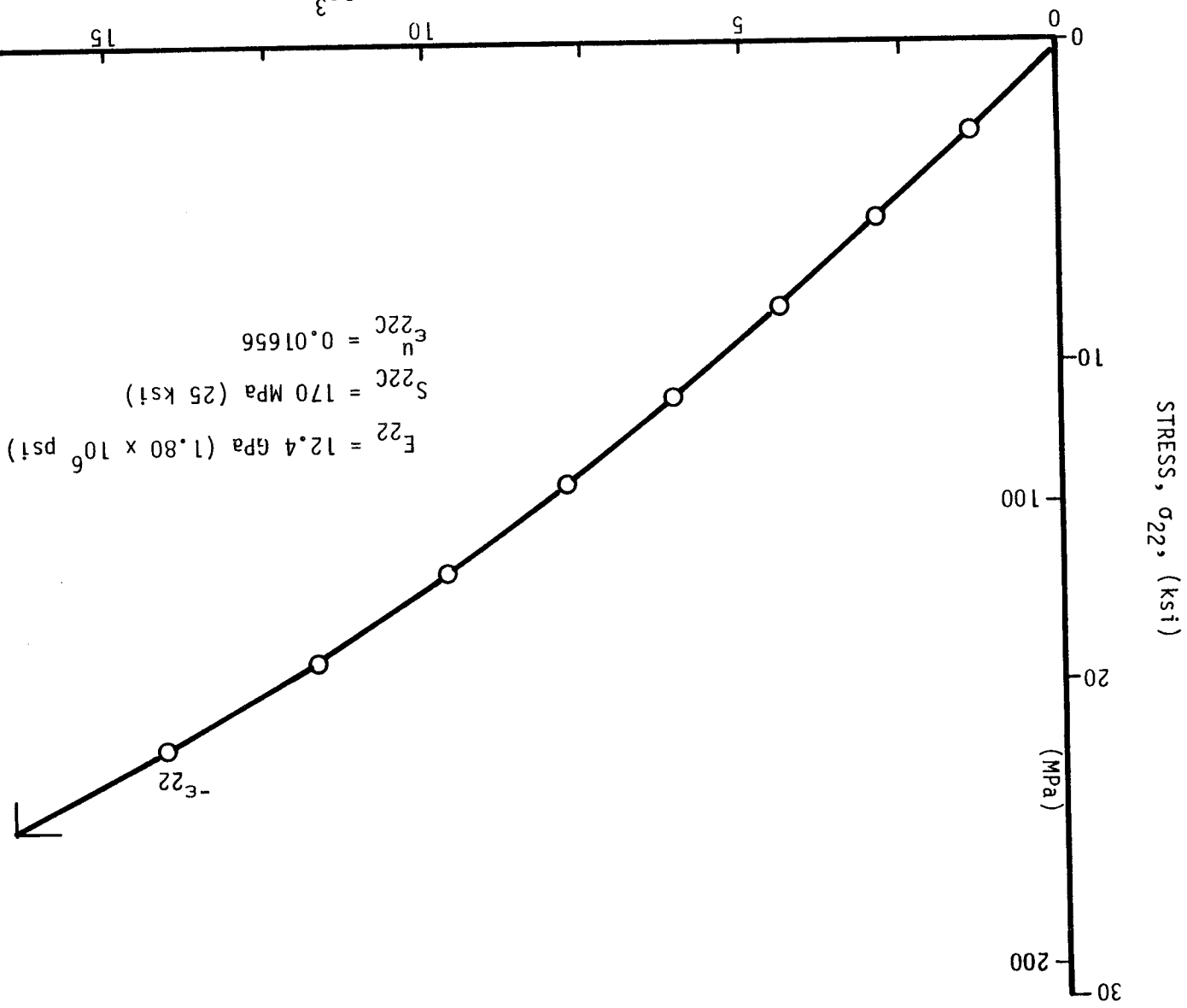


Figure 2-30. Stress-strain curve for unidirectional 90-deg 80AS/20S/PR288 specimen under compressive loading.

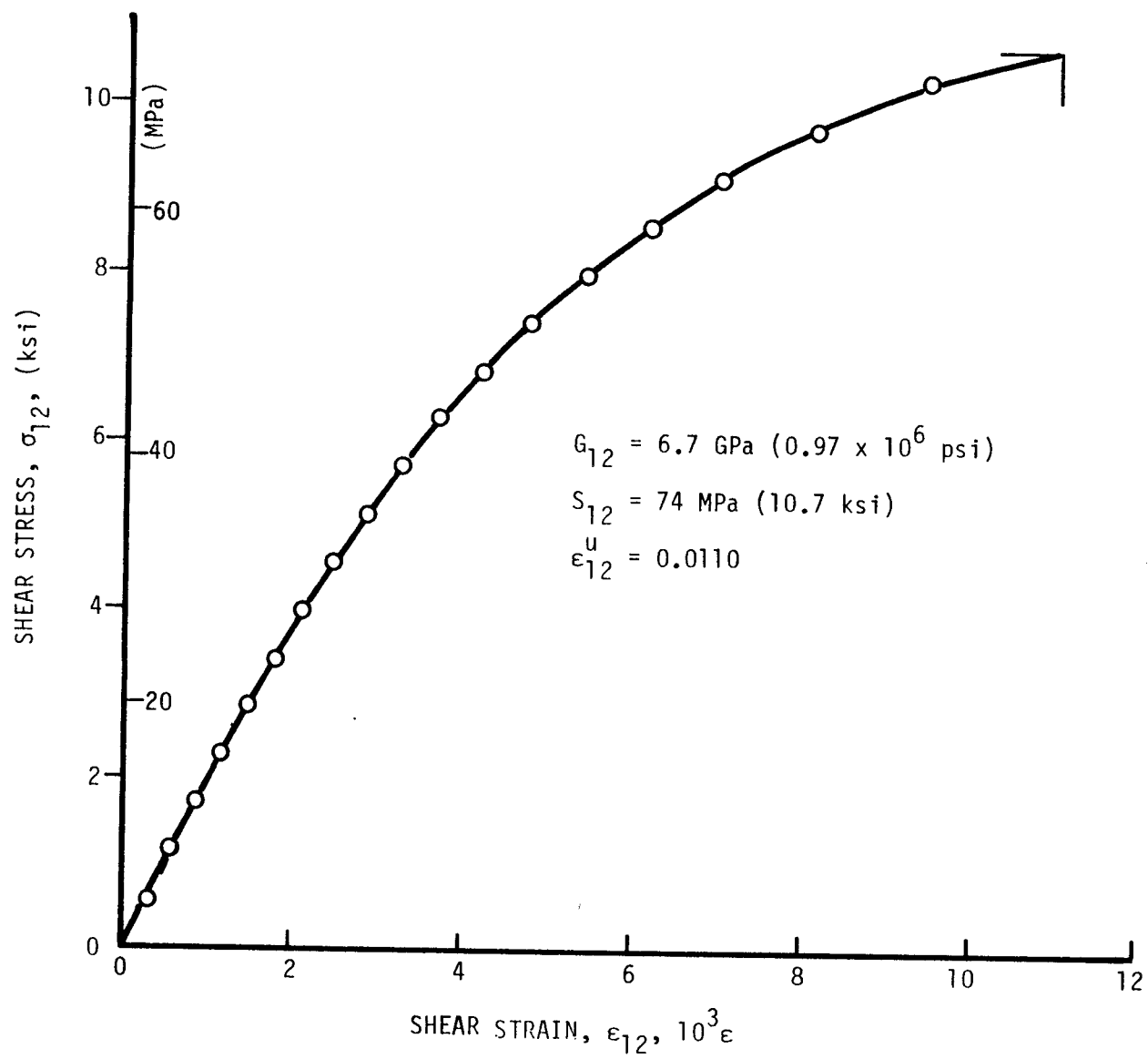


Figure 2-31. Shear stress versus shear strain for unidirectional 10-deg off-axis SP288/T300 specimen.

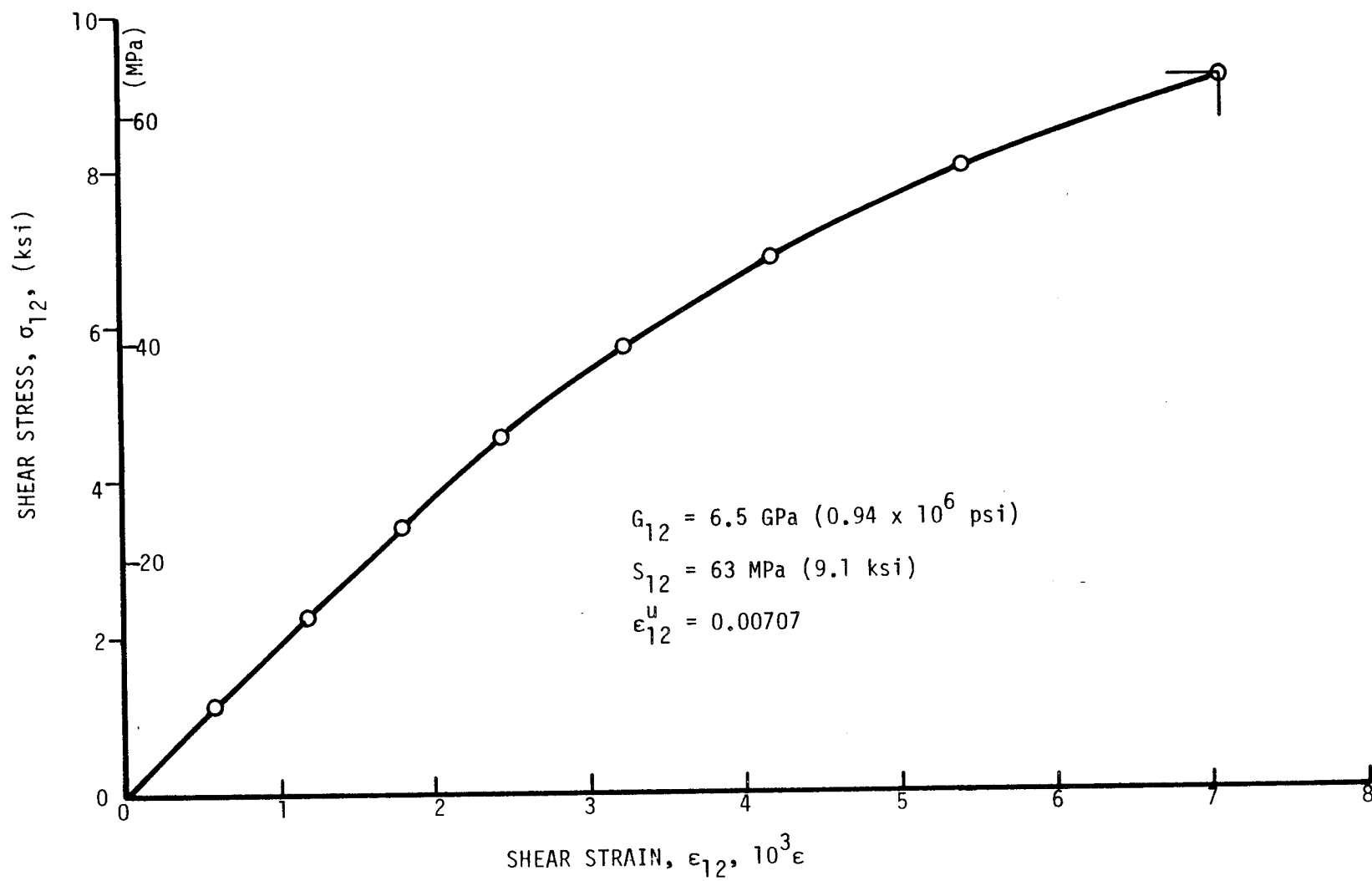


Figure 2-32. Shear stress versus shear strain for unidirectional 10-deg off-axis SP288/T300 specimen.

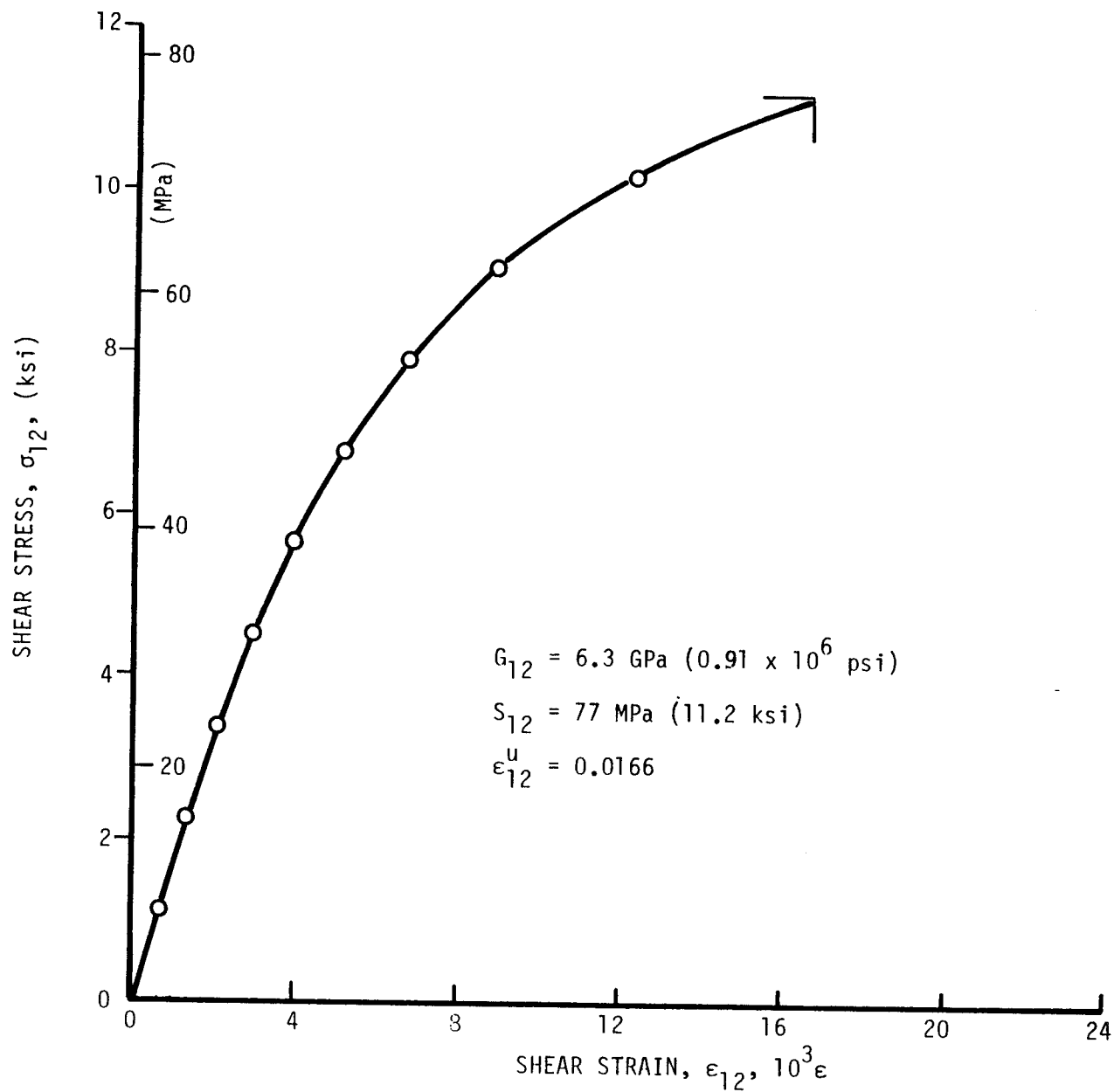


Figure 2-33. Shear stress versus shear strain for unidirectional 10-deg off-axis SP288/AS specimen.

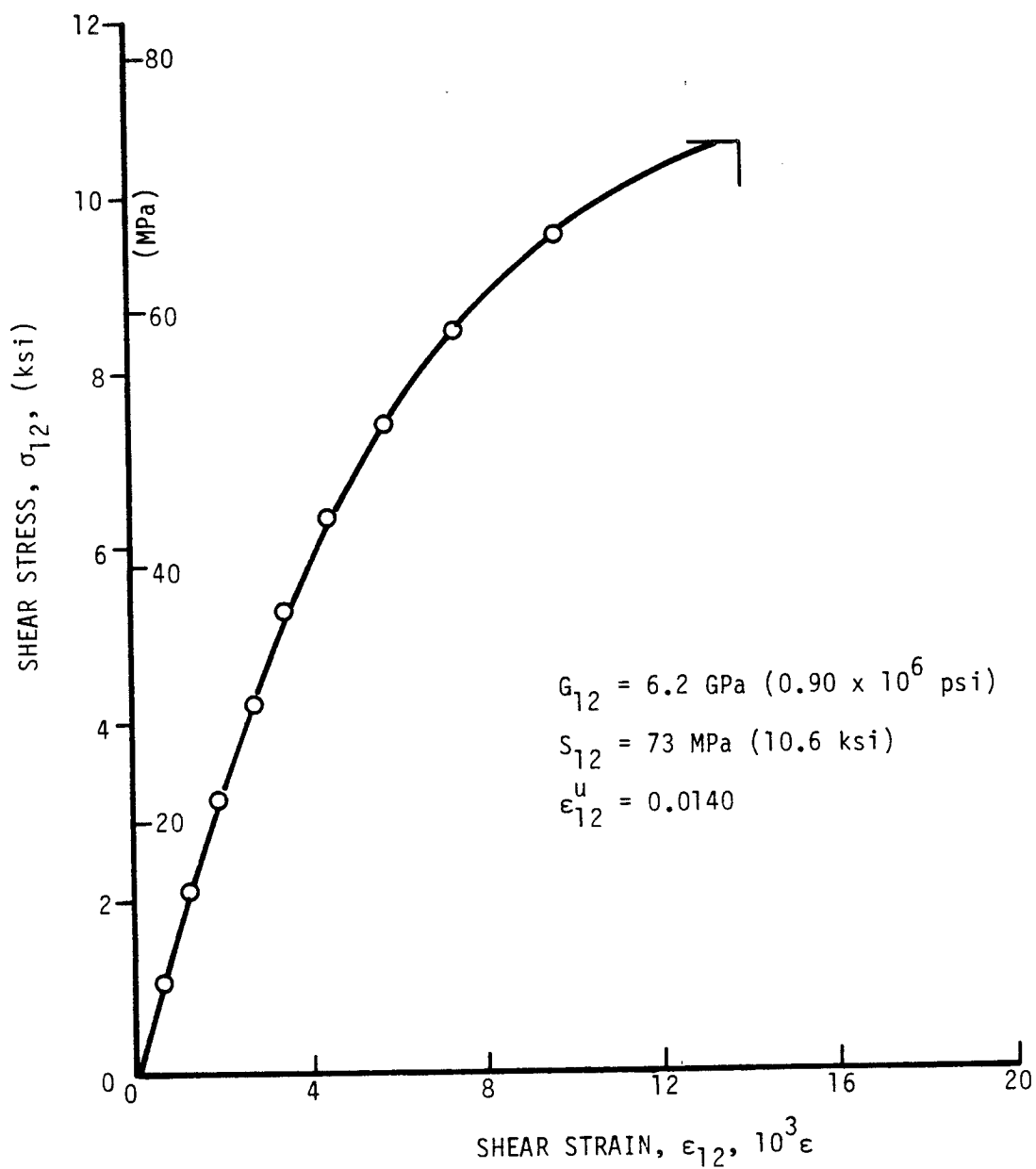


Figure 2-34. Shear stress versus shear strain for unidirectional 10-deg off-axis SP288/AS specimen.

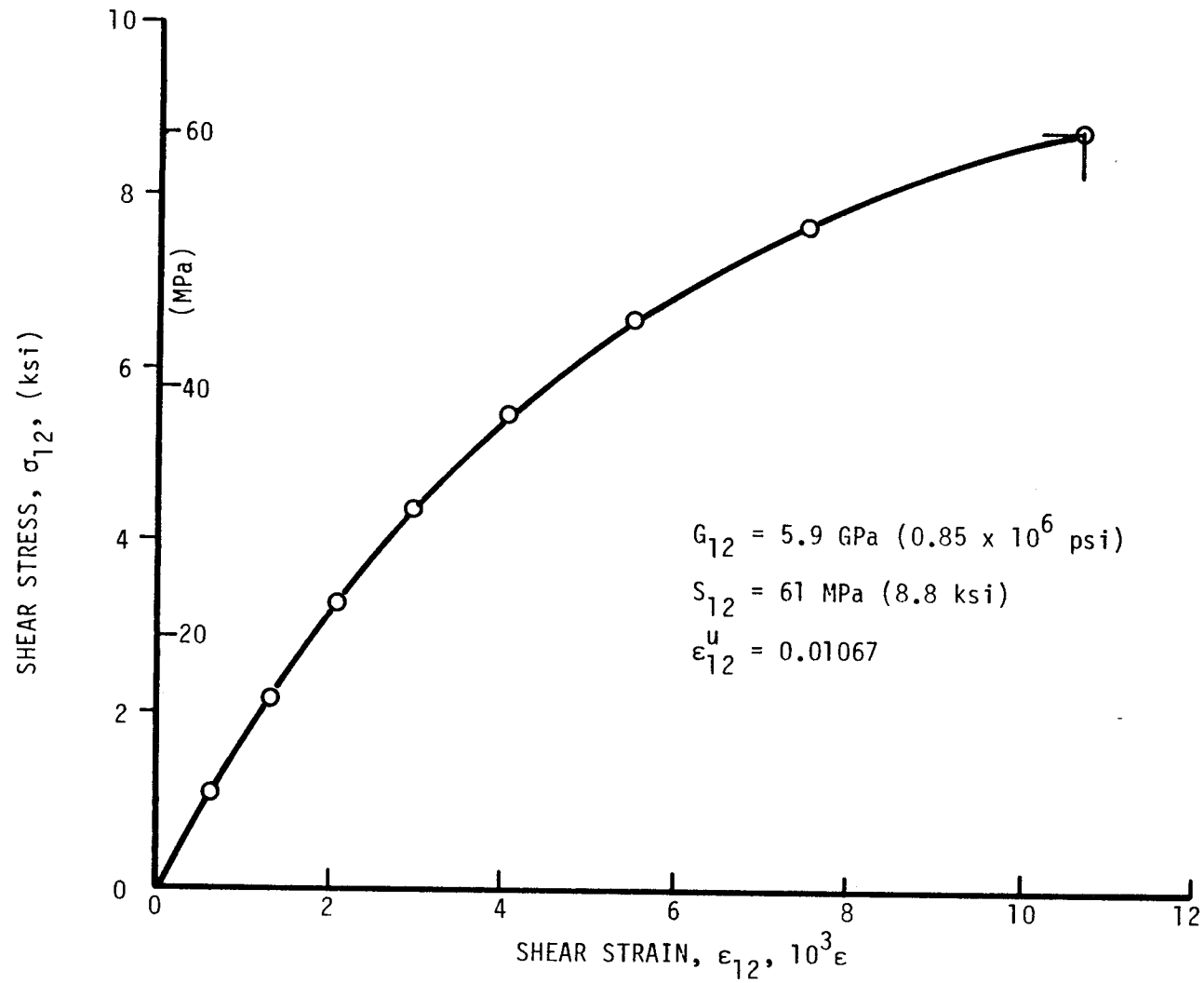


Figure 2-35. Shear stress versus shear strain for unidirectional 10-deg off-axis 80AS/20S/PR288 specimen.

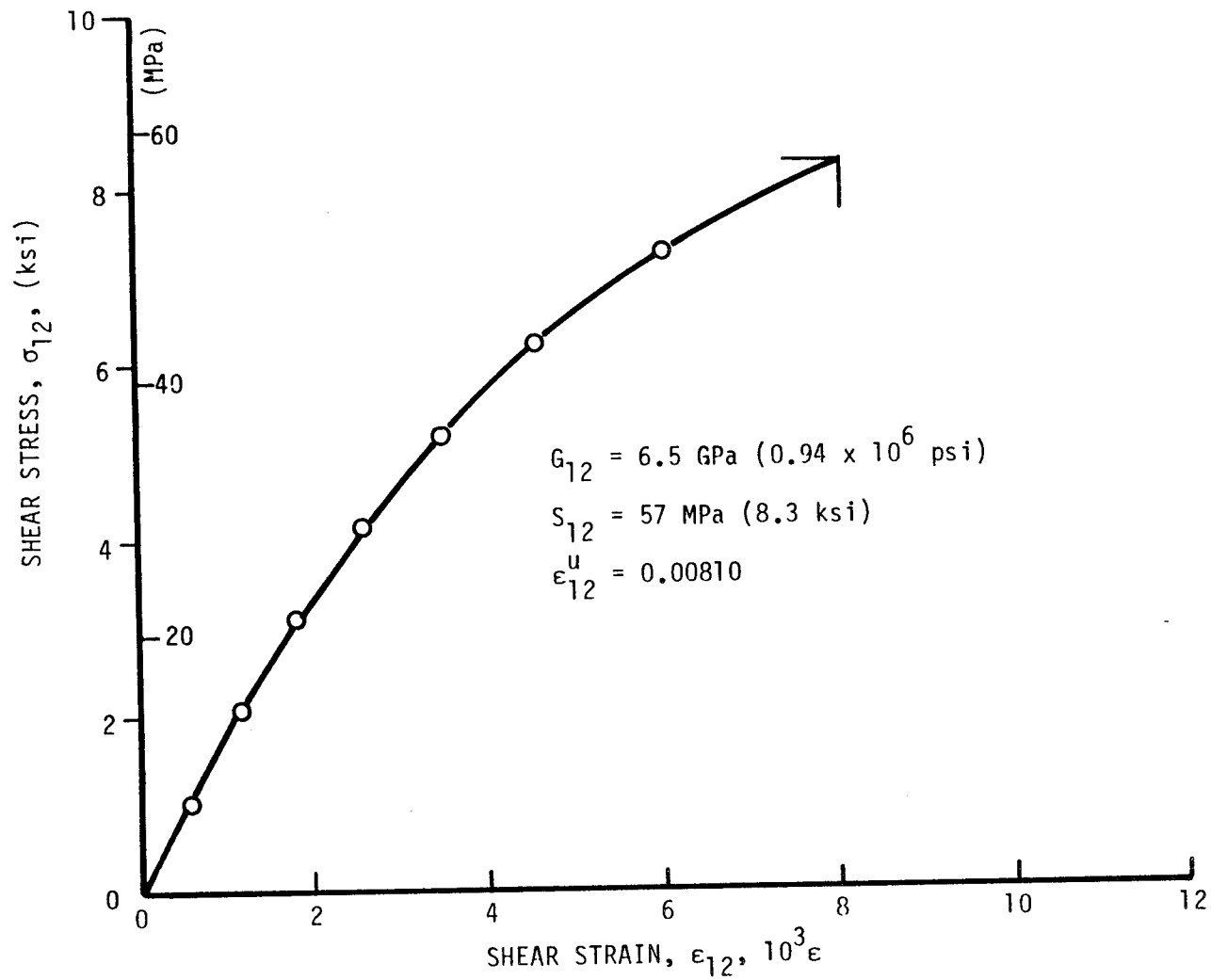


Figure 2-36. Shear stress versus shear strain for unidirectional 10-deg off-axis 80AS/20S/PR288 specimen.

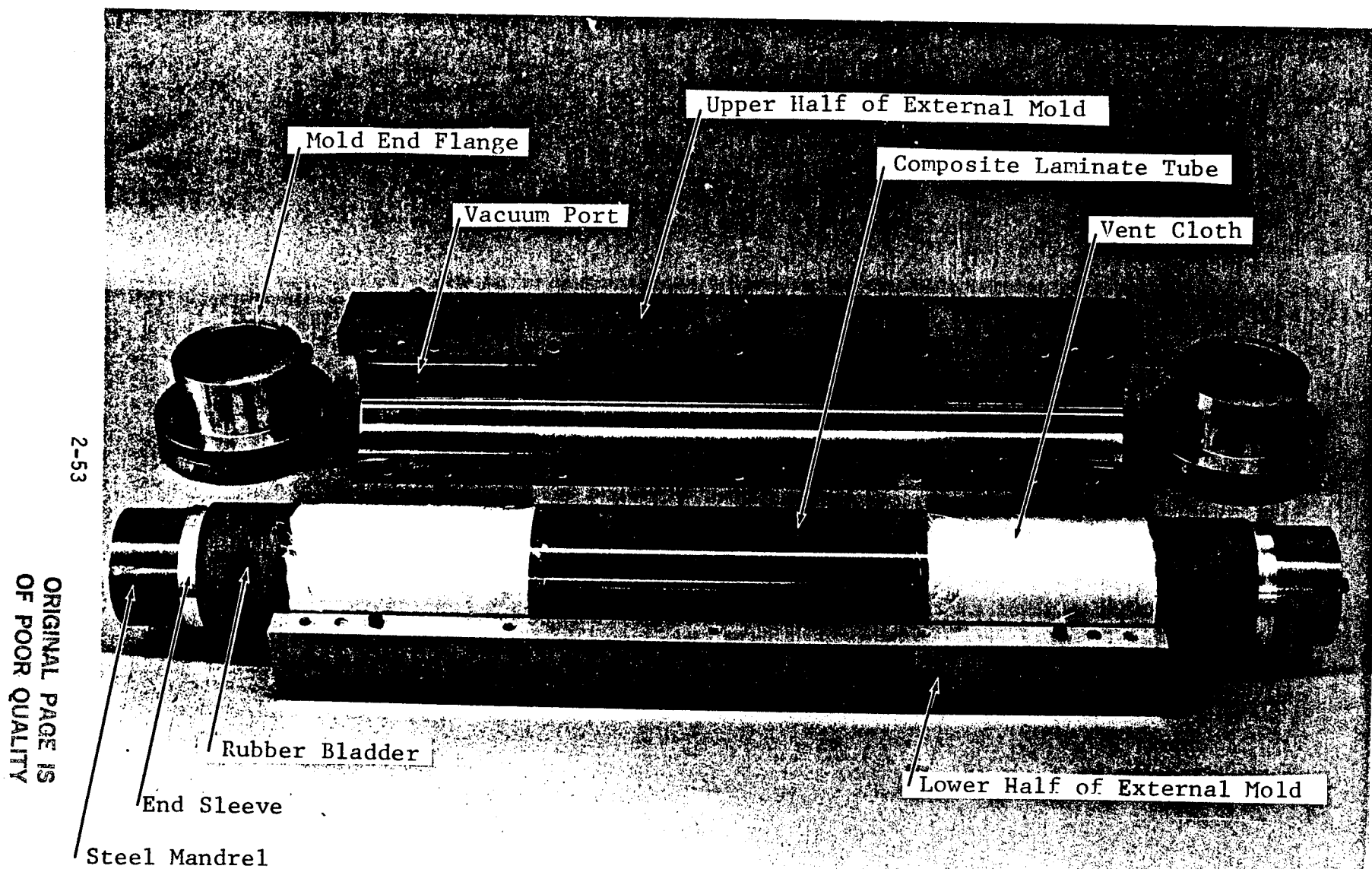


Figure 2-37. Components of cavity mold tool for fabricating composite laminate tubes.

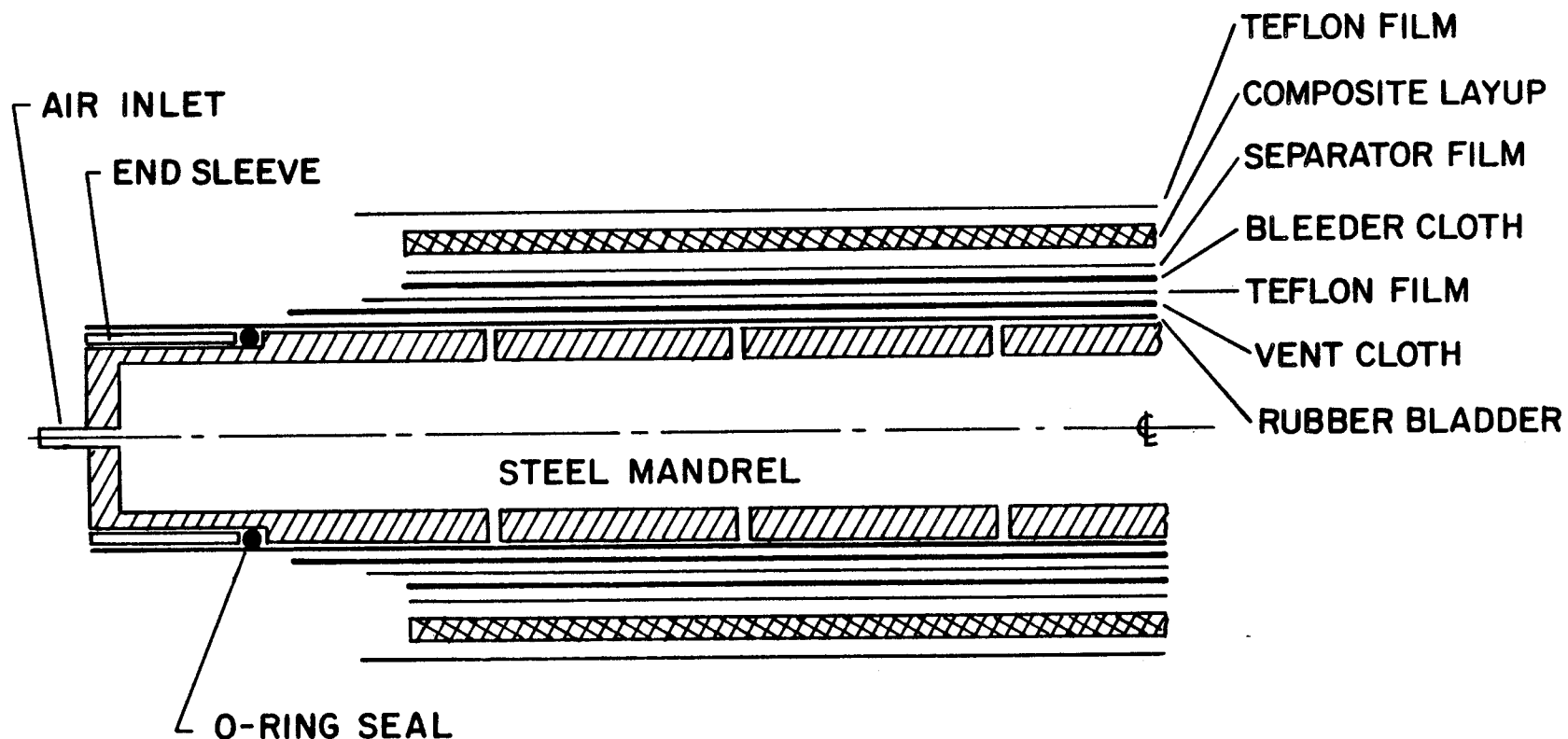


Figure 2-38. Sketch showing the center steel mandrel and the sequence of material layers employed in the composite laminate tube fabrication.

2-55

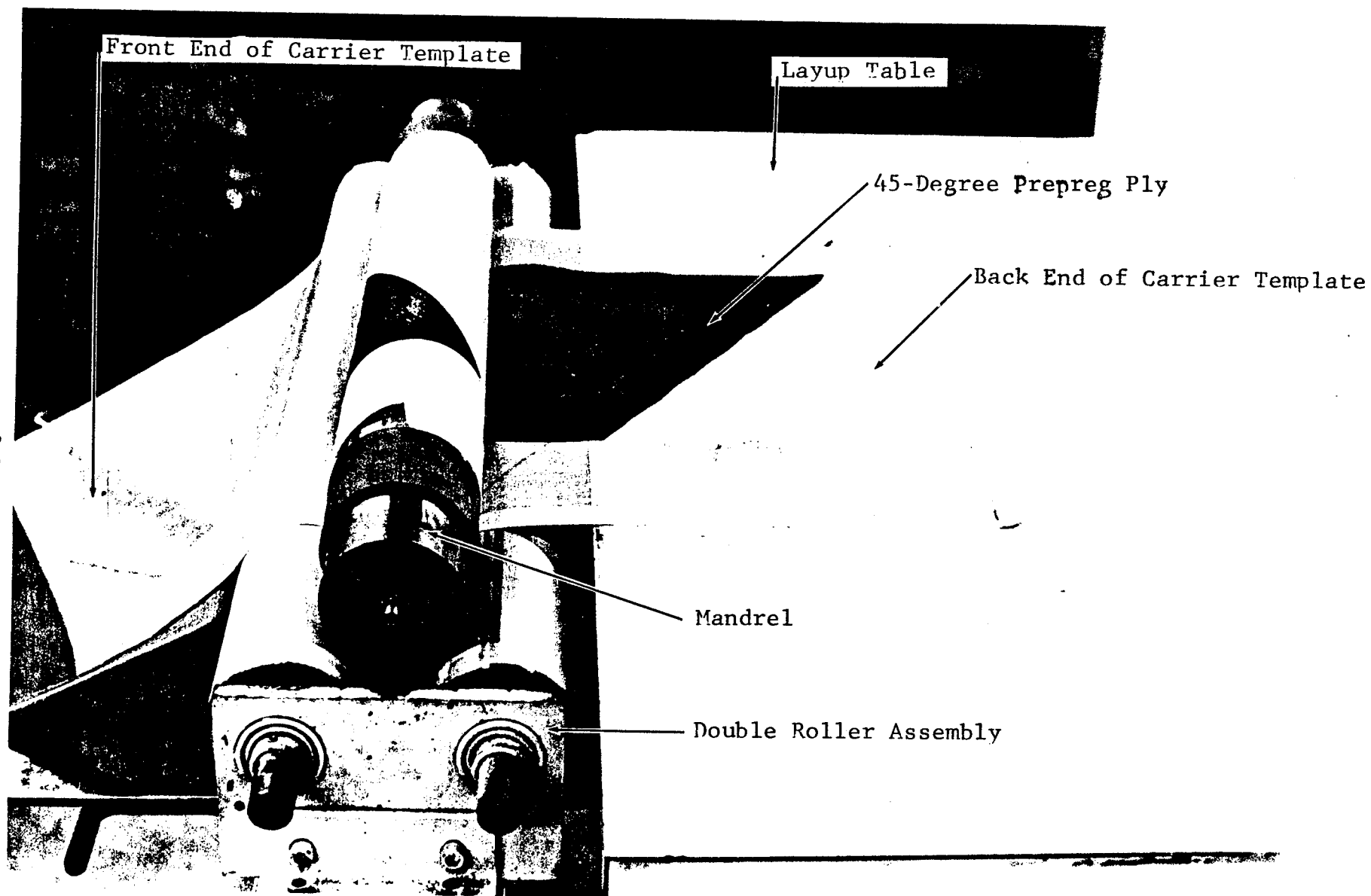


Figure 2-39. Roller and carrier template system for wrapping prepreg plies on the tube layup mandrel.
(The photograph shows partial layup of a 45-deg fist ply.)

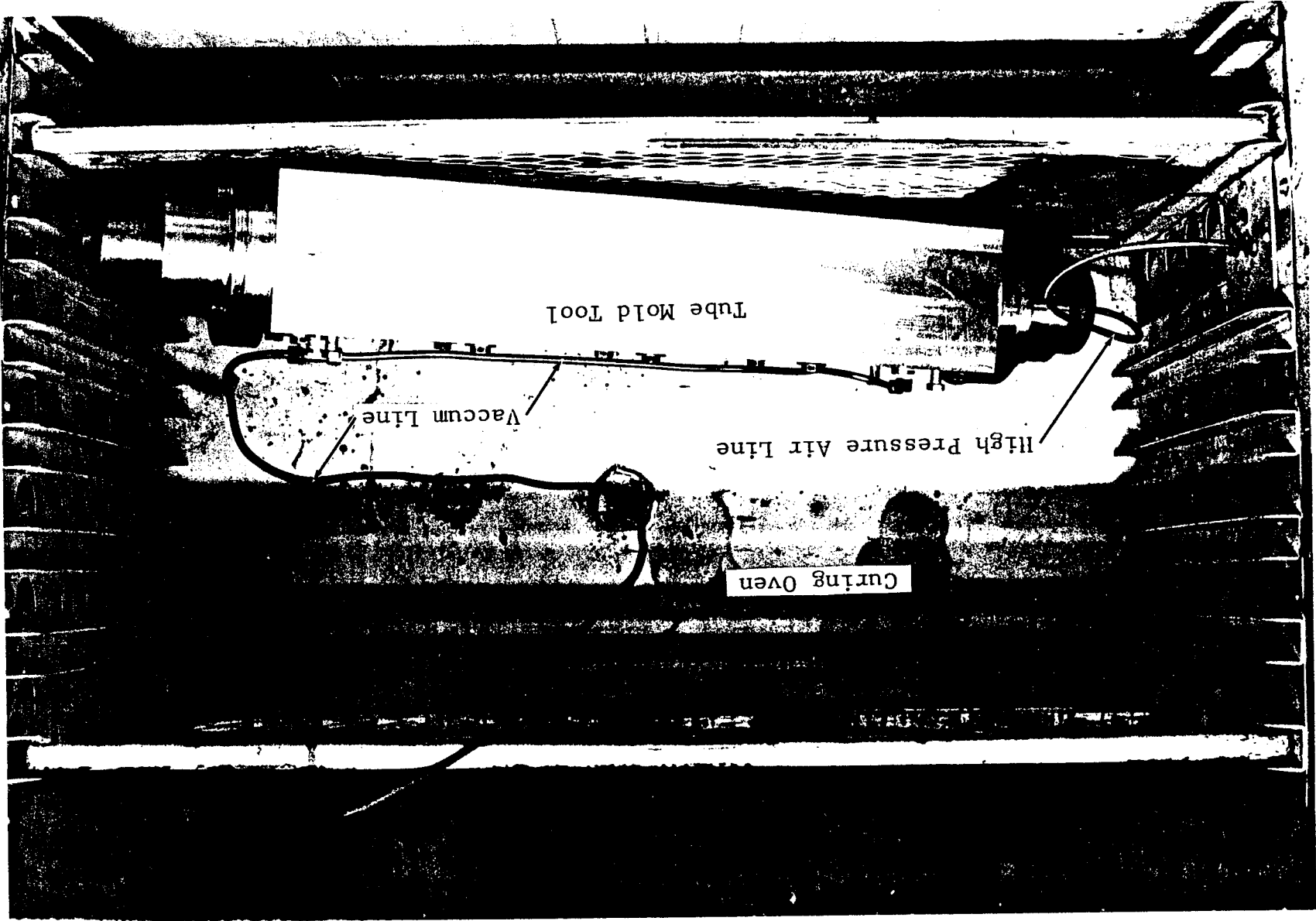


Figure 2-40. Assembled cavity mold tool for composite tube fabrication shown in curing oven with air and vacuum lines attached.

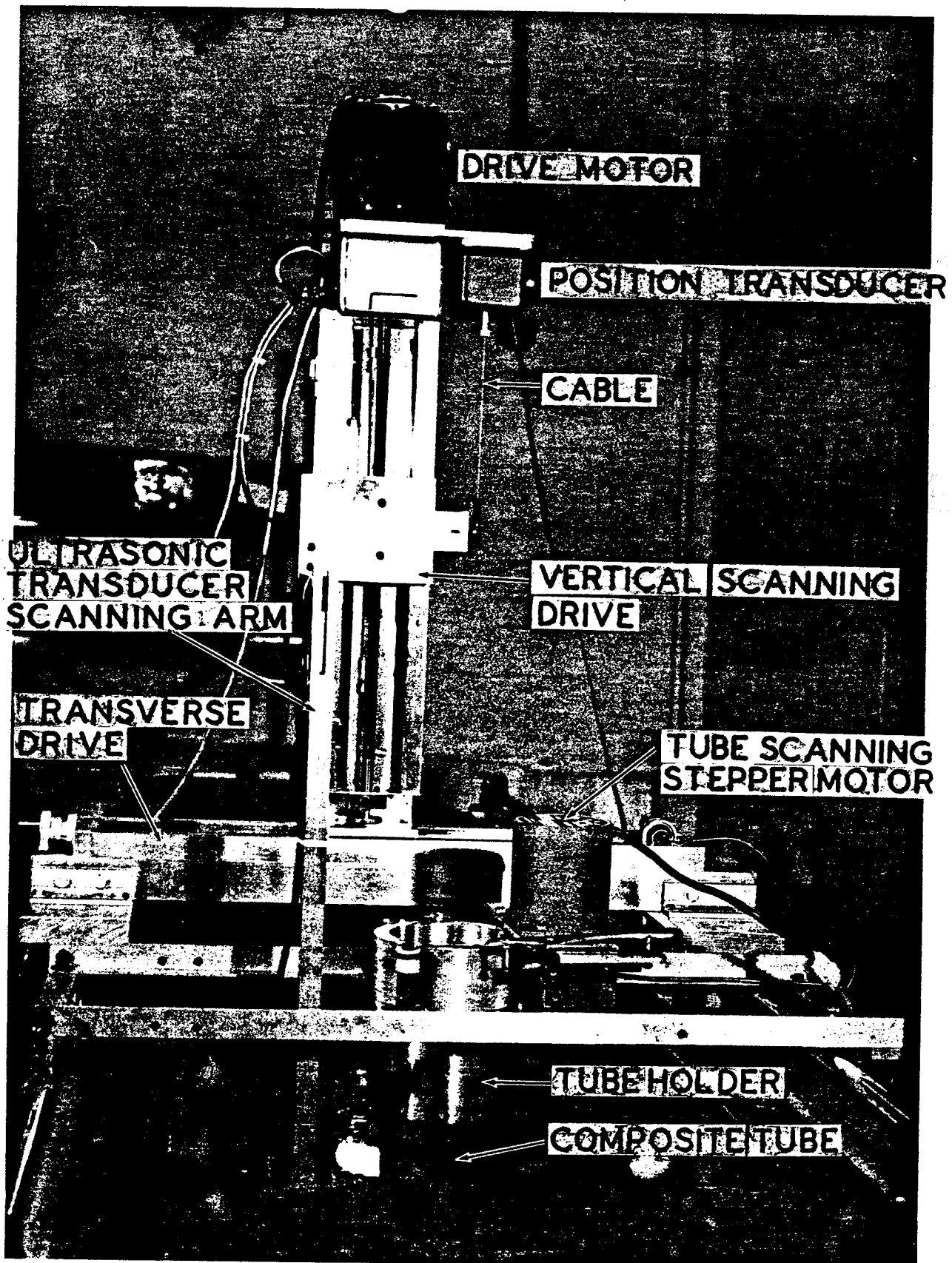


Figure 2-41. Ultrasonic system for scanning tubular specimens.

ORIGINAL PAGE IS
OF POOR QUALITY

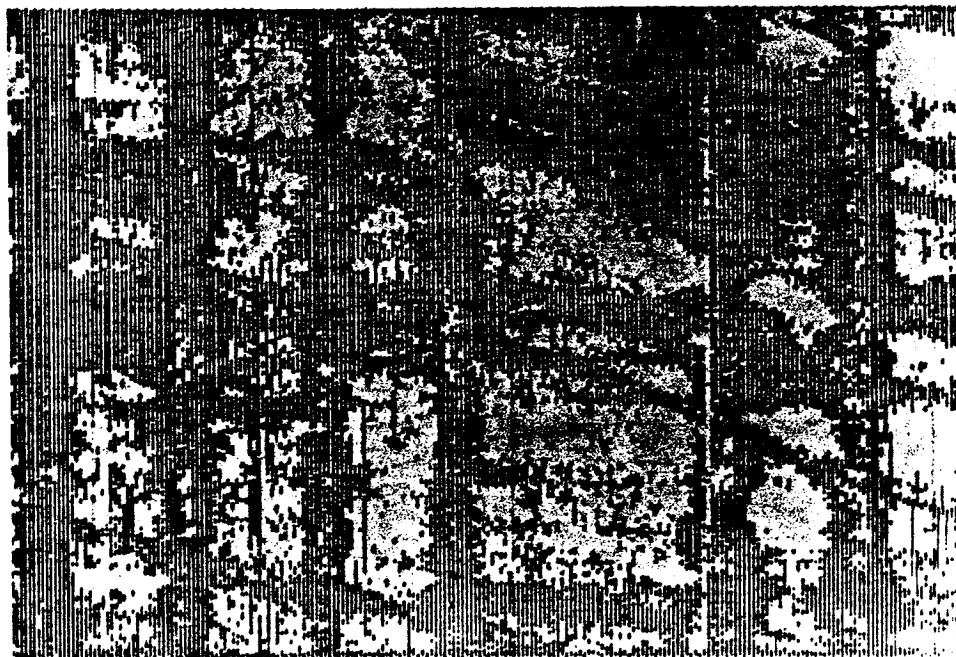
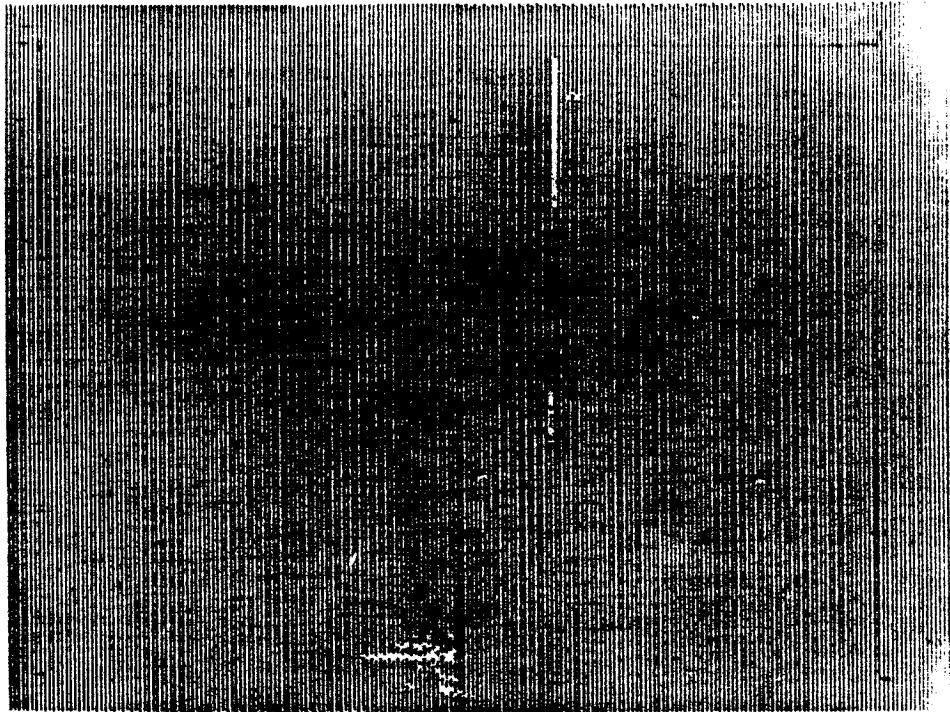


Figure 2-42. Typical ultrasonic C-scans of acceptable and unacceptable $[0_6]$ graphite/epoxy (SP288/T300) tubes.

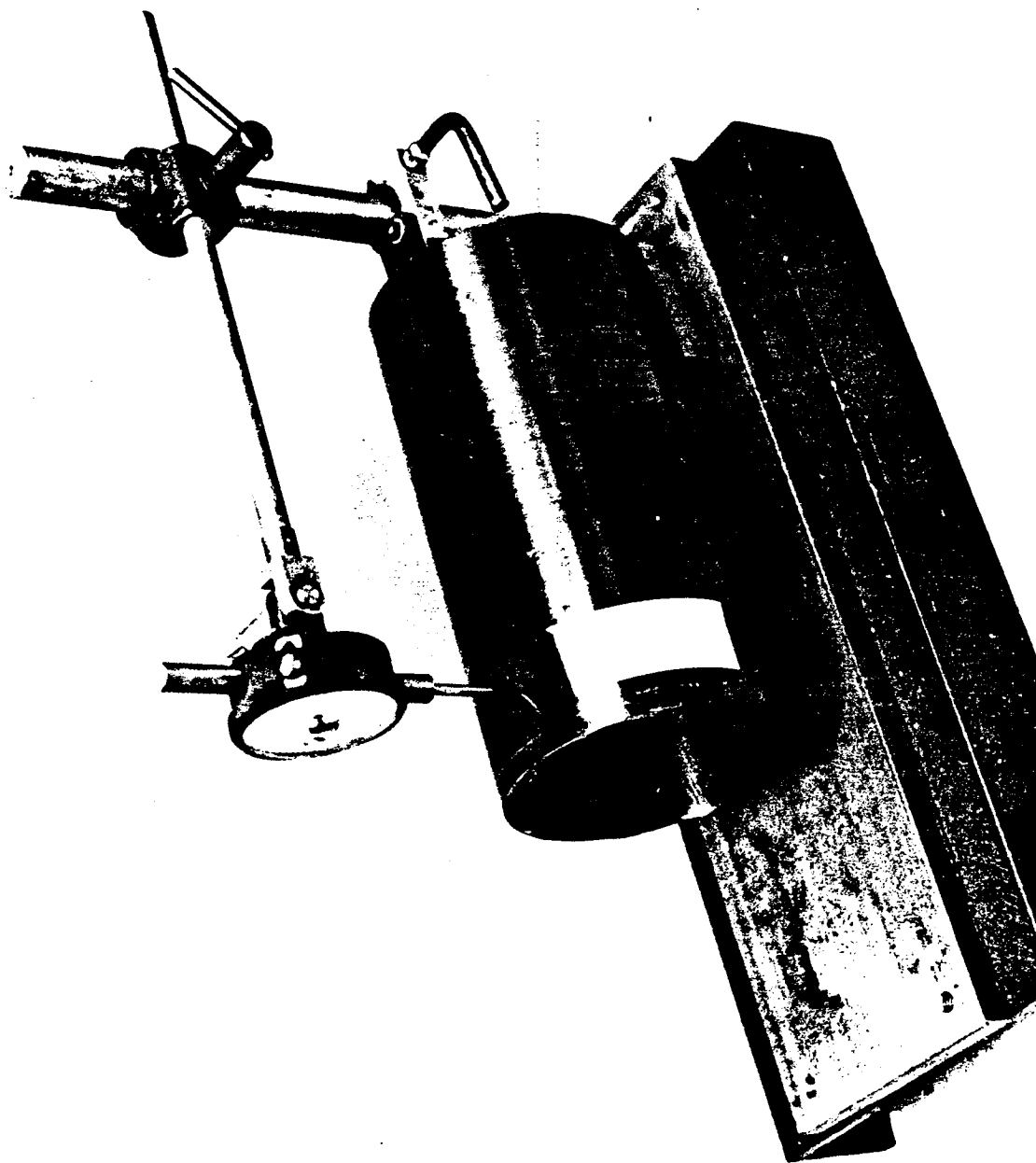


Figure 2-43. Fixture for measuring the wall thickness of composite tubes.

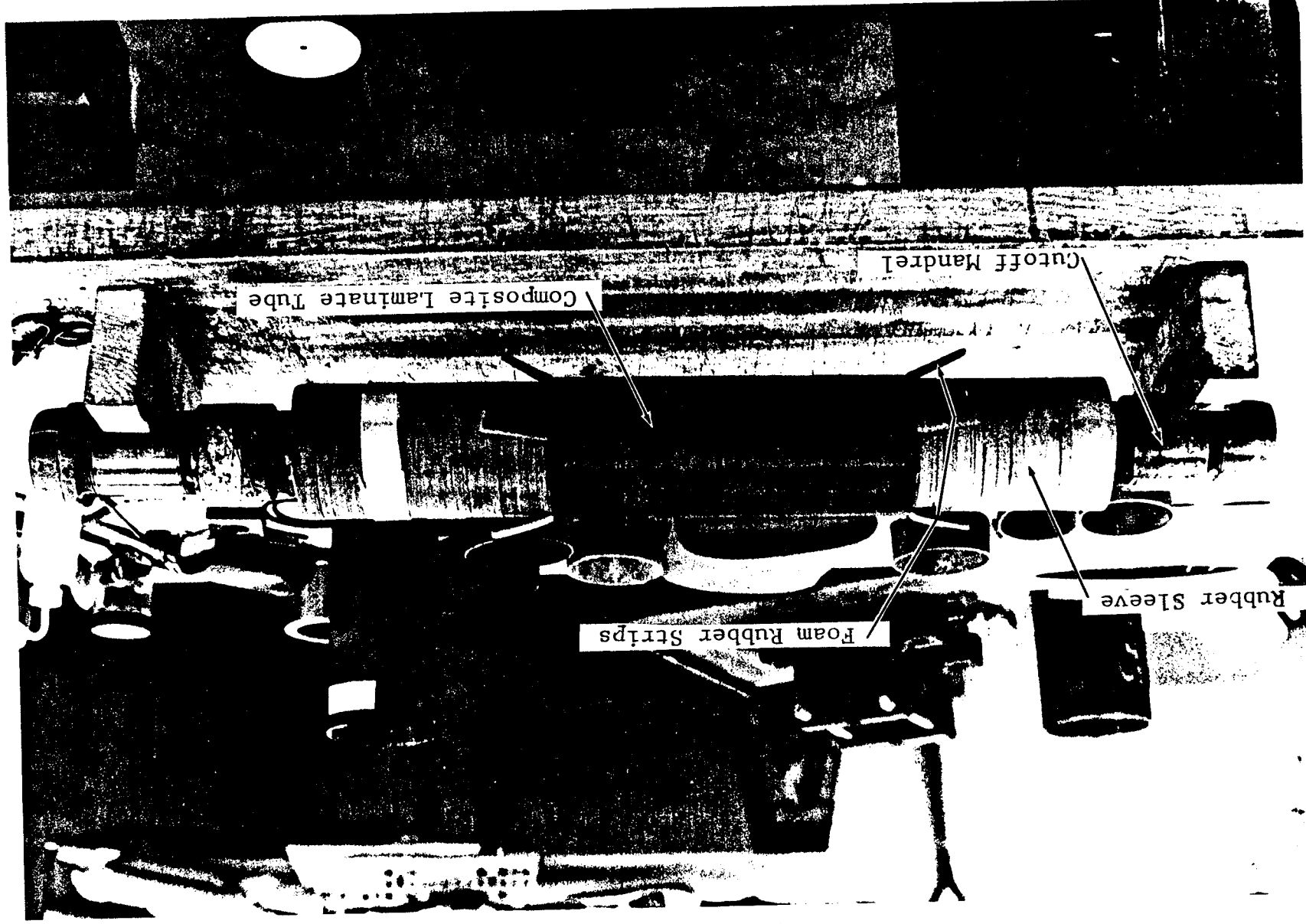


Figure 2-44. Composite laminate tube mounted on a rubber-sleeve-covered cutoff mandrel in preparation for cutting ring specimens.

2-60

ORIGINAL PAGE IS
OF POOR QUALITY

C-2



2-61

ORIGINAL PAGE IS
OF POOR QUALITY

Figure 2-45. Cutting of composite tube on a lathe into rings using a high speed diamond cutoff wheel.

3. TEST METHOD DEVELOPMENT

3.1 PRELIMINARY TESTING

Preliminary testing to establish test methods and procedures was conducted using metallic and composite ring specimens. These were mounted between two thick rigid metal disks held together with bolts and forming with the specimen a cylindrical vessel. In one configuration used, one of the disks was perforated and connected to a cylinder with a piston. The cavity between the disks and the cylinder was filled with fluid (a solution of water and water-soluble oil). The piston was loaded dynamically to produce a pressure surge in the liquid to load the ring specimens dynamically. The liquid pressure was measured with a piezoelectric transducer and the specimen deformation was measured with strain gages mounted on the specimen.

All strain gage and transducer data were recorded with a four channel digital processing oscilloscope (Norland 2001A Waveform and Data Analysis System). It has sampling rates as fast as one point per microsecond. It is equipped with a minicomputer and Flexible Disk Memory (floppy disk) for storage and retrieval of data and keyboard programs. The storage capacity of the floppy disk is 99 plies (array, register, or program files). Any signal that is recorded or processed by the oscilloscope or stored in the floppy disk can be plotted to any desired scale by an X-Y point plotter connected to the oscilloscope.

In the first series of tests graphite/epoxy rings of $[90_2/\pm 45]_S$ layup were used. Pressure and strain signals for such a specimen are shown in Figure 3-1. A peak strain of approximately 5400 $\mu\epsilon$ was reached in 800 μsec at an initial strain rate of 8 ϵ/sec . This is approximately two orders of magnitude lower than the desired rate. The pressure signal shows an oscillatory modulation superimposed on a ramp function. The following elastic and strength values were obtained for this graphite/epoxy layup:

Strain rate:	$\dot{\epsilon} = 8s^{-1}$
Modulus:	$E = 24.6 \text{ GPa } (3.56 \times 10^6 \text{ psi})$
Strength:	$S = 163 \text{ MPa } (23.6 \text{ ksi})$
Ultimate Strain:	$\epsilon^u = 5.4 \times 10^{-3}$

The corresponding values obtained under quasi-static loading for the same material and layup, but different batch, are:

$E = 24.0 \text{ GPa } (3.46 \times 10^6 \text{ psi})$
$S = 139 \text{ MPa } (20 \text{ ksi})$
$\epsilon^u = 7.5 \times 10^{-3}$

Additional tests with a hydraulic cylinder were conducted by loading the piston with a falling weight. A weight of 187N (42 lb) falling from a height of 59 cm (22 in.) produced a peak pressure of approximately 48,300 Pa (7,000 psi) in 2 msec. Increasing the height of drop to 122 cm (48 in.) increased the peak pressure to 67,900 Pa (9,800 psi) in the same length of time (2 msec). The preliminary conclusion from the falling weight tests was that for some low strength composite laminates it might be possible to achieve sufficiently high strain rates.

The loading fixture described before was subsequently modified. The disk supporting the piston was replaced with another steel disk with a 5.08 cm (2 in.) diameter threaded hole. A plug containing a detonator was threaded in this hole with the detonator exposed to the liquid reservoir and the leads coming out from the other end of the plug. A pressure transducer was mounted at the bottom disk of the fixture (Figure 3-2). Tests were conducted with $[90_2/\pm 45]_s$ graphite/epoxy rings using 50 mg detonators. These detonators produced sufficient pressure in the liquid to fracture these composite rings in approximately 12 μs corresponding to a strain rate of over 650 ϵ/sec . A typical strain record from such a test is shown in Figure 3-3.

A similar test with a similar graphite/epoxy ring was conducted and signals from four strain gages were recorded with the digital processing oscilloscope. Strain records from 4 gages around the circumference are shown in Figure 3-4. The sampling rate was one point per microsecond. The time duration between load initiation and the first indication of failure was 9 μs . The measured corresponding strain was 0.0077. All four strain records show the same average

strain rate of approximately 850 ϵ /sec. As can be seen in the record of Figure 3-4 these data are acquired digitally and stored in the system for further processing. The numerical data appearing in the record are referred to cursors P and Q on the lower trace. The ordinates are expressed in volts (or they can be scaled to any other units) and the abscissas are expressed in microseconds.

A similar test was conducted with an aluminum ring 10 cm (4 in.) in diameter, 1.57 mm (0.062 in.) thick, and 2.54 cm (1 in.) wide. Signals from two circumferential (hoop) and one axial strain gage and from a hoop conductive band are shown in Figure 3-5. In the upper figure the cursors are placed on the trace of the circumferential strain. The ordinate differential is expressed directly in $\mu\epsilon$ as $Q-P=\epsilon_{\theta}=17,773 \mu\epsilon$. The abscissa differential is $T=27 \mu s$ and the strain rate is displayed as $D=658.28 \epsilon$ /sec. In the lower figure the cursors are placed on the trace for the axial strain which reaches a value at failure of approximately $\epsilon_x = -6090 \mu\epsilon$. The corresponding average Poisson's ratio is $\nu=0.34$. A lower value would result if Poisson's ratio were based on the initial portion of the axial strain curve. The upper trace appears erratic either because of some localized yielding or a defective gage. A photograph of the failed specimen is shown in Figure 3-6. In addition to the cracked region, regions of localized yielding and reduced thickness appeared all around the ring.

Although the loading system described before produced sufficiently high strain rates, the fixture was not considered satisfactory because of the multiple reflections of the pressure waves in the liquid and the inability to record the pressure pulse to which the specimen itself is subjected. It was decided to design a new dynamic loading fixture to provide for a much larger fluid reservoir.

3.2 QUASI-STATIC TESTING

Quasi-static testing was conducted in a fixture which applies circumferential tension to the composite ring specimens by means of internal hydraulic pressure.¹⁵ Figure 3-7 is a sketch of the fixture used for quasi-static loading. It consists of a central steel core containing the fluid passages and ports. The core is threaded at both ends. They form the seats for the

two pressure retaining collars. The core has a pair of O-ring grooves where O-rings seal off the space between the core and the retaining collars. A thin latex tubular membrane fits tightly over the core between the threaded ends. The O-rings shown in Figure 3-7 fit over this membrane. Thus, when the retaining collars are screwed into place, the latex membrane and O-rings provide a leak proof barrier for the specimen pressurization fluid.

The test section contains a thick wall rubber tube, somewhat longer than the width of the ring specimen as shown in Figure 3-7. The tube fits over the rubber membrane and has an outer diameter somewhat smaller than the inner diameter of the ring specimen. The ends of the rubber tube fit into recesses provided for it in the retaining collars. Since the rubber is soft and compliant the hydraulic pressure is transmitted uniformly, and for all practical purposes, undiminished to the inside surface of the specimen. The rubber tube acts not only as the pressure transmission medium, but also as an extrusion barrier for the latex membrane. As with any hydraulic seal system, if the pressure is sufficiently high, the rubber tube can be extruded between the specimen ends and the retaining collars. To guard against this, the ends of the ring specimen should be parallel and flat.

To perform a test, the upper retaining collar is removed and the ring specimen is slipped over the rubber tube. The upper retaining collar is next screwed back into place and tightened up until the ring specimen is in contact with the end surfaces of both retaining collars. The hydraulic lines, a pressure gage, and a hydraulic hand pump are next connected to the test fixture as shown in Figure 3-8. The pressure is applied in steps until the ring fails. Strain gage readings are recorded at every step. Typical ring specimens instrumented with strain gages and after failure are shown in Figure 3-9.

3.3 DYNAMIC TESTING

3.3.1 Experimental Procedures

Ring specimens were loaded by an internal pressure pulse applied explosively through a liquid in a specially designed fixture. This fixture consists of two thick cylinders and two disks assembled together with the ring specimen between them (Figures 3-10 to 3-12). The reservoir was filled with a

mixture of water and water-soluble oil. The pressure pulse in the chamber was produced by detonating an explosive charge in the liquid reservoir. The explosive charges varied according to the laminate layup of the test specimen (or expected failure pressure) and the desired strain rate. Two types of explosive charges were used: pistol powder in quantities ranging between 260 mg and 1,560 mg, and PETN detonators (50 mg, 100 mg, and 330 mg). The explosive amounts were varied with the various specimens to obtain strain rates in the same range.

The dynamic internal pressure originally was measured with a piezoelectric transducer mounted on the side of the cylinder. This transducer had a resonant frequency higher than 500 kHz. Tests were conducted with unidirectional and angle-ply graphite/epoxy, steel, and aluminum rings instrumented with strain gages to check out the system. Strain gage signals from the composite and metallic rings and signals from the piezoelectric pressure transducer were recorded.

Figure 3-13 shows strain and pressure signals obtained from a $[0_8]$ graphite/epoxy (SP288/T300) specimen, and a 1.27 cm (0.50 in.) wide, and 0.56 cm (0.219 in.) thick steel ring. The upper trace represents the circumferential strain in the graphite/epoxy ring and reaches a peak of 4670 $\mu\epsilon$, due to premature failure around a known defect. The second and third traces represent circumferential strain measurements at two locations on the steel ring. The average peak strain was 965 $\mu\epsilon$. This peak occurs beyond the point of fracture of the graphite/epoxy ring. The bottom trace represents the pressure measured by the piezoelectric transducer. It shows a small initial peak followed by a much longer peak of 29,640 kPa (4300 psi), which occurs near the point of maximum rate change in the composite ring strain. An X-Y plot of the above data is shown in Figure 3-14. Failure occurred in approximately 28 μs .

Figure 3-15 shows circumferential strain and pressure records for a $[90_8]$ graphite/epoxy ring loaded in the fixture with a 50 mg detonator. The peak strain recorded in the upper trace is 4,880 $\mu\epsilon$. The pressure pulse shows two peaks with the larger exceeding 26,400 kPa (4400 psi). Recorded time to failure was 17 μs , corresponding to an average strain rate of 290 s^{-1} .

Figure 3-16 shows two sets of records for a $[\pm 45]_{2s}$ graphite/epoxy ring loaded dynamically with a 50 mg charge. The upper two traces in each photograph represent strain readings with average peaks of 9300 $\mu\epsilon$ and 11,170 $\mu\epsilon$. The lower trace represents the pressure pulse which appears different in the two tests. Peak pressures of 37,880 kPa (5490 psi) and 29,390 kPa (4260 psi) were recorded. The corresponding times to failure were 30 μs and 36 μs , corresponding to average strain rates of $310 s^{-1}$ in both cases.

Because of the large noise of the signals obtained with the pressure transducer, it was decided to replace it with an instrumented calibration ring placed next to the composite ring specimen. Several tests were conducted with steel rings of two thicknesses, 2.77 mm (0.109 in.) and 1.24 mm (0.049 in.). For the low pressures necessary to fracture 90-deg composite rings, the strains in the steel rings were approximately inversely proportional to their thickness and there was correlation between the effective pressure computed from the steel ring strains and the pressure measured with the piezoelectric transducer. However, at the higher pressures necessary to fracture 0-deg composite rings, the steel rings above deform into the plastic range (Figure 3-17). A new set of rings made of Vascomax steel was fabricated. The material is an 18% Nickel maraging steel with a 2415 MPa (350 ksi) yield point and a 193 GPa (28×10^6 psi) modulus. It is heat treated at 810°K (1000°F) for 3 hours. These pressure-cell rings have an internal diameter of 9.957 cm (3.920 in.), a width of 1.27 cm (0.5 in.), and thicknesses of 0.64 mm (0.025 in.) and 1.42 mm (0.056 in.). These rings were instrumented with foil and semiconductor strain gages. The latter were Kulite Semiconductor strain gages with a resistance of 119 ± 2 ohms and a gage factor of 110 (Type DCP-120-500). The instrumented rings were mounted and calibrated in the static ring testing fixture discussed before. Calibration results are shown in Figure 3-18. The static modulus determined from these calibration tests was computed as $E = 193$ GPa (28.0×10^6 psi).

To answer the question of any possible strain rate dependence of the Vasomax steel modulus, a bar of this material 0.620 cm (0.244 in.) x 0.617 cm (0.243 in.) x 9.406 cm (3.703 in.) instrumented with strain gages was tested dynamically. It was loaded with a 50 mg detonator at one end and the strain history at the gage location was recorded. The resulting strain rate, the measured wave propagation velocity, and the computed modulus were:

$$\dot{\epsilon} = 1151 \text{ s}^{-1}$$

$$c_0 = 4852 \text{ ms}^{-1} (191,020 \text{ in./sec})$$

$$E = 190.5 \text{ GPa} (27.6 \times 10^6 \text{ psi})$$

The result above indicates that there is no strain rate effect on the modulus of Vascomax steel for the range of interest.

3.3.2 Data Processing

Data analysis and interpretation are based on the mechanics of a dynamically pressurized elastic ring. The equation of motion for axisymmetric loading is:

$$\frac{\partial \sigma_r}{\partial r} + \frac{\sigma_r - \sigma_\theta}{r} = \rho \ddot{u} \quad (3-1)$$

where σ_r , σ_θ the radial and circumferential stresses, r the radial distance, ρ the material mass density, and u the radial displacement. Using the Lamé equations for an internally pressurized cylinder:

$$\begin{aligned} \sigma_r &= \frac{pa^2}{b^2 - a^2} \left(1 - \frac{b^2}{r^2} \right) \\ \sigma_\theta &= \frac{pa^2}{b^2 - a^2} \left(1 + \frac{b^2}{r^2} \right) \end{aligned} \quad (3-2)$$

the equation of motion at $r = b$ is written as:

$$p \left(\frac{2a^2}{b^2 - a^2} \right) = \sigma_\theta + \rho b \ddot{u} = \sigma_\theta + \rho b^2 \ddot{\epsilon}_\theta \quad (3-3)$$

where a and b are the inner and outer radii of the ring.

The primary data recorded in the dynamic ring tests are:

ϵ_{θ}^S - circumferential strain in steel ring
(pressure cell) at the outer radius, b.

ϵ_{θ}^C - circumferential strain in composite ring
at the outer radius, b.

ϵ_x^C - axial strain in composite ring at the
outer radius, b.

Assuming a uniaxial state of stress in the circumferential direction, the stress in the elastic ring is computed as

$$\sigma_{\theta}^S = E^S \epsilon_{\theta}^S \quad (3-4)$$

and then, the dynamic pressure is obtained in terms of this stress and the second derivative of ϵ_{θ}^S

$$p = \left[\sigma_{\theta}^S + \rho_s b_s^2 \ddot{\epsilon}_{\theta}^S \right] \left(\frac{b_s^2 - a_s^2}{2a_s^2} \right) \quad (3-5)$$

where E^S and ρ_s are the modulus and density of steel.

The circumferential stress in the composite ring is obtained in terms of the pressure above and the second derivative of ϵ_{θ}^C

$$\sigma_{\theta}^C = p \left(\frac{2a_c^2}{b_c^2 - a_c^2} \right) - \rho_c b_c^2 \ddot{\epsilon}_{\theta}^C \quad (3-6)$$

The dynamic stress strain curve for the composite material is obtained by plotting σ_{θ}^C versus ϵ_{θ}^C . Moduli, Poisson's ratios, strength, and ultimate strain for the composite material are thus obtained from the recorded and computed data.

In the case of the 10-deg off-axis rings used for determination of in-plane shear properties 3-gage rosettes were mounted on the outer surface of the composite rings. The measurements made were:

- ϵ_{θ}^S - circumferential strain in steel ring
- ϵ_{θ}^C - circumferential strain in composite ring
- ϵ_x^C - axial strain in composite ring
- ϵ_{45}^C - 45-deg strain in composite ring.

The circumferential stress in the composite ring was obtained from Equation 3-6 as before. The in-plane shear stress, referred to the fiber direction, is given by

$$\sigma_{12}^C = \sigma_{\theta}^C \sin\phi \cos\phi \quad (3-7)$$

where $\phi = 10$ -deg, the fiber orientation with respect to the circumferential direction. The in-plane shear strain is obtained from the three strain components as follows:

$$\epsilon_{12}^C = \frac{\epsilon_{\theta}^C - \epsilon_x^C}{2} \sin 2\phi + \left[\epsilon_{45}^C - \frac{\epsilon_x^C + \epsilon_{\theta}^C}{2} \right] \cos 2\phi \quad (3-8)$$

A dynamic shear stress versus shear strain curve is obtained by plotting σ_{12}^C versus ϵ_{12}^C . The shear modulus is given by

$$G_{12} = \frac{\sigma_{12}}{2\epsilon_{12}} \quad (3-9)$$

which can be taken from the initial slope or the secant of the curve.

In the computation above, it is necessary to obtain second derivatives of experimental data, a task which is very difficult to do with precision. The procedure adopted here involves smoothing operations and approximations. The original strain data are smoothed by a three-point averaging technique. Each point on the record, except the first and last ones, is replaced by the average of its two neighboring points. Subsequently, the smoothed curve is differentiated directly on the processing oscilloscope and the derivative curve (strain rate) is smoothed. The smoothed strain rate curve is then divided into four

equal segments and a straight line is fitted in each segment by the least squares method. Thus, a four-step approximation is obtained of the second derivative (strain acceleration). This four-segment approximation procedure was chosen as it gave results in agreement with those obtained by graphical (manual) smoothing and differentiation based on experienced judgment and discretion. The discontinuous stepwise curve for the strain acceleration is smoothed by applying the three-point averaging technique seven consecutive times. In this case, an initial point fixed at zero was added to insure that the acceleration correction on the pressure and stress is zero at zero time and strain. The sequence of all these operations is illustrated in Figure 3-19 for the circumferential strain in the steel ring, from the as-recorded strain to the smoothed second derivative.

The circumferential strain in the composite ring is treated in an identical manner to arrive at the first and second derivatives.

All smoothing and computational operations were programmed and done automatically in every case. The computer program was stored in the floppy disk memory of the processing oscilloscope.

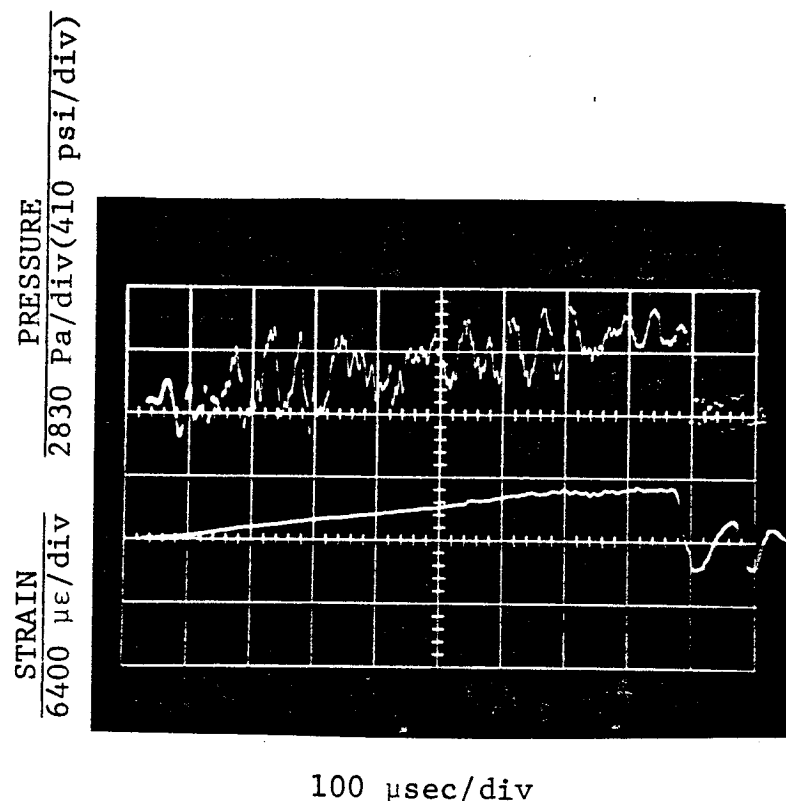


Figure 3-1. Pressure and strain signals for $[90_2/\pm 45]_s$ graphite/epoxy ring loaded by hammer impact on piston of pressure vessel.

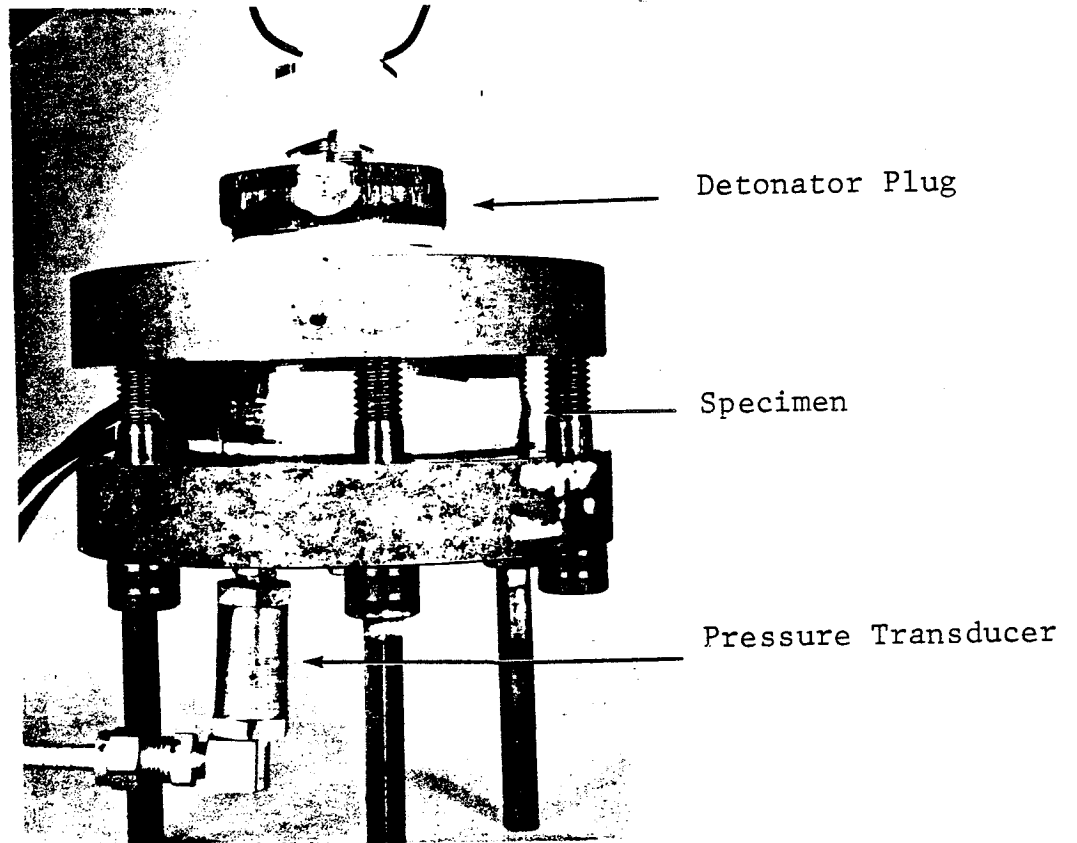


Figure 3-2. Fixture for dynamic loading of composite ring specimens.

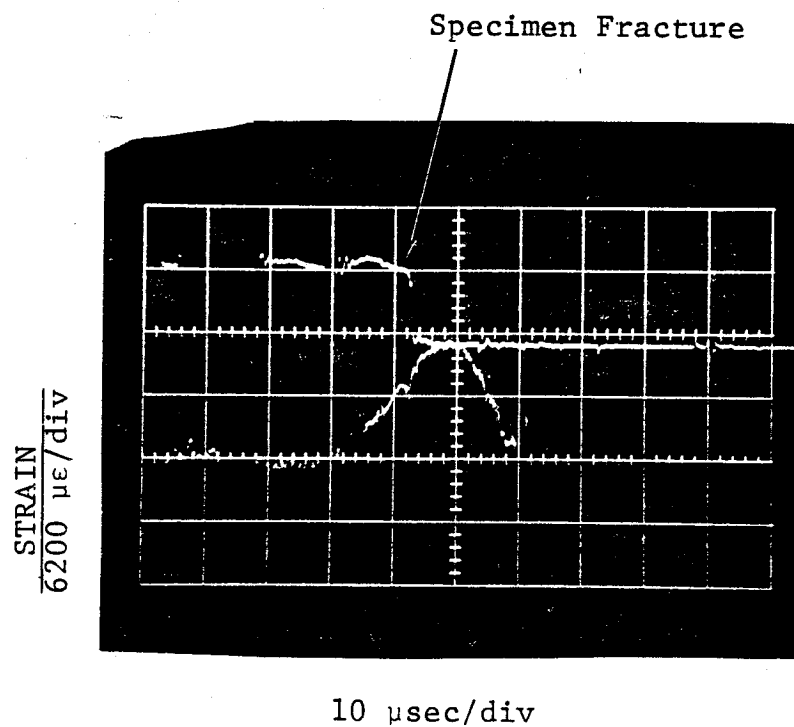


Figure 3-3. Circumferential strain record in dynamically loaded $[90_2/\pm 45]_s$ graphite/epoxy ring specimen.

ORIGINAL PAGE IS
OF POOR QUALITY

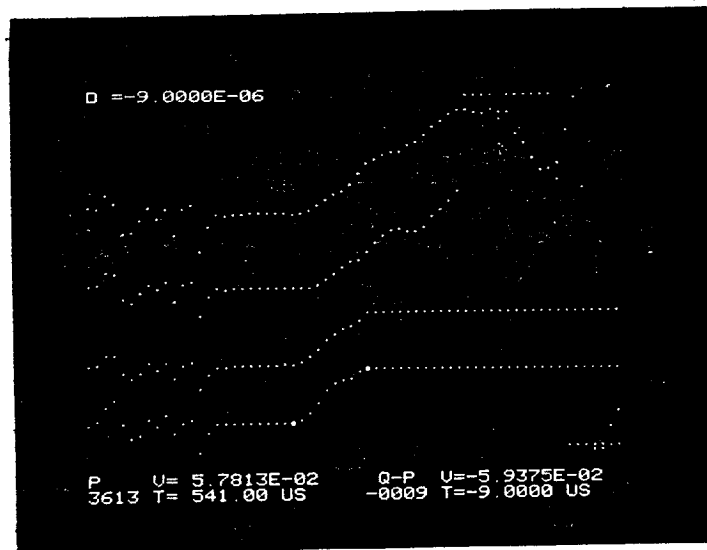


Figure 3-4. Circumferential strain records in dynamically loaded $[90_2/\pm 45]_s$ graphite/epoxy ring specimen.

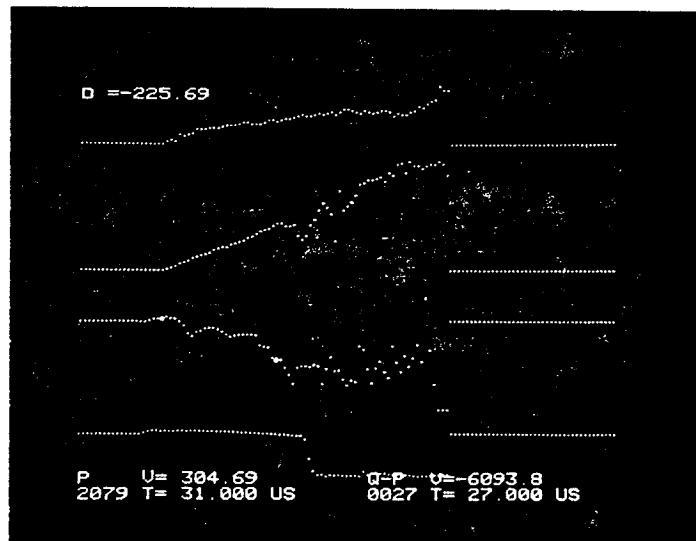
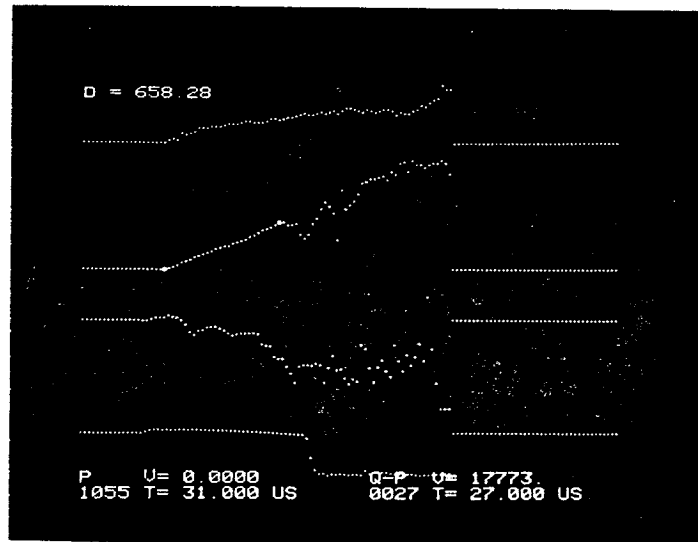


Figure 3-5. Strain records in dynamically loaded aluminum ring (second trace from top is circumferential strain, third trace is axial strain).

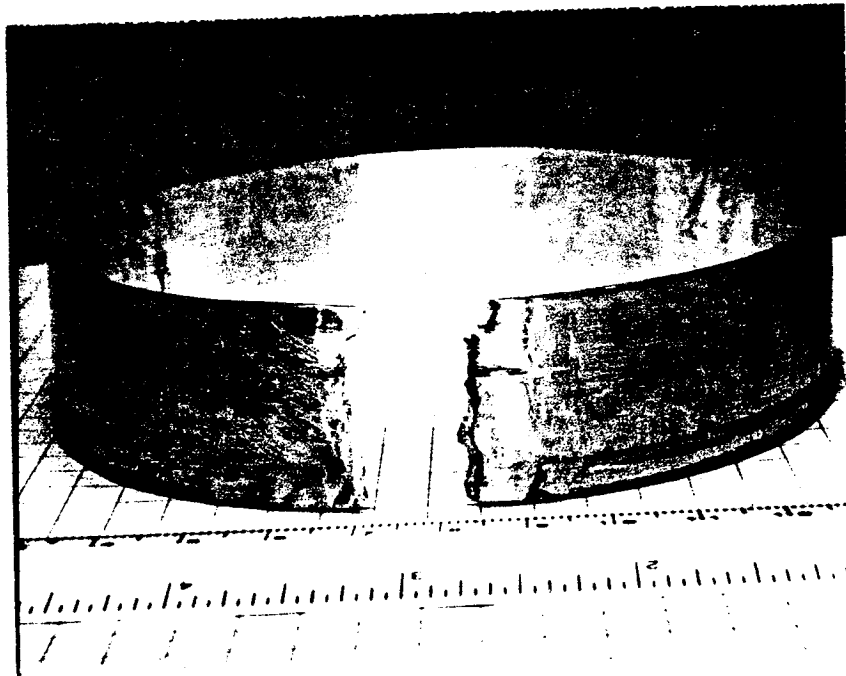


Figure 3-6. Failure of dynamically loaded aluminum ring.

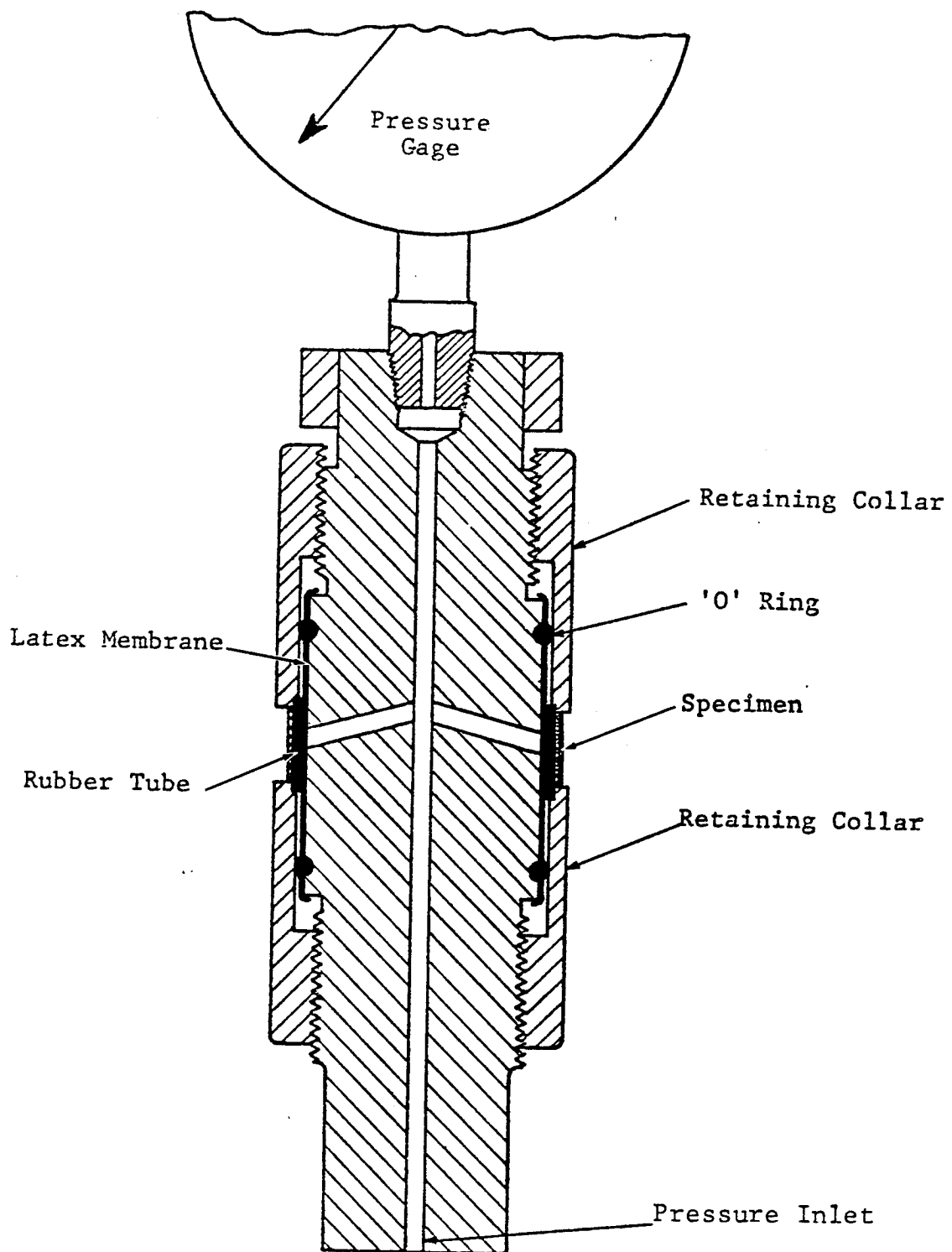


Figure 3-7. Fixture for quasi-static loading of composite ring specimens.

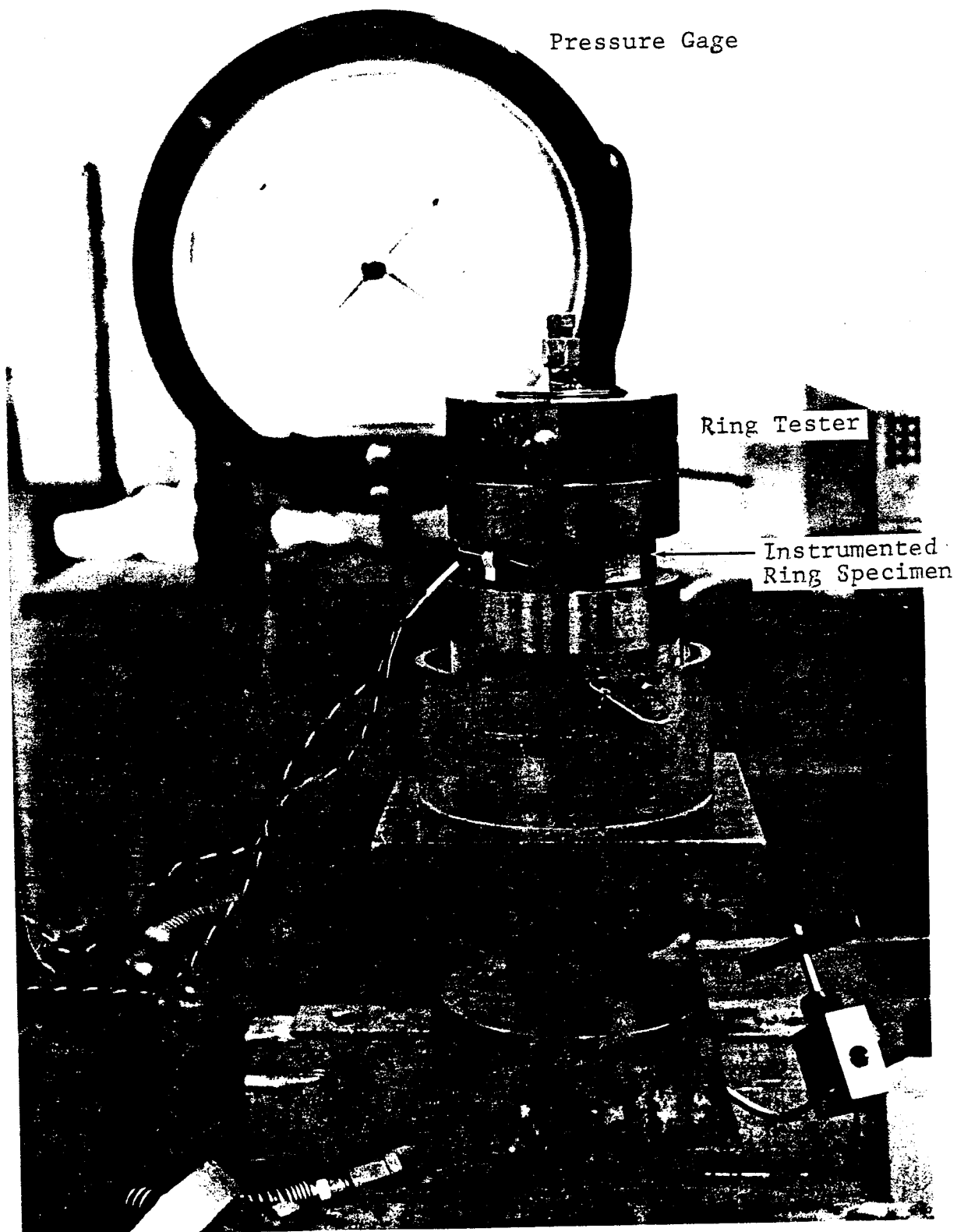


Figure 3-8. Photograph of assembled fixture for quasi-static loading of composite ring specimens.

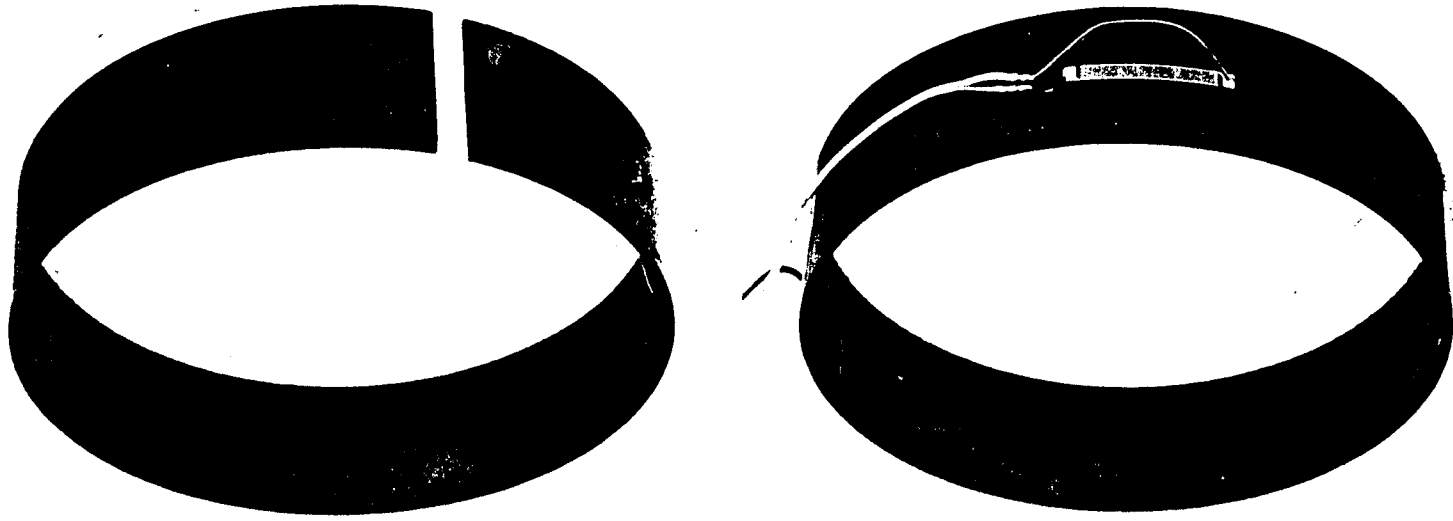


Figure 3-9. Graphite/epoxy ring specimens with strain gages and after failure.

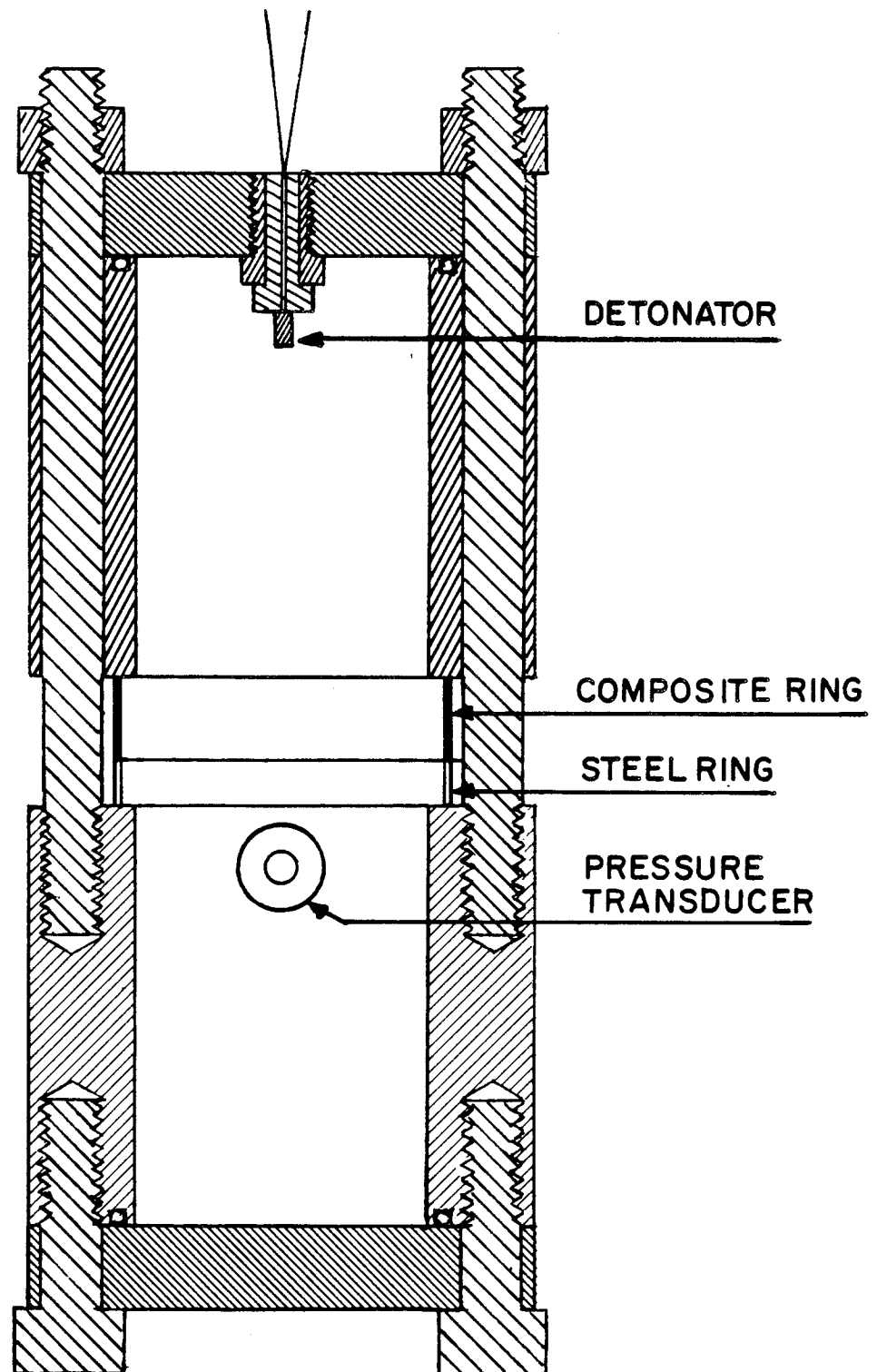


Figure 3-10. Fixture for dynamic loading of composite ring specimens.

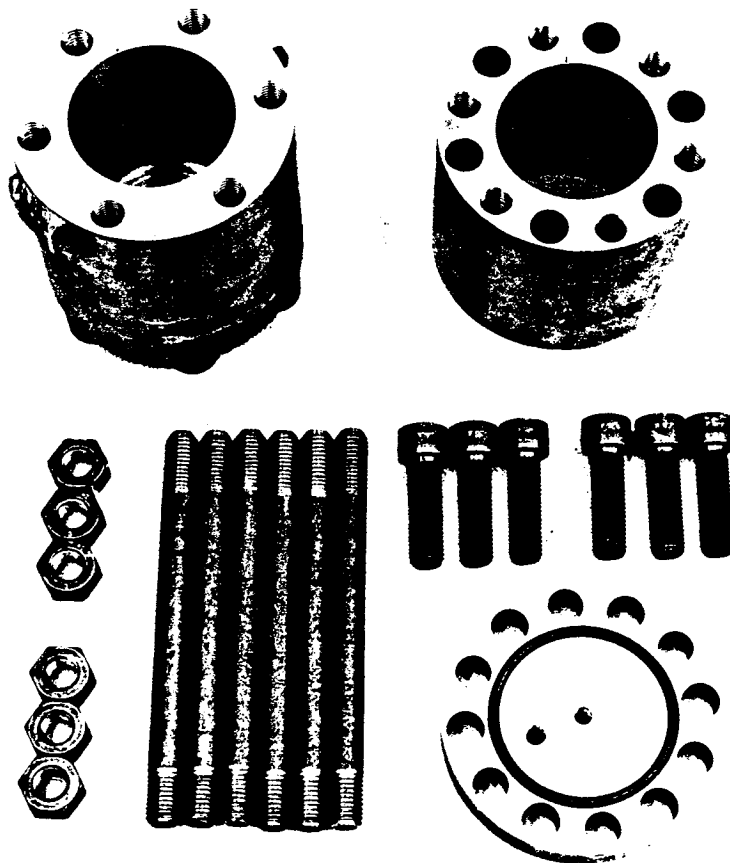


Figure 3-11. Photograph of components of fixture for dynamic loading of composite ring specimens.

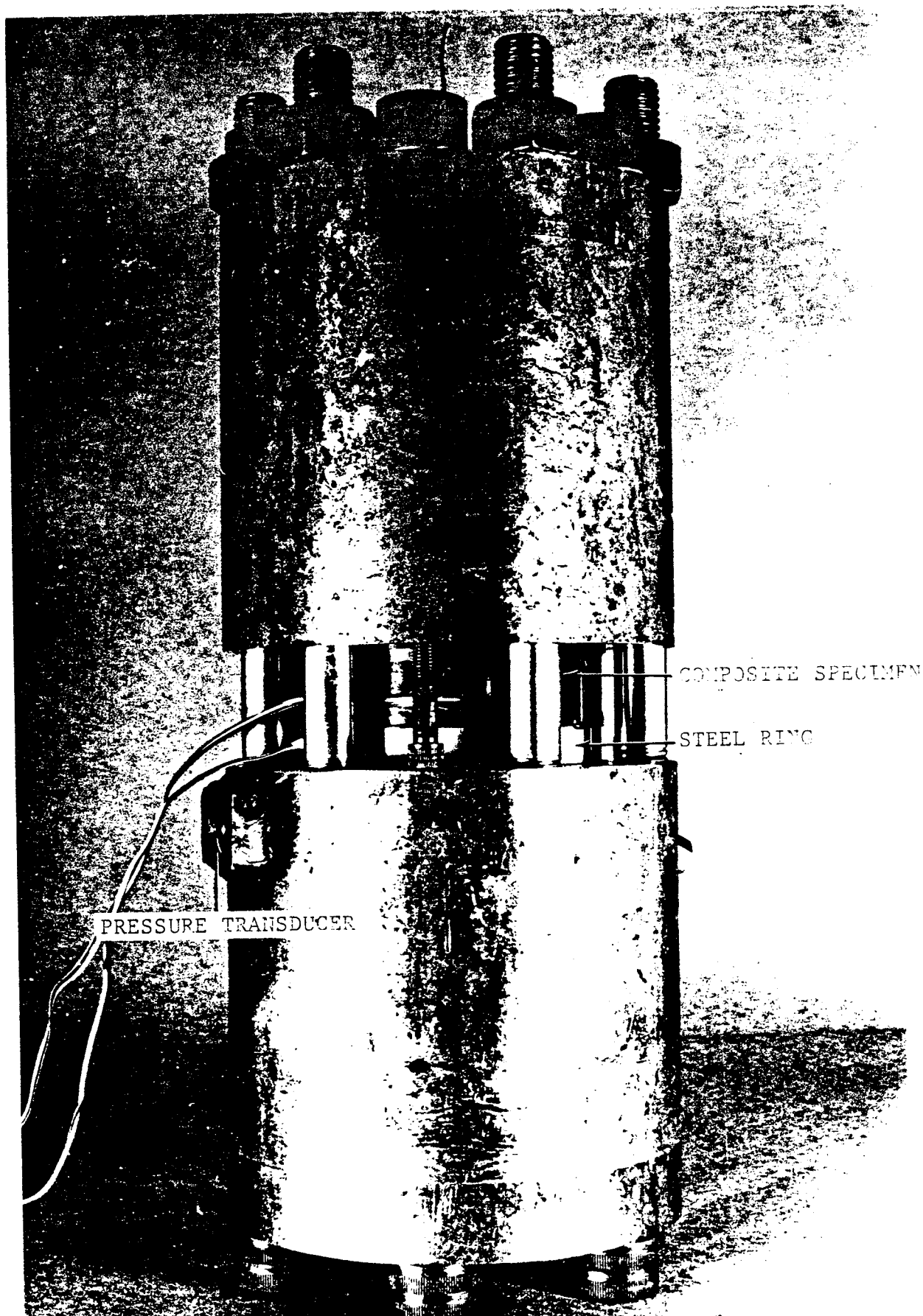


Figure 3-12. Photograph of assembled fixture for dynamic loading of composite ring specimen.

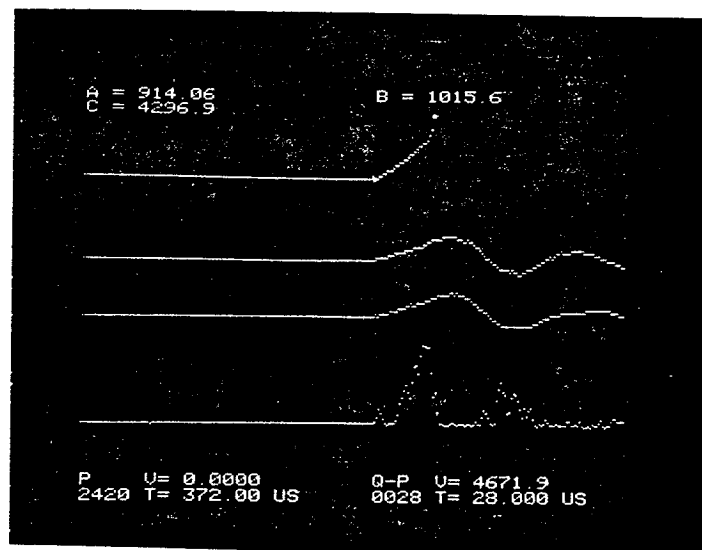


Figure 3-13. Circumferential strain and pressure records (top trace: strain in [0g] graphite/epoxy ring; second and third traces: strains in steel ring; bottom trace: pressure transducer).

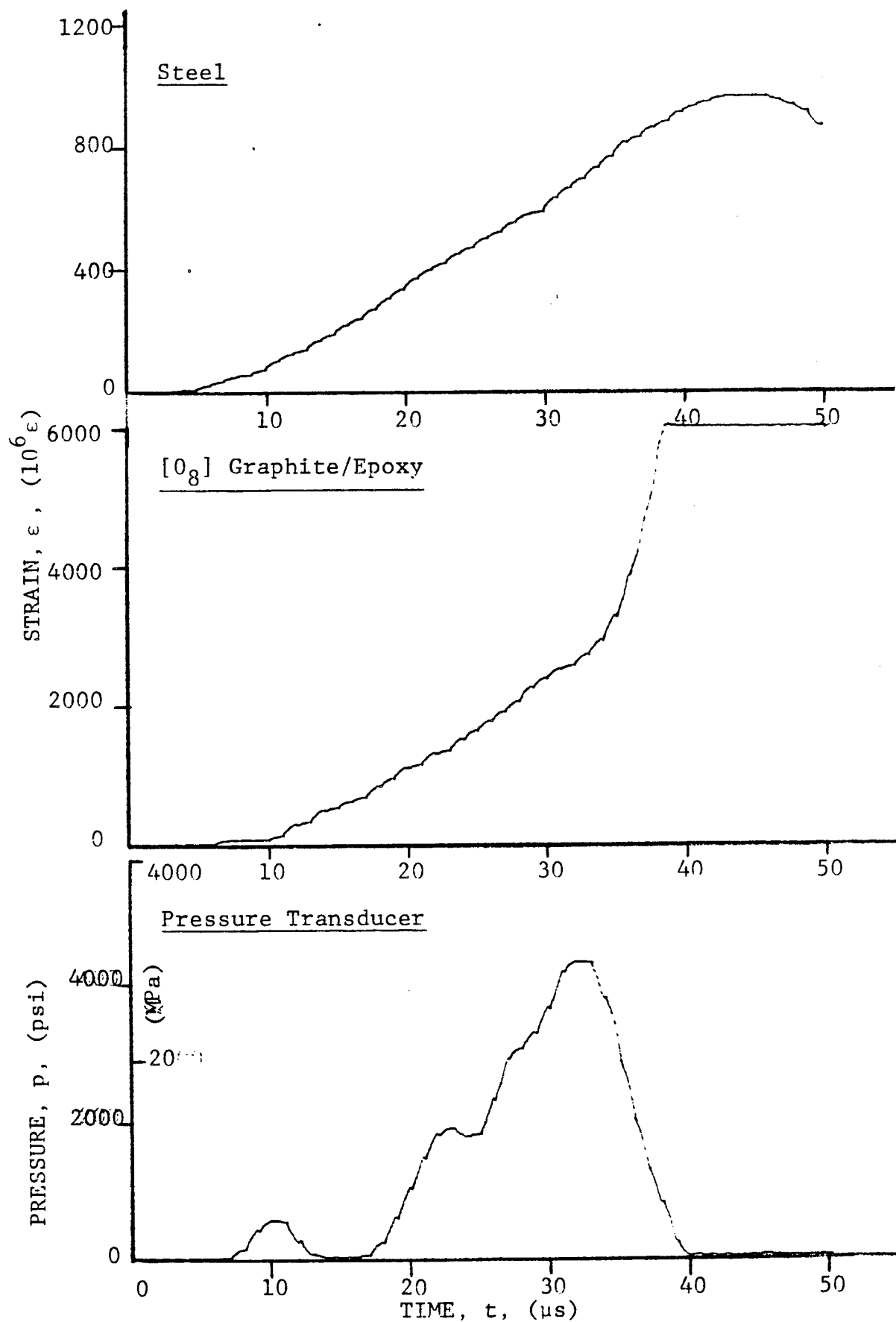


Figure 3-14. Strain and pressure signals for dynamic loading of steel and [0_g] graphite/epoxy ring specimens.

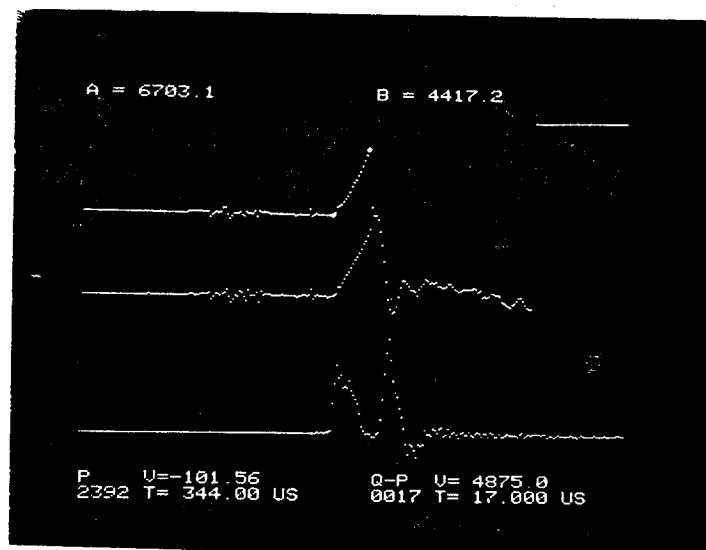


Figure 3-15. Circumferential strain and pressure records for dynamically loaded $[90_8]$ graphite/epoxy ring.

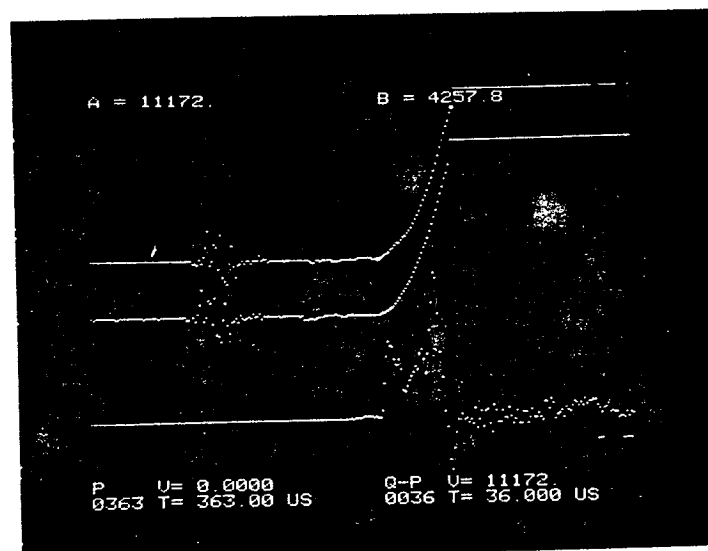
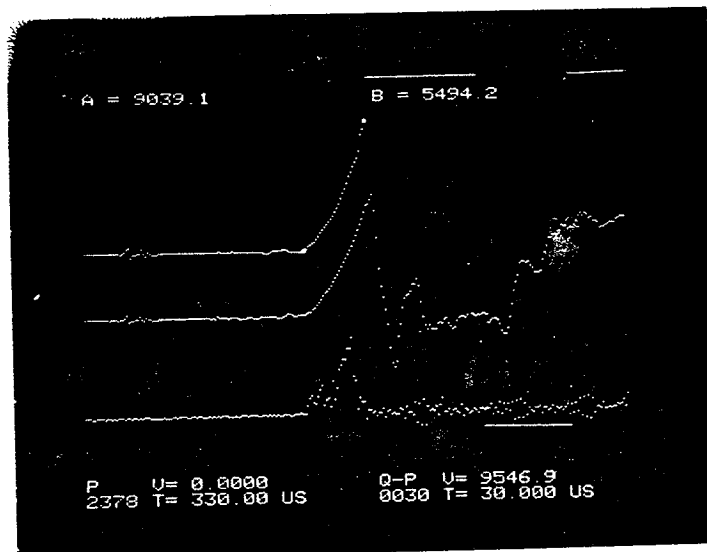


Figure 3-16. Circumferential strain and pressure records for dynamically loaded $[\pm 45]_2$ graphite/epoxy ring.

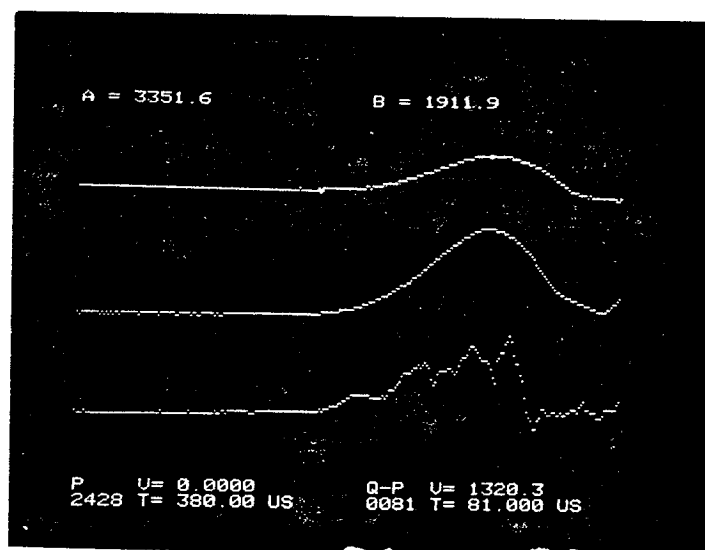


Figure 3-17. Circumferential strain and pressure records for dynamically loaded 0.277 cm (0.109 in.) and 0.124 cm (0.049 in.) thick steel rings.

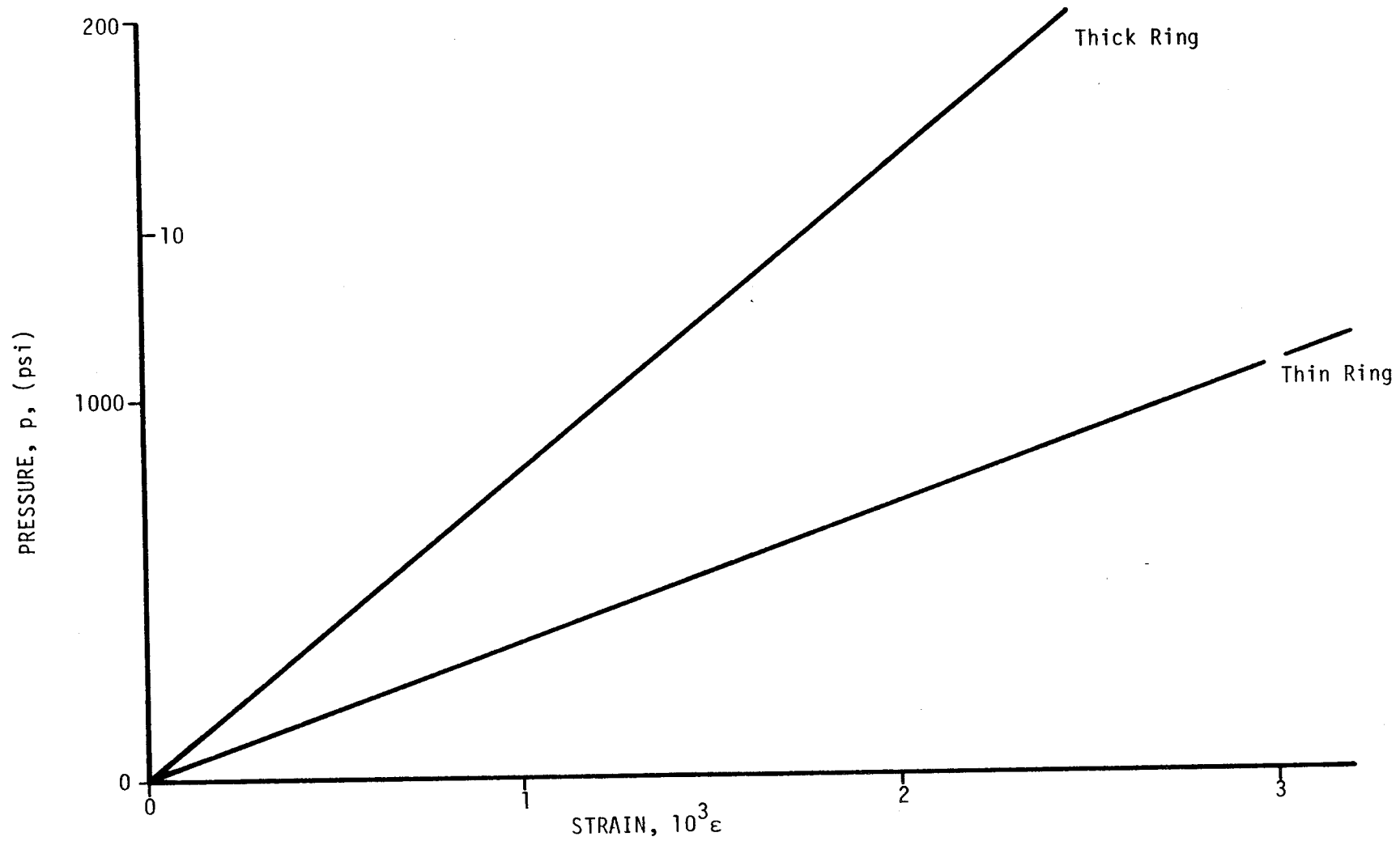


Figure 3-18. Pressure-strain calibration of Vascomax steel rings used as pressure cells.

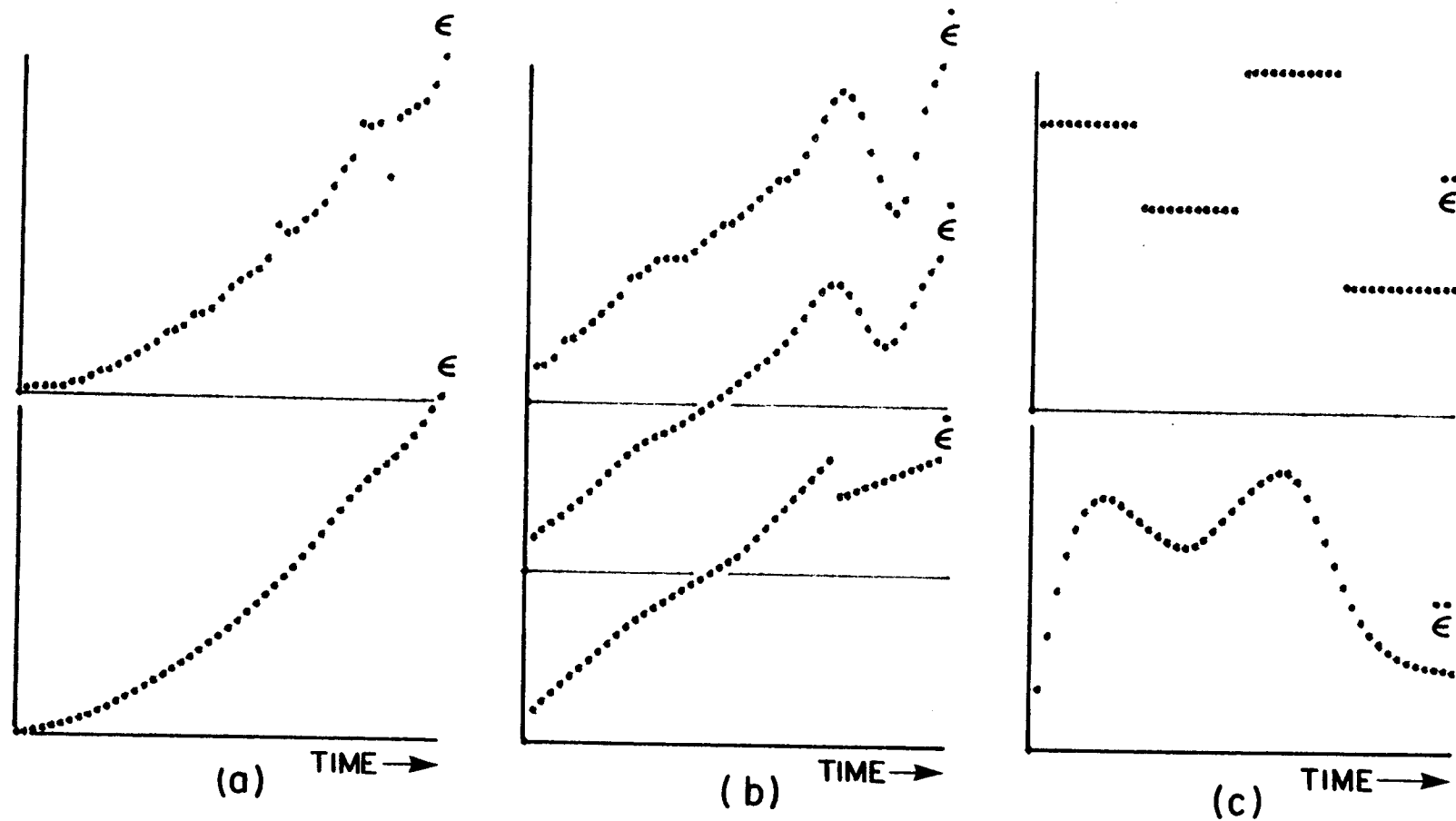


Figure 3-19. Illustration of smoothing and approximation operations. a) As recorded and smoothed strains, b) strain rate, smoothed strain rate and piecewise linear approximation, and c) stepwise and smoothed strain acceleration.

4. STRAIN RATE CHARACTERIZATION OF UNIDIRECTIONAL COMPOSITES

4.1 INTRODUCTION

The objective of this task is to determine the longitudinal, transverse, and in-plane shear unidirectional properties of the three materials, discussed previously in Section 2, at three strain rates. The materials characterized are SP288/T300 graphite/epoxy, SP288/AS graphite/epoxy, and 80AS/20S/PR288 graphite/S-Glass/epoxy. The three strain rates selected are quasi-static, intermediate, and high rates ranging from 10^{-4} s^{-1} to over 500 s^{-1} . All characterization tests were conducted with the same type of thin ring specimen under internal pressure. This was the case for the quasi-static rate as well for consistency, although quasi-static properties were obtained from flat coupon specimens (see Section 2). In all cases, with few exceptions, three replications per test were used. In all cases results were presented in the form of stress-strain curves to failure and properties determined included initial, secant, and terminal strain rate; initial, secant, and terminal modulus and Poisson's ratio; and strength and ultimate strain. The effects of strain rate on the various properties are discussed below.

4.2 LONGITUDINAL TENSILE PROPERTIES

4.2.1 Graphite/Epoxy (SP288/T300)

Quasi-static longitudinal properties were obtained by testing three $[0_6]$ rings instrumented with strain gages. The fiber orientation of these specimens was in the circumferential direction. The specimens were tested according to the procedure described in Section 3.2. Stress-strain curves to failure, as well as modulus, Poisson's ratio, strength, and ultimate strain, for the three specimens tested are shown in Figures 4-1, 4-2, and 4-3. Results for the three specimens tested are tabulated in Table 4-1.

The 0-deg rings above tend to close in a little after failure indicating the presence of residual stresses. It is assumed that the self-equilibrated state of residual stress is equivalent to a bending moment M in the circumferential

TABLE 4-1. QUASI-STATIC TENSILE PROPERTIES OF $[0_6]$
SP288/T300 GRAPHITE/EPOXY

Specimen Number	Strain Rate $(\dot{\epsilon}_{11}), s^{-1}$	Modulus $(E_{11}),$ GPa (10^6 psi)	Poisson's Ratio (ν_{12})
<u>Initial Properties</u>			
19-2	1×10^{-4}	141 (20.4)	0.30
19-3	1×10^{-4}	136 (19.7)	0.25
19-10	1×10^{-4}	137 (19.8)	0.26
<u>Secant Properties</u>			
19-2	1×10^{-4}	141 (20.4)	0.30
19-3	1×10^{-4}	136 (19.7)	0.25
19-10	1×10^{-4}	137 (19.8)	0.26
<u>Terminal Properties</u>			
19-2	1×10^{-4}	141 (20.4)	0.30
19-3	1×10^{-4}	136 (19.7)	0.25
19-10	1×10^{-4}	137 (19.8)	0.26
<u>Ultimate Properties</u>			
	Time to Failure $(t_f), \mu s$	Strength $(S_{11T}),$ MPa (ksi)	Strain (ϵ_{11T}^u)
19-2	1×10^8	1528 (221)	0.0110
19-3	1×10^8	1445 (209)	0.0106
19-10	1×10^8	1340 (194)	0.0099

direction. If the broken ends of the ring specimen move past each other a distance 2δ , the residual bending moment is computed from the relation

$$M = \frac{E_{11} I \delta}{\pi a^2} \quad (4-1)$$

where I = moment of inertia of ring cross section
 a = ring radius.

The outer fiber residual stress is then

$$\sigma_{11R} = \frac{E_{11} \delta t}{2\pi a^2} \quad (4-2)$$

where t is the specimen thickness. In the case of the rings above a maximum residual stress of $\sigma_{11R} = 90$ MPa (13 ksi) was calculated. This is the amount by which the measured strength values must be increased to obtain more realistic values.

Intermediate rate longitudinal properties were obtained by testing three $[0_6]$ rings in the fixture described in Section 3.3.1. To achieve strain rates in the desired range 650 mg of slow-burning pistol powder (red dot) was used in the pressure chamber of the fixture. The circumferential and axial strains in the composite ring and the circumferential strain in the steel calibration ring were recorded in every case. Strain records for the three rings tested (Specimens 40-3, 40-4, and 40-5) are shown in Figures 4-4, 4-5, and 4-6. These data were analyzed following the procedures described in Section 3.3.2. Results in the form of dynamic stress-strain curves are shown in Figures 4-7, 4-8, and 4-9. Results for the three rings tested are tabulated in Table 4-2. The initial strain rates range between $10s^{-1}$ and $24s^{-1}$ and the average (secant) strain rates between $40s^{-1}$ and $58s^{-1}$. The times to failure range between 188 μs and 250 μs .

High strain rate properties were obtained by testing three $[0_6]$ rings under dynamic internal pressure produced by two 100 mg PETN detonators in the pressure chamber. The circumferential and axial strains in the composite

TABLE 4-2. INTERMEDIATE STRAIN RATE TENSILE PROPERTIES
OF [0₆] SP288/T300 GRAPHITE/EPOXY

Specimen Number	Strain Rate ($\dot{\epsilon}_{11}$), s ⁻¹	Modulus (E ₁₁), GPa (10 ⁶ psi)	Poisson's Ratio (ν_{12})
<u>Initial Properties</u>			
40-3	10	151.1 (21.9)	0.35
40-4	11	148.4 (21.5)	0.25
40-5	24	132.5 (19.2)	0.41
<u>Secant Properties</u>			
40-3	40	146.3 (21.2)	0.33
40-4	46	144.9 (21.0)	0.23
40-5	58	122.8 (17.8)	0.40
<u>Terminal Properties</u>			
40-3	103	165.6 (24.0)	0.35
40-4	175	167.7 (24.3)	0.24
40-5	230	107.6 (15.6)	0.26
<u>Ultimate Properties</u>			
	Time to Failure (t_f), μ s	Strength (S _{11T}), MPa (ksi)	Strain (ϵ_{11T}^u)
40-3	222	1242 (180)	0.0085
40-4	250	1711 (248)	0.0115
40-5	188	1325 (192)	0.0111

ring and the circumferential strain in the steel calibration ring were recorded in every case. Strain, strain rate, and strain acceleration records for the three rings tested (Specimens 19-4, 19-5, and 19-6) are shown in Figures 4-10 to 4-18. The corresponding dynamic stress-strain curves are shown in Figures 4-19, 4-20, and 4-21. Results are tabulated in Table 4-3. The initial strain rates range between 150s^{-1} and 200s^{-1} and the secant strain rates between 180s^{-1} and 265s^{-1} . The times to failure range between 34 μs and 51 μs .

Average results for the three ranges of strain rate investigated are tabulated in Table 4-4. The initial and secant moduli increase with strain rate, up to 12% in the case of the secant modulus. No significant trend is evident in Poisson's ratio. Dynamic strength values showed considerable scatter, but on the average, the strength does not vary with strain rate. The same is true for the ultimate tensile strain, although the value at the highest strain rate is the lowest.

4.2.2 Graphite/Epoxy (SP288/AS)

Quasi-static longitudinal properties were obtained by testing three $[0_6]$ rings instrumented with strain gages according to the procedures described earlier in Section 3.2. Stress-strain curves to failure, as well as modulus, Poisson's ratio, strength, and ultimate strain for the three specimens tested are shown in Figures 4-22, 4-23, and 4-24. In two of the three cases the circumferential (longitudinal) strain shows some apparent stiffening and the axial (transverse to the fibers) strain shows nonlinear response at stress levels of 1035 MPa to 1170 MPa (150 ksi to 170 ksi). Results for the three specimens tested are tabulated in Table 4-5. As in the case of SP288/T300, the rings tested tended to close in after failure because of residual stresses. In this case a maximum residual stress on the outer fibers of $\sigma_{11R} = 76\text{ MPa}$ (11 ksi) was calculated from the measured overlap of the broken ends after failure.

Intermediate rate longitudinal properties were obtained by testing three $[0_6]$ rings as described before in Section 3.3.1. A charge of 650 mg of pistol powder was used in the pressure chamber of the fixture. The circumferential and axial strains in the composite ring and the circumferential strain in the steel calibration ring were recorded. Strain records for the three rings tested

TABLE 4-3. HIGH STRAIN RATE TENSILE PROPERTIES OF $[0_6]$
SP288/T300 GRAPHITE/EPOXY

Specimen Number	Strain Rate ($\dot{\epsilon}_{11}$), s^{-1}	Modulus (E_{11}), GPa (10^6 psi)	Poisson's Ratio (ν_{12})
<u>Initial Properties</u>			
19-4	200	152.8 (22.15)	--
19-5	160	214.6 (31.10)	--
19-6	150	201.5 (29.20)	0.30
<u>Secant Properties</u>			
19-4	265	125.0 (18.12)	0.18
19-5	241	194.9 (28.24)	0.17
19-6	180	143.6 (20.81)	0.30
<u>Terminal Properties</u>			
19-4	480	98.7 (14.30)	--
19-5	270	187.7 (27.20)	--
19-6	210	73.1 (10.60)	0.29
<u>Ultimate Properties</u>			
	Time to Failure (t_f), μs	Strength (S_{11T}), MPa (ksi)	Strain (ϵ_{11T}^u)
19-4	34	1113 (161)	0.0090
19-5	40	1880 (272)	0.0096
19-6	51	1325 (192)	0.0092

TABLE 4-4. LONGITUDINAL TENSILE PROPERTIES OF UNIDIRECTIONAL
SP288/T300 GRAPHITE/EPOXY AT VARIOUS STRAIN RATES

Specimen Numbers	Strain Rate ($\dot{\epsilon}_{11}$), s ⁻¹	Modulus (E_{11}), GPa (10 ⁶ psi)	Poisson's Ratio (ν_{12})
<u>Initial Properties</u>			
19-2,3,10	1 X 10 ⁻⁴	138 (20.0)	0.27
40-3,4,5	15	144 (20.9)	0.34
19-4,5,6	170	190 (27.5)	0.30
<u>Secant Properties</u>			
19-2,3,10	1 X 10 ⁻⁴	138 (20.0)	0.27
40-3,4,5	48	138 (20.0)	0.32
19-4,5,6	229	154 (22.4)	0.22
<u>Terminal Properties</u>			
19-2,3,10	1 X 10 ⁻⁴	138 (20.0)	0.27
40-3,4,5	169	147 (21.3)	0.28
19-4,5,6	320	120 (17.4)	0.29
<u>Ultimate Properties</u>			
	Time to Failure (t_f), μ s	Strength (S_{11T}), MPa (ksi)	Strain (ϵ_{11T}^u)
19-2,3,10	1 X 10 ⁸	1435 (208)	0.0105
40-3,4,5	220	1426 (207)	0.0104
19-4,5,6	42	1438 (208)	0.0093

TABLE 4-5. QUASI-STATIC TENSILE PROPERTIES OF $[0_6]$
SP288/AS GRAPHITE/EPOXY

Specimen Number	Strain Rate ($\dot{\epsilon}_{11}$), s^{-1}	Modulus (E_{11}), GPa (10^6 psi)	Poisson's Ratio (ν_{12})
<u>Initial Properties</u>			
7-1	1×10^{-4}	138 (20.0)	0.39
7-5	1×10^{-4}	140 (20.3)	0.32
7-10	1×10^{-4}	129 (18.8)	0.37
<u>Secant Properties</u>			
7-1	1×10^{-4}	142 (20.5)	0.40
7-5	1×10^{-4}	140 (20.3)	0.55
7-10	1×10^{-4}	132 (19.1)	0.43
<u>Terminal Properties</u>			
7-1	1×10^{-4}	147 (21.2)	0.41
7-5	1×10^{-4}	140 (20.0)	--
7-10	1×10^{-4}	137 (19.8)	0.53
<u>Ultimate Properties</u>			
	Time to Failure (t_f), μs	Strength (S_{11T}), MPa (ksi)	Strain (ϵ_{11T}^u)
7-1	1×10^8	1368 (198)	0.0097
7-5	1×10^8	1547 (224)	0.0110
7-10	1×10^8	1460 (212)	0.0111

(Specimens 45-9, 45-10, and 45-11) are shown in Figures 4-25, 4-26, and 4-27. The corresponding dynamic stress-strain curves are shown in Figures 4-28, 4-29, and 4-30. Results are tabulated in Table 4-6. The initial strain rates range between 8s^{-1} and 24s^{-1} and the average (secant) strain rate between 36s^{-1} and 56s^{-1} . The times to failure range between $185\text{ }\mu\text{s}$ and $225\text{ }\mu\text{s}$.

High strain rate properties were obtained by testing four $[0_6]$ rings. Specimens 7-7 and 7-8 were loaded with a 330 mg PETN detonator; Specimen 7-6 was loaded with two 100 mg detonators; and Specimen 7-9 was loaded with a 100 mg detonator in the pressure chamber. The circumferential and axial strains in the composite ring and the circumferential strain in the steel calibration ring were recorded. Strain, strain rate, and strain acceleration records for the four rings tested are shown in Figures 4-31 to 4-42. The corresponding dynamic stress-strain curves are shown in Figures 4-43 to 4-46. Results are tabulated in Table 4-7. The initial strain rates range between 170s^{-1} and 450s^{-1} and the secant strain rates between 240s^{-1} and 328s^{-1} . The times to failure range between $31\text{ }\mu\text{s}$ and $37\text{ }\mu\text{s}$.

Average results for the three ranges of strain rate investigated are tabulated in Table 4-8. The moduli (initial, secant, and terminal) all increase with strain rate by up to 20% at the high rate. No significant trend is evident in Poisson's ratio. Dynamic strength values showed considerable scatter, but on the average, the strength does not vary significantly with strain rate. The same is true for the ultimate tensile strain.

4.2.3 Graphite/S-Glass/Epoxy (80AS/20S/PR288)

Quasi-static longitudinal properties were obtained by testing $[0_6]$ rings instrumented with strain gages. Stress-strain curves to failure, as well as modulus, Poisson's ratio, strength, and ultimate strain are shown in Figures 4-47 and 4-48. Three additional tests were conducted, but they gave low strength values because of asymmetrical distribution of the glass strips in the ring specimens. Strains are linear up to approximately 830 MPa (120 ksi); thereafter, an apparent stiffening of the specimen occurs. Results for the two specimens of Figures 4-47 and 4-48 are tabulated in Table 4-9. As in the case of the graphite/epoxy rings before, the hybrid rings tended to close in

TABLE 4-6. INTERMEDIATE STRAIN RATE TENSILE PROPERTIES
OF $[O_6]$ SP288/AS GRAPHITE/EPOXY

Specimen Number	Strain Rate ($\dot{\epsilon}_{11}$), s^{-1}	Modulus (E_{11}), GPa (10^6 psi)	Poisson's Ratio (ν_{12})
<u>Initial Properties</u>			
45-9	8	155.9 (22.6)	0.31
45-10	24	148.4 (21.5)	--
45-11	15	128.3 (18.6)	0.40
<u>Secant Properties</u>			
45-9	36	161.5 (23.4)	0.44
45-10	45	158.7 (23.0)	0.35
45-11	56	120.8 (17.5)	0.34
<u>Terminal Properties</u>			
45-9	110	160.8 (23.3)	0.37
45-10	113	203.6 (29.5)	0.42
45-11	225	106.3 (15.4)	0.40
<u>Ultimate Properties</u>			
	Time to Failure (t_f), μs	Strength (S_{11T}) MPa (ksi)	Strain (ϵ_{11T}^u)
45-9	225	1325 (192)	0.0082
45-10	185	1318 (191)	0.0083
45-11	198	1325 (192)	0.0110

TABLE 4-7. HIGH STRAIN RATE TENSILE PROPERTIES OF
[0₆] SP288/AS GRAPHITE/EPOXY

Specimen Number	Strain Rate ($\dot{\epsilon}_{11}$), s ⁻¹	Modulus (E ₁₁), GPa (10 ⁶ psi)	Poisson's Ratio (ν_{12})
<u>Initial Properties</u>			
7-6	170	155.9 (22.60)	0.25
7-7	250	176.6 (25.60)	0.55
7-8	260	163.7 (23.72)	0.41
7-9	450	151.8 (22.00)	0.40
<u>Secant Properties</u>			
7-6	240	134.9 (19.56)	0.22
7-7	328	203.5 (29.49)	0.32
7-8	316	163.3 (23.67)	0.54
7-9	314	165.6 (24.00)	0.55
<u>Terminal Properties</u>			
7-6	370	110.4 (16.00)	0.32
7-7	410	248.4 (36.00)	0.31
7-8	390	180.8 (26.20)	0.44
7-9	210	96.6 (14.00)	--
<u>Ultimate Properties</u>			
	Time to Failure (t_f), μ s	Strength (S _{11T}) MPa (ksi)	Strain (ϵ_{11T}^u)
7-6	37	1214 (176)	0.0090
7-7	32	2136 (310)	0.0105
7-8	31	1601 (232)	0.0098
7-9	35	1090 (158)	0.0110

TABLE 4-8. LONGITUDINAL TENSILE PROPERTIES OF UNIDIRECTIONAL
SP288/AS GRAPHITE/EPOXY AT VARIOUS STRAIN RATES

Specimen Number	Strain Rate ($\dot{\epsilon}_{11}$), s ⁻¹	Modulus (E_{11}), GPa (10 ⁶ psi)	Poisson's Ratio (ν_{12})
<u>Initial Properties</u>			
7-1,5,10	1 X 10 ⁻⁴	136 (19.7)	0.36
45-9,10,11	16	144 (20.9)	0.36
7-6,7,8,9	280	162 (23.5)	0.40
<u>Secant Properties</u>			
7-1,5,10	1 X 10 ⁻⁴	138 (20.0)	0.46
45-9,10,11	46	147 (21.3)	0.38
7-6,7,8,9	300	167 (24.2)	0.41
<u>Terminal Properties</u>			
7-1,5,10	1 X 10 ⁻⁴	140 (20.3)	0.47
45-9,10,11	150	157 (22.7)	0.40
7-6,7,8,9	345	159 (23.1)	0.36
<u>Ultimate Properties</u>			
	Time to Failure (t_f), μ s	Strength (S_{11T}) MPa (ksi)	Strain (ϵ_{11T}^u)
7-1,5,10	1 X 10 ⁸	1458 (211)	0.0106
45-9,10,11	203	1322 (192)	0.0092
7-6,7,8,9	34	1511 (219)	0.0101

TABLE 4-9. QUASI-STATIC TENSILE PROPERTIES OF $[0_6]$
80AS/20S/PR288 GRAPHITE/S-GLASS/EPOXY

Specimen Number	Strain Rate ($\dot{\epsilon}_{11}$), s^{-1}	Modulus (E_{11}), GPa (10^6 psi)	Poisson's Ratio (ν_{12})
<u>Initial Properties</u>			
10-1	1×10^{-4}	113 (16.4)	0.18
10-5	1×10^{-4}	101 (14.7)	--
<u>Secant Properties</u>			
10-1	1×10^{-4}	116 (16.9)	0.20
10-5	1×10^{-4}	101 (14.7)	--
<u>Terminal Properties</u>			
10-1	1×10^{-4}	121 (17.5)	0.30
10-5	1×10^{-4}	101 (14.7)	--
<u>Ultimate Properties</u>			
	Time to Failure (t_f), μs	Strength (S_{11T}) MPa (ksi)	Strain (ϵ_{11T}^u)
10-1	1×10^8	1237 (179)	0.0107
10-5	1×10^8	1242 (180)	0.0122

after failure because of residual stresses. The maximum tensile residual stress for the hybrid rings computed as before is $\sigma_{11R} = 75 \text{ MPa}$ (11 ksi).

Intermediate rate longitudinal properties were obtained by testing three $[0_6]$ rings as described before. A charge of 650 mg of pistol powder was used in the pressure chamber of the fixture. Strain records for the three hybrid rings tested and the steel calibration ring are shown in Figures 4-49, 4-50, and 4-51. The corresponding dynamic stress-strain curves are shown in Figures 4-52, 4-53, and 4-54. Results are tabulated in Table 4-10. The initial strain rates range between 9s^{-1} and 18s^{-1} and the average (secant) strain rates between 45s^{-1} and 52s^{-1} . The times to failure range between $186 \mu\text{s}$ and $218 \mu\text{s}$. Considerable scatter exists in the values of both moduli and strength.

High strain rate properties were obtained by testing three $[0_6]$ rings. A 100 mg PETN detonator, two 100 mg PETN detonators, and a 330 mg PETN detonator were used in the pressure chamber for Specimens 10-8, 10-9, and 10-10, respectively. Strain and strain derivative records for the three hybrid rings tested and the steel calibration ring are shown in Figures 4-55 to 4-63. The corresponding dynamic stress-strain curves are shown in Figures 4-64, 4-65, and 4-66. Results are tabulated in Table 4-11. The initial strain rates range between 70s^{-1} and 200s^{-1} and the average (secant) strain rates between 186s^{-1} and 370s^{-1} . The times to failure range between $34 \mu\text{s}$ and $51 \mu\text{s}$. Considerable scatter exists in the values of moduli and strength.

Average results for the three ranges of strain rate investigated are tabulated in Table 4-12. Because of the scatter and the small number of specimens involved, the average values shown can only be viewed as general indicators of trends. There is an appreciable increase in initial modulus with strain rate, however, the secant modulus shows only a slight increase. The strength appears to be decreasing with strain rate; however, the trend would appear differently if the lowest values for the intermediate and high strain rates were dropped. No significant variations with strain rate can be detected in the ultimate strain values.

TABLE 4-10. INTERMEDIATE STRAIN RATE TENSILE PROPERTIES OF
[0₆] 80AS/20S/PR288 GRAPHITE/S-GLASS/EPOXY

Specimen Number	Strain Rate ($\dot{\epsilon}_{11}$), s ⁻¹	Modulus (E_{11}), GPa (10 ⁶ psi)	Poisson's Ratio (ν_{12})
<u>Initial Properties</u>			
43-2	9	143 (20.7)	0.56
43-3	16	87 (12.6)	--
43-4	18	121 (17.5)	0.35
<u>Secant Properties</u>			
43-2	45	139 (20.1)	0.72
43-3	50	84 (12.2)	--
43-4	52	131 (19.0)	0.39
<u>Terminal Properties</u>			
43-2	235	136 (19.7)	0.68
43-3	140	75 (10.9)	--
43-4	120	166 (24.0)	0.79
<u>Ultimate Properties</u>			
	Time to Failure (t_f), μ s	Strength (S_{11T}) MPa (ksi)	Strain (ϵ_{11T}^u)
43-2	218	1366 (198)	0.0098
43-3	204	861 (125)	0.0103
43-4	186	1256 (182)	0.0096

TABLE 4-11. HIGH STRAIN RATE TENSILE PROPERTIES OF [0₆]
80AS/20S/PR288 GRAPHITE/S-GLASS/EPOXY

Specimen Number	Strain Rate ($\dot{\epsilon}_{11}$), s ⁻¹	Modulus (E_{11}), GPa (10 ⁶ psi)	Poisson's Ratio (ν_{12})
<u>Initial Properties</u>			
10-8	70	161 (23.3)	--
10-9	180	166 (24.1)	0.20
10-10	200	184 (26.6)	0.40
<u>Secant Properties</u>			
10-8	186	102 (14.7)	0.16
10-9	249	136 (19.7)	0.40
10-10	370	99 (14.3)	0.40
<u>Terminal Properties</u>			
10-8	260	33 (4.8)	--
10-9	380	104 (15.0)	--
10-10	600	84 (12.1)	--
<u>Ultimate Properties</u>			
	Time to Failure (t_f), μ s	Strength (S_{11T}) MPa (ksi)	Strain (ϵ_{11T}^u)
10-8	51	966 (140)	0.0095
10-9	35	1180 (171)	0.0087
10-10	34	1242 (180)	0.0126

TABLE 4-12. LONGITUDINAL TENSILE PROPERTIES OF UNIDIRECTIONAL 80AS/20S/PR288 GRAPHITE/S-GLASS/EPOXY AT VARIOUS STRAIN RATES

Specimen Numbers	Strain Rate ($\dot{\epsilon}_{11}$), s ⁻¹	Modulus (E_{11}), GPa (10 ⁶ psi)	Poisson's Ratio (ν_{12})
<u>Initial Properties</u>			
10-1,2	1 X 10 ⁻⁴	107 (15.6)	0.18
43-2,3,4	14	117 (16.9)	0.45
10-8,9,10	150	170 (24.7)	0.30
<u>Secant Properties</u>			
10-1,2	1 X 10 ⁻⁴	109 (15.8)	0.20
43-2,3,4	49	118 (17.1)	0.55
10-8,9,10	268	112 (16.2)	0.32
<u>Terminal Properties</u>			
10-1,2	1 X 10 ⁻⁴	111 (16.1)	0.30
43-2,3,4	165	126 (18.2)	0.73
10-8,9,10	413	73 (10.6)	--
<u>Ultimate Properties</u>			
	Time to Failure (t_f), μ s	Strength (S_{11T}) MPa (ksi)	Strain (ϵ_{11T}^u)
10-1,2	1 X 10 ⁸	1240 (180)	0.0115
43-2,3,4	203	1162 (168)	0.0099
10-8,9,10	40	1129 (164)	0.0103

4.3 TRANSVERSE TENSILE PROPERTIES

4.3.1 Graphite/Epoxy (SP288/T300)

Quasi-static transverse properties were obtained by testing four $[90_g]$ rings instrumented with strain gages. The fiber orientation of these specimens was in the axial direction. The specimens were tested according to the procedure described in Section 3.2. Stress-strain curves to failure, as well as modulus, Poisson's ratio, strength, and ultimate strain, are shown in Figures 4-67 through 4-70. Strains are linear up to stress levels between 28 MPa and 35 MPa (4 and 5 ksi) corresponding to strains between 0.003 and 0.004. The moduli and strengths are somewhat lower than those obtained previously using flat coupon specimens (see Section 2.2). Results for the three specimens tested are tabulated in Table 4-13.

Intermediate rate transverse properties were obtained by testing three $[90_g]$ rings using 650 mg of pistol powder in the pressure chamber. The circumferential and axial strains in the composite rings and the circumferential strain in the steel calibration ring were recorded as shown in Figures 4-71, 4-72, and 4-73. The corresponding dynamic stress-strain curves are shown in Figures 4-74, 4-75, and 4-76. Results are tabulated in Table 4-14. The axial strain records appeared erratic and as a result no Poisson's ratios were computed. The initial strain rates vary between $18s^{-1}$ and $20s^{-1}$ and the average (secant) rates between $50s^{-1}$ and $58s^{-1}$. The times to failure range between 111 μs and 120 μs .

High strain rate properties were obtained by testing three $[90_g]$ rings. Specimen No. 3-1 was loaded with 260 mg fast-burning pistol powder and Specimen Nos. 3-2 and 3-5 with 50 mg PETN detonators in the pressure chamber. Strain and strain derivative records for the three graphite/epoxy rings and the steel calibration ring are shown in Figures 4-77 through 4-85. The corresponding dynamic stress-strain curves are shown in Figures 4-86, 4-87, and 4-88. Results are tabulated in Table 4-15. The strain rates achieved for Specimen No. 3-1 are relatively low, with values of $15s^{-1}$ and $89s^{-1}$ for the initial and secant rates, respectively. Initial and secant rates for the other two specimens vary between $100s^{-1}$ and $140s^{-1}$, and $197s^{-1}$ and $202s^{-1}$, respectively. Times to failure range between 35 μs and 89 μs .

TABLE 4-13. QUASI-STATIC TENSILE PROPERTIES OF [90₈]
SP288/T300 GRAPHITE/EPOXY

Specimen Numbers	Strain Rate ($\dot{\epsilon}_{22}$), s ⁻¹	Modulus (E_{22}), GPa (10 ⁶ psi)	Poisson's Ratio (ν_{21})
<u>Initial Properties</u>			
3-3	1 X 10 ⁻⁴	9.6 (1.39)	0.01
3-4	1 X 10 ⁻⁴	9.4 (1.36)	0.02
3-7	1 X 10 ⁻⁴	9.4 (1.37)	0.02
3-11	1 X 10 ⁻⁴	9.1 (1.32)	0.02
<u>Secant Properties</u>			
3-3	1 X 10 ⁻⁴	9.4 (1.37)	0.01
3-4	1 X 10 ⁻⁴	8.7 (1.26)	0.03
3-7	1 X 10 ⁻⁴	9.1 (1.32)	0.03
3-11	1 X 10 ⁻⁴	8.9 (1.28)	0.02
<u>Terminal Properties</u>			
3-3	1 X 10 ⁻⁴	8.8 (1.28)	0.01
3-4	1 X 10 ⁻⁴	7.9 (1.15)	0.04
3-7	1 X 10 ⁻⁴	8.8 (1.27)	0.03
3-11	1 X 10 ⁻⁴	8.6 (1.25)	0.02
<u>Ultimate Properties</u>			
	Time to Failure (t_f), μ s	Strength (S_{22T}), MPa (ksi)	Strain (ϵ_{22T}^u)
3-3	1 X 10 ⁸	56 (8.2)	0.0060
3-4	1 X 10 ⁸	57 (8.3)	0.0066
3-7	1 X 10 ⁸	46 (6.8)	0.0052
3-11	1 X 10 ⁸	54 (7.9)	0.0062

TABLE 4-14. INTERMEDIATE STRAIN RATE TENSILE PROPERTIES OF
[90₈] SP288/T300 GRAPHITE/EPOXY

Specimen Numbers	Strain Rate ($\dot{\epsilon}_{22}$), s ⁻¹	Modulus (E_{22}), GPa (10 ⁶ psi)	Poisson's Ratio (ν_{21})
<u>Initial Properties</u>			
44-5	18	26.9 (3.90)	
44-6	20	30.5 (4.42)	
44-7	18	28.8 (4.17)	
<u>Secant Properties</u>			
44-5	50	19.4 (2.81)	
44-6	58	14.8 (2.14)	
44-7	51	14.5 (2.10)	
<u>Terminal Properties</u>			
44-5	100	26.9 (3.90)	
44-6	116	14.8 (2.15)	
44-7	105	11.9 (1.73)	
<u>Ultimate Properties</u>			
	Time to Failure (t_f), μ s	Strength (S_{22T}), MPa (ksi)	Strain (ϵ_{22T}^u)
44-5	114	110.4 (16.0)	0.0057
44-6	111	92.5 (13.4)	0.0064
44-7	120	88.3 (12.8)	0.0061

TABLE 4-15. HIGH STRAIN RATE TENSILE PROPERTIES OF $[90_8]$
SP288/T300 GRAPHITE/EPOXY

<u>Specimen Numbers</u>	<u>Strain Rate ($\dot{\epsilon}_{22}$), s^{-1}</u>	<u>Modulus (E_{22}), GPa (10^6 psi)</u>	<u>Poisson's Ratio (ν_{21})</u>
<u>Initial Properties</u>			
3-1	15	27.3 (3.95)	--
3-2	100	50.4 (7.30)	--
3-5	140	31.6 (4.58)	--
<u>Secant Properties</u>			
3-1	89	21.7 (3.14)	0.04
3-2	202	22.7 (3.28)	0.02
3-5	197	23.7 (3.43)	0.06
<u>Terminal Properties</u>			
3-1	225	12.4 (1.80)	0.04
3-2	360	13.8 (2.00)	0.05
3-5	330	15.0 (2.17)	--
<u>Ultimate Properties</u>			
	<u>Time to Failure (t_f), μs</u>	<u>Strength (S_{22T}), MPa (ksi)</u>	<u>Strain (ϵ_{22T}^u)</u>
3-1	89	169 (24.5)	0.0079
3-2	40	184 (26.6)	0.0081
3-5	35	164 (23.7)	0.0069

Average results for the three ranges of strain rate investigated are tabulated in Table 4-16. The initial and secant moduli increase sharply with strain rate, reaching values more than twice the static modulus. The transverse tensile strength follows a similar trend, increasing from 54 MPa (7.8 ksi) under quasi-static loading to 172 MPa (24.9 ksi) under high strain rate loading. The ultimate strain remains constant up to the intermediate rate level, but shows a noticeable increase at high strain rates.

4.3.2 Graphite/Epoxy (SP288/AS)

Quasi-static transverse properties were obtained by testing four $[90_8]$ rings. Stress-strain curves to failure, as well as modulus, Poisson's ratio, strength, and ultimate strain, are shown in Figures 4-89 through 4-92. Strains are linear up to stress levels of between 28 MPa (4 ksi) and 35 MPa (5 ksi) corresponding to strains between 0.0030 and 0.0037. Results are comparable with those obtained using flat coupons except that strength values are a little lower. Results are tabulated in Table 4-17.

Intermediate rate transverse properties were obtained by testing three $[90_8]$ rings using 650 mg of pistol powder in the pressure chamber. Strain records are shown in Figures 4-93, 4-94, and 4-95. The corresponding dynamic stress-strain curves are shown in Figures 4-96, 4-97, and 4-98. Results are tabulated in Table 4-18. No Poisson's ratios were computed as the axial strain records appeared erratic. The initial strain rates range between $28s^{-1}$ and $33s^{-1}$ and the secant strain rates between $39s^{-1}$ and $50s^{-1}$. The times to failure range between 100 μs and 137 μs .

High strain rate properties were obtained by testing three $[90_8]$ rings. Specimen Nos. 5-9, 5-10, and 5-11 were loaded with 260 mg pistol powder, a 50 mg detonator, and a 20 mg PETN detonator, respectively. Strain and strain derivative records are shown in Figures 4-99 through 4-107. The corresponding dynamic stress-strain curves are shown in Figures 4-108, 4-109, and 4-110. Results are tabulated in Table 4-19. The initial strain rates vary between $25s^{-1}$ and $120s^{-1}$ and the secant rates between $128s^{-1}$ and $195s^{-1}$. The times to failure range between 40 μs and 50 μs .

Average results for the three ranges of strain rate investigated are tabulated in Table 4-20. The initial and secant moduli increase sharply with strain rate. At the highest rate the secant modulus is more than double the

TABLE 4-16. TRANSVERSE TENSILE PROPERTIES OF UNIDIRECTIONAL
SP288/T300 GRAPHITE/EPOXY AT VARIOUS STRAIN RATES

<u>Specimen Numbers</u>	<u>Strain Rate ($\dot{\epsilon}_{22}$), s⁻¹</u>	<u>Modulus (E_{22}), GPa (10⁶ psi)</u>	<u>Poisson's Ratio (ν_{21})</u>
<u>Initial Properties</u>			
3-3,4,7,11	1 x 10 ⁻⁴	9.4 (1.36)	0.02
44-5,6,7	19	28.7 (4.16)	--
3-1,2,5	85	36.4 (5.28)	--
<u>Secant Properties</u>			
3-3,4,7,11	1 x 10 ⁻⁴	9.0 (1.31)	0.02
44-5,6,7	53	16.2 (2.35)	--
3-1,2,5	163	22.7 (3.28)	0.04
<u>Terminal Properties</u>			
3-3,4,7,11	1 x 10 ⁻⁴	8.5 (1.24)	0.03
44-5,6,7	107	17.9 (2.59)	--
3-1,2,5	305	13.7 (1.99)	0.05
<u>Ultimate Properties</u>			
	<u>Time to Failure (t_f), μs</u>	<u>Strength (S_{22T}), MPa (ksi)</u>	<u>Strain (ϵ_{22T}^u)</u>
3-3,4,7,11	1 x 10 ⁸	54 (7.8)	0.0060
44-5,6,7	115	97 (14.1)	0.0061
3-1,2,5	55	172 (24.9)	0.0076

TABLE 4-17. QUASI-STATIC TENSILE PROPERTIES OF $[90_8]$
SP288/AS GRAPHITE/EPOXY

Specimen Numbers	Strain Rate ($\dot{\epsilon}_{22}$), s^{-1}	Modulus (E_{22}), GPa (10^6 psi)	Poisson's Ratio (ν_{21})
<u>Initial Properties</u>			
4-3	1×10^{-4}	9.8 (1.43)	0.02
5-5	1×10^{-4}	10.6 (1.54)	0.03
5-6	1×10^{-4}	10.2 (1.48)	0.03
5-10	1×10^{-4}	10.5 (1.52)	0.03
<u>Secant Properties</u>			
4-3	1×10^{-4}	9.8 (1.43)	0.02
5-5	1×10^{-4}	10.6 (1.54)	0.03
5-6	1×10^{-4}	10.2 (1.48)	0.03
5-10	1×10^{-4}	10.5 (1.52)	0.03
<u>Terminal Properties</u>			
4-3	1×10^{-4}	9.8 (1.43)	0.02
5-5	1×10^{-4}	10.6 (1.54)	0.03
5-6	1×10^{-4}	10.2 (1.48)	0.03
5-10	1×10^{-4}	10.5 (1.52)	0.03
<u>Ultimate Properties</u>			
	Time to Failure (t_f), μs	Strength (S_{22T}), MPa (ksi)	Strain (ϵ_{22T}^u)
4-3	1×10^8	49 (7.2)	0.0051
5-5	1×10^8	52 (7.6)	0.0050
5-6	1×10^8	56 (8.2)	0.0057
5-10	1×10^8	50 (7.3)	0.0050

TABLE 4-18. INTERMEDIATE STRAIN RATE TENSILE PROPERTIES OF
[90₈] SP288/AS GRAPHITE/EPOXY

<u>Specimen Numbers</u>	<u>Strain Rate ($\dot{\epsilon}_{22}$), s⁻¹</u>	<u>Modulus (E_{22}), GPa (10⁶ psi)</u>	<u>Poisson's Ratio (ν_{21})</u>
<u>Initial Properties</u>			
38-7	33	16.0 (2.32)	
38-9	29	23.6 (3.42)	
38-10	28	14.6 (2.11)	
<u>Secant Properties</u>			
38-7	50	11.7 (1.70)	
38-9	47	16.1 (2.34)	
38-10	39	19.7 (2.85)	
<u>Terminal Properties</u>			
38-7	96	16.8 (2.43)	
38-9	69	19.2 (2.78)	
38-10	86	20.2 (2.93)	
<u>Ultimate Properties</u>			
	<u>Time to Failure (t_f), μs</u>	<u>Strength (S_{22T}), MPa (ksi)</u>	<u>Strain (ϵ_{22T}^u)</u>
38-7	100	59 (8.5)	0.0050
38-9	111	83 (12.1)	0.0052
38-10	137	104 (15.1)	0.0053

TABLE 4-19. HIGH STRAIN RATE TENSILE PROPERTIES OF [90₈]
SP288/AS GRAPHITE/EPOXY

Specimen Numbers	Strain Rate ($\dot{\epsilon}_{22}$), s ⁻¹	Modulus (E_{22}), GPa (10 ⁶ psi)	Poisson's Ratio (ν_{21})
<u>Initial Properties</u>			
5-9	25	28.6 (4.15)	0.06
5-10	120	42.8 (6.20)	--
5-11	70	52.6 (7.62)	--
<u>Secant Properties</u>			
5-9	128	24.8 (3.59)	0.05
5-10	195	18.9 (2.74)	--
5-11	136	19.2 (2.78)	--
<u>Terminal Properties</u>			
5-9	220	23.8 (3.45)	--
5-10	300	9.7 (1.40)	--
5-11	210	--	--
<u>Ultimate Properties</u>			
	Time to Failure (t_f), μ s	Strength (S_{22T}), MPa (ksi)	Strain (ϵ_{22T}^u)
5-9	50	159 (23.0)	0.0064
5-10	40	157 (22.8)	0.0078
5-11	47	122 (17.8)	0.0064

TABLE 4-20. TRANSVERSE TENSILE PROPERTIES OF UNIDIRECTIONAL SP288/AS GRAPHITE/EPOXY AT VARIOUS STRAIN RATES

<u>Specimen Numbers</u>	<u>Strain Rate ($\dot{\epsilon}_{22}$), s^{-1}</u>	<u>Modulus (E_{22}), GPa (10^6 psi)</u>	<u>Poisson's Ratio (ν_{21})</u>
<u>Initial Properties</u>			
4-3,5-5,6	1×10^{-4}	10.3 (1.49)	0.03
38-7,9,10	30	18.1 (2.62)	--
5-9,10,11	72	41.3 (5.99)	0.06
<u>Secant Properties</u>			
4-3,5-5,6	1×10^{-4}	10.3 (1.49)	0.03
38-7,9,10	45	15.8 (2.30)	--
5-9,10,11	153	21.0 (3.04)	0.05
<u>Terminal Properties</u>			
4-3,5-5,6	1×10^{-4}	10.3 (1.49)	0.03
38-7,9,10	84	18.7 (2.71)	--
5-9,10,11	243	16.7 (2.43)	--
<u>Ultimate Properties</u>			
	<u>Time to Failure (t_f), μs</u>	<u>Strength (S_{22T}), MPa (ksi)</u>	<u>Strain (ϵ_{22T}^u)</u>
4-3,5-5,6	1×10^8	52 (7.6)	0.0052
38-7,9,10	116	82 (11.9)	0.0052
5-9,10,11	46	146 (21.2)	0.0069

static modulus. The transverse tensile strength follows a similar trend, increasing from 52 MPa (7.6 ksi) under quasi-static loading to 146 MPa (21.2 ksi) under high strain rate loading. The ultimate strain increases somewhat at the high strain rate, but it is believed that the differences observed are not significant.

4.3.3 Graphite/S-Glass/Epoxy (80AS/20S/PR288)

Quasi-static transverse properties were obtained by testing three $[90_g]$ rings. Stress-strain curves to failure are shown in Figures 4-111, 4-112, and 4-113. Strains are linear up to stress levels between 21 MPa (3 ksi) and 31 MPa (4.5 ksi) corresponding to axial strains between 0.0015 and 0.003. There is no explanation for the higher modulus of Specimen No. 1A-4. It is probably due to a higher local concentration of S-glass at the gage location. Results are tabulated in Table 4-21.

Intermediate rate transverse properties were obtained by testing three $[90_g]$ rings using 650 mg of pistol powder in the pressure chamber. Strain records are shown in Figures 4-114, 4-115, and 4-116. The corresponding dynamic stress-strain curves are shown in Figures 4-117, 4-118, and 4-119. Results are tabulated in Table 4-22. No Poisson's ratios were computed as the axial strain records appeared erratic. The initial strain rates vary between $20s^{-1}$ and $43s^{-1}$ and the secant strain rates between $30s^{-1}$ and $65s^{-1}$. The times to failure range between 46 μs and 68 μs .

High strain rate properties were obtained by testing three $[90_g]$ rings. Specimen Nos. 1A-1 and 1A-2 were loaded with 130 mg and Specimen No. 1A-3 with 260 mg of fast-burning pistol powder in the pressure chamber. Strain and strain derivative records for the three hybrid rings and the steel calibration ring are shown in Figures 4-120 through 4-128. The corresponding dynamic stress-strain curves are shown in Figures 4-129, 4-130, and 4-131. Results are tabulated in Table 4-23. Initial strain rates vary between $20s^{-1}$ and $40s^{-1}$ and secant strain rates between $90s^{-1}$ and $103s^{-1}$, not much higher than those achieved for the intermediate rate tests. Times to failure range between 61 μs and 67 μs .

TABLE 4-21. QUASI-STATIC TENSILE PROPERTIES OF [90₈]
80AS/20S/PR288 GRAPHITE/S-GLASS/EPOXY

<u>Specimen Numbers</u>	<u>Strain Rate ($\dot{\epsilon}_{22}$), s⁻¹</u>	<u>Modulus (E_{22}), GPa (10⁶ psi)</u>	<u>Poisson's Ratio (ν_{21})</u>
<u>Initial Properties</u>			
1A-4	1 X 10 ⁻⁴	13.8 (2.00)	0.02
1A-5	1 X 10 ⁻⁴	11.1 (1.61)	0.03
1A-6	1 X 10 ⁻⁴	10.5 (1.52)	0.02
<u>Secant Properties</u>			
1A-4	1 X 10 ⁻⁴	12.6 (1.82)	0.01
1A-5	1 X 10 ⁻⁴	10.5 (1.53)	0.03
1A-6	1 X 10 ⁻⁴	10.2 (1.48)	0.02
<u>Terminal Properties</u>			
1A-4	1 X 10 ⁻⁴	11.3 (1.64)	0.01
1A-5	1 X 10 ⁻⁴	9.8 (1.42)	0.02
1A-6	1 X 10 ⁻⁴	9.9 (1.44)	0.03
<u>Ultimate Properties</u>			
	<u>Time to Failure (t_f), μs</u>	<u>Strength (S_{22T}), MPa (ksi)</u>	<u>Strain (ϵ_{22T}^u)</u>
1A-4	1 X 10 ⁸	45 (6.5)	0.0036
1A-5	1 X 10 ⁸	53 (7.7)	0.0050
1A-6	1 X 10 ⁸	49 (7.1)	0.0048

TABLE 4-22. INTERMEDIATE STRAIN RATE TENSILE PROPERTIES
OF [90₈] 80AS/20S/PR288 GRAPHITE/S-GLASS/EPOXY

Specimen Numbers	Strain Rate ($\dot{\epsilon}_{22}$), s ⁻¹	Modulus (E_{22}), GPa (10 ⁶ psi)	Poisson's Ratio (ν_{21})
<u>Initial Properties</u>			
39-4	43	24.1 (3.50)	
39-5	30	30.0 (4.35)	
39-6	20	24.1 (3.50)	
<u>Secant Properties</u>			
39-4	51	18.8 (2.72)	
39-5	31	23.8 (3.45)	
39-6	25	19.5 (2.82)	
<u>Terminal Properties</u>			
39-4	65	20.4 (2.95)	
39-5	43	24.1 (3.50)	
39-6	30	21.4 (3.10)	
<u>Ultimate Properties</u>			
	Time to Failure (t_f), μ s	Strength (S_{22T}), MPa (ksi)	Strain (ϵ_{22T}^u)
39-4	46	44 (6.4)	0.0023
39-5	54	39 (5.7)	0.0016
39-6	68	33 (4.8)	0.0017

TABLE 4-23. HIGH STRAIN RATE TENSILE PROPERTIES OF $[90_8]$
80AS/20S/PR288 GRAPHITE/S-GLASS/EPOXY

Specimen Numbers	Strain Rate ($\dot{\epsilon}_{22}$), s^{-1}	Modulus (E_{22}), GPa (10^6 psi)	Poisson's Ratio (ν_{21})
<u>Initial Properties</u>			
1A-1	40	37.6 (5.45)	--
1A-2	40	46.7 (6.77)	--
1A-3	20	44.2 (6.41)	--
<u>Secant Properties</u>			
1A-1	100	23.3 (3.38)	--
1A-2	103	28.6 (4.15)	--
1A-3	90	31.9 (4.62)	--
<u>Terminal Properties</u>			
1A-1	180	10.0 (1.45)	--
1A-2	150	20.4 (2.95)	--
1A-3	190	15.5 (2.25)	--
<u>Ultimate Properties</u>			
	Time to Failure (t_f), μs	Strength (S_{22T}), MPa (ksi)	Strain (ϵ_{22T}^u)
1A-1	61	142 (20.6)	0.0061
1A-2	64	189 (27.4)	0.0066
1A-3	67	191 (27.7)	0.0060

TABLE 4-24. TRANSVERSE TENSILE PROPERTIES OF UNIDIRECTIONAL 30AS/20S/PR288 GRAPHITE/S-GLASS/EPOXY AT VARIOUS STRAIN RATES

Specimen Numbers	Strain Rate ($\dot{\epsilon}_{22}$), s^{-1}	Modulus (E_{22}), GPa (10^6 psi)	Poisson's Ratio (ν_{21})
<u>Initial Properties</u>			
1A-4,5,6	1×10^{-4}	11.8 (1.71)	0.02
39-4,5,6	31	26.1 (3.78)	--
1A-1,2,3	33	42.8 (6.21)	--
<u>Secant Properties</u>			
1A-4,5,6	1×10^{-4}	11.1 (1.61)	0.02
39-4,5,6	36	20.7 (3.00)	--
1A-1,2,3	98	27.9 (4.05)	--
<u>Terminal Properties</u>			
1A-4,5,6	1×10^{-4}	10.4 (1.50)	0.02
39-4,5,6	46	22.0 (3.18)	--
1A-1,2,3	173	15.3 (2.22)	--
<u>Ultimate Properties</u>			
	Time to Failure (t_f), μs	Strength (S_{22T}), MPa (ksi)	Strain (ϵ_{22T}^u)
1A-4,5,6	1×10^8	49 (7.1)	0.0045
39-4,5,6	56	39 (5.6)	0.0019
1A-1,2,3	64	174 (25.2)	0.0062

Average results for the three ranges of strain rate investigated are tabulated in Table 4-24. The initial and secant moduli increase sharply even for the intermediate strain rates. The strength at the high strain rate is more than three times the static strength, whereas the ultimate strain is only 44% higher. In the case of the intermediate strain rate tests, the strength, as well as the ultimate strain, are appreciably lower than corresponding static values. This is not indicative of any trend, but is the result of premature failures in the specimens cut from a different tube (Tube 34).

4.4 IN-PLANE SHEAR PROPERTIES

4.4.1 Graphite/Epoxy (SP288/T300)

Quasi-static in-plane shear properties were obtained by testing four $[10_6]$ rings under internal pressure. These rings, with the fibers at 10-deg with the circumferential direction, were instrumented with 3-gage rosettes. The gage elements were oriented in the circumferential direction, in the axial direction, and at 45-deg with the circumferential direction. The in-plane (along the fiber direction) shear stress and shear strain were determined from measured data as discussed in Section 3.3.2. Shear stress versus shear strain curves are shown in Figures 4-132 through 4-135. Results are tabulated in Table 4-25.

Intermediate rate in-plane shear properties were obtained by testing three $[10_6]$ rings using 650 mg of pistol powder in the pressure chamber. The circumferential, axial, and 45-deg strains in the composite rings and the circumferential strain in the steel calibration ring were recorded as shown in Figures 4-136, 4-137, and 4-138. The corresponding dynamic shear stress versus shear strain curves are shown in Figures 4-139, 4-140, and 4-141. Results are tabulated in Table 4-26. The initial strain rates range between $16s^{-1}$ and $27s^{-1}$ and the secant rates between $37s^{-1}$ and $69s^{-1}$. The times to failure range between 125 μs and 187 μs .

High strain rate in-plane shear properties were obtained by testing four $[10_6]$ rings. Specimen Nos. 17-7, 17-8, and 17-10 were loaded with 100 mg PETN detonators and Specimen No. 17-9 with 455 mg of pistol powder in the pressure chamber. Strain and strain derivative records for the three graphite/epoxy rings and the steel calibration ring are shown in Figures 4-142 through

TABLE 4-25. QUASI-STATIC IN-PLANE SHEAR PROPERTIES
OF UNIDIRECTIONAL SP288/T300 GRAPHITE/EPOXY

<u>Specimen Number</u>	<u>Strain Rate ($\dot{\epsilon}_{12}$), s⁻¹</u>	<u>Shear Modulus (G₁₂), GPa (10⁶ psi)</u>	
<u>Initial Properties</u>			
17-1	1 X 10 ⁻⁴	7.1 (1.02)	
17-2	1 X 10 ⁻⁴	6.3 (0.91)	
17-3	1 X 10 ⁻⁴	6.3 (0.91)	
17-4	1 X 10 ⁻⁴	5.5 (0.80)	
<u>Secant Properties</u>			
17-1	1 X 10 ⁻⁴	5.0 (0.72)	
17-2	1 X 10 ⁻⁴	3.5 (0.50)	
17-3	1 X 10 ⁻⁴	3.0 (0.44)	
17-4	1 X 10 ⁻⁴	3.6 (0.53)	
<u>Terminal Properties</u>			
17-1	1 X 10 ⁻⁴	3.1 (0.44)	
17-2	1 X 10 ⁻⁴	1.7 (0.25)	
17-3	1 X 10 ⁻⁴	1.5 (0.21)	
17-4	1 X 10 ⁻⁴	2.0 (0.30)	
<u>Ultimate Properties</u>			
	<u>Time to Failure (t_f), μs</u>	<u>Strength (S₁₂), MPa (ksi)</u>	<u>Strain (ε₁₂^u)</u>
17-1	1 X 10 ⁸	66 (9.5)	0.0066
17-2	1 X 10 ⁸	73 (10.6)	0.0105
17-3	1 X 10 ⁸	73 (10.6)	0.0121
17-4	1 X 10 ⁸	66 (9.5)	0.0090

TABLE 4-26. INTERMEDIATE STRAIN RATE IN-PLANE SHEAR
PROPERTIES OF UNIDIRECTIONAL SP288/T300 GRAPHITE/EPOXY

<u>Specimen Number</u>	<u>Strain Rate ($\dot{\epsilon}_{12}$), s⁻¹</u>	<u>Shear Modulus (G_{12}), GPa (10⁶ psi)</u>	
<u>Initial Properties</u>			
57-2	24	6.0 (0.87)	
57-3	27	6.4 (0.93)	
57-5	16	6.3 (0.92)	
<u>Secant Properties</u>			
57-2	37	5.2 (0.75)	
57-3	69	6.0 (0.87)	
57-5	47	5.3 (0.76)	
<u>Terminal Properties</u>			
57-2	84	4.9 (0.70)	
57-3	144	4.4 (0.63)	
57-5	118	4.6 (0.67)	
<u>Ultimate Properties</u>			
	<u>Time to Failure (t_f), μs</u>	<u>Strength (S_{12}), MPa (ksi)</u>	<u>Strain (ϵ_{12}^u)</u>
57-2	187	72 (10.5)	0.0070
57-3	125	103 (15.0)	0.0086
57-5	171	85 (12.4)	0.0081

4-153. The corresponding dynamic stress-strain curves are shown in Figures 4-154 through 4-157. Results are tabulated in Table 4-27. Initial strain rates range between 284s^{-1} and 292s^{-1} for the three specimens loaded with PETN detonators. The times to failure for the same three specimens range between $34\text{ }\mu\text{s}$ and $39\text{ }\mu\text{s}$. Strain rates for Specimen No. 17-9 fall between the high rate and intermediate rate ranges. For this reason properties for this specimen were not averaged with those of the other specimens.

Average results for the four ranges of strain rate investigated are tabulated in Table 4-28. The initial shear modulus remains unchanged for the static and intermediate rate conditions, but it increases sharply to more than twice the static value at high strain rates. The secant shear modulus increases more noticeably with strain rate, from 3.8 GPa ($0.55 \times 10^6\text{ psi}$) under static conditions to 5.5 GPa ($0.79 \times 10^6\text{ psi}$) under intermediate and high rate conditions. The in-plane shear strength increases with strain rate by up to 65% over the static value. The ultimate shear strain shows a slight increase with strain rate, from 0.0096 under static conditions to 0.0106 under high rate conditions.

4.4.2 Graphite/Epoxy (SP288/AS)

Quasi-static in-plane shear properties were obtained by testing three $[10_g]$ rings under internal pressure as described before. Shear stress versus shear strain curves are shown in Figures 4-158, 4-159, and 4-160. Results are tabulated in Table 4-29.

Intermediate rate in-plane shear properties were obtained by testing three $[10_g]$ rings using 650 mg of pistol powder in the pressure chamber. The circumferential, axial, and 45-deg strains in the composite rings and the circumferential strain in the steel calibration ring were recorded as shown in Figures 4-161, 4-162, and 4-163. The corresponding dynamic shear stress versus shear strain curves are shown in Figures 4-164, 4-165, and 4-166. Results are tabulated in Table 4-30. The initial strain rates range between 7s^{-1} and 25s^{-1} and the secant rates between 39s^{-1} and 68s^{-1} . The times to failure range between $180\text{ }\mu\text{s}$ and $240\text{ }\mu\text{s}$.

High strain rate in-plane shear properties were obtained by testing three $[10_g]$ rings. Specimen Nos. 15-5 and 15-7 were loaded with 50 mg PETN detonators,

TABLE 4-27. HIGH STRAIN RATE IN-PLANE SHEAR PROPERTIES
OF UNIDIRECTIONAL SP288/T300 GRAPHITE/EPOXY

<u>Specimen Number</u>	<u>Strain Rate ($\dot{\epsilon}_{12}$), s⁻¹</u>	<u>Shear Modulus (G_{12}), GPa (10⁶ psi)</u>	
<u>Initial Properties</u>			
17-7	136	14.3 (2.07)	
17-8	150	13.9 (2.02)	
17-9	119	7.0 (1.02)	
17-10	180	12.2 (1.78)	
<u>Secant Properties</u>			
17-7	291	7.0 (1.02)	
17-8	292	5.0 (0.72)	
17-9	87	5.5 (0.80)	
17-10	284	4.1 (0.59)	
<u>Terminal Properties</u>			
17-7	520	6.3 (0.91)	
17-8	490	2.4 (0.35)	
17-9	78	8.8 (1.28)	
17-10	500	0.9 (0.14)	
<u>Ultimate Properties</u>			
	<u>Time to Failure (t_f), μs</u>	<u>Strength (S_{12}), MPa (ksi)</u>	<u>Strain (ϵ_{12}^u)</u>
17-7	34	139 (20.2)	0.0099
17-8	39	113 (16.4)	0.0114
17-9	120	115 (16.6)	0.0104
17-10	37	86 (12.4)	0.0105

TABLE 4-28. IN-PLANE SHEAR PROPERTIES OF UNIDIRECTIONAL
SP288/T300 GRAPHITE/EPOXY AT VARIOUS STRAIN RATES

<u>Specimen Number</u>	<u>Strain Rate ($\dot{\epsilon}_{12}$), s⁻¹</u>	<u>Shear Modulus (G_{12}), GPa (10⁶ psi)</u>	
<u>Initial Properties</u>			
17-1,2,3,4	1 X 10 ⁻⁴	6.3 (0.91)	
57-2,3,5	22	6.3 (0.91)	
17-9	119	7.0 (1.02)	
17-7,8,10	155	13.5 (1.96)	
<u>Secant Properties</u>			
17-1,2,3,4	1 X 10 ⁻⁴	3.8 (0.55)	
57-2,3,5	51	5.5 (0.79)	
17-9	87	5.5 (0.80)	
17-7,8,10	289	5.4 (0.78)	
<u>Terminal Properties</u>			
17-1,2,3,4	1 X 10 ⁻⁴	2.1 (0.30)	
57-2,3,5	115	4.6 (0.67)	
17-9	78	8.8 (1.28)	
17-7,8,10	503	3.2 (0.47)	
<u>Ultimate Properties</u>			
	<u>Time to Failure (t_f), μs</u>	<u>Strength (S₁₂), MPa (ksi)</u>	<u>Strain (ϵ_{12}^u)</u>
17-1,2,3,4	1 X 10 ⁸	69 (10.1)	0.0096
57-2,3,5	161	87 (12.6)	0.0079
17-9	120	115 (16.6)	0.0104
17-7,8,10	37	113 (16.3)	0.0106

TABLE 4-29. QUASI-STATIC IN-PLANE SHEAR PROPERTIES
OF UNIDIRECTIONAL SP288/AS GRAPHITE/EPOXY

<u>Specimen Number</u>	<u>Strain Rate ($\dot{\epsilon}_{12}$), s⁻¹</u>	<u>Shear Modulus (G_{12}), GPa (10⁶ psi)</u>	
<u>Initial Properties</u>			
15-2	1 X 10 ⁻⁴	5.5 (0.79)	
15-3	1 X 10 ⁻⁴	6.0 (0.88)	
15-4	1 X 10 ⁻⁴	6.8 (0.98)	
<u>Secant Properties</u>			
15-2	1 X 10 ⁻⁴	3.2 (0.46)	
15-3	1 X 10 ⁻⁴	3.2 (0.47)	
15-4	1 X 10 ⁻⁴	3.1 (0.45)	
<u>Terminal Properties</u>			
15-2	1 X 10 ⁻⁴	1.6 (0.24)	
15-3	1 X 10 ⁻⁴	1.3 (0.20)	
15-4	1 X 10 ⁻⁴	1.3 (0.19)	
<u>Ultimate Properties</u>			
	<u>Time to Failure (t_f), μs</u>	<u>Strength (S_{12}), MPa (ksi)</u>	<u>Strain (ϵ_{12}^u)</u>
15-2	1 X 10 ⁸	83 (12.1)	0.0131
15-3	1 X 10 ⁸	86 (12.5)	0.0133
15-4	1 X 10 ⁸	90 (13.1)	0.0146

TABLE 4-30. INTERMEDIATE STRAIN RATE IN-PLANE SHEAR PROPERTIES OF UNIDIRECTIONAL SP288/AS GRAPHITE/EPOXY

<u>Specimen Number</u>	<u>Strain Rate ($\dot{\epsilon}_{12}$), s⁻¹</u>	<u>Shear Modulus (G_{12}), GPa (10⁶ psi)</u>	
<u>Initial Properties</u>			
15-9	25	6.6 (0.96)	
15-10	13	5.7 (0.82)	
15-11	7	6.0 (0.88)	
<u>Secant Properties</u>			
15-9	68	4.7 (0.68)	
15-10	61	4.3 (0.63)	
15-11	39	4.7 (0.68)	
<u>Terminal Properties</u>			
15-9	114	2.7 (0.39)	
15-10	190	4.1 (0.59)	
15-11	96	3.5 (0.51)	
<u>Ultimate Properties</u>			
	<u>Time to Failure (t_f), μs</u>	<u>Strength (S_{12}), MPa (ksi)</u>	<u>Strain (ϵ_{12}^u)</u>
15-9	180	114 (16.5)	0.0122
15-10	235	125 (18.1)	0.0143
15-11	240	89 (12.9)	0.0094

and Specimen No. 15-8 with a 100 mg PETN detonator in the pressure chamber. Strain and strain derivative records for the composite and steel calibration rings are shown in Figures 4-167 through 4-175. The corresponding dynamic stress-strain curves are shown in Figures 4-176, 4-177, and 4-178. Results are tabulated in Table 4-31. The initial strain rates range between 140s^{-1} and 170s^{-1} and the secant rates between 223s^{-1} and 282s^{-1} . The times to failure range between $40\text{ }\mu\text{s}$ and $47\text{ }\mu\text{s}$.

Average results for the three ranges of strain rate investigated are tabulated in Table 4-32. The initial shear modulus remains essentially unchanged for the static and intermediate rate conditions (6.1 GPa ; $0.89 \times 10^6\text{ psi}$), but it increases to 8.3 GPa ($1.21 \times 10^6\text{ psi}$) under high strain rate loading. The secant modulus increases more noticeably with strain rate, from 3.2 GPa ($0.46 \times 10^6\text{ psi}$) under static conditions to 5.2 GPa ($0.76 \times 10^6\text{ psi}$) under high rate conditions. The shear strength shows a similar trend, although not as pronounced. The ultimate shear strain decreases with strain rate from 0.0137 under static conditions to 0.0108 under high rate conditions.

4.4.3 Graphite/S-Glass/Epoxy (80AS/20S/PR288)

Quasi-static in-plane shear properties were obtained by testing three $[10_6]$ rings under internal pressure as described before. Shear stress versus shear strain curves are shown in Figures 4-179, 4-180, and 4-181. Results are tabulated in Table 4-33.

Intermediate rate in-plane shear properties were obtained by testing three $[10_6]$ rings using 650 mg of pistol powder in the pressure chamber. Recorded strains are shown in Figures 4-182, 4-183, and 4-184. The corresponding dynamic shear stress versus strain curves are shown in Figures 4-185, 4-186, and 4-187. Results are tabulated in Table 4-34. The initial strain rates vary between 11s^{-1} and 19s^{-1} and the secant rates between 33s^{-1} and 66s^{-1} . The times to failure range between $134\text{ }\mu\text{s}$ and $203\text{ }\mu\text{s}$.

High strain rate in-plane shear properties were obtained by testing three $[10_6]$ rings. Specimen Nos. 18-5 and 18-8 were loaded with 100 mg PETN detonators, and Specimen No. 18-6 with 455 mg of pistol powder in the pressure chamber. Strain and strain derivative records for the three hybrid rings and the steel calibration ring are shown in Figures 4-188 through 4-196. The

TABLE 4-31. HIGH STRAIN RATE IN-PLANE SHEAR PROPERTIES
OF UNIDIRECTIONAL SP288/AS GRAPHITE/EPOXY

<u>Specimen Number</u>	<u>Strain Rate ($\dot{\epsilon}_{12}$), s⁻¹</u>	<u>Shear Modulus (G_{12}), GPa (10⁶ psi)</u>	
<u>Initial Properties</u>			
15-5	170	7.08 (1.03)	
15-7	140	10.09 (1.46)	
15-8	160	7.80 (1.13)	
<u>Secant Properties</u>			
15-5	223	5.34 (0.77)	
15-7	230	4.77 (0.69)	
15-8	282	5.56 (0.81)	
<u>Terminal Properties</u>			
15-5	380	3.11 (0.45)	
15-7	500	3.71 (0.54)	
15-8	660	3.64 (0.53)	
<u>Ultimate Properties</u>			
	<u>Time to Failure (t_f), μs</u>	<u>Strength (S_{12}), MPa (ksi)</u>	<u>Strain (ϵ_{12}^u)</u>
15-5	47	112 (16.3)	0.0105
15-7	46	100 (14.6)	0.0106
15-8	40	126 (18.2)	0.0113

TABLE 4-32. IN-PLANE SHEAR PROPERTIES OF UNIDIRECTIONAL
SP288/AS GRAPHITE/EPOXY AT VARIOUS STRAIN RATES

<u>Specimen Numbers</u>	<u>Strain Rate ($\dot{\epsilon}_{12}$), s⁻¹</u>	<u>Shear Modulus (G_{12}), GPa (10⁶ psi)</u>	
<u>Initial Properties</u>			
15-2,3,4	1 X 10 ⁻⁴	6.1 (0.88)	
15-9,10,11	15	6.1 (0.89)	
15-5,7,8	157	8.3 (1.21)	
<u>Secant Properties</u>			
15-2,3,4	1 X 10 ⁻⁴	3.2 (0.46)	
15-9,10,11	56	4.6 (0.66)	
15-5,7,8	245	5.2 (0.76)	
<u>Terminal Properties</u>			
15-2,3,4	1 X 10 ⁻⁴	1.4 (0.21)	
15-9,10,11	133	3.4 (0.50)	
15-5,7,8	513	3.5 (0.51)	
<u>Ultimate Properties</u>			
	<u>Time to Failure (t_f), μs</u>	<u>Strength (S_{12}), MPa (ksi)</u>	<u>Strain (ϵ_{12}^u)</u>
15-2,3,4	1 X 10 ⁸	87 (12.6)	0.0137
15-9,10,11	218	109 (15.8)	0.0120
15-5,7,8	44	113 (16.4)	0.0108

TABLE 4-33. QUASI-STATIC IN-PLANE SHEAR PROPERTIES
OF UNIDIRECTIONAL 80AS/20S/PR288 GRAPHITE/S-GLASS/EPOXY

<u>Specimen Number</u>	<u>Strain Rate ($\dot{\epsilon}_{12}$), s⁻¹</u>	<u>Shear Modulus (G₁₂), GPa (10⁶ psi)</u>	
<u>Initial Properties</u>			
18-2	1 X 10 ⁻⁴	8.2 (1.18)	
18-3	1 X 10 ⁻⁴	6.6 (0.95)	
18-4	1 X 10 ⁻⁴	6.0 (0.87)	
<u>Secant Properties</u>			
18-2	1 X 10 ⁻⁴	4.8 (0.69)	
18-3	1 X 10 ⁻⁴	4.0 (0.57)	
18-4	1 X 10 ⁻⁴	4.2 (0.61)	
<u>Terminal Properties</u>			
18-2	1 X 10 ⁻⁴	2.7 (0.39)	
18-3	1 X 10 ⁻⁴	2.1 (0.30)	
18-4	1 X 10 ⁻⁴	2.6 (0.38)	
<u>Ultimate Properties</u>			
	<u>Time to Failure (t_f), μs</u>	<u>Strength (S₁₂), MPa (ksi)</u>	<u>Strain (ε₁₂^u)</u>
18-2	1 X 10 ⁸	66 (9.5)	0.0069
18-3	1 X 10 ⁸	69 (10.1)	0.0088
18-4	1 X 10 ⁸	64 (9.3)	0.0076

TABLE 4-34. INTERMEDIATE STRAIN RATE IN-PLANE SHEAR PROPERTIES OF UNIDIRECTIONAL 80AS/20S/PR288 GRAPHITE/S-GLASS/EPOXY

<u>Specimen Number</u>	<u>Strain Rate ($\dot{\epsilon}_{12}$), s⁻¹</u>	<u>Shear Modulus (G_{12}), GPa (10⁶ psi)</u>	
<u>Initial Properties</u>			
18-9	11	10.8 (1.56)	
18-10	13	8.6 (1.25)	
18-11	19	6.8 (0.99)	
<u>Secant Properties</u>			
18-9	55	5.9 (0.86)	
18-10	33	6.9 (1.00)	
18-11	66	5.5 (0.80)	
<u>Terminal Properties</u>			
18-9	170	3.6 (0.53)	
18-10	83	5.8 (0.83)	
18-11	150	3.8 (0.56)	
<u>Ultimate Properties</u>			
	<u>Time to Failure (t_f), μs</u>	<u>Strength (S_{12}), MPa (ksi)</u>	<u>Strain (ϵ_{12}^u)</u>
18-9	175	115 (16.7)	0.0097
18-10	203	93 (13.4)	0.0067
18-11	134	97 (14.1)	0.0089

corresponding dynamic stress-strain curves are shown in Figures 4-197, 4-198, and 4-199. Results are tabulated in Table 4-35. Initial strain rates vary between 112s^{-1} and 220s^{-1} and secant strain rates between 90s^{-1} and 240s^{-1} . The times to failure range between $32\text{ }\mu\text{s}$ and $75\text{ }\mu\text{s}$. The lowest secant rate and the longest failure time correspond to Specimen No. 18-6 which was loaded with the slower burning explosive.

Average results for the three ranges of strain rate investigated are tabulated in Table 4-36. The initial shear modulus increases at the intermediate and high strain rates by approximately the same amount. The secant shear modulus increases at the intermediate rate, but not so much at the high strain rates. The in-plane shear strength shows a similar trend, increasing sharply at the intermediate rates, but only moderately at the high strain rates. The ultimate shear strain shows some variations with strain rate which may not be significant.

4.5 COMPRESSIVE PROPERTIES

4.5.1 Compression Fixture

Dynamic compressive properties of unidirectional composites were obtained by testing rings under dynamic external pressure. A new test system was designed and fabricated for this purpose. Components of this fixture and the assembled fixture are shown in Figures 4-200, 4-201, and 4-202. A cross section of the assembled fixture is shown in Figure 4-203.

Figure 4-200 shows the arbor for holding the test and calibration ring specimens inside the fixture. It is a short cylinder with a base diameter approximately equal to that of the ring specimens, i.e., 10.16 cm (4 in.). This arbor has a reduced diameter section with a threaded end. The composite and steel calibration specimens are supported on the shoulder of the base section and held in place by means of a retaining ring shown in Figure 4-200b. The arbor has radial holes in the reduced section at the specimen location which connect to an axial central hole extending to the bottom of the arbor. These passages serve to vent the space inside the ring specimen to atmosphere and are used to take the leads out from the strain gages inside the specimens. The arbor with the specimens is attached to a base flange plate as shown in Figure 4-201.

TABLE 4-35. HIGH STRAIN RATE IN-PLANE SHEAR PROPERTIES
OF UNIDIRECTIONAL 80AS/20S/PR288 GRAPHITE/S-GLASS/EPOXY

<u>Specimen Number</u>	<u>Strain Rate ($\dot{\epsilon}_{12}$), s⁻¹</u>	<u>Shear Modulus (G_{12}), GPa (10⁶ psi)</u>	
<u>Initial Properties</u>			
18-5	175	7.9 (1.15)	
18-6	112	9.9 (1.43)	
18-8	220	9.5 (1.38)	
<u>Secant Properties</u>			
18-5	228	5.7 (0.83)	
18-6	90	5.0 (0.72)	
18-8	240	5.3 (0.77)	
<u>Terminal Properties</u>			
18-5	270	3.8 (0.56)	
18-6	88	4.9 (0.71)	
18-8	255	3.9 (0.56)	
<u>Ultimate Properties</u>			
	<u>Time to Failure (t_f), μs</u>	<u>Strength (S_{12}), MPa (ksi)</u>	<u>Strain (ϵ_{12}^u)</u>
18-5	32	83 (12.0)	0.0073
18-6	75	67 (9.8)	0.0067
18-8	32	82 (11.9)	0.0077

TABLE 4-36. IN-PLANE SHEAR PROPERTIES OF UNIDIRECTIONAL
80AS/20S/PR288 GRAPHITE/S-GLASS/EPOXY AT VARIOUS STRAIN RATES

<u>Specimen Numbers</u>	<u>Strain Rate ($\dot{\epsilon}_{12}$), s⁻¹</u>	<u>Shear Modulus (G₁₂), GPa (10⁶ psi)</u>	
<u>Initial Properties</u>			
18-2,3,4	1 X 10 ⁻⁴	6.9 (1.00)	
18-9,10,11	14	8.7 (1.27)	
18-5,6,8	169	9.1 (1.32)	
<u>Secant Properties</u>			
18-2,3,4	1 X 10 ⁻⁴	4.3 (0.62)	
18-9,10,11	51	6.1 (0.89)	
18-5,6,8	186	5.3 (0.77)	
<u>Terminal Properties</u>			
18-2,3,4	1 X 10 ⁻⁴	2.5 (0.36)	
18-9,10,11	134	4.4 (0.64)	
18-5,6,8	204	4.2 (0.61)	
<u>Ultimate Properties</u>			
	<u>Time to Failure (t_f), μs</u>	<u>Strength (S₁₂), MPa (ksi)</u>	<u>Strain (ε₁₂^u)</u>
18-2,3,4	1 X 10 ⁸	66 (9.6)	0.0078
18-9,10,11	171	102 (14.7)	0.0084
18-5,6,8	46	78 (11.2)	0.0072

A cone wave deflector is threaded to the arbor over the specimens and retaining ring (Figure 4-202). This cone helps to guide the pressure wave in the surrounding liquid so that a uniform dynamic pressure is generated on the outside of the ring specimens. The assembly of the arbor with the specimens and cone deflector is enclosed in a pressure chamber of 15.24 cm (6 in.) diameter (Figure 4-202). A smaller diameter extension of this chamber at the top contains the detonator which initiates the pressure wave in the fluid filled chamber.

4.5.2 Longitudinal Compressive Properties

Quasi-static longitudinal compressive properties were obtained using the IITRI compression fixture with 15-ply thick coupon specimens as described in Section 2.2. Results for the two graphite/epoxy and the hybrid materials are incorporated in Tables 2-7, 2-8, and 2-9.

Dynamic compressive properties of SP288/T300 graphite/epoxy were obtained by testing $[0_6]$ rings under dynamic external pressure in the fixture described above. Four rings were loaded dynamically using a 1.56 g mixture of pistol powder, potassium perchlorate, and aluminum dust in the pressure chamber. Strains in the composite and steel calibration rings, obtained from strain gages mounted on the inside surface of these rings, were recorded in every case. Strain and strain derivative records for the four rings above (Specimen Nos. 19-8, 19-9, 40-1, and 40-2) are shown in Figures 4-204 through 4-215. These data were analyzed following the procedures described earlier for dynamic tensile tests. Dynamic stress-strain curves obtained by the digital processing oscilloscope are shown in Figures 4-216 through 4-219.

Results for the four graphite/epoxy specimens above are tabulated in Table 4-37. The initial and secant moduli of 150.6 GPa (21.8×10^6 psi) and 135.2 GPa (19.6×10^6 psi), respectively, are not appreciably different from the static modulus of 145 GPa (21.1×10^6 psi). This is because the strain rates achieved in these tests are not very high, ranging from $15s^{-1}$ to $93s^{-1}$. The secant Poisson's ratio of 0.35 is somewhat higher than the static value of 0.30. The average dynamic strength of 1175 MPa (170 ksi) is lower than the static compressive strength of 1297 MPa (188 ksi) obtained by testing small coupons with the IITRI compression fixture. The difference may be due to the

TABLE 4-37. HIGH STRAIN RATE COMPRESSIVE PROPERTIES OF $[0_6]$
SP288/T300 GRAPHITE/EPOXY

Specimen Number	Strain Rate ($\dot{\epsilon}_{11}$), s^{-1}	Modulus (E_{11}), GPa (10^6 psi)	Poisson's Ratio (ν_{12})
<u>Initial Properties</u>			
19-8	20	132.0 (19.1)	--
19-9	15	164.6 (23.9)	0.50
40-1	30	147.3 (21.4)	--
40-2	25	157.7 (22.9)	0.32
<u>Secant Properties</u>			
19-8	93	142.8 (20.7)	--
19-9	84	146.3 (21.2)	0.35
40-1	80	135.4 (19.6)	--
40-2	93	116.8 (16.9)	0.35
<u>Terminal Properties</u>			
19-8	80	180.1 (26.1)	--
19-9	100	115.6 (16.8)	0.55
40-1	100	112.8 (16.4)	--
40-2	100	86.9 (12.6)	0.66
<u>Ultimate Properties</u>			
	Time to Failure (t_f), μs	Strength (S_{11C}), MPa (ksi)	Strain (ϵ_{11C}^u)
19-8	96	1277 (185)	0.0089
19-9	100	1216 (176)	0.0083
40-1	97	1070 (155)	0.0079
40-2	105	1139 (165)	0.0098

different methods of testing, as there was no evidence of buckling of the 6-ply rings under dynamic external pressure. The average dynamic ultimate strain of 0.0088 is also lower than the static value of 0.0114, following the same trend as the strength values.

Attempts were made to increase the strain rate in these tests, by shortening the distance between detonator and specimen and by using more powerful detonators (PETN). However, the strain rates did not increase noticeably. They appear to be governed by the specimen layup and the dimensions of the pressure chamber.

Dynamic compressive properties of SP288/AS graphite/epoxy were obtained in a similar manner as described above. Strain and strain derivative records for the three rings tested (Specimen Nos. 45-2, 45-3, and 45-4) are shown in Figures 4-220 through 4-228. These data were analyzed as discussed before. Dynamic stress-strain curves are shown in Figures 4-229, 4-230, and 4-231. They show more nonlinearity than corresponding static stress-strain curves. Results for the three graphite/epoxy specimens above are tabulated in Table 4-38. The initial and secant moduli are 179.2 GPa (26.0×10^6 psi) and 122.8 GPa (17.8×10^6 psi), which are respectively higher and lower than the static modulus of 137 GPa (19.9×10^6 psi). The average initial Poisson's ratio of 0.34 is somewhat higher than the static value of 0.32. The secant and terminal values of Poisson's ratio do not appear to be reliable as they are affected by the unexplainable sharp increase in axial strain at later times. The average dynamic compressive strength of 1219 MPa (177 ksi) is very close to the static compressive strength of 1235 MPa (179 ksi) obtained by testing small coupons with the IITRI compression fixture. The average dynamic ultimate strain of 0.0101 is lower than the static value of 0.0108. The longitudinal dynamic properties, in general, are not appreciably different from quasi-static properties with the exception of the initial modulus. This is probably due to the relatively lower strain rates achieved.

4.5.3 Transverse Compressive Properties

Quasi-static transverse compressive properties were obtained using the IITRI compression fixture with 15-ply thick coupon specimens as described in Section 2.2. Results for the two graphite/epoxy and the hybrid materials are incorporated in Tables 2-7, 2-8, and 2-9.

TABLE 4-38. HIGH STRAIN RATE COMPRESSIVE PROPERTIES OF
[0₆] SP288/AS GRAPHITE/EPOXY

Specimen Number	Strain Rate ($\dot{\epsilon}_{11}$), s ⁻¹	Modulus (E_{11}), GPa (10 ⁶ psi)	Poisson's Ratio (ν_{12})
<u>Initial Properties</u>			
45-2	20	169.1 (24.5)	0.32
45-3	20	158.7 (23.0)	0.43
45-4	20	209.8 (30.4)	0.27
<u>Secant Properties</u>			
45-2	87	110.1 (16.0)	0.43
45-3	80	115.6 (16.8)	0.30
45-4	73	142.3 (20.6)	0.46
<u>Terminal Properties</u>			
45-2	170	89.7 (13.0)	--
45-3	120	117.3 (17.0)	0.49
45-4	100	117.3 (17.0)	--
<u>Ultimate Properties</u>			
	Time to Failure (t_f), μ s	Strength (S_{11C}), MPa (ksi)	Strain (ϵ_{11C}^u)
45-2	130	1233 (179)	0.0113
45-3	130	1225 (178)	0.0106
45-4	115	1195 (173)	0.0084

Dynamic compressive properties of SP288/T300 graphite/epoxy were obtained by testing $[90_g]$ rings under dynamic external pressure in the fixture described above. Three rings were loaded dynamically using a 1.56 g mixture of pistol powder, potassium perchlorate, and aluminum dust in the pressure chamber. Strains in the composite and steel calibration rings, obtained from strain gages mounted on the inside surface of these rings, were recorded in every case. Strain and strain derivative records for the three rings above (Specimen Nos. 44-1, 44-3, and 44-4) are shown in Figures 4-232 through 4-240. These data were analyzed following the procedures described earlier for dynamic tensile tests. Dynamic stress-strain curves obtained by the digital processing oscilloscope are shown in Figures 4-241, 4-242, and 4-243.

Results for the three graphite/epoxy specimens above are tabulated in Table 4-39. The initial and secant moduli of 34.5 GPa (5.00×10^6 psi) and 18.5 GPa (2.68×10^6 psi), respectively, are much higher than the static modulus of 10.4 GPa (1.50×10^6 psi). The average dynamic strength of 393 MPa (57.0 ksi) is also higher than the static strength of 251 MPa (36 ksi). The average secant Poisson's ratio of 0.03 is close to the static value of 0.02. The dynamic ultimate strain of 0.0213 is appreciably lower than the static ultimate strain of 0.0336.

Dynamic compressive properties of SP288/AS graphite/epoxy were obtained by testing three $[90_g]$ rings in a similar manner as described before. Strain and strain derivative records for the three rings above (Specimen Nos. 38-1, 38-2, and 38-3) are shown in Figures 4-244 through 4-252. These data were analyzed following the procedures described earlier for dynamic tensile tests. Dynamic stress-strain curves obtained by the digital processing oscilloscope are shown in Figures 4-253, 4-254, and 4-255.

Results for the three graphite/epoxy specimens above are tabulated in Table 4-40. The initial and secant moduli of 28.5 GPa (4.12×10^6 psi) and 18.4 GPa (2.66×10^6 psi), respectively, are much higher than the static modulus of 10.7 GPa (1.56×10^6 psi). The average dynamic strength of 362 MPa (52.2 ksi) is also higher than the static strength of 244 MPa (35 ksi). The average Poisson's secant ratio of 0.033 is close to the static value of 0.03. The dynamic ultimate strain of 0.0198 is much lower than the static ultimate strain of 0.0317.

TABLE 4-39. HIGH STRAIN RATE COMPRESSIVE PROPERTIES OF
[90₈] SP288/T300 GRAPHITE/EPOXY

Specimen Number	Strain Rate ($\dot{\epsilon}_{22}$), s ⁻¹	Modulus (E_{22}), GPa (10 ⁶ psi)	Poisson's Ratio (ν_{21})
<u>Initial Properties</u>			
44-1	25	29.0 (4.20)	--
44-3	25	30.6 (4.43)	--
44-4	35	44.0 (6.37)	--
<u>Secant Properties</u>			
44-1	229	18.3 (2.65)	0.02
44-3	219	15.2 (2.20)	0.03
44-4	228	22.0 (3.18)	0.03
<u>Terminal Properties</u>			
44-1	450	14.1 (2.05)	0.09
44-3	450	14.8 (2.15)	0.08
44-4	510	9.5 (1.37)	0.12
<u>Ultimate Properties</u>			
	Time to Failure (t_f), μ s	Strength (S_{22C}), MPa (ksi)	Strain (ϵ_{22C}^u)
44-1	95	398 (57.7)	0.0218
44-3	95	315 (45.7)	0.0208
44-4	93	466 (67.5)	0.0212

TABLE 4-40. HIGH STRAIN RATE COMPRESSIVE PROPERTIES OF
[90_g] SP288/AS GRAPHITE/EPOXY

Specimen Number	Strain Rate ($\dot{\epsilon}_{22}$), s ⁻¹	Modulus (E ₂₂), GPa (10 ⁶ psi)	Poisson's Ratio (ν_{21})
<u>Initial Properties</u>			
38-1	25	27.6 (4.00)	0.04
38-2	20	29.3 (4.25)	--
38-3	35	--	--
<u>Secant Properties</u>			
38-1	215	17.7 (2.56)	0.03
38-2	196	17.3 (2.50)	0.04
38-3	219	20.2 (2.93)	0.03
<u>Terminal Properties</u>			
38-1	450	10.0 (1.45)	0.10
38-2	400	10.7 (1.55)	0.09
38-3	480	7.9 (1.15)	0.08
<u>Ultimate Properties</u>			
	Time to Failure (t _f), μ s	Strength (S _{22C}), MPa (ksi)	Strain (ϵ_{22C}^u)
38-1	100	376 (54.5)	0.0215
38-2	99	335 (48.5)	0.0194
38-3	85	376 (54.5)	0.0186

Dynamic compressive properties of $[90_g]$ 80AS/20S/PR288 graphite/S-glass/epoxy were obtained similarly as those of the graphite/epoxy materials above. Strain and strain derivative records for the three hybrid rings tested (Specimen Nos. 39-1, 39-2, and 39-3) are shown in Figures 4-256 through 4-264. Dynamic stress-strain curves are shown in Figures 4-265, 4-266, and 4-267.

Results for the three hybrid specimens above are tabulated in Table 4-41. The initial and secant moduli of 55.0 GPa (7.98×10^6 psi) and 28.5 GPa (4.14×10^6 psi), respectively, are much higher than the static modulus of 11.8 GPa (1.71×10^6 psi). The average dynamic strength of 305 MPa (44.1 ksi) is also much higher than the static strength of 166 MPa (24 ksi). The dynamic ultimate strain of 0.0111 is lower than the static ultimate strain of 0.0157.

Attempts were made to increase the strain rate in the compression tests above by shortening the distance between detonator and specimen and by using more powerful detonators (PETN). However, the strain rates did not increase noticeably. They appear to be governed by the specimen layup and the dimensions of the pressure chamber.

TABLE 4-41. HIGH STRAIN RATE COMPRESSIVE PROPERTIES OF [90₈]
80AS/20S/PR288 GRAPHITE/S-GLASS/EPOXY

Specimen Number	Strain Rate ($\dot{\epsilon}_{22}$), s ⁻¹	Modulus (E_{22}), GPa (10 ⁶ psi)	Poisson's Ratio (ν_{21})
<u>Initial Properties</u>			
39-1	50	57.4 (8.31)	--
39-2	20	58.5 (8.47)	--
39-3	20	49.3 (7.15)	--
<u>Secant Properties</u>			
39-1	180	22.0 (3.19)	--
39-2	135	26.9 (3.89)	--
39-3	102	36.7 (5.33)	--
<u>Terminal Properties</u>			
39-1	500	6.0 (0.87)	--
39-2	250	14.1 (2.05)	0.11
39-3	200	29.9 (4.33)	--
<u>Ultimate Properties</u>			
	Time to Failure (t_f), μ s	Strength (S_{22C}), MPa (ksi)	Strain (ϵ_{22C}^u)
39-1	75	297 (43.0)	0.0135
39-2	83	301 (43.6)	0.0112
39-3	84	316 (45.8)	0.0086

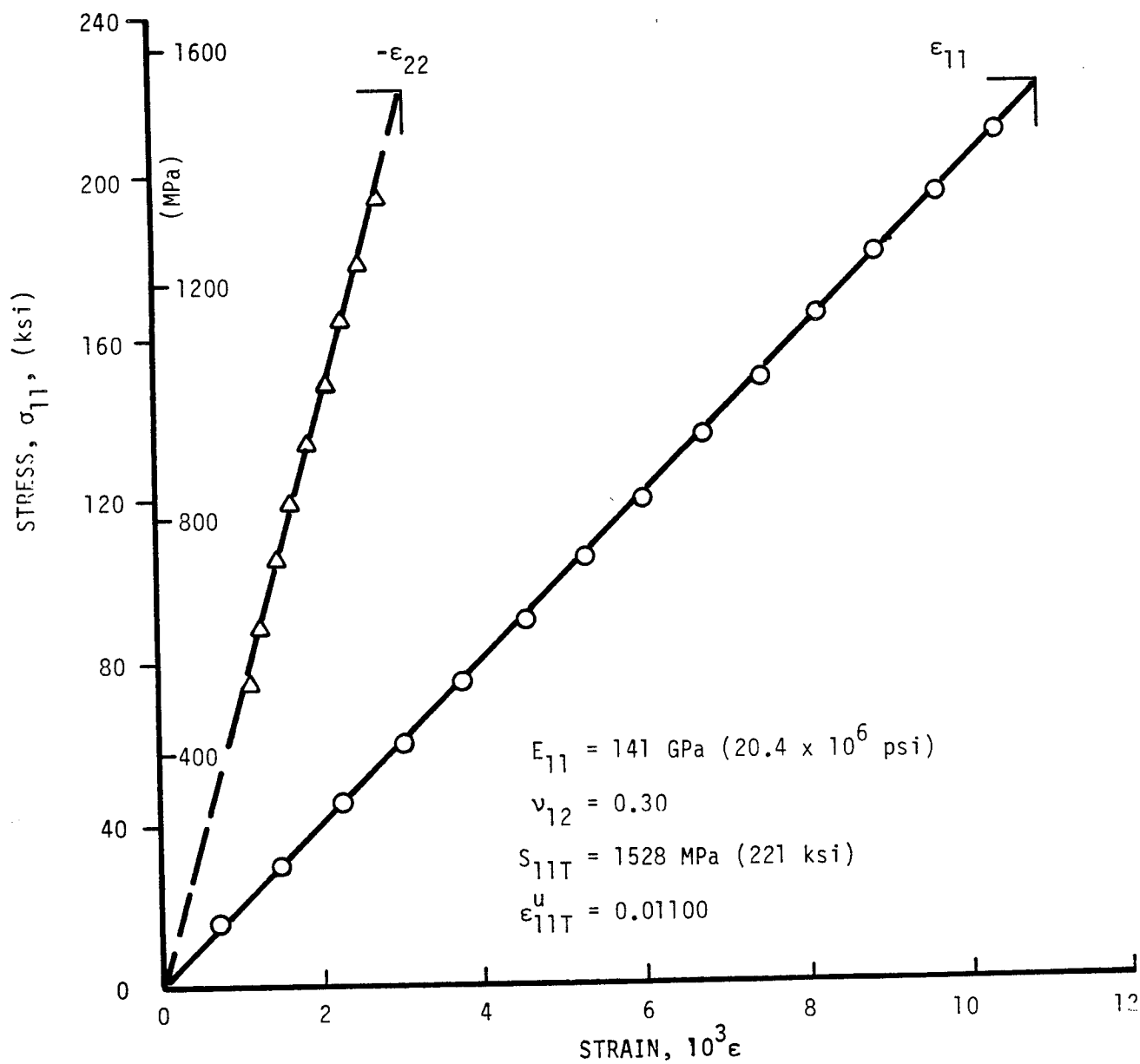


Figure 4-1. Strains in unidirectional 0-deg SP288/T300 ring specimen under static tensile loading (Specimen No. 19-2).

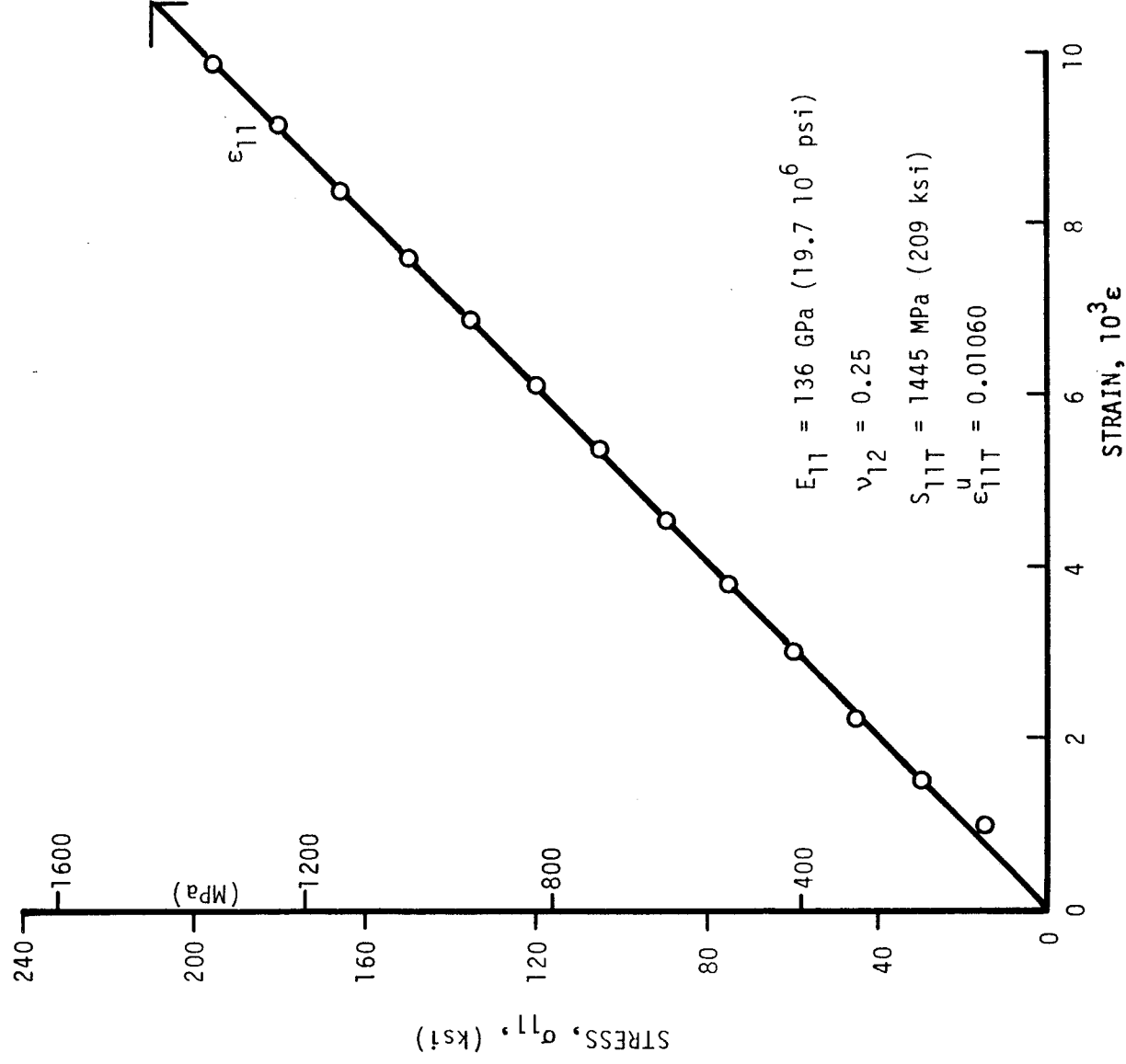


Figure 4-2. Stress-strain curve in unidirectional 0-deg SP288/T300 ring specimen under static tensile loading (Specimen No. 19-3).

Figure 4-3. Strains in unidirectional 0-deg SP288/T300 ring specimen under static tensile loading (Specimen No. 19-10).

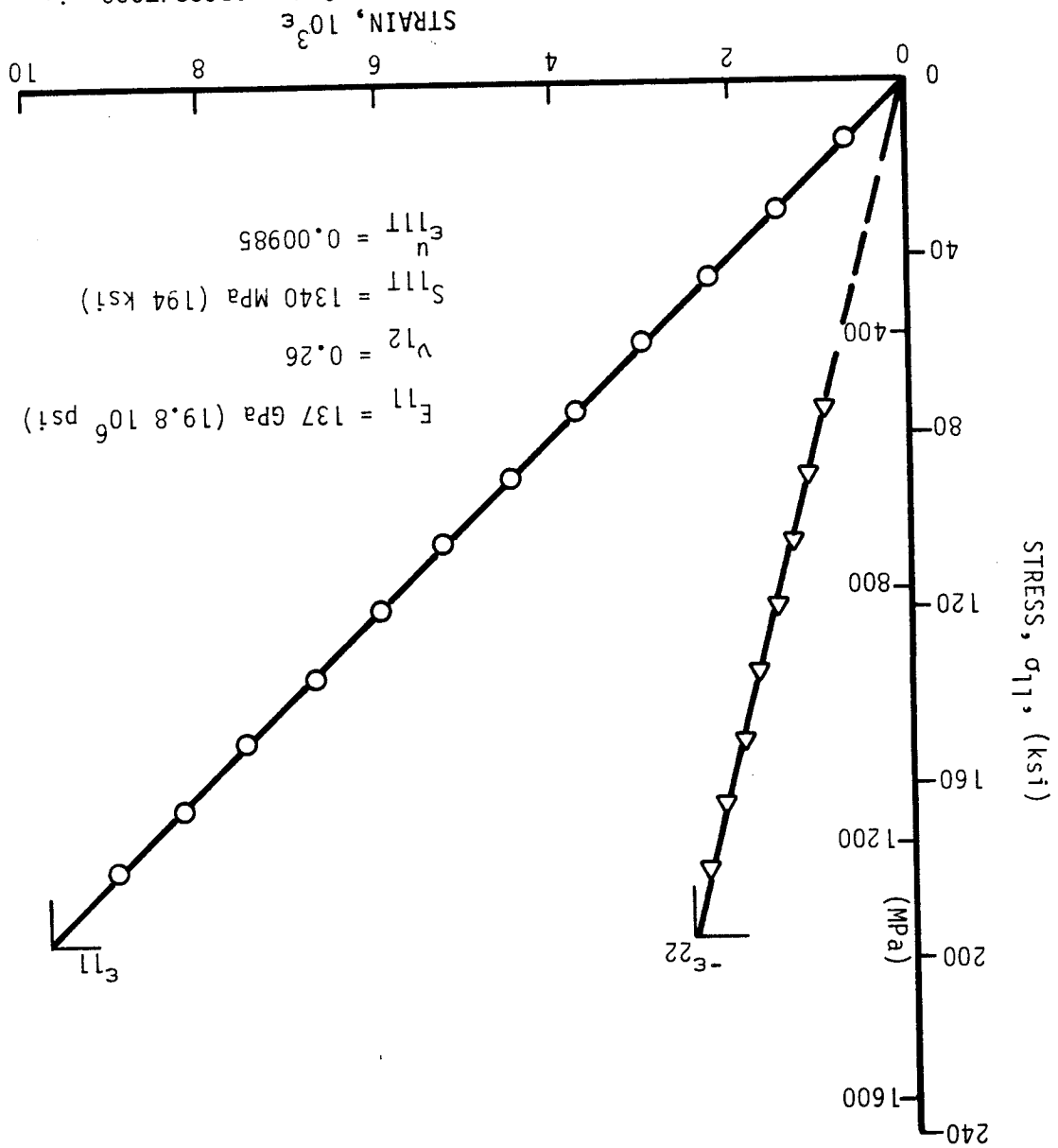
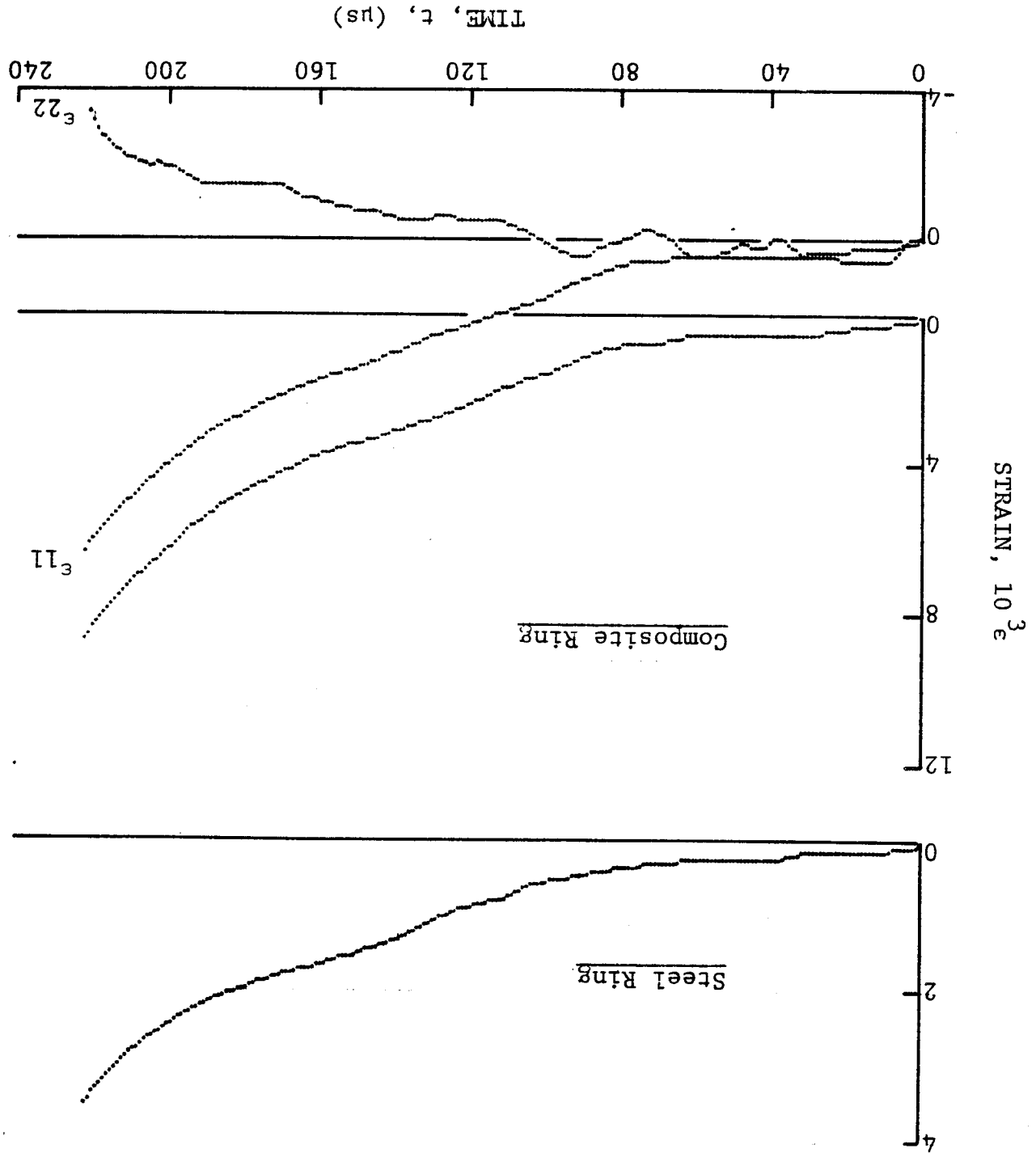


Figure 4-4. Strain records in steel ring and [06] SP288/T300 graphite/epoxy ring under dynamic loading for Specimen 40-3 (650 mg pistol powder).



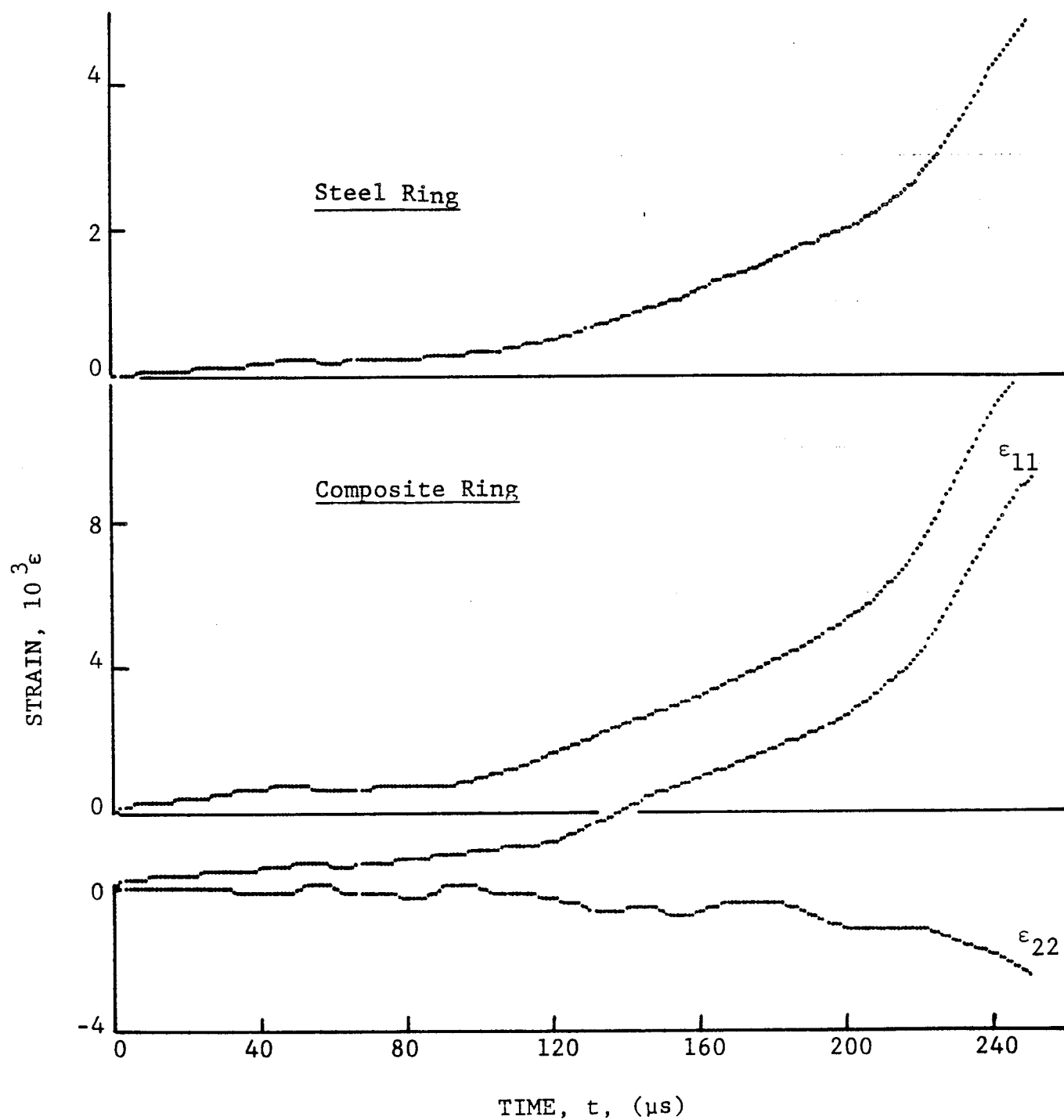


Figure 4-5. Strain records in steel ring and $[0_6]$ SP288/T300 graphite/epoxy ring under dynamic loading for Specimen 40-4 (650 mg pistol powder).

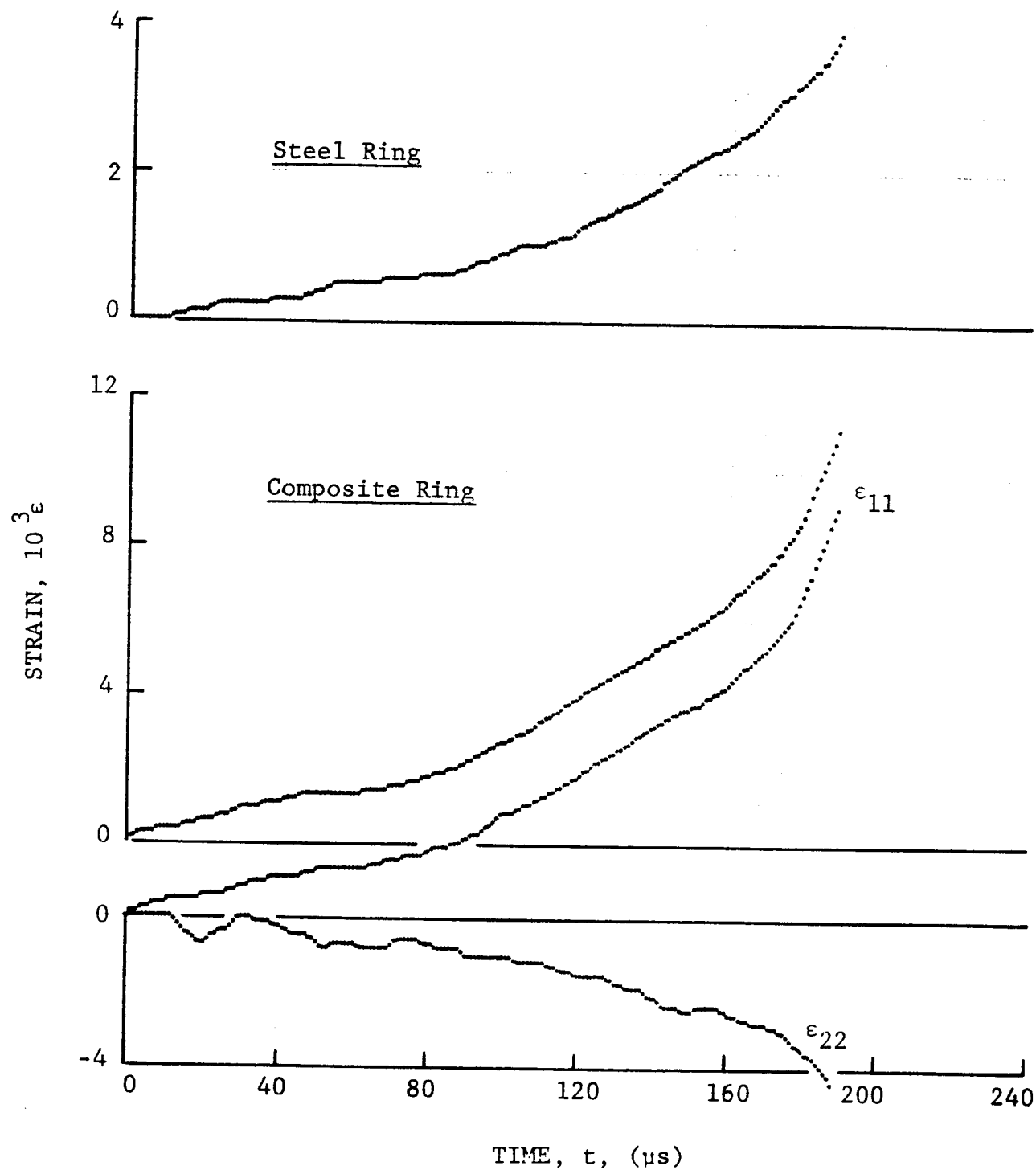


Figure 4-6. Strain records in steel ring and $[0_6]$ SP288/T300 graphite/epoxy ring under dynamic loading for Specimen 40-5 (650 mg pistol powder).

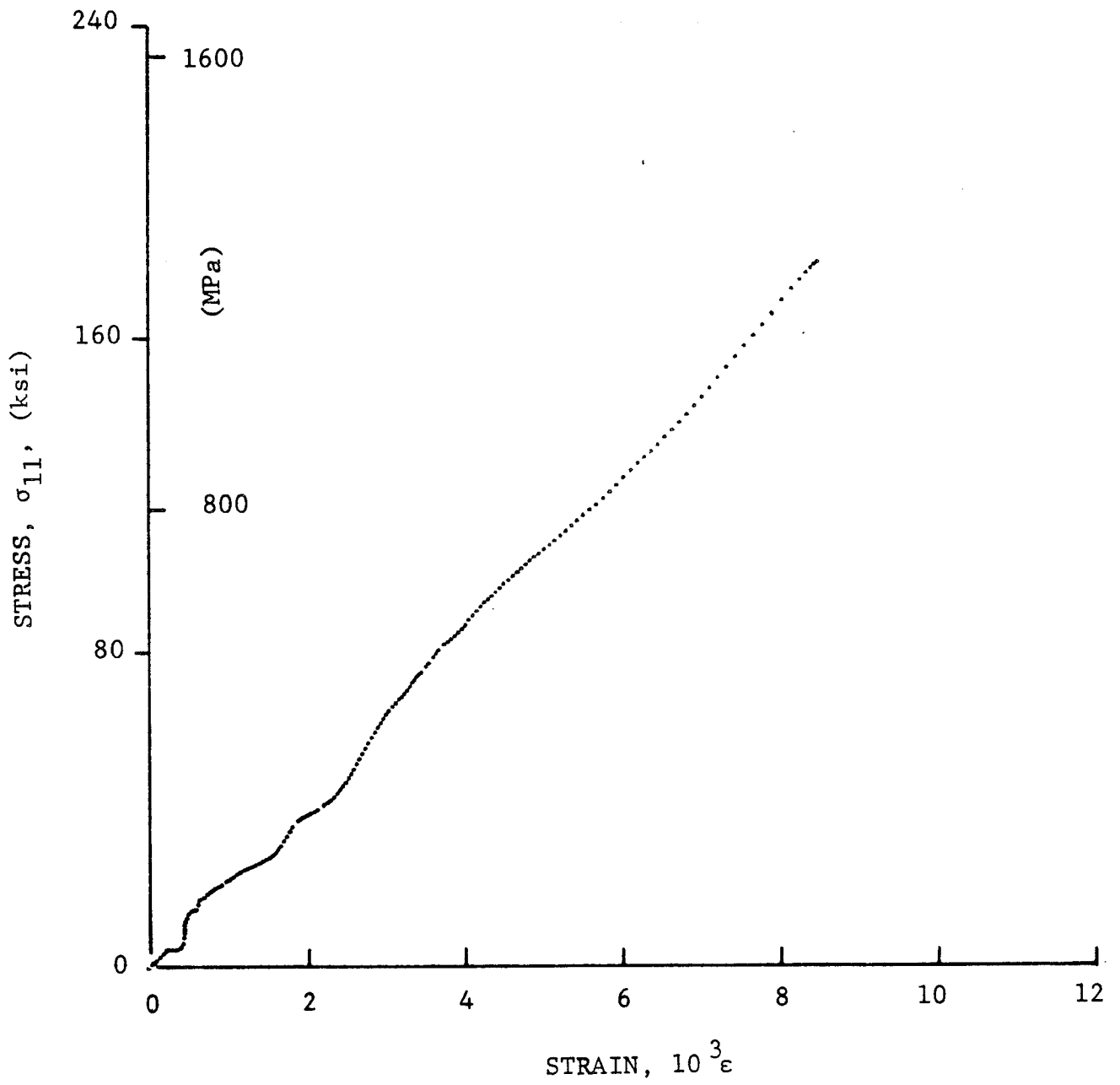


Figure 4-7. Stress-strain curve for dynamically loaded $[0_6]$ SP288/T300 graphite/epoxy ring, Specimen 40-3 (650 mg pistol powder).

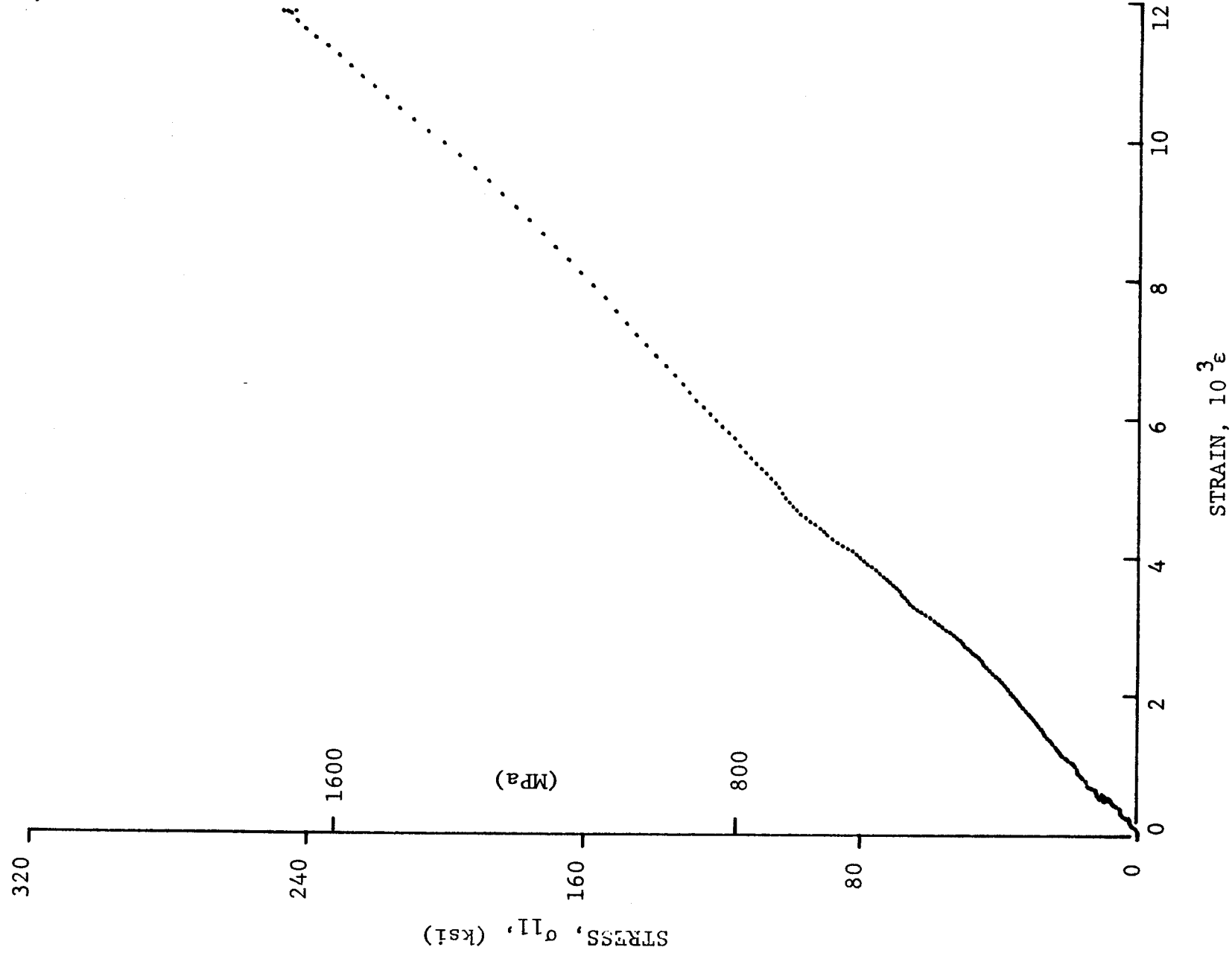


Figure 4-8. Stress-strain curve for dynamically loaded [O₆] SP288/T300 graphite/epoxy ring, Specimen 40-4 (650 mg pistol powder).

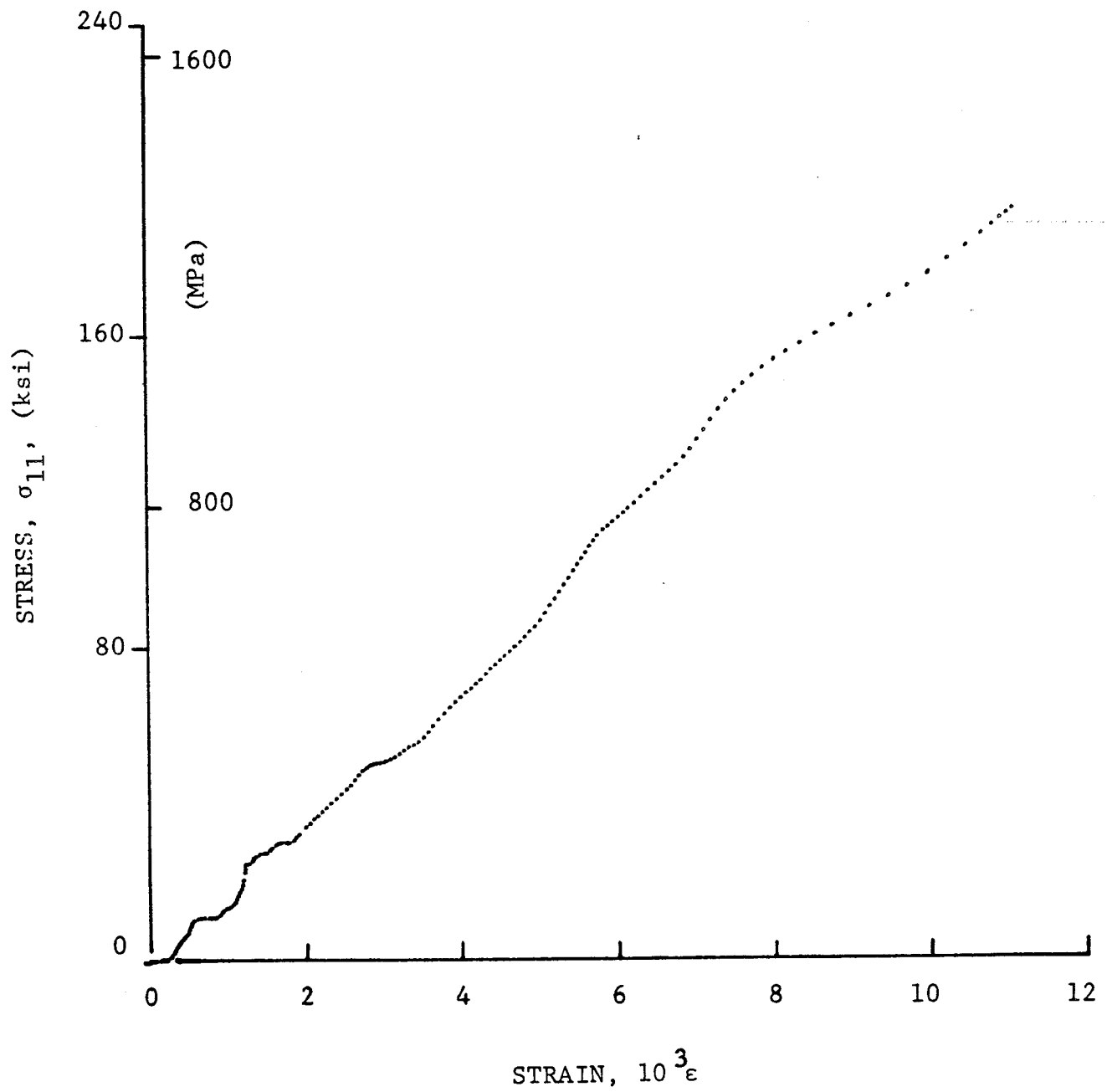


Figure 4-9. Stress-strain curve for dynamically loaded $[0_6]$ SP288/T300 graphite/epoxy ring, Specimen 40-5 (650 mg pistol powder).

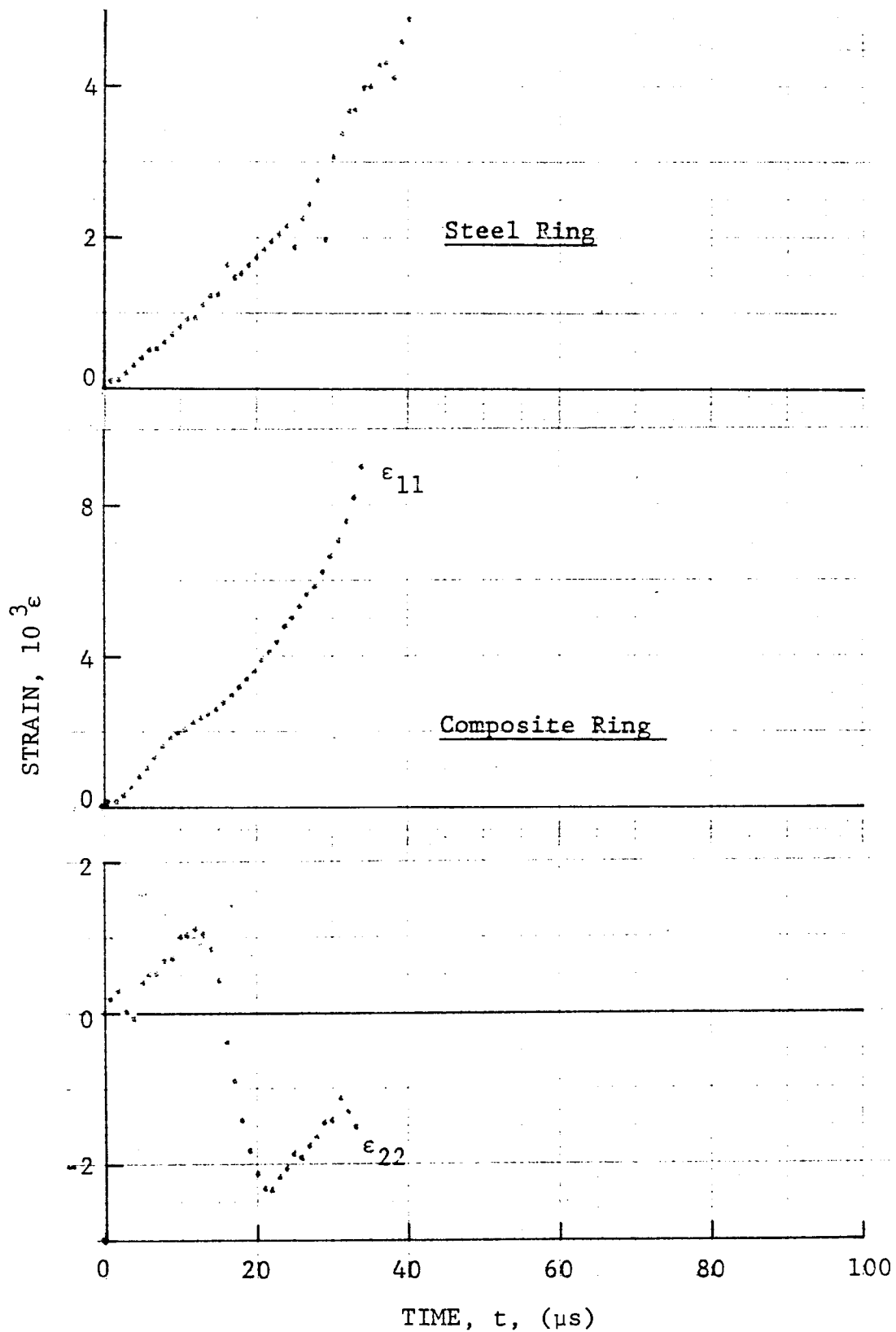


Figure 4-10. Strain records in steel ring and [0₆] SP288/T300 graphite/epoxy ring under dynamic loading for Specimen 19-4 (two 100 mg PETN detonators).

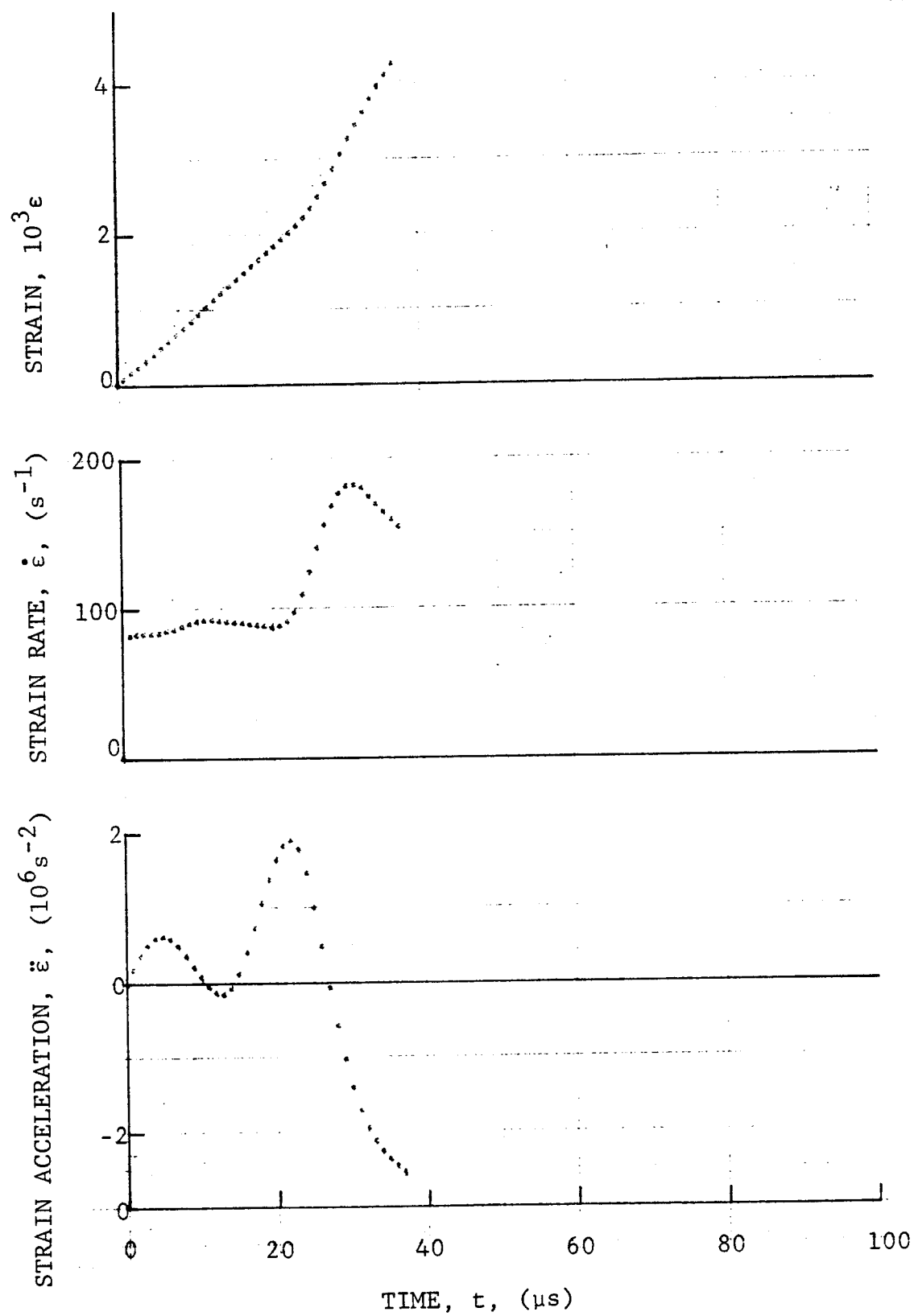
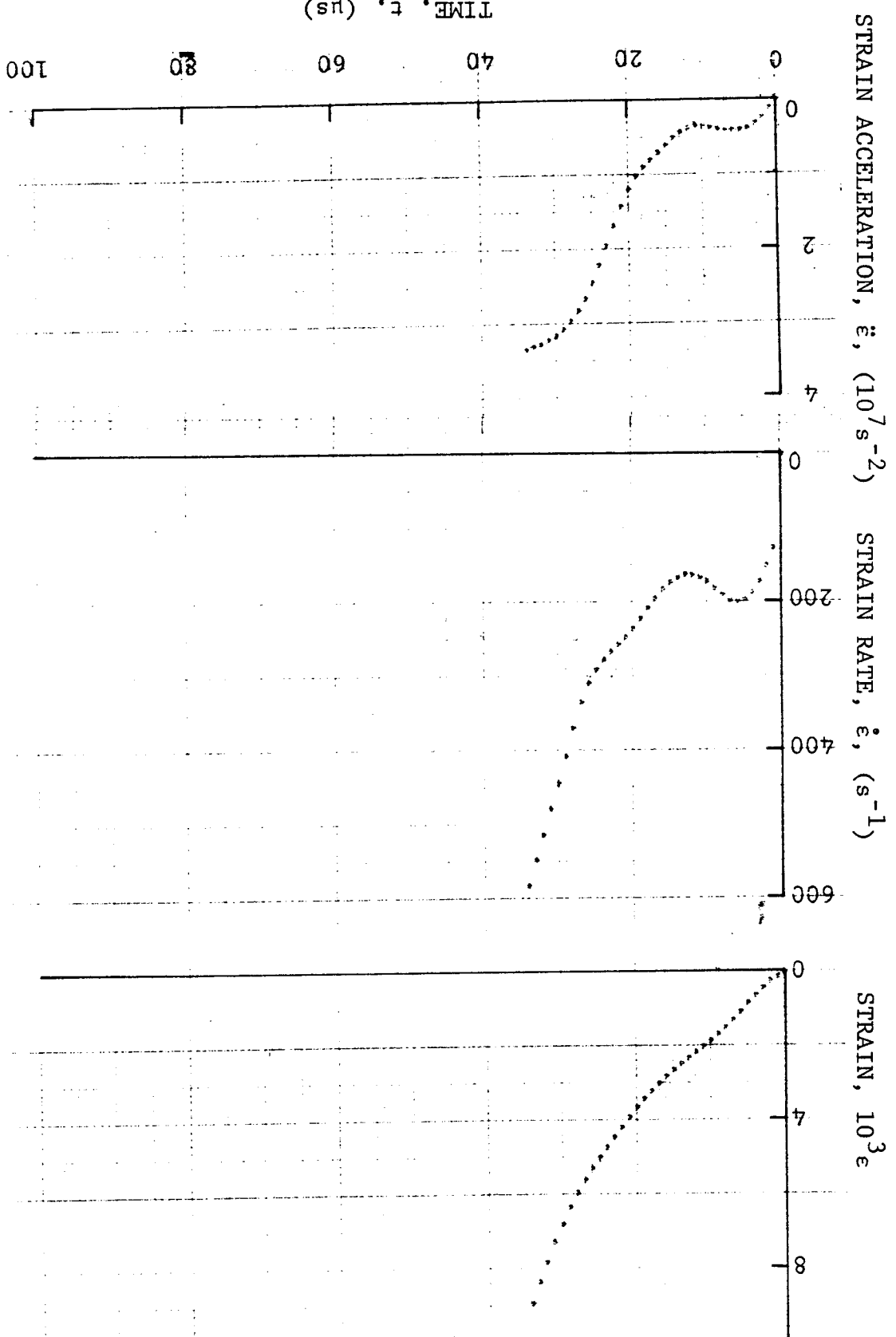


Figure 4-11. Strain and its derivatives in steel ring for Specimen 19-4.

Figure 4-12. Circumferential strain and its derivatives for [0₆] SP288/T300 graphite/epoxy ring under dynamic loading for Specimen 19-4.

4-69



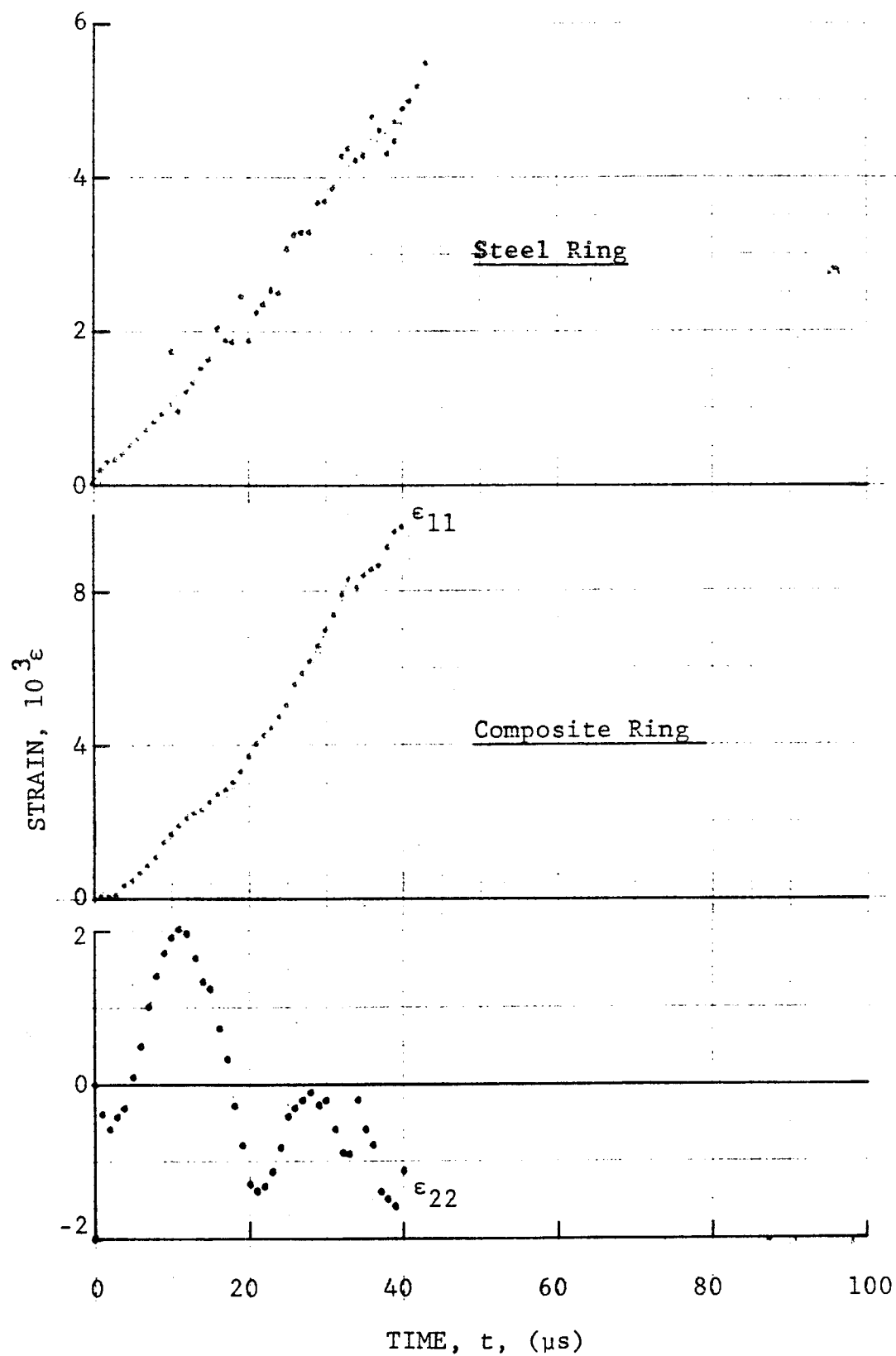


Figure 4-13. Strain records in steel ring and [0₆] SP288/T300 graphite/epoxy ring under dynamic loading for Specimen 19-5 (two 100 mg PETN detonators).

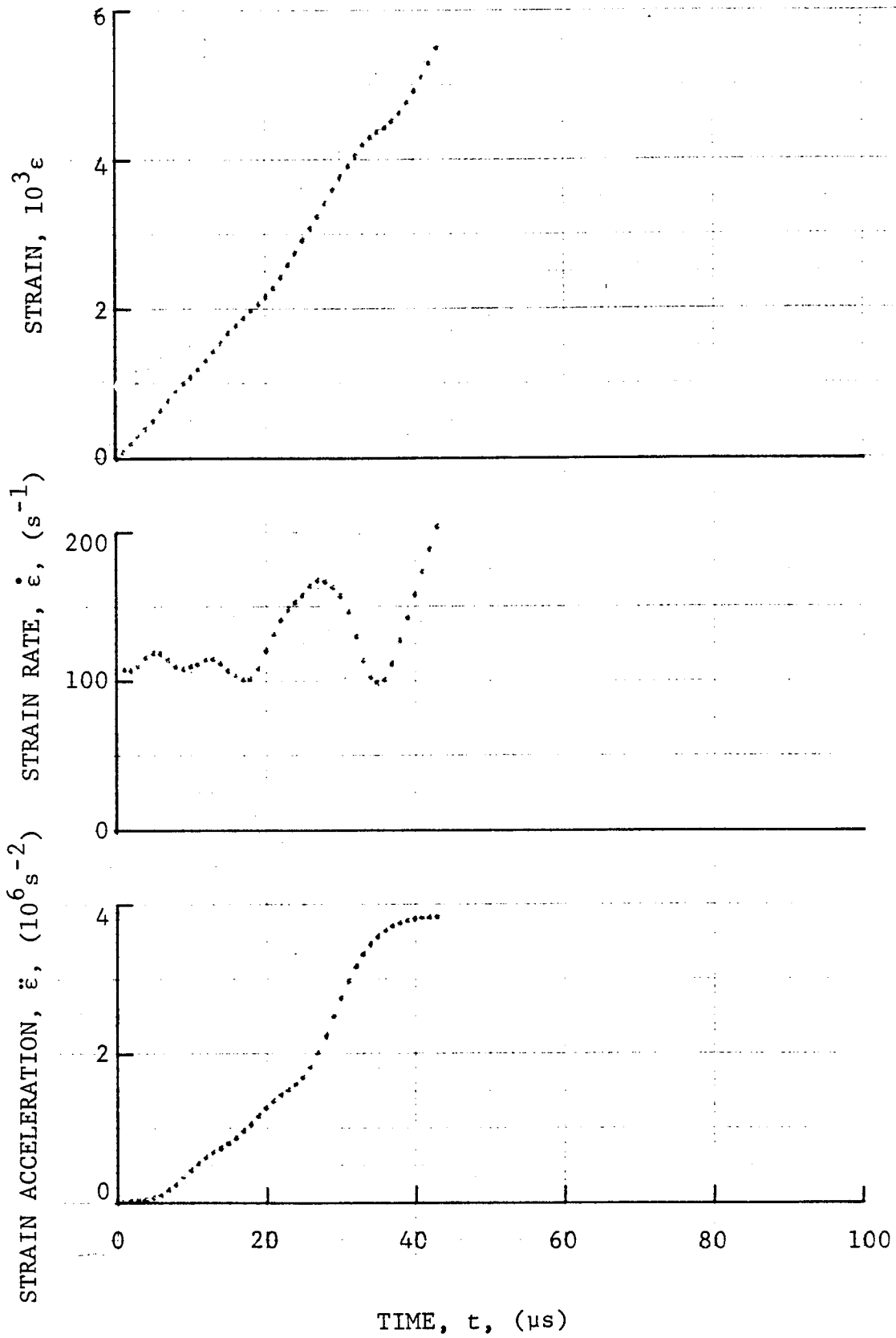


Figure 4-14. Strains and its derivatives in steel ring for Specimen 19-5.

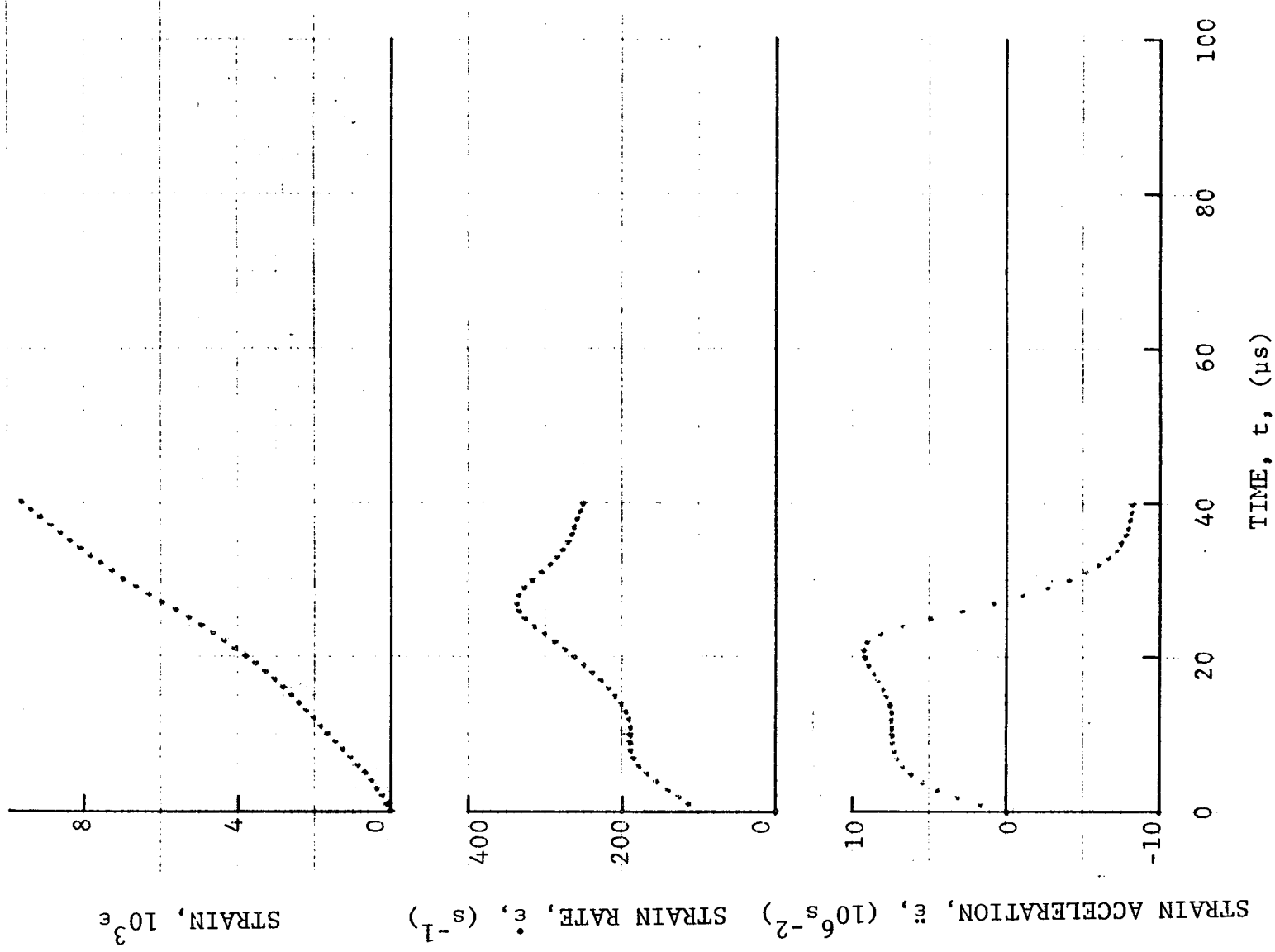


Figure 4-15. Circumferential strain and its derivatives for $[0_6]$ SP288/T300 graphite/epoxy ring under dynamic loading for Specimen 19-5.

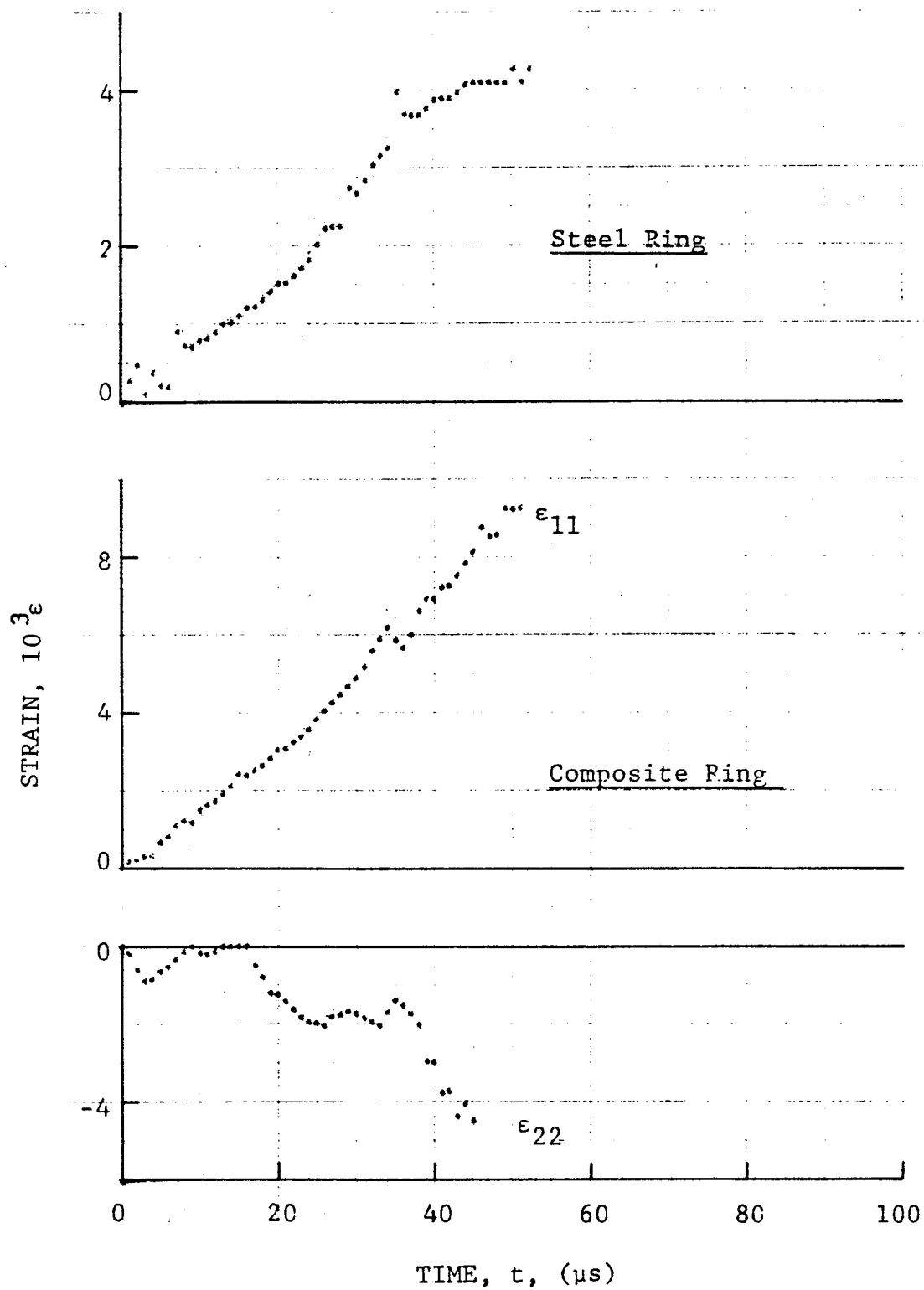
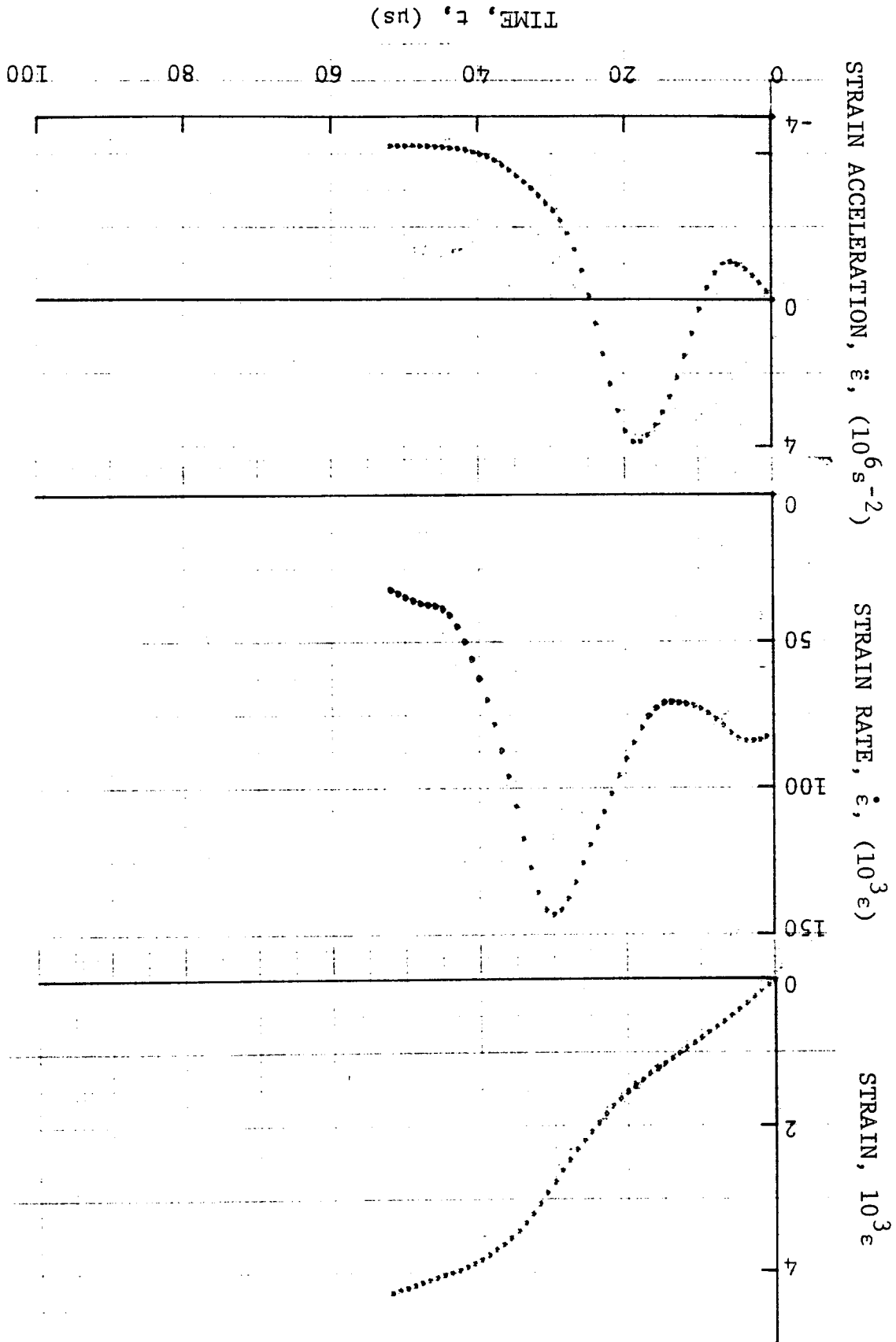


Figure 4-16. Strain records in steel ring and $[0_6]$ SP288/T300 graphite/epoxy ring under dynamic loading for Specimen 19-6 (two 100 mg PETN detonators).

Figure 4-17. Strain and its derivatives in steel ring for Specimen 19-6.



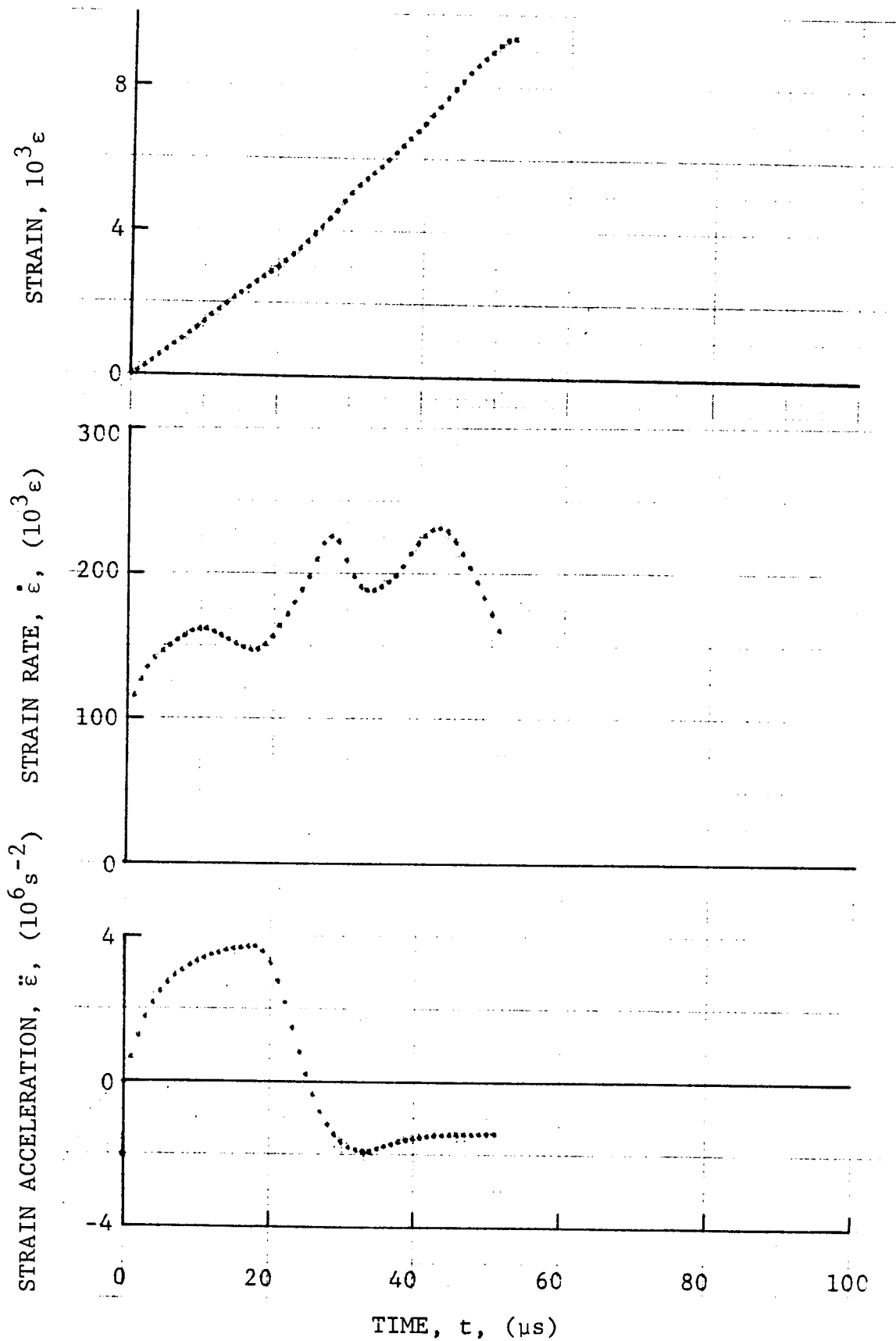
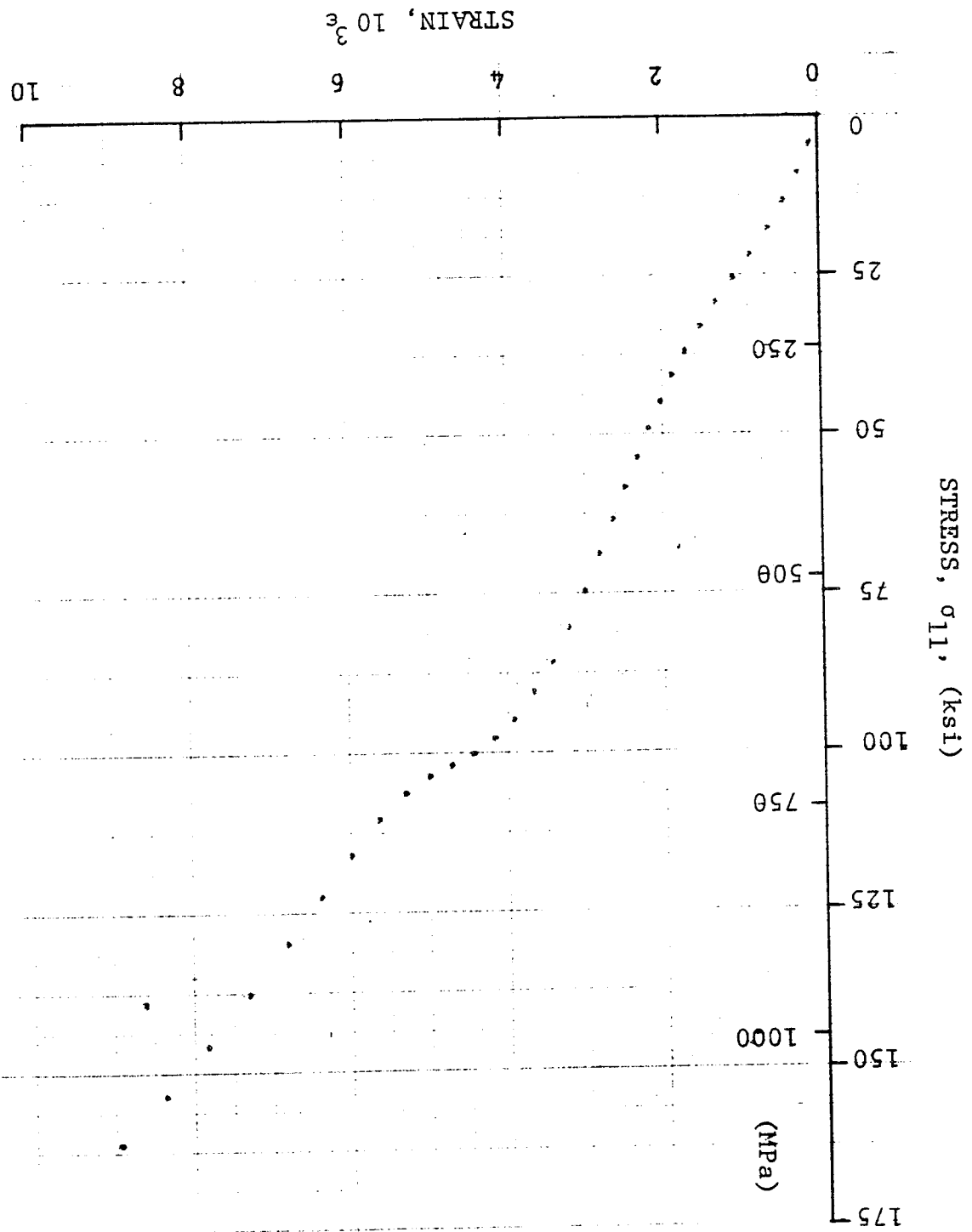


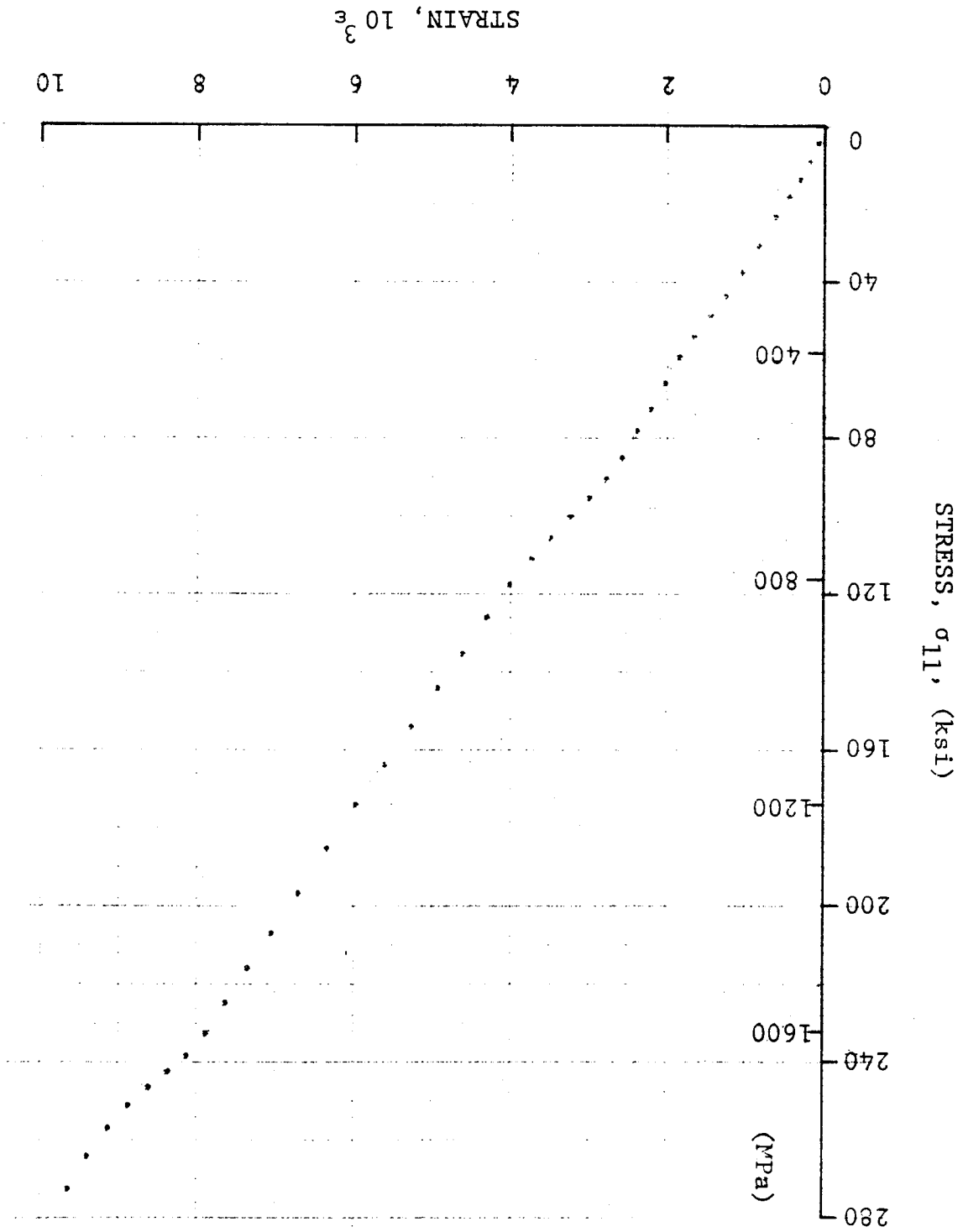
Figure 4-18. Circumferential strain and its derivatives for $[0_6]$ SP288/T300 graphite/epoxy ring under dynamic loading for Specimen 19-6.

Figure 4-19. Stress-strain curve for dynamically loaded [0₆] SP288/T300 graphite/epoxy ring, Specimen 19-4 (two 100 mg PETN detonators).



4-77

Figure 4-20. Stress-strain curve for dynamically loaded [0₆] SP288/T300 graphite/epoxy ring, Specimen 19-5 (two 100 mg PETN detonators).



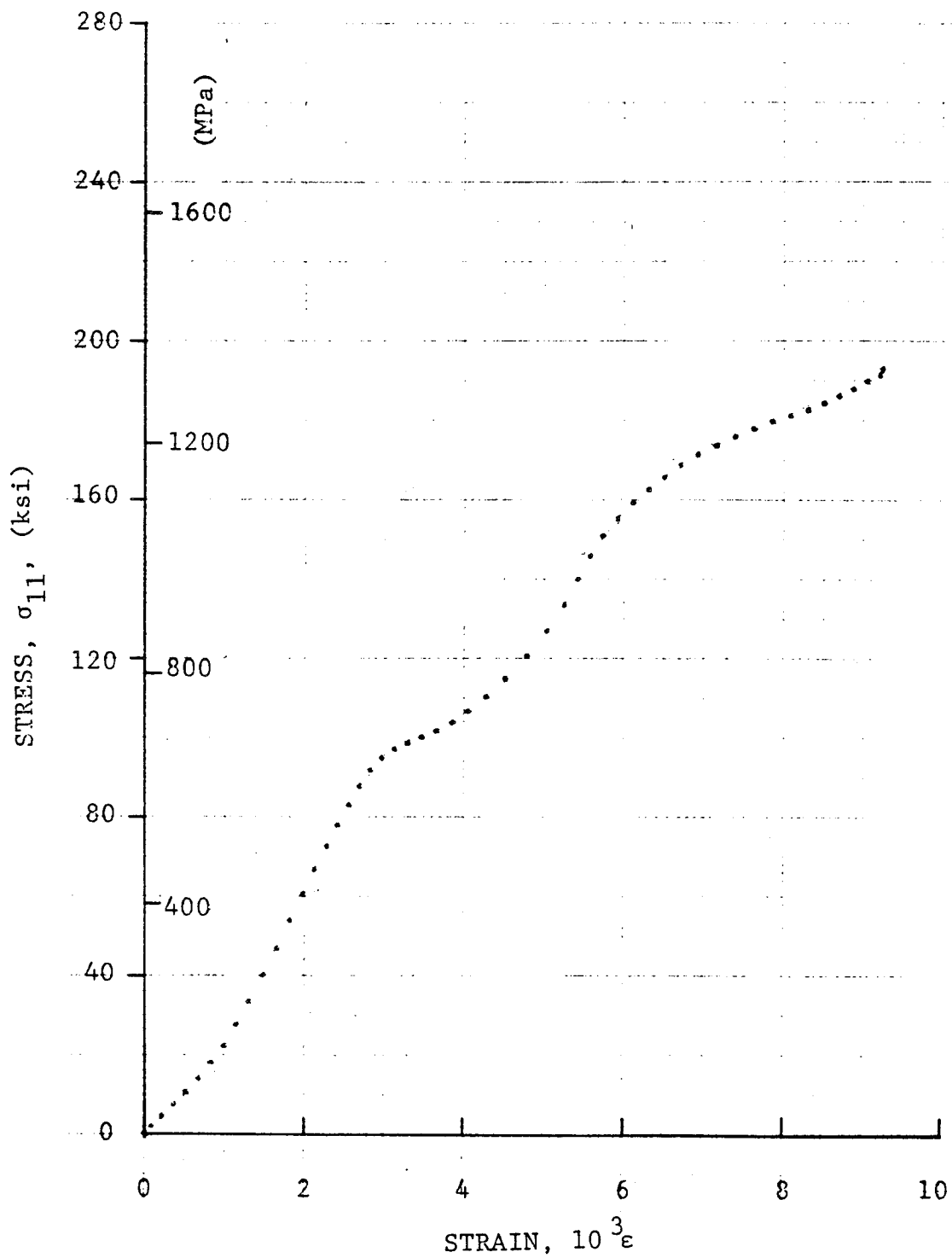


Figure 4-21. Stress-strain curve for dynamically loaded $[0_6]$ SP288/T300 graphite/epoxy ring, Specimen 19-6 (two 100 mg PETN detonators).

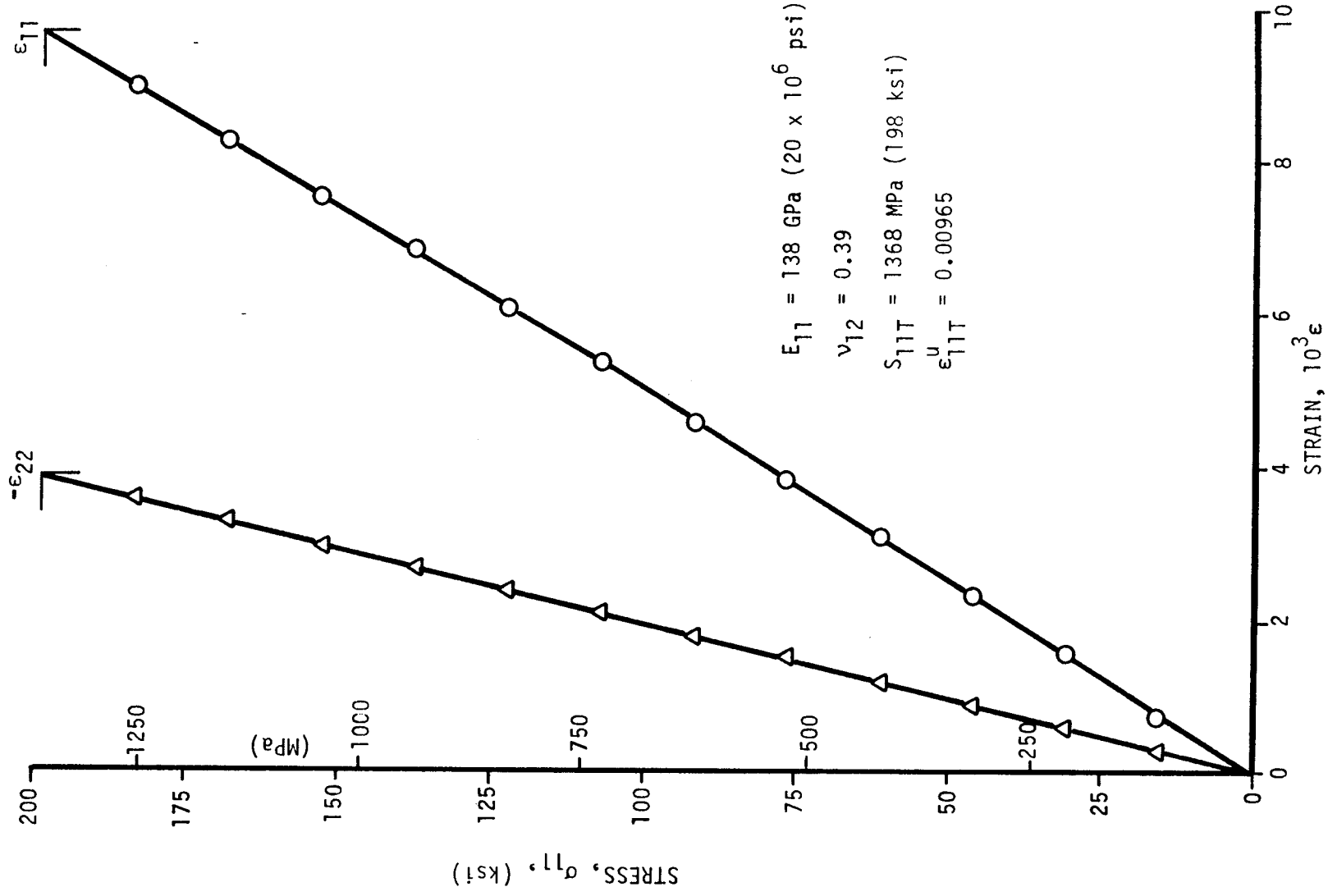


Figure 4-22. Strains in unidirectional 0-deg SP288/AS ring specimen under static tensile loading (Specimen No. 7-1).

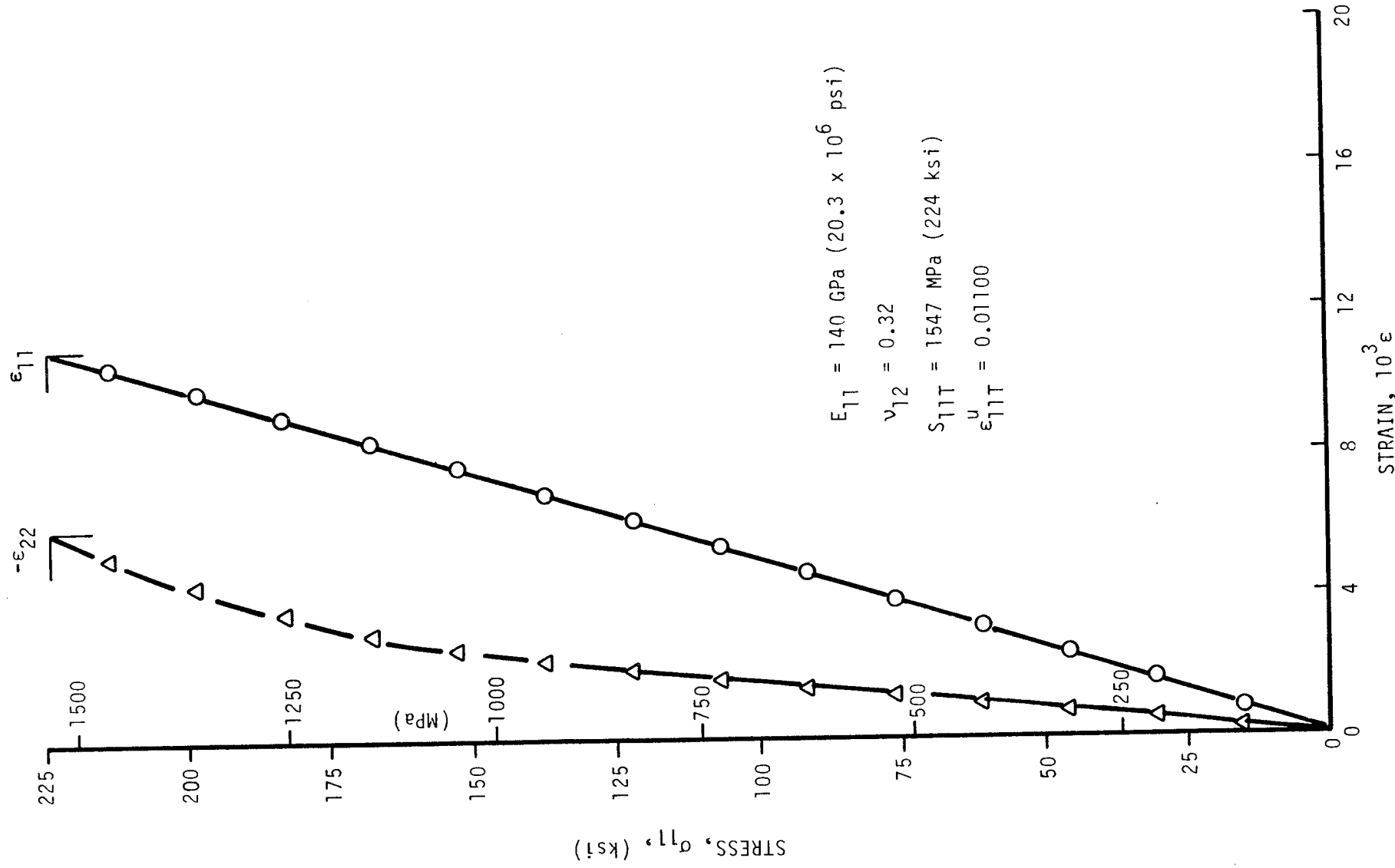


Figure 4-23. Strains in unidirectional 0-deg SP288/AS ring specimen under static tensile loading (Specimen No. 7-5).

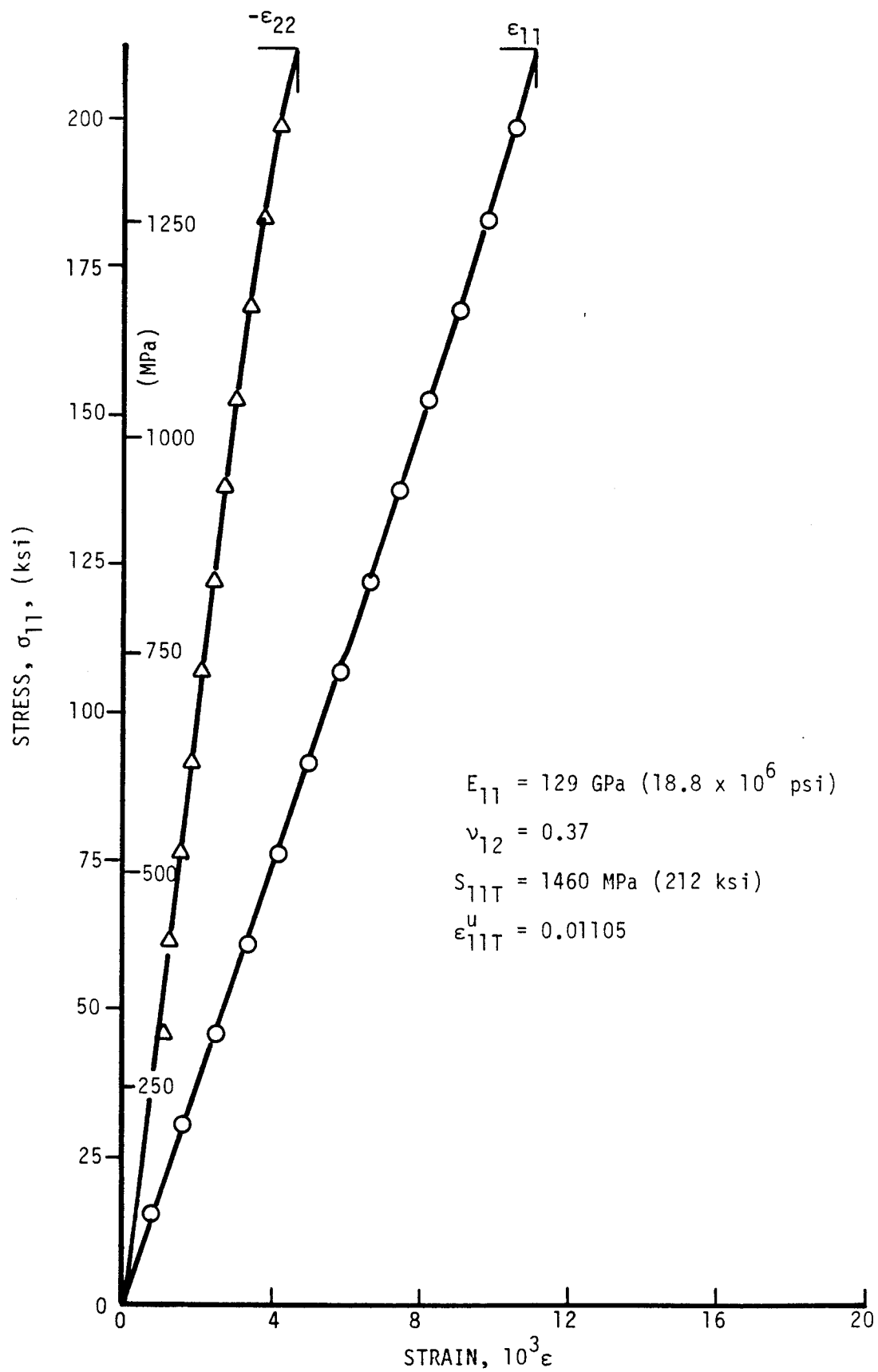


Figure 4-24. Strains in unidirectional 0-deg SP288/AS ring specimen under static tensile loading (Specimen No. 7-10).

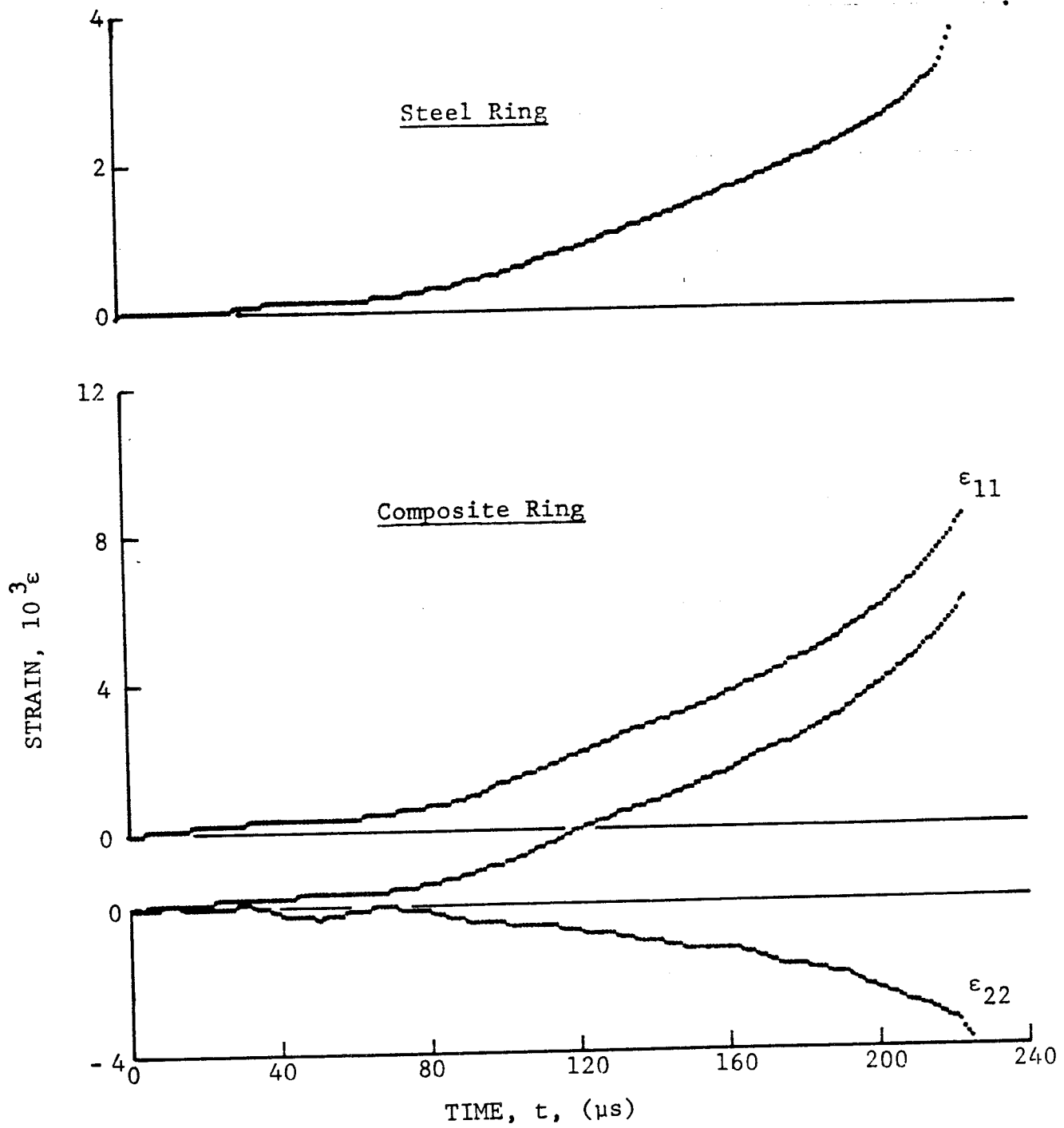


Figure 4-25. Strain records in steel ring and [0₆] SP288/AS graphite/epoxy ring under dynamic loading for Specimen 45-9 (650 mg pistol powder).

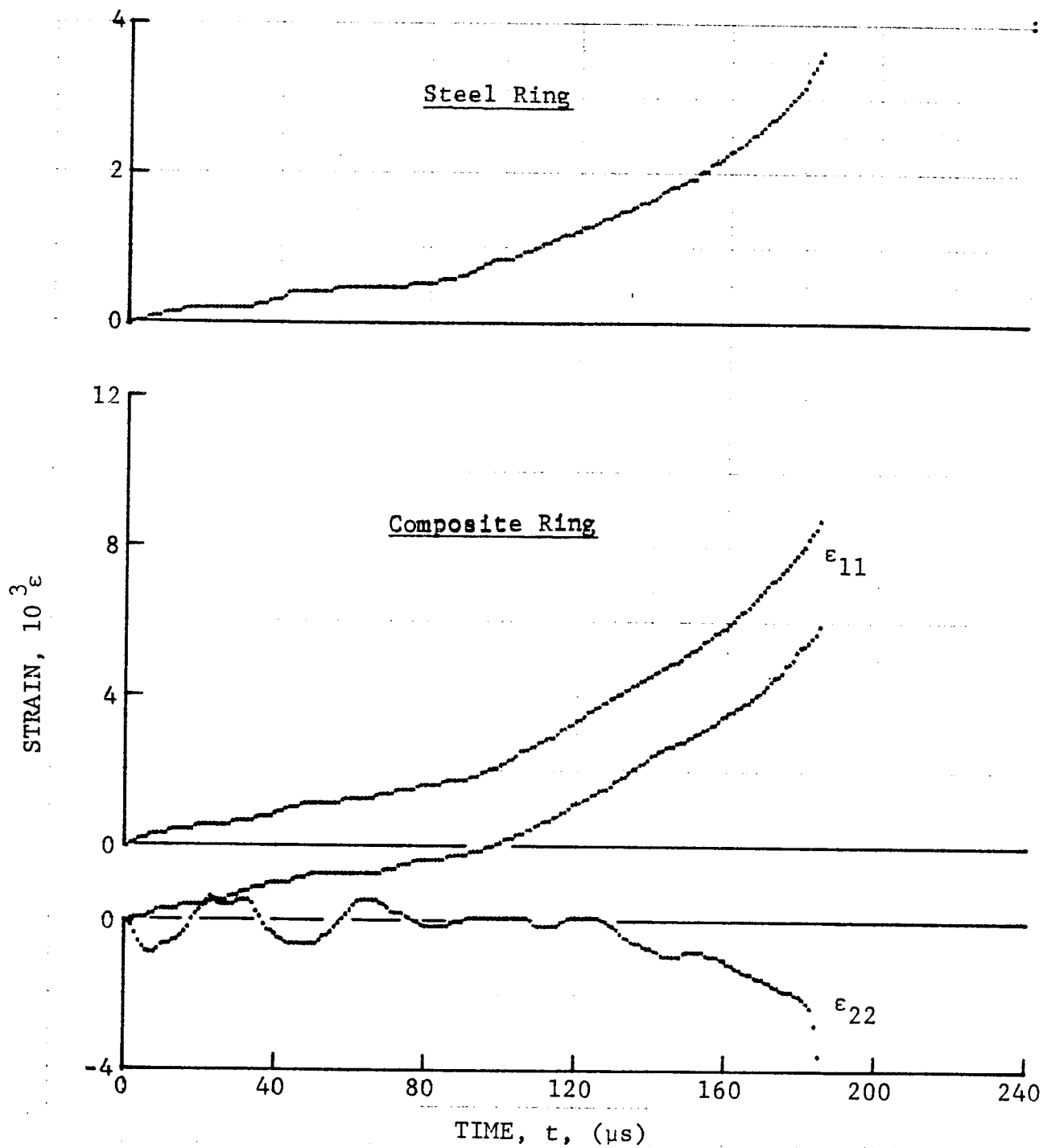


Figure 4-26. Strain records in steel ring and $[0_6]$ SP288/AS graphite/epoxy ring under dynamic loading for Specimen 45-10 (650 mg pistol powder).

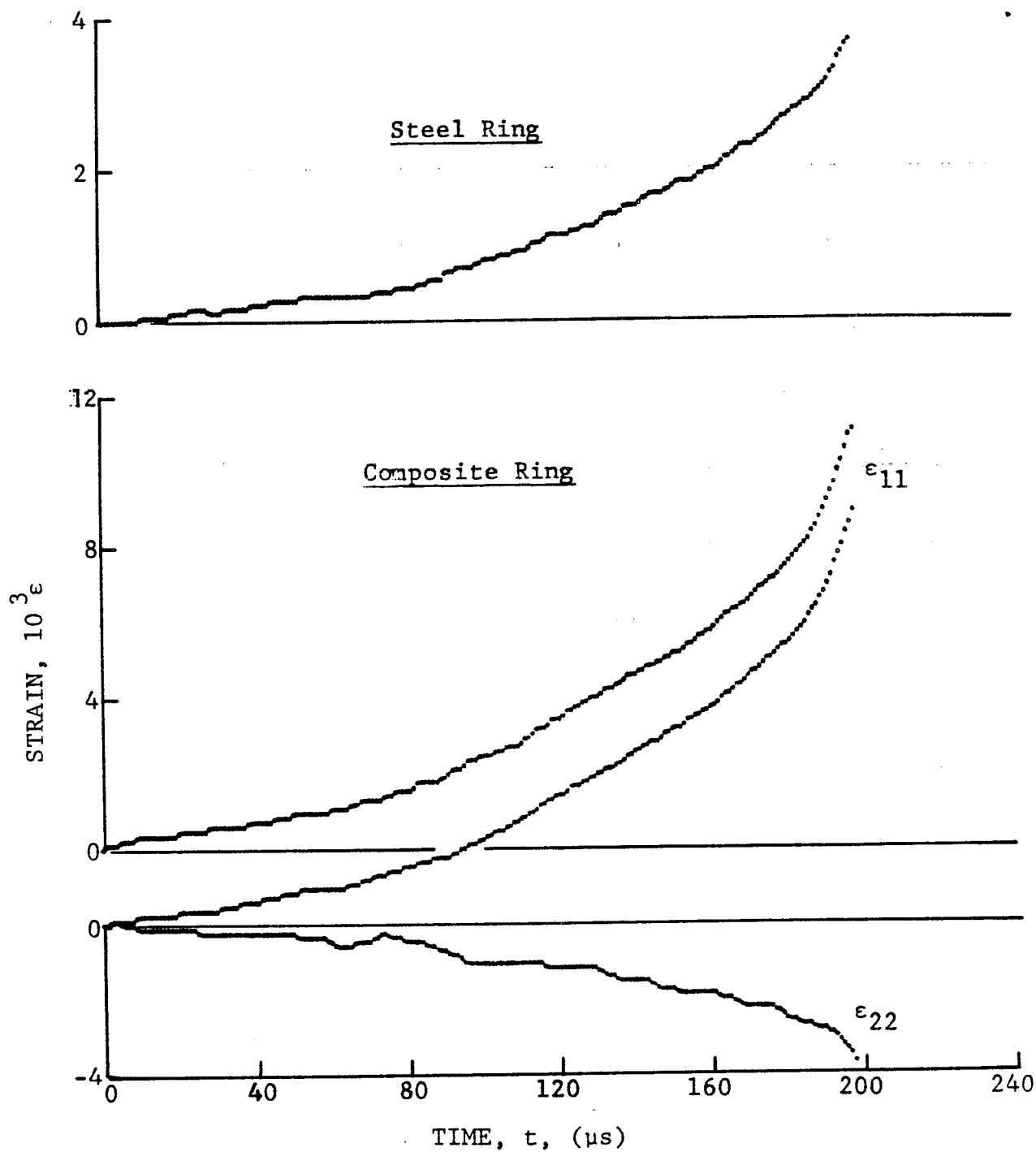


Figure 4-27. Strain records in steel ring and $[0_6]$ SP288/AS graphite/epoxy ring under dynamic loading for Specimen 45-11 (650 mg pistol powder).

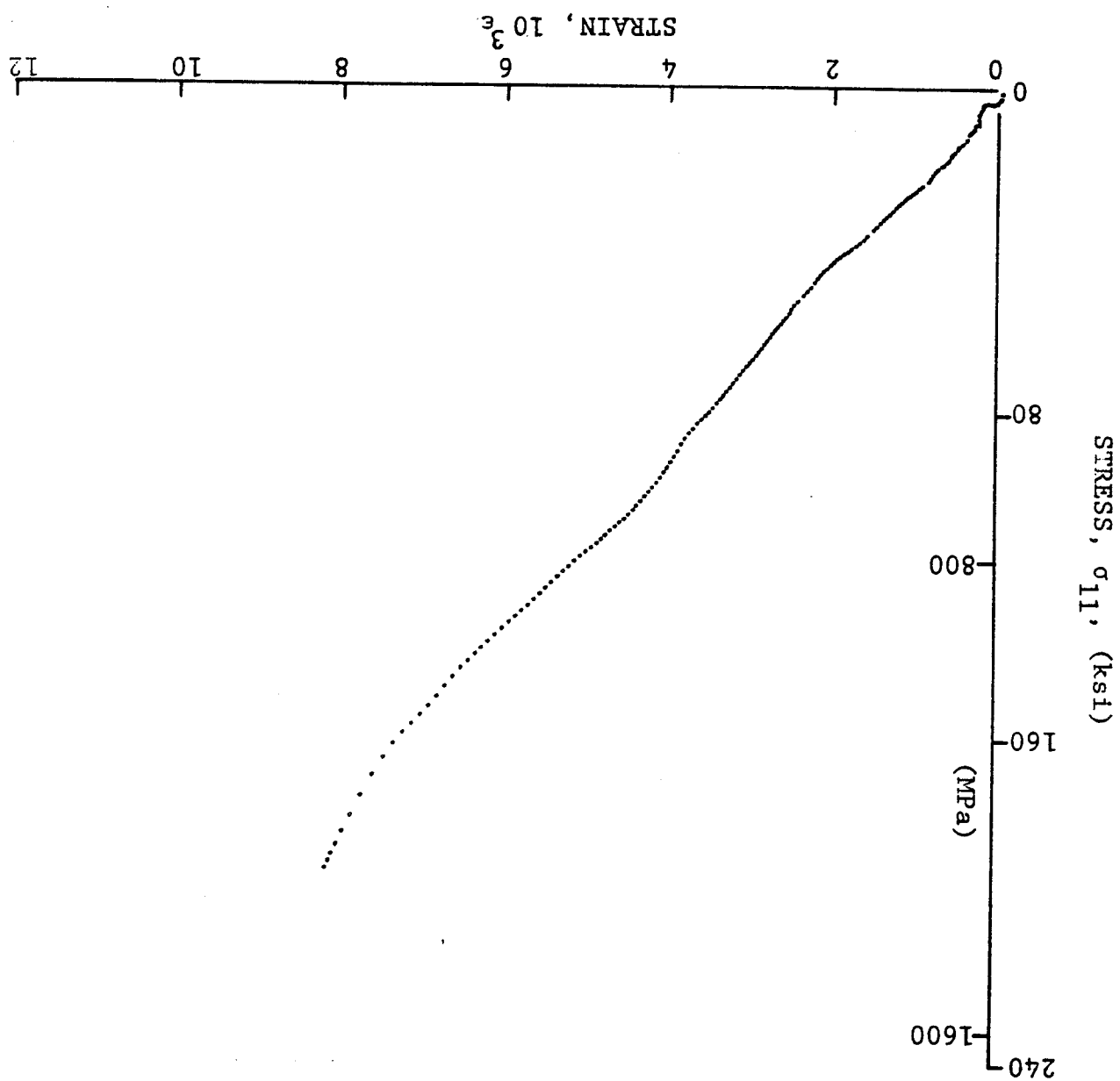


Figure 4-28. Stress-strain curve for dynamically loaded $[0_6]$ SP288/AS graphite/epoxy ring, Specimen 45-9 (650 mg pistol powder).

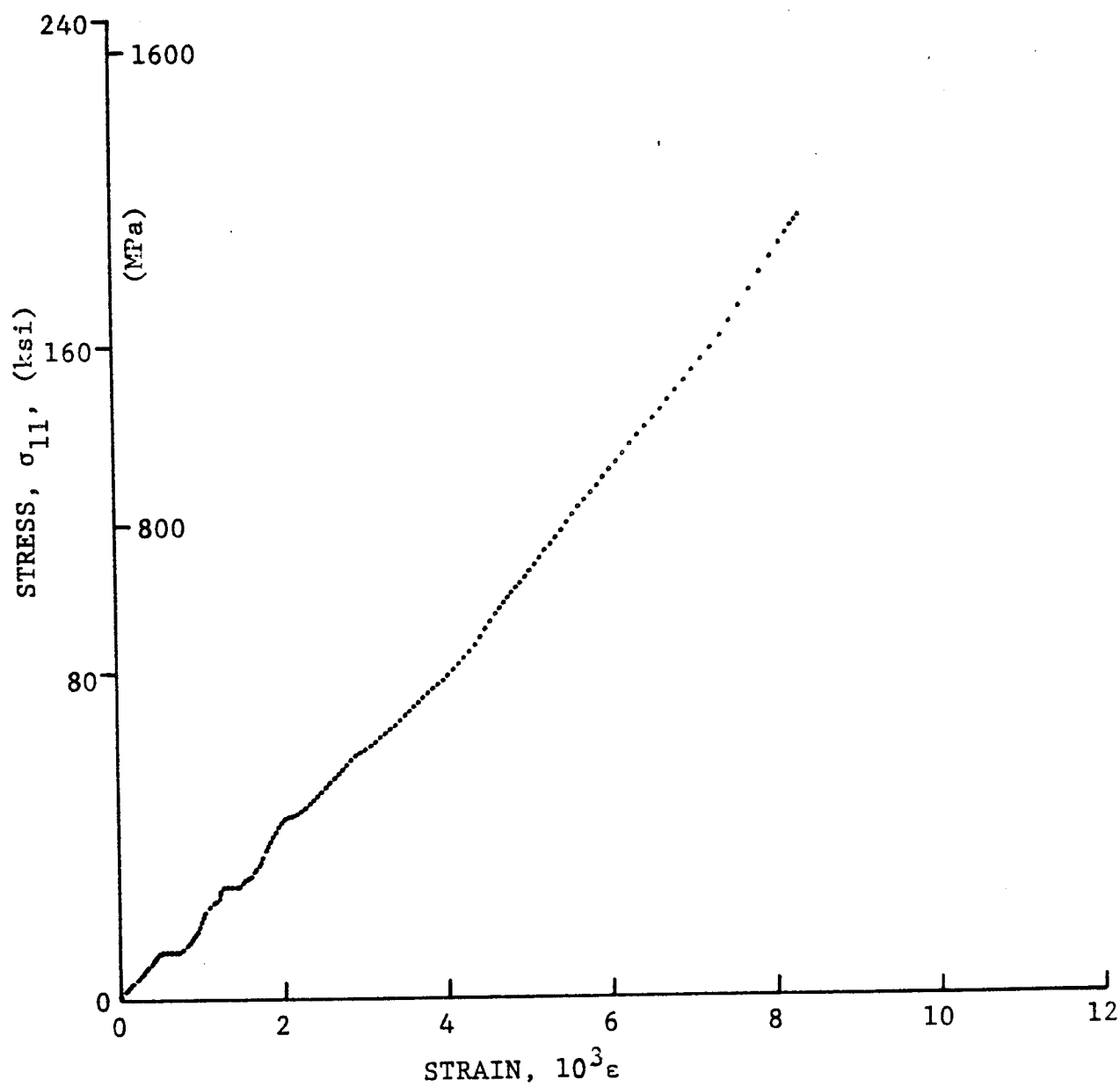


Figure 4-29. Stress-strain curve for dynamically loaded $[0_6]$ SP288/AS graphite/epoxy ring, Specimen 45-10 (650 mg pistol powder).

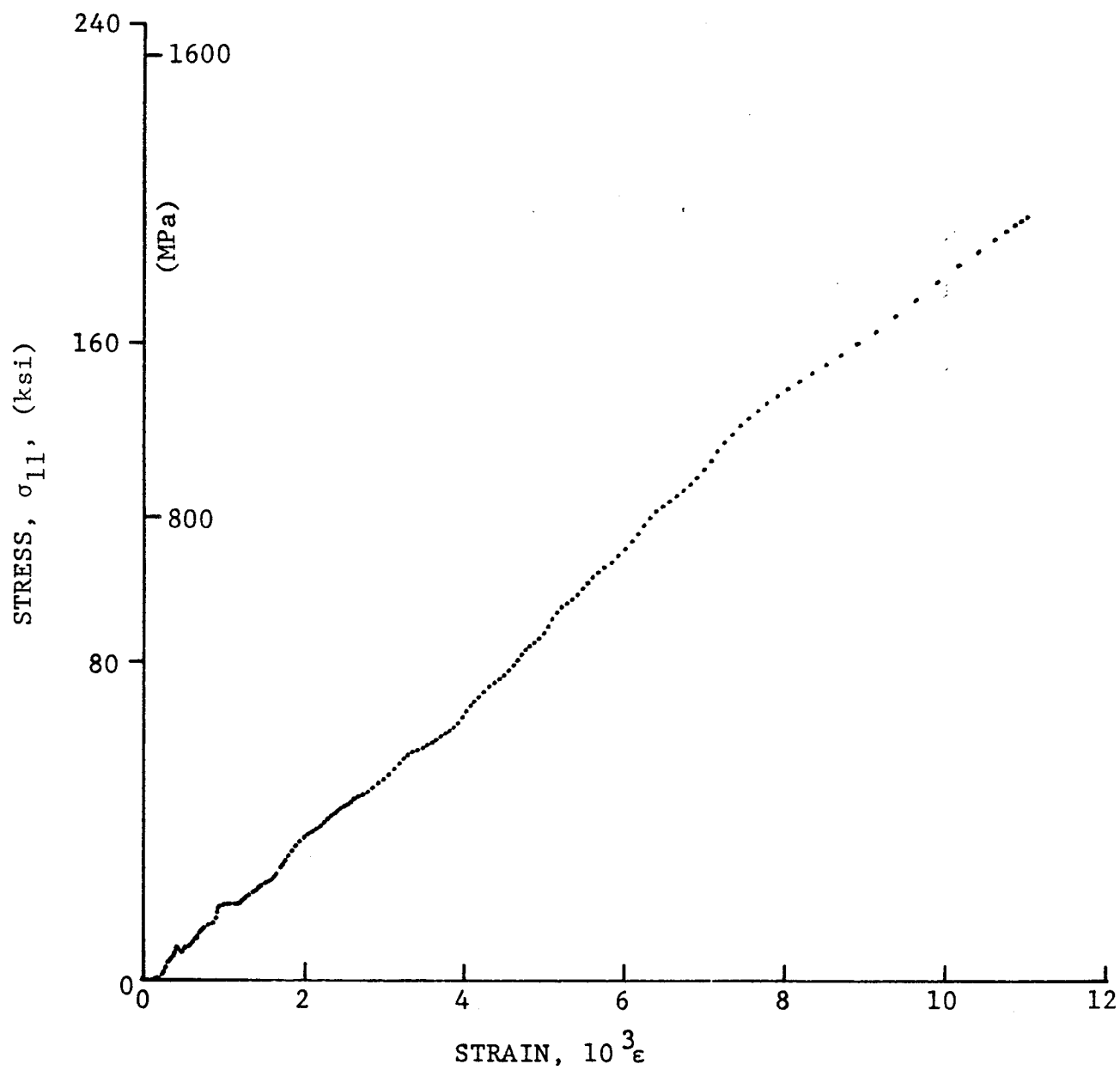


Figure 4-30. Stress-strain curve for dynamically loaded $[0_6]$ SP288/AS graphite/epoxy ring, Specimen 45-11 (650 mg pistol powder).

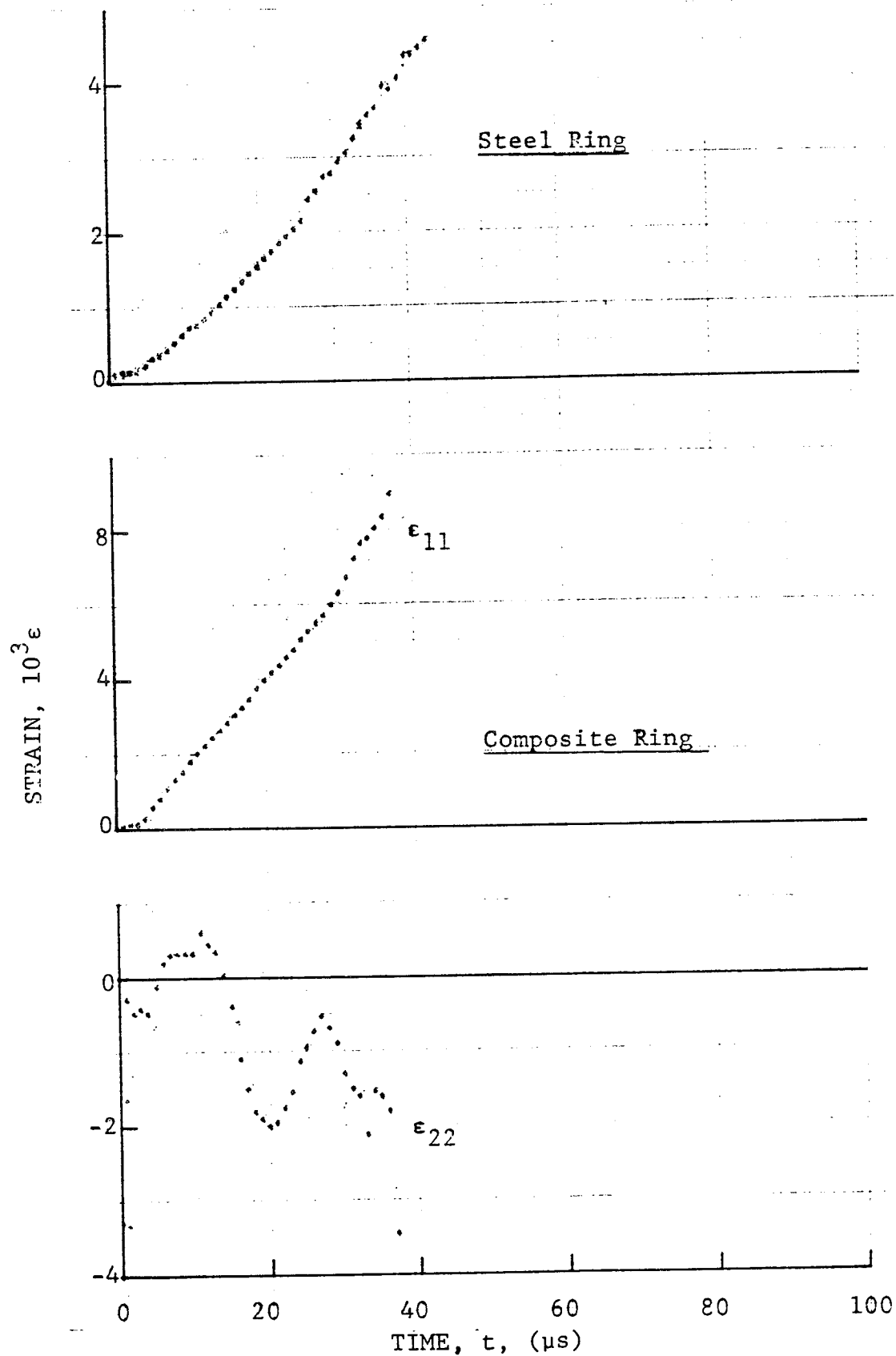


Figure 4-31. Strain records in steel ring and $[0_6]$ SP288/AS graphite/epoxy ring under dynamic loading for Specimen 7-6 (two 100 mg PETN detonators).

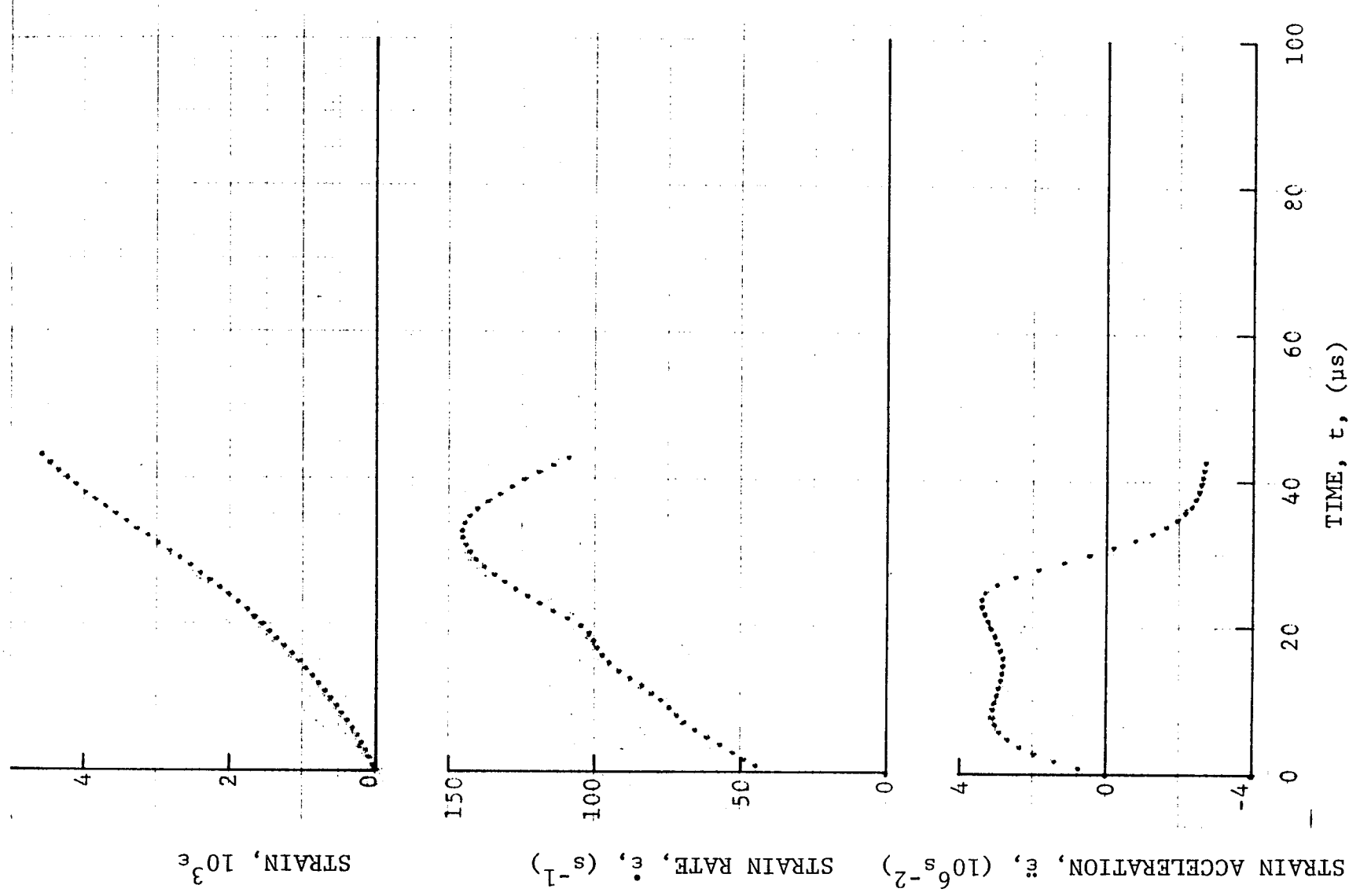


Figure 4-32. Strain and its derivatives in steel ring for Specimen 7-6.

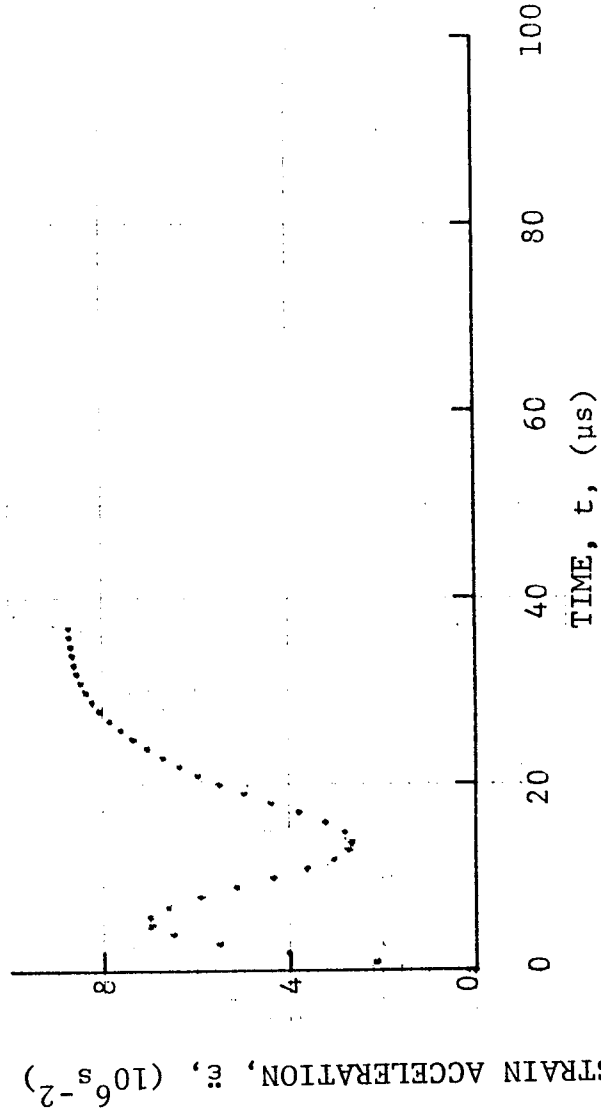
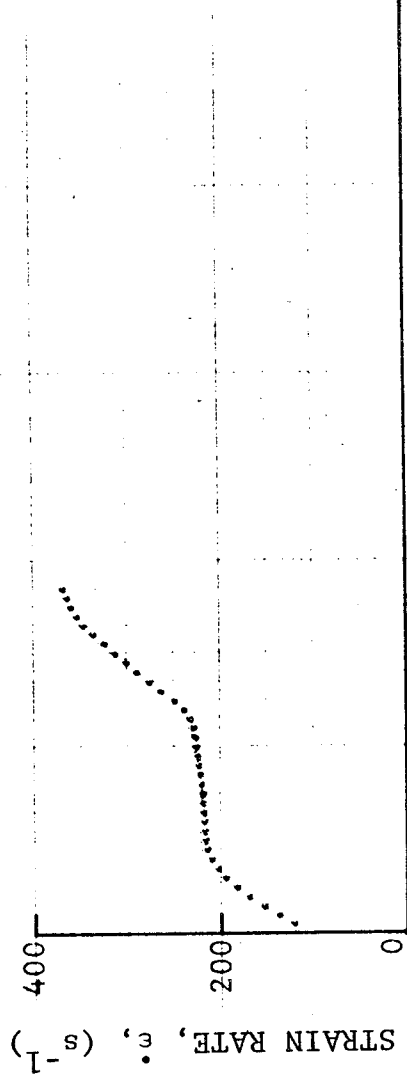
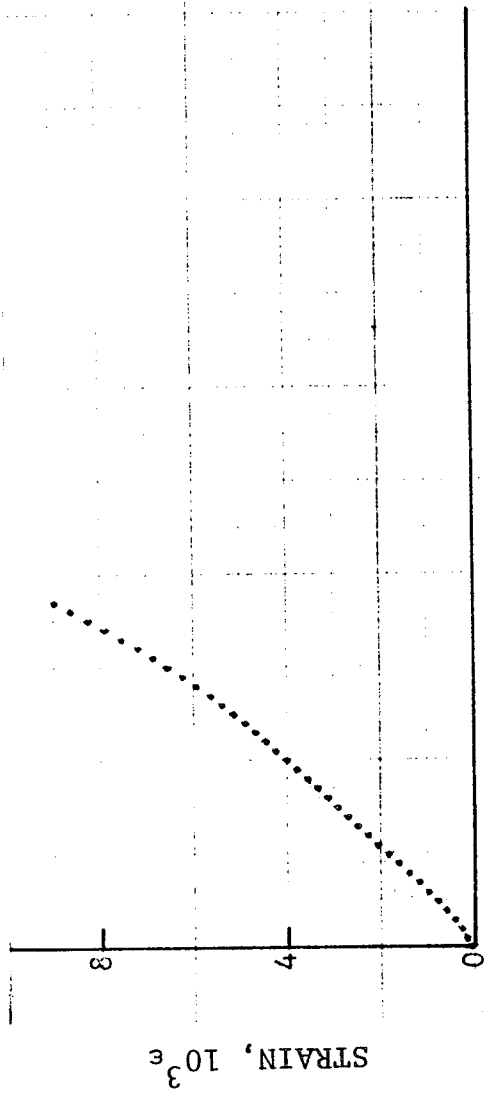


Figure 4-33. Circumferential strain and its derivatives for [0₆] SP288/AS graphite/epoxy ring under dynamic loading for Specimen 7-6.

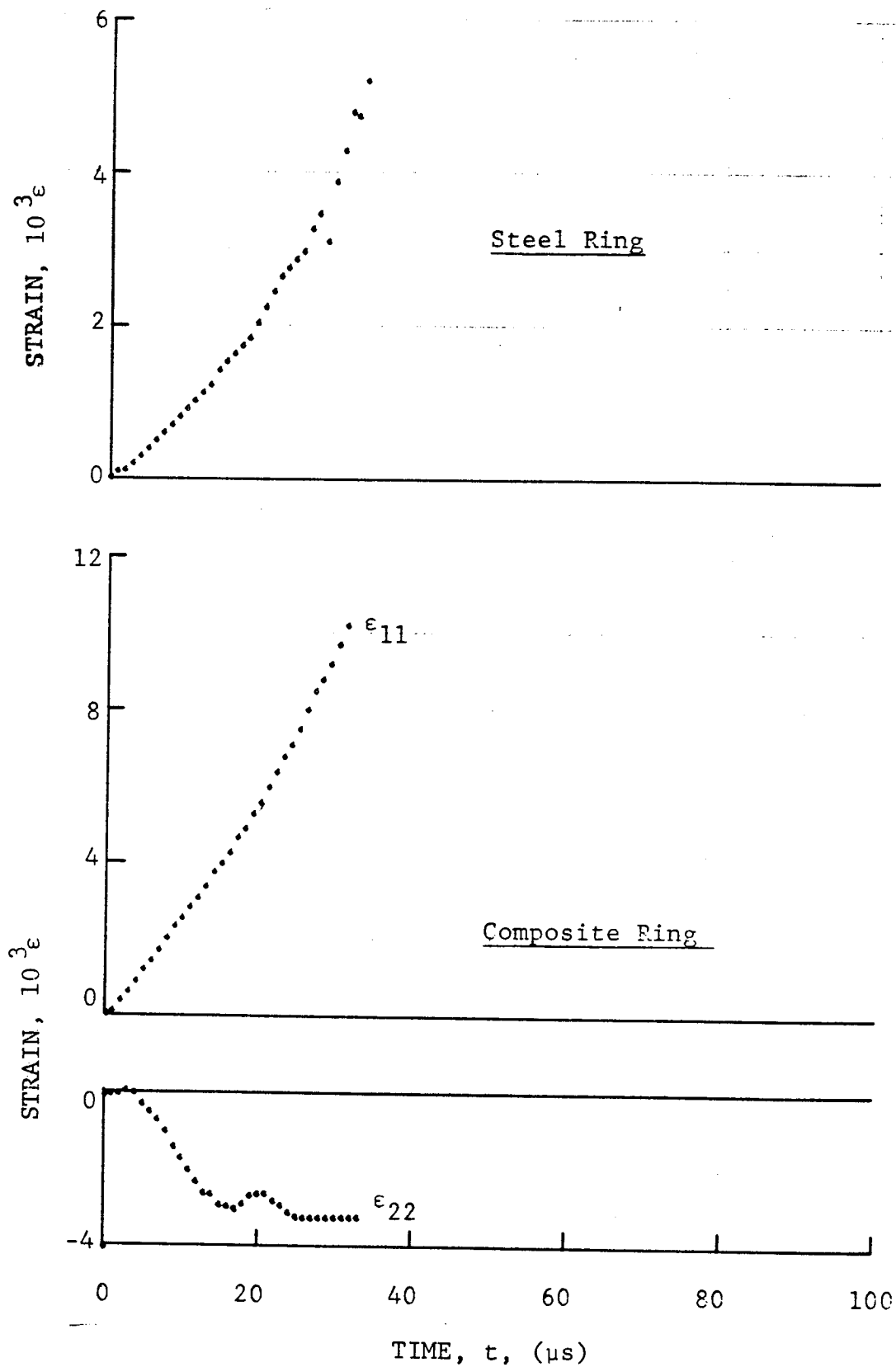


Figure 4-34. Strain records in steel ring and [0₆] SP288/AS graphite/epoxy ring under dynamic loading for Specimen 7-7 (330 mg PETN detonator).

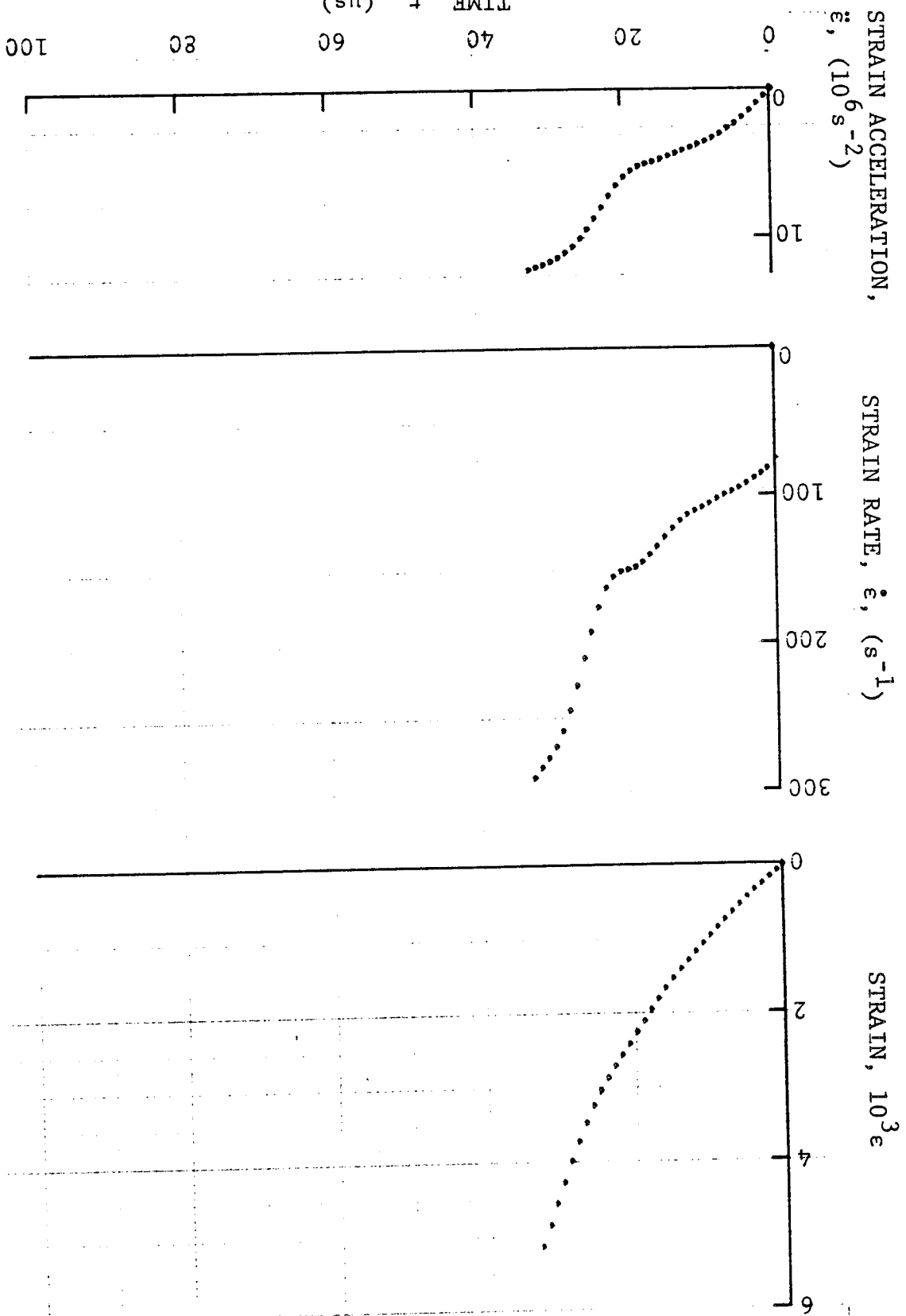


Figure 4-35. Strain and its derivatives in steel ring for Specimen 7-7.

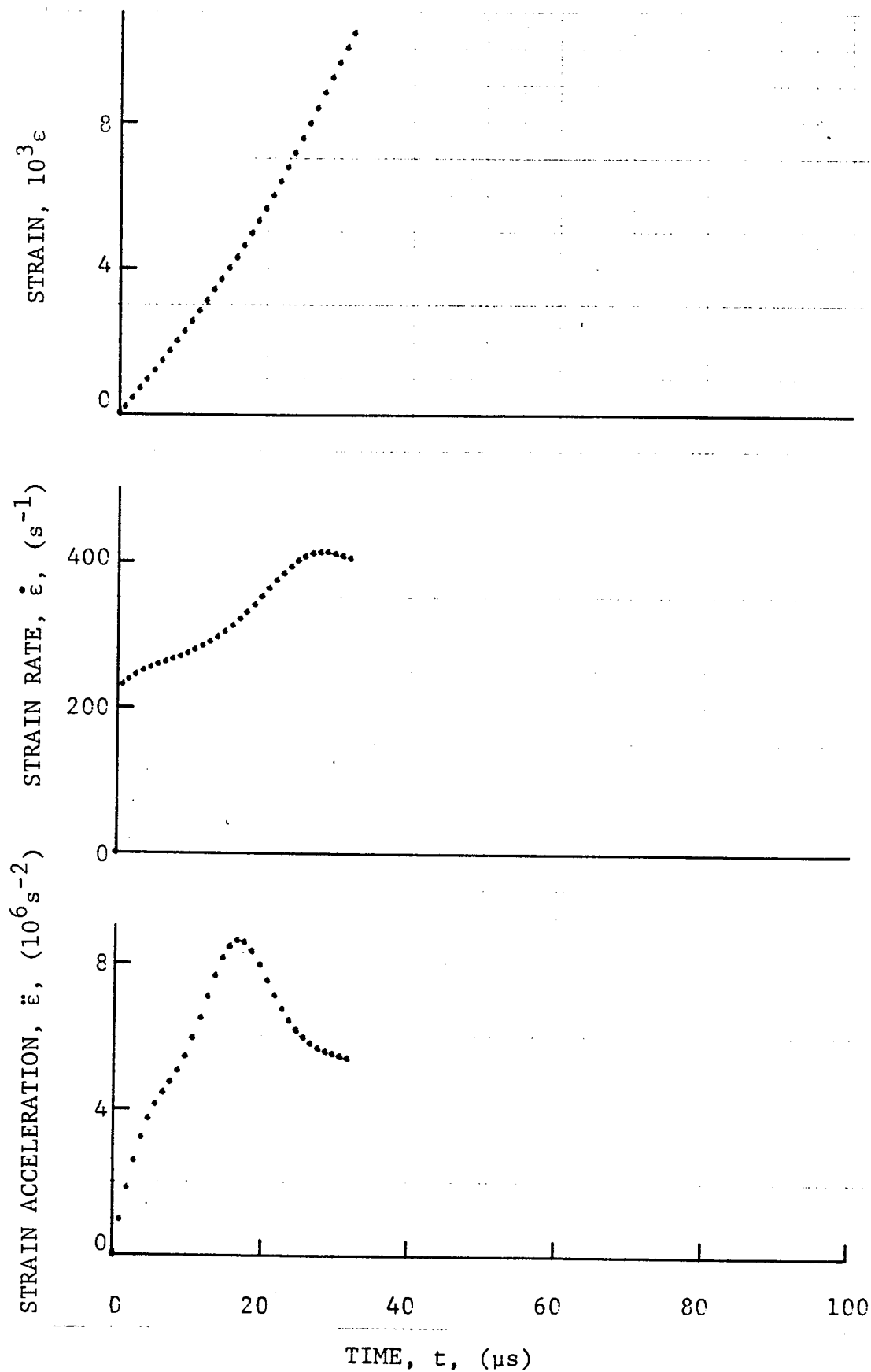


Figure 4-36. Circumferential strain and its derivatives for $[0_6]$ SP288/AS graphite/epoxy ring under dynamic loading for Specimen 7-6.

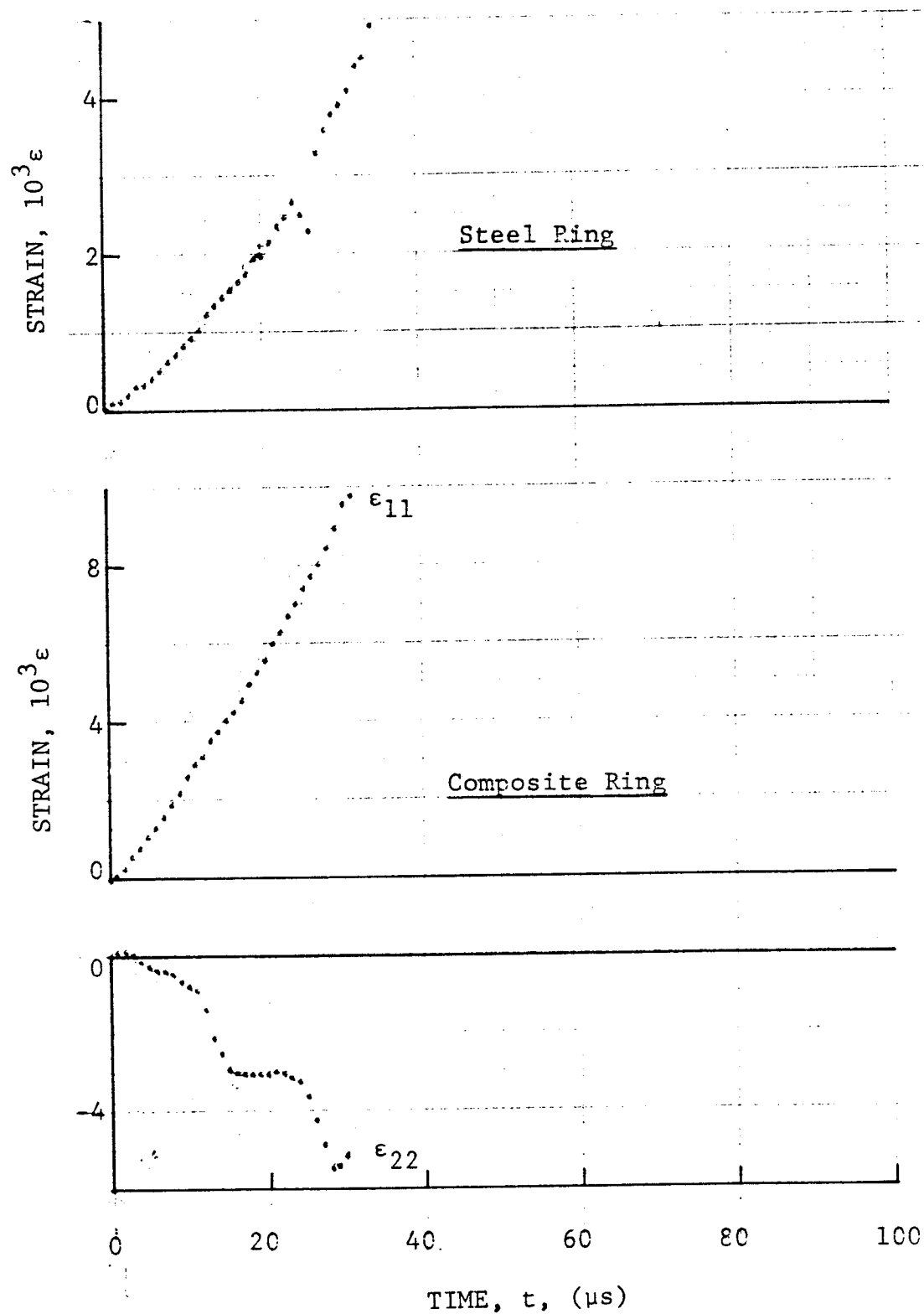


Figure 4-37. Strain records in steel ring and [0₆] SP288/AS graphite/epoxy ring under dynamic loading for Specimen 7-8 (330 mg PETN detonator).

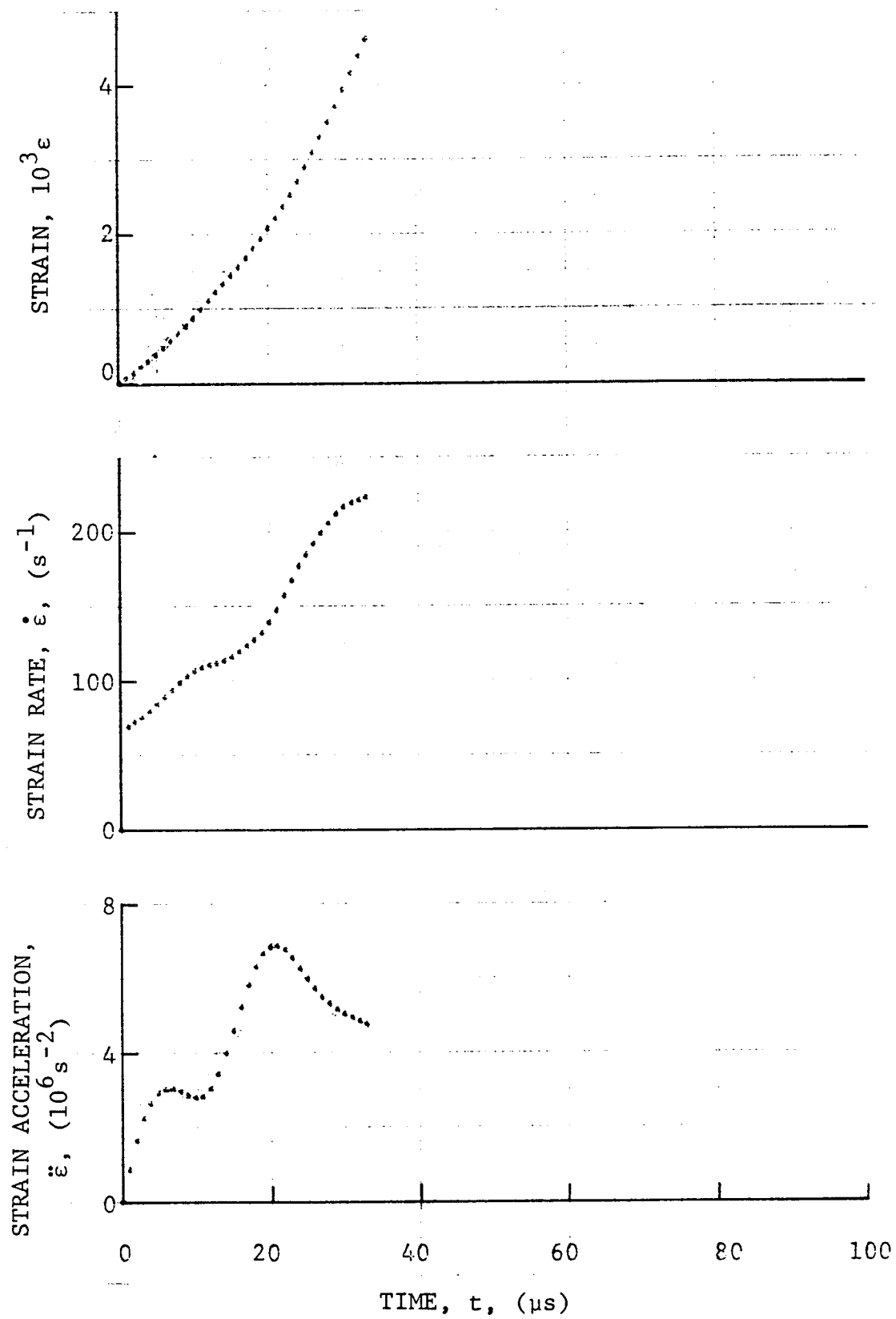


Figure 4-38. Strain and its derivatives in steel ring for Specimen 7-8.

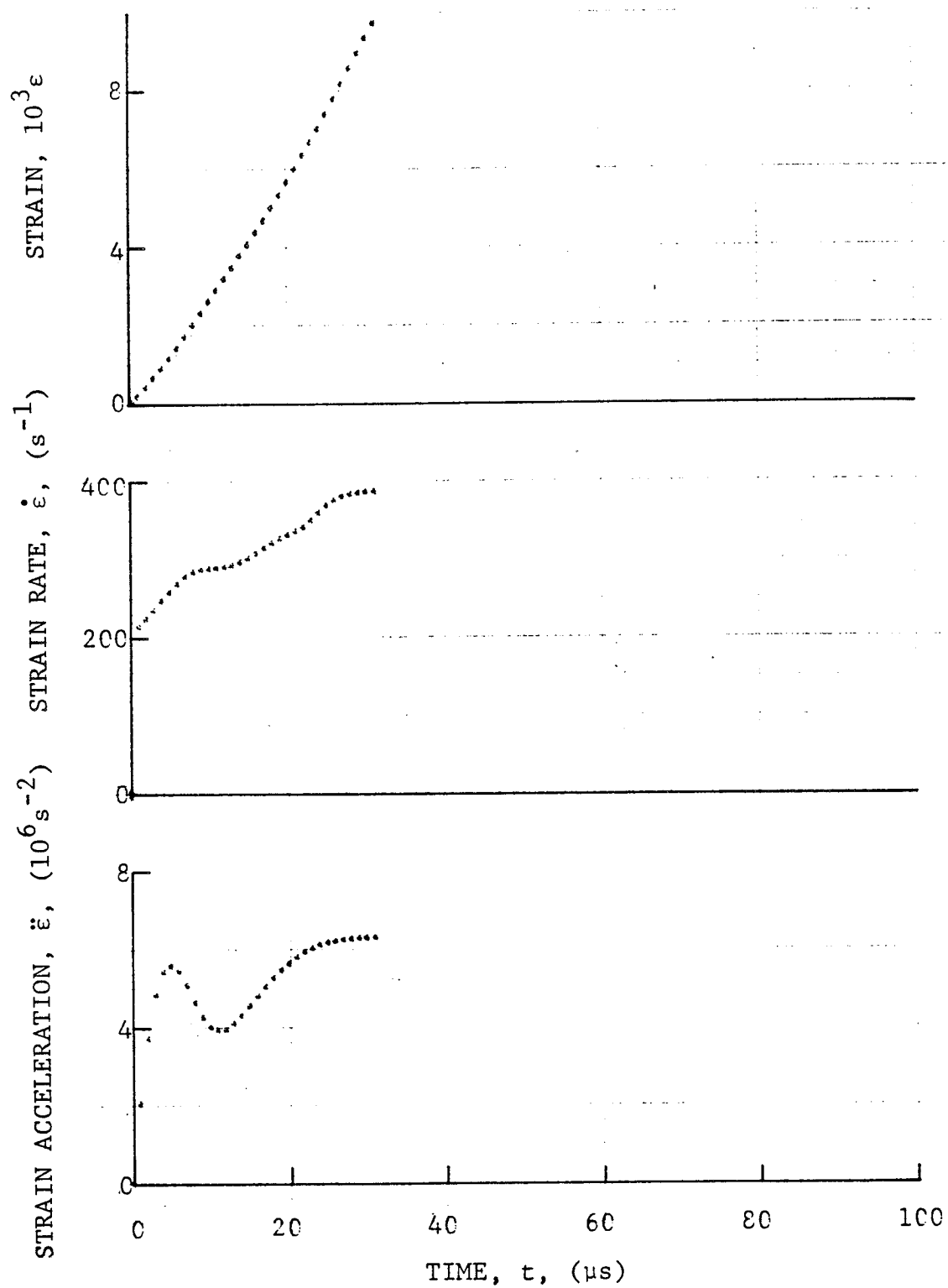


Figure 4-39. Circumferential strain and its derivatives for $[0_6]$ SP288/AS graphite/epoxy ring under dynamic loading for Specimen 7-8.

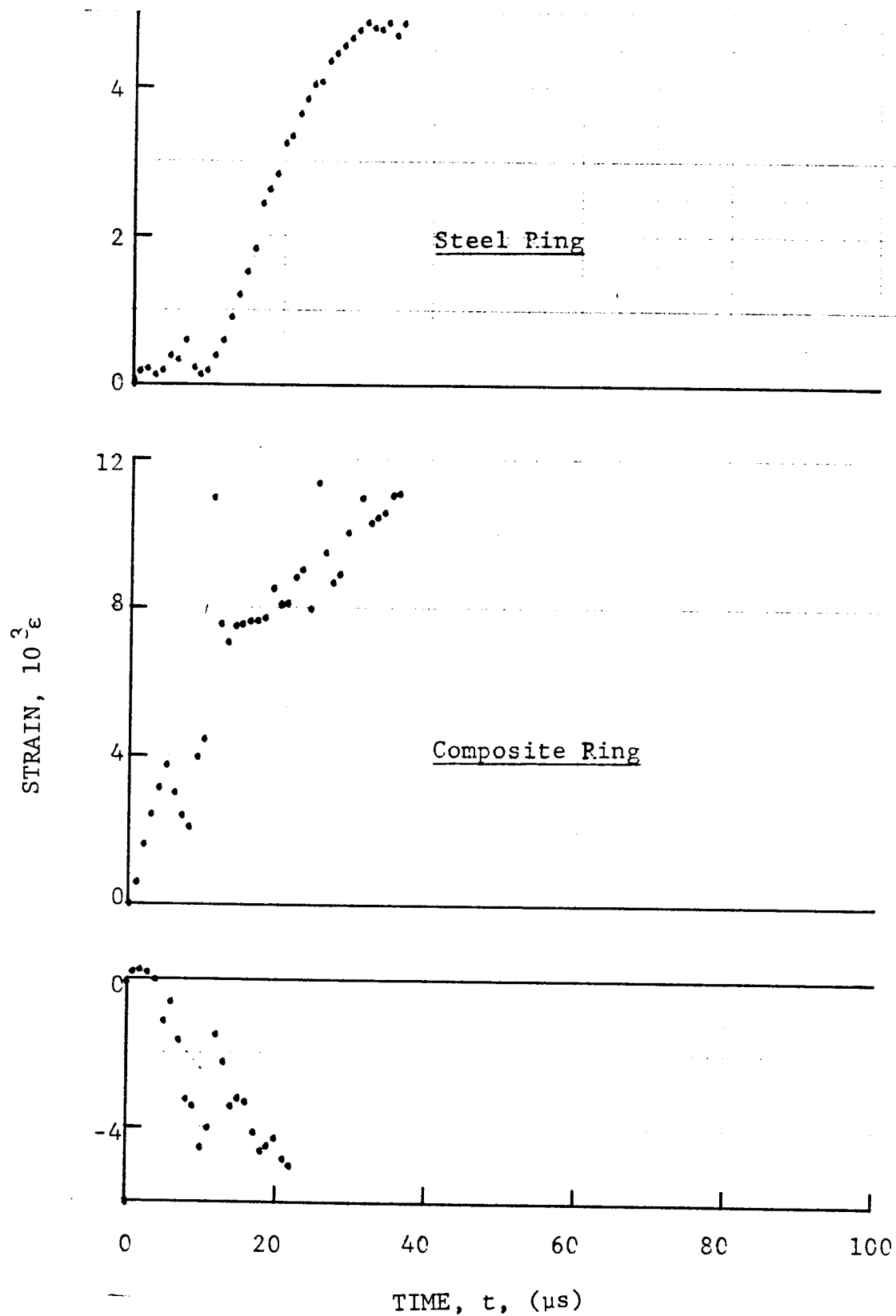


Figure 4-40. Strain records in steel ring and [0₆] SP288/AS graphite/epoxy ring under dynamic loading for Specimen 7-9 (100 mg PETN detonator).

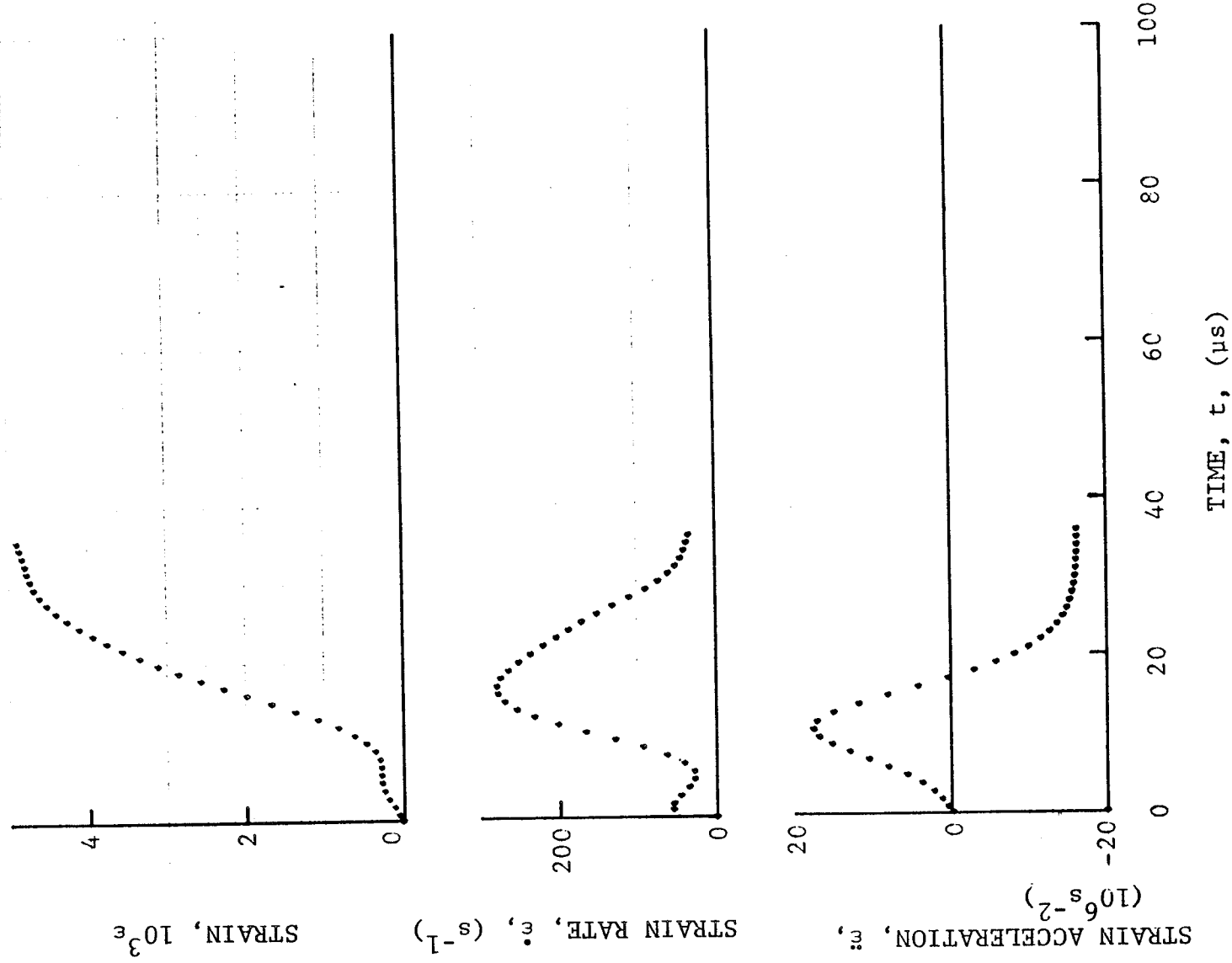


Figure 4-41. Strain and its derivatives in steel ring for Specimen 7-9.

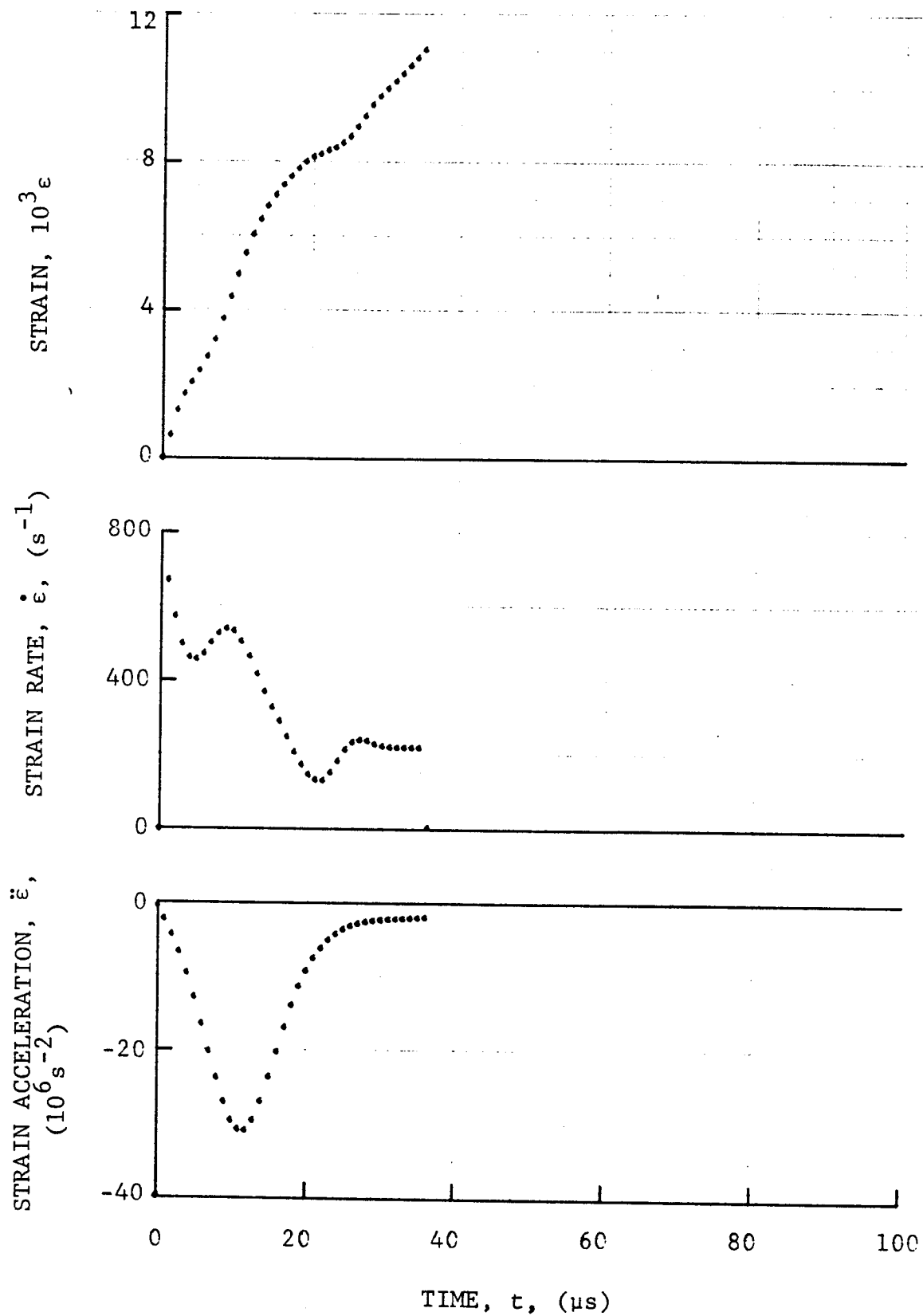


Figure 4-42. Circumferential strain and its derivatives for $[0_6]$ SP288/AS graphite/epoxy ring under dynamic loading for Specimen 7-9.

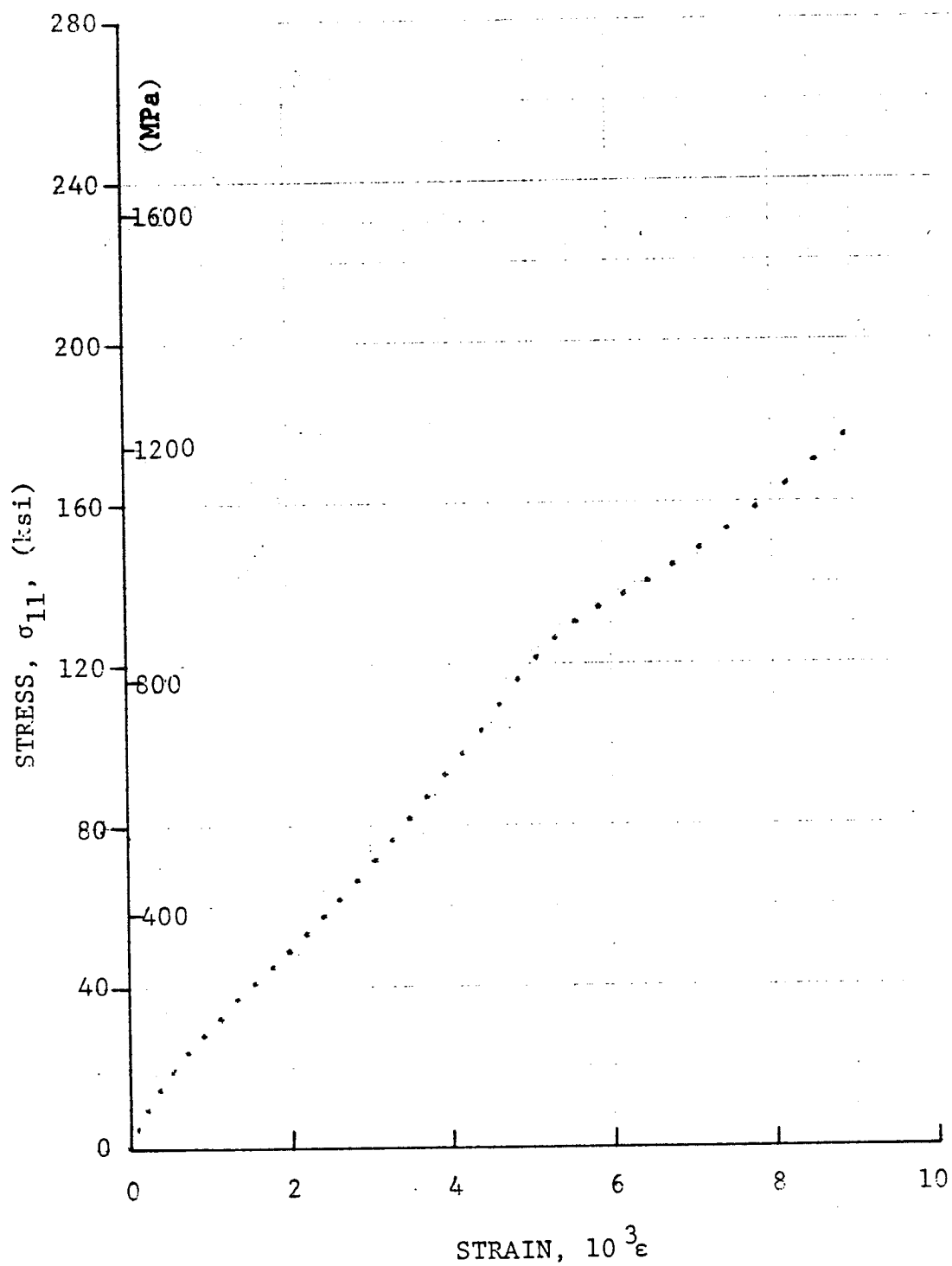


Figure 4-43. Stress-strain curve for dynamically loaded [0₆] SP288/AS graphite/epoxy ring for Specimen 7-6 (two 100 mg PETN detonators).

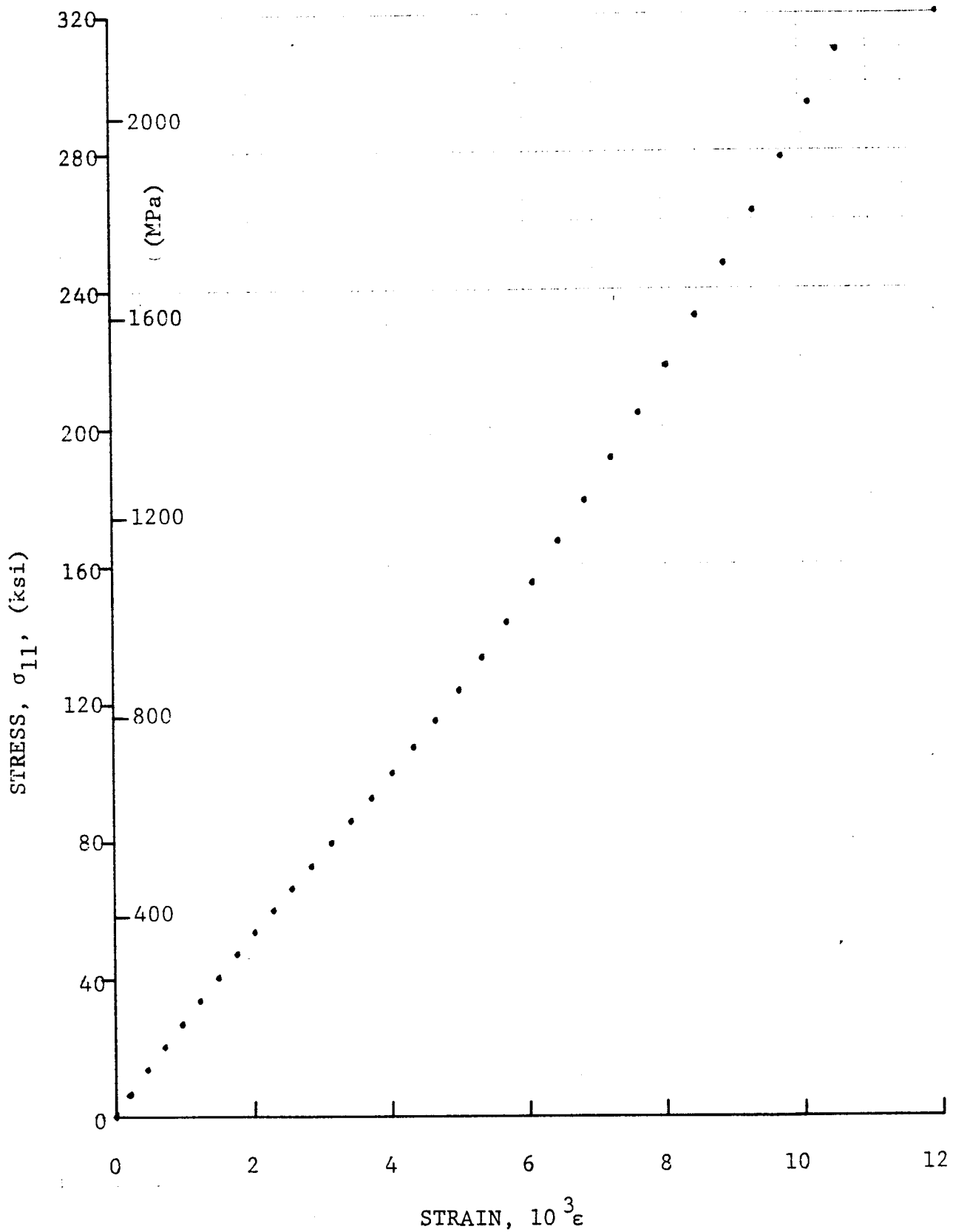


Figure 4-44. Stress-strain curve for dynamically loaded $[0_6]$ SP288/AS graphite/epoxy ring for Specimen 7-7 (330 mg PETN detonator).

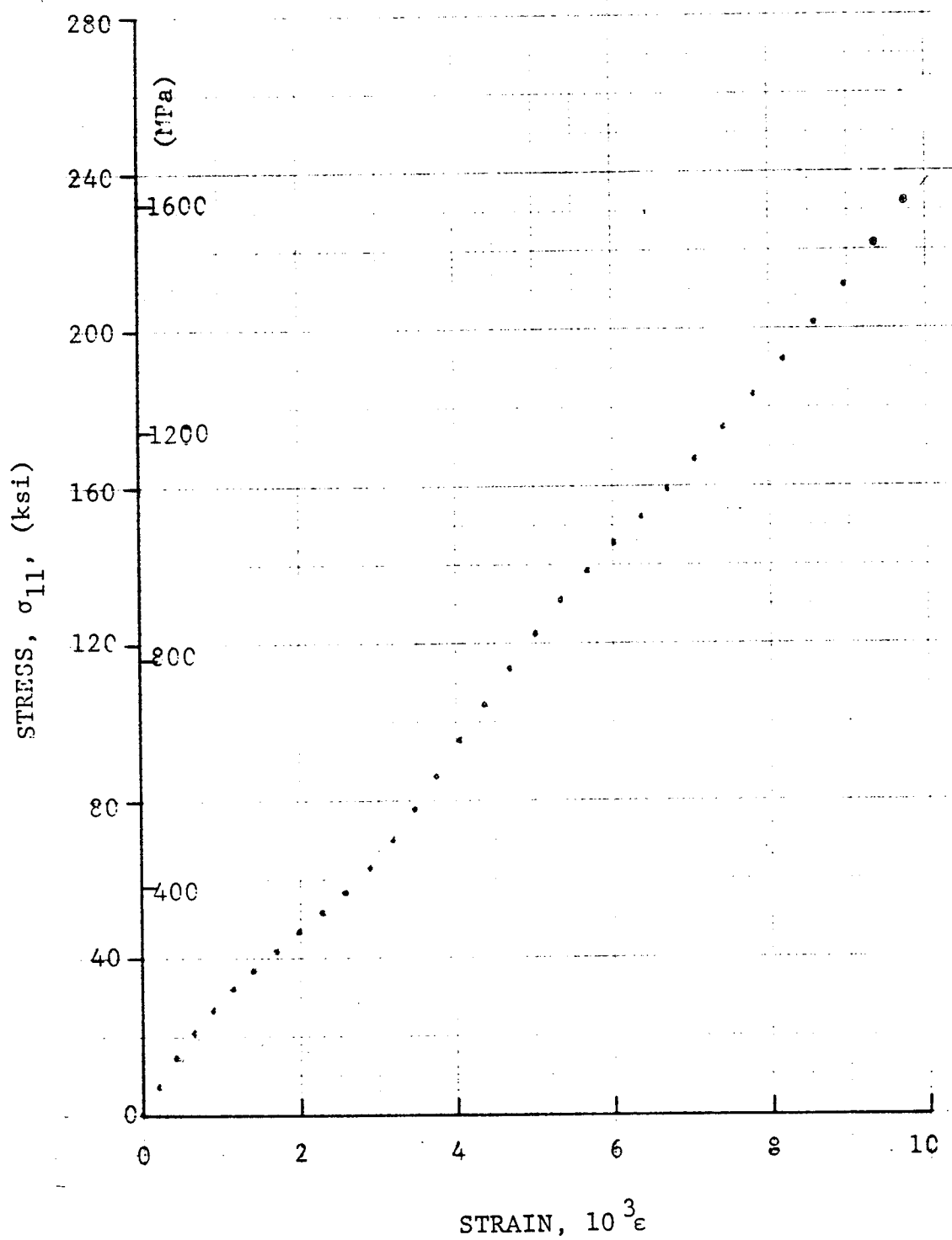


Figure 4-45. Stress-strain curve for dynamically loaded [0₆] SP288/AS graphite/epoxy ring for Specimen 7-8 (330 mg PETN detonator).

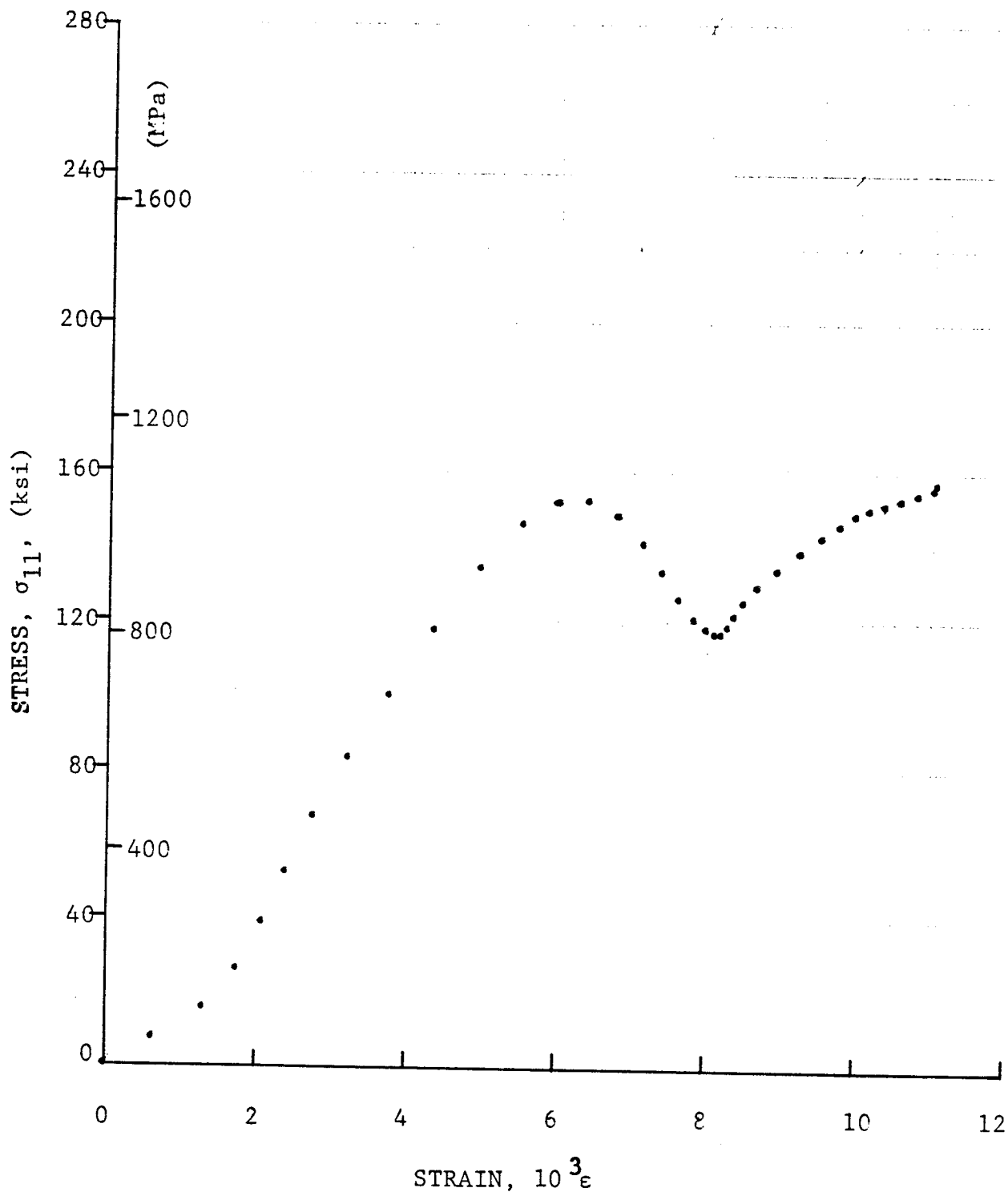


Figure 4-46. Stress-strain curve for dynamically loaded [0₆] SP288/AS graphite/epoxy ring for Specimen 7-9 (100 mg PETN detonator).

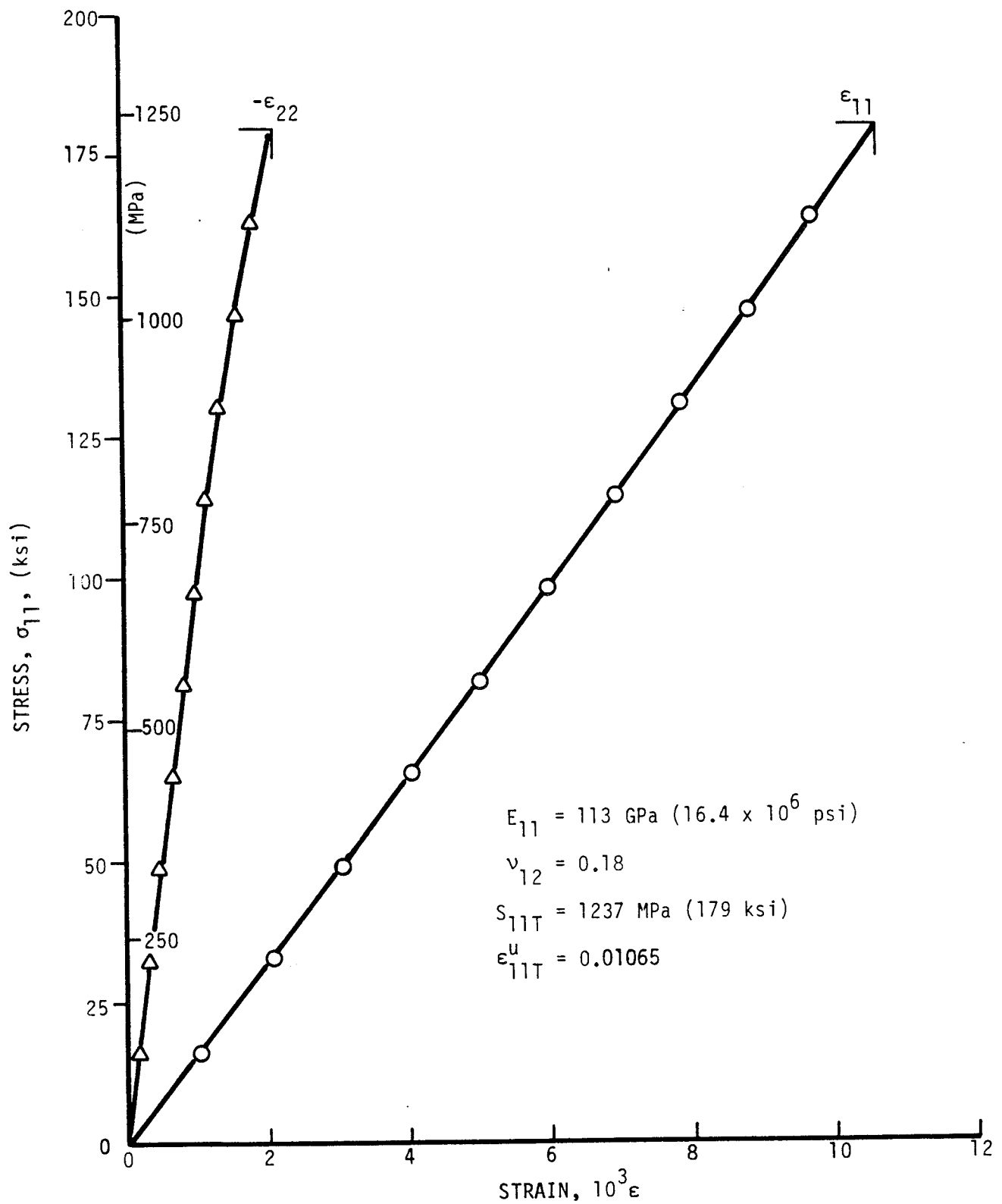


Figure 4-47. Strains in unidirectional 0-deg 80AS/20S/PR288 specimen under static tensile loading (Specimen No. 10-1).

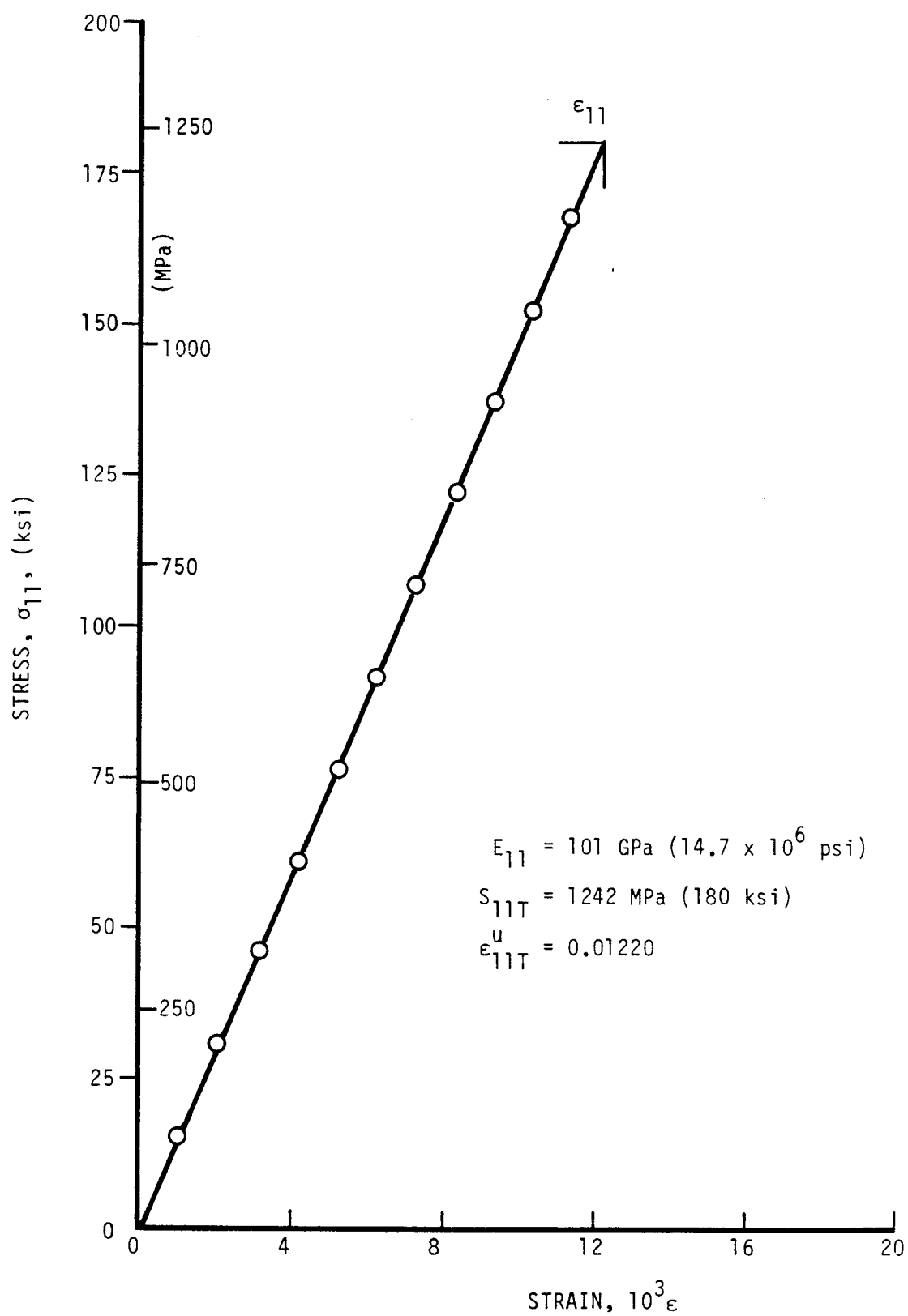


Figure 4-48. Stress-strain curve in unidirectional 0-deg 80AS/20S/PR288 ring specimen under static tensile loading (Specimen No. 10-5).

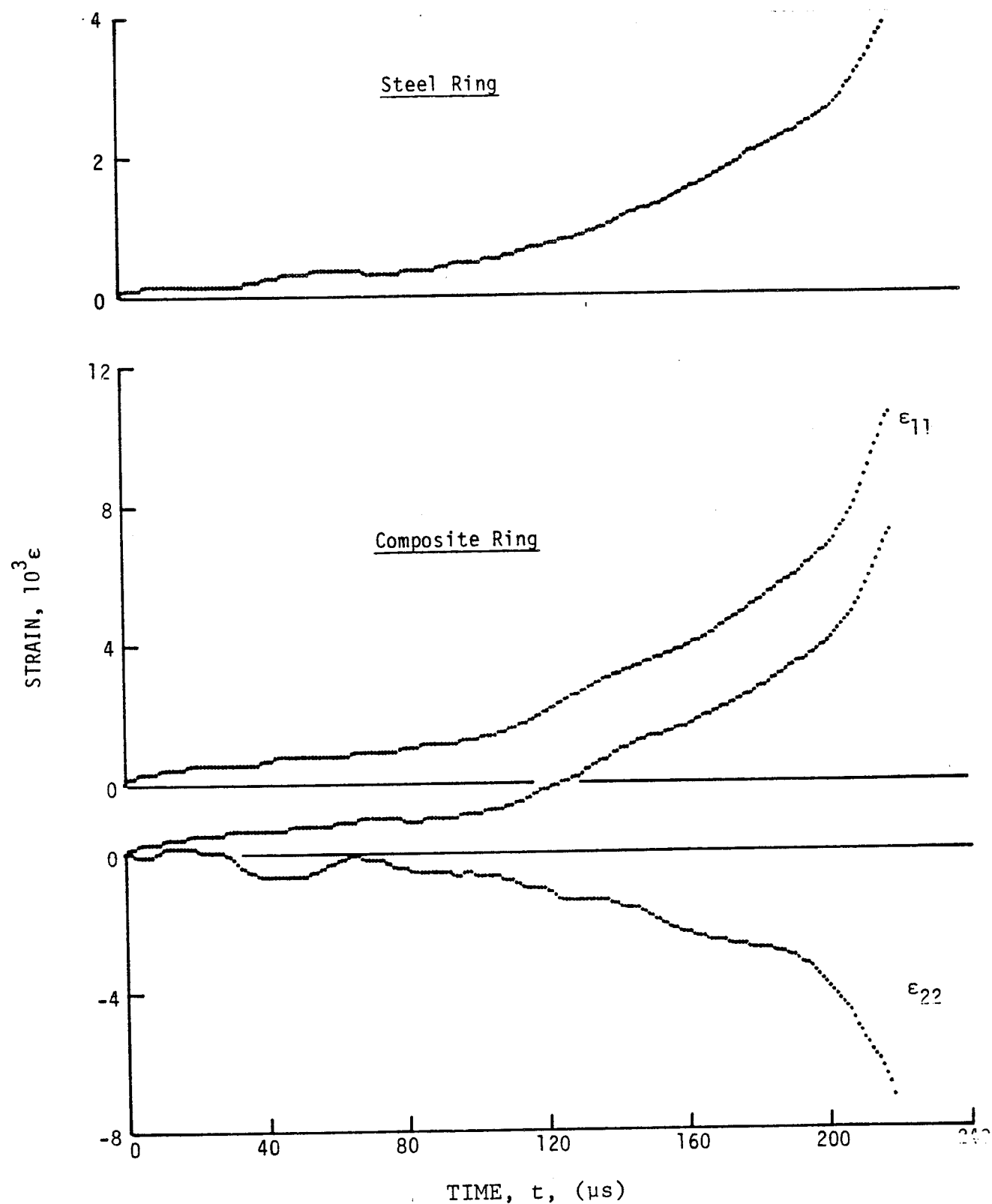


Figure 4-49. Strain records in steel ring and $[0_6]$ 80AS/20S/PR288 graphite/S-glass/epoxy ring under dynamic loading for Specimen 43-2 (650 mg pistol powder).

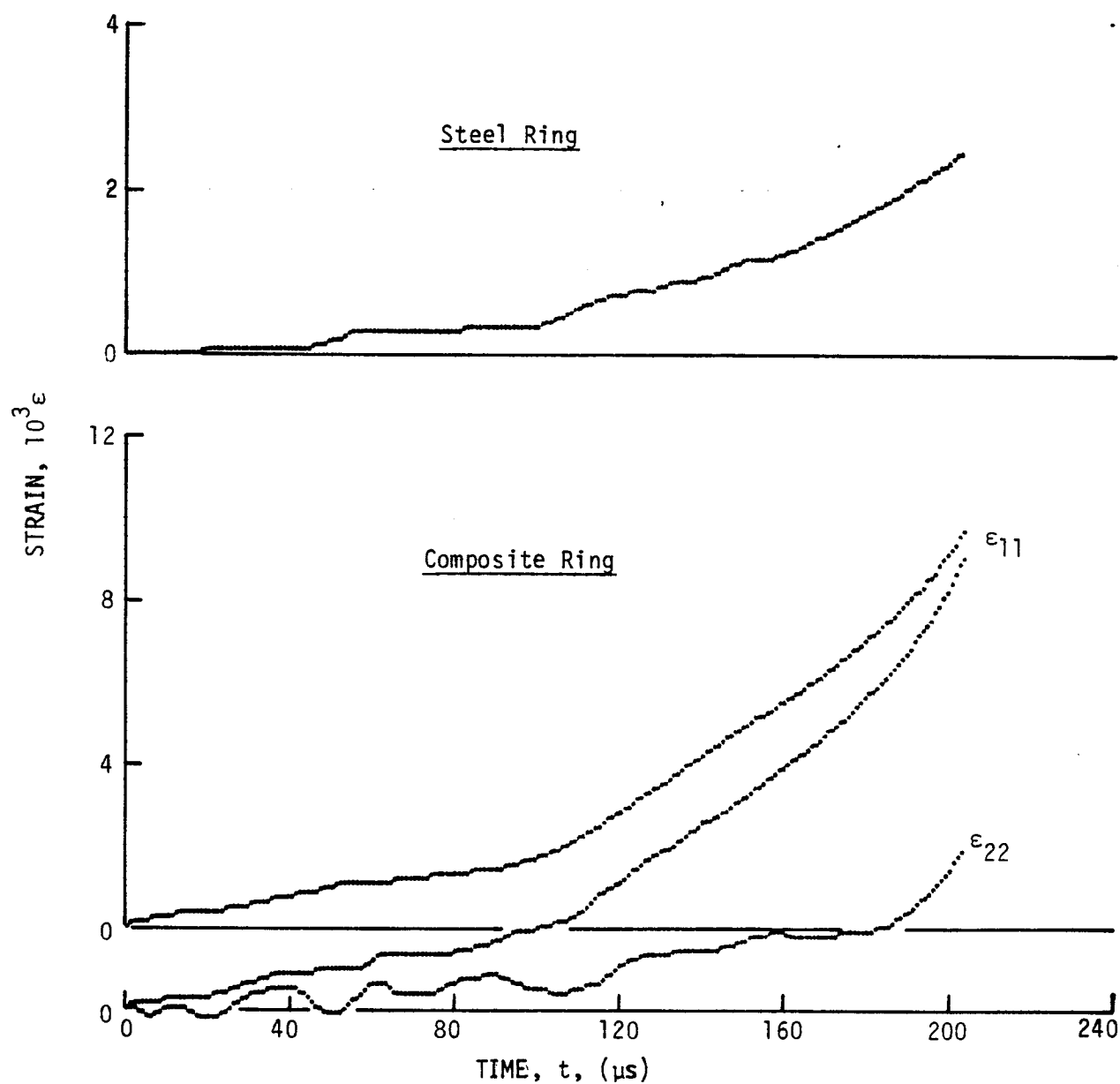


Figure 4-50. Strain records in steel ring and $[0_6]$ 80AS/20S/PR288 graphite/S-glass/epoxy ring under dynamic loading for Specimen 43-3 (650 mg pistol powder).

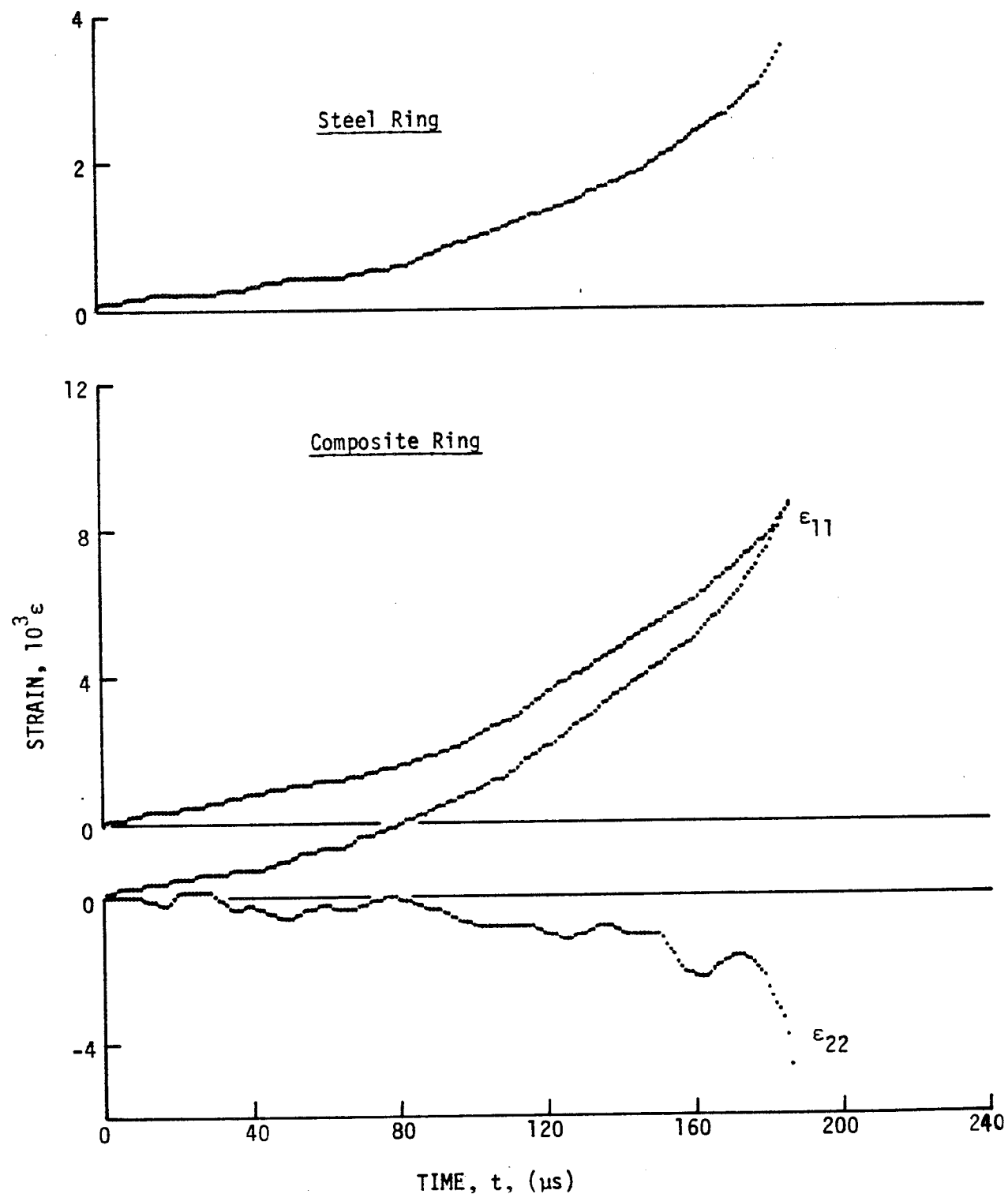


Figure 4-51. Strain records in steel ring and $[0_6]$ 80AS/20S/PR288 graphite/S-glass/epoxy ring under dynamic loading for Specimen 43-4 (650 mg pistol powder).

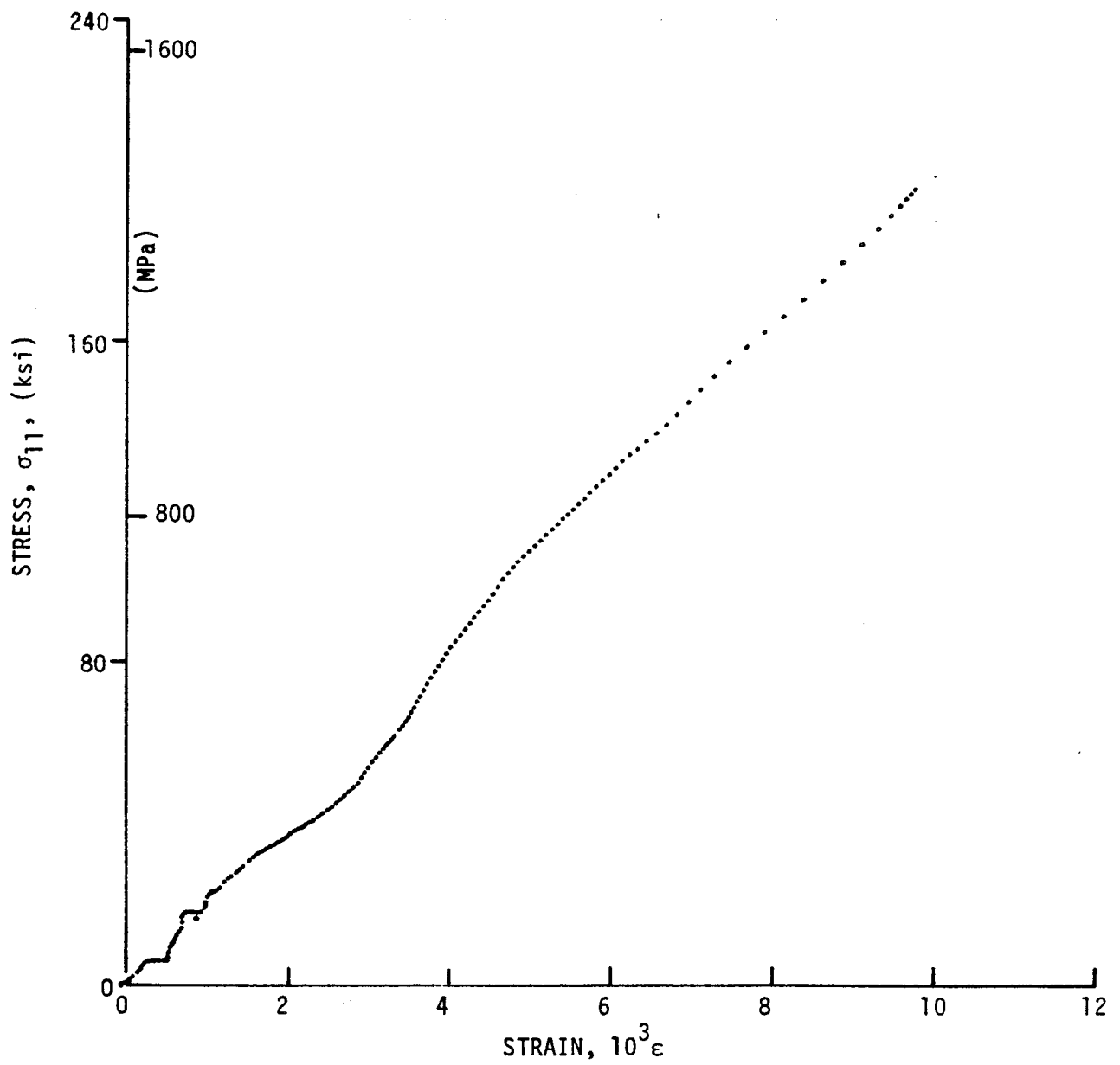


Figure 4-52. Stress-strain curve for dynamically loaded $[0_6]$ 80AS/20S/PR288 graphite/S-glass/epoxy ring for Specimen 43-2.

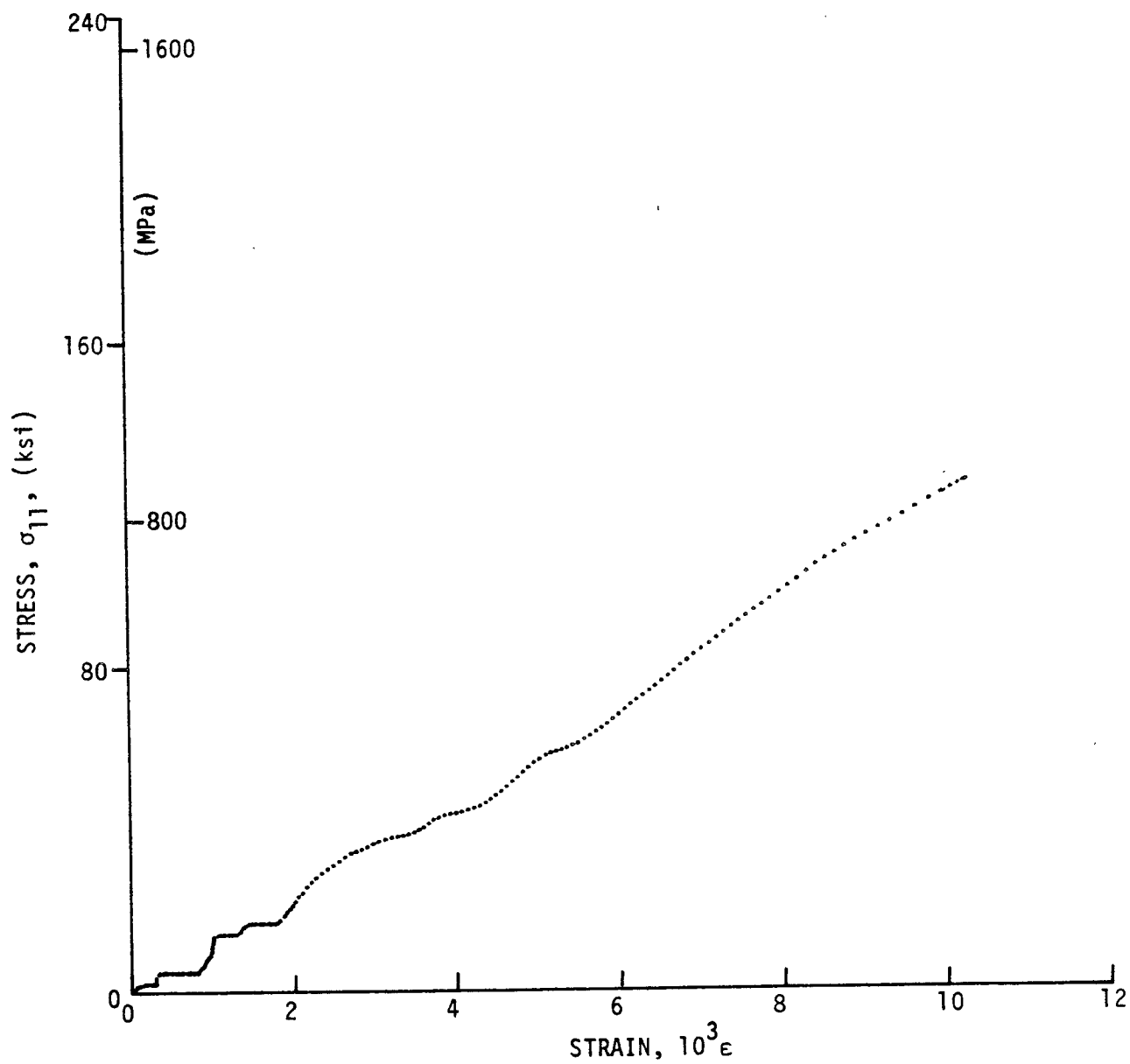


Figure 4-53. Stress-strain curve for dynamically loaded $[0_6]$ 80AS/20S/PR288 graphite/S-glass/epoxy ring for Specimen 43-3.

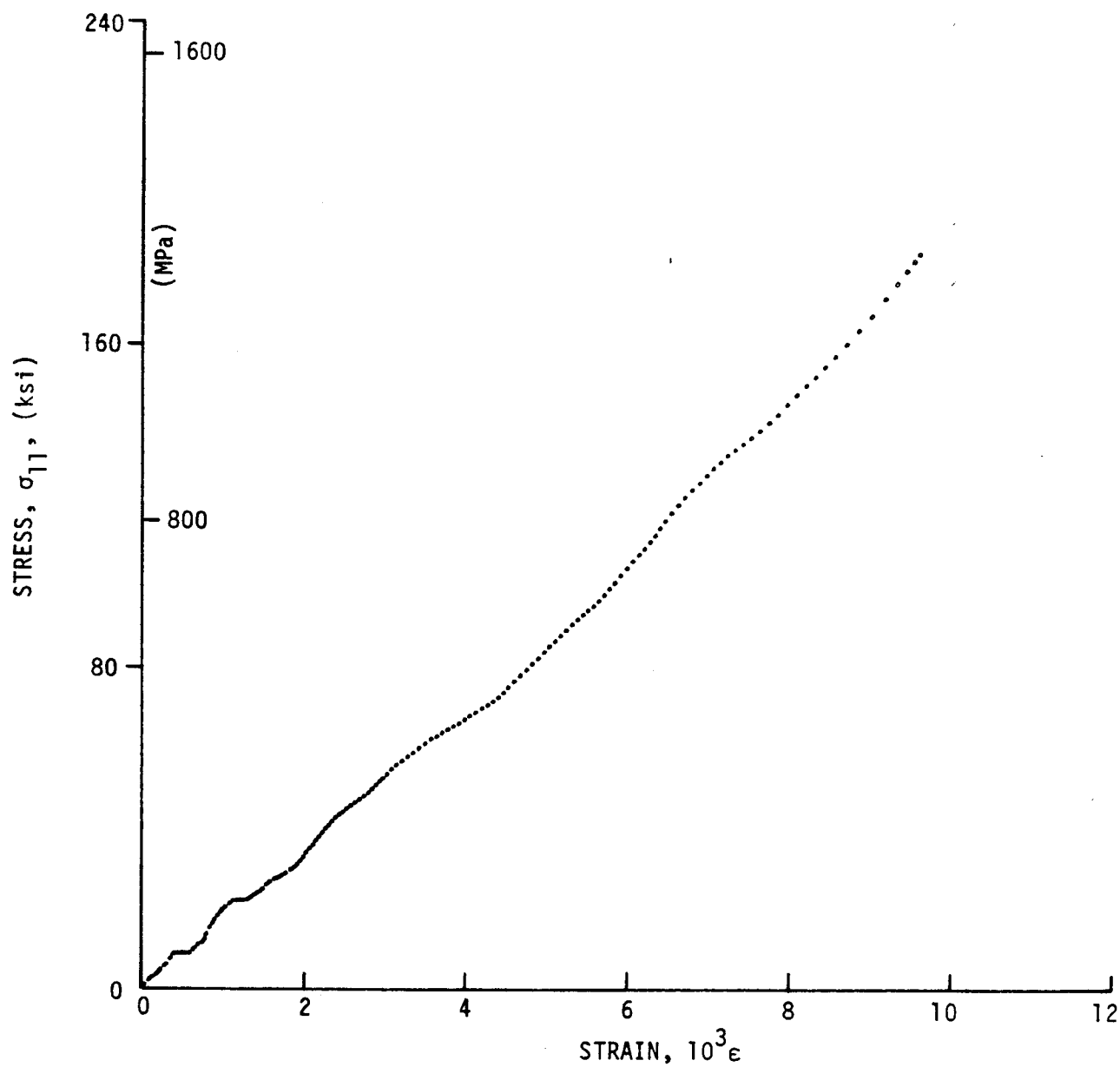


Figure 4-54. Stress-strain curve for dynamically loaded $[0_6]$ 80AS/20S/PR288 graphite/S-glass/epoxy ring for Specimen 43-4.

STRAIN, $10^3 \epsilon$

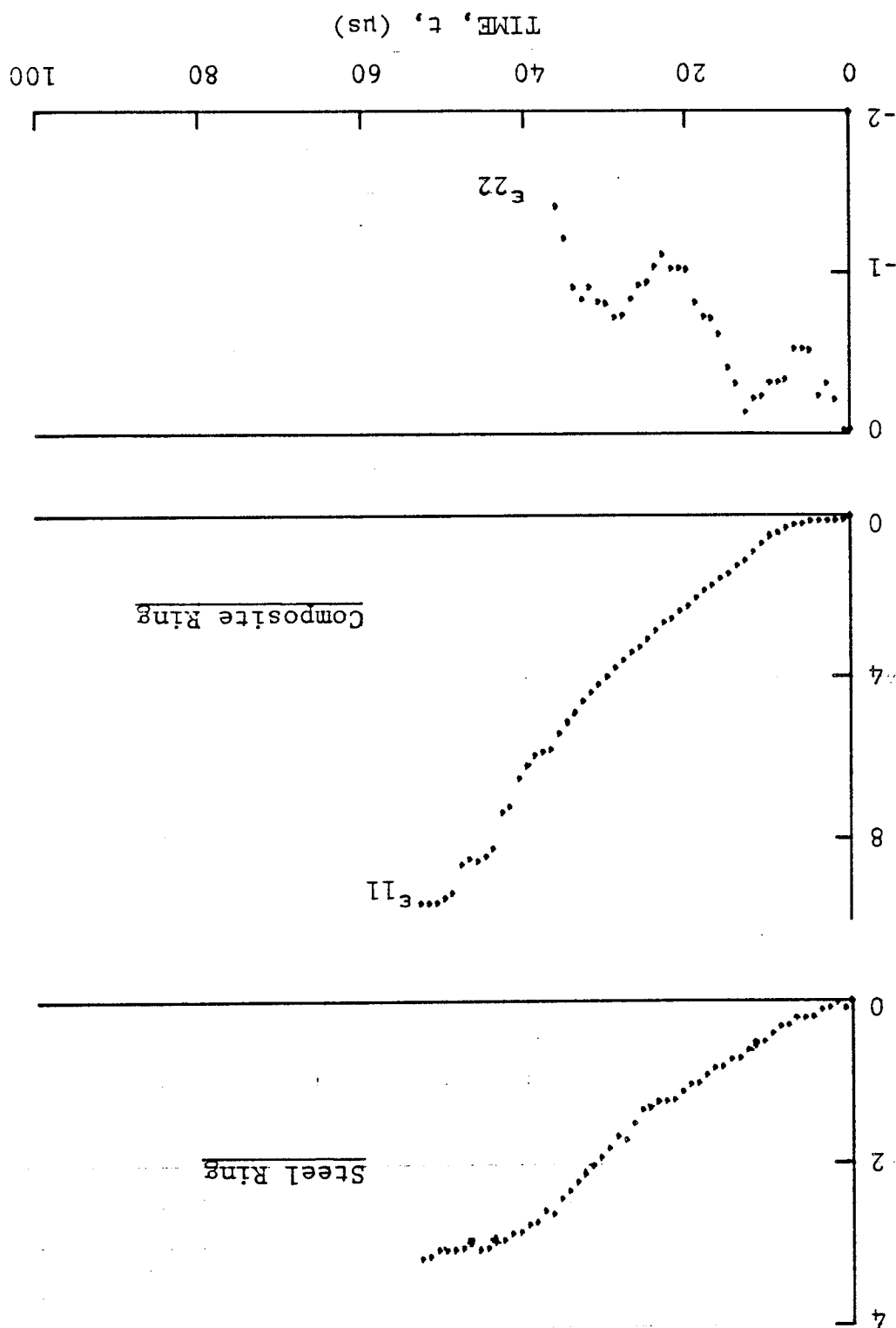


Figure 4-55. Strain records in steel ring and [0₆] 80AS/20S/PR288 graphite/S-glass/epoxy ring under dynamic loading for Specimen 10-8 (100 mg PETN detonator).

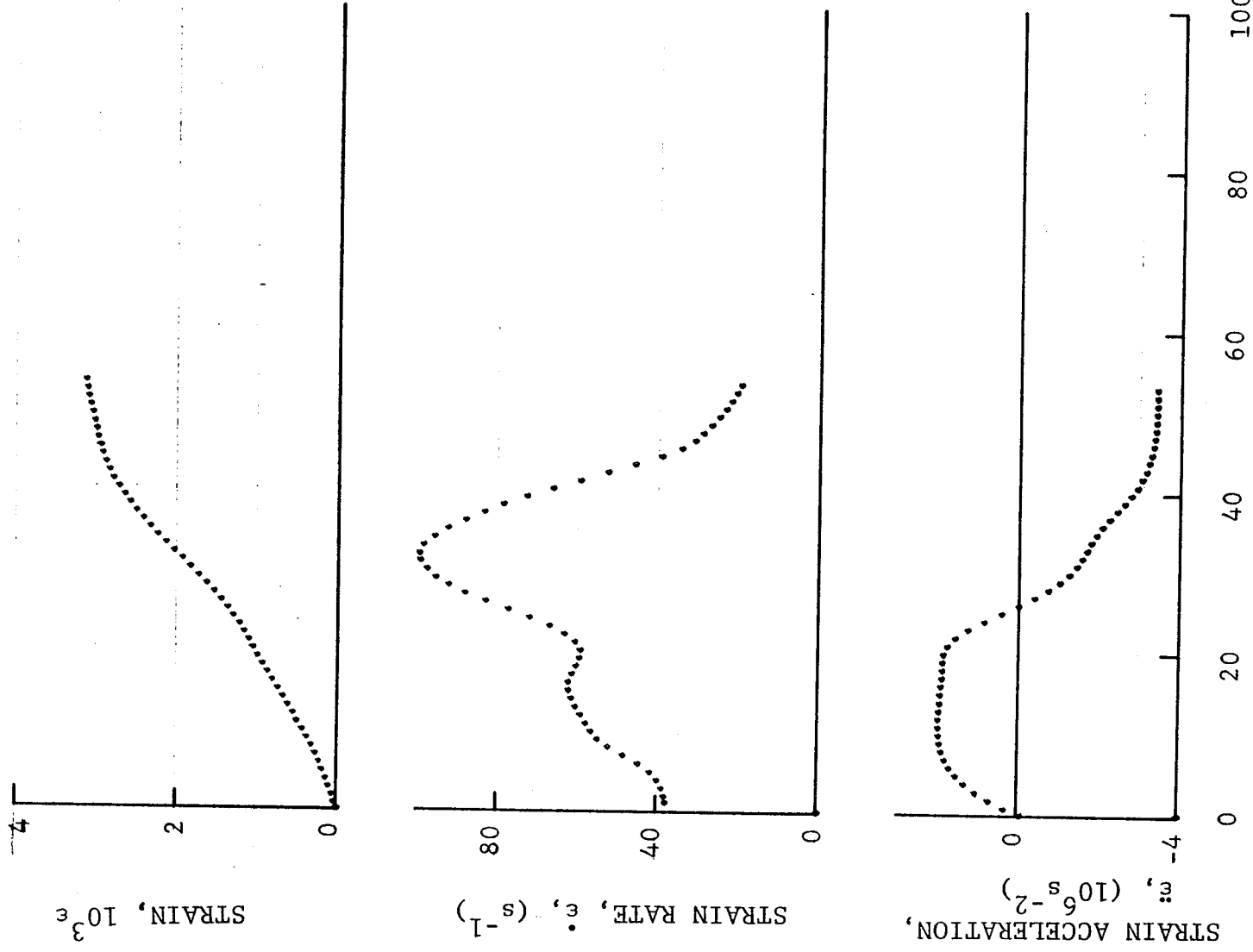


Figure 4-56. Strain and its derivatives in steel ring for Specimen 10-8.

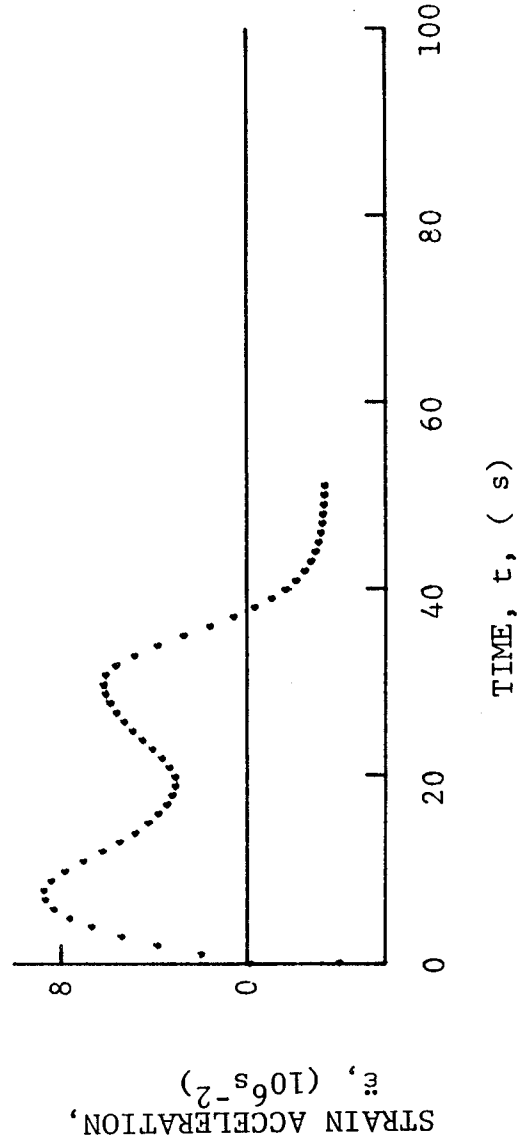
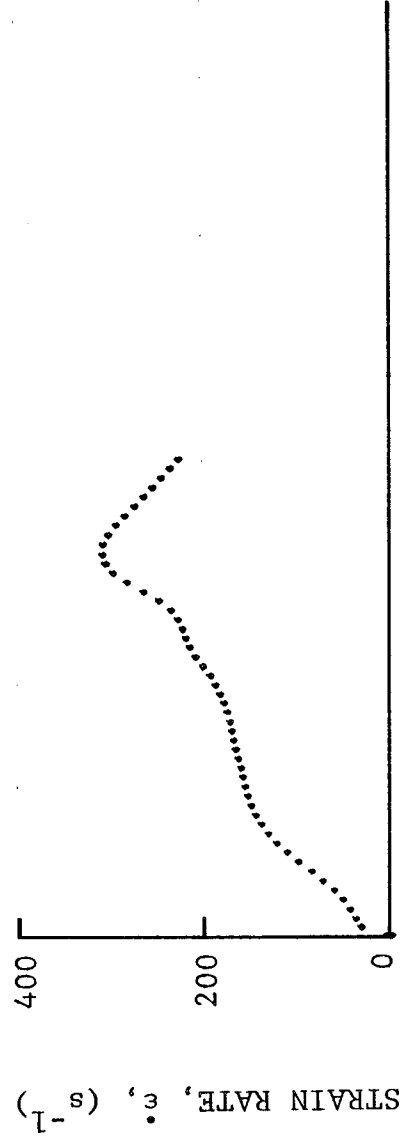
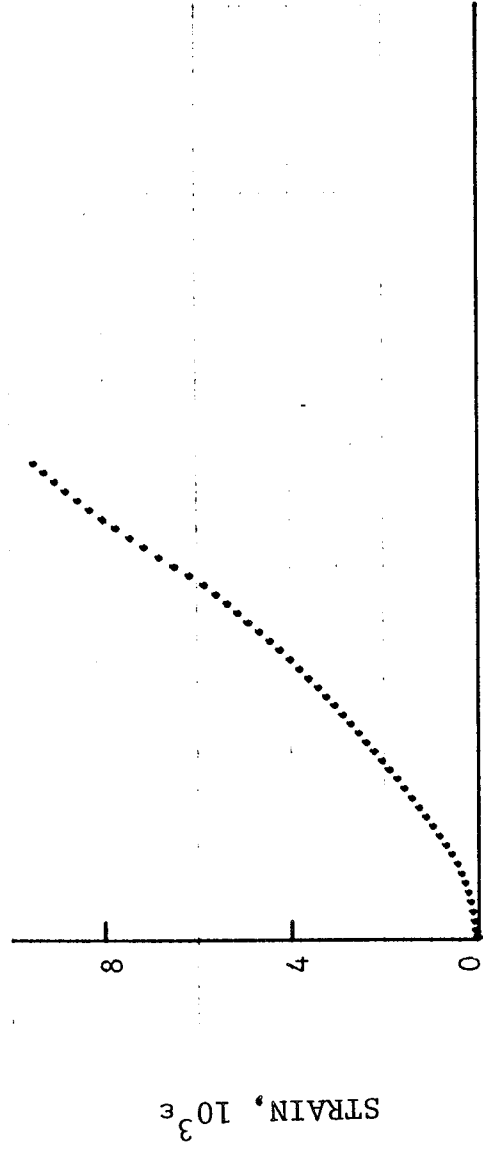


Figure 4-57. Circumferential strain and its derivatives for [0₆] 80AS/20S/PR288 graphite/S-glass/epoxy ring under dynamic loading for Specimen 10-8.

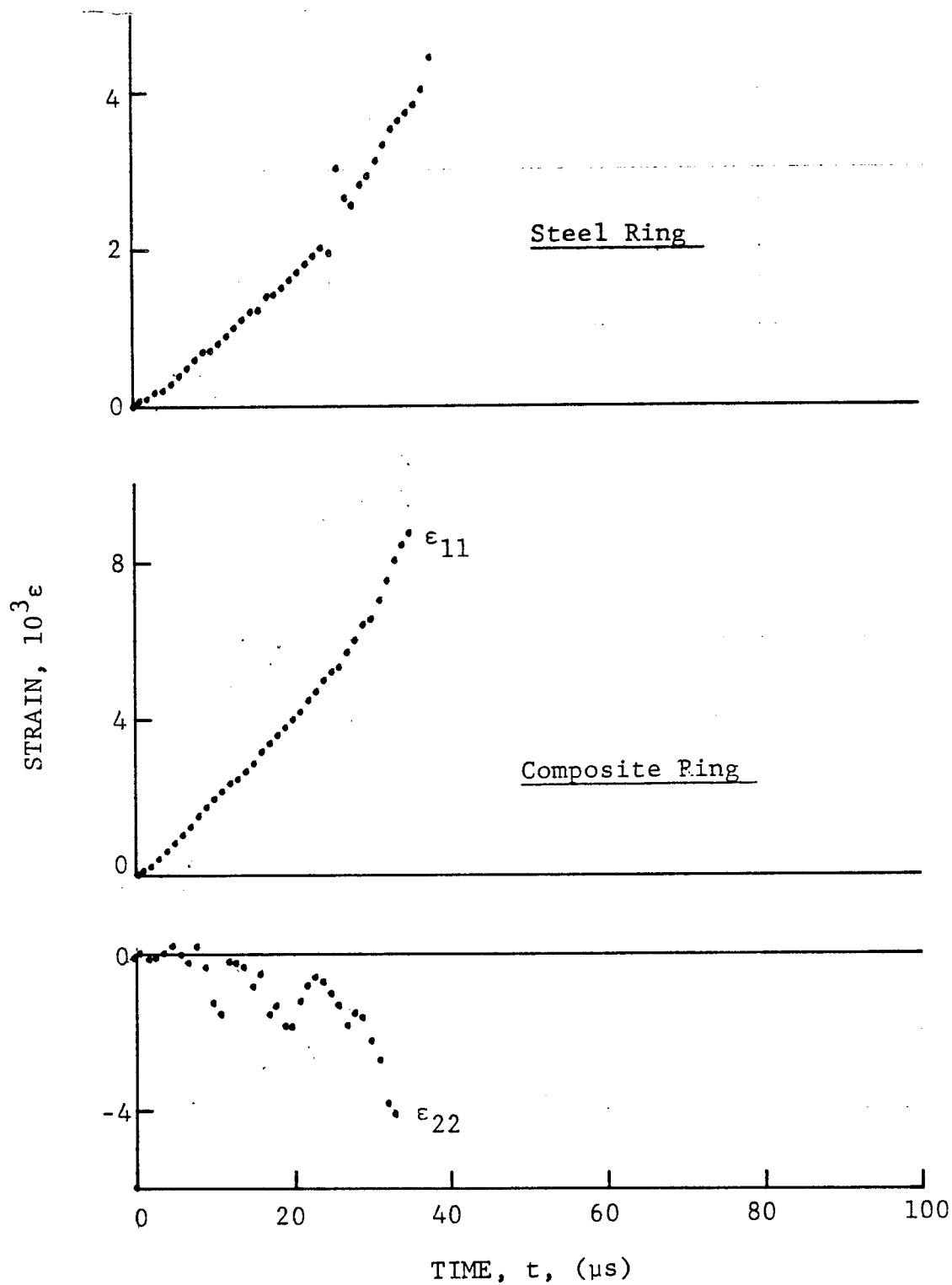


Figure 4-58. Strain records in steel ring and $[0_6]$ 80AS/20S/PR288 graphite/S-glass/epoxy ring under dynamic loading for Specimen 10-9 (two 100 mg PETN detonators).

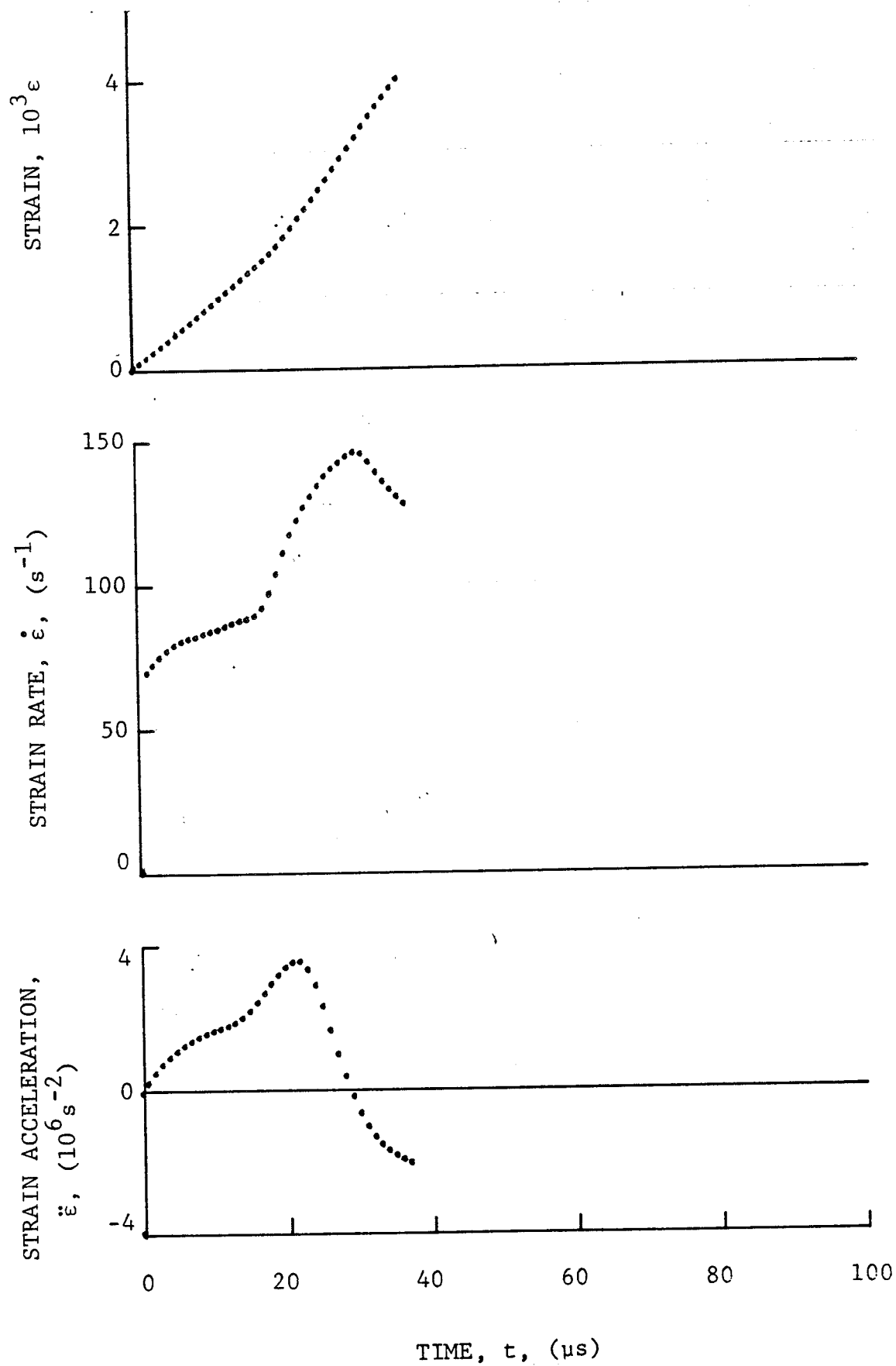


Figure 4-59. Strain and its derivatives in steel ring for Specimen 10-9.

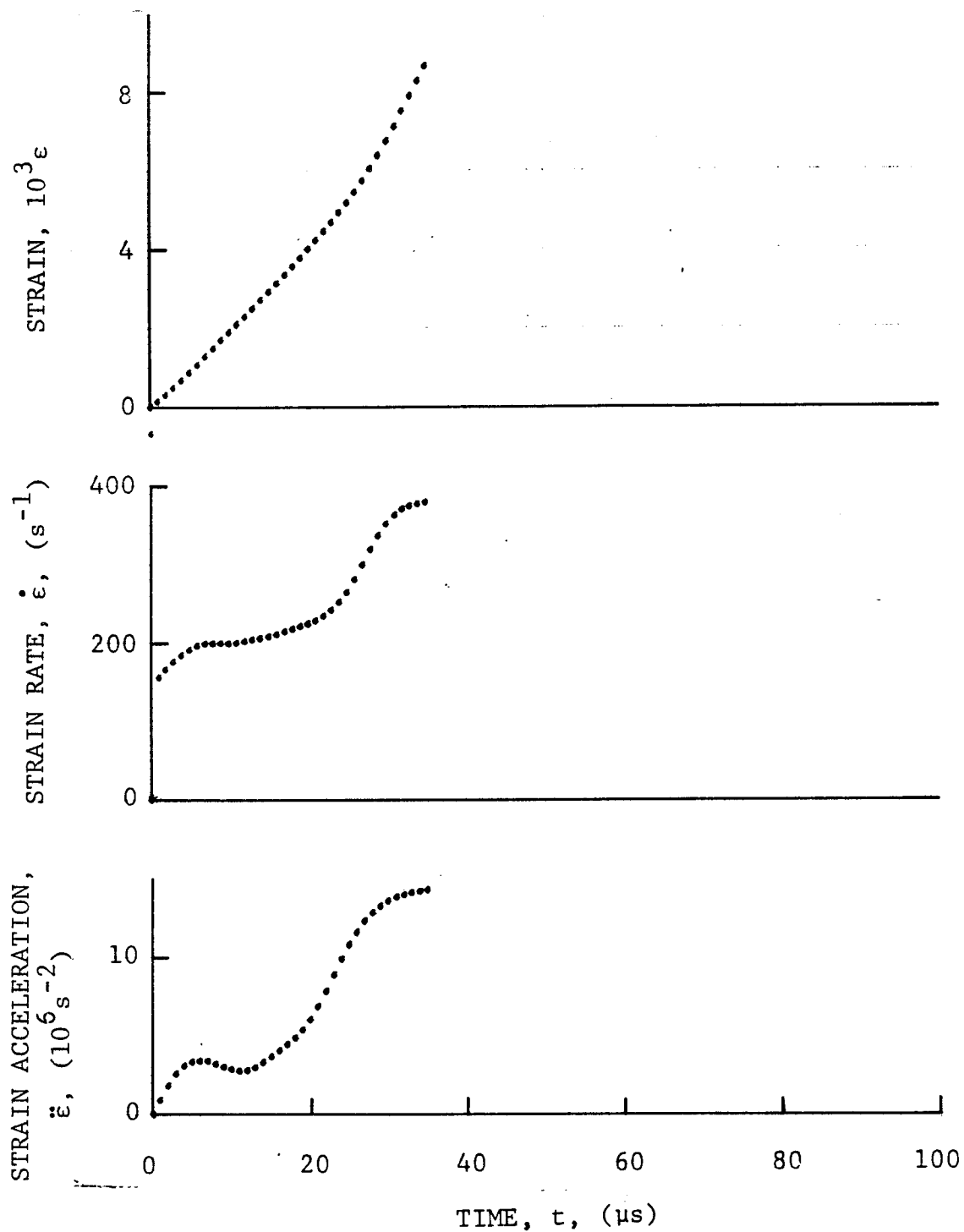


Figure 4-60. Circumferential strain and its derivatives for $[0_6]$ 80AS/20S/PR288 graphite/S-glass/epoxy ring under dynamic loading for Specimen 10-9.

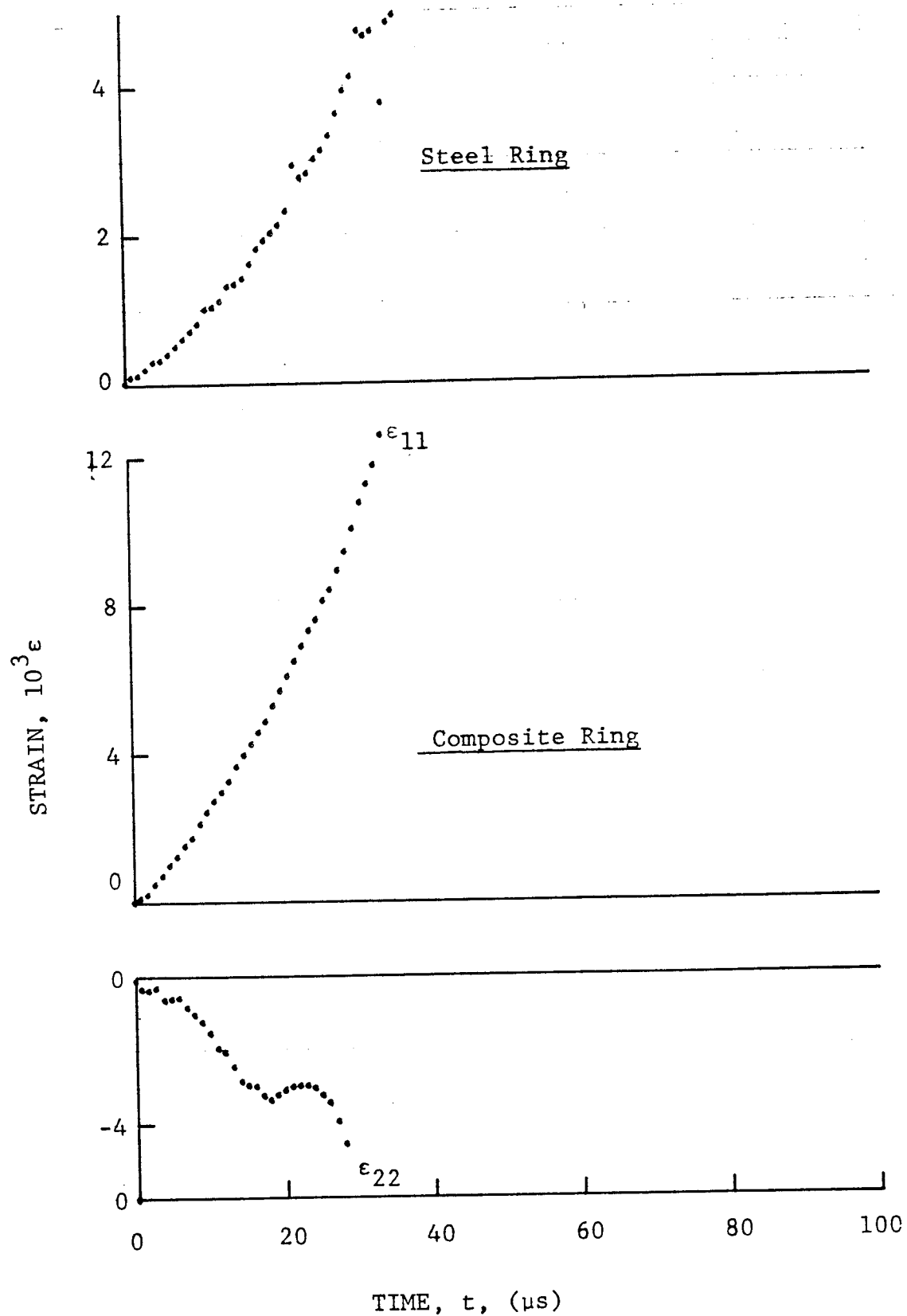
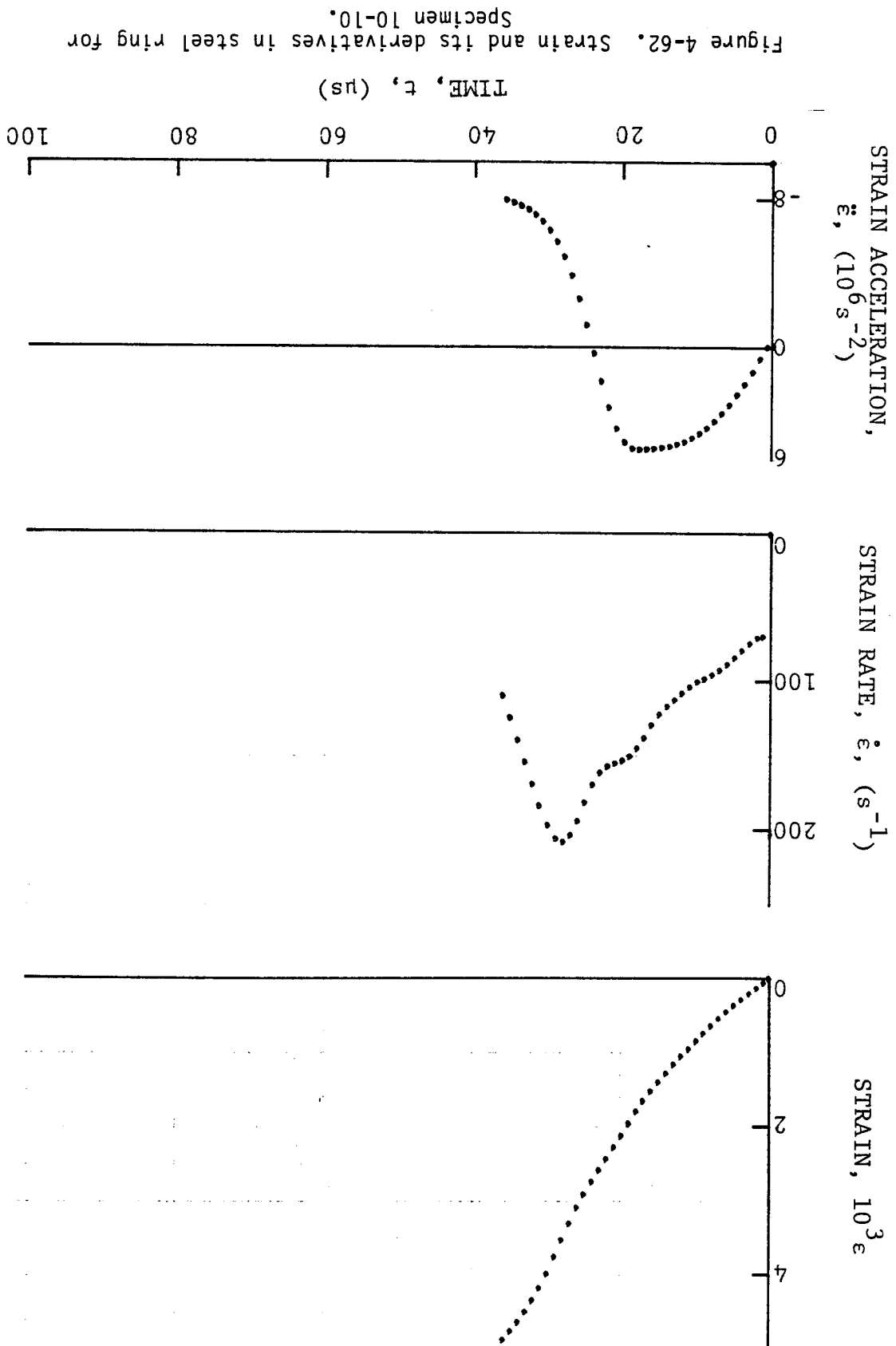


Figure 4-61. Strain records in steel ring and $[0_6]$ 80AS/20S/PR288 graphite/S-glass/epoxy ring under dynamic loading for Specimen 10-10 (330 mg PETN detonator).



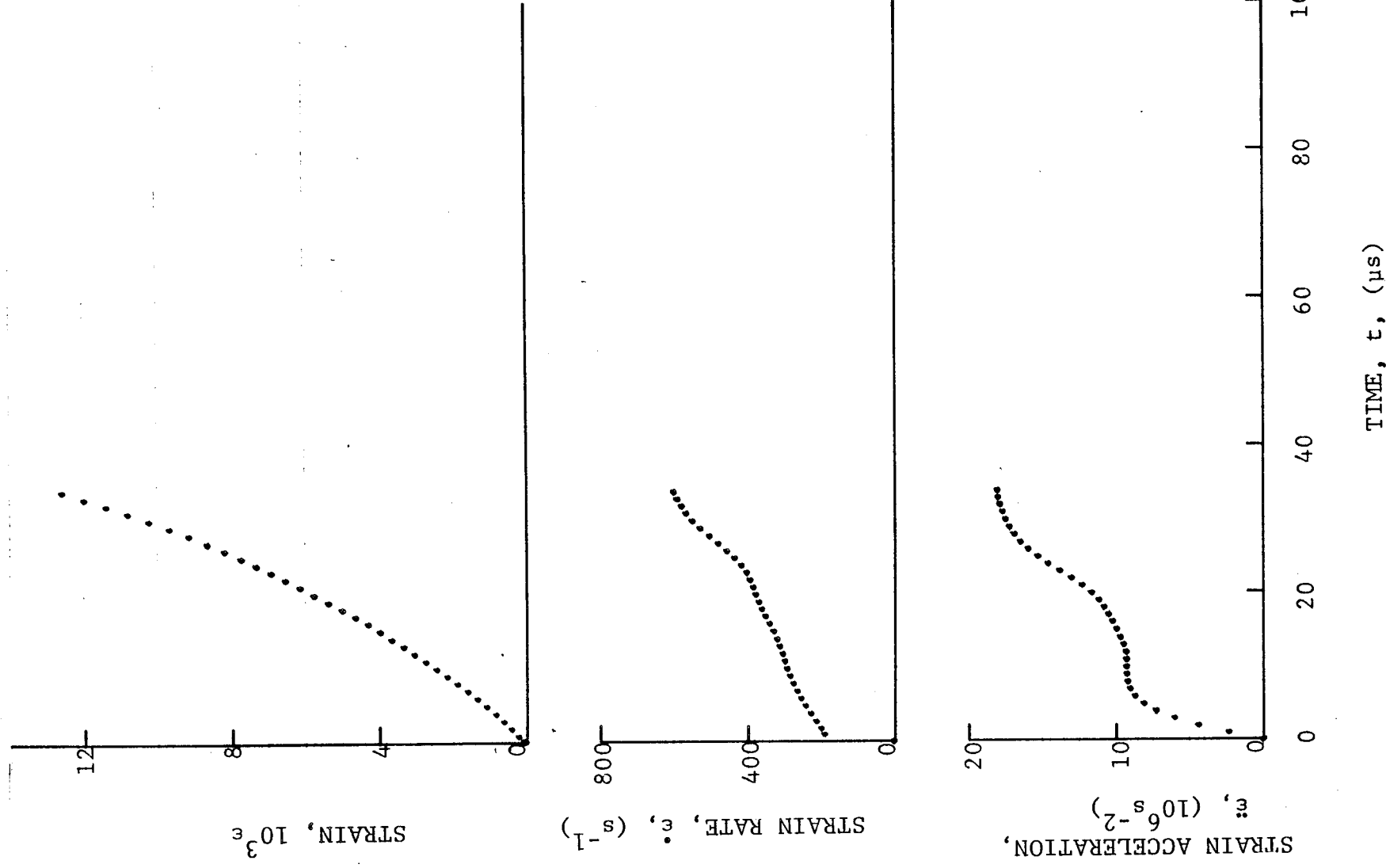
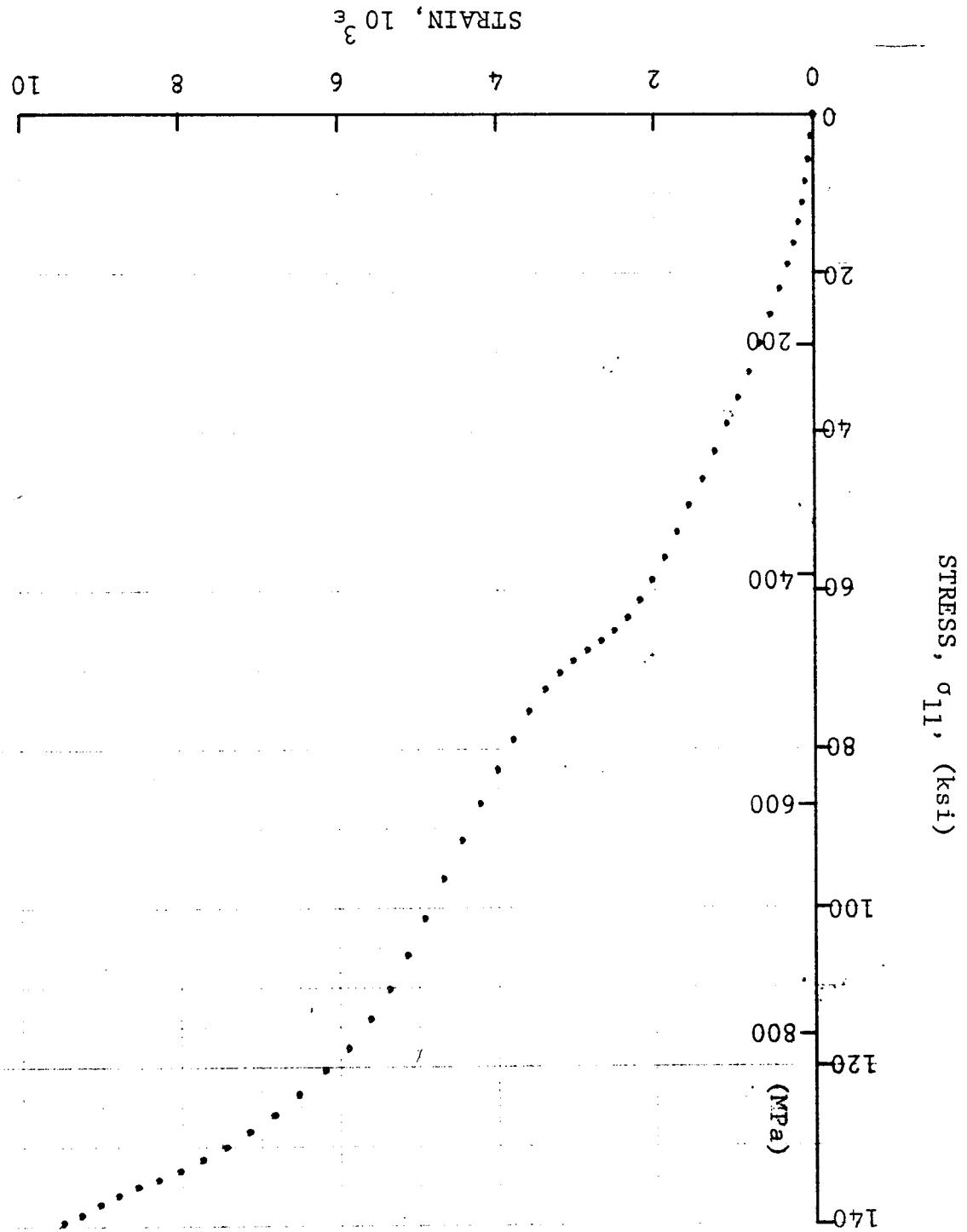


Figure 4-63. Circumferential strain and its derivatives for [06] 80AS/20S/PR288 graphite/S-glass/epoxy ring under dynamic loading for Specimen 10-10.

Figure 4-64. Stress-strain curve for dynamically loaded [0₆] 80AS/20S/PR288 graphite/S-glass/epoxy ring for Specimen 10-8 (100 mg PETN detonator).



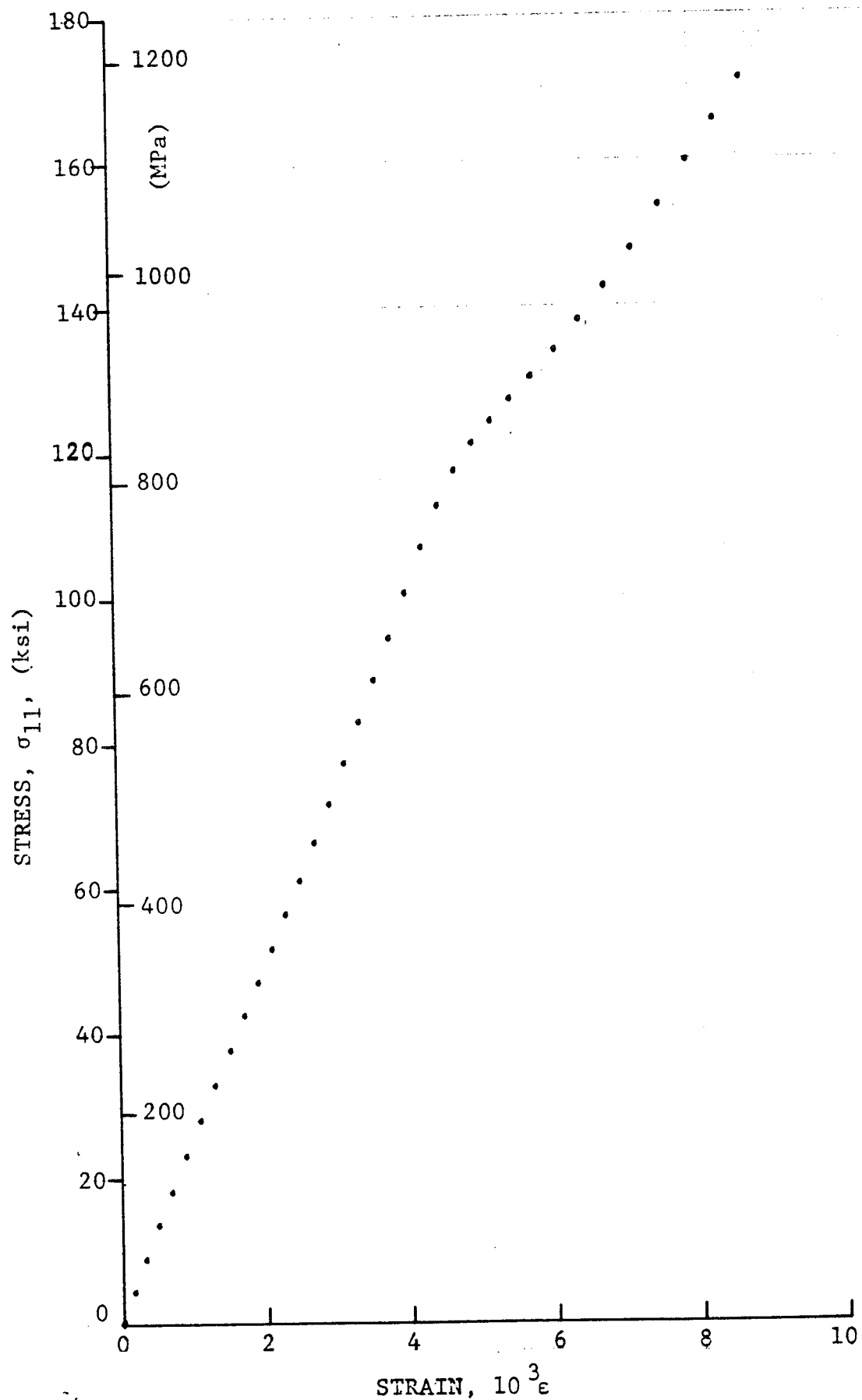
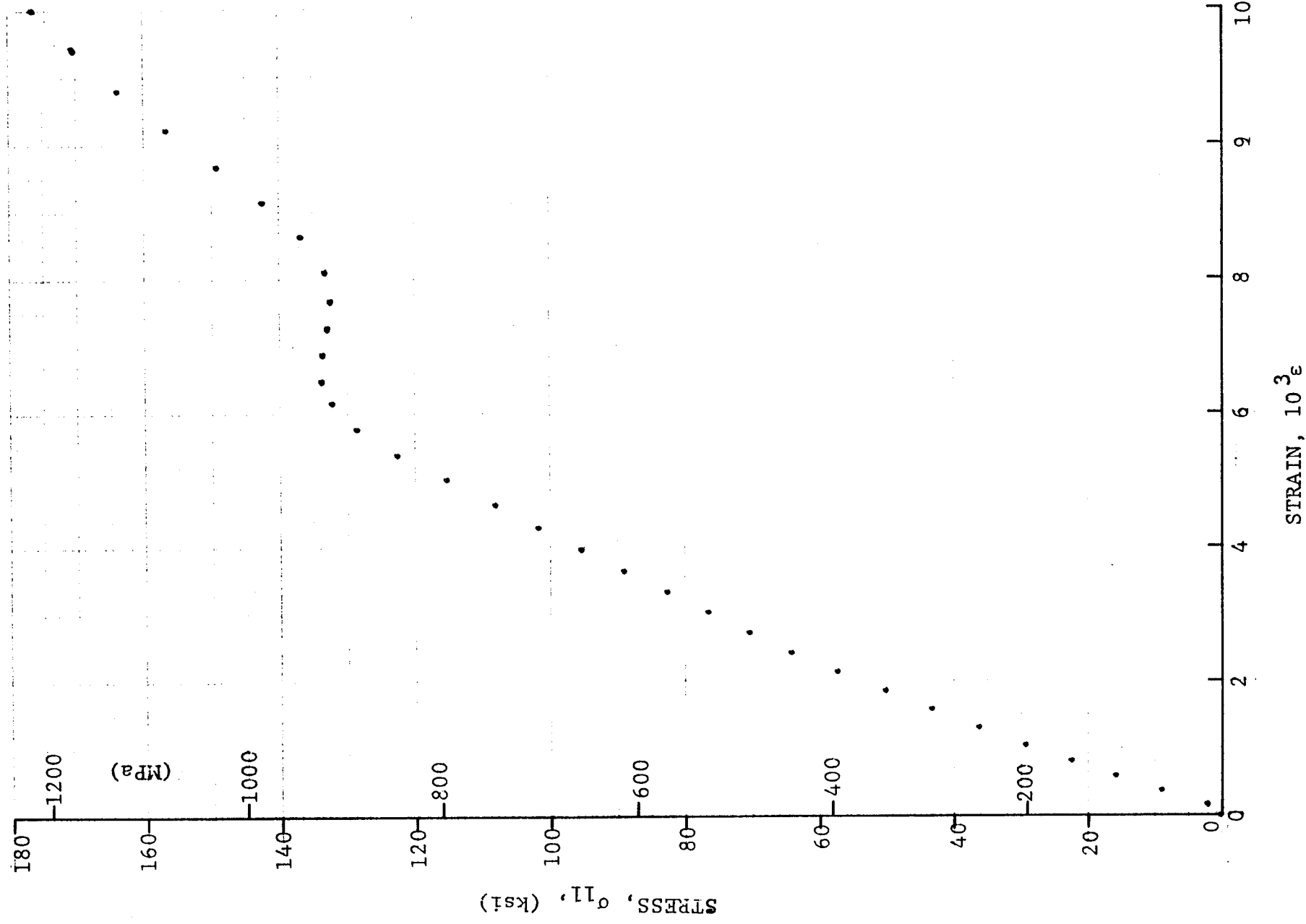


Figure 4-65. Stress-strain curve for dynamically loaded $[0_6]$ 80AS/20S/PR288 graphite/S-glass/epoxy ring for Specimen 10-9 (two 100 mg PETN detonators).



STRAIN, $10^3 \epsilon$

Figure 4-66. Stress-strain curve for dynamically loaded [O₆] 80AS/20S/PR288 graphite/S-glass/epoxy ring for Specimen 10-10 (330 mg PETN detonator).

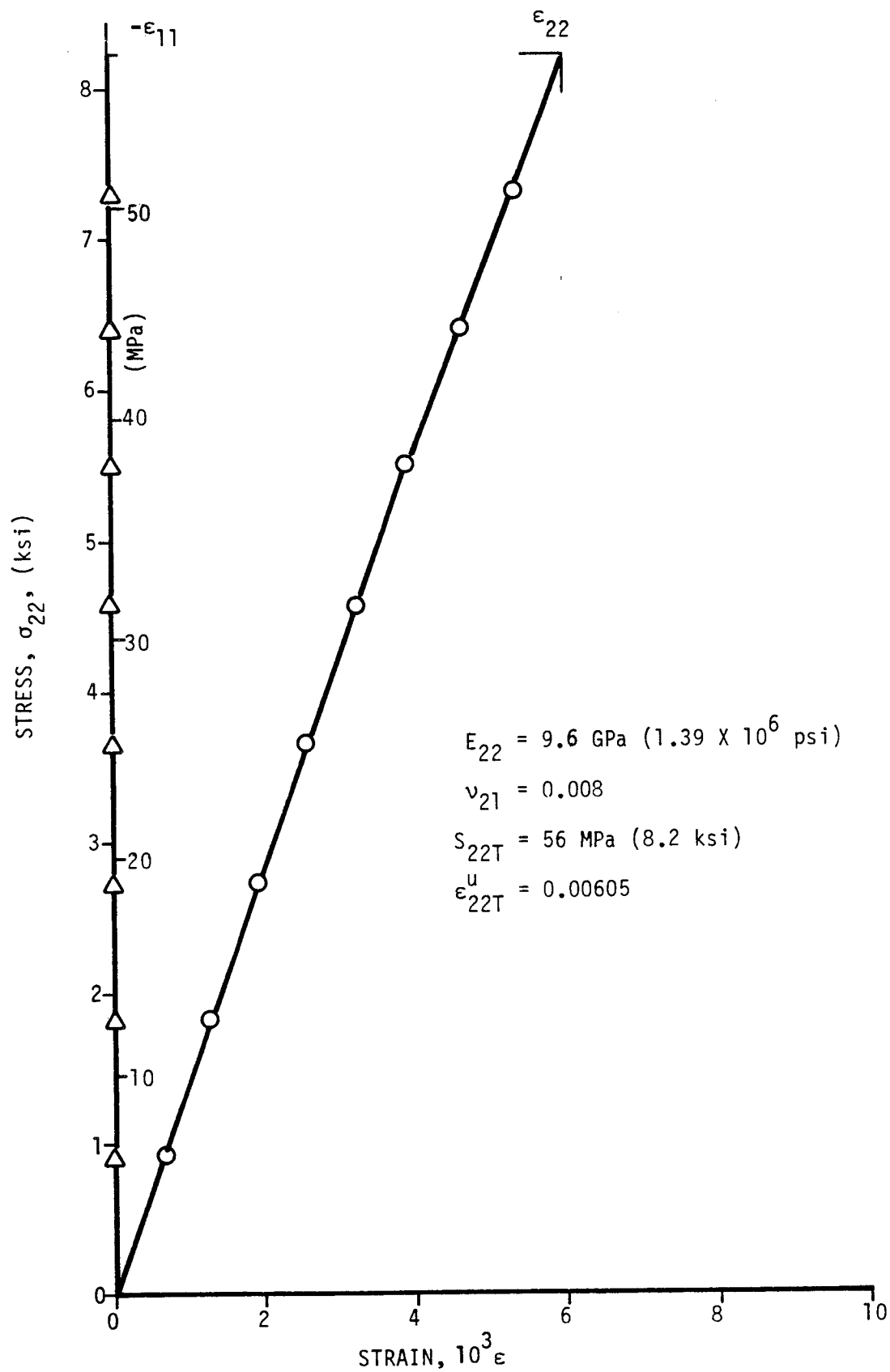
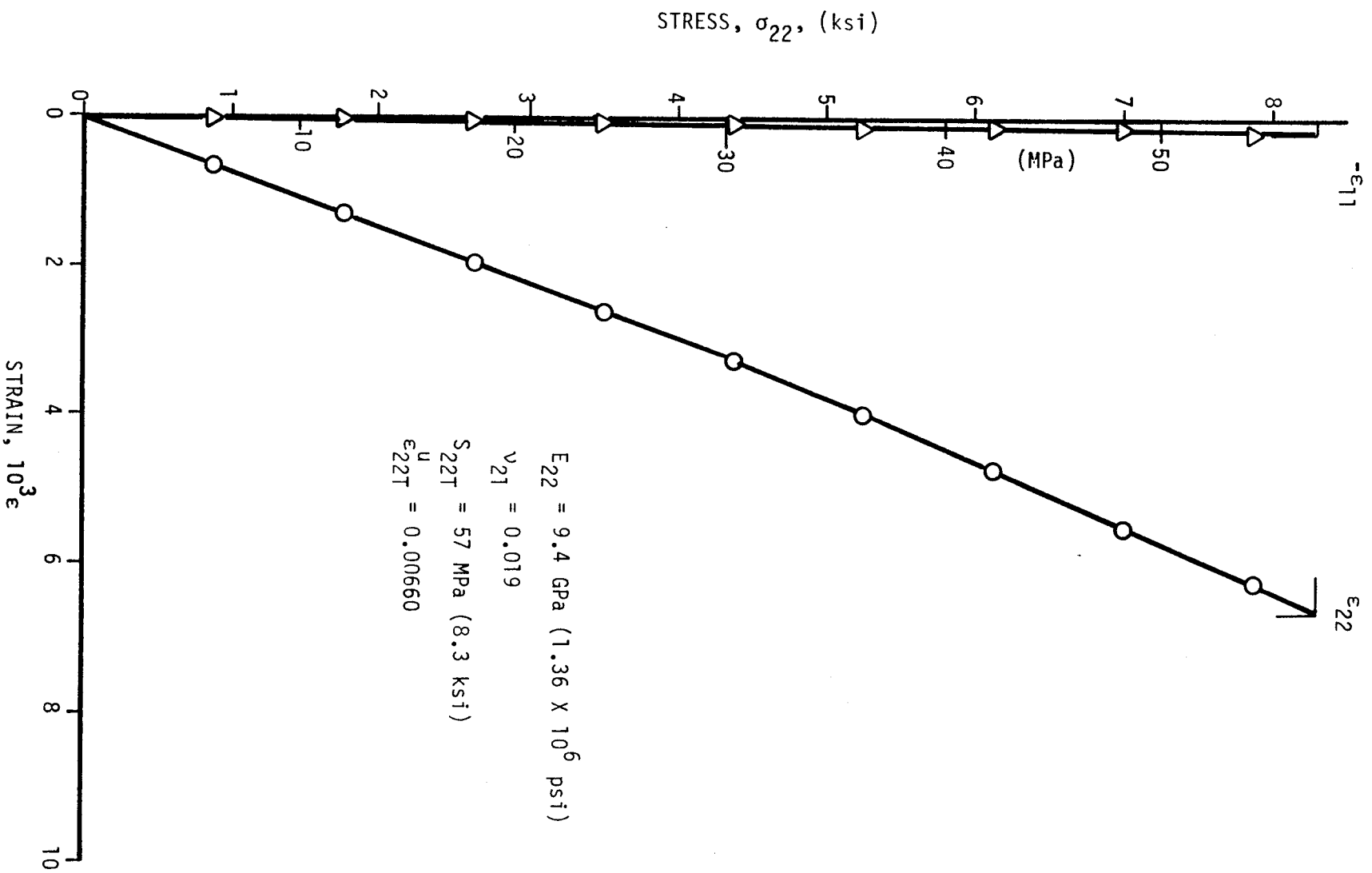


Figure 4-67. Strains in unidirectional 90-deg SP288/T300 ring specimen under static tensile loading (Specimen No. 3-3).



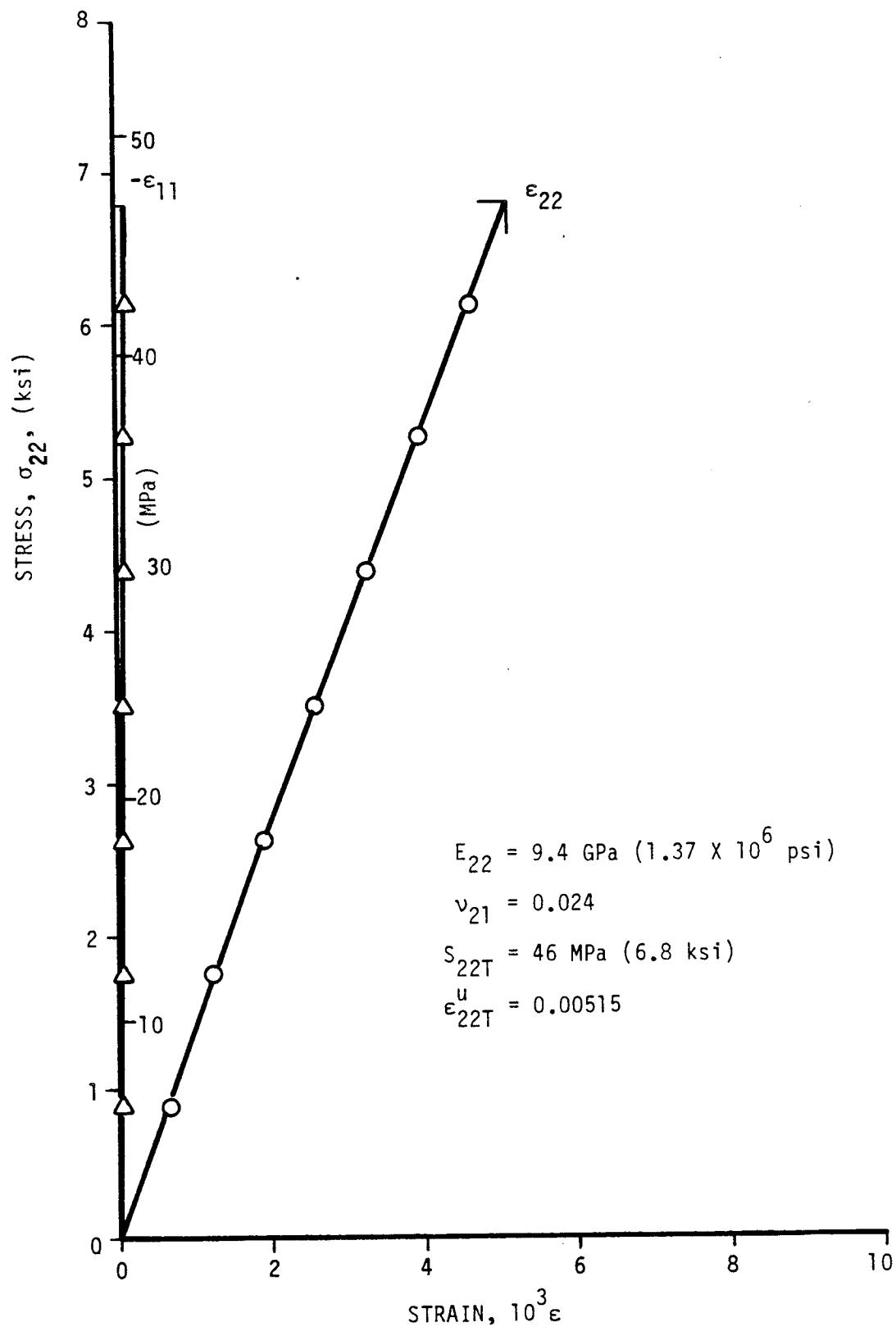


Figure 4-69. Strains in unidirectional 90-deg SP288/T300 ring specimen under static tensile loading (Specimen No. 3-7).

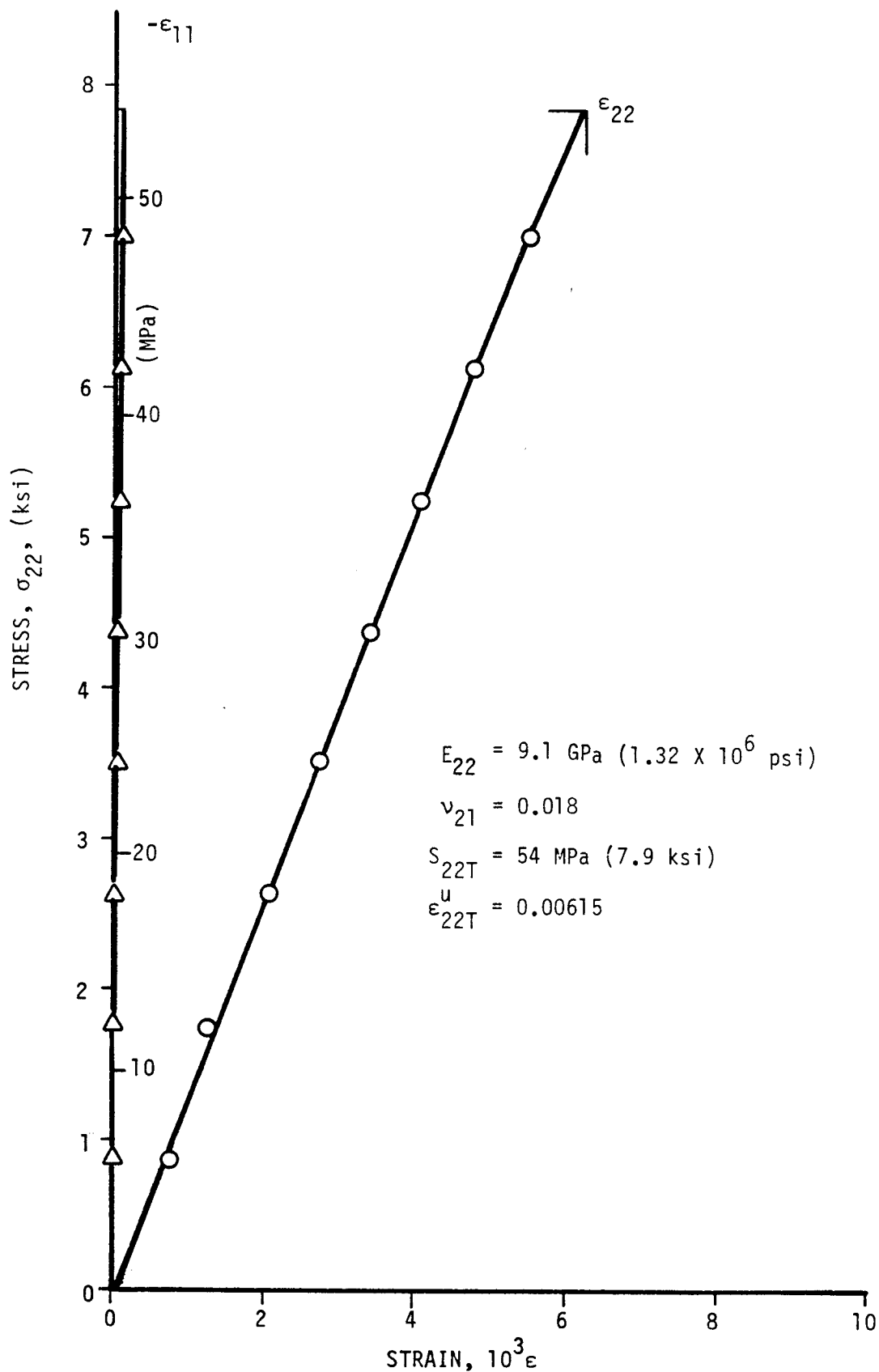


Figure 4-70. Strains in unidirectional 90-deg SP288/T300 ring specimen under static tensile loading (Specimen No. 3-11).

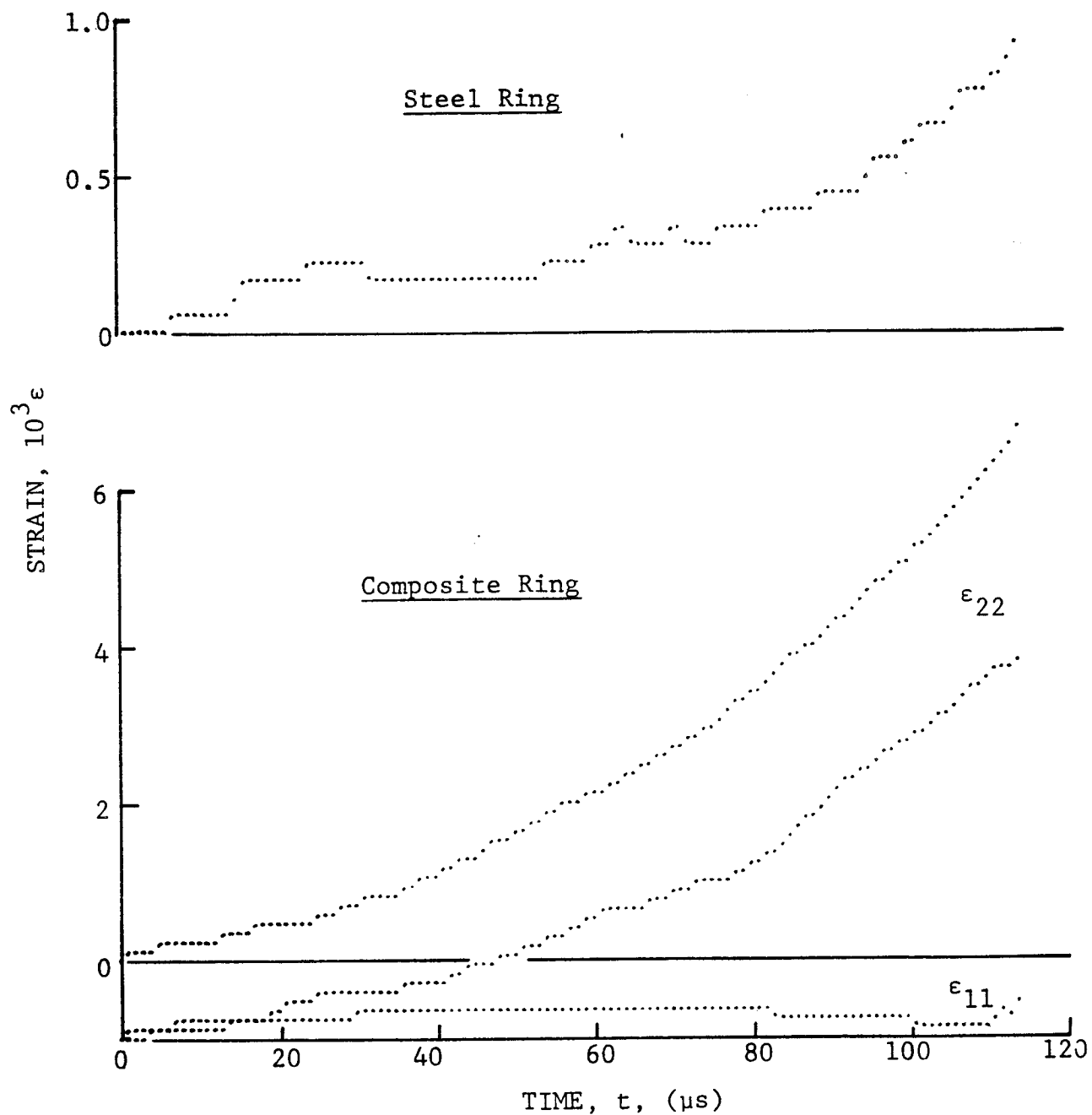


Figure 4-71. Strain record in steel ring and [90_g] SP288/T300 graphite/epoxy ring under dynamic loading for Specimen No. 44-5 (650 mg pistol powder).

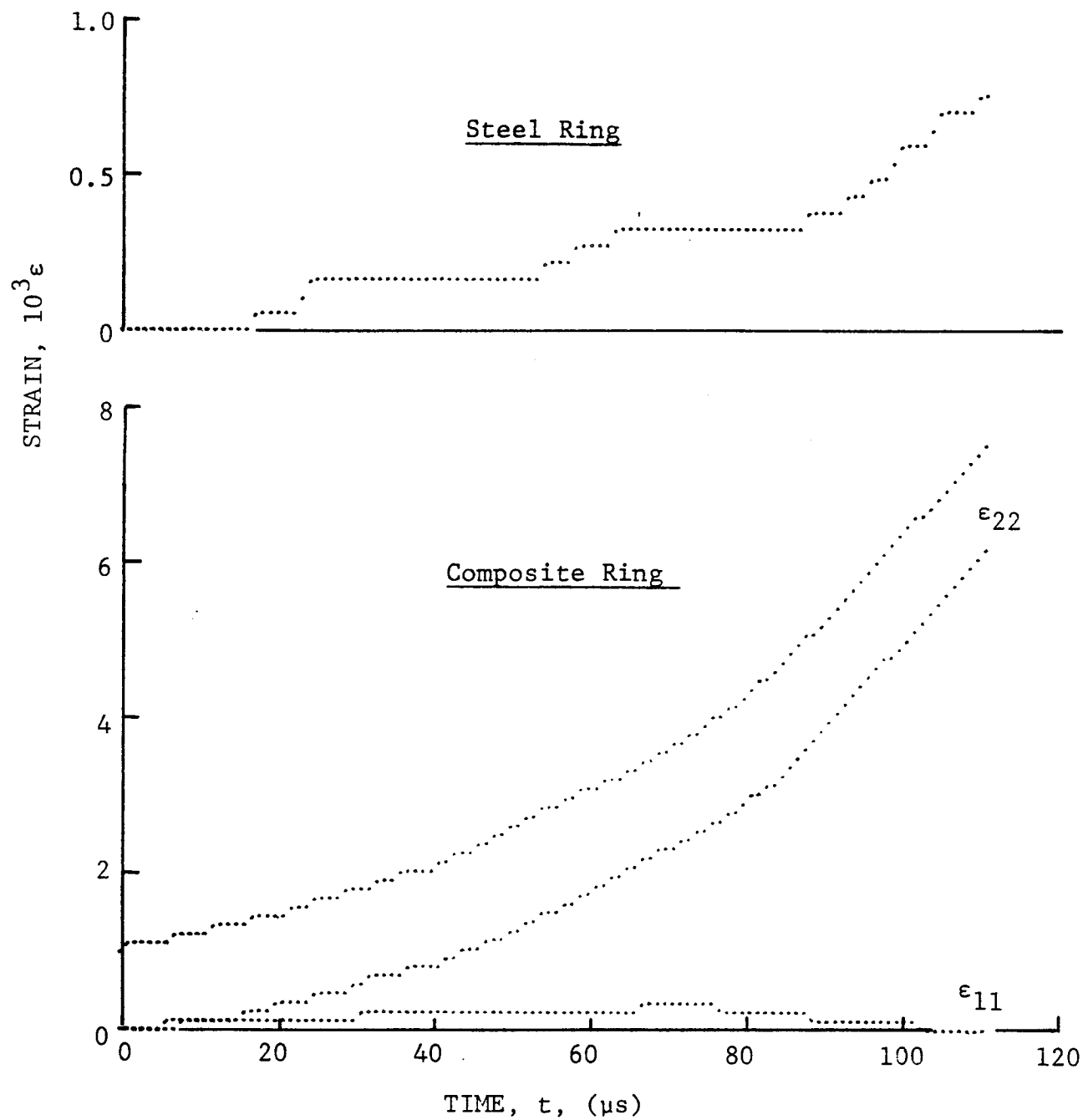


Figure 4-72. Strain records in steel ring and [90_g] SP288/T300 graphite/epoxy ring under dynamic loading for Specimen No. 44-6 (650 mg pistol powder).

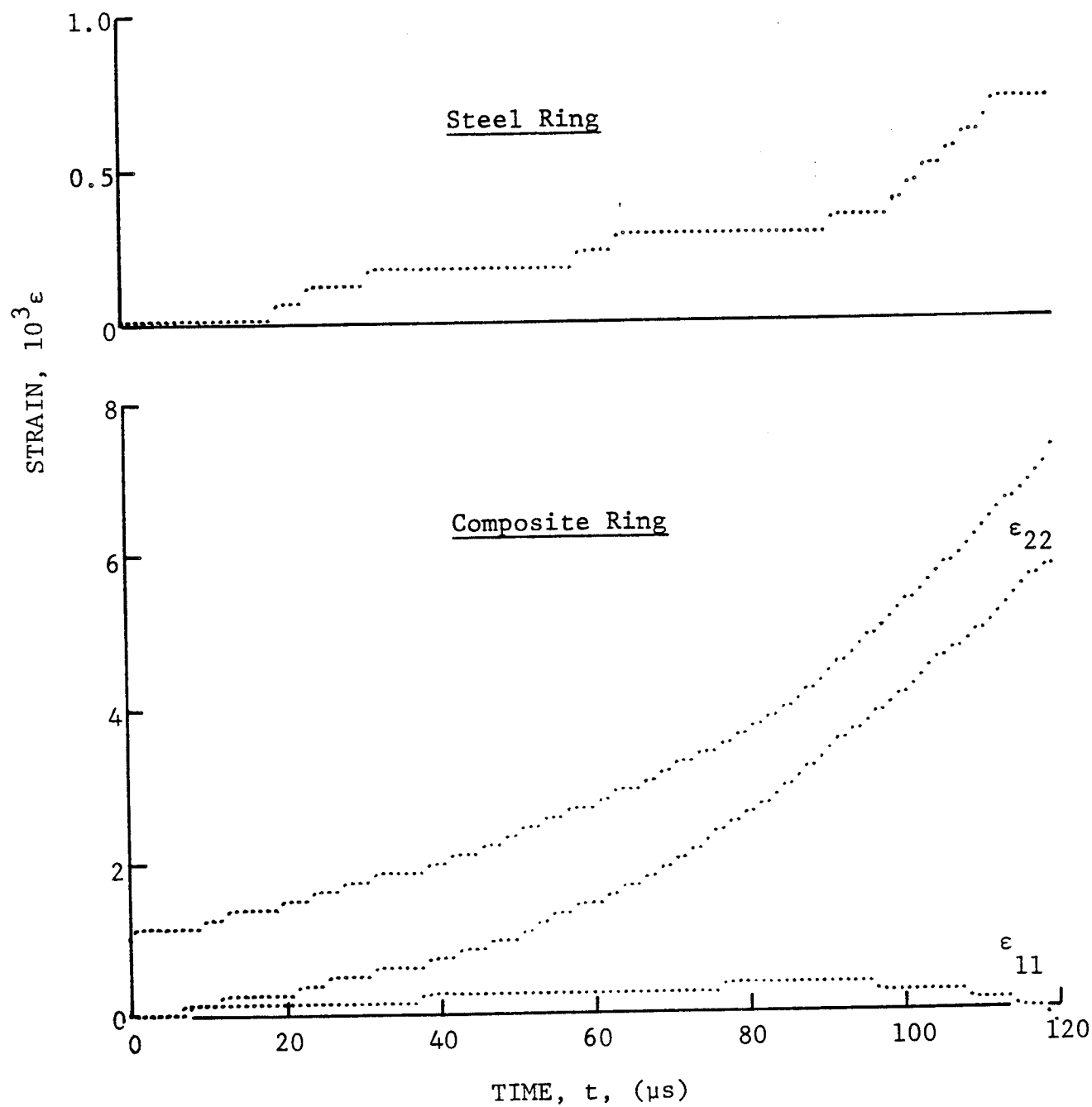


Figure 4-73. Strain records in steel ring and [90_g] SP288/T300 graphite/epoxy ring under dynamic loading for Specimen No. 44-7 (650 mg pistol powder).

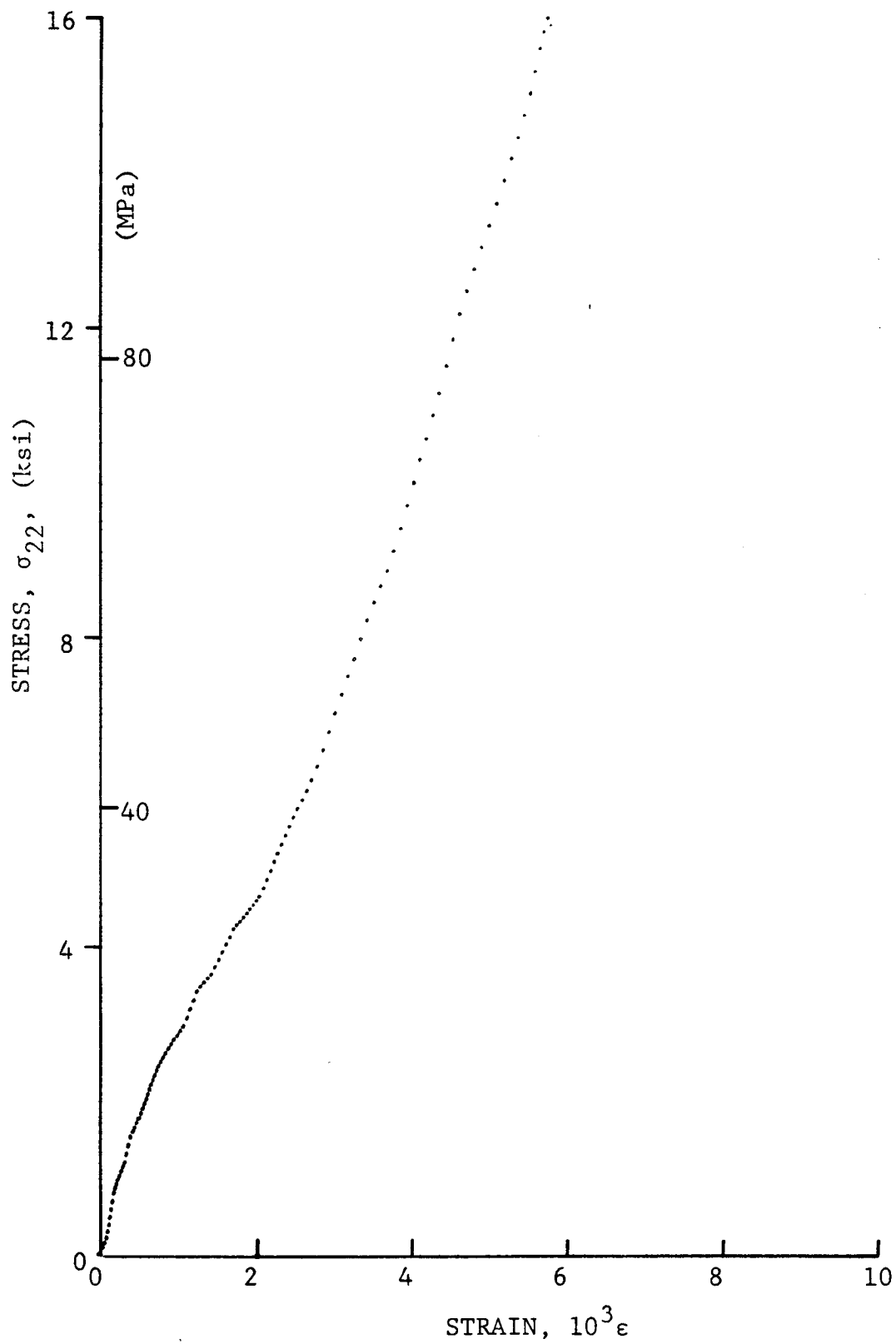


Figure 4-74. Stress-strain curve for dynamically loaded [90°] SP288/T300 graphite/epoxy ring for Specimen No. 44-5 (650 mg pistol powder).

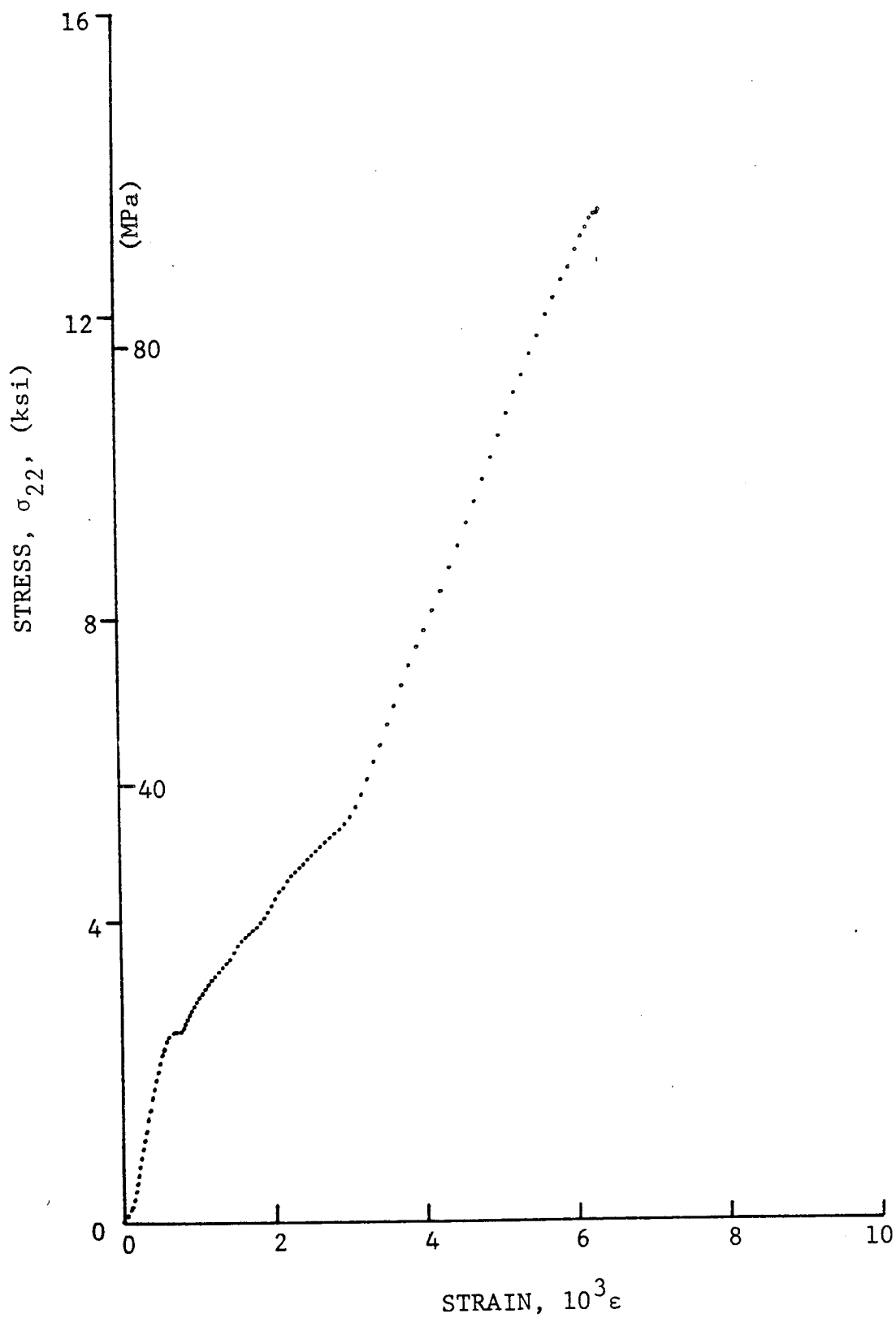


Figure 4-75. Stress-strain curve for dynamically loaded [90g] SP288/T300 graphite/epoxy ring for Specimen No. 44-6 (650 mg pistol powder).

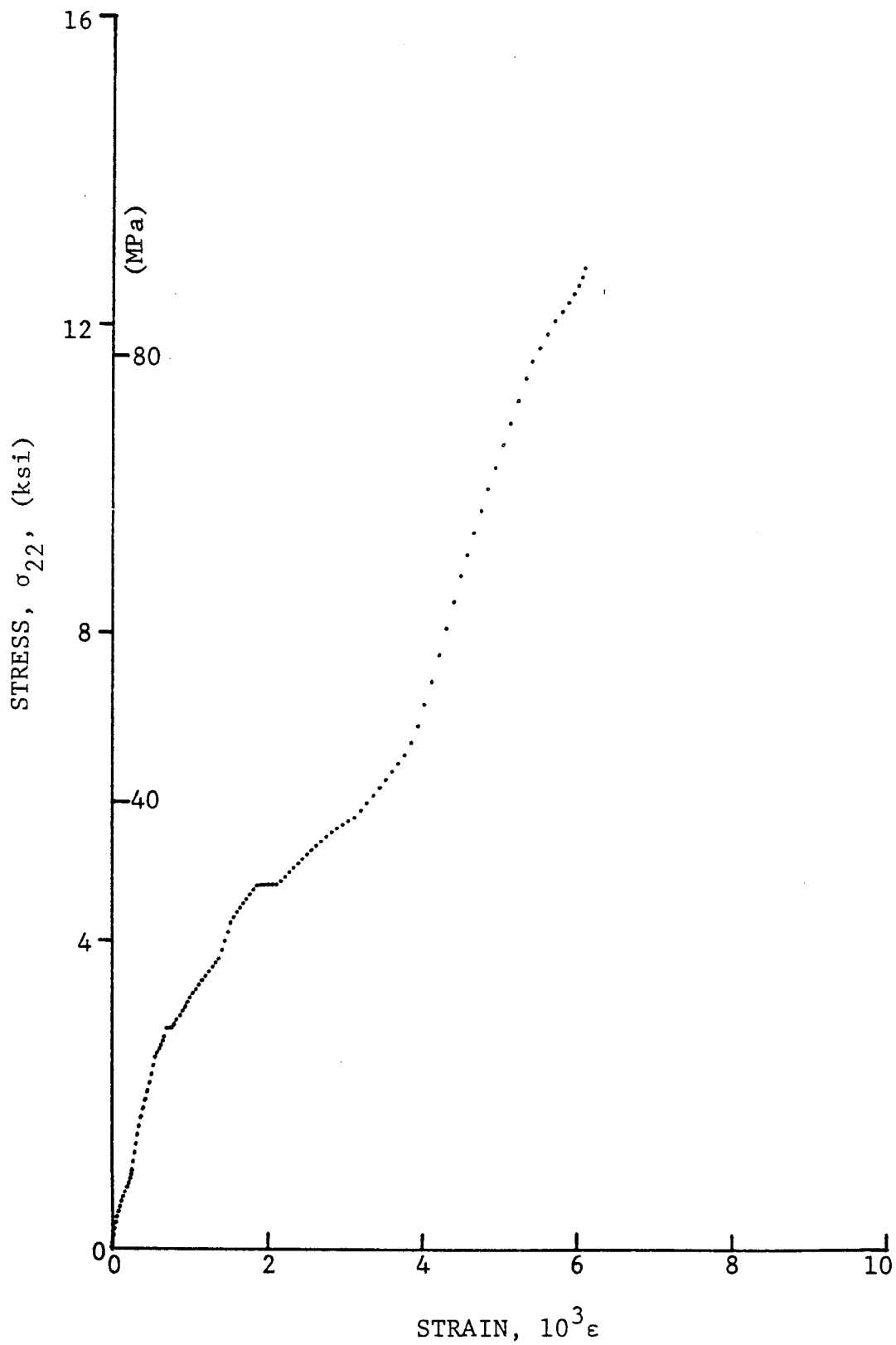


Figure 4-76. Stress-strain curve for dynamically loaded [90g] SP288/T300 graphite/epoxy ring for Specimen No. 44-7 (650 mg pistol powder).

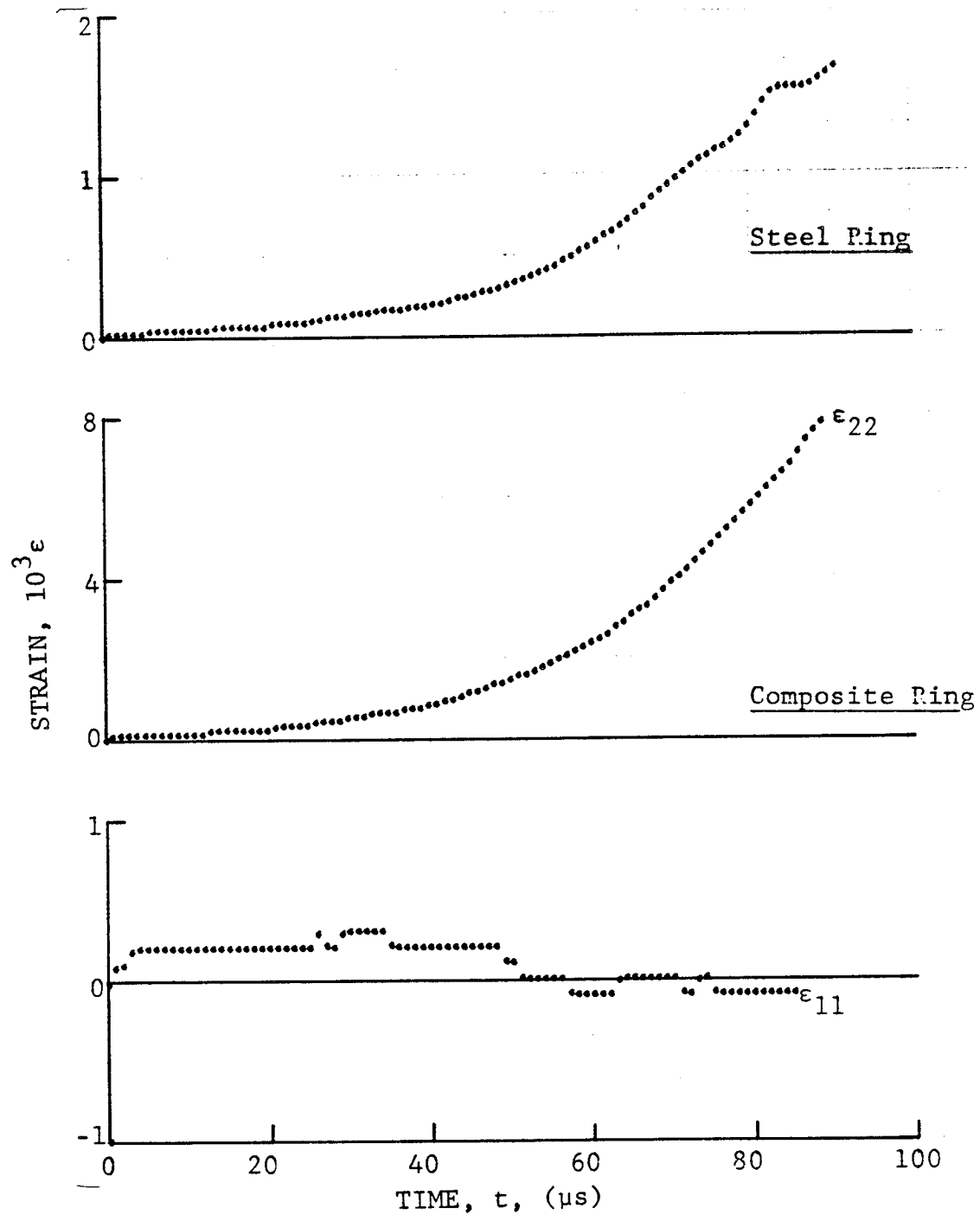


Figure 4-77. Strain records in steel ring and [90_g] SP288/T300 graphite/epoxy ring under dynamic loading for Specimen No. 3-1 (260 mg pistol powder).

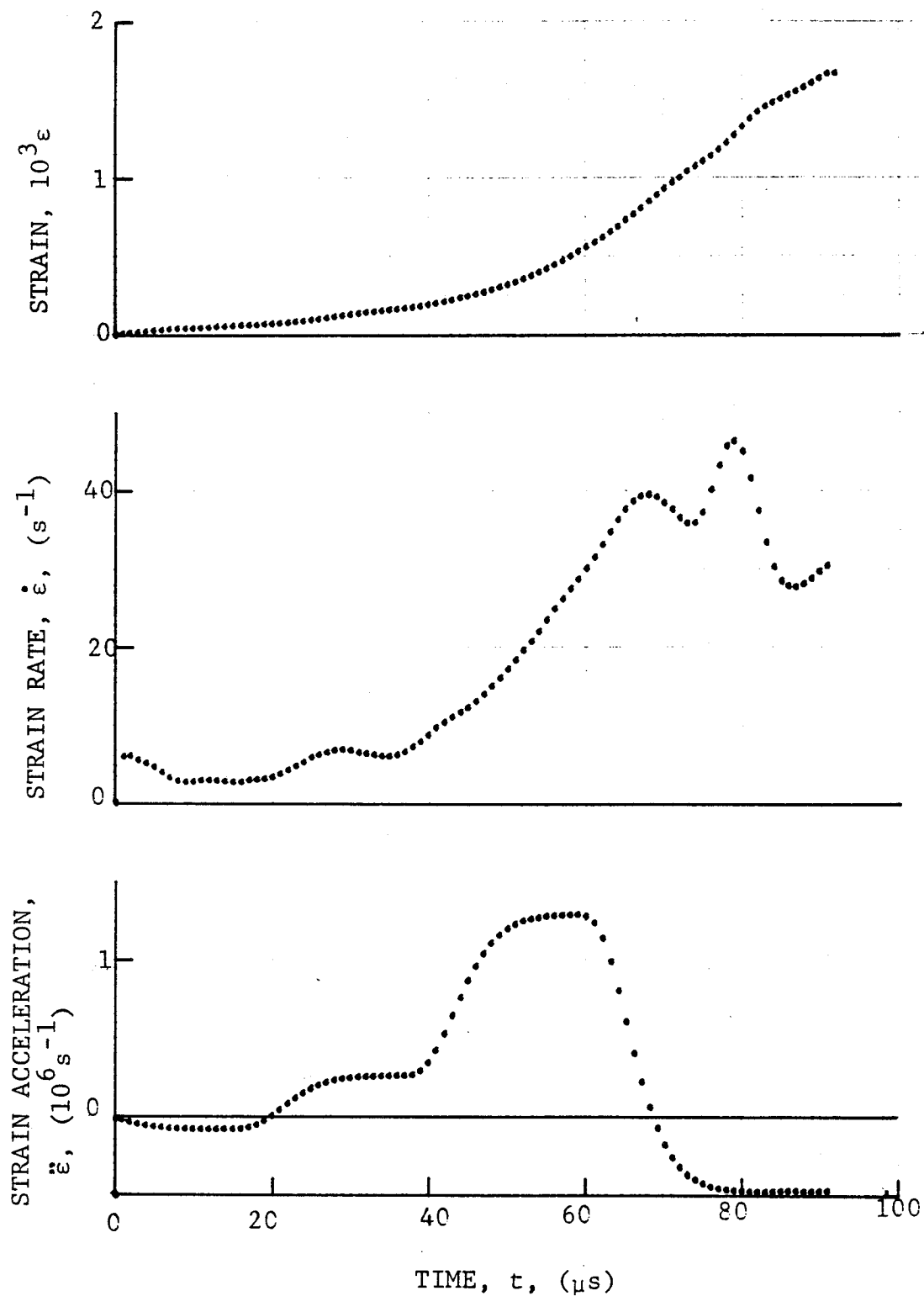


Figure 4-78. Strain and its derivatives in steel ring for Specimen No. 3-1.

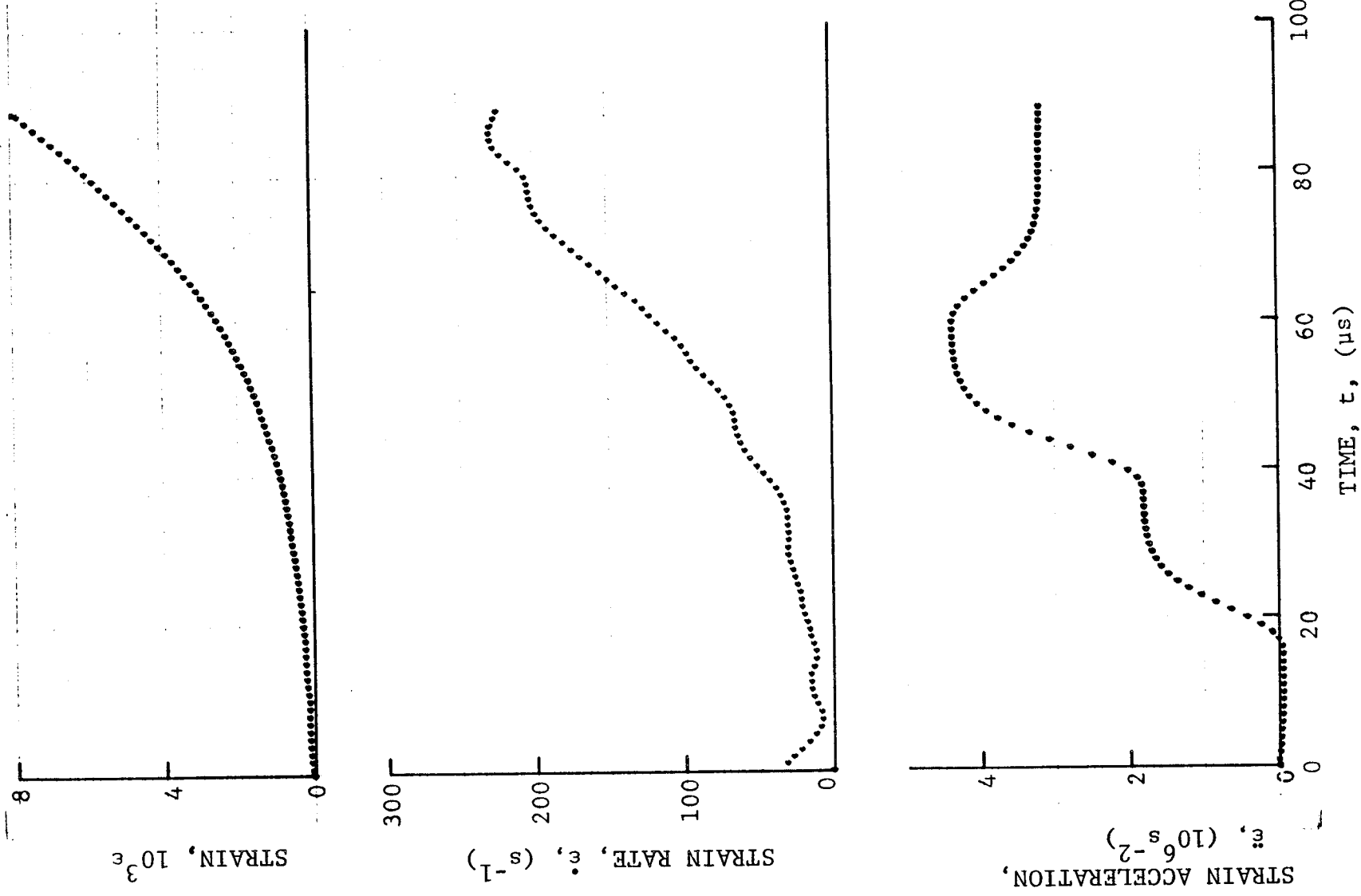


Figure 4-79. Circumferential strain and its derivatives in [90g] SP288/T300 graphite/epoxy ring under dynamic loading for Specimen No. 3-1 (260 mg pistol powder).

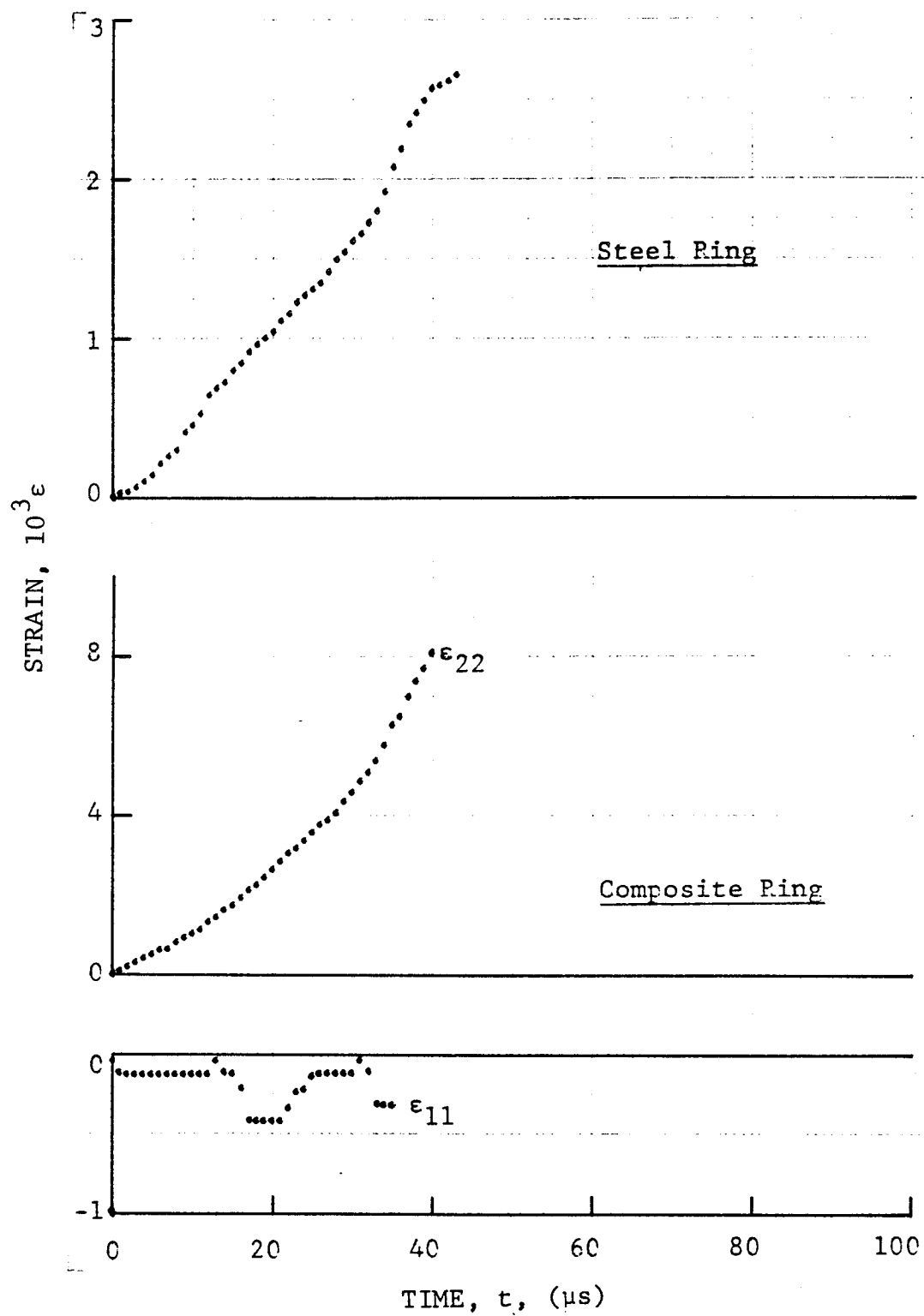


Figure 4-80. Strain records in steel ring and [90_g] SP288/T300 graphite/epoxy ring under dynamic loading for Specimen No.3-2 (50 mg PETN detonator).

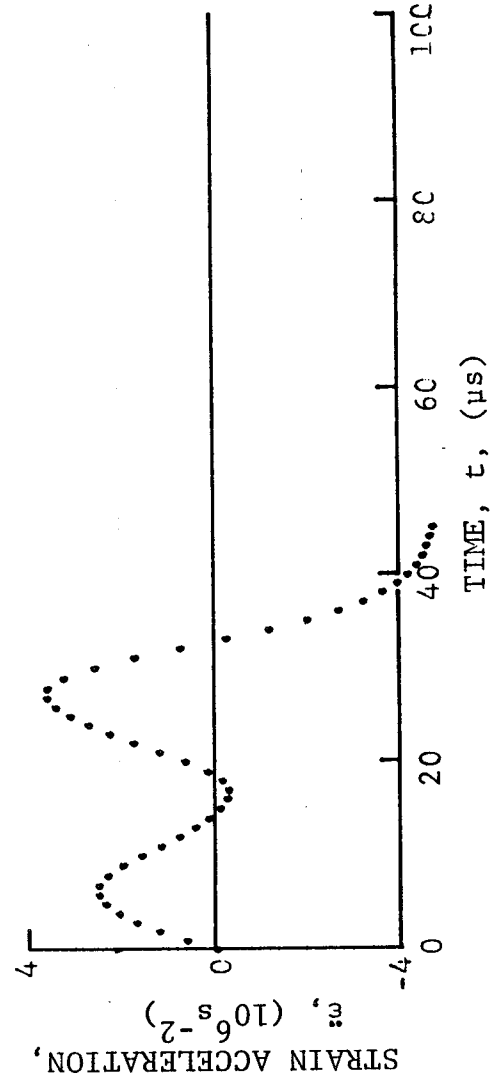
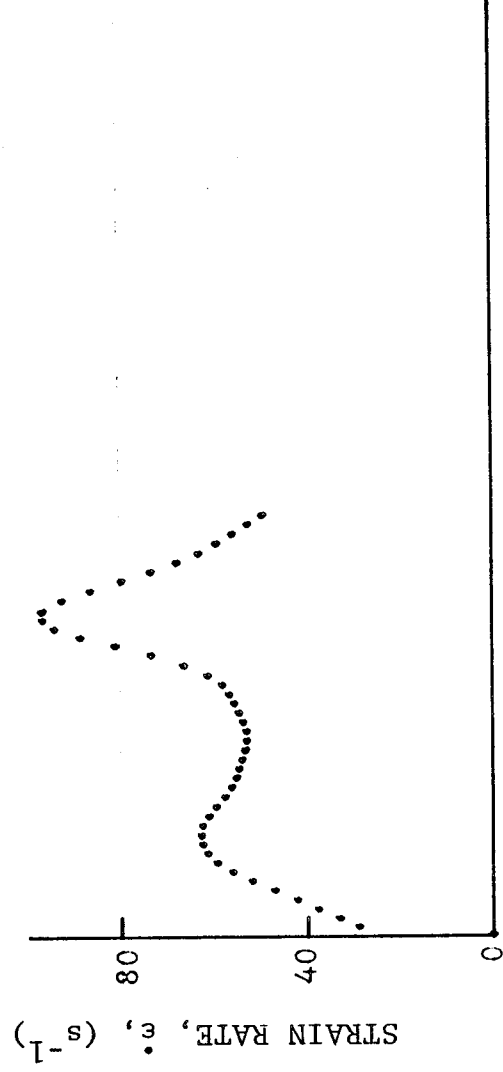
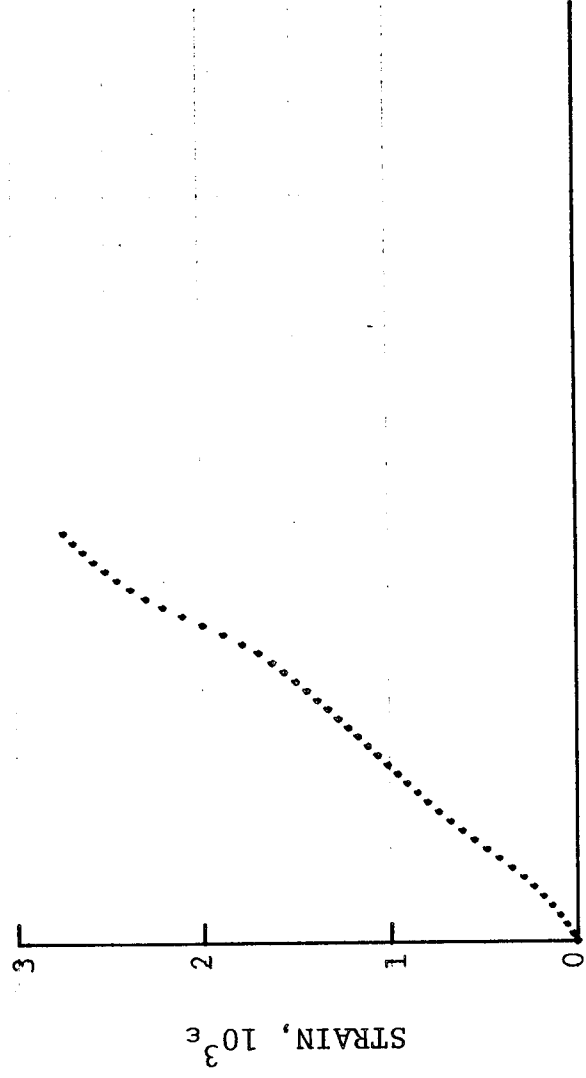


Figure 4-81. Strain and its derivatives in steel ring for Specimen No. 3-2.

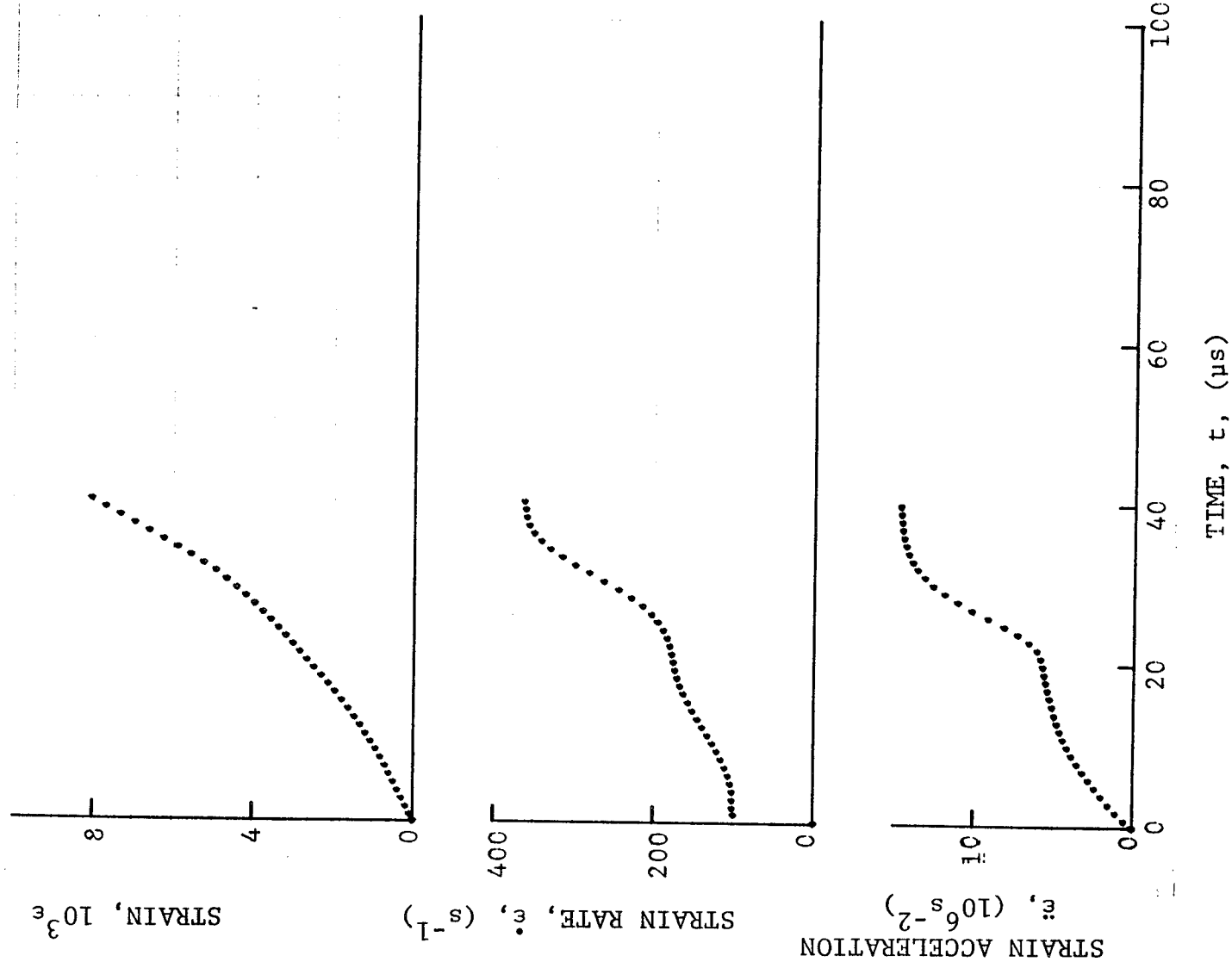


Figure 4-82. Circumferential strain and its derivatives in [90g] SP288/T300 graphite/epoxy ring under dynamic loading for Specimen No. 3-2 (50 mg PETN detonator).

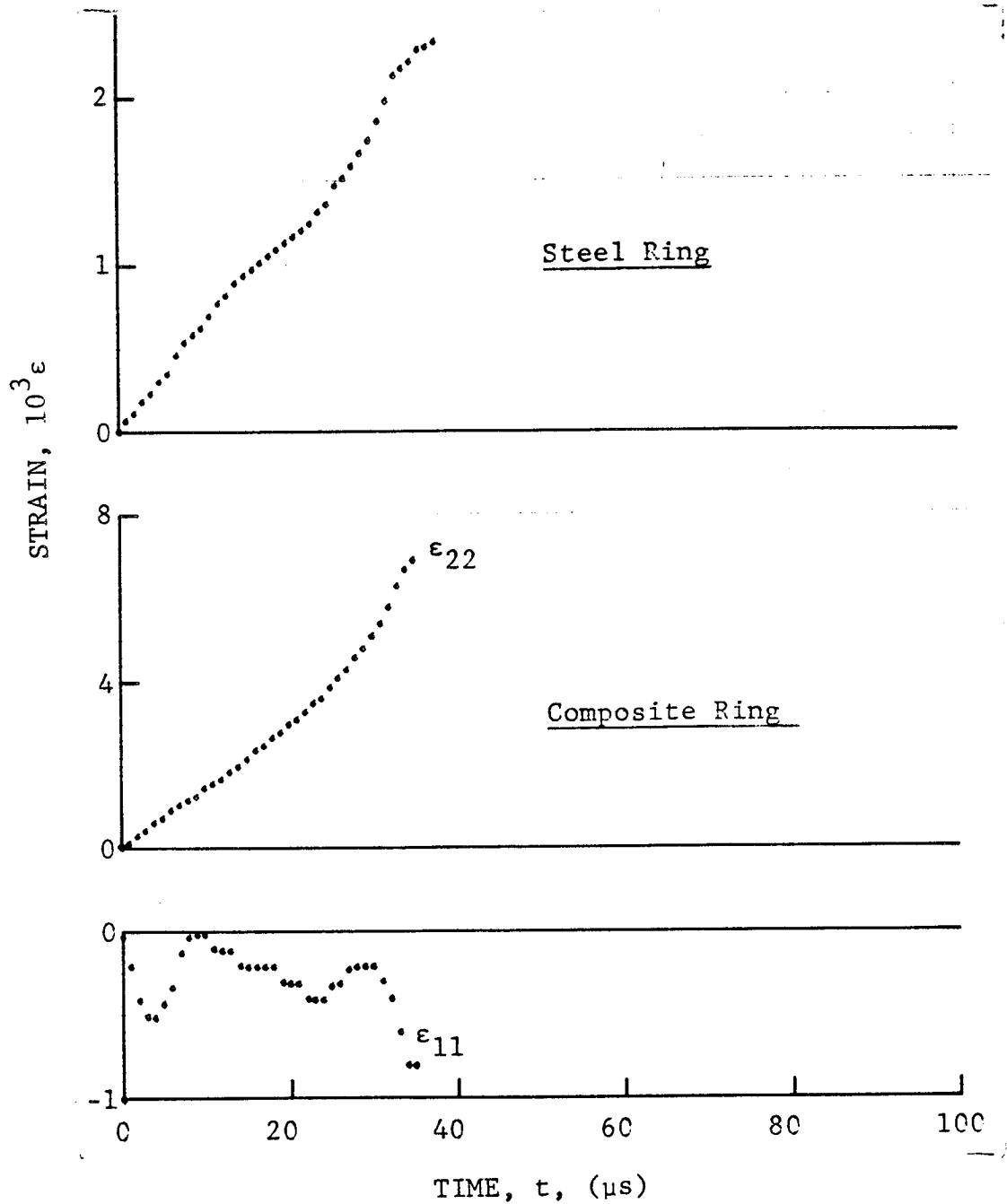


Figure 4-83. Strain records in steel ring and [90_g] SP288/T300 graphite/epoxy ring under dynamic loading for Specimen No. 3-5 (50 mg PETN detonator).

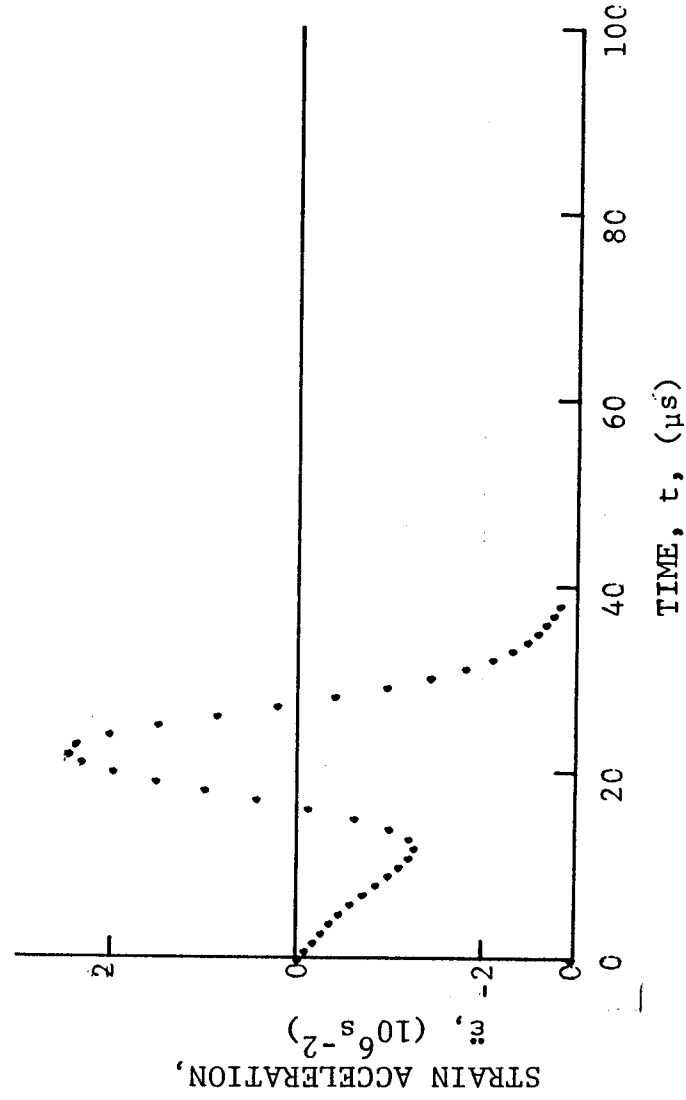
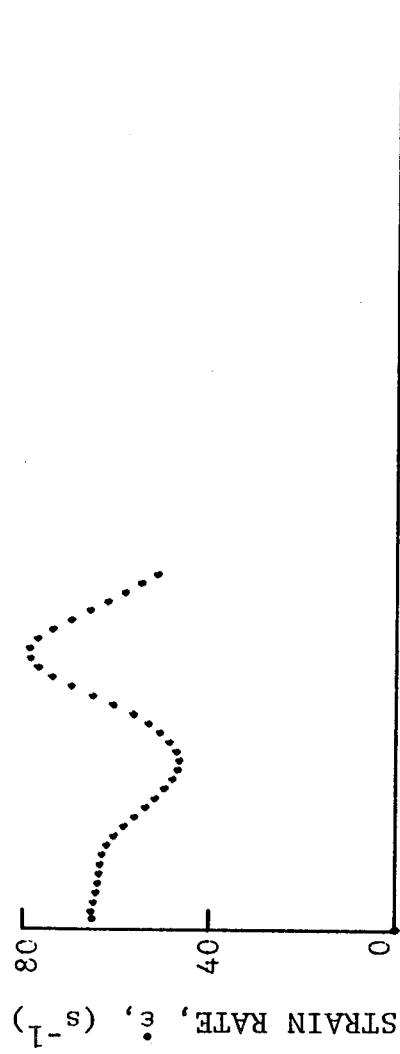
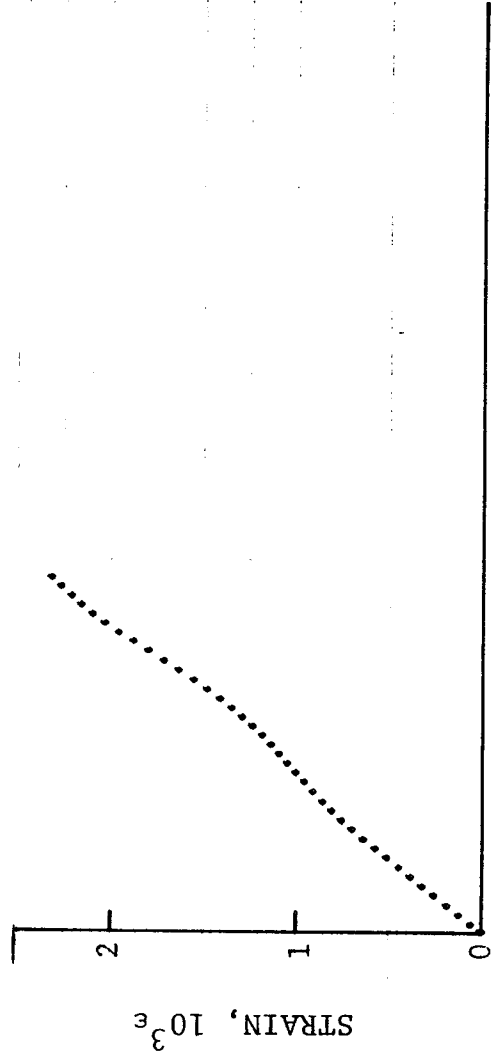


Figure 4-84. Strain and its derivatives in steel ring for Specimen No. 3-5.

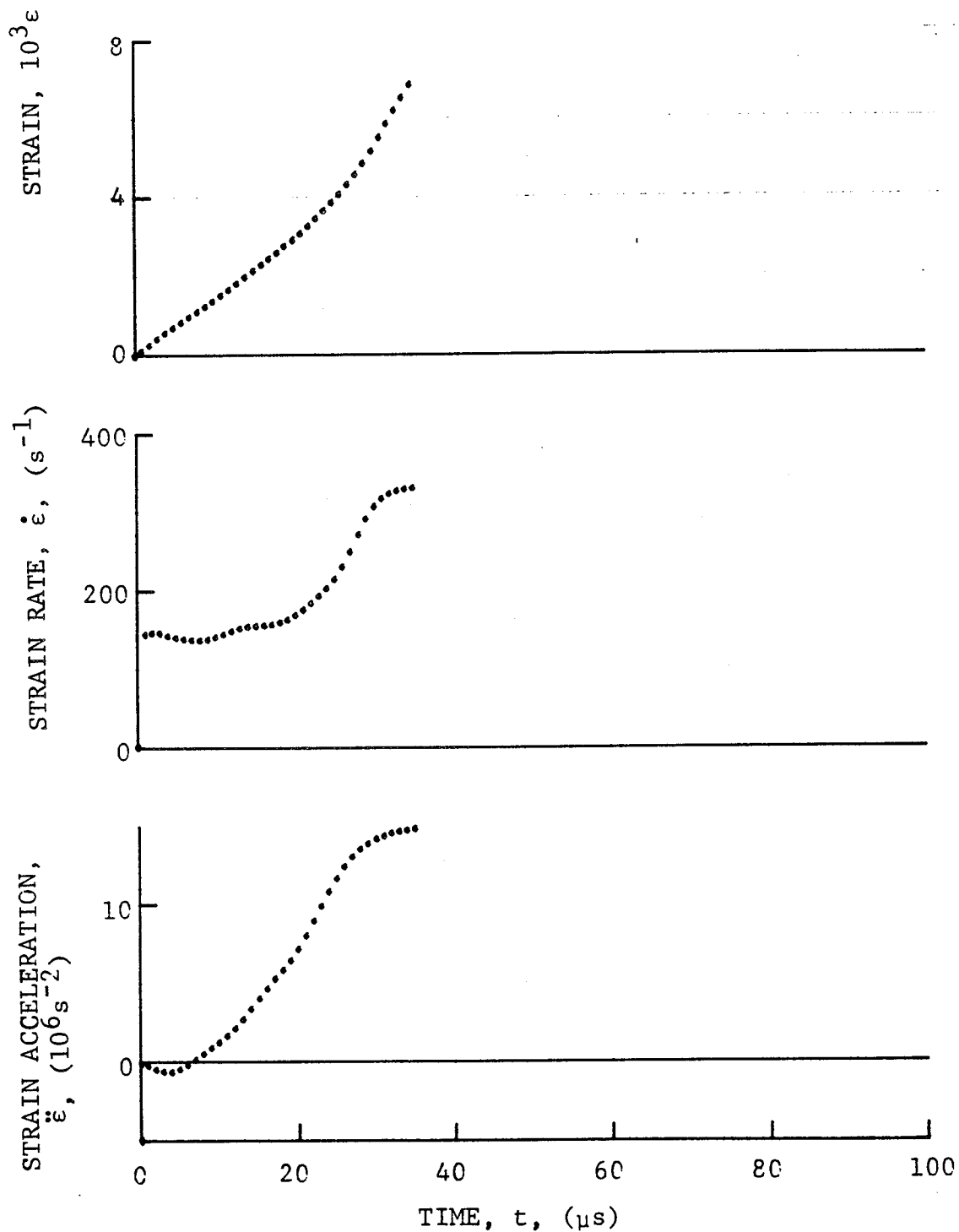


Figure 4-85. Circumferential strain and its derivatives in [90g] SP288/T300 graphite/epoxy ring under dynamic loading for Specimen No. 3-5 (50 mg PETN detonator).

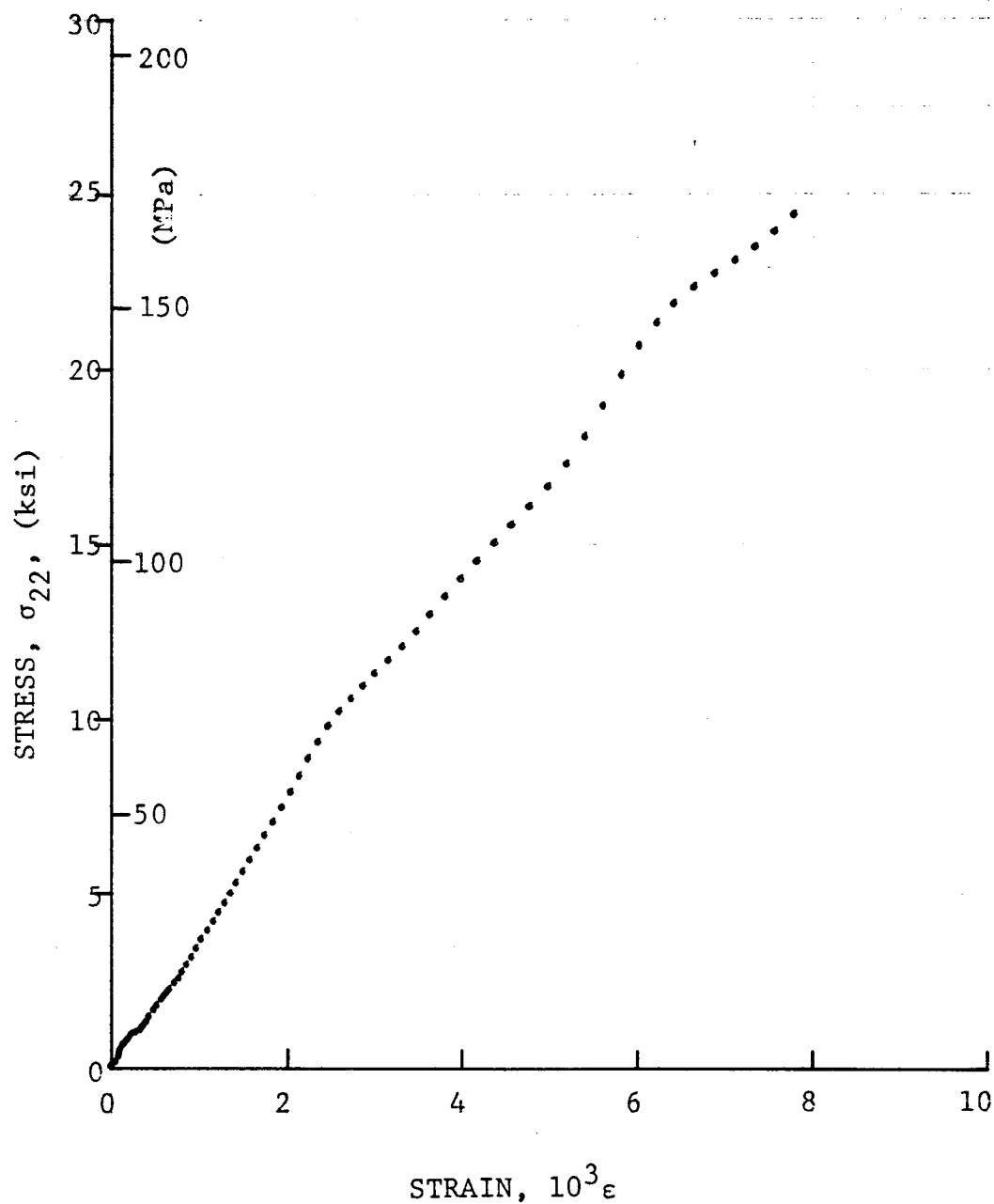


Figure 4-86. Stress-strain curve for dynamically loaded [90g]
SP288/T300 graphite/epoxy ring for Specimen No. 3-1
(260 mg pistol powder).

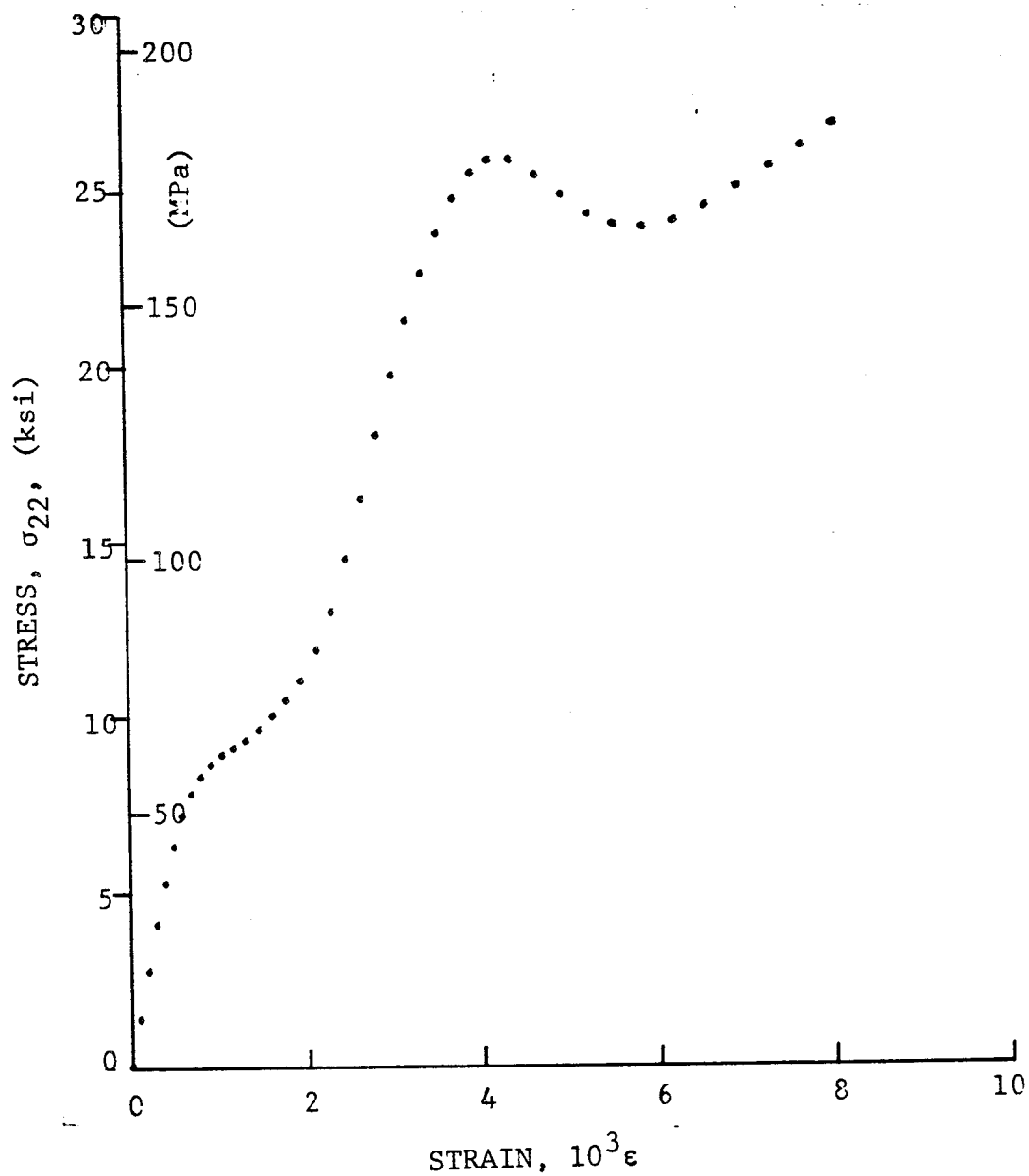


Figure 4-87. Stress-strain curve for dynamically loaded [90_g] SP288/T300 graphite/epoxy ring for Specimen No. 3-2 (50 mg PETN detonator).

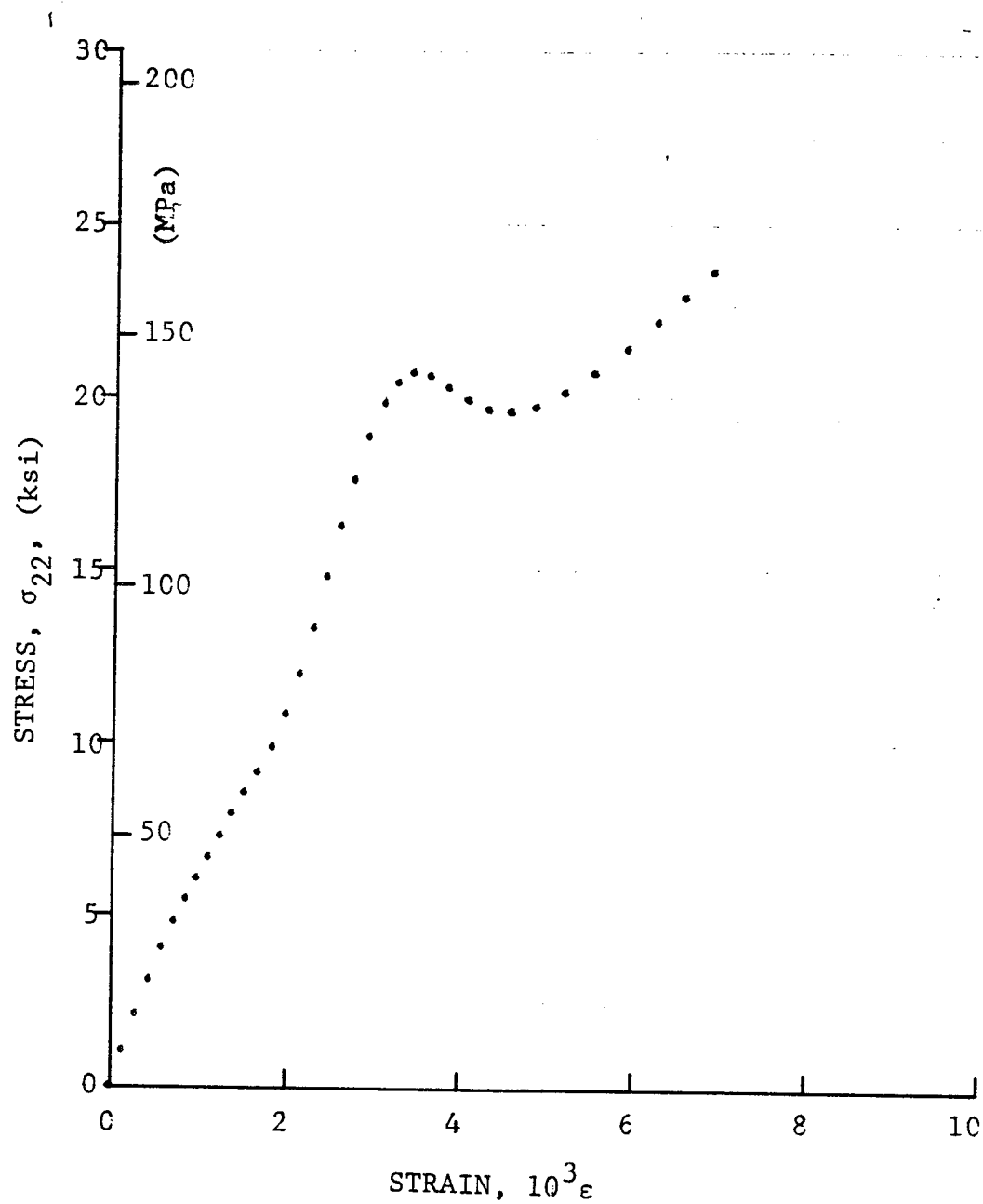


Figure 4-88. Stress-strain curve for dynamically loaded [90g] SP288/T300 graphite/epoxy ring for Specimen No. 3-5 (50 mg PETN detonator).

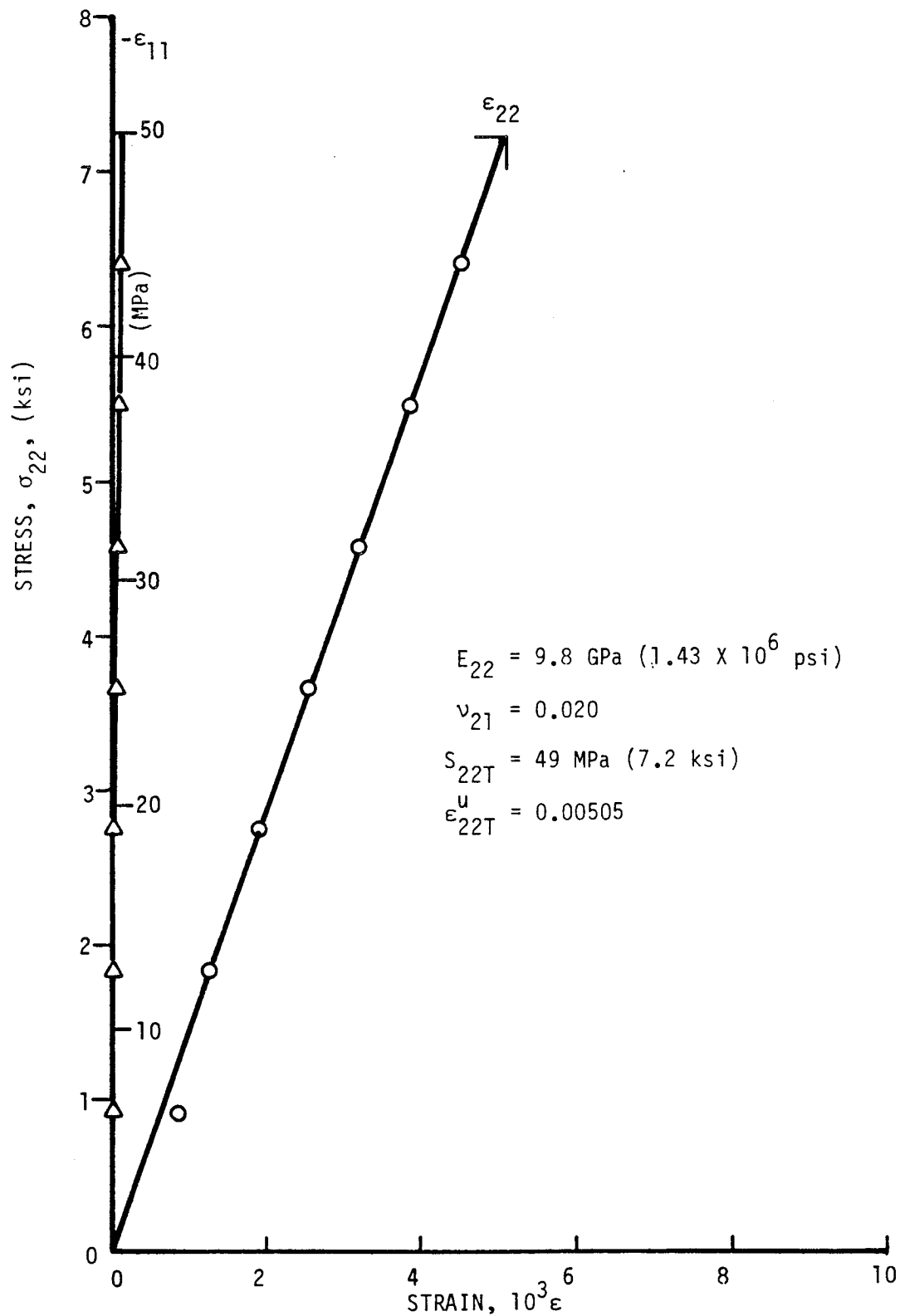


Figure 4-89. Strains in unidirectional 90-deg SP288/AS ring specimen under static tensile loading (Specimen No. 4-3).

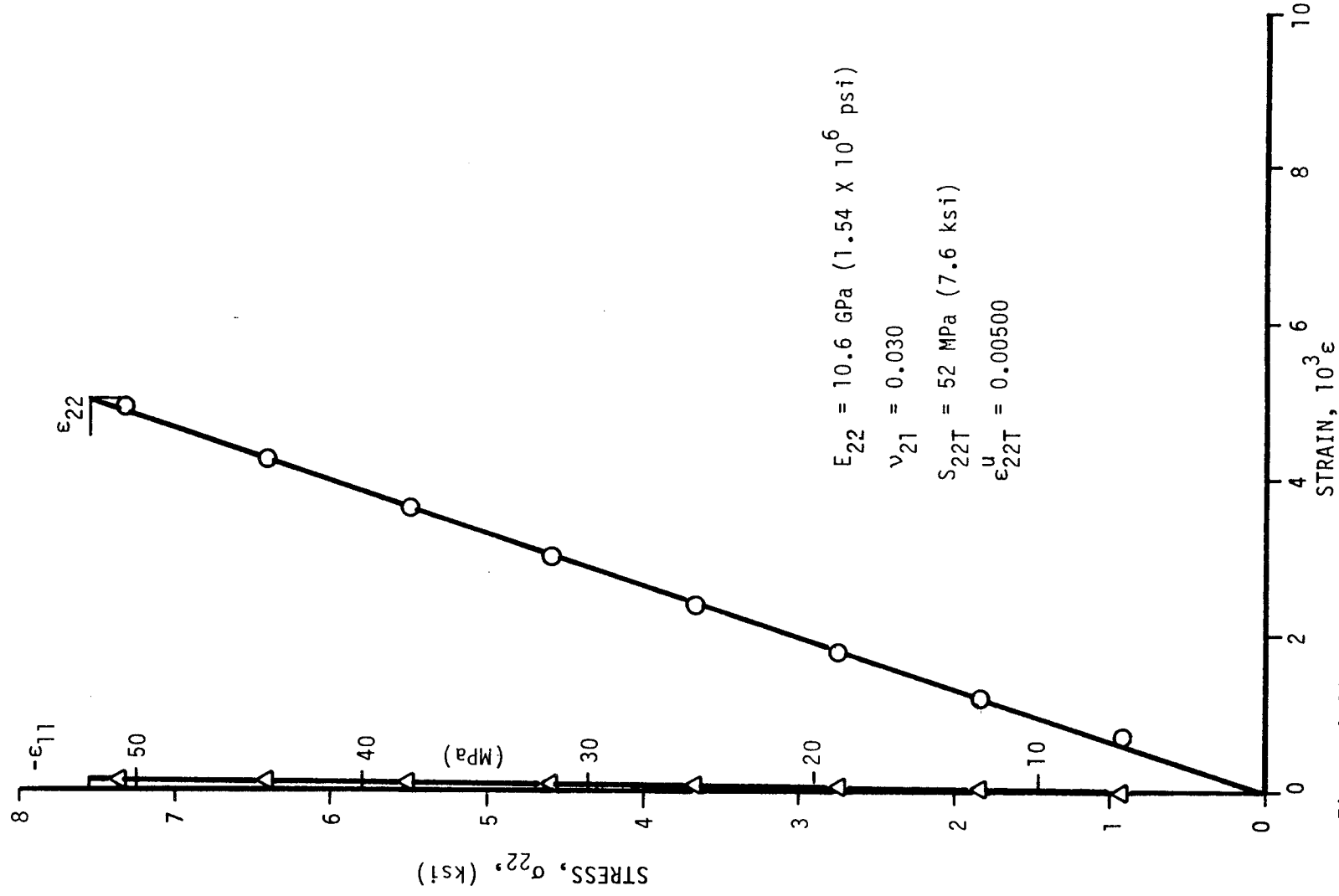


Figure 4-90. Strains in unidirectional 90-deg SP288/AS ring specimen under static tensile loading (Specimen No. 5-5).

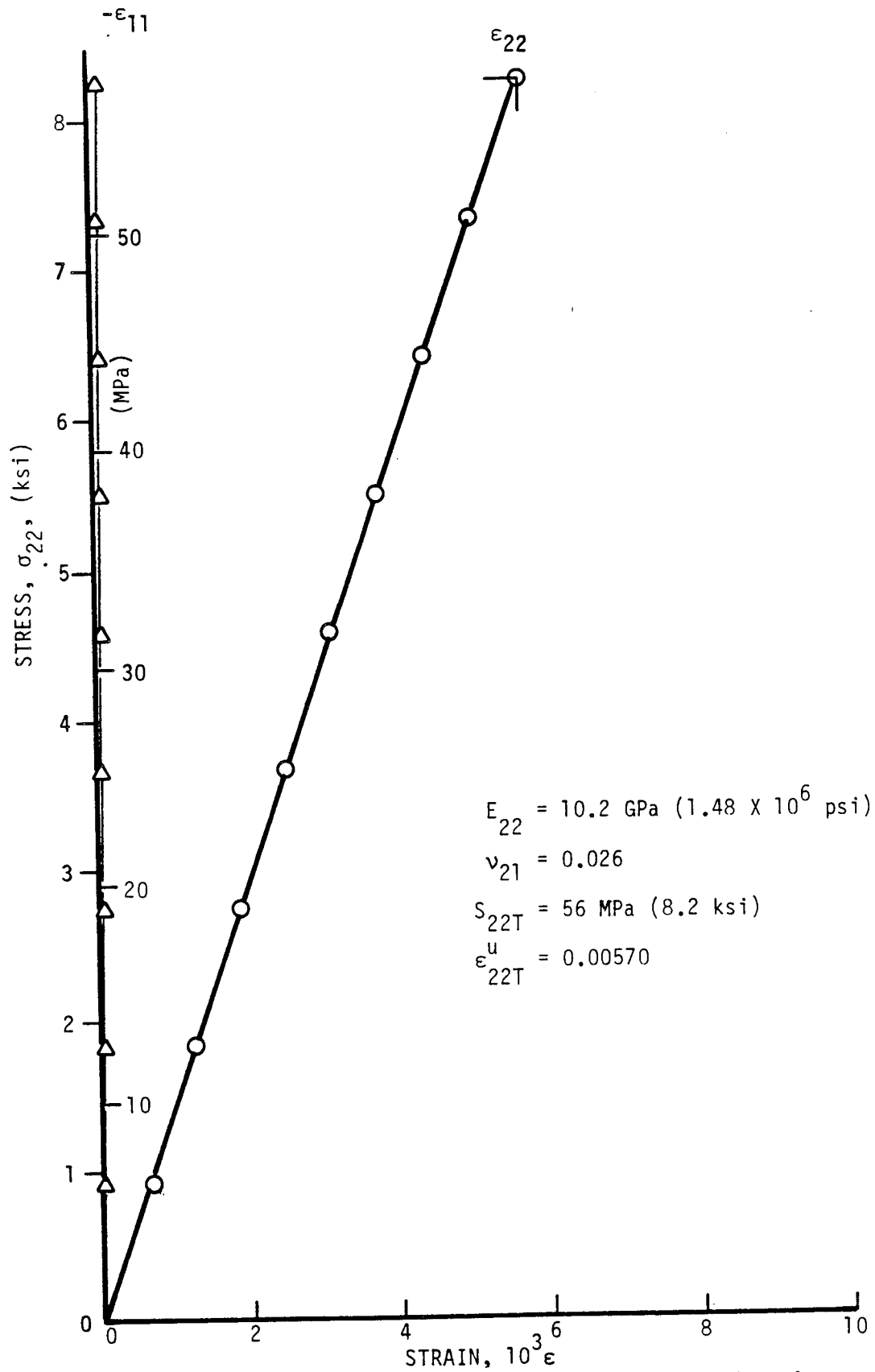


Figure 4-91. Strains in unidirectional 90-deg SP288/AS ring specimen under static tensile loading (Specimen No. 5-6).

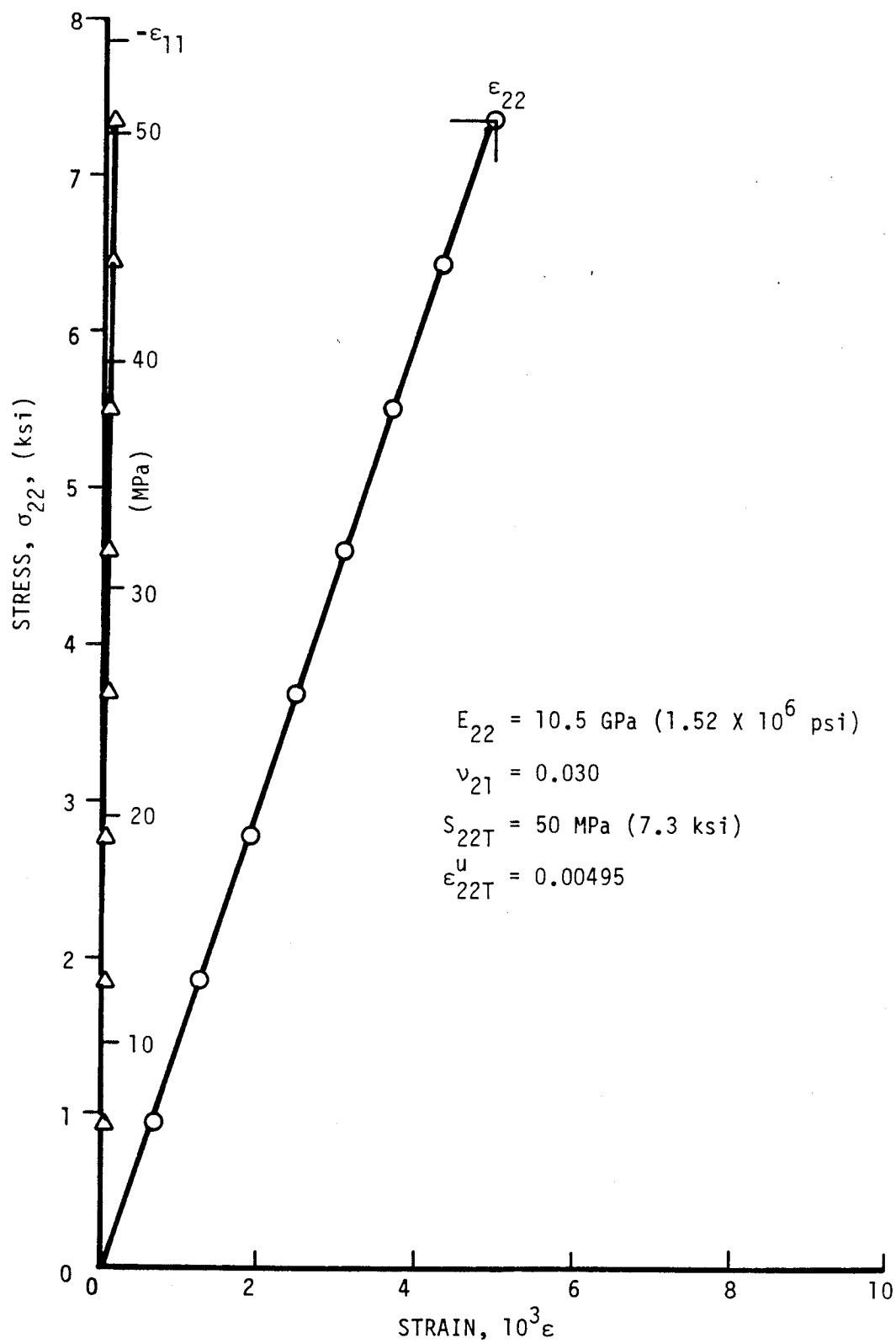


Figure 4-92. Strains in unidirectional 90-deg SP288/AS ring specimen under static tensile loading (Specimen No. 5-10).

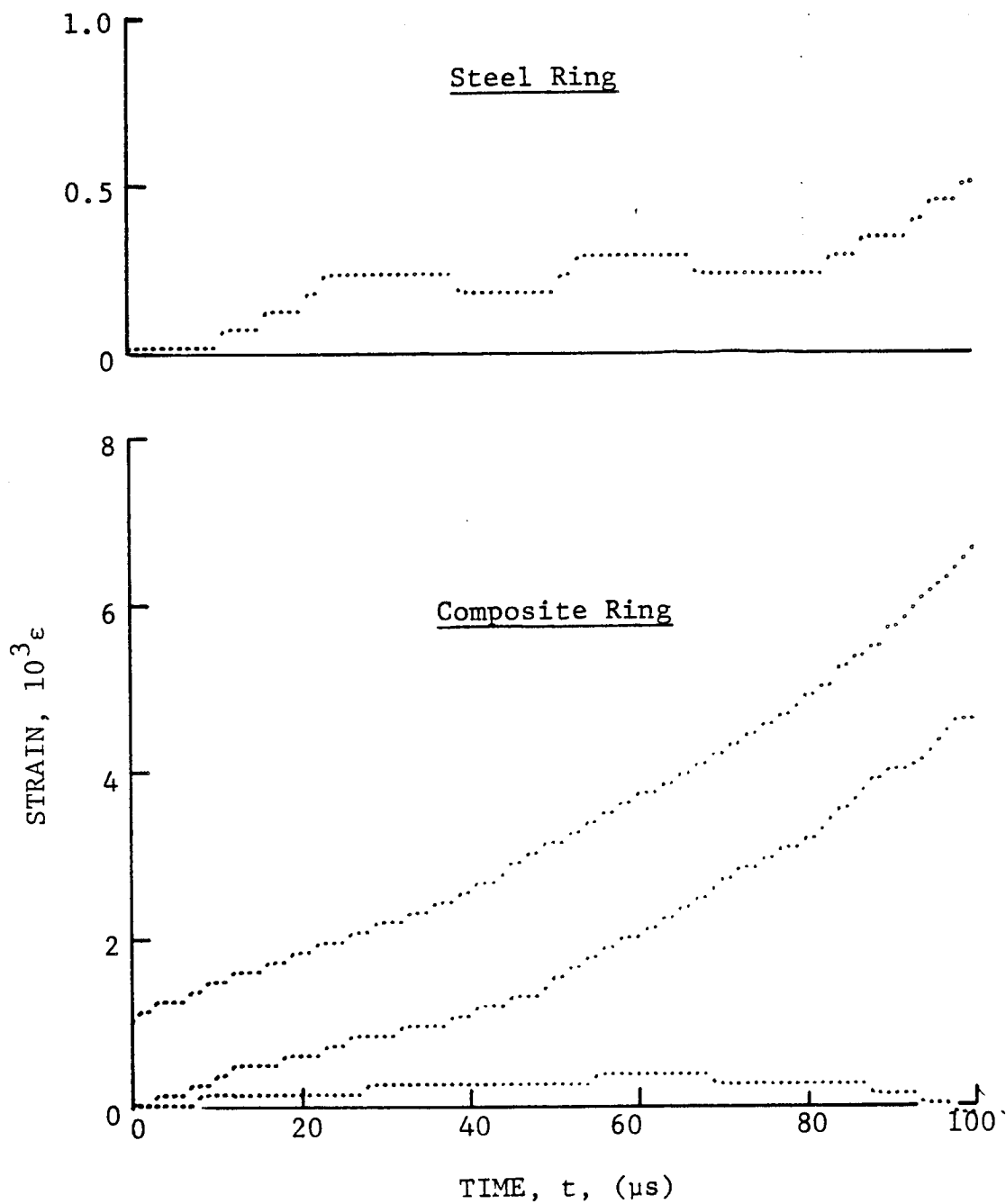


Figure 4-93. Strain records in steel ring and [90g] SP288/AS graphite/epoxy ring under dynamic loading for Specimen No. 38-7 (650 mg pistol powder).

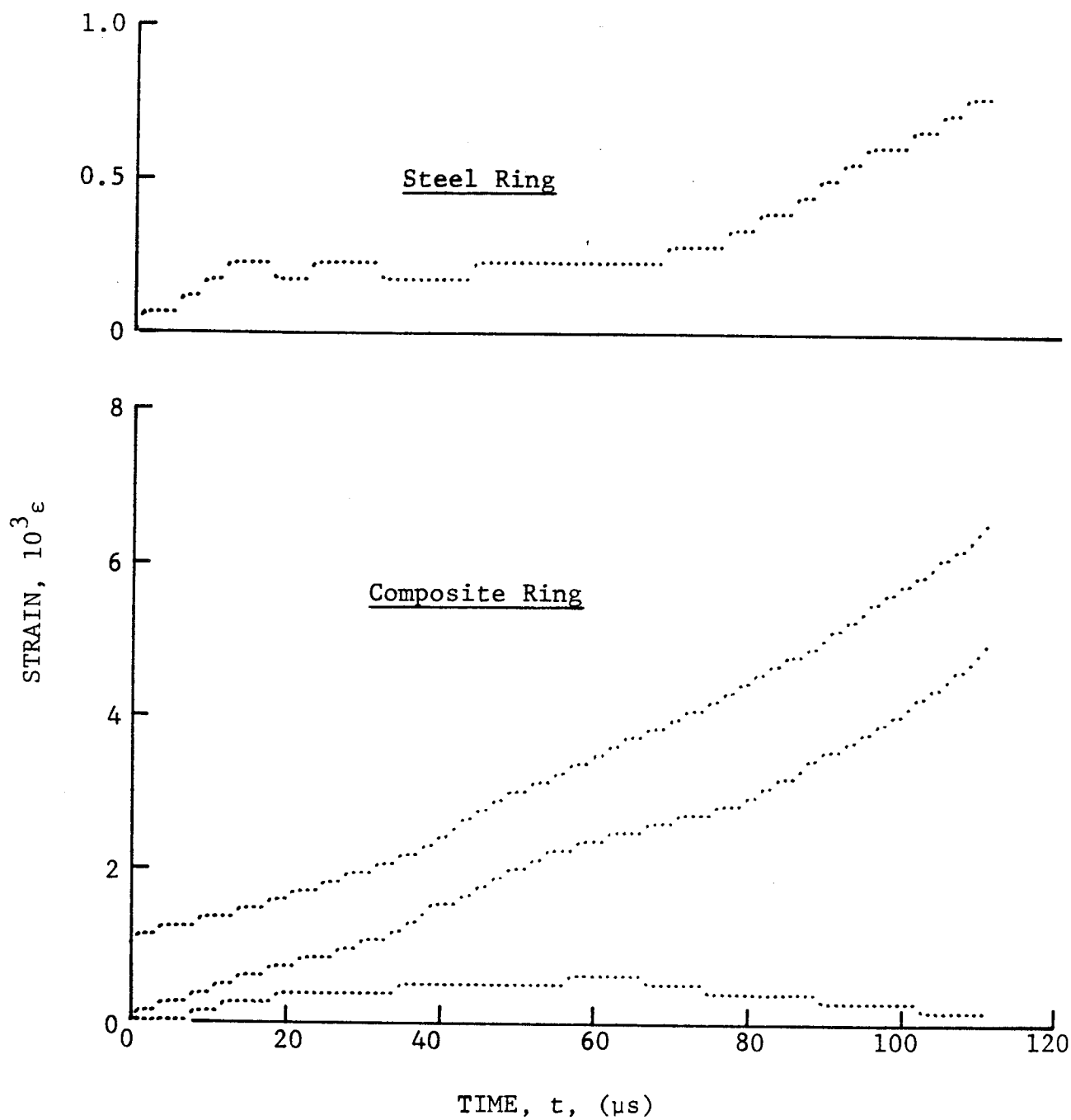


Figure 4-94. Strain records in steel ring and [90_g] SP288/AS graphite/epoxy ring under dynamic loading for Specimen No. 38-9 (650 mg pistol powder)

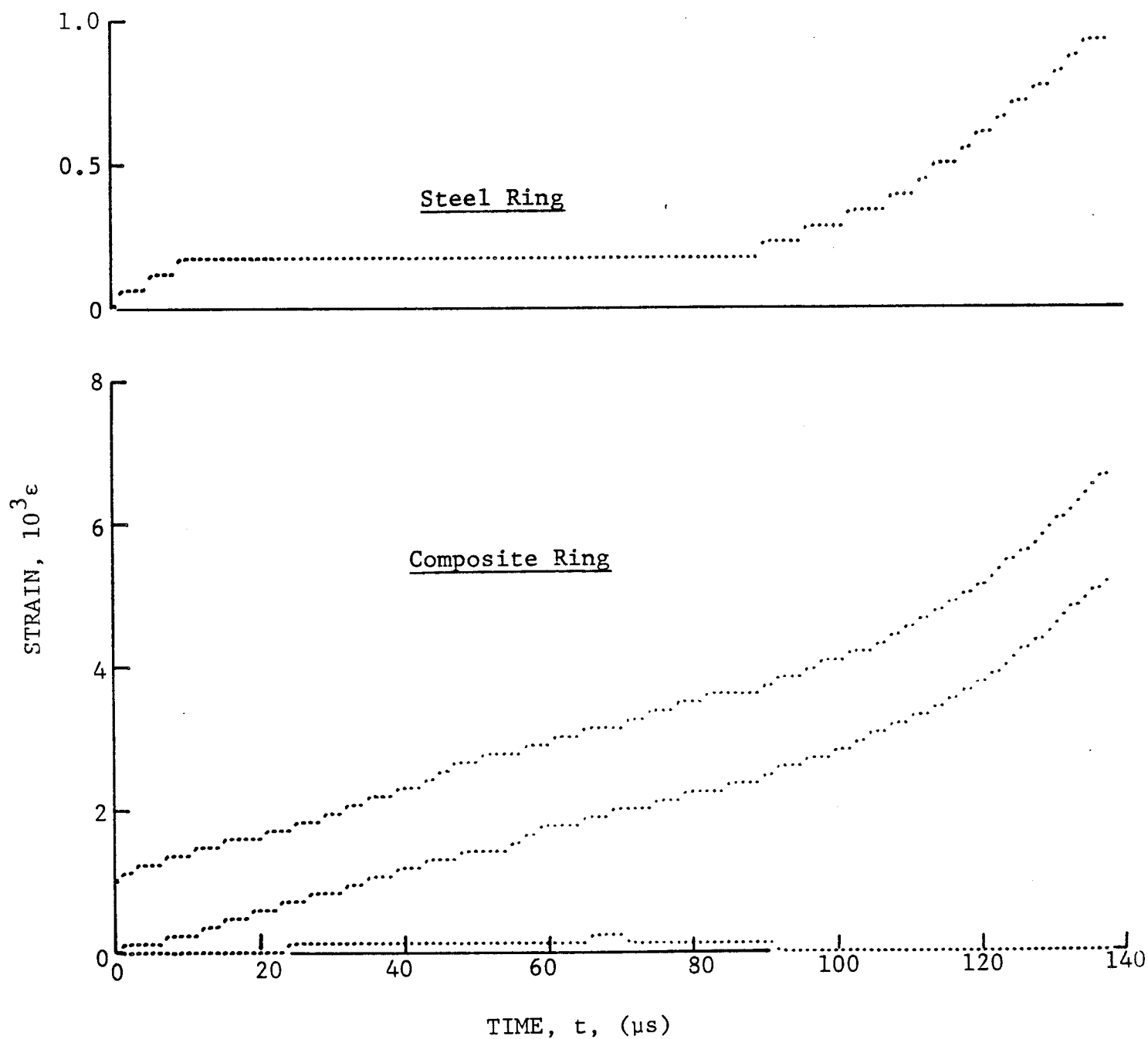


Figure 4-95. Strain records in steel ring and [90_g] SP288/AS graphite/epoxy ring under dynamic loading for Specimen No. 38-10 (650 mg pistol powder).

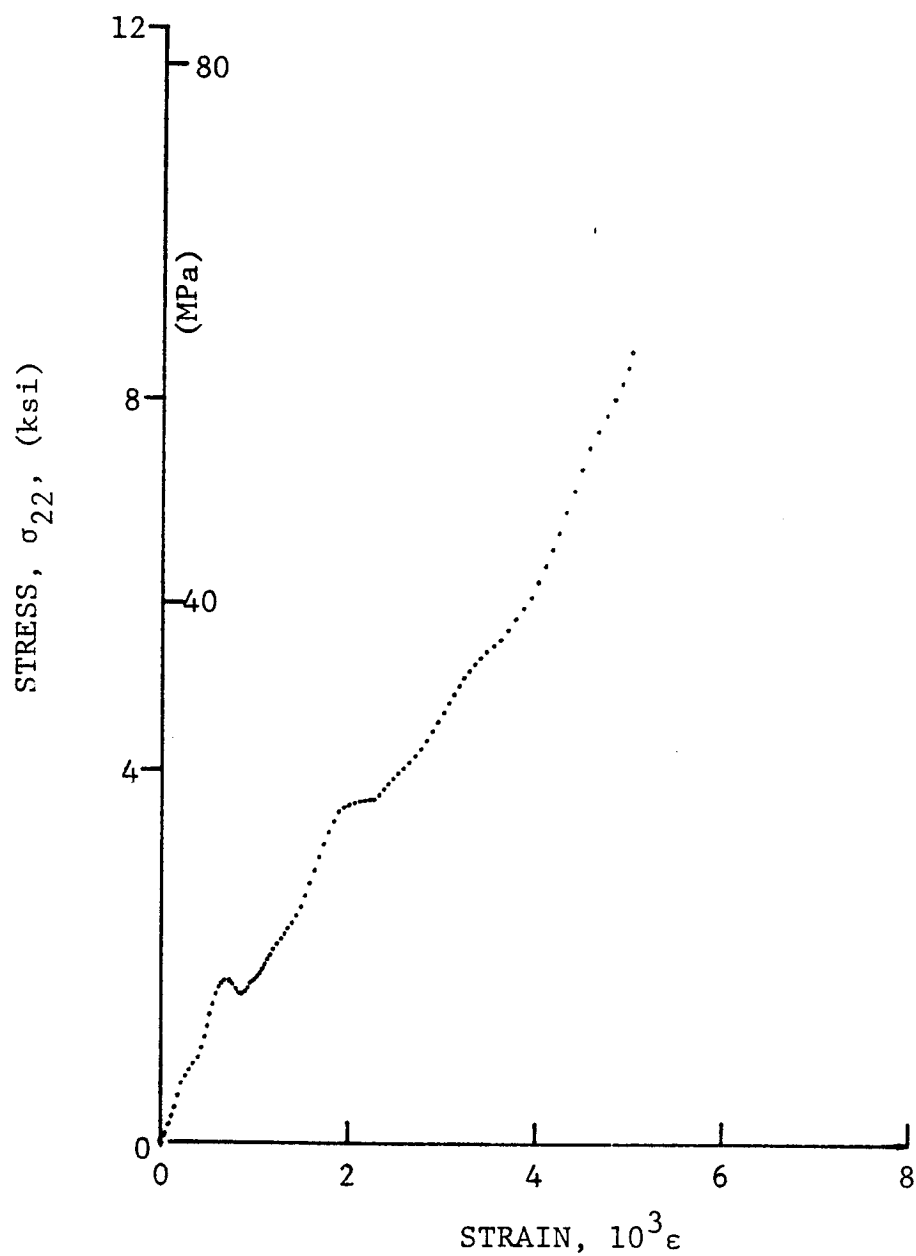


Figure 4-96. Stress-strain curve for dynamically loaded
 $[90_8]$ SP288/AS graphite/epoxy ring, Specimen No. 38-7
 (650 mg pistol powder).

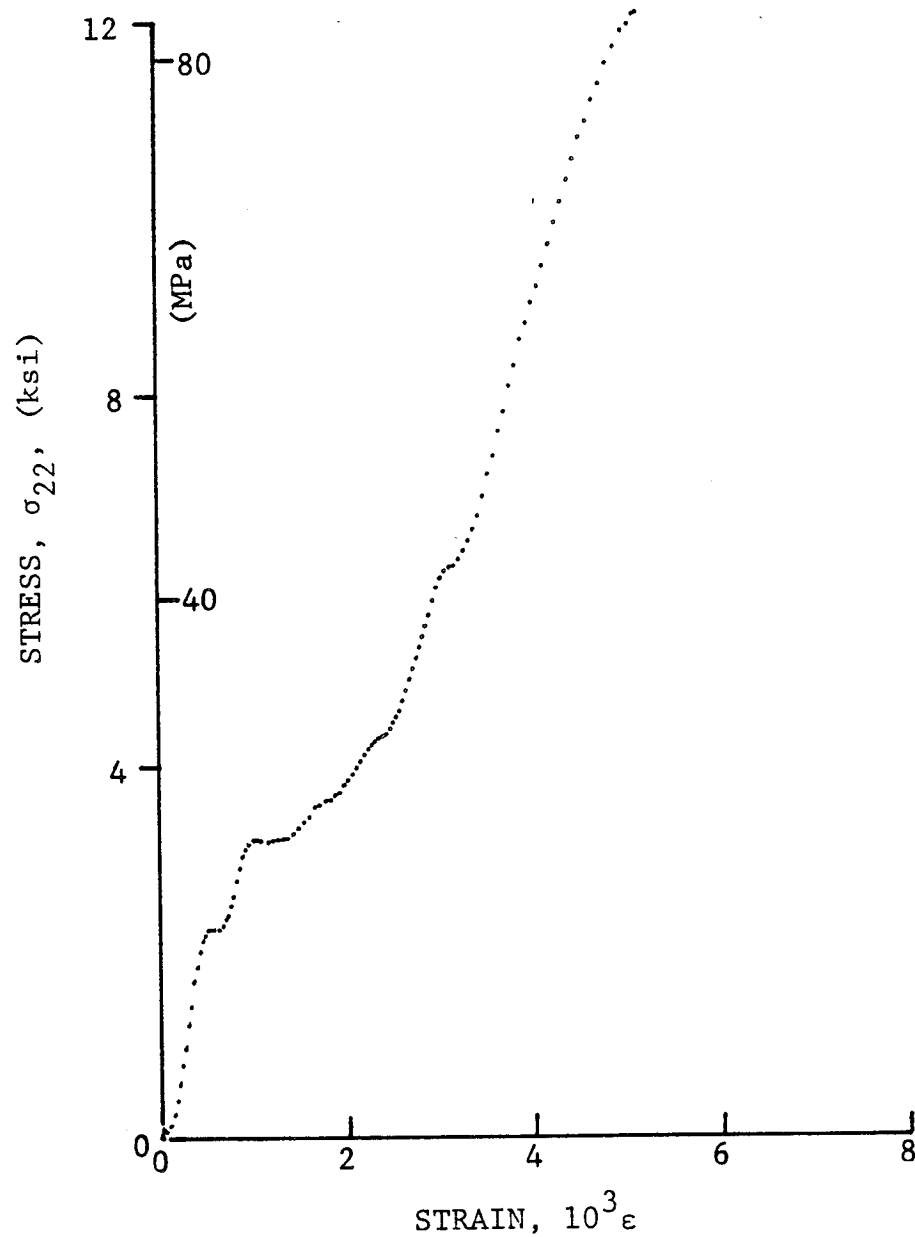


Figure 4-97. Stress-strain curve for dynamically loaded $[90_8]$ SP288/AS graphite/epoxy ring, Specimen No. 38-9 (650 mg pistol powder).

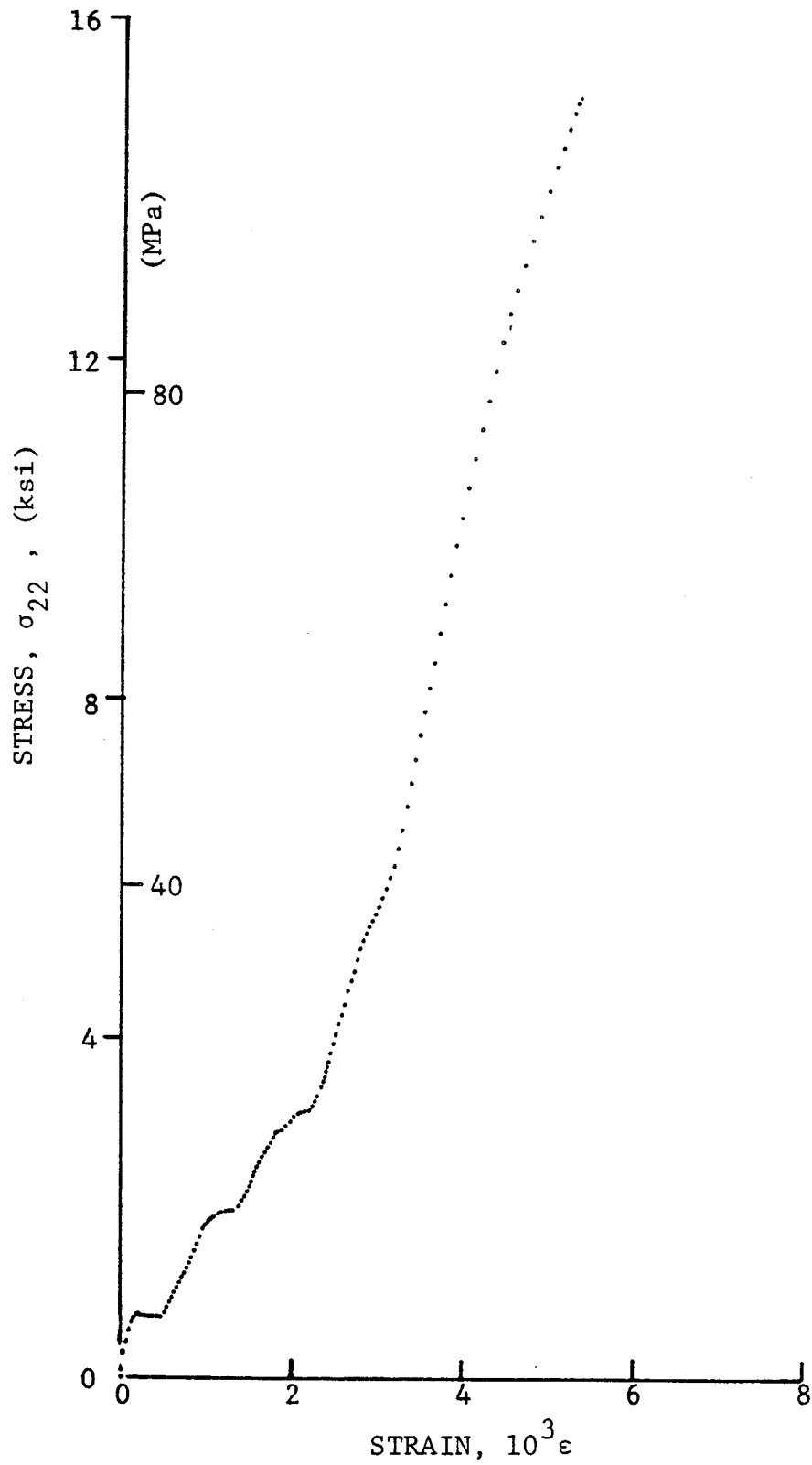


Figure 4-98. Stress-strain curve for dynamically loaded $[90_8]$ SP288/AS graphite/epoxy ring, Specimen No. 38-10 (650 mg pistol powder).

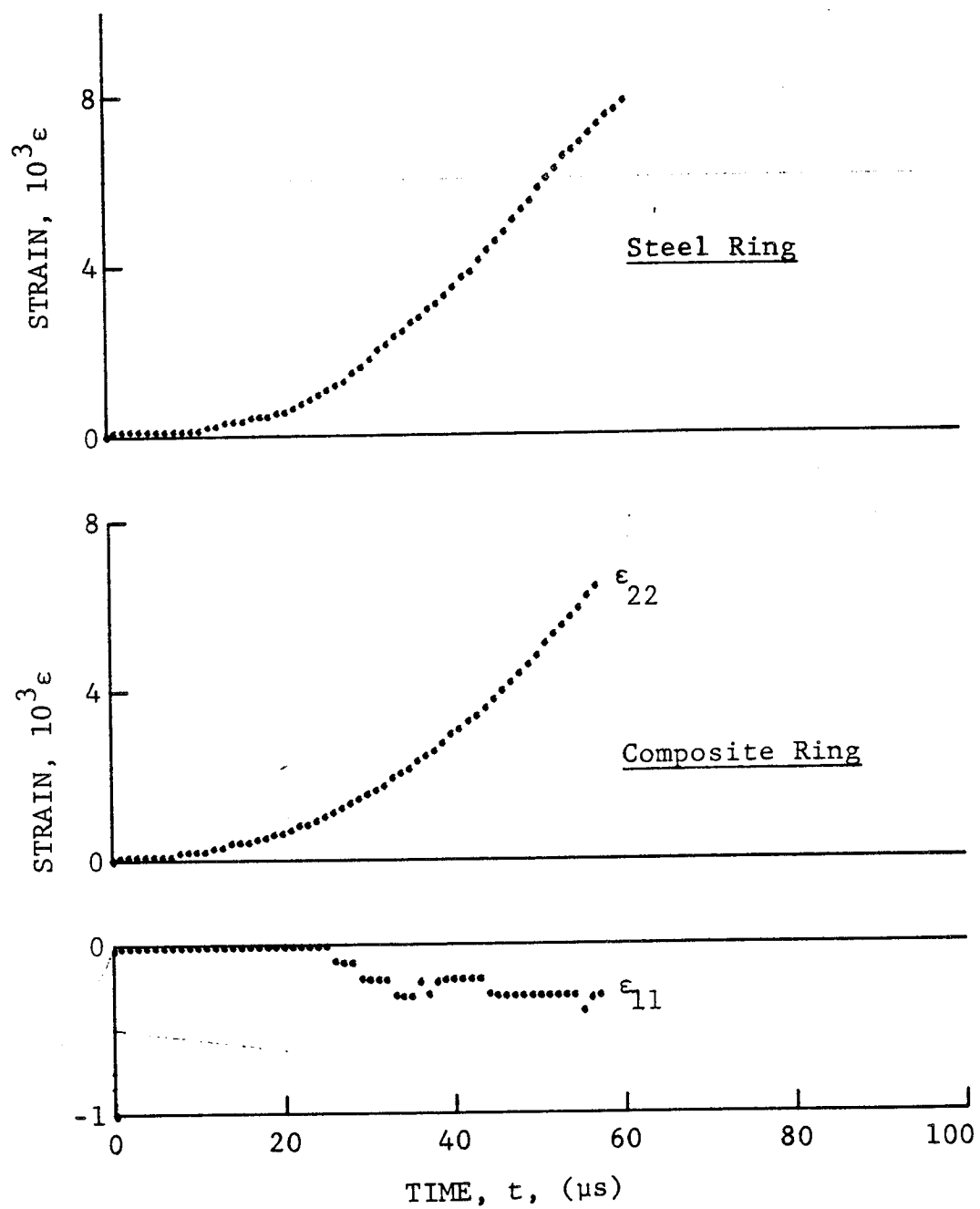


Figure 4-99. Strain records in steel ring and [90_g] SP288/AS graphite/epoxy ring under dynamic loading for Specimen No. 5-9 (260 mg pistol powder).

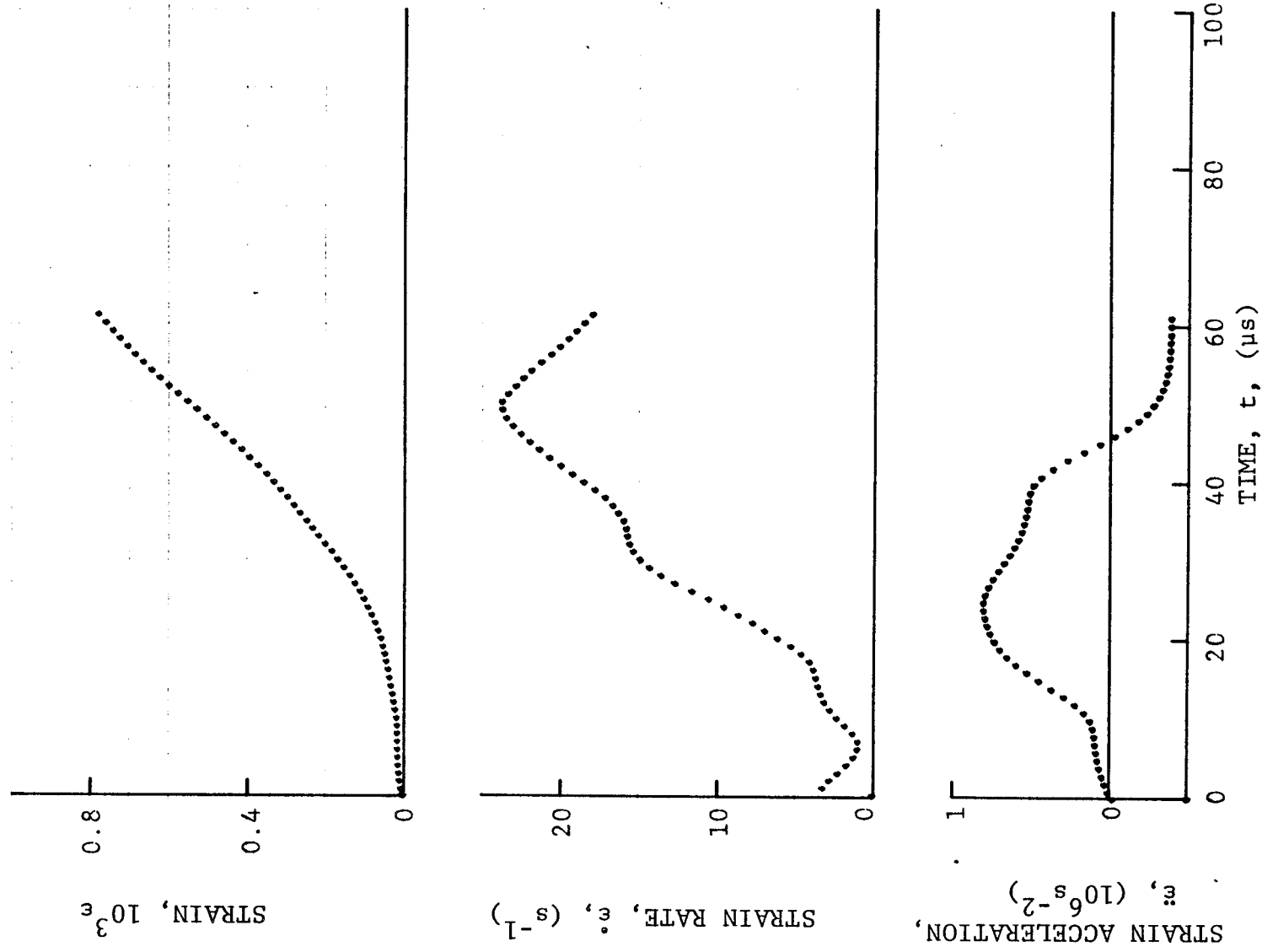


Figure 4-100. Strain and its derivatives in steel ring for Specimen No. 5-9.

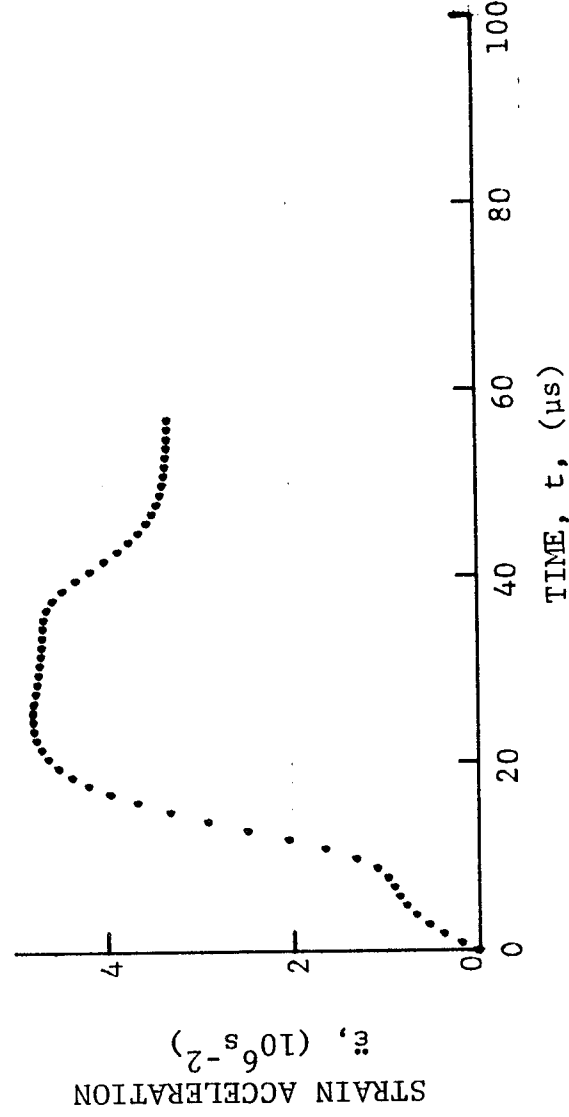
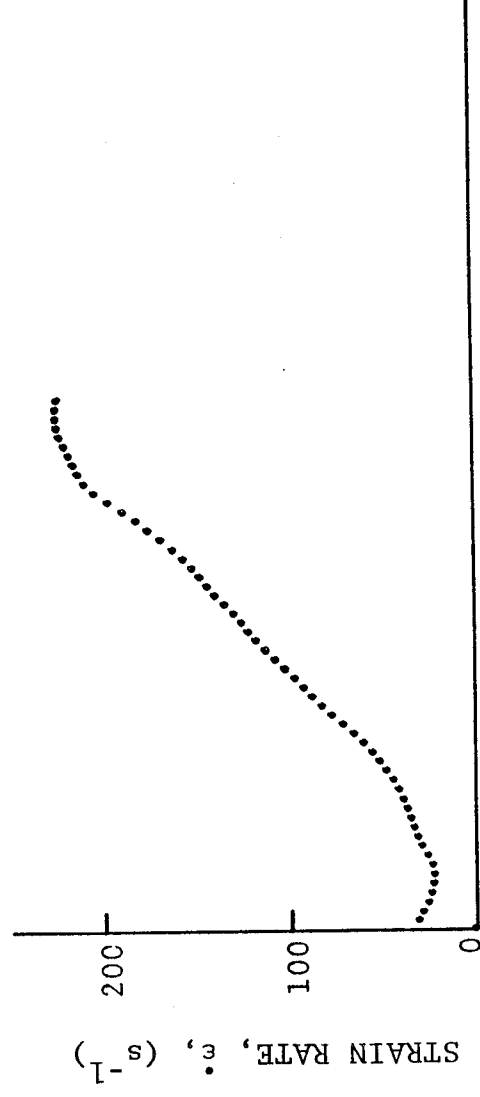
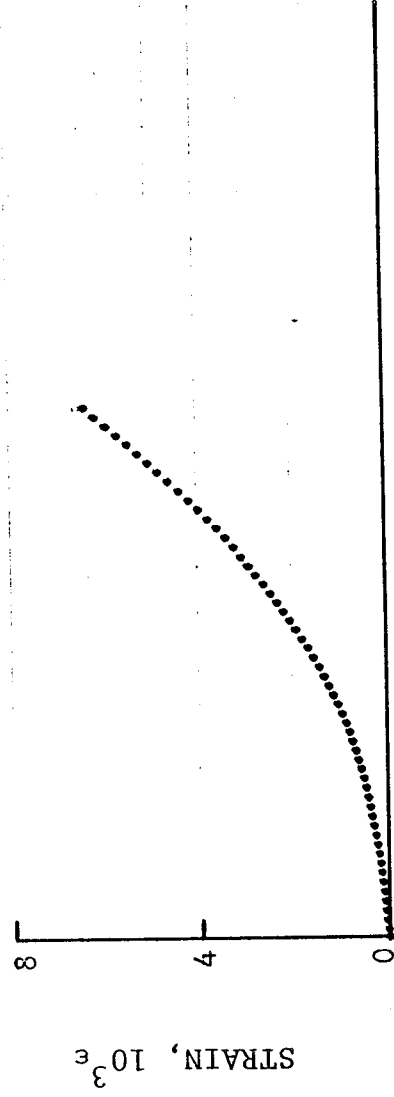


Figure 4-101. Circumferential strain and its derivatives in [90g] SP288/AS graphite/epoxy ring under dynamic loading for Specimen No. 5-9 (260 mg pistol powder).

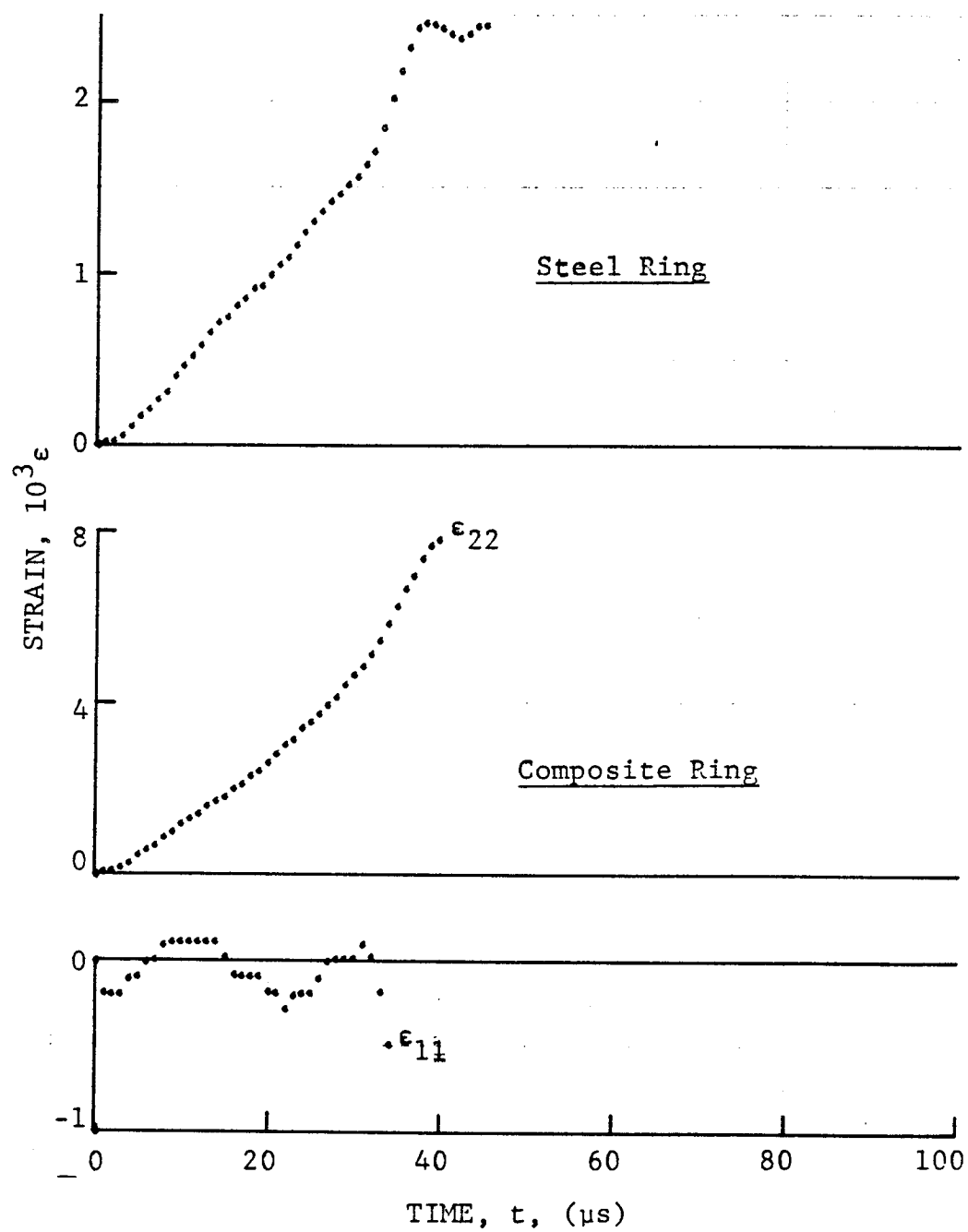


Figure 4-102. Strain records in steel ring and [90_g] SP288/AS graphite/epoxy ring under dynamic loading for Specimen No. 5-10 (50 mg PETN detonator).

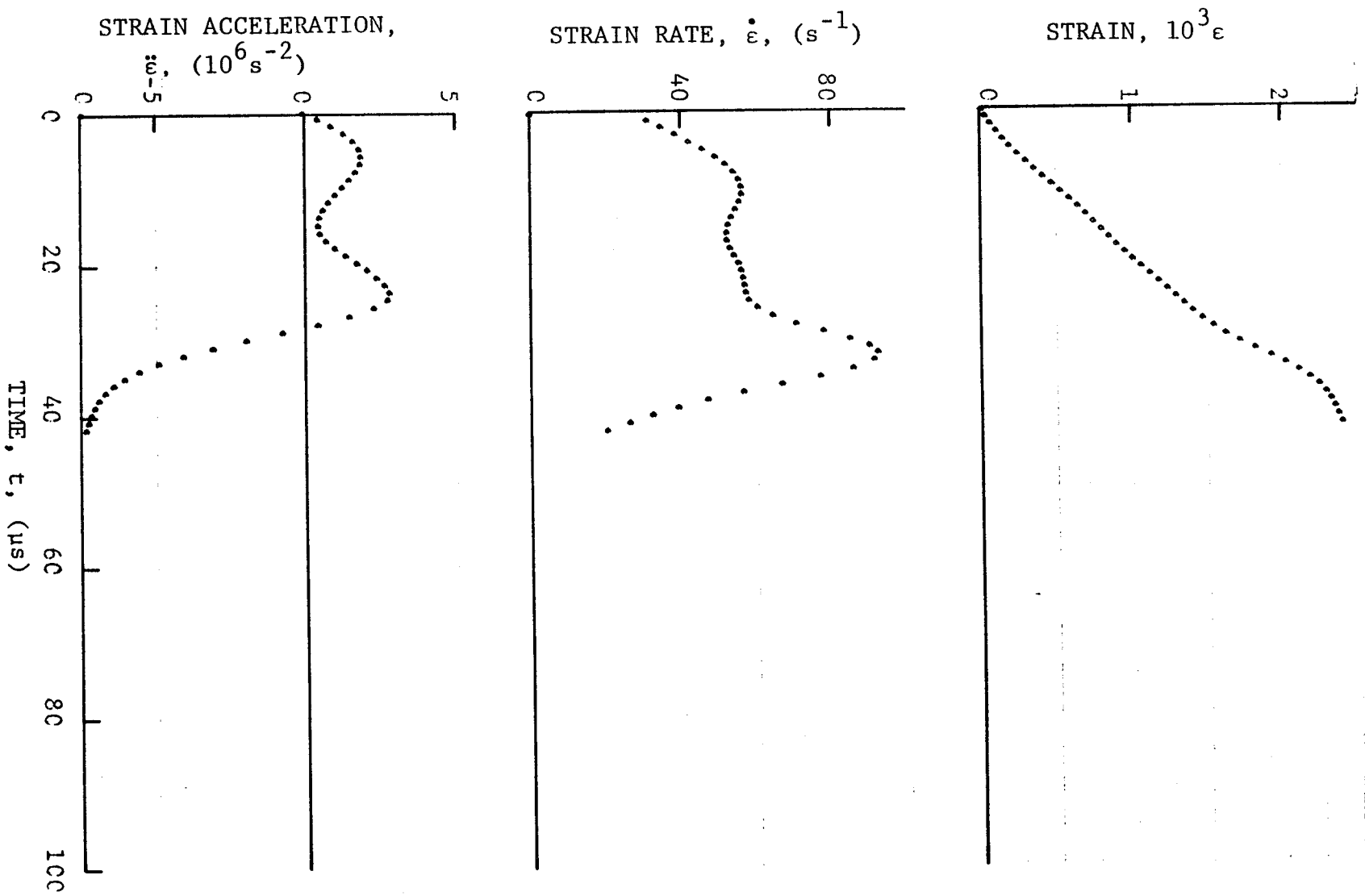


Figure 4-103. Strain and its derivatives in steel ring for Specimen No. 5-10.

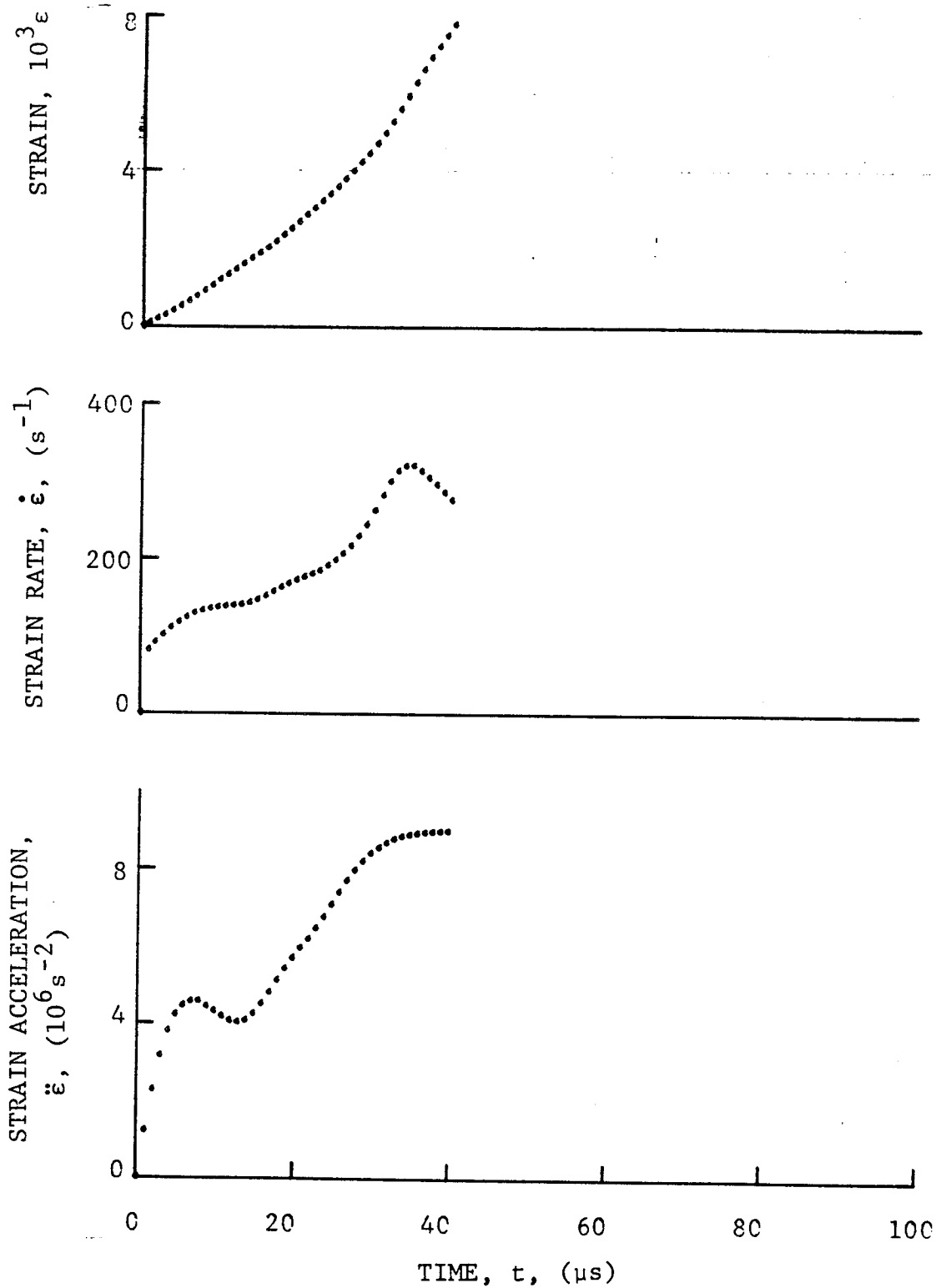


Figure 4-104. Circumferential strain and its derivatives in [90g] SP288/AS graphite/epoxy ring under dynamic loading for Specimen No. 5-10 (50 mg PETN detonator).

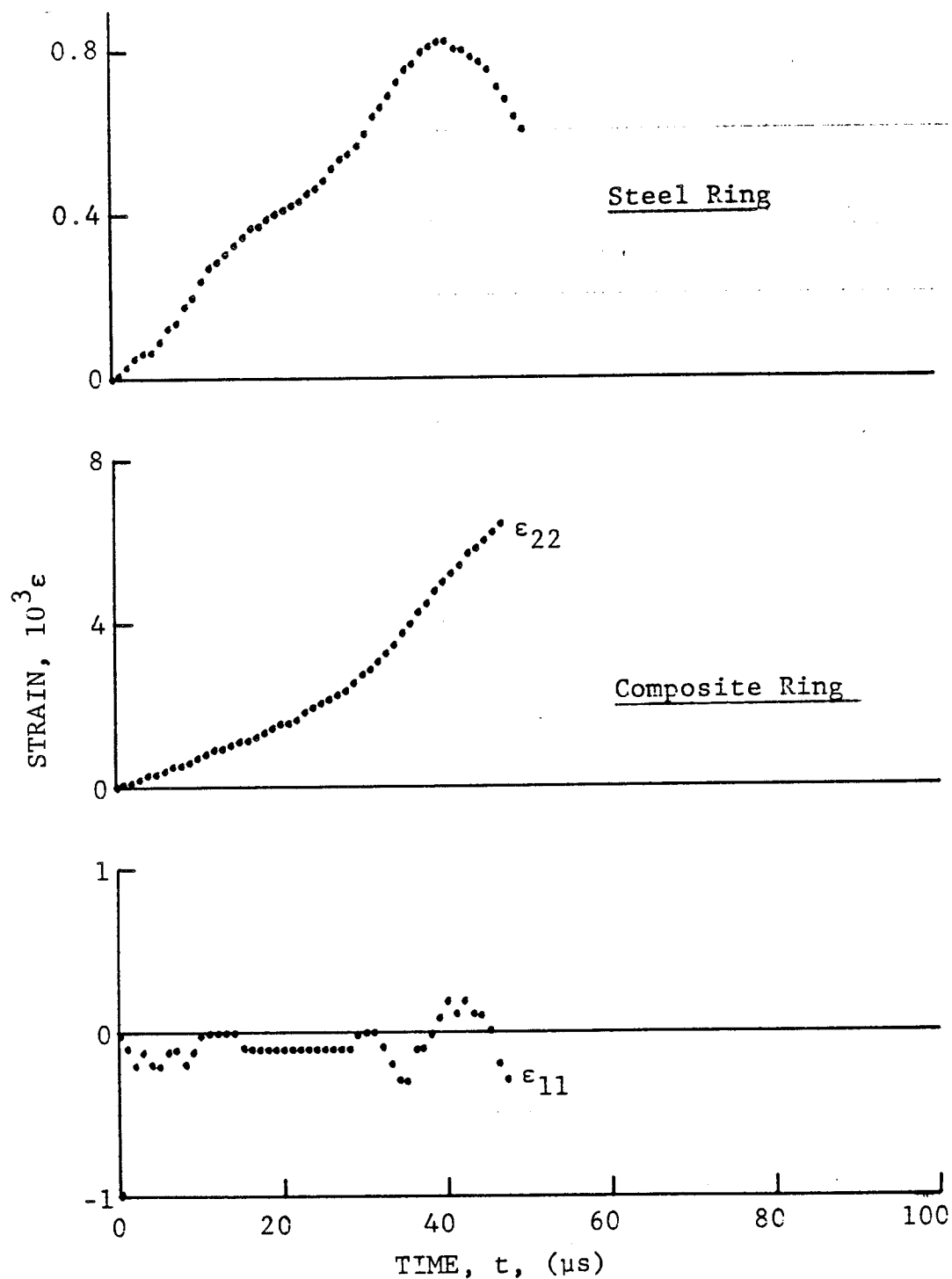


Figure 4-105. Strain records in steel ring and [90g] SP288/AS graphite/epoxy ring under dynamic loading for Specimen No. 5-11 (20 mg PETN detonator).

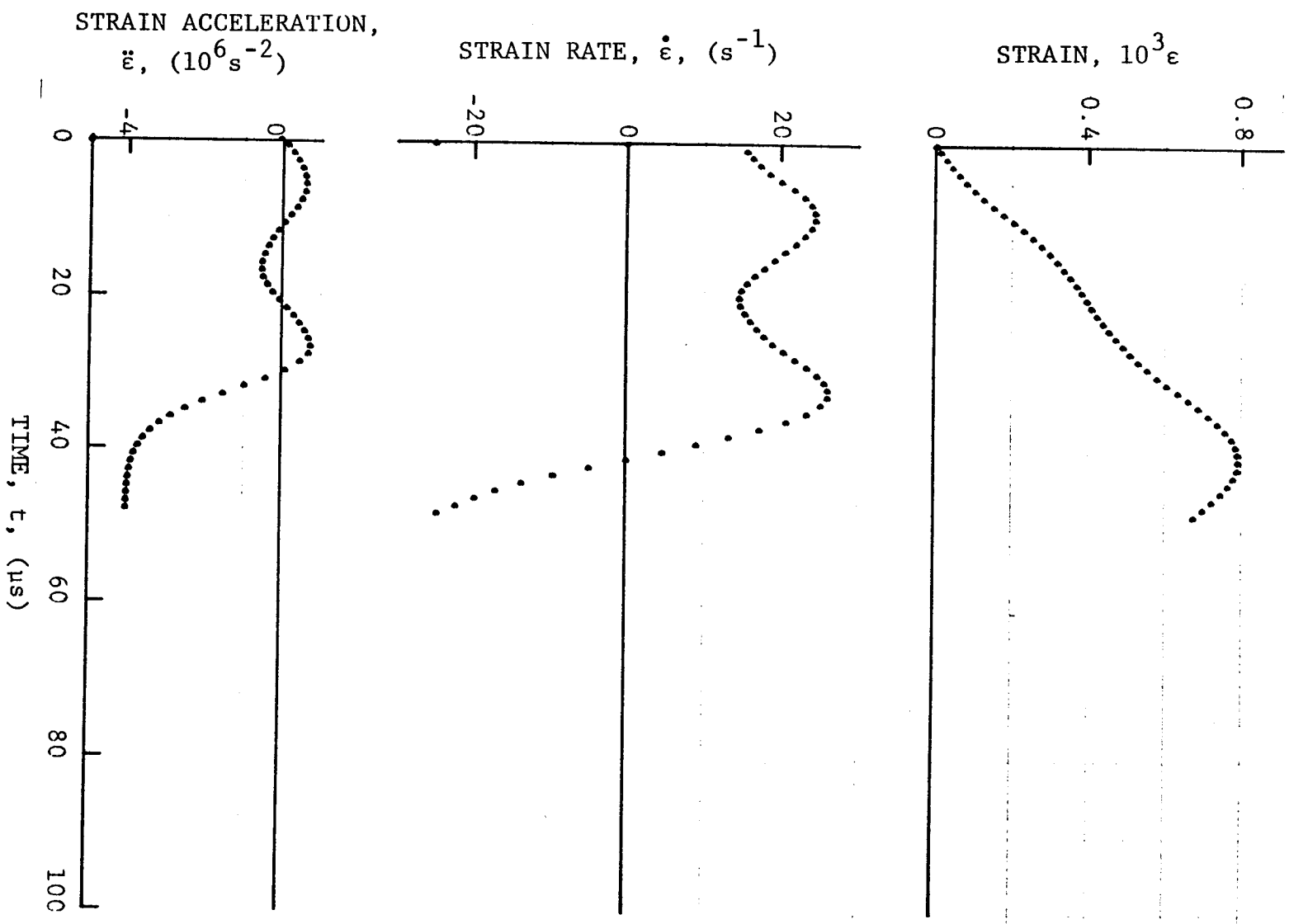


Figure 4-106. Strain and its derivatives in steel ring for Specimen No. 5-17.

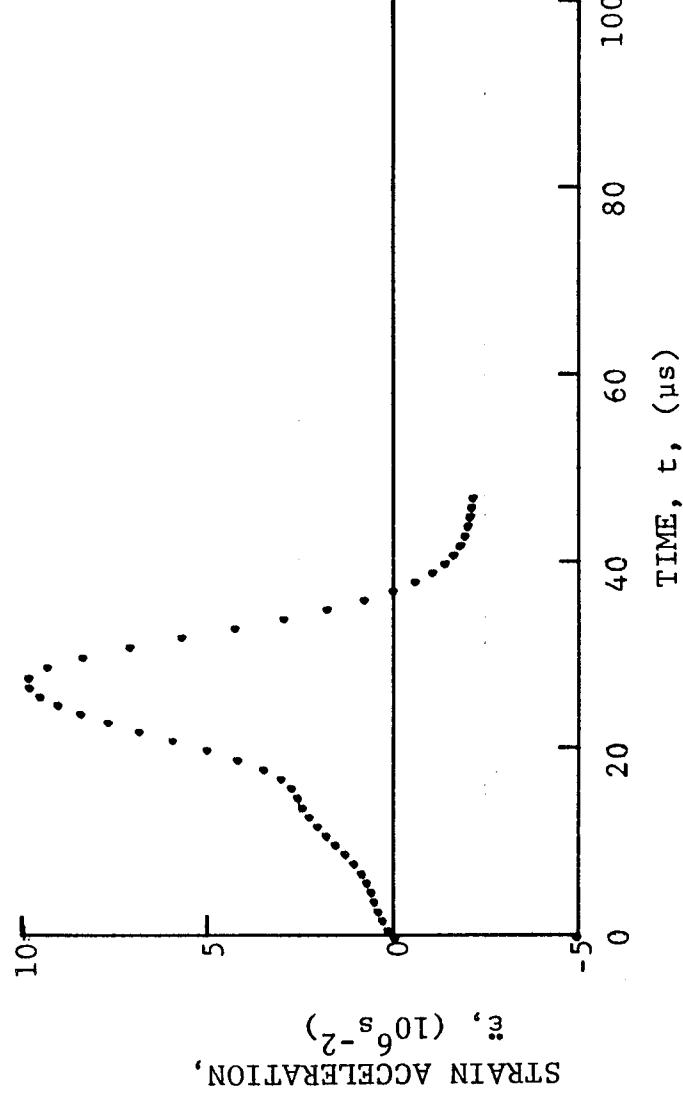
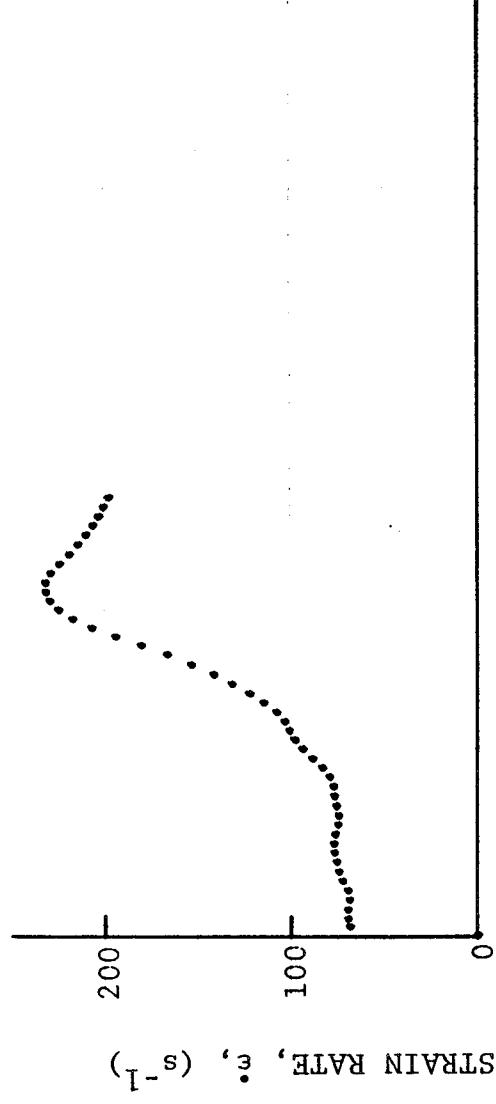
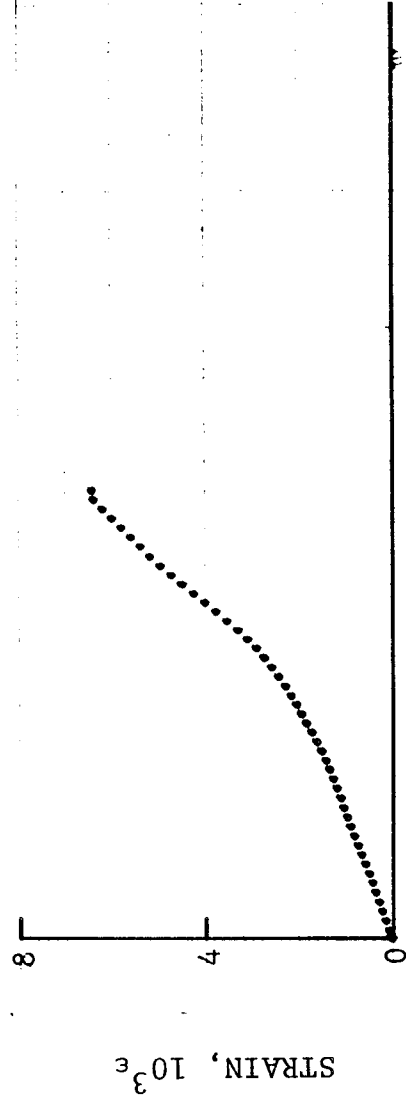


Figure 4-107. Circumferential strain and its derivatives in [908]
graphite/epoxy ring under dynamic loading for Specimen No. 5-11
(20 mg PETN detonator).

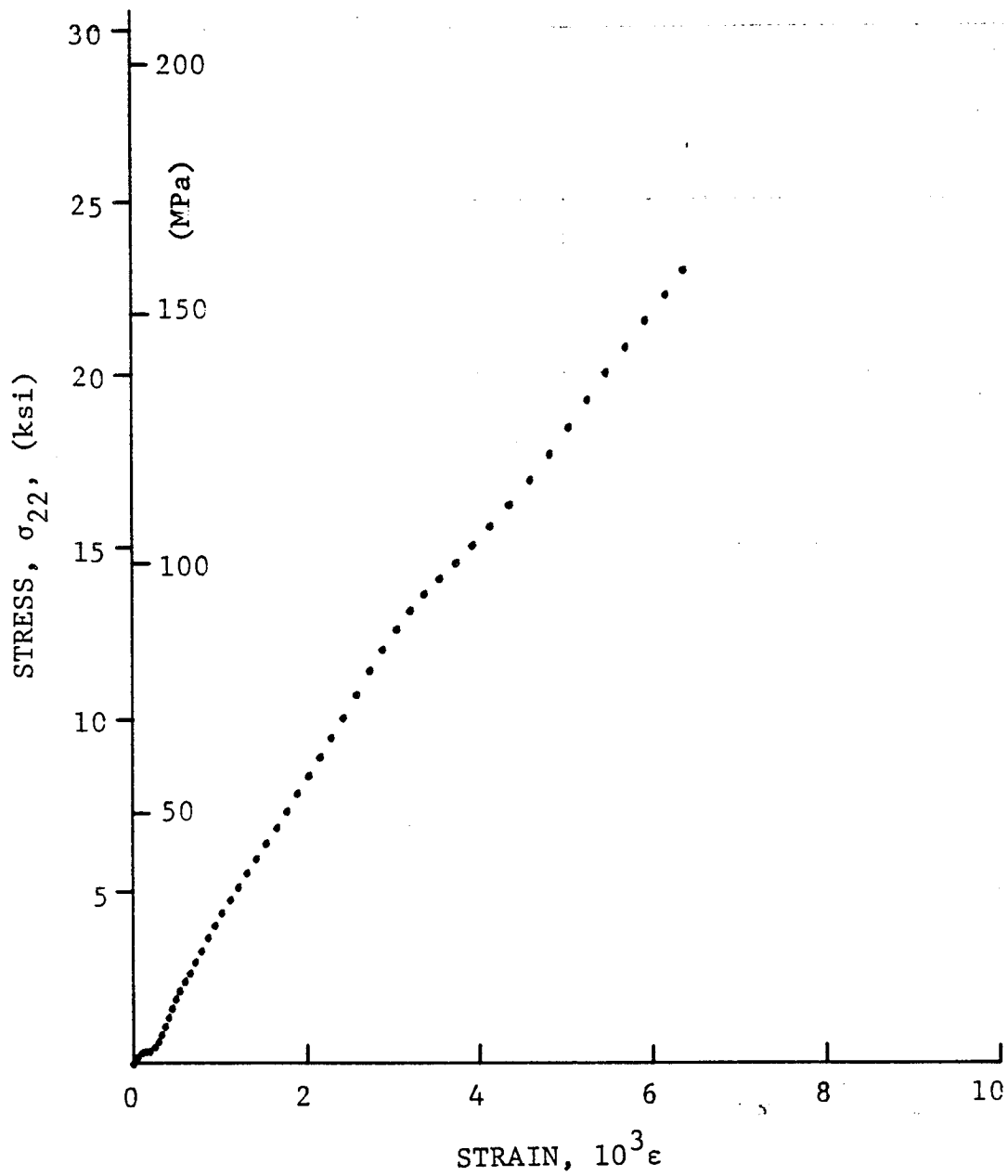


Figure 4-108. Stress-strain curve for dynamically loaded [90g] SP288/AS graphite/epoxy ring for Specimen No. 5-9 (260 mg pistol powder).

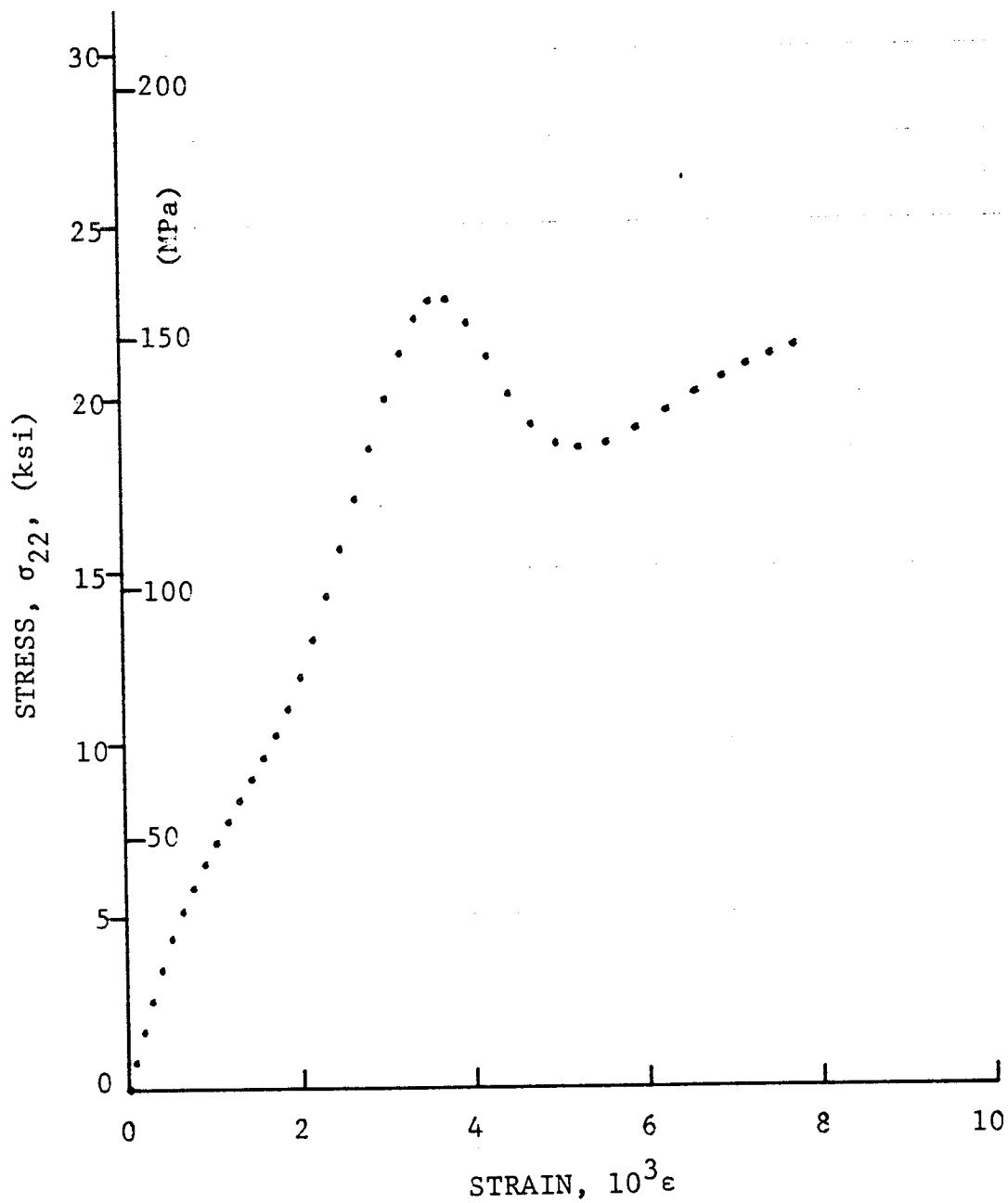


Figure 4-109. Stress-strain curve for dynamically loaded [90₈]
SP288/AS graphite/epoxy ring for Specimen No. 5-10
(50 mg PETN detonator).

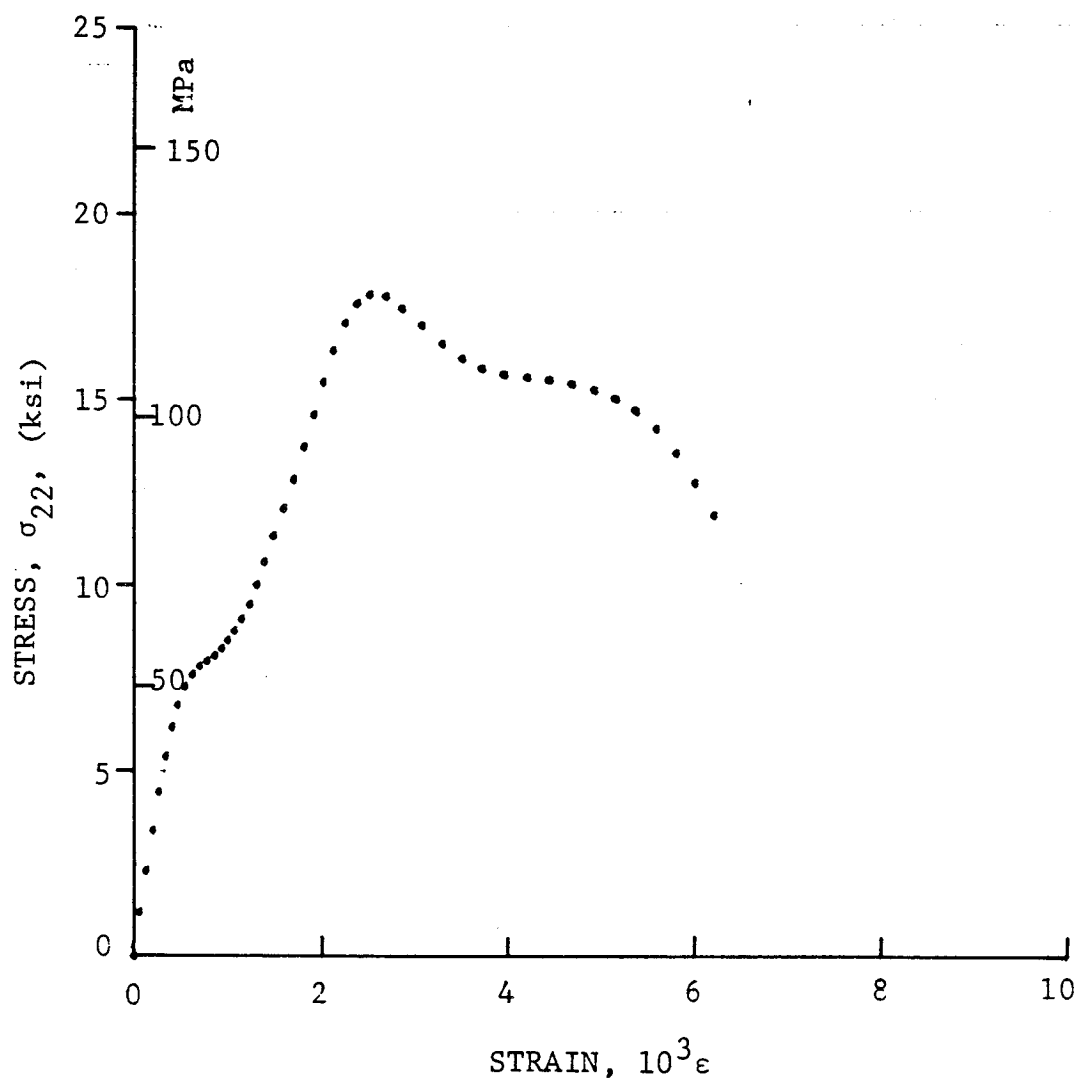


Figure 4-110. Stress-strain curve for dynamically loaded $[90_8]$ SP288/AS graphite/epoxy ring for Specimen No. 5-11 (20 mg PETN detonator).

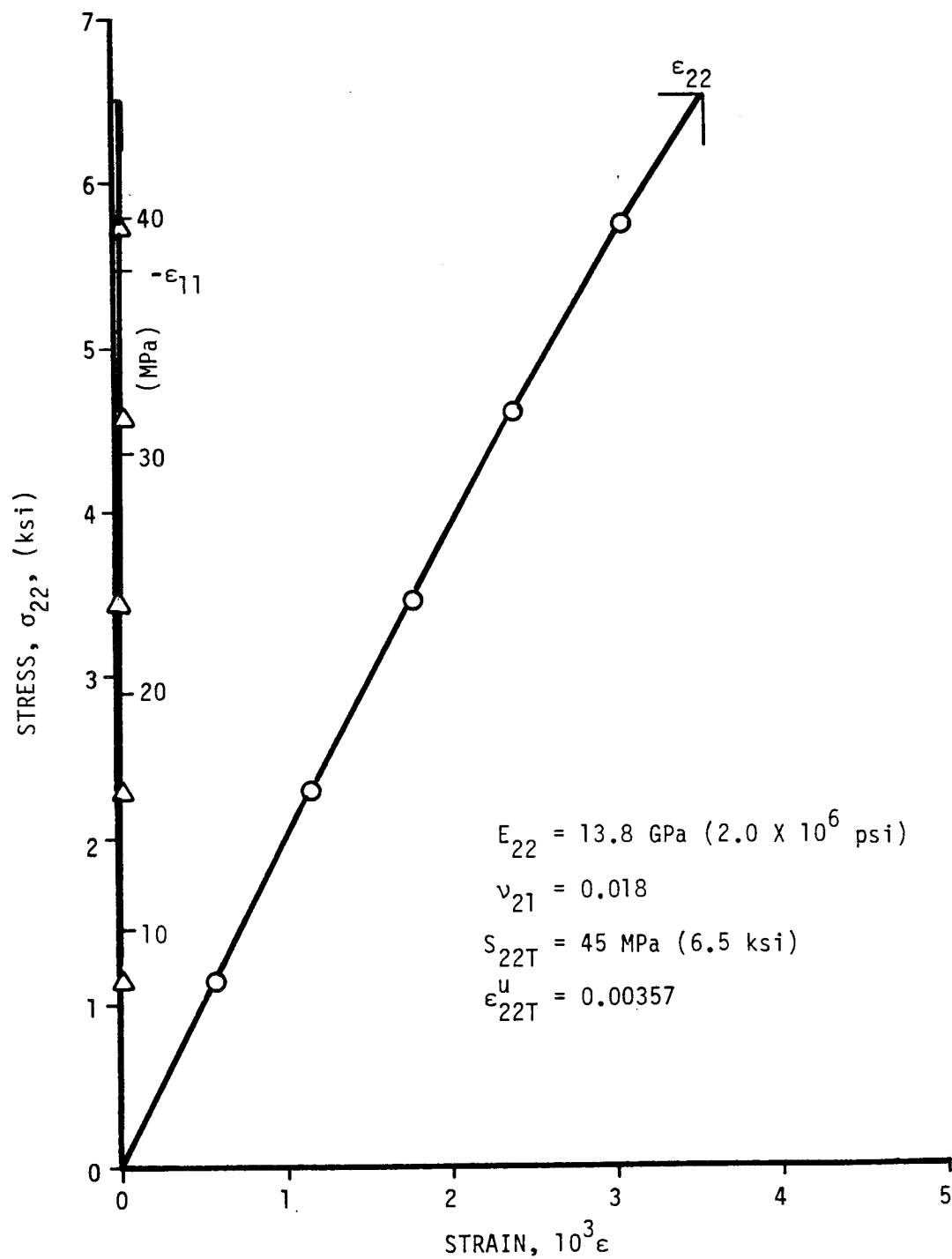


Figure 4-111. Strains in unidirectional 90-deg 80AS/20S/PR288 ring specimen under static tensile loading (Specimen No. 1A-4).

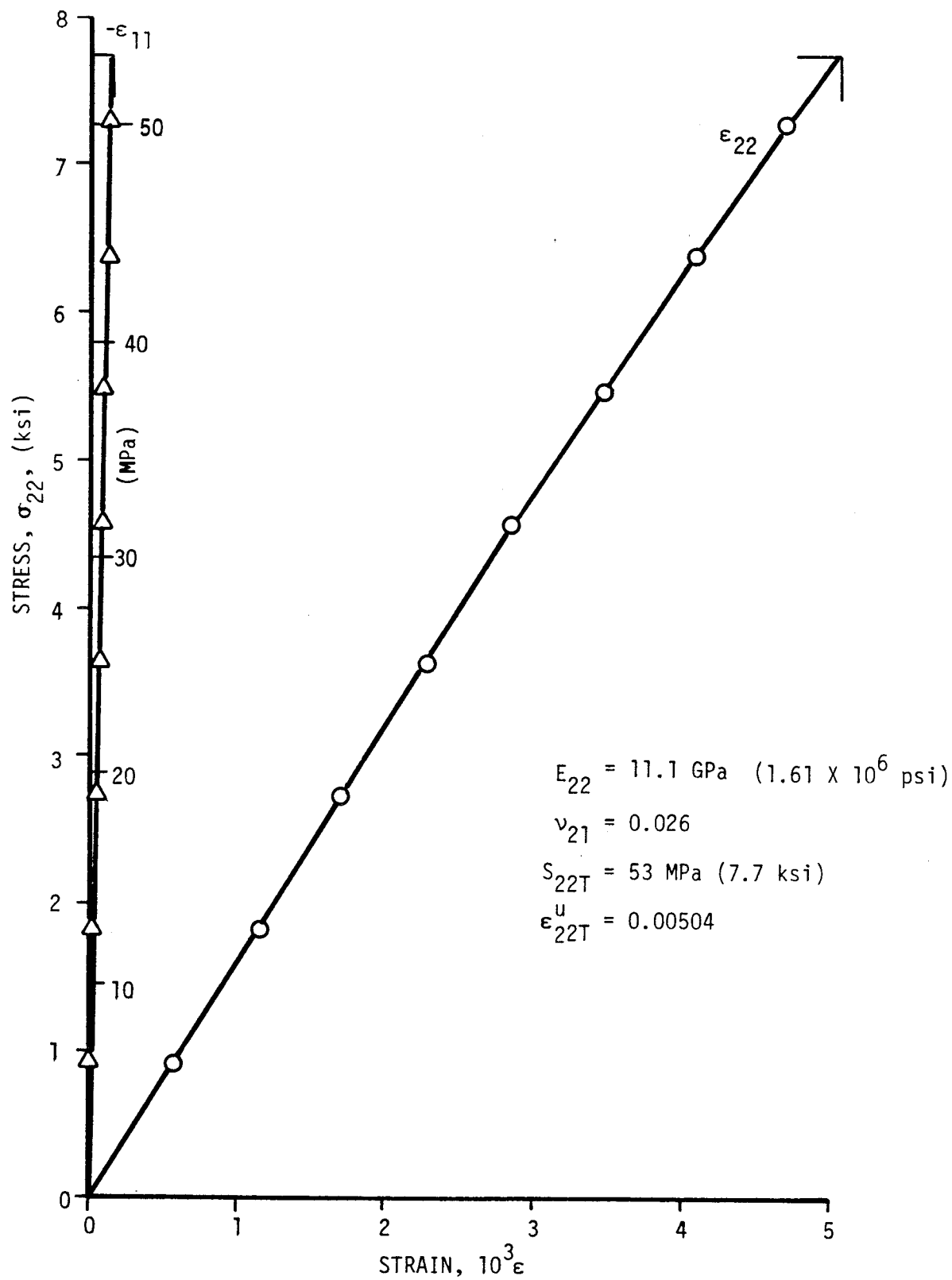
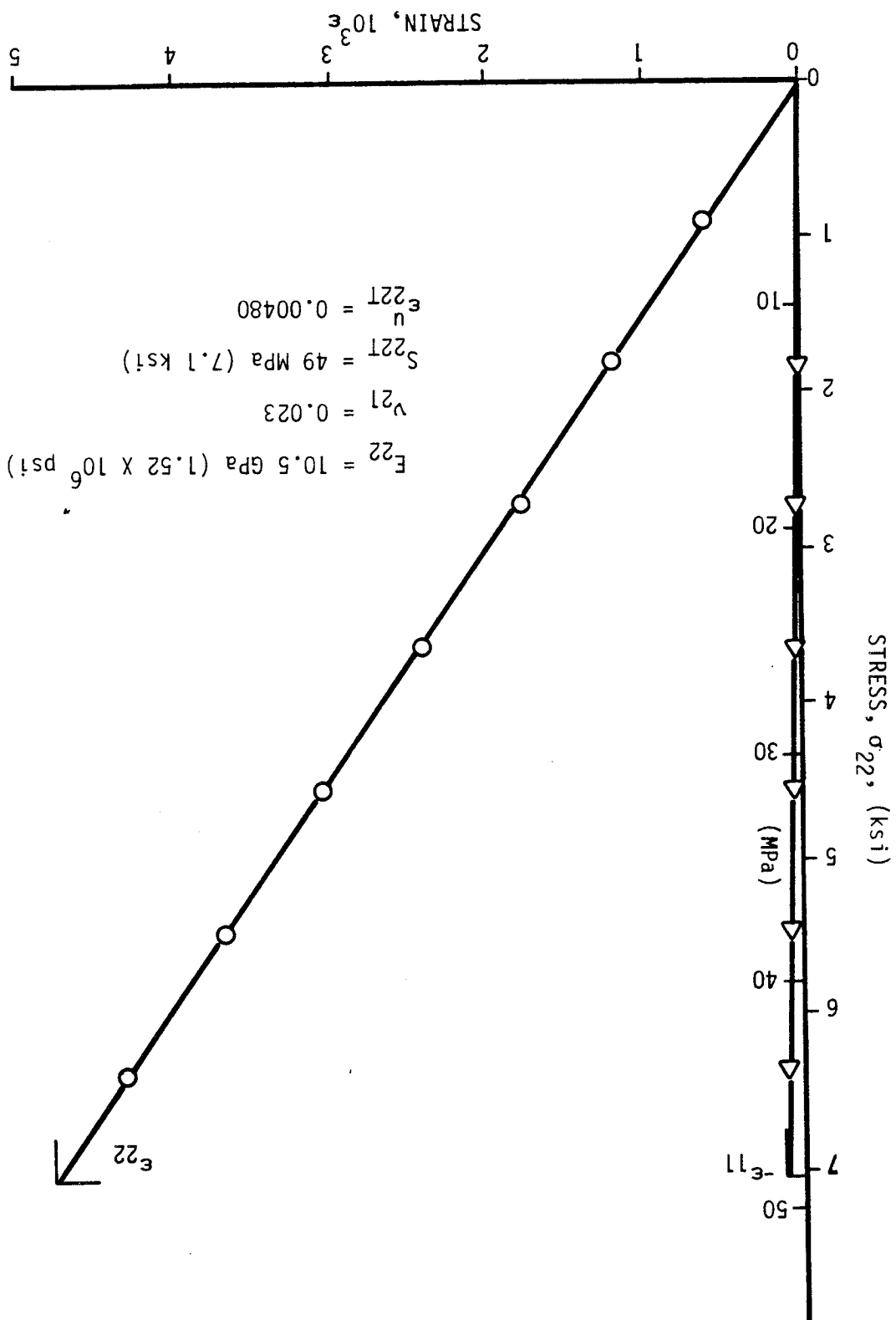


Figure 4-112. Strains in unidirectional 90-deg 80AS/20S/PR288 ring specimen under static tensile loading (Specimen No. 1A-5).

Figure 4-113. Strains in unidirectional 90-deg '80AS/20S/PR288 ring specimen under static tensile loading (Specimen No. 1A-6).



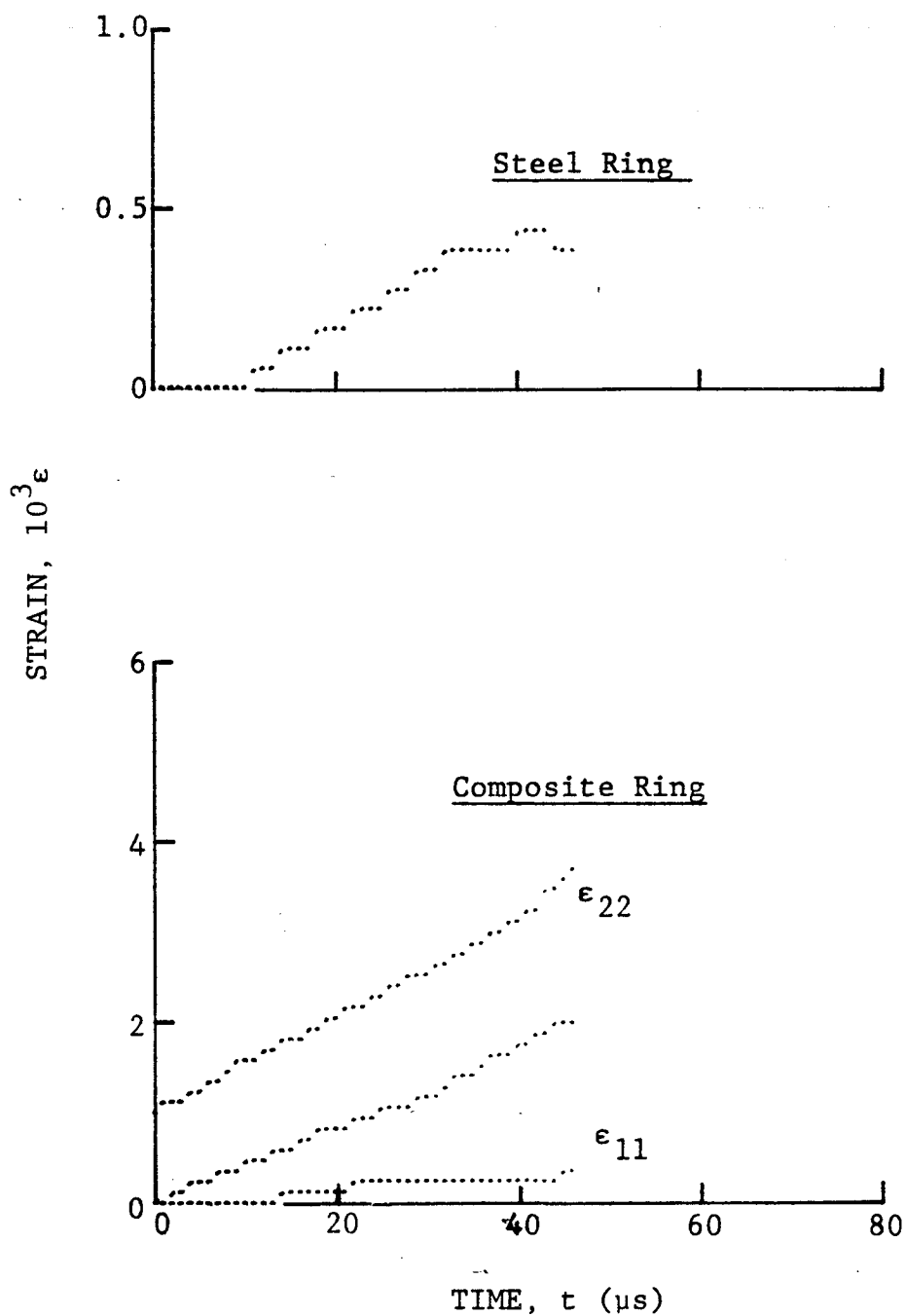


Figure 4-114. Strain records in steel ring and 80AS/20S/PR288 [90_g] graphite/S-glass/epoxy ring under dynamic loading for Specimen No. 39-4 (650 mg pistol powder).

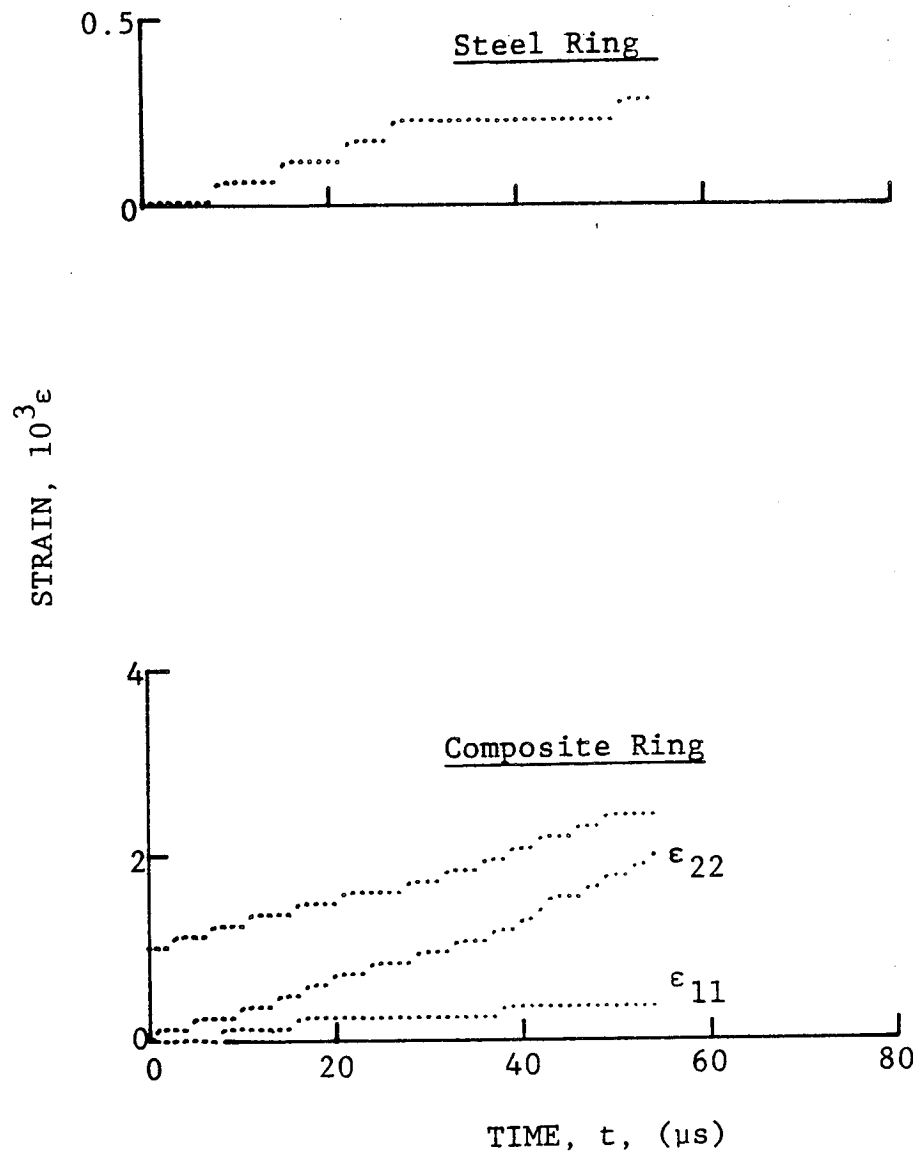


Figure 4-115. Strain records in steel ring and 80AS/20S/PR288 [90_g] graphite/S-glass/epoxy ring under dynamic loading for Specimen No. 39-5 (650 mg pistol powder).

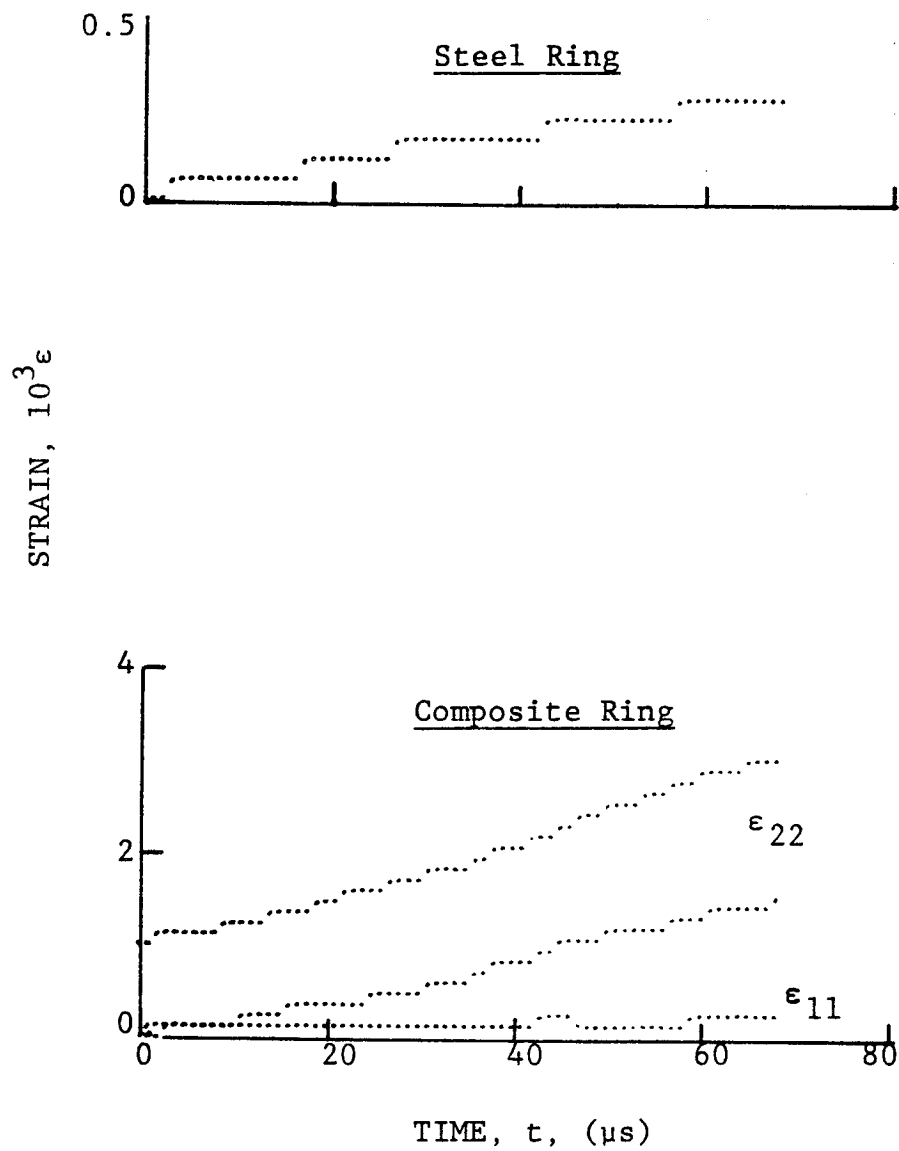


Figure 4-116. Strain records in steel ring and 80AS/20S/PR288 [90_g] graphite/S-glass/epoxy ring under dynamic loading for Specimen No. 39-6 (650 mg pistol powder).

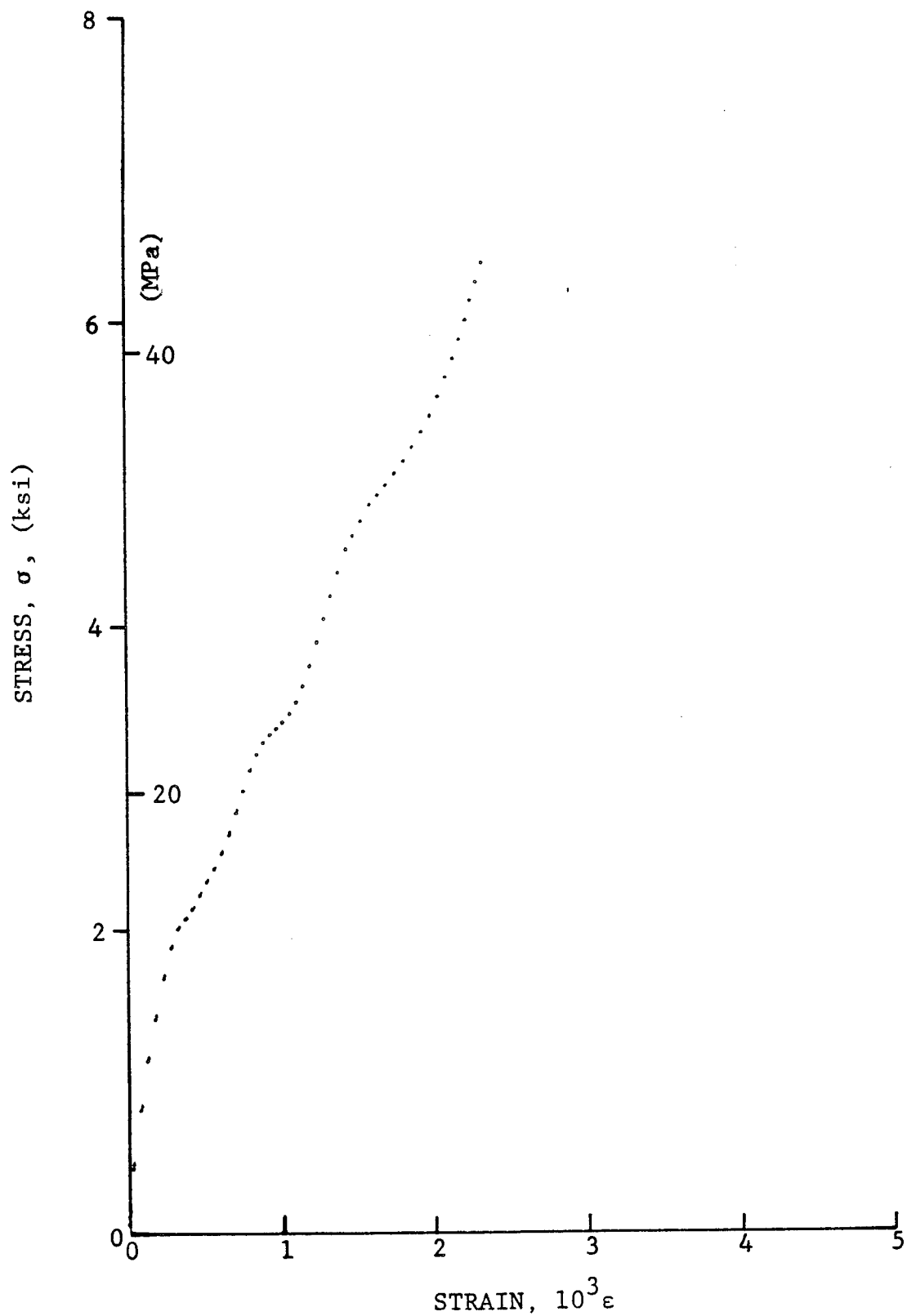


Figure 4-117. Stress-strain curve for dynamically loaded [90g] 80AS/20S/PR288 graphite/S-glass/epoxy ring for Specimen No. 39-4.

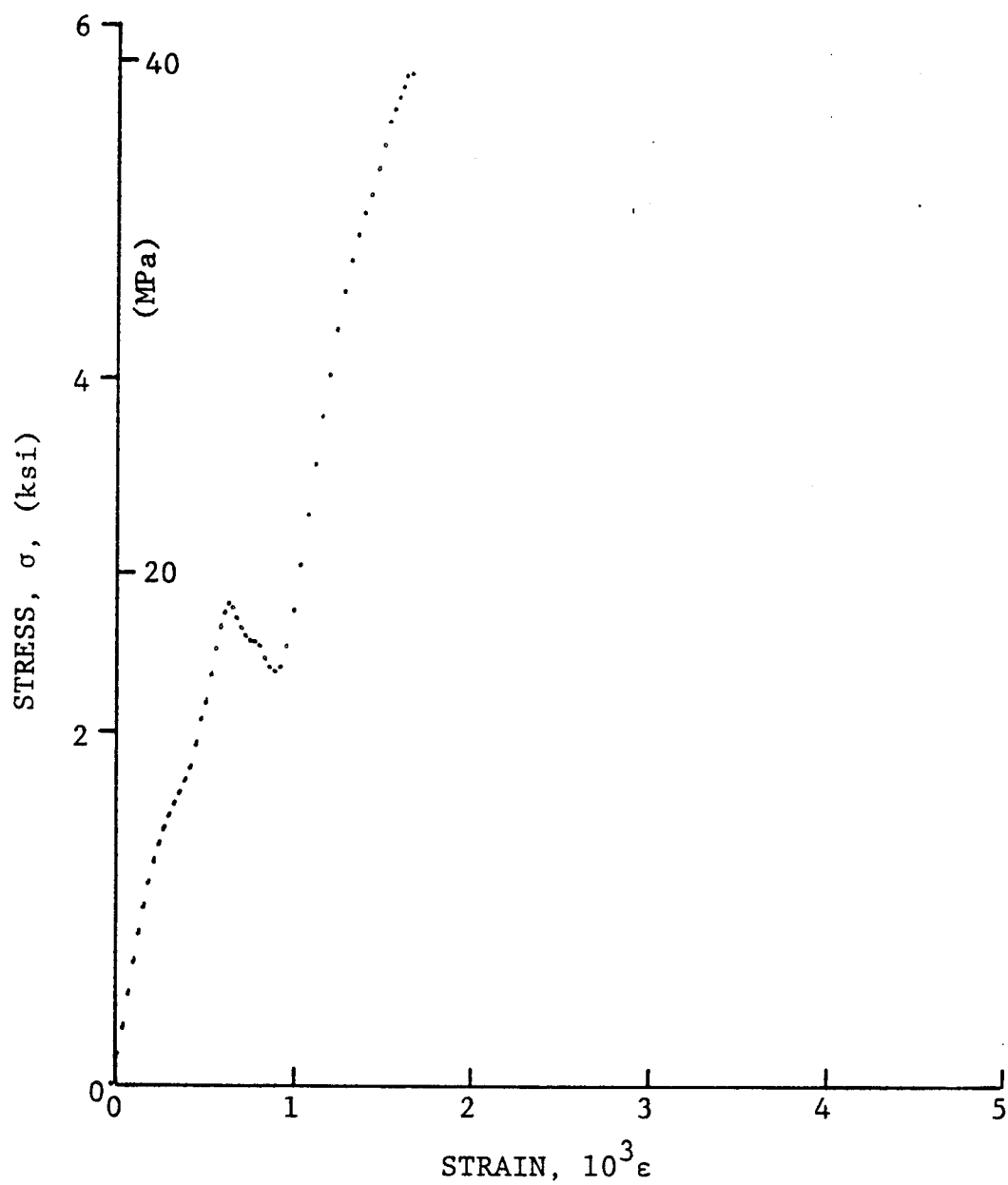


Figure 4-118. Stress-strain curve for dynamically loaded [90g] 80AS/20S/PR288 graphite/S-glass/epoxy ring for Specimen No. 39-5.

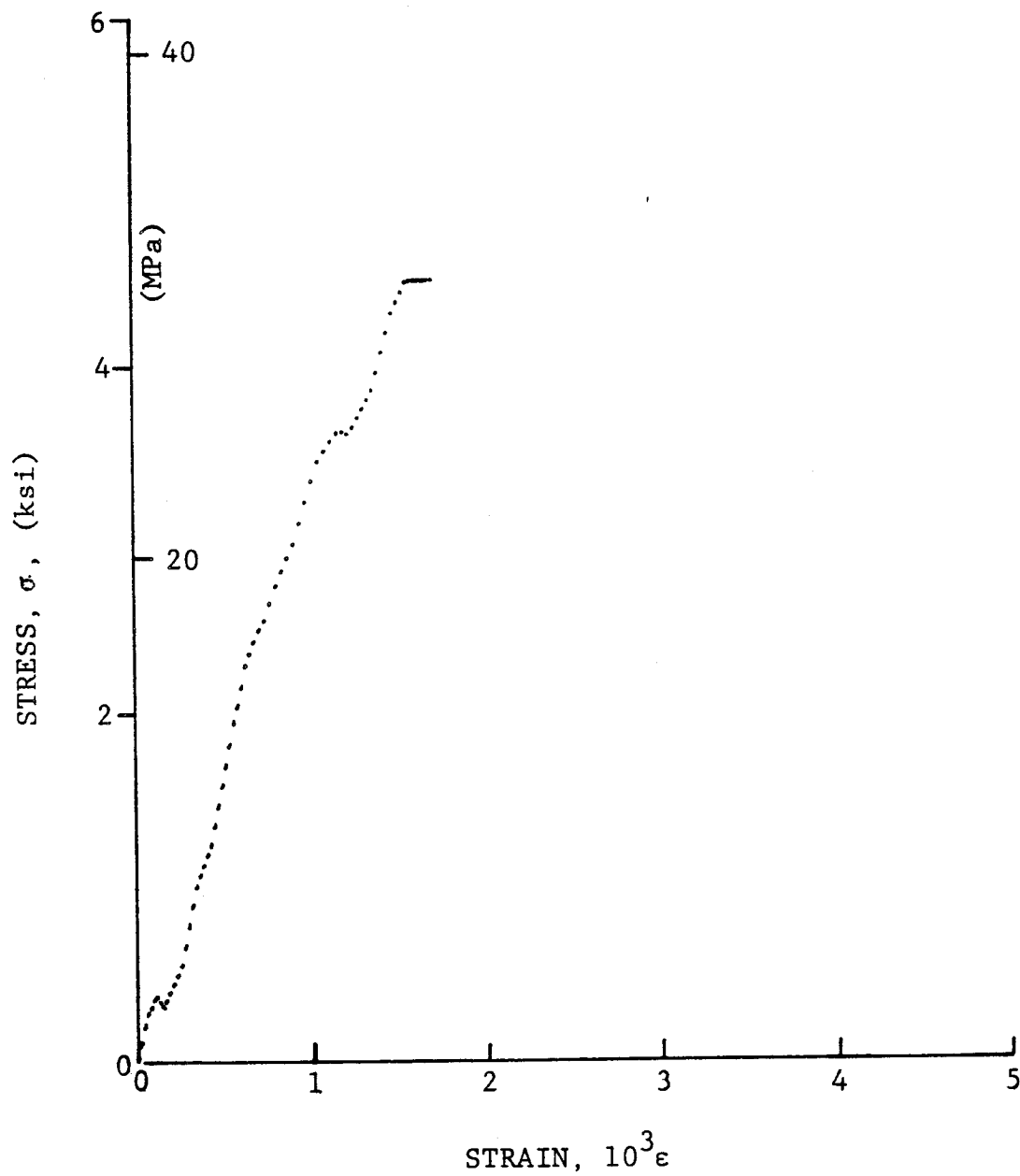


Figure 4-119. Stress-strain curve for dynamically loaded [90_g] 80AS/20S/PR288 graphite/S-glass/epoxy ring for Specimen No. 39-6.

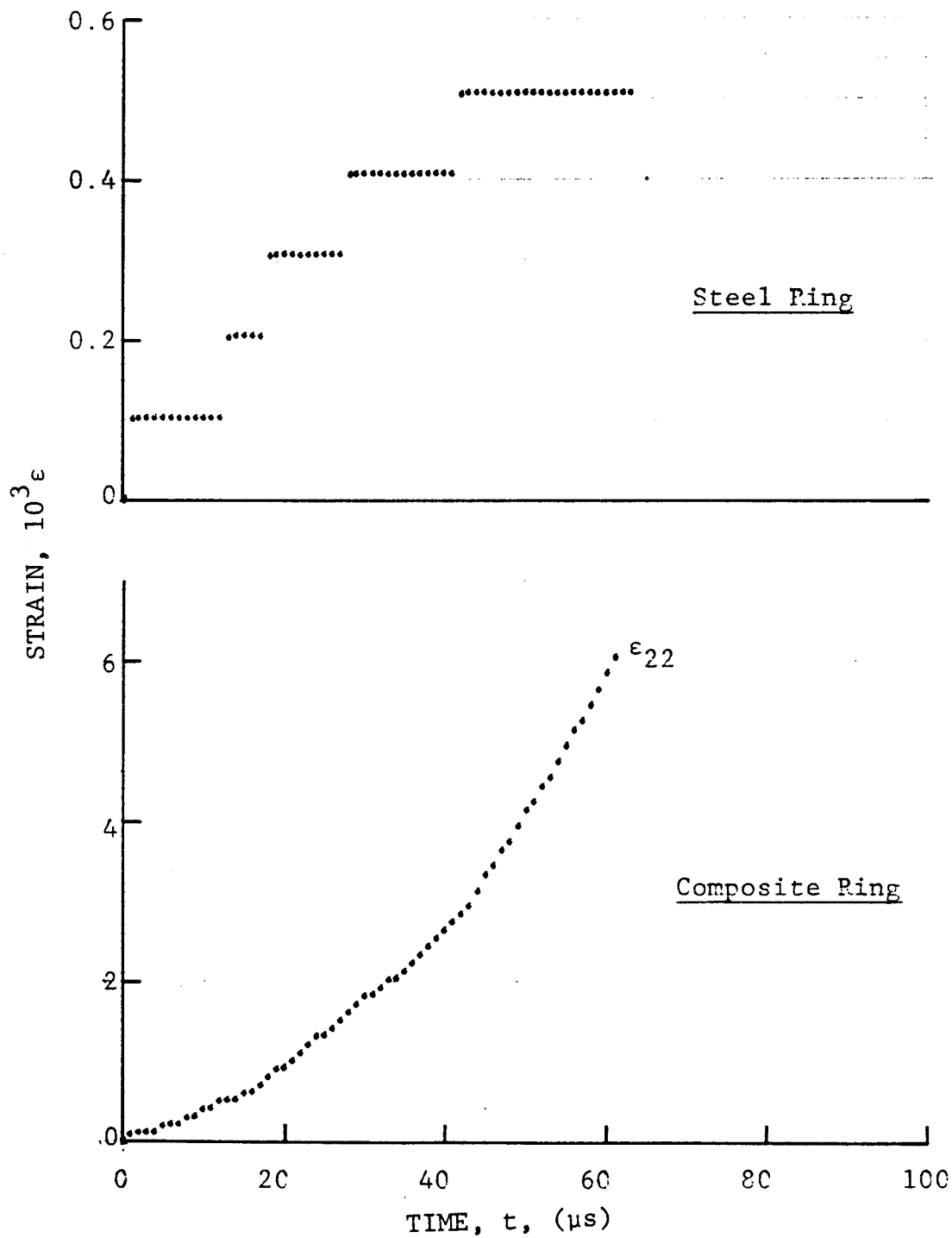


Figure 4-120. Strain records in steel ring and [90g] 80AS/20S/PR288 graphite/S-glass/epoxy ring under dynamic loading for Specimen No. 1A-1 (130 mg pistol powder).

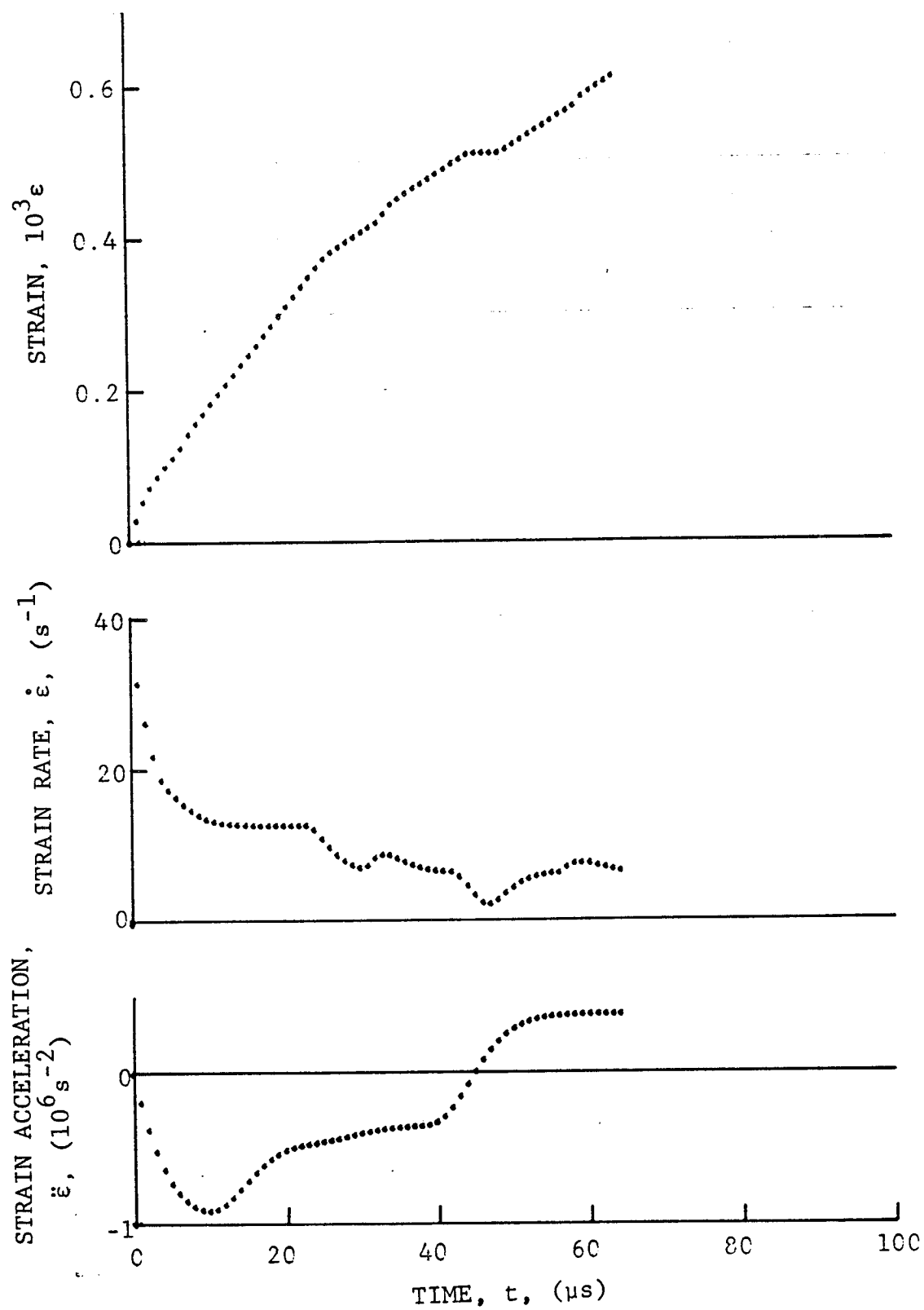


Figure 4-121. Strain and its derivatives in steel ring for Specimen No. 1A-1.

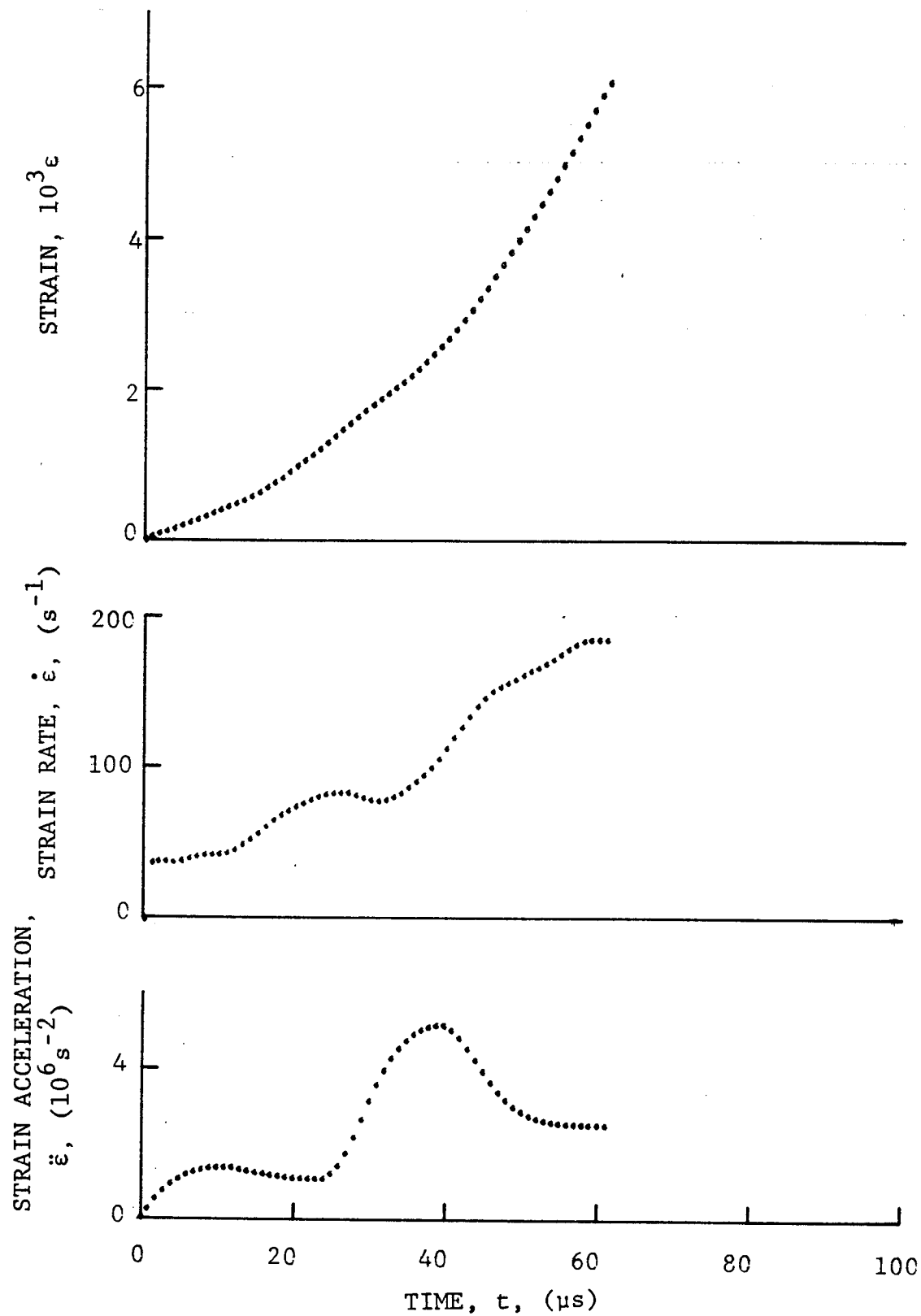


Figure 4-122. Circumferential strain and its derivatives in $[90_8]$ 80AS/20S/PR288 graphite/S-glass/epoxy ring under dynamic loading for Specimen No. 1A-1.

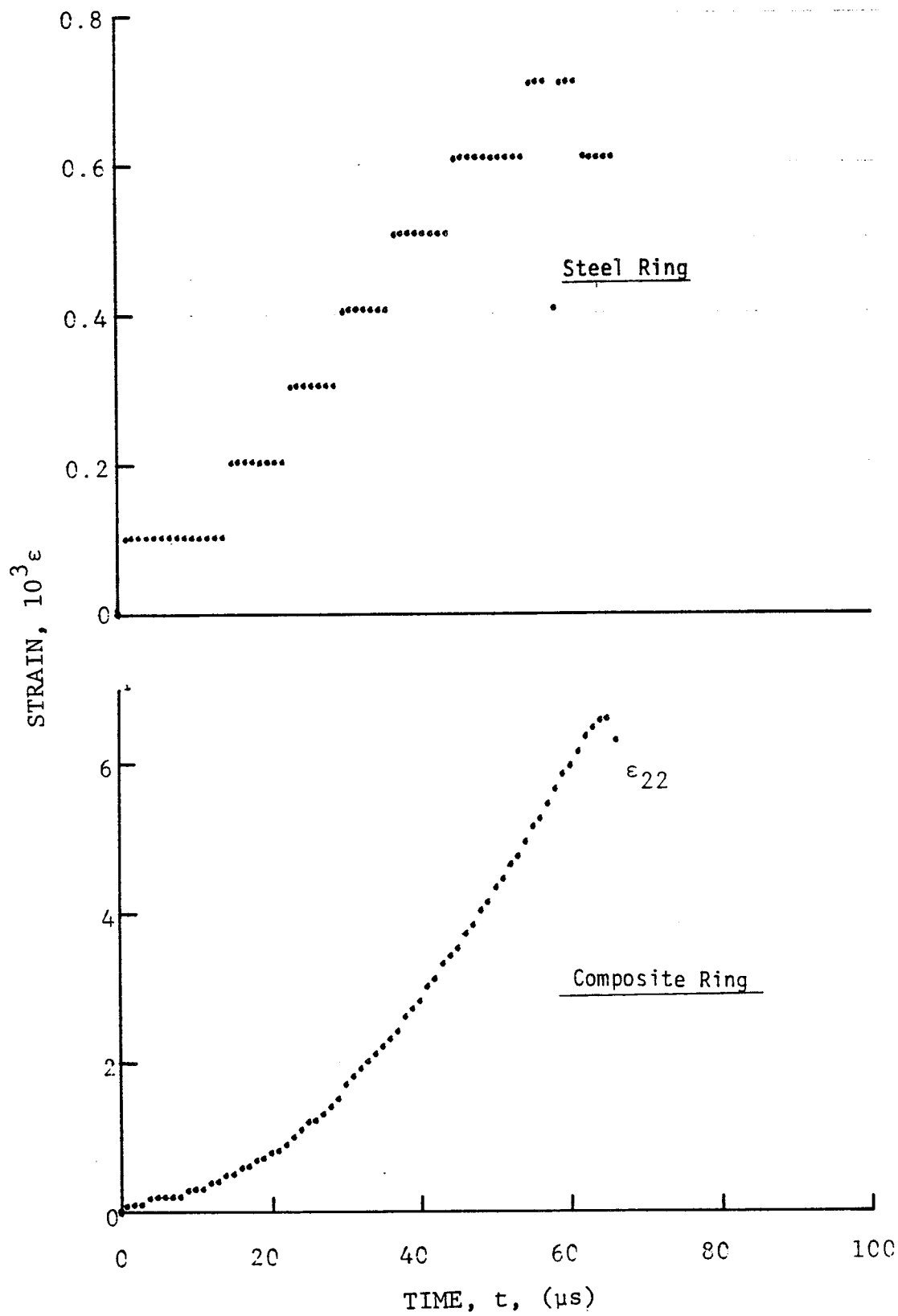


Figure 4-123. Strain records in steel ring and [90_g] 80AS/20S/PR288 graphite/S-glass/epoxy ring under dynamic loading for Specimen No. 1A-2 (130 mg pistol powder).

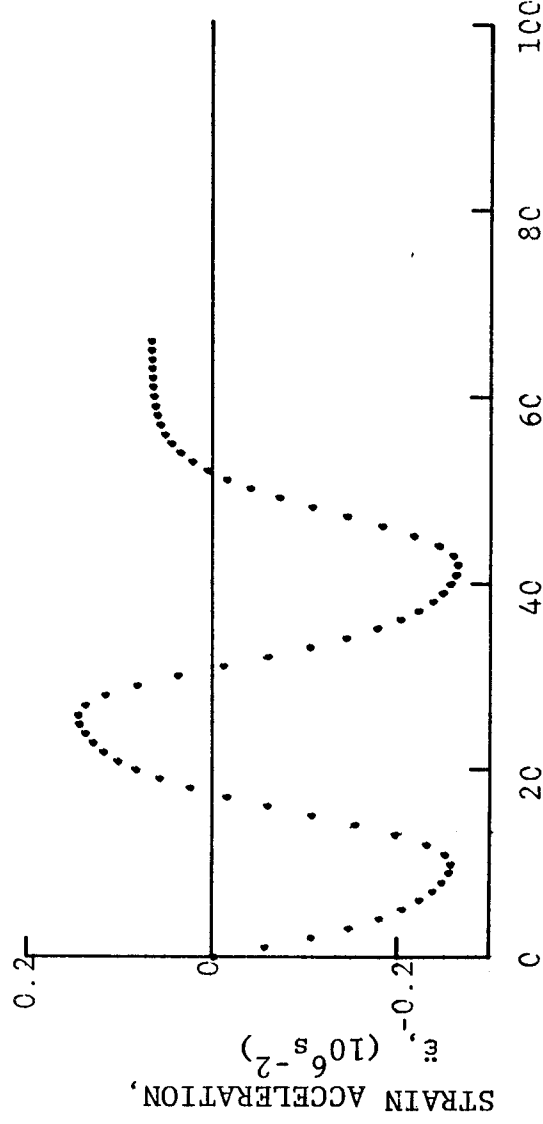
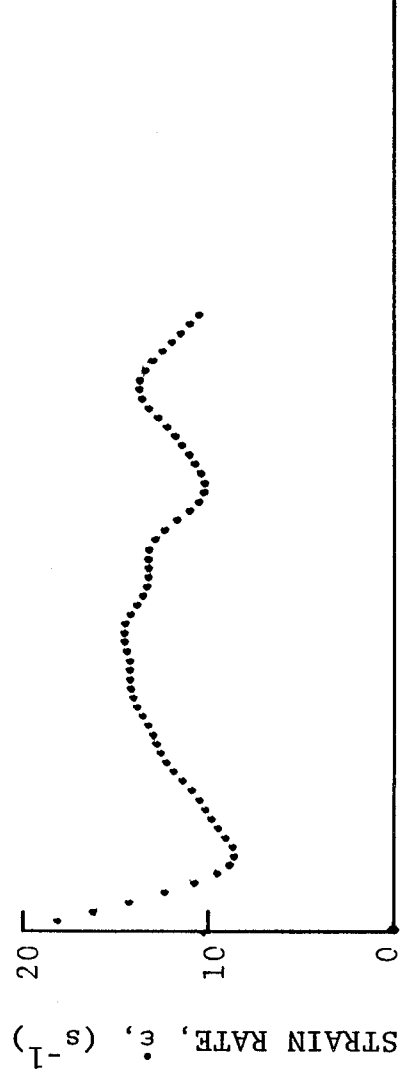
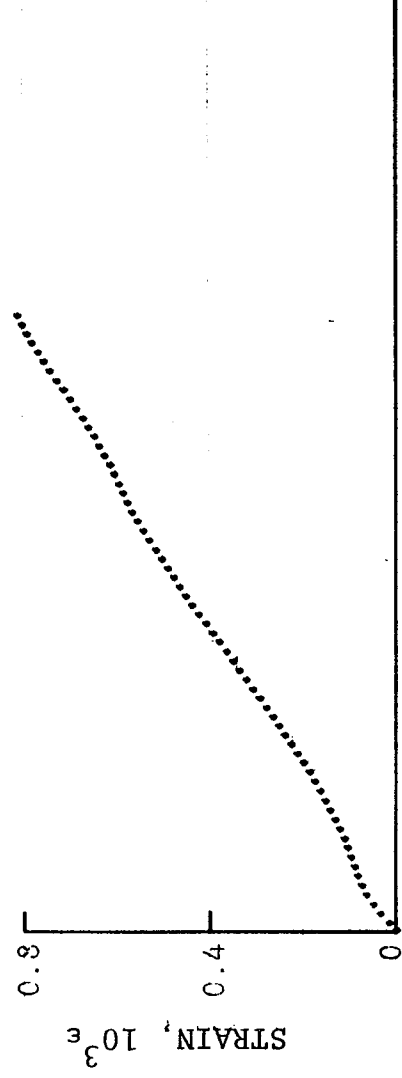


Figure 4-124. Strain and its derivatives in steel ring for Specimen No. 1A-2.

Figure 4-125. Circumferential strain and its derivatives in [908]
80AS/20S/PR288 graphite/S-glass/epoxy ring under dynamic loading
for Specimen No. 1A-2.

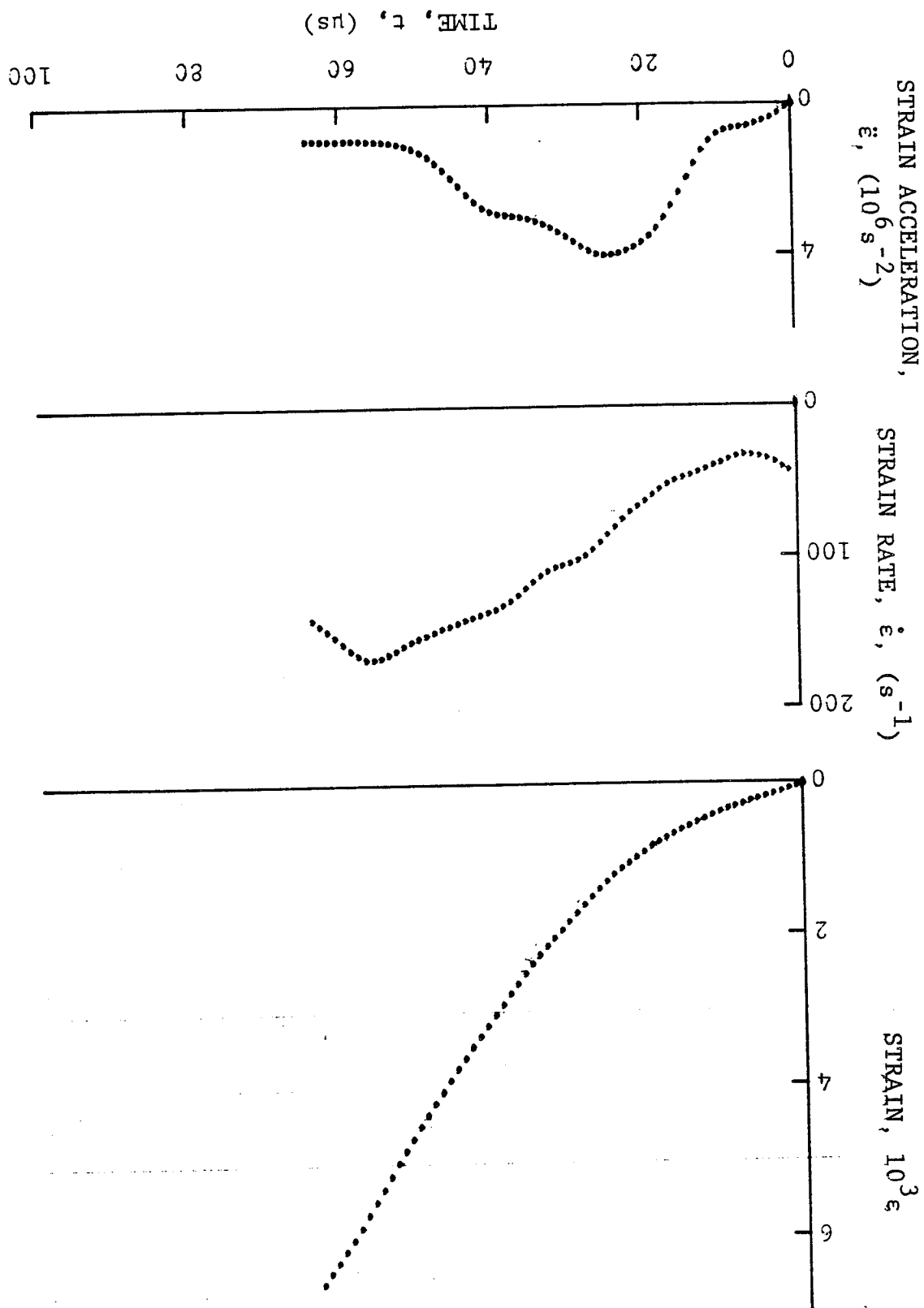
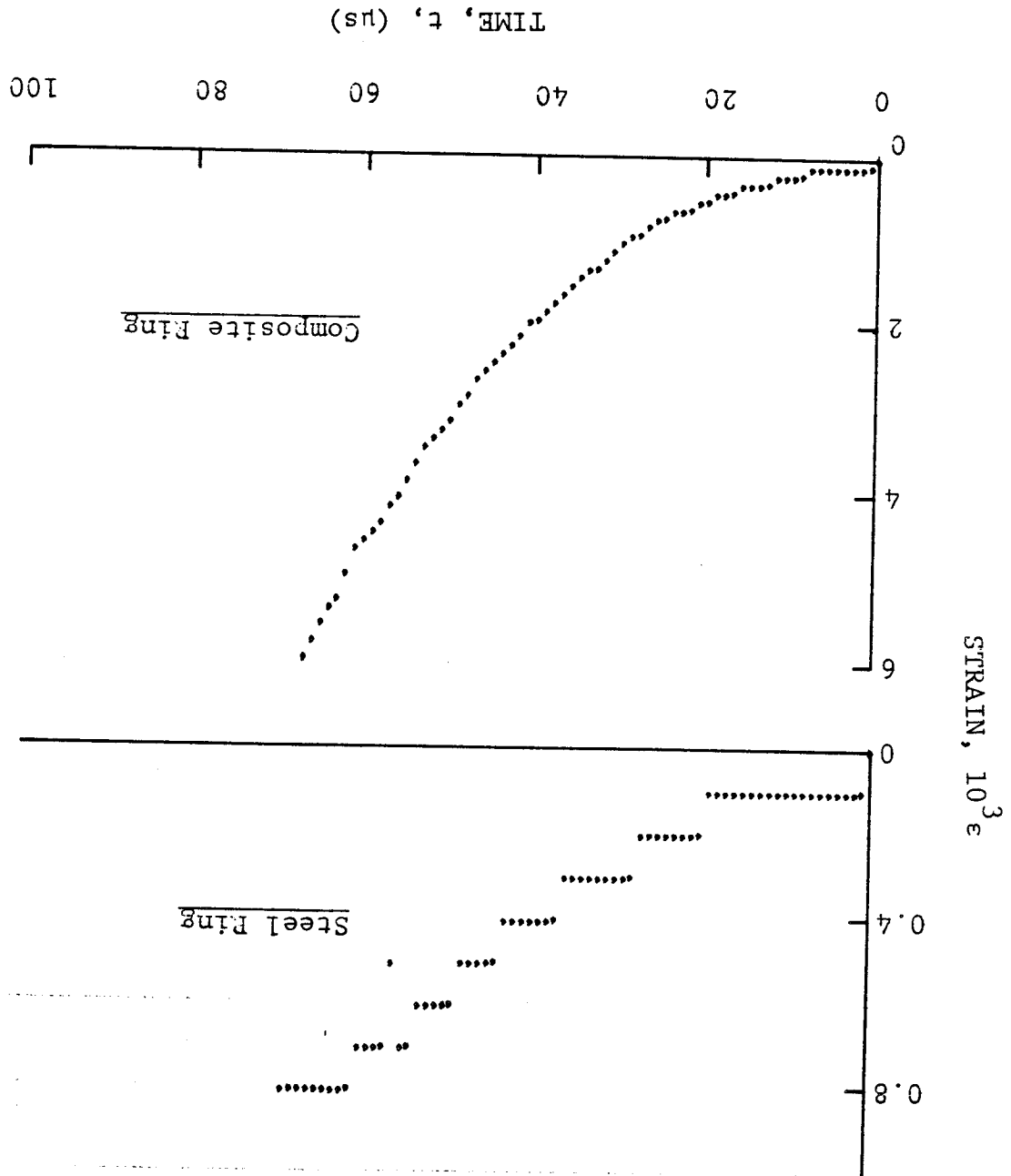


Figure 4-126. Strain records in steel ring and [90°] 80AS/20S/PR288 graphite/S-glass/epoxy ring under dynamic loading for Specimen No. 1A-3 (260 mg pistol powder).



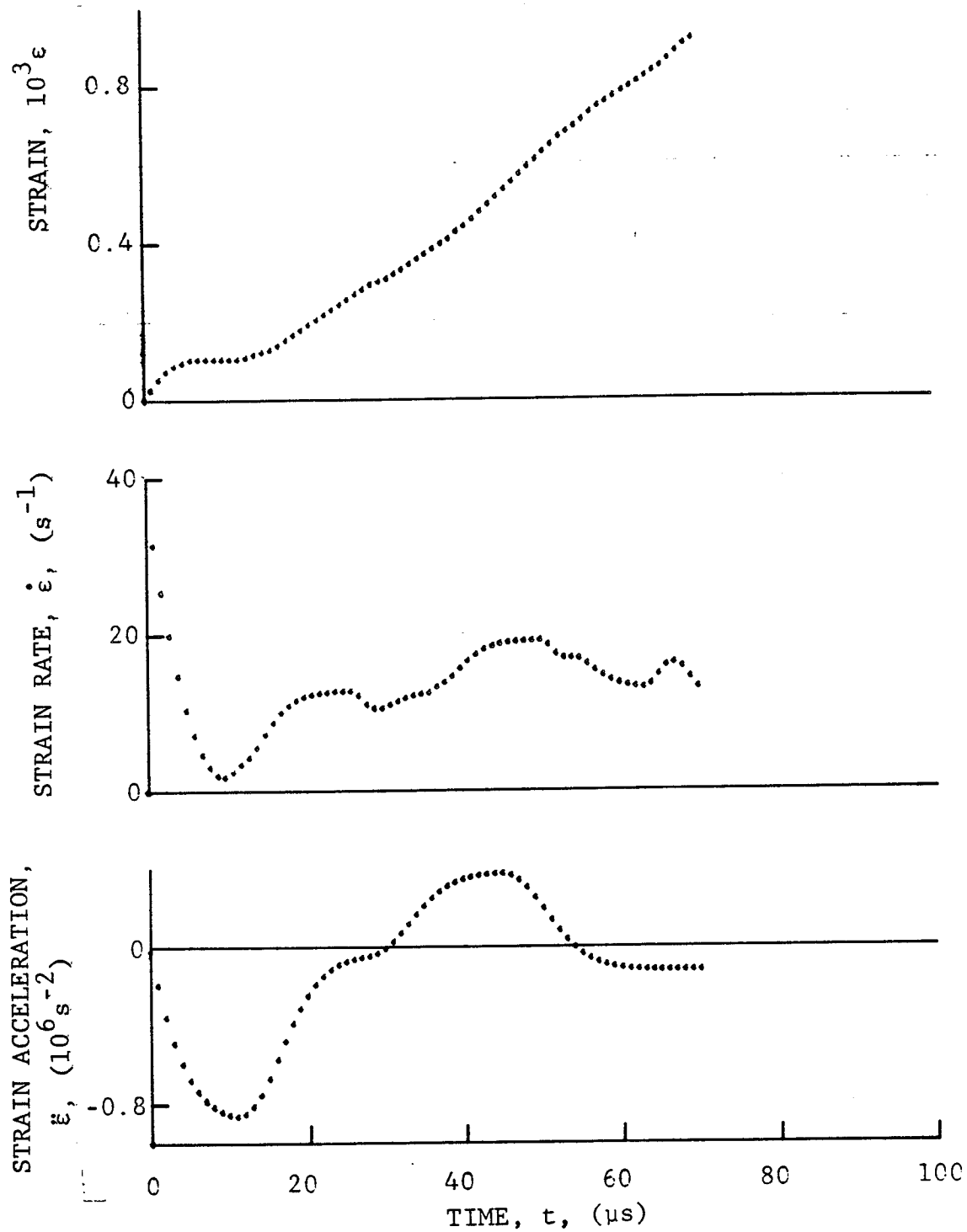


Figure 4-127. Strain and its derivatives in steel ring for Specimen No. 1A-3.

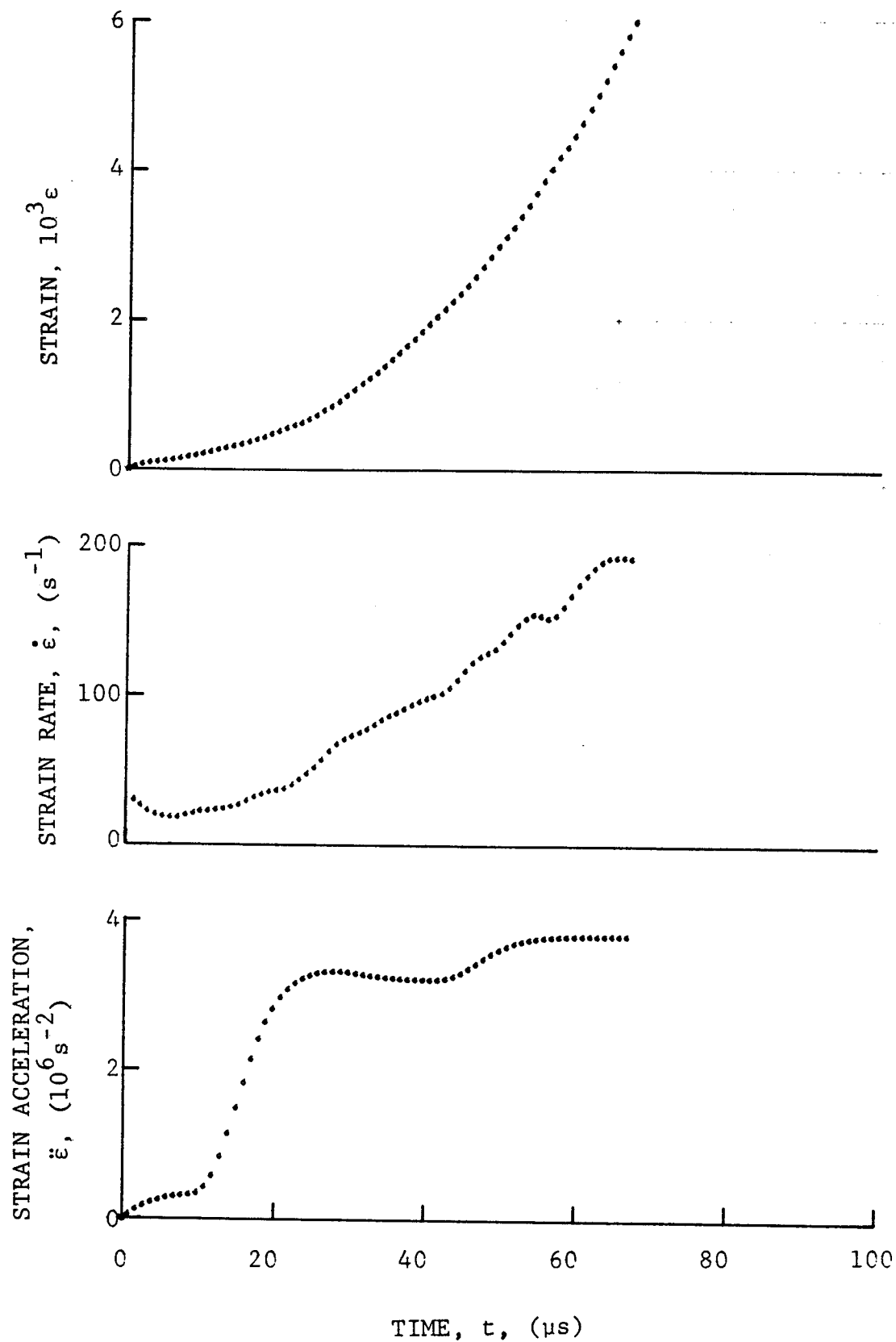


Figure 4-128. Circumferential strain and its derivatives in [90_g] 80AS/20S/PR288 graphite/S-glass/epoxy ring under dynamic loading for Specimen No. 1A-3.

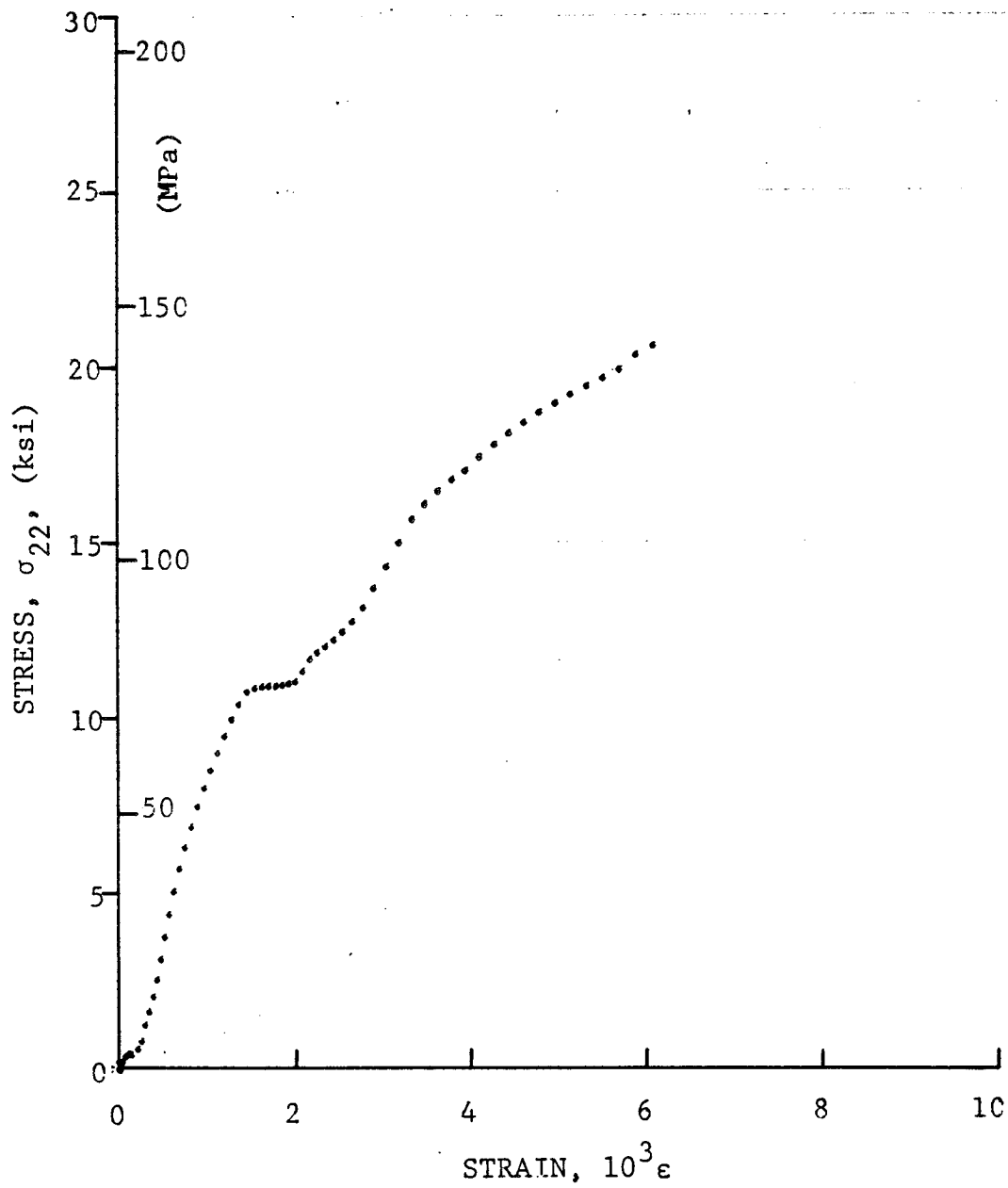


Figure 4-129. Stress-strain curve for dynamically loaded [90g] 80AS/20S/PR288 graphite/S-glass/epoxy ring for Specimen No. 1A-1 (130 mg pistol powder).

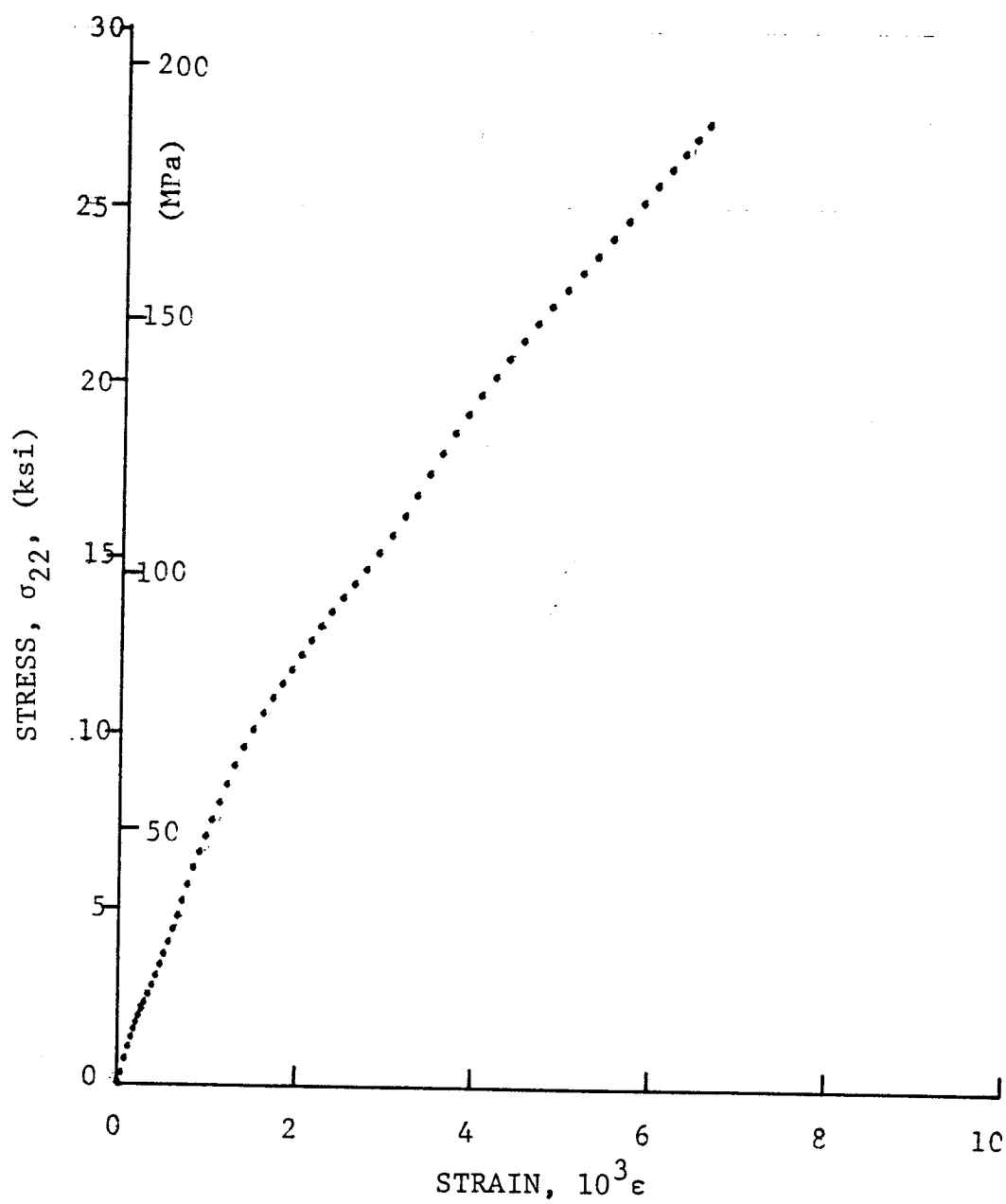


Figure 4-130. Stress-strain curve for dynamically loaded $[90_8]$ 80AS/20S/PR288 graphite/S-glass/epoxy ring for Specimen No. 1A-2.

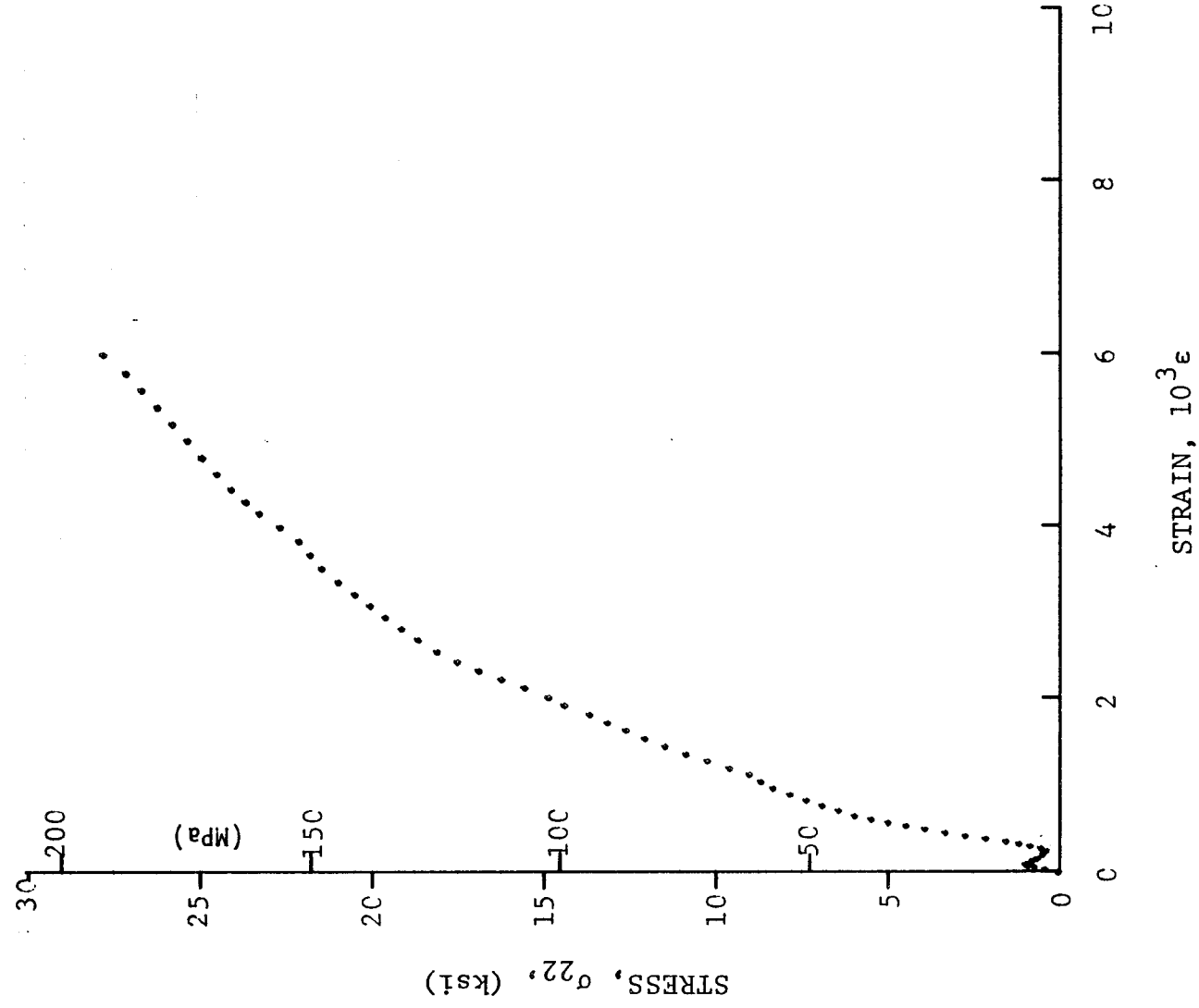


Figure 4-131. Stress-strain curve for dynamically loaded [90g]
80AS/20S/PR288 graphite/S-glass/epoxy ring for Specimen
No. 1A-3 (260 mg pistol powder).

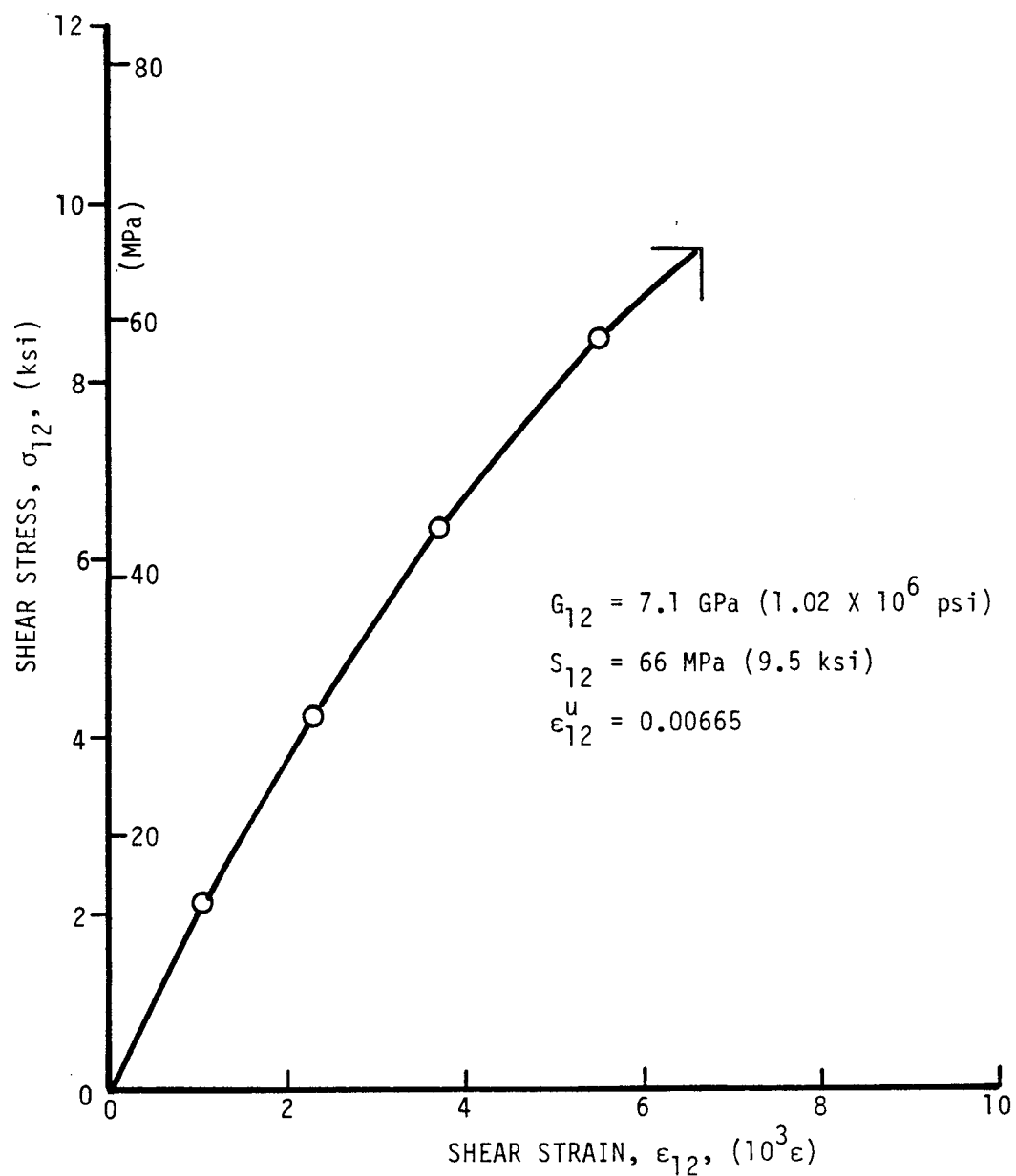


Figure 4-132. Shear stress versus shear strain for unidirectional 10-deg off-axis SP288/T300 ring specimen (Specimen No. 17-1).

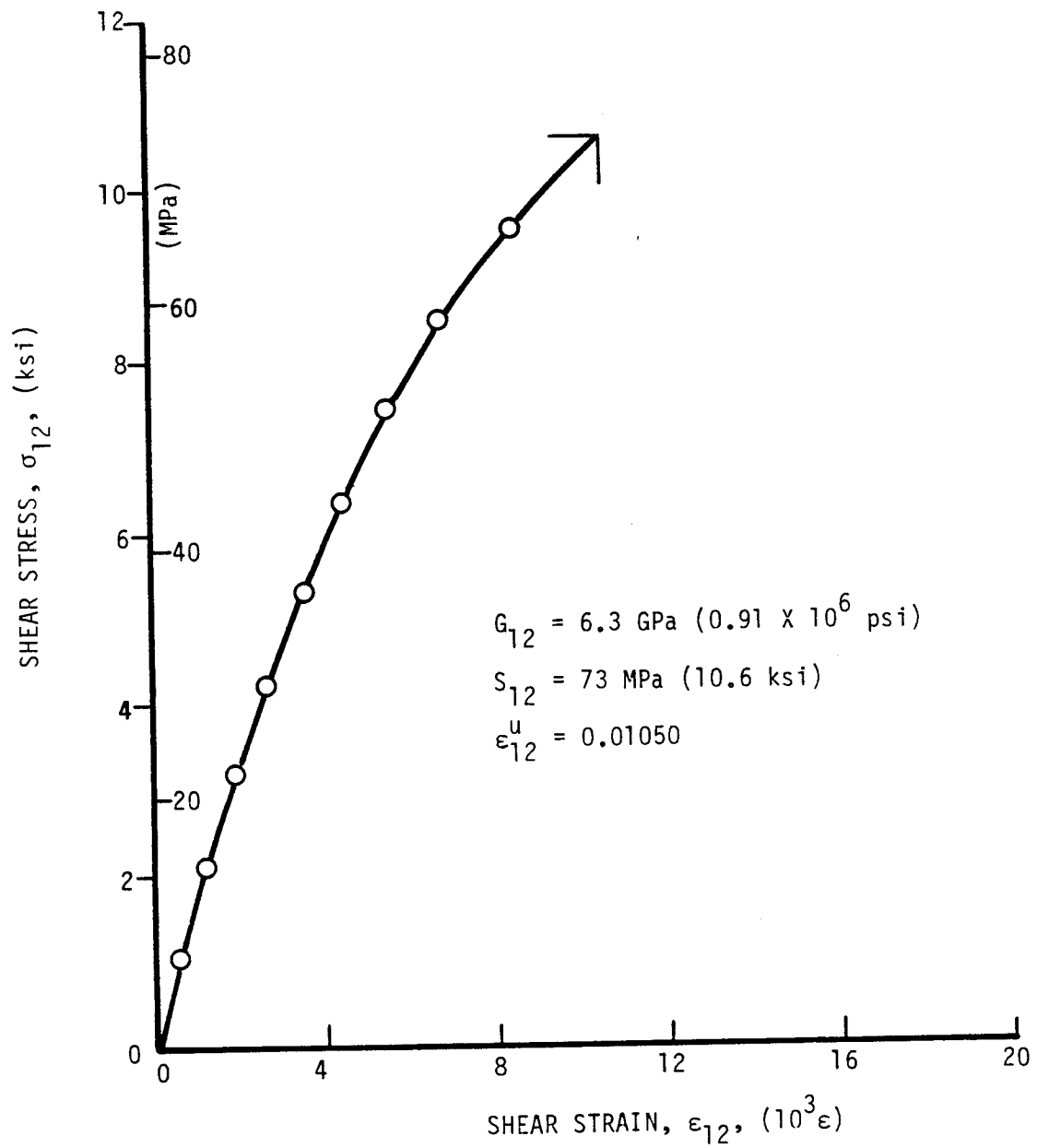


Figure 4-133. Shear stress versus shear strain for unidirectional 10-deg off-axis SP288/T300 ring specimen (Specimen No. 17-2).

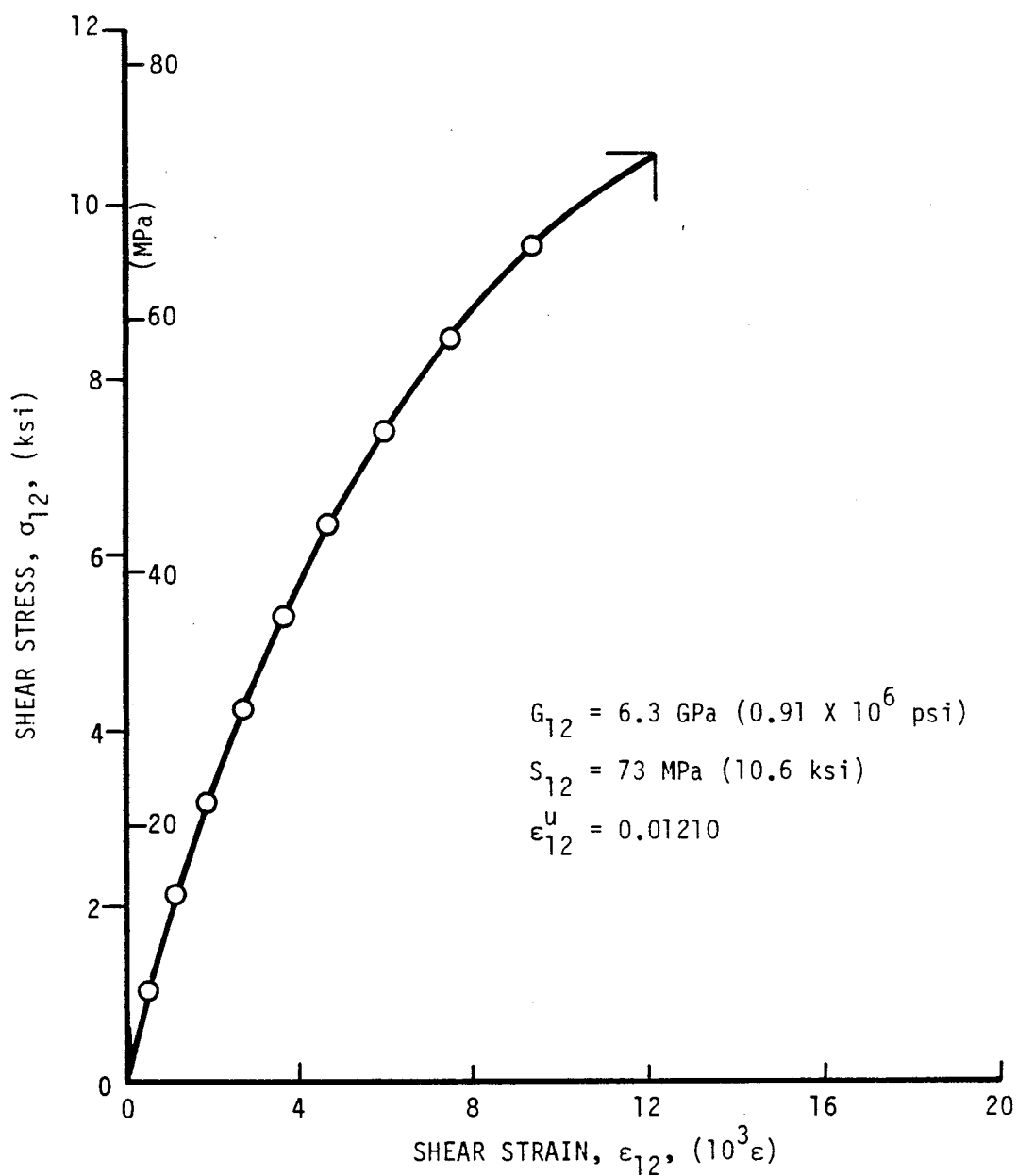


Figure 4-134. Shear stress versus shear strain for unidirectional 10-deg off-axis SP288/T300 ring specimen (Specimen No. 17-3).

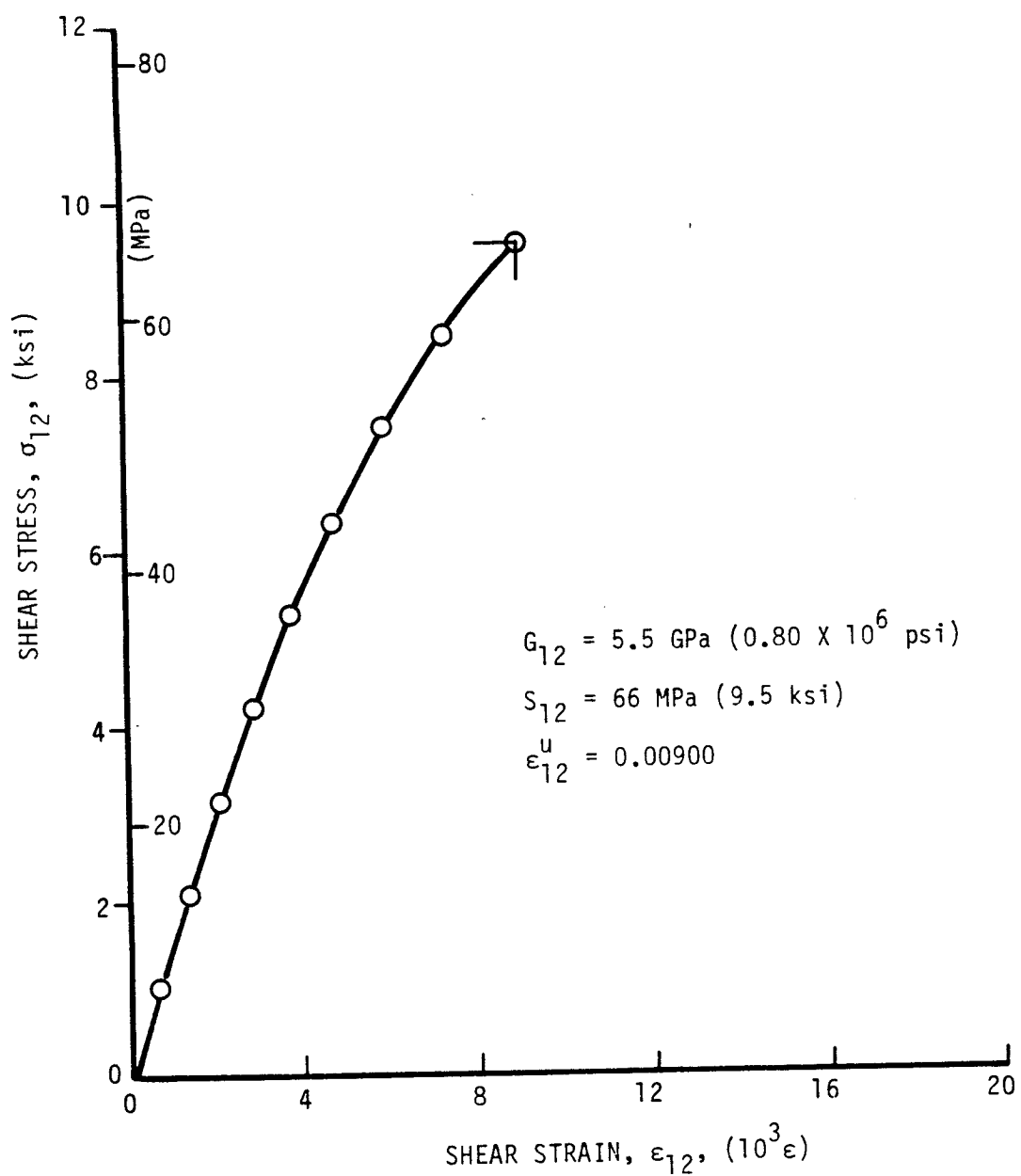


Figure 4-135. Shear stress versus shear strain for unidirectional 10-deg off-axis SP288/T300 ring specimen (Specimen No. 17-4).

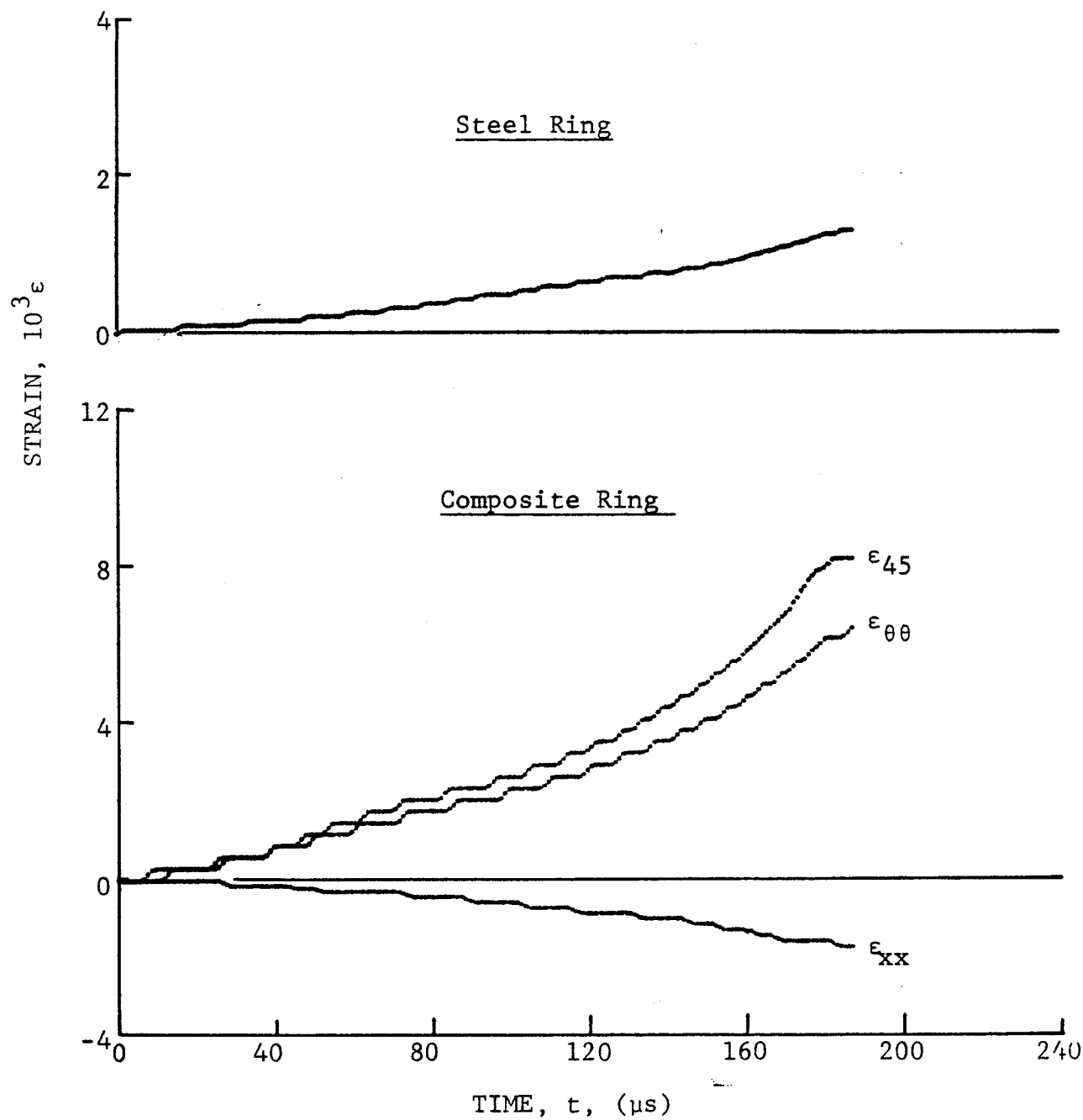


Figure 4-136. Strain records in steel ring and in [10₆] SP288/T300 graphite/epoxy ring under dynamic loading for Specimen No. 57-2 (650 mg pistol powder).

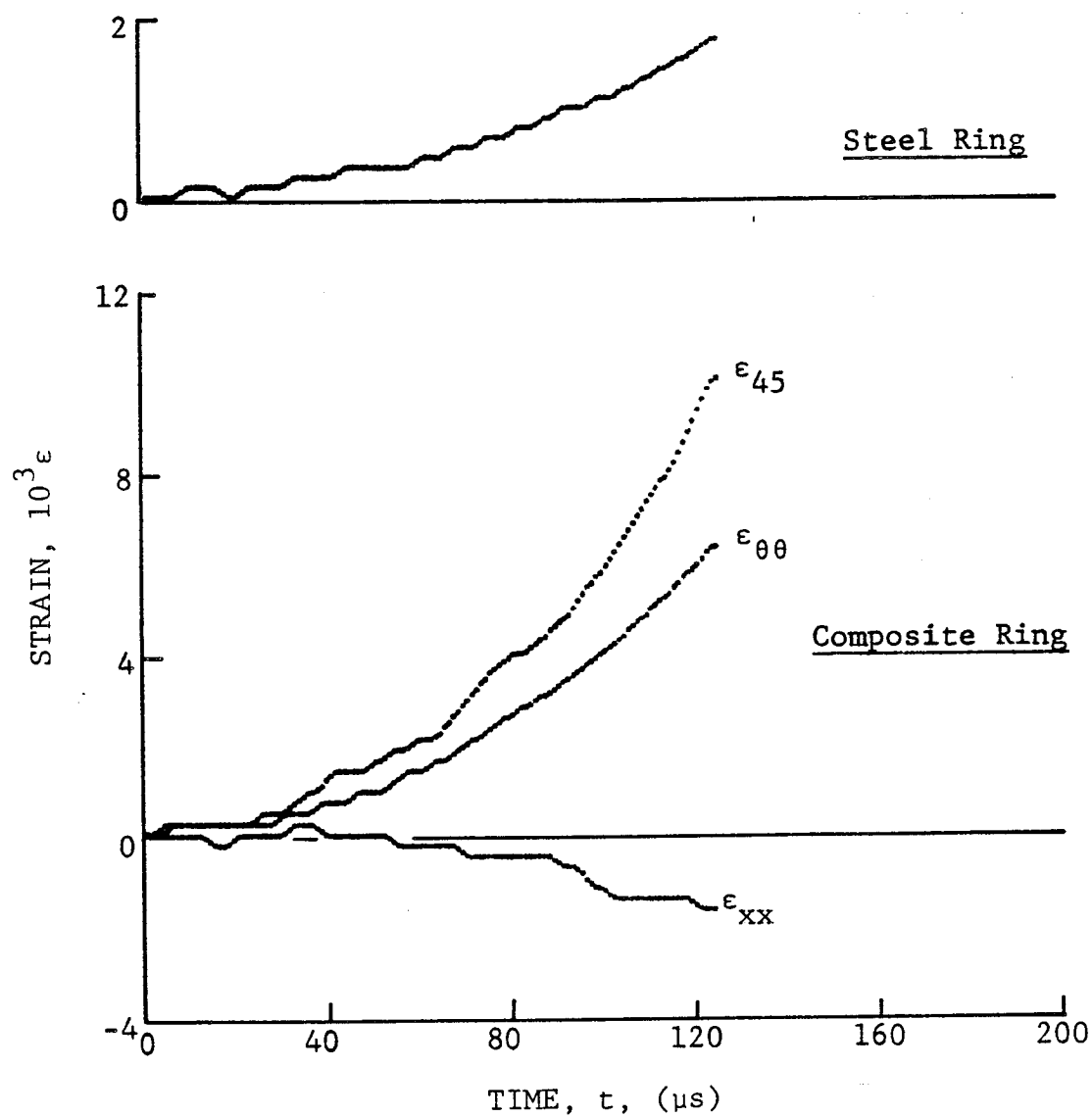


Figure 4-137. Strain records in steel ring and in $[10_6]$ SP288/T300 graphite/epoxy ring under dynamic loading for Specimen No. 57-3 (650 mg pistol powder).

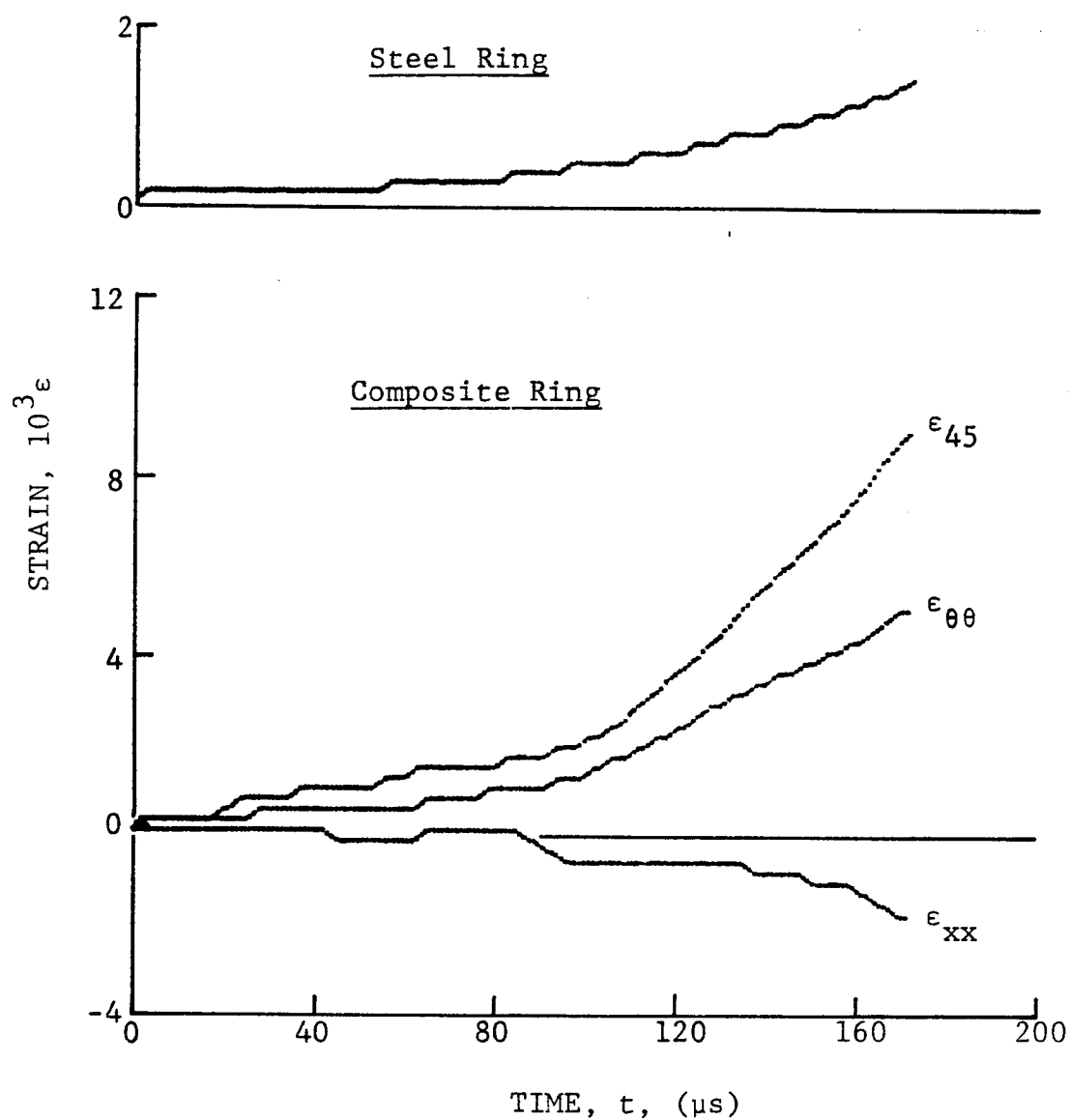


Figure 4-138. Strain records in steel ring and in $[10_6]$ SP288/T300 graphite/epoxy ring under dynamic loading for Specimen No. 57-5 (650 mg pistol powder).

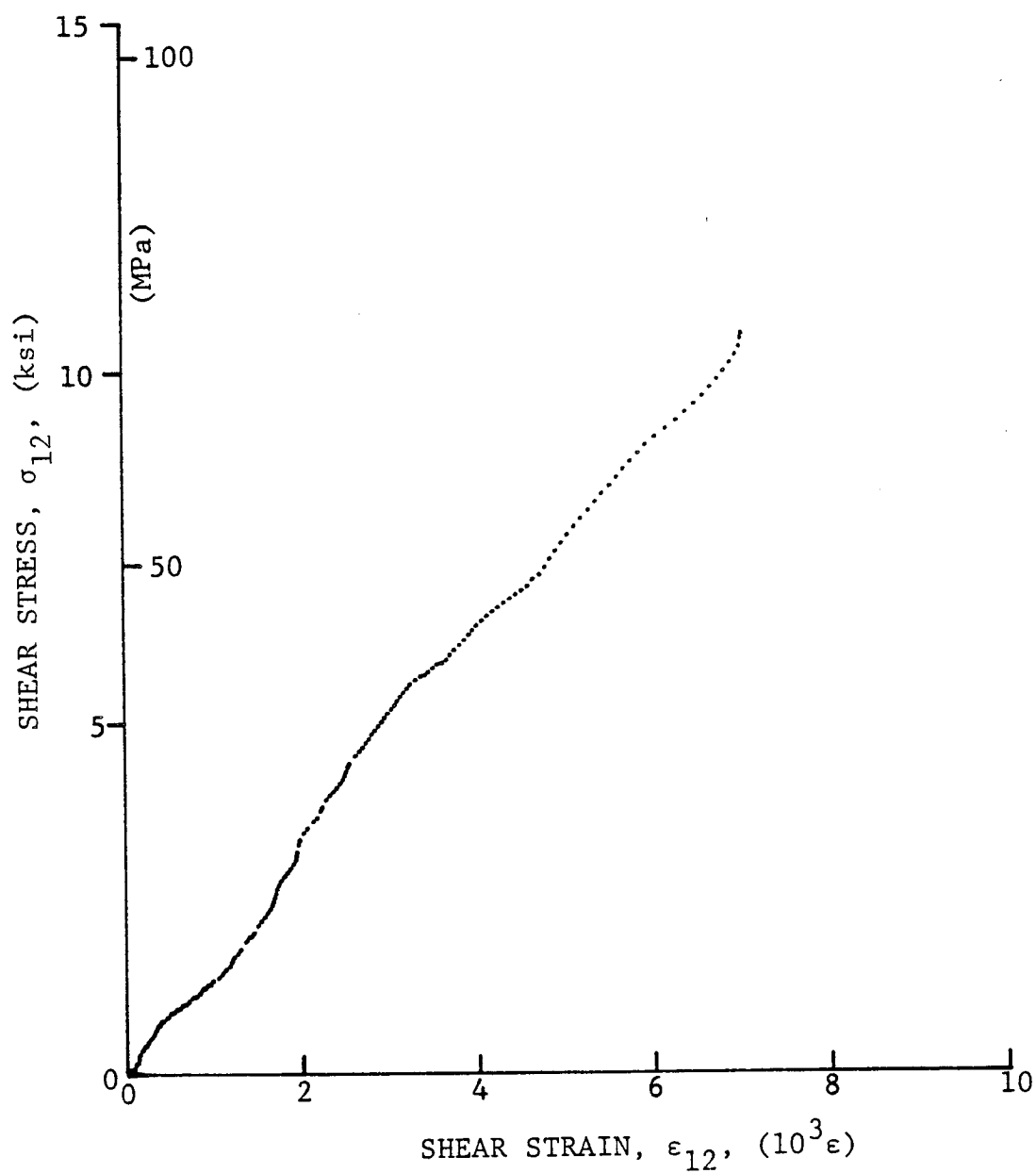


Figure 4-139. Shear stress versus shear strain curve for dynamically loaded $[10_6]$ SP288/T300 graphite/epoxy ring for Specimen No. 57-2 (650 mg pistol powder).

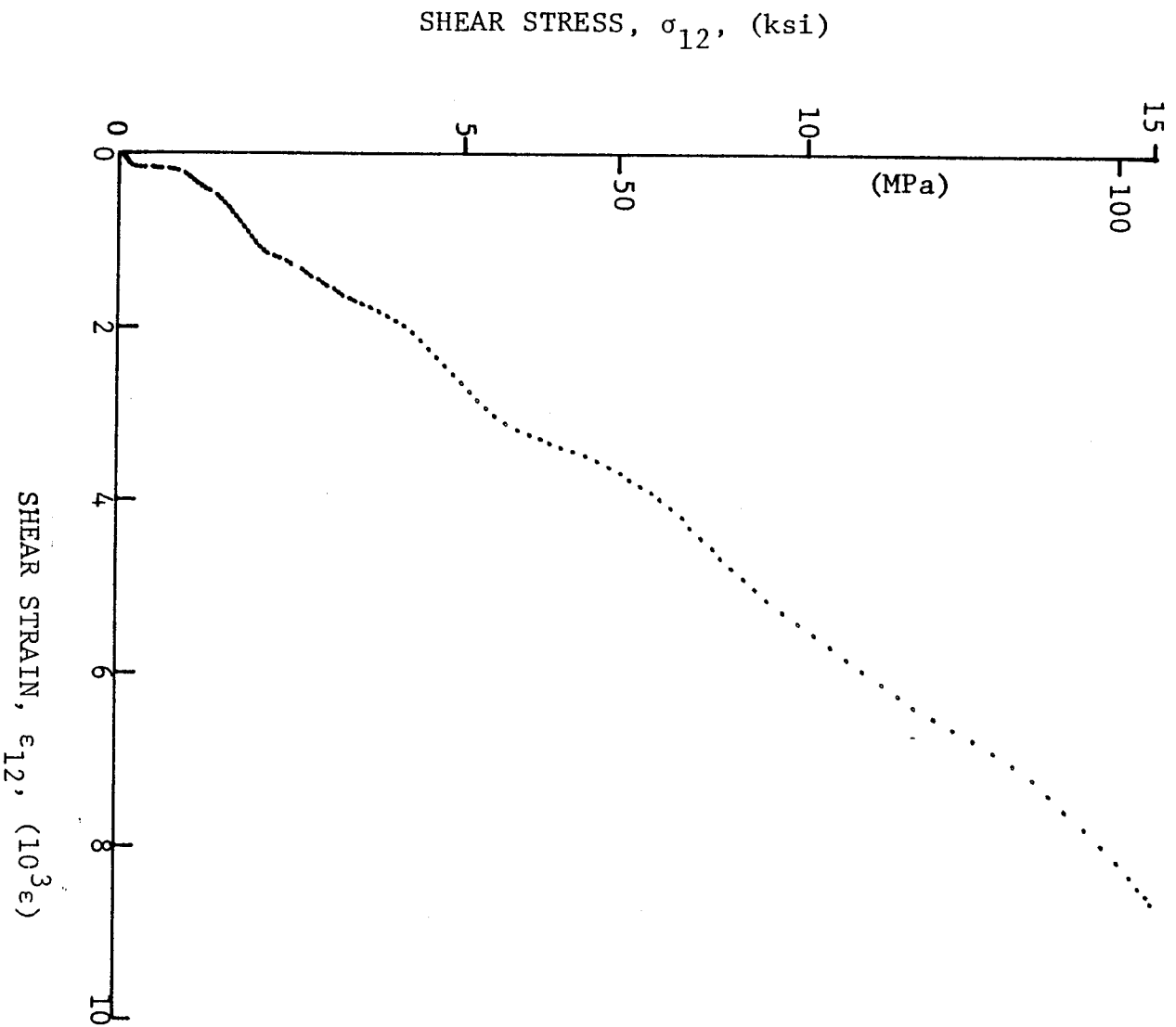


Figure 4-140. Shear stress versus shear strain curve for dynamically loaded $[10_6]$ SP288/T300 graphite/epoxy ring for Specimen No. 57-3 (650 mg pistol powder).

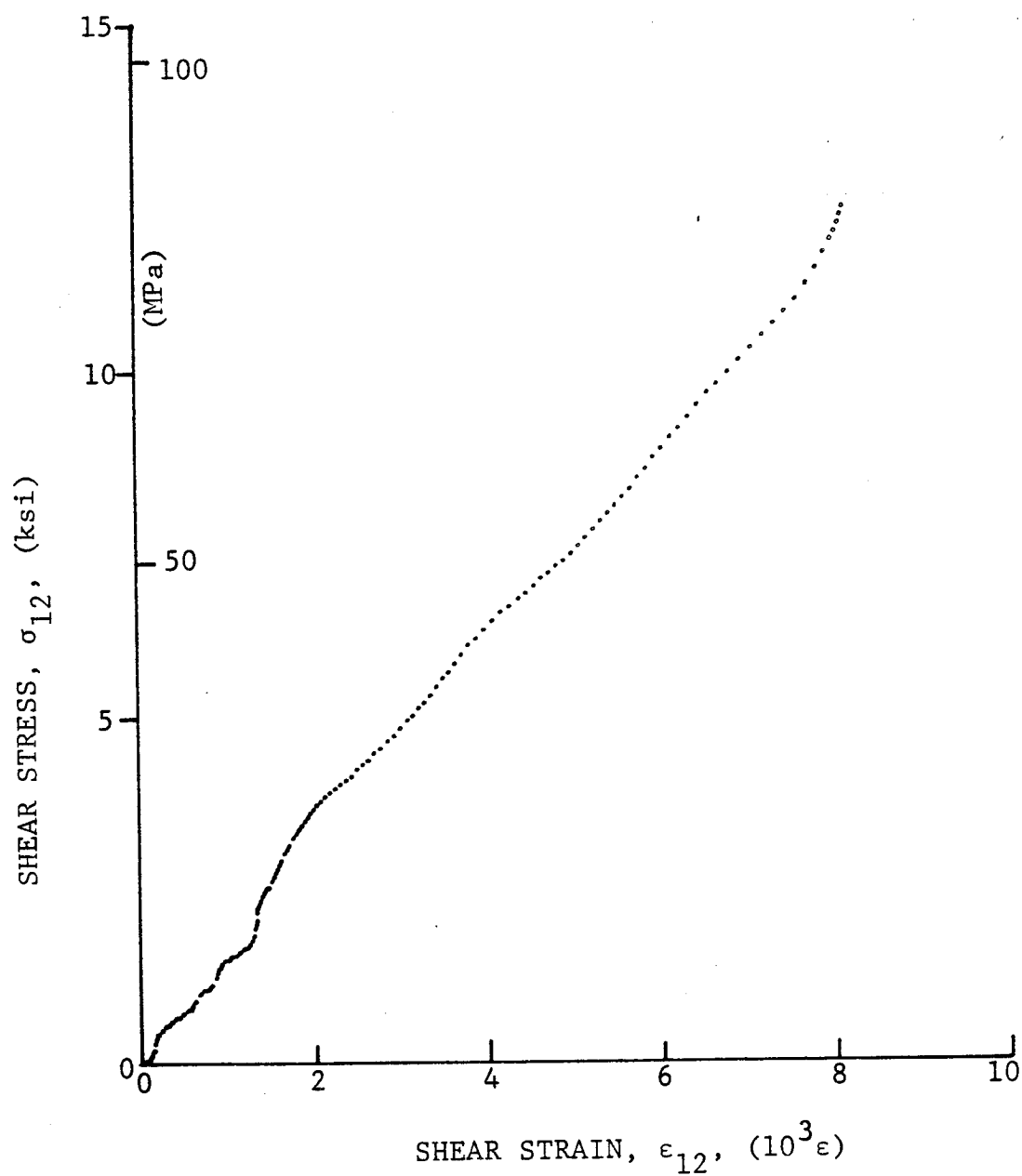
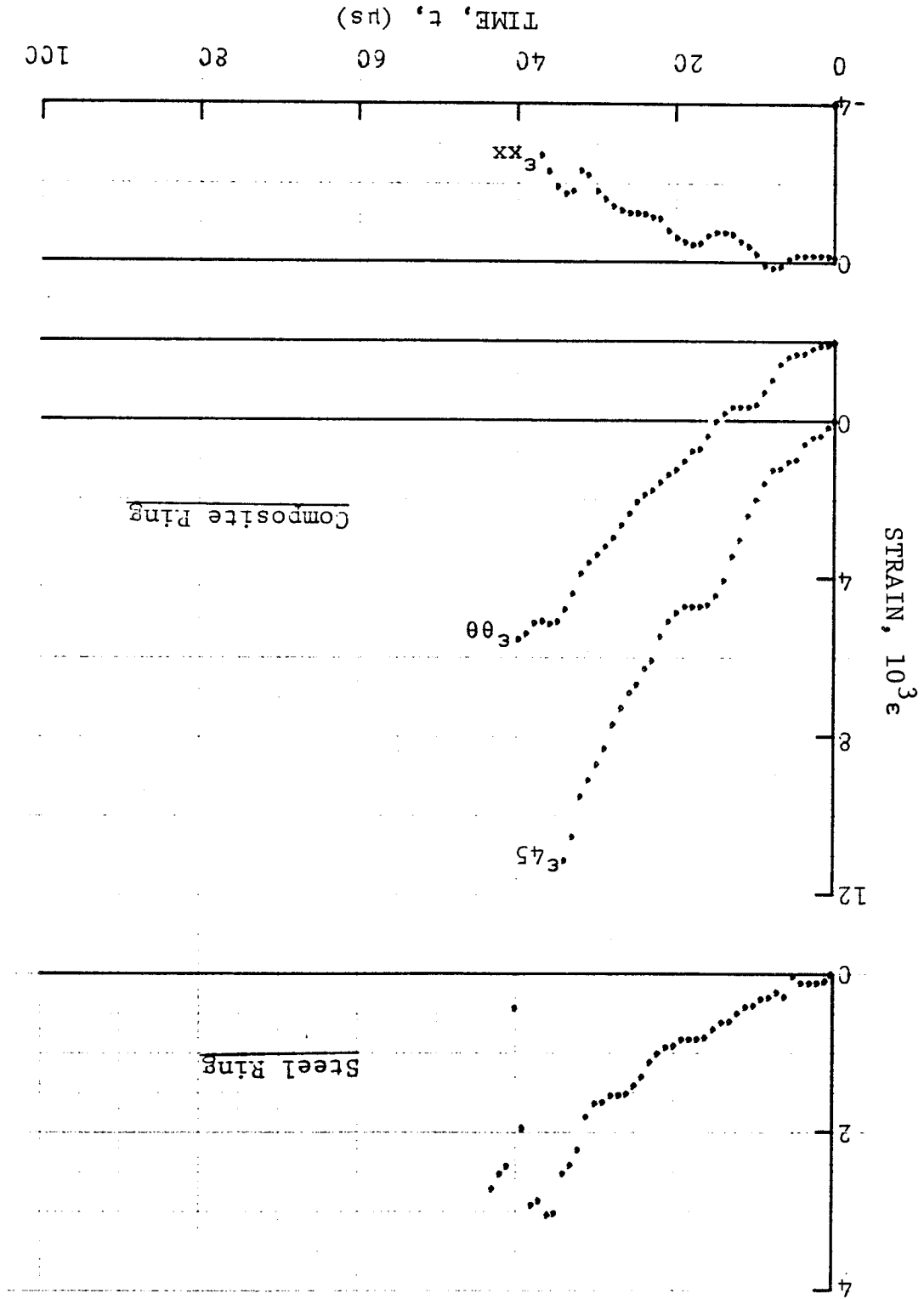


Figure 4-141. Shear stress versus shear strain curve for dynamically loaded $[10_6]$ SP288/T300 graphite/epoxy ring for Specimen No. 57-5 (650 mg pistol powder).

Figure 4-142. Strain records in steel ring and [106] SP288/T300 graphite/epoxy ring under dynamic loading for Specimen No. 17-7 (100 mg PETN detonator).



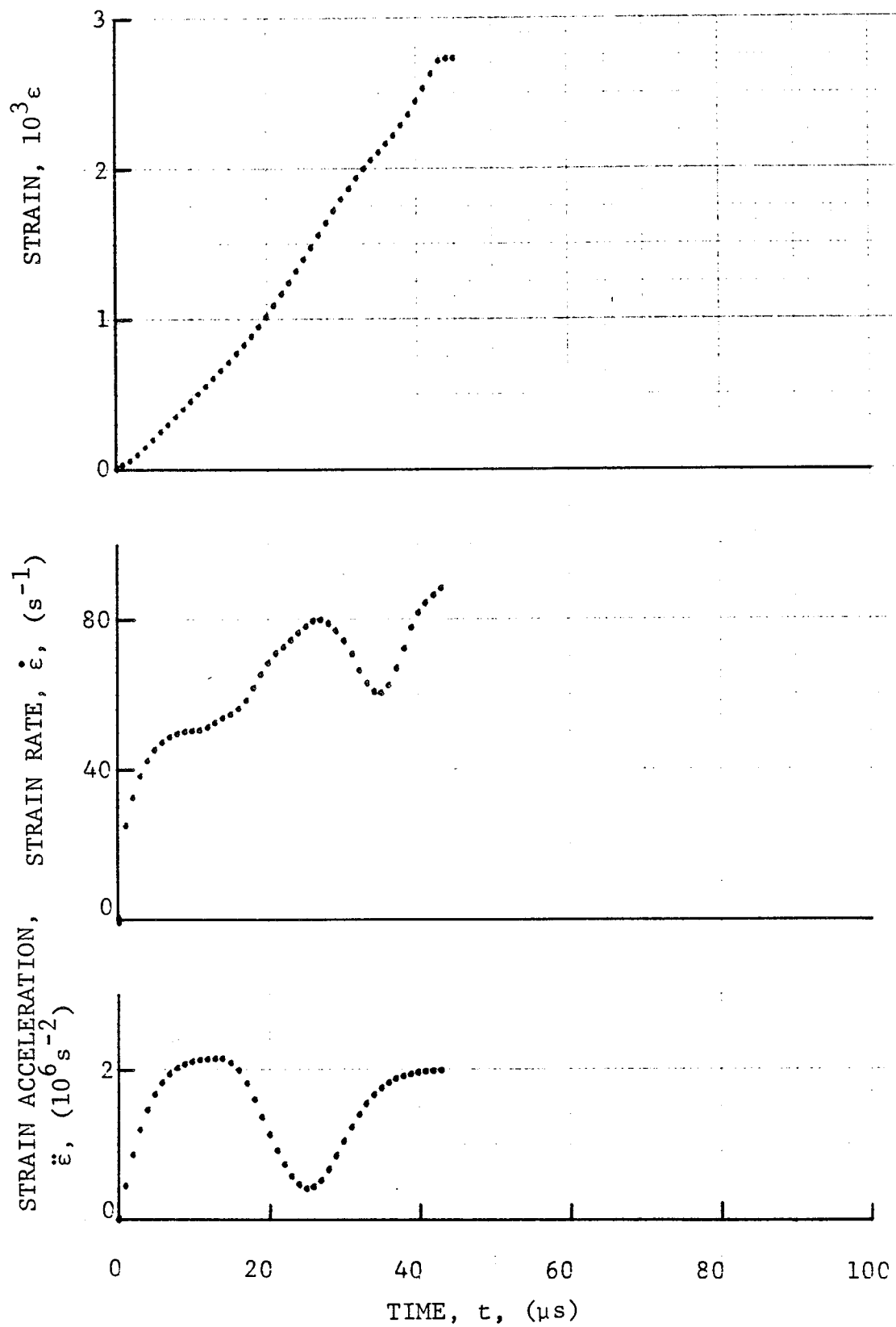


Figure 4-143. Strain and its derivatives in steel ring for Specimen No. 17-7.

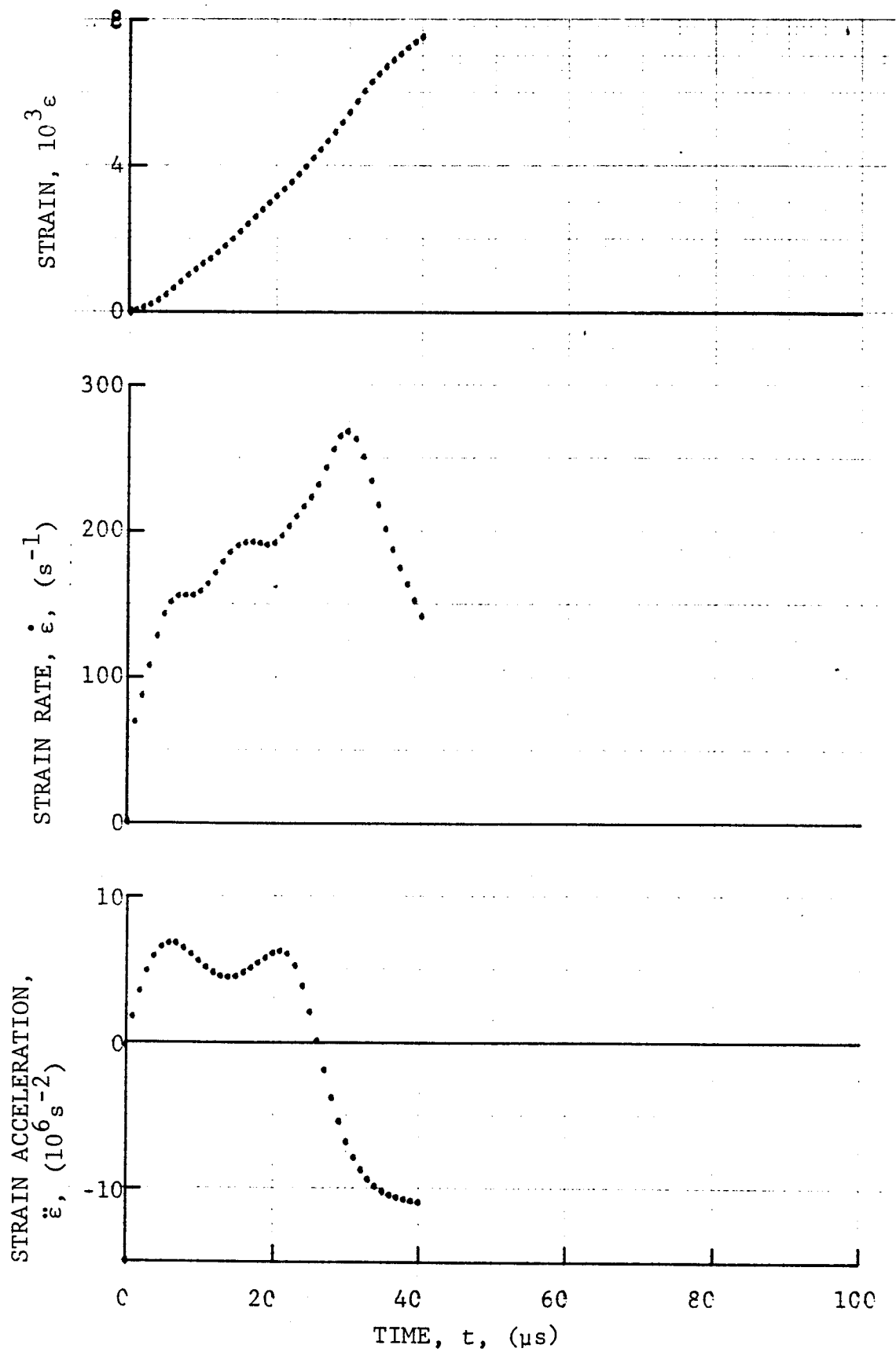


Figure 4-144. Circumferential strain and its derivatives in $[10_6]$ SP288/T300 graphite/epoxy ring under dynamic loading for Specimen No. 17-7.

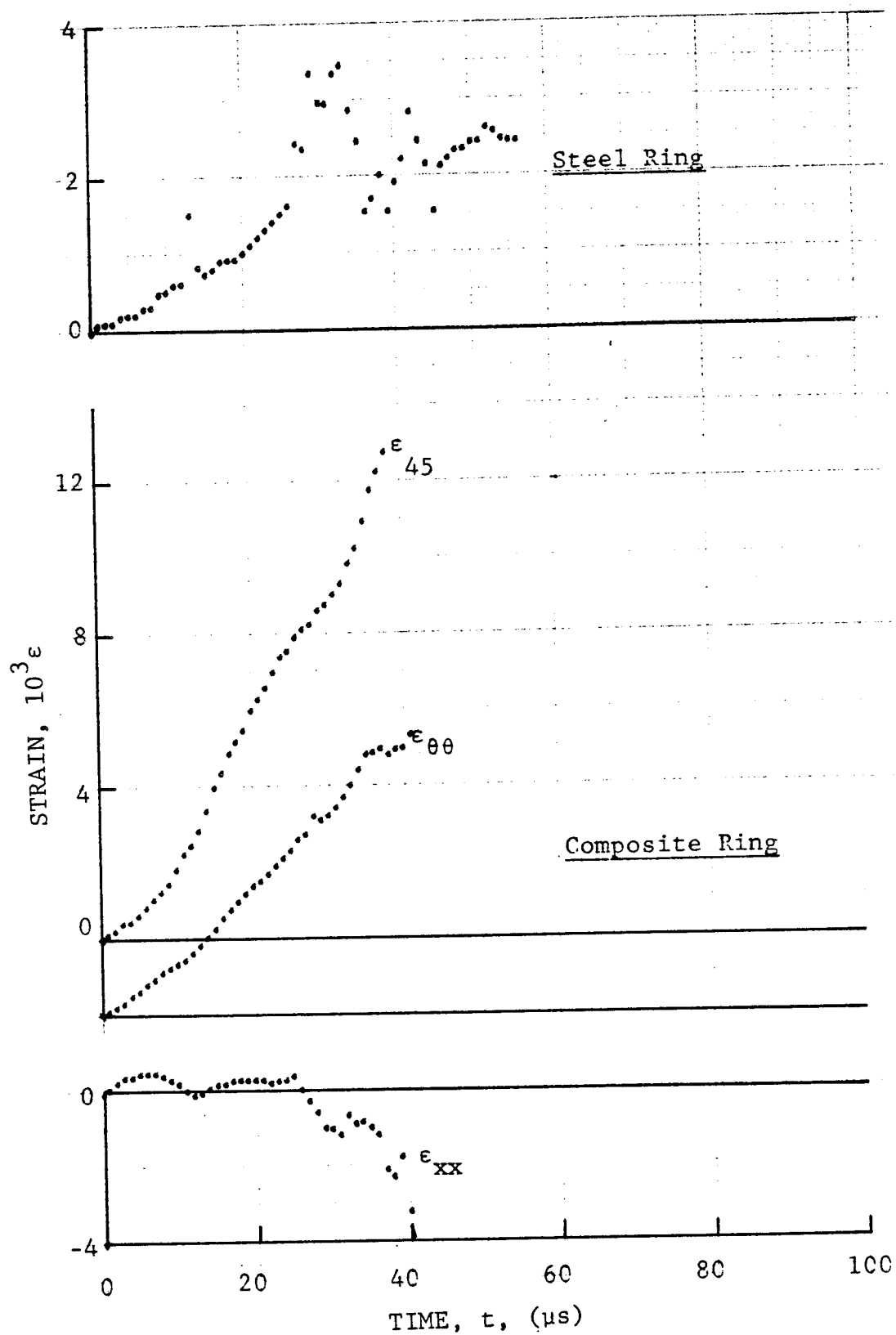


Figure 4-145. Strain records in steel ring and [10₆] SP288/T300 graphite/epoxy ring under dynamic loading for Specimen No. 17-8 (100 mg PETN detonator).

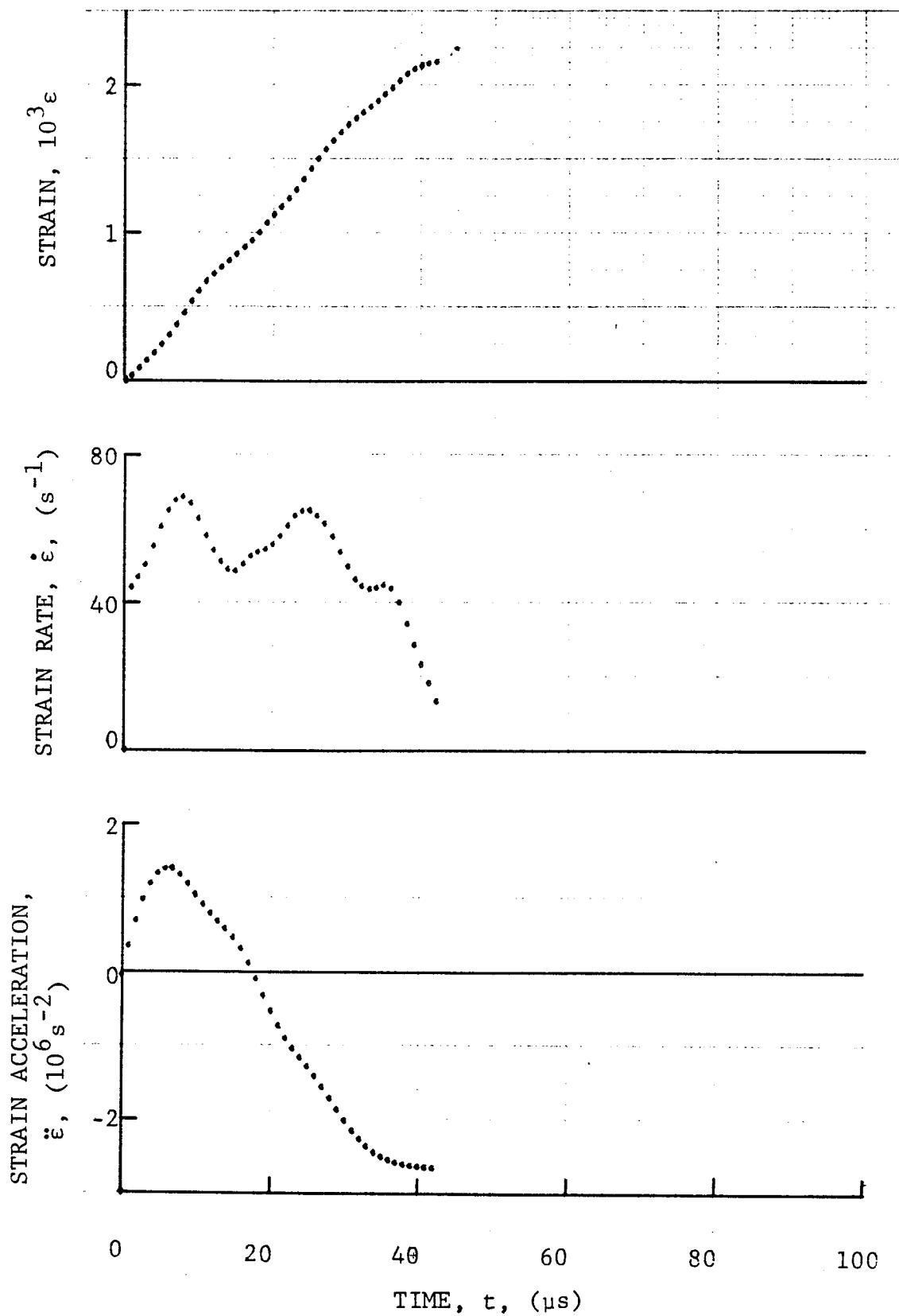


Figure 4-146. Strain and its derivatives in steel ring for Specimen No. 17-8.

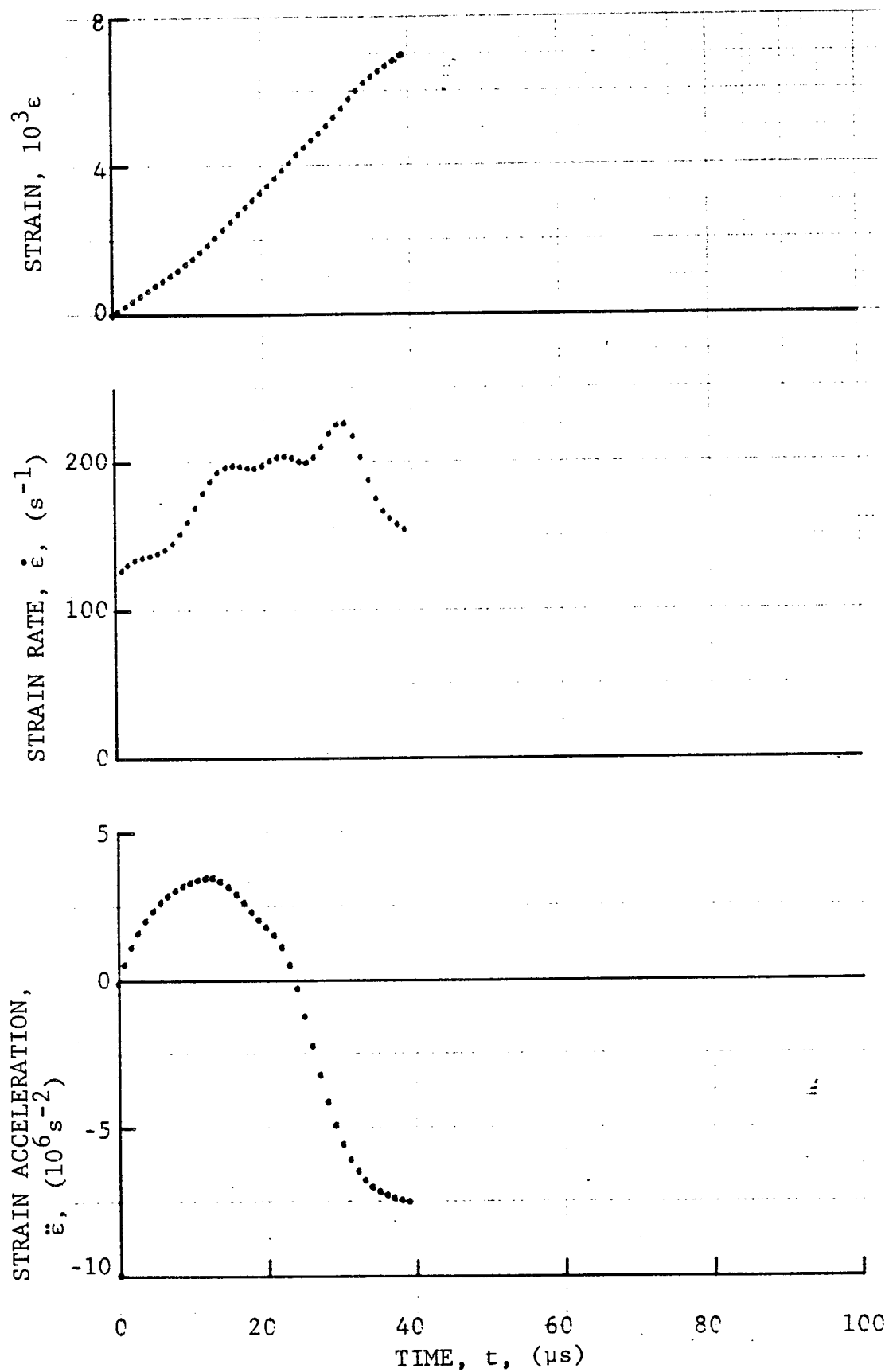


Figure 4-147. Circumferential strain and its derivatives in $[10_6]$ SP288/T300 graphite/epoxy ring under dynamic loading for Specimen No. 17-8.

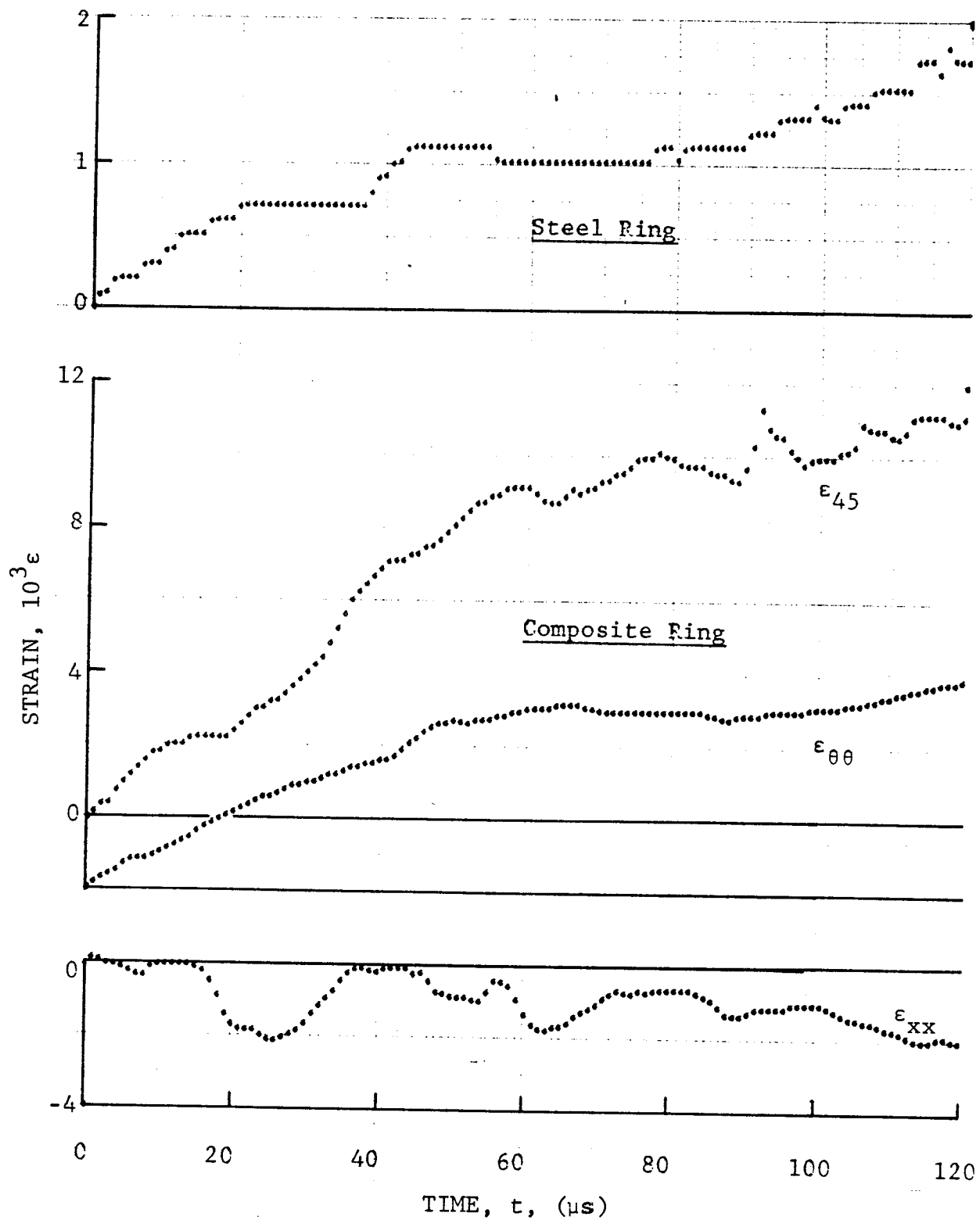


Figure 4-148. Strain records in steel ring and $[10_6]$ SP288/T300 graphite/epoxy ring under dynamic loading for Specimen No. 17-9 (455 mg pistol powder).

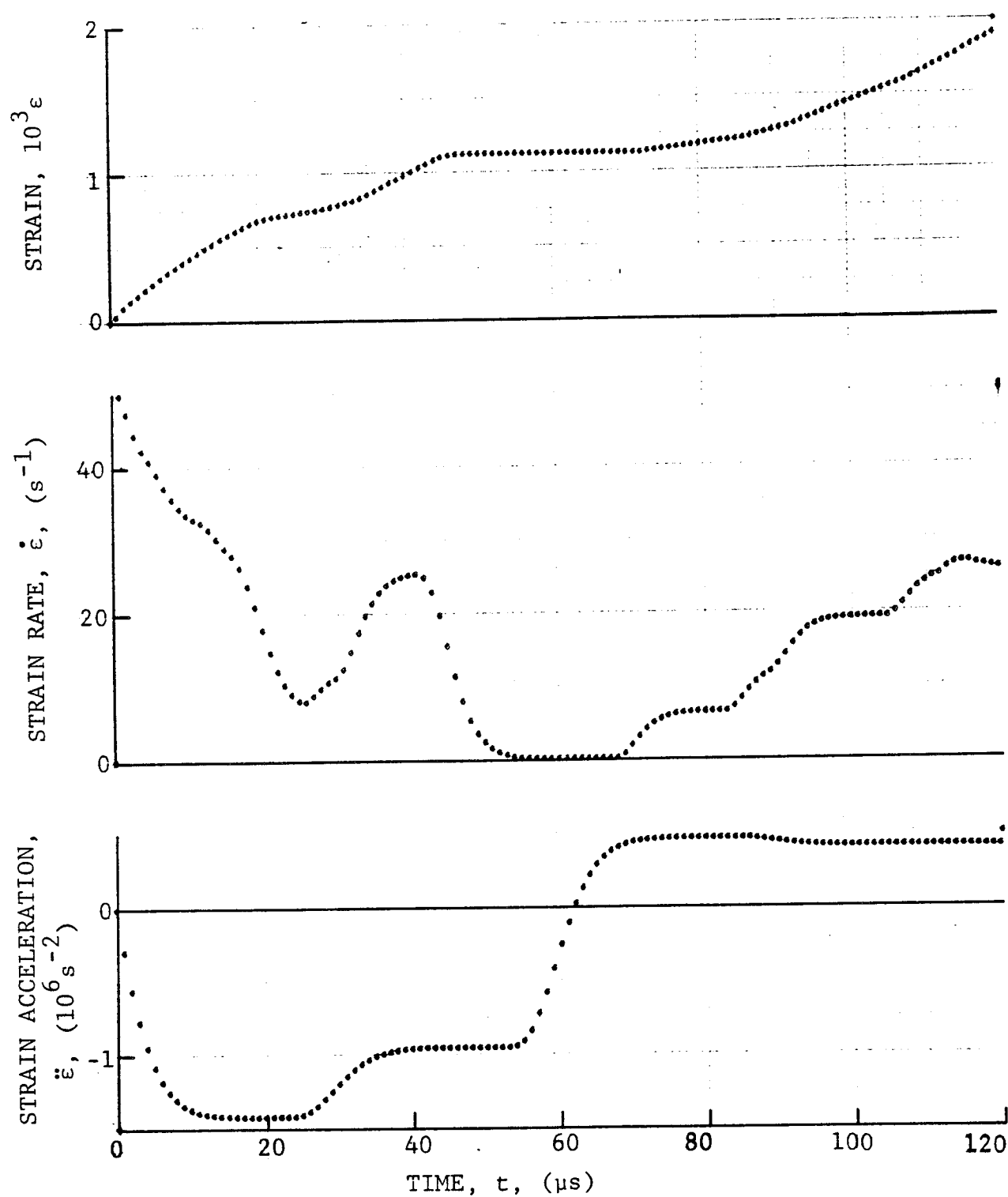


Figure 4-149. Strain and its derivatives in steel ring for Specimen No. 17-9.

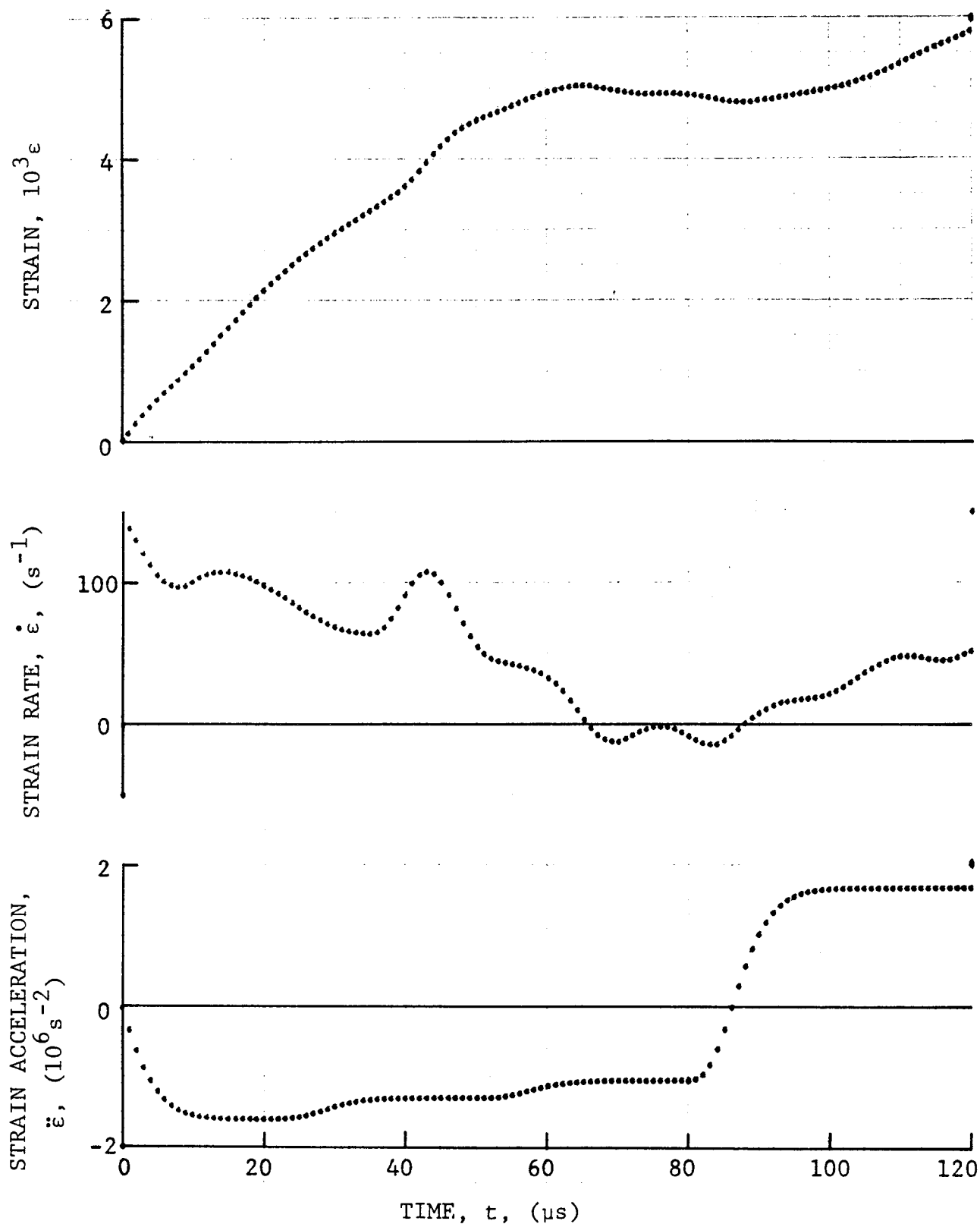
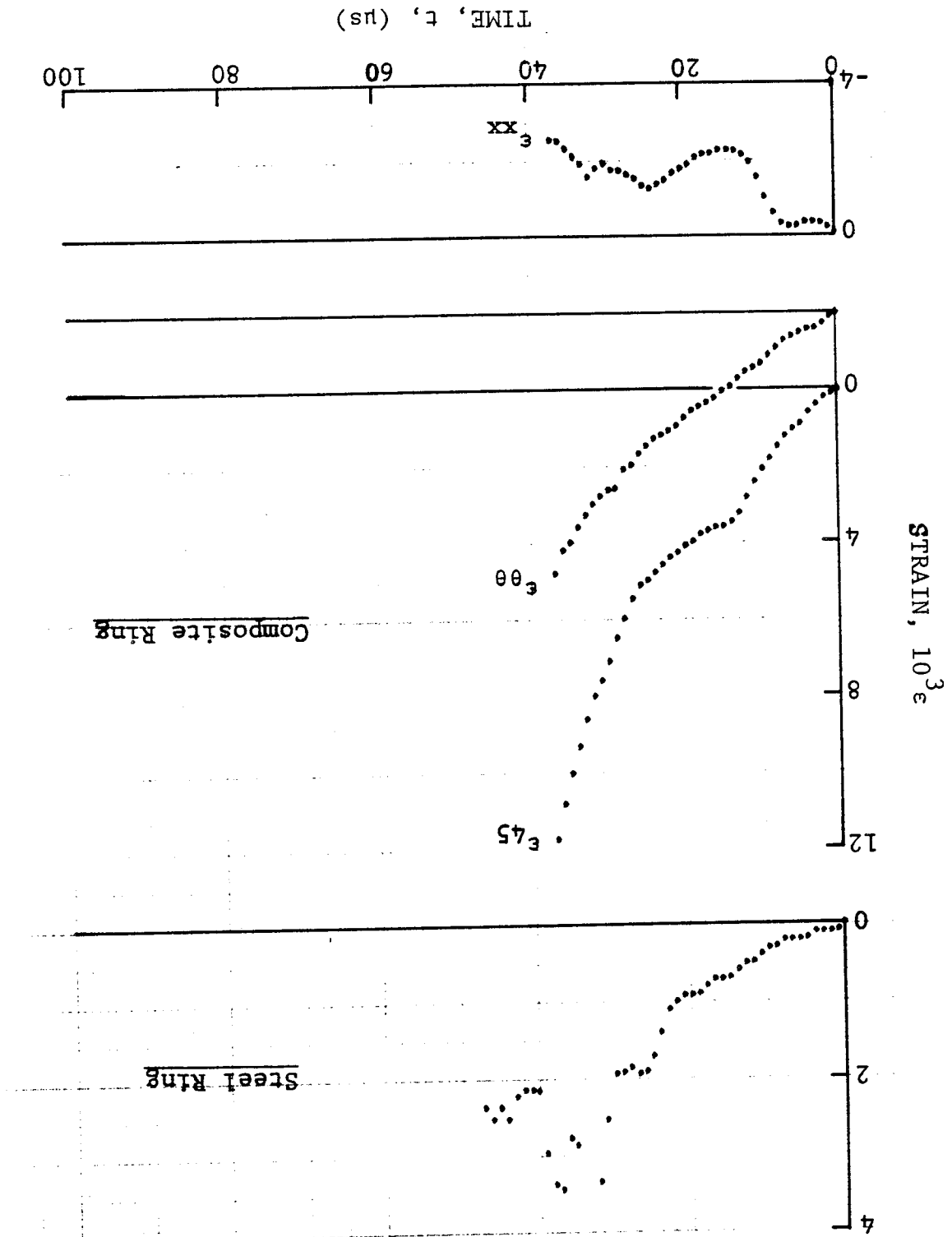


Figure 4-150. Circumferential strain and its derivatives in $[10_6]$ SP288/T300 graphite/epoxy ring under dynamic loading for Specimen No. 17-9.

Figure 4-151. Strain records in steel ring and [106] SP288/T300 graphite/epoxy ring under dynamic loading for Specimen No. 17-10.



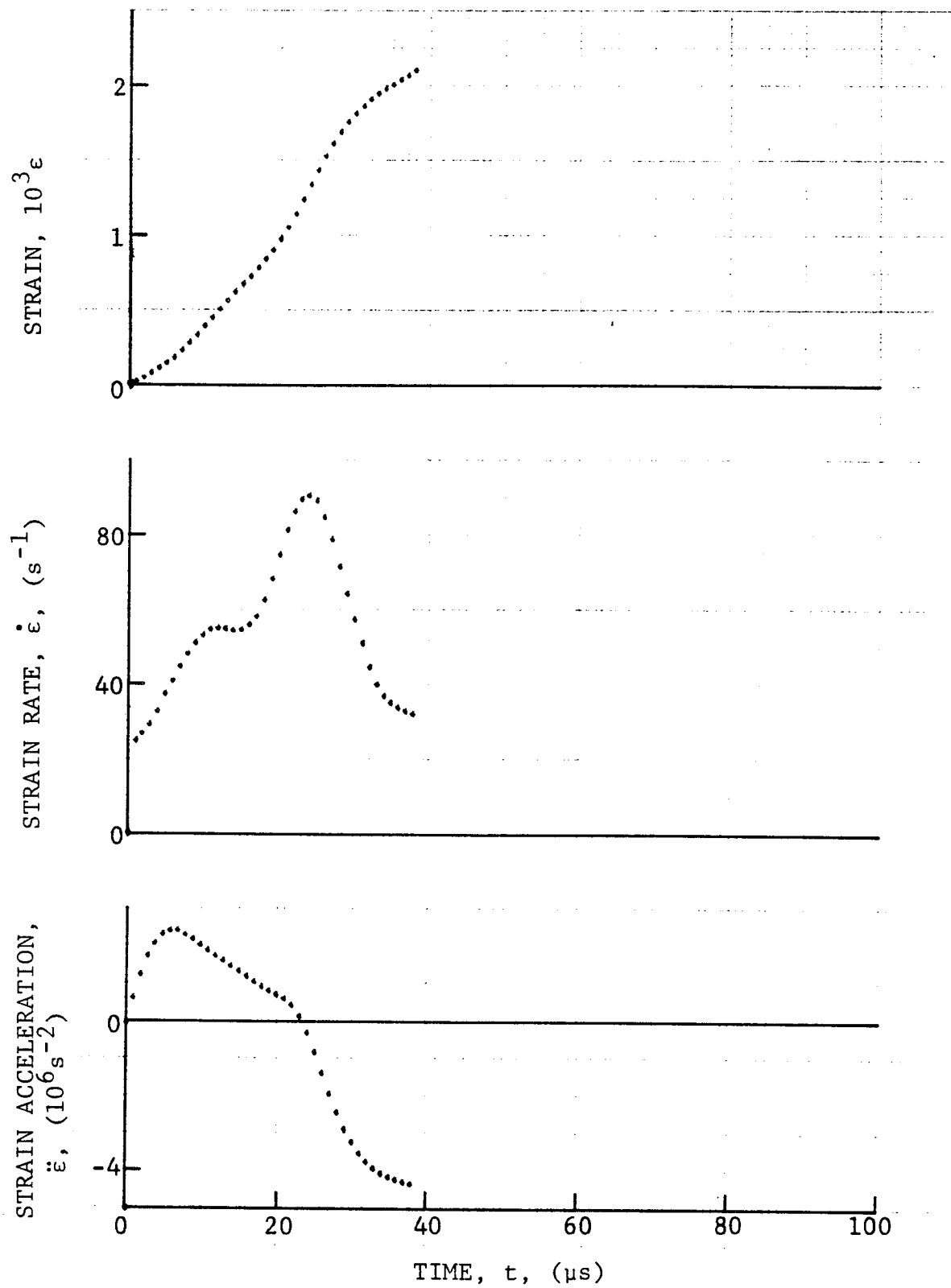
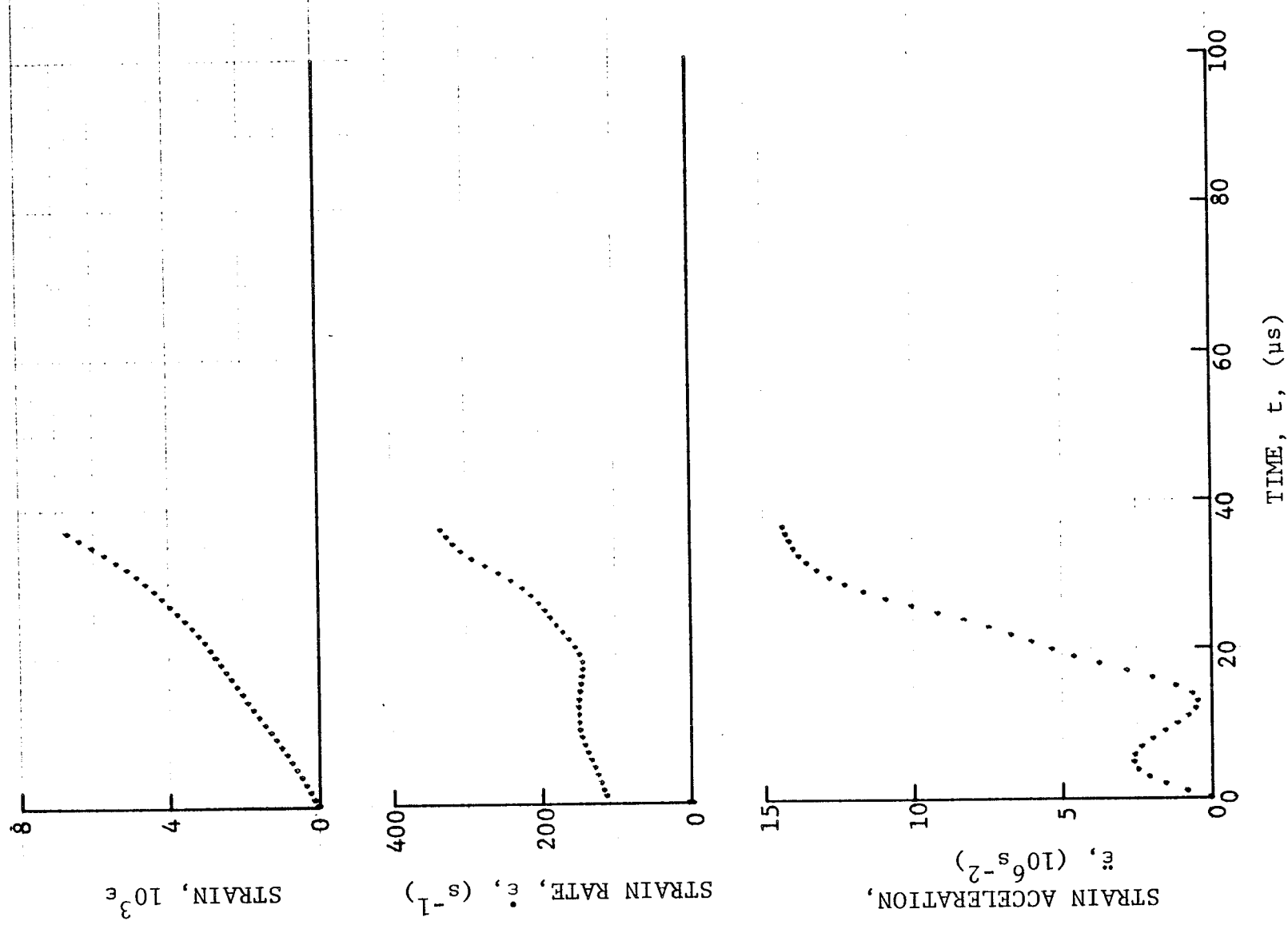


Figure 4-152. Strain and its derivatives in steel ring for Specimen No. 17-10.



TIME, t , (μs)

Figure 4-153. Circumferential strain and its derivatives in [10₆] SP288/T300 graphite/epoxy ring under dynamic loading for Specimen No. 17-10.

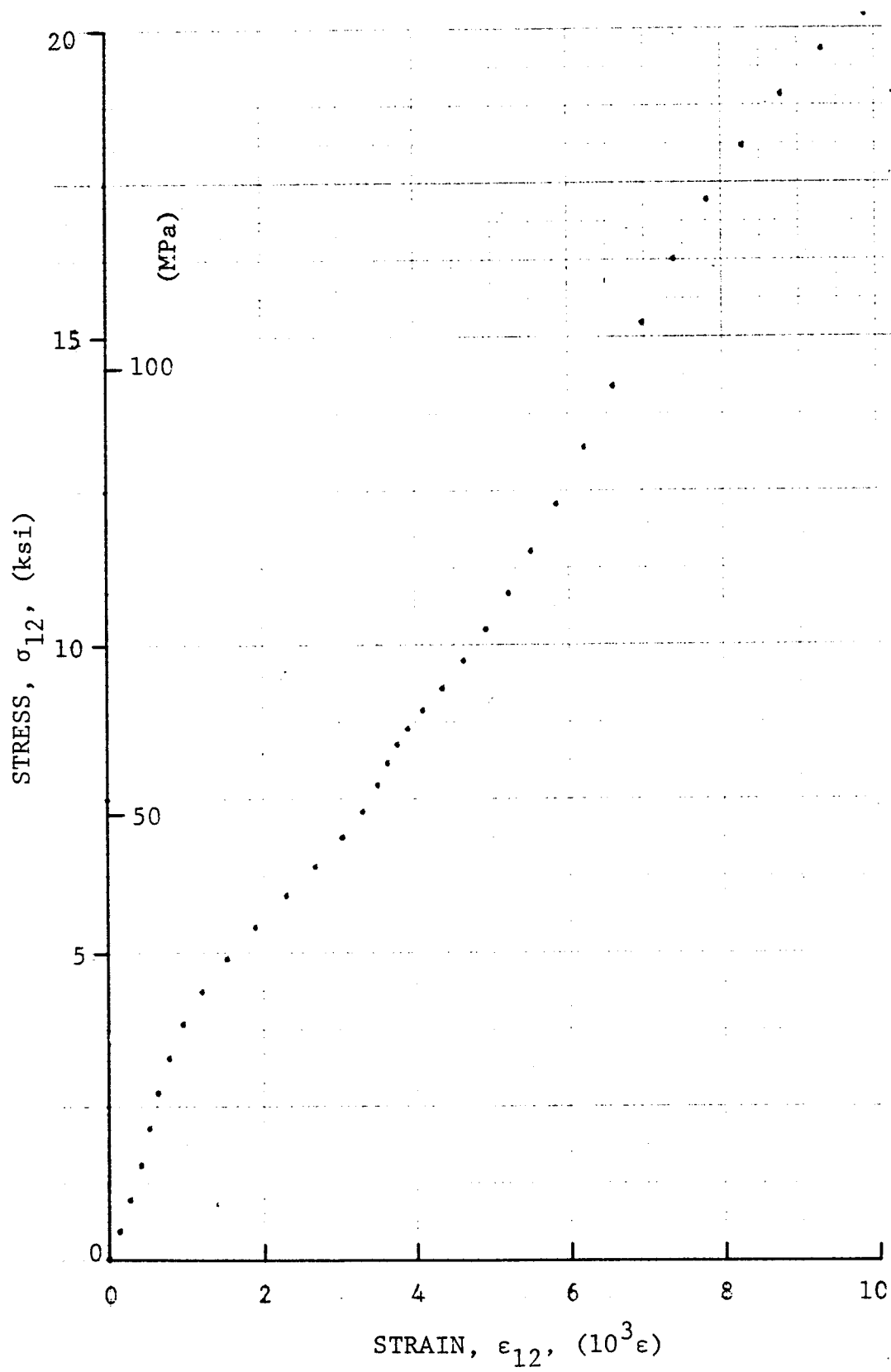


Figure 4-154. Stress-strain curve for dynamically loaded $[10_6]$ SP288/T300 graphite/epoxy ring for Specimen No. 17-7.

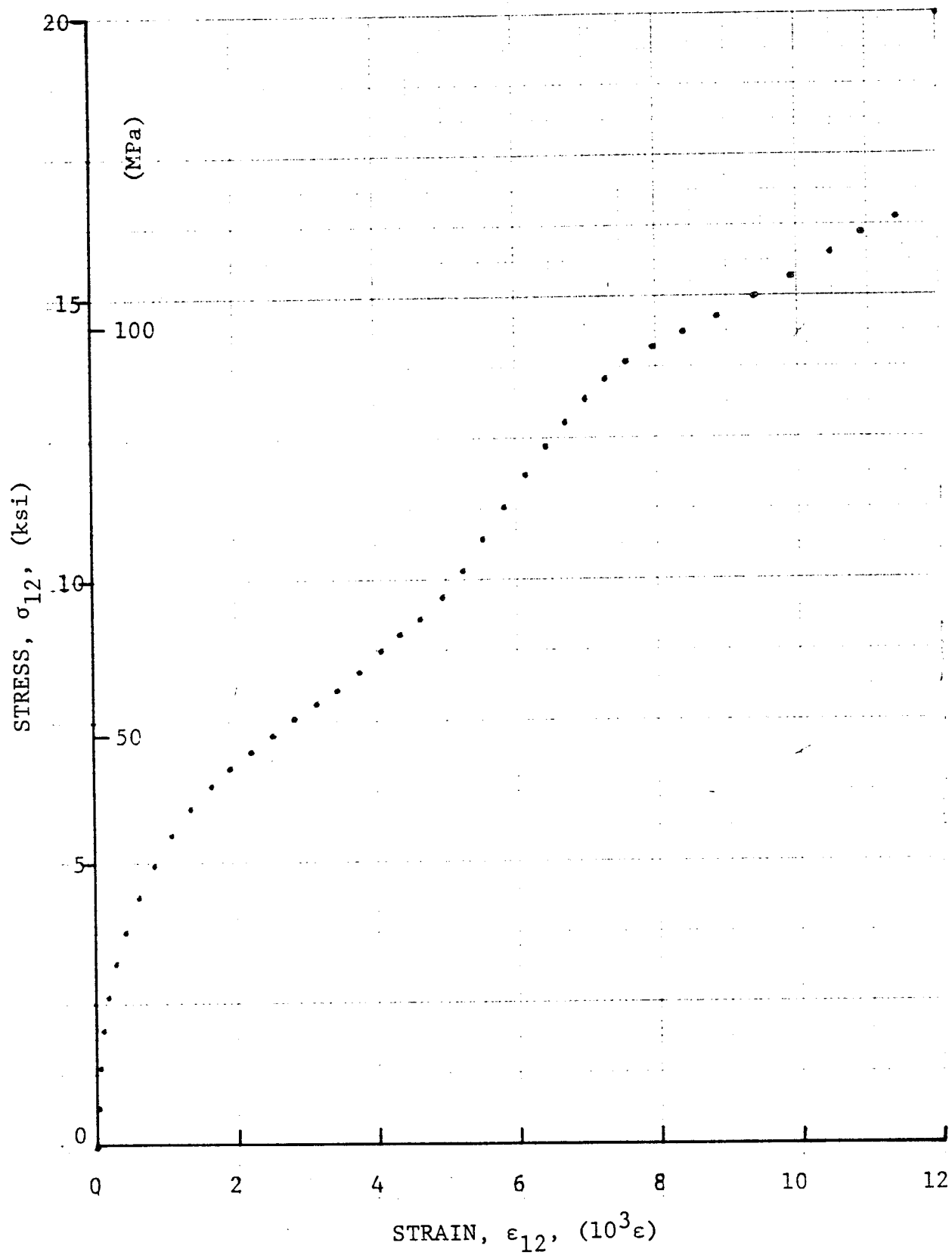


Figure 4-155. Stress-strain curve for dynamically loaded [106]
 SP288/T300 graphite/epoxy ring for Specimen No. 17-8
 (100 mg PETN detonator).

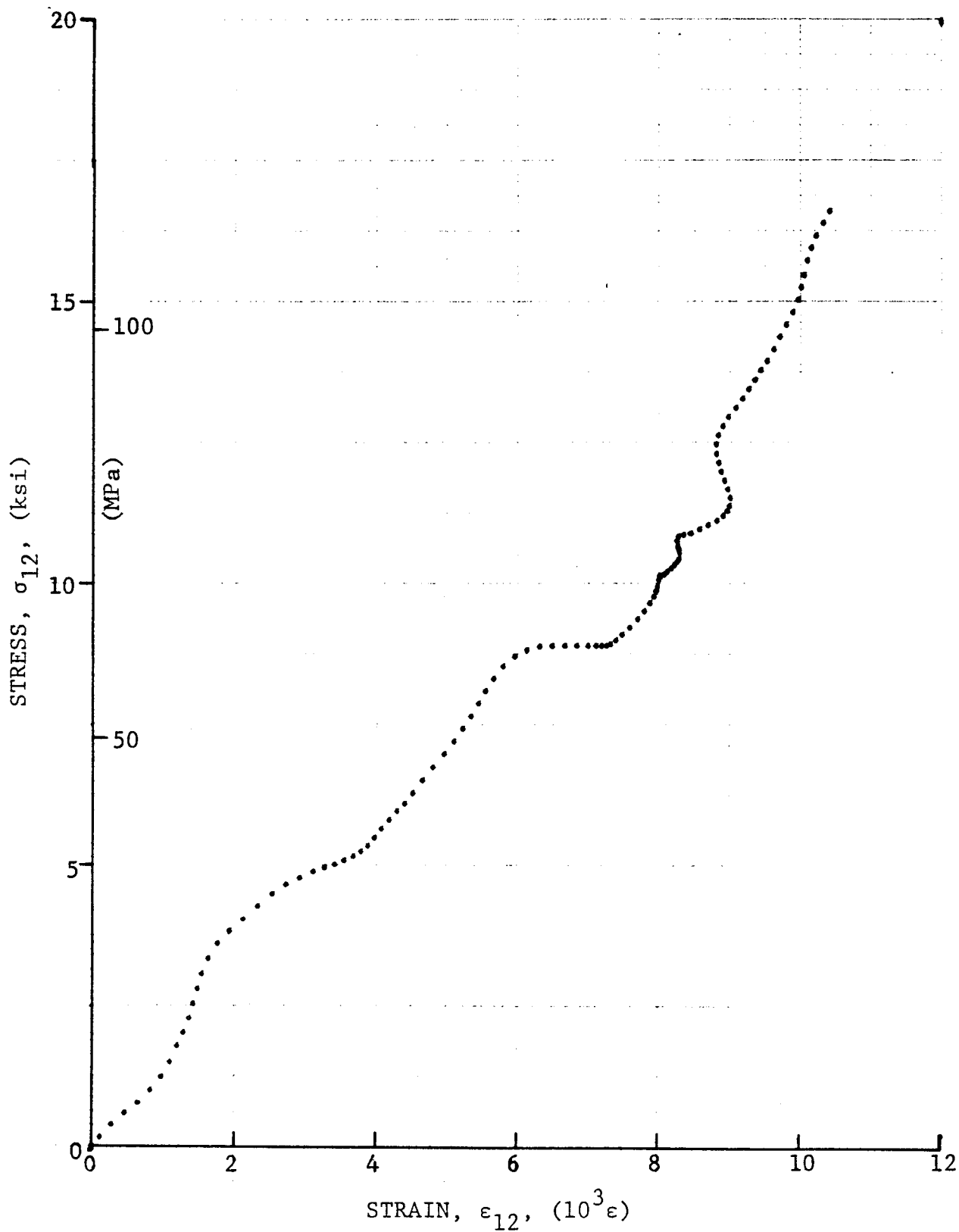


Figure 4-156. Stress-strain curve for dynamically loaded [10₆] SP288/T300 graphite/epoxy ring for Specimen No. 17-9 (455 mg pistol powder).

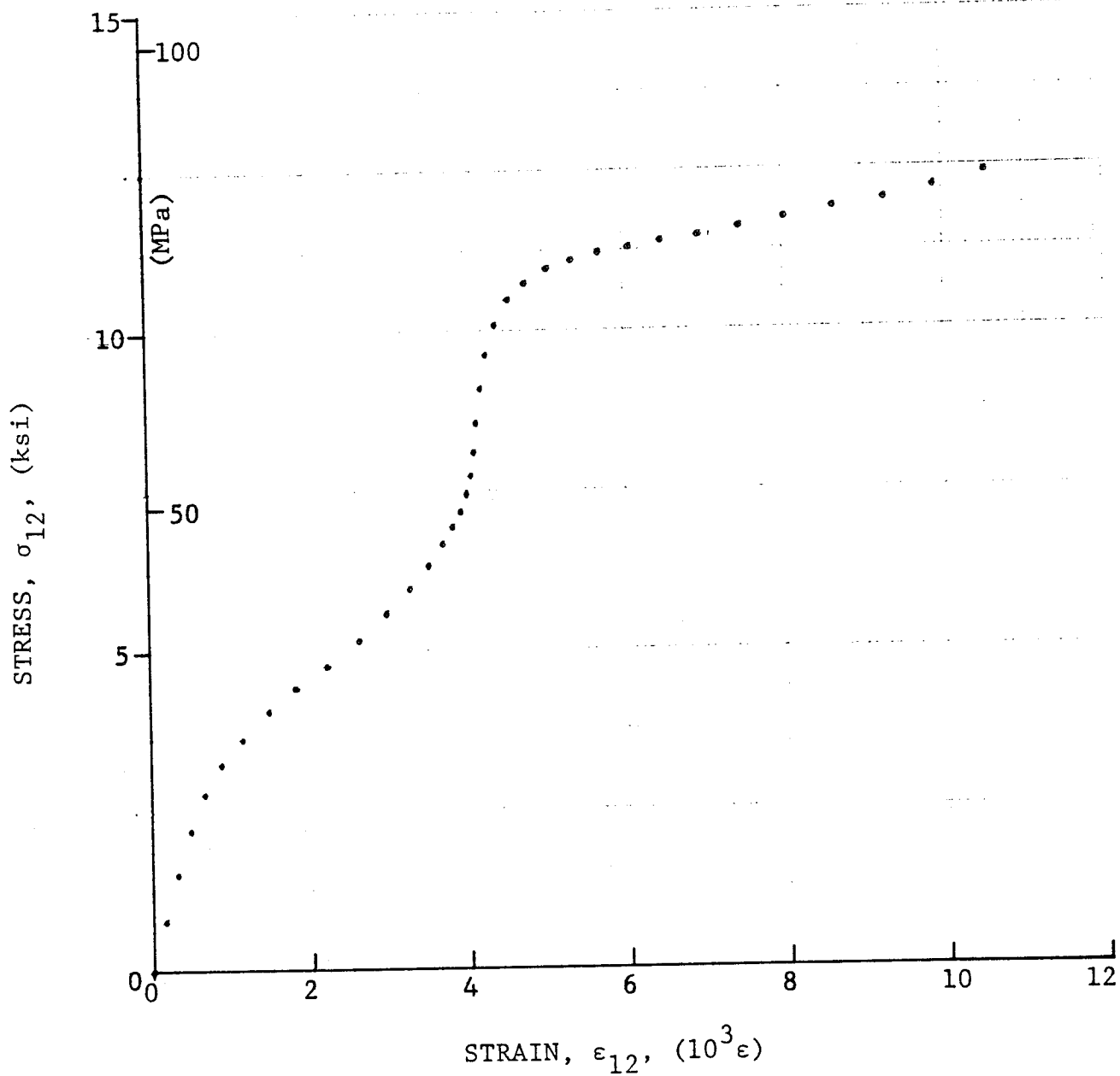


Figure 4-157. Stress-strain curve for dynamically loaded [10₆] SP288/T300 graphite/epoxy ring for Specimen No. 17-10.

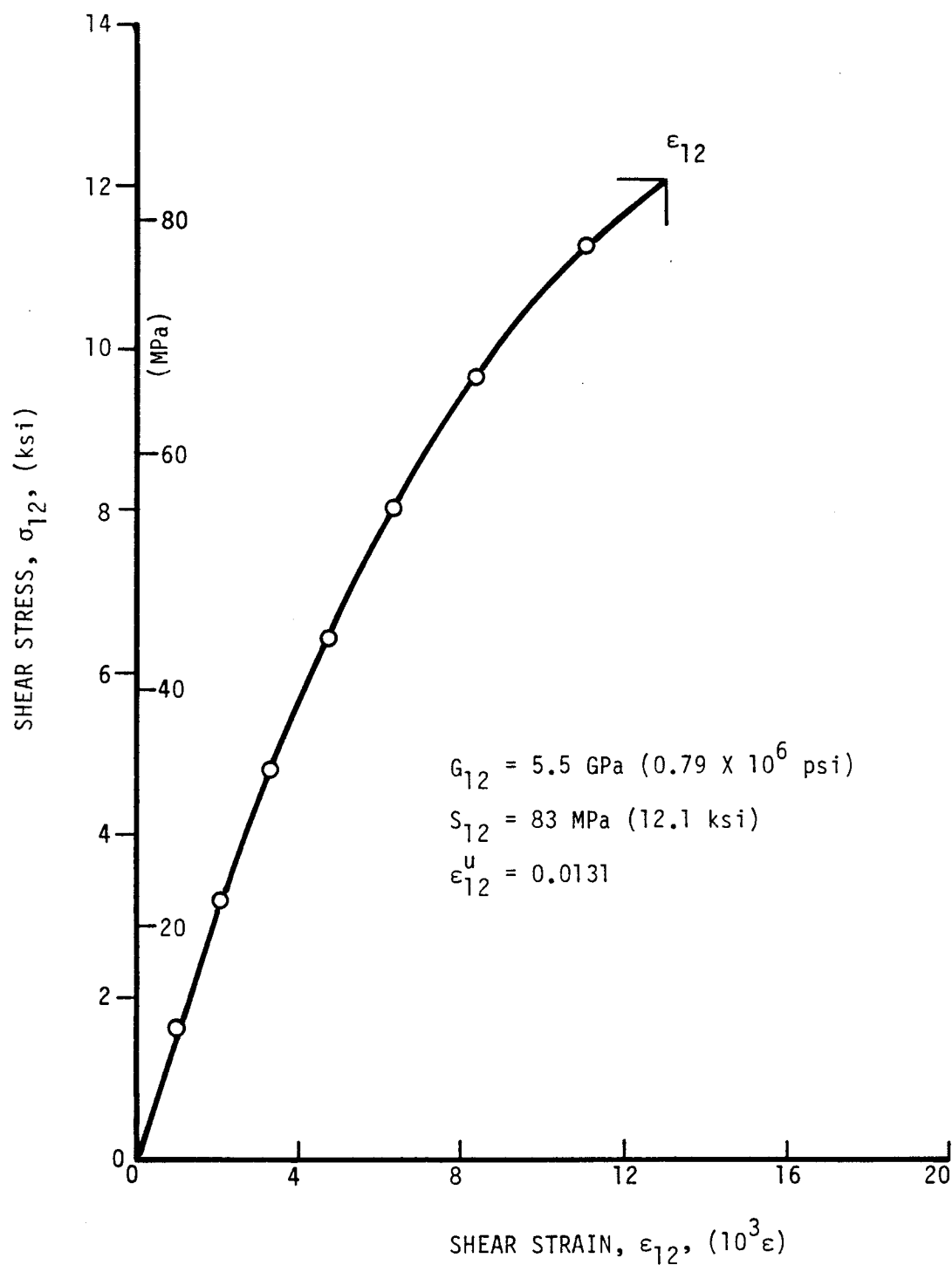


Figure 4-158. Shear stress versus shear strain for unidirectional 10-deg off-axis SP288/AS ring specimen (Specimen No. 15-2).

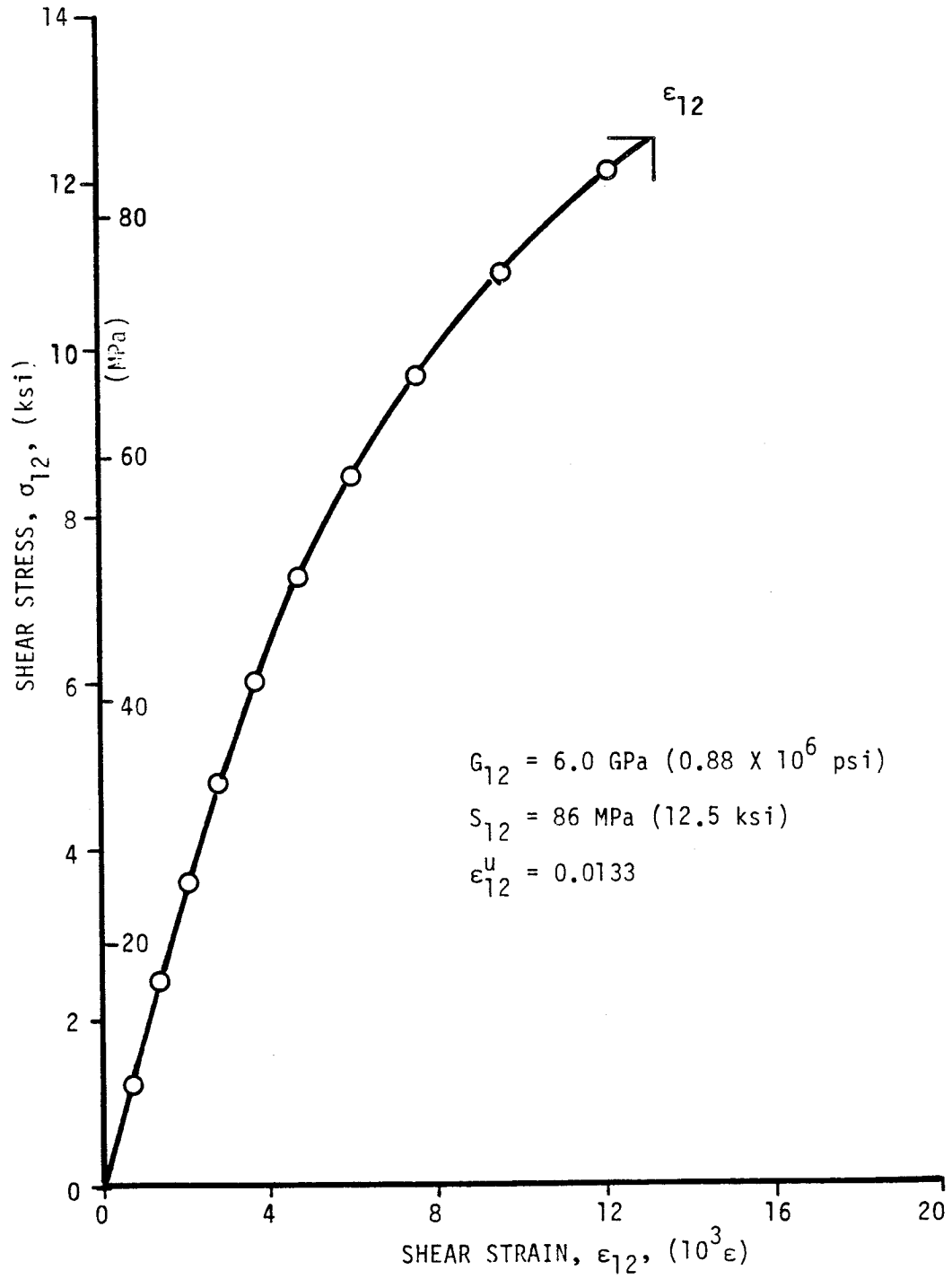


Figure 4-159. Shear stress versus shear strain for unidirectional 10-deg off-axis SP288/AS ring specimen (Specimen No. 15-3).

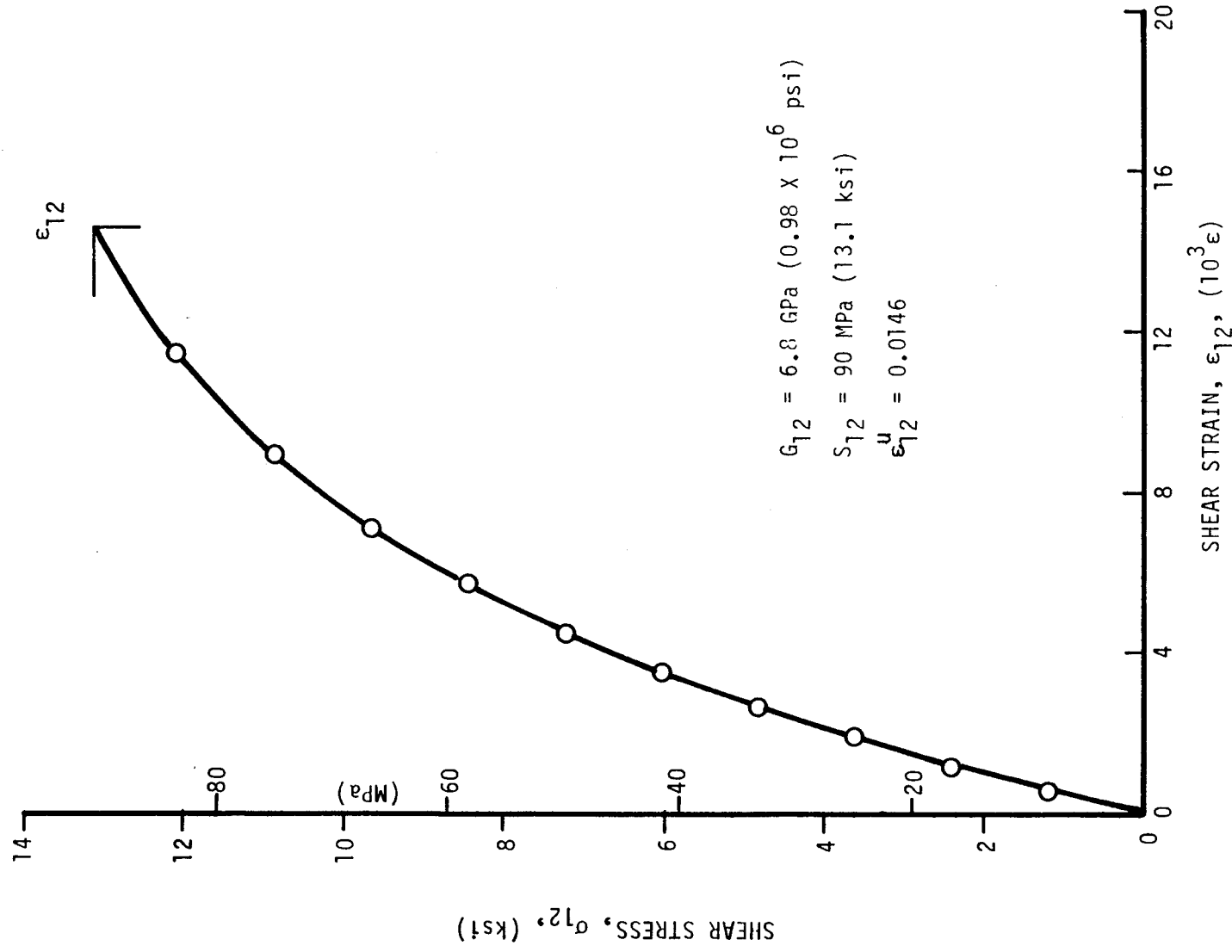


Figure 4-160. Shear stress versus shear strain for unidirectional 10-deg off-axis SP288/AS ring specimen (Specimen No. 15-4).

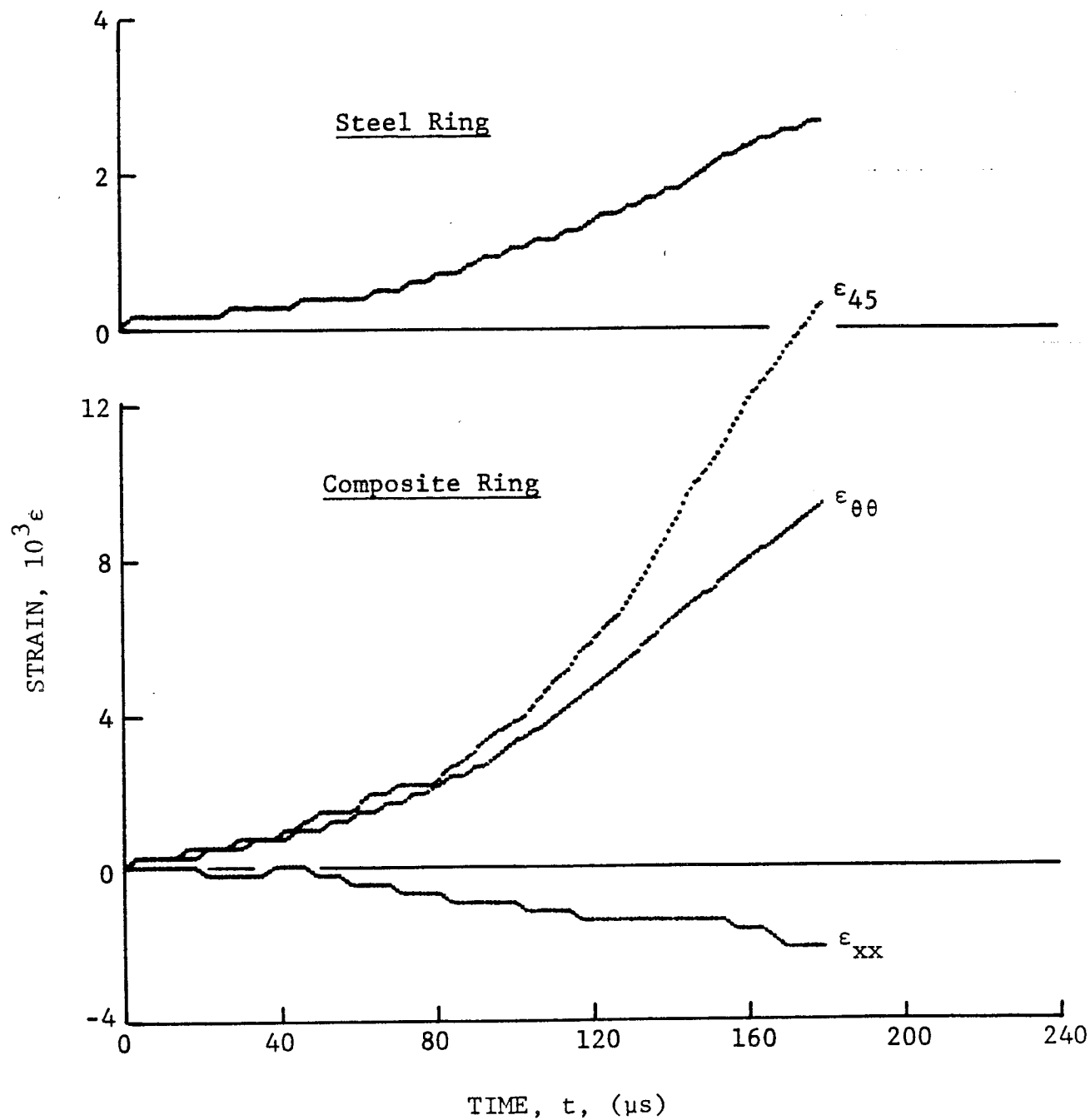


Figure 4-161. Strain records in steel ring and in [10_g] SP288/AS graphite/epoxy ring under dynamic loading for Specimen No. 15-9 (650 mg pistol powder).

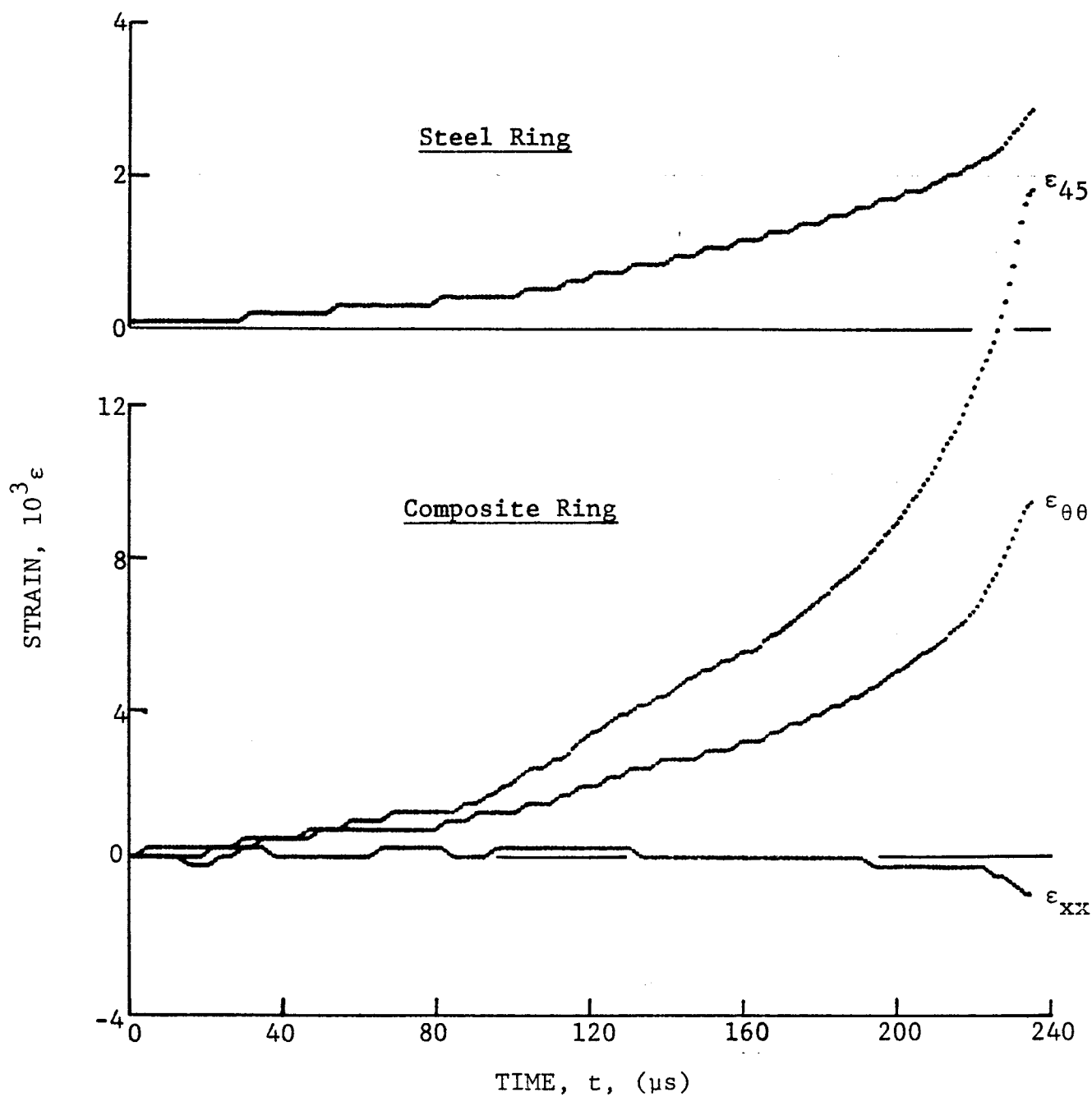


Figure 4-162. Strain records in steel ring and in $[10_8]$ SP288/AS graphite/epoxy ring under dynamic loading for Specimen No. 15-10 (650 mg pistol powder).

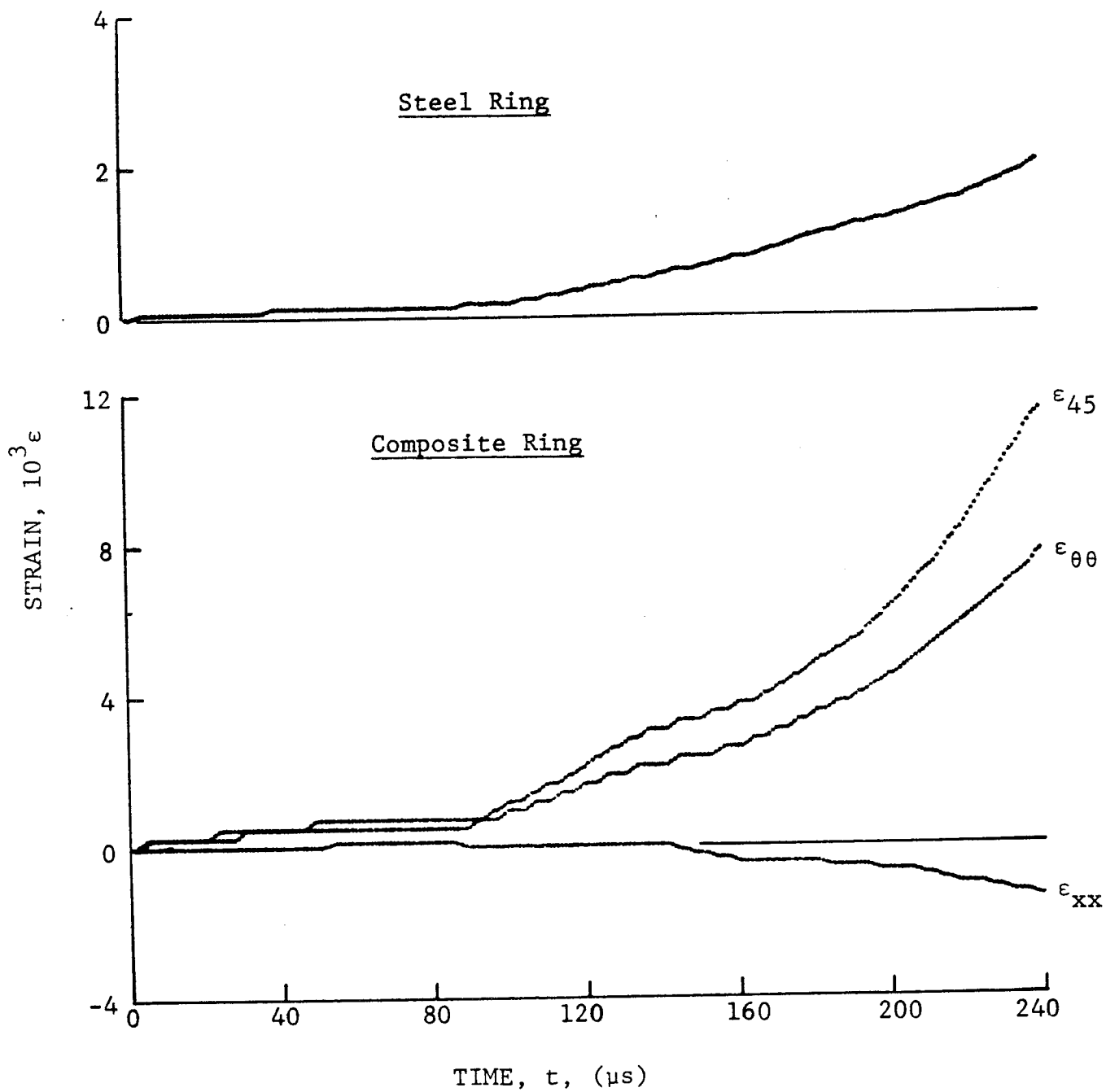


Figure 4-163. Strain records in steel ring and in $[10_8]$ SP288/AS graphite/epoxy ring under dynamic loading for Specimen No. 15-11 (650 mg pistol powder).

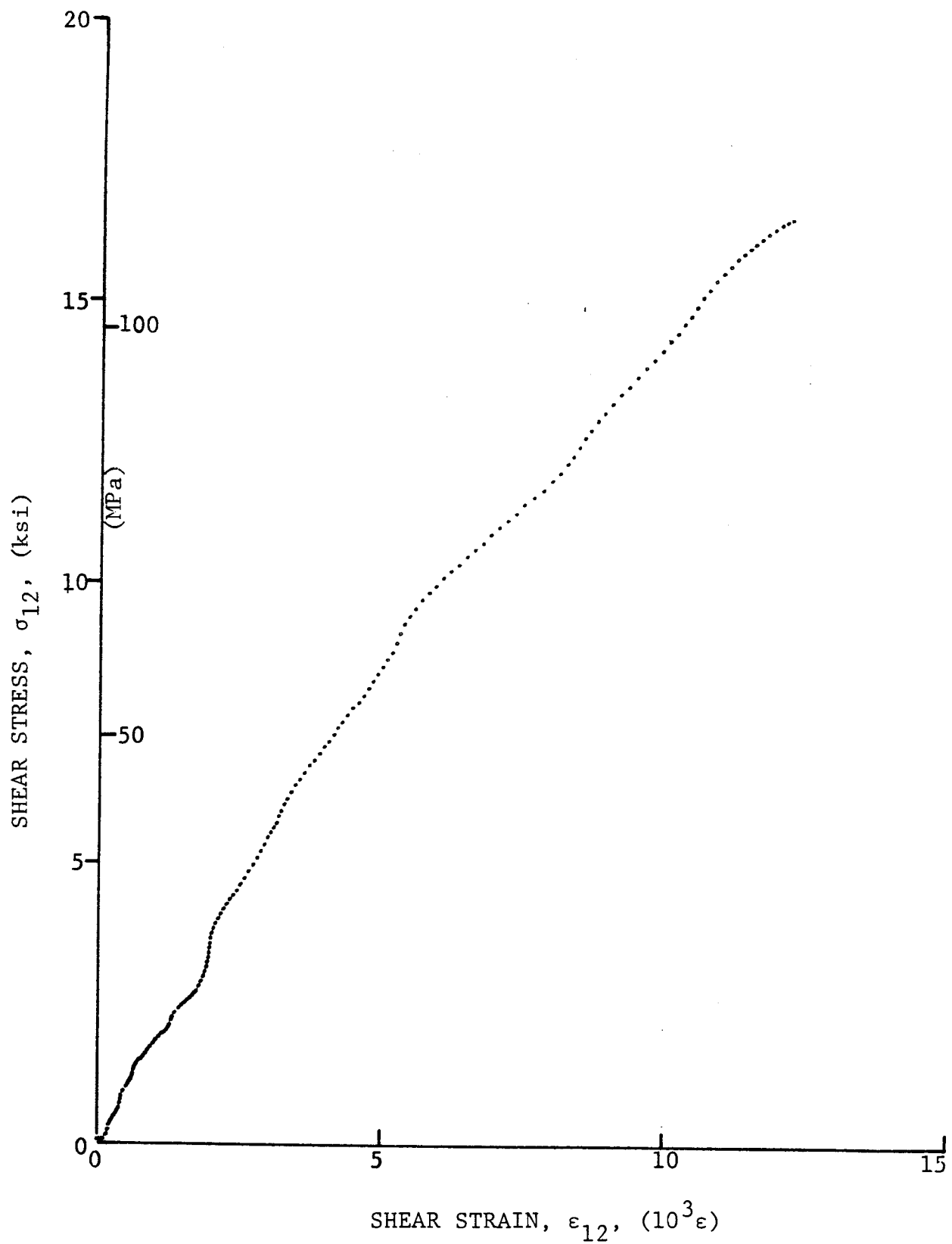


Figure 4-164. Shear stress versus shear strain curve for dynamically loaded $[10_8]$ SP288/AS graphite/epoxy ring for Specimen No. 15-9 (650 mg pistol powder).

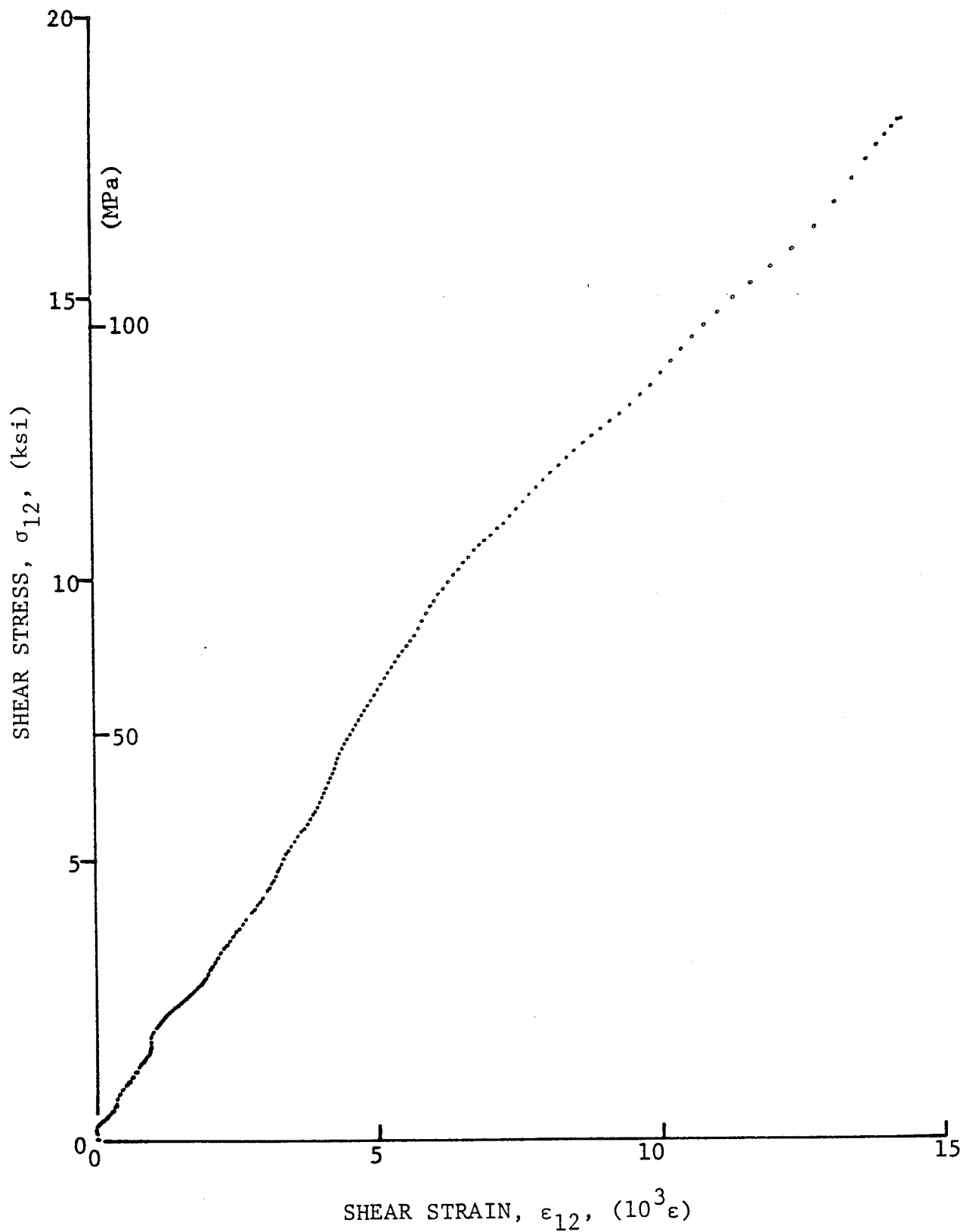


Figure 4-165. Shear stress versus shear strain curve for dynamically loaded [10_g] SP288/AS graphite/epoxy ring for Specimen No. 15-10 (650 mg pistol powder).

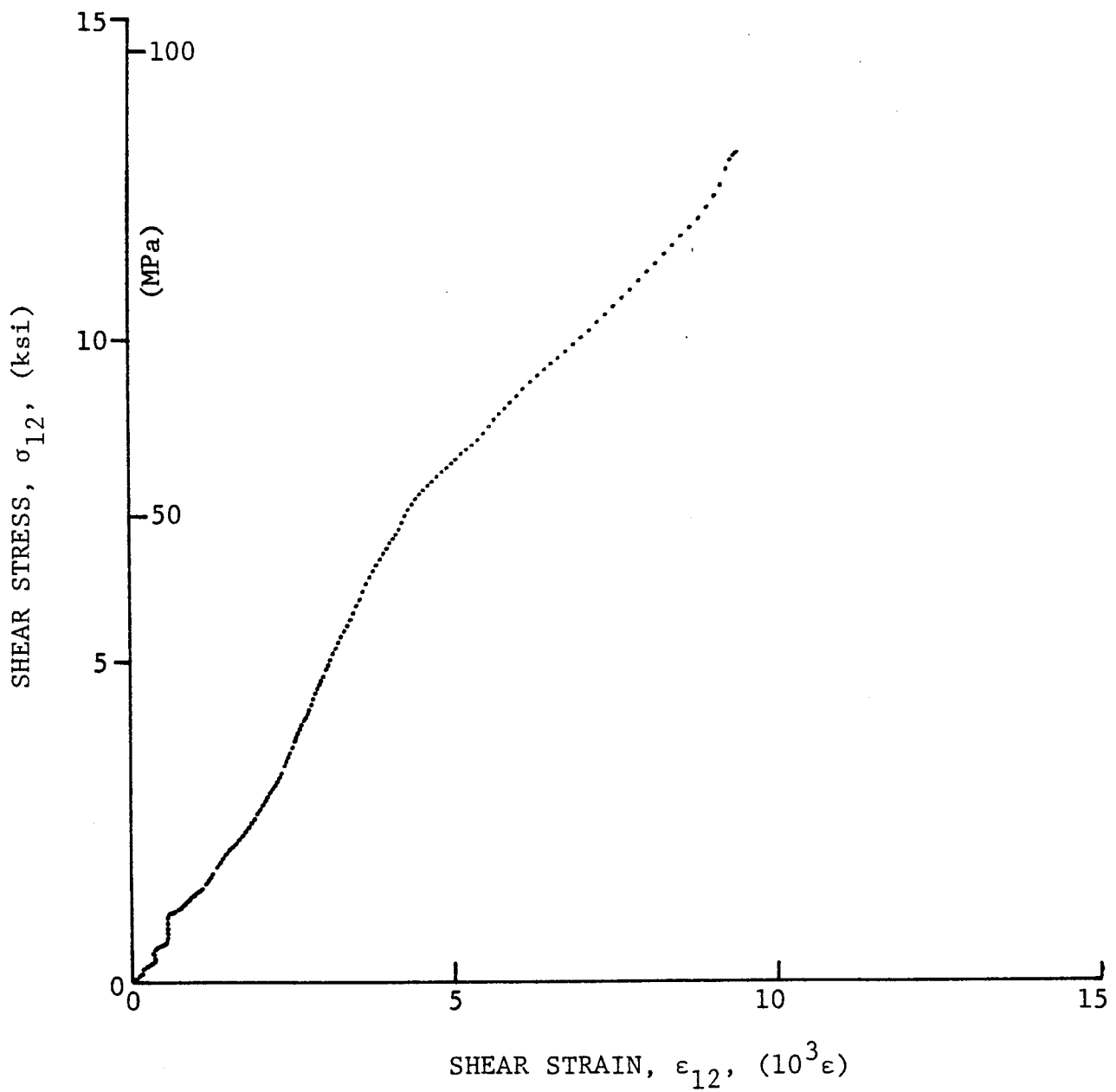


Figure 4-166. Shear stress versus shear strain curve for dynamically loaded [10g] SP288/AS graphite/epoxy ring for Specimen No. 15-11 (650 mg pistol powder).

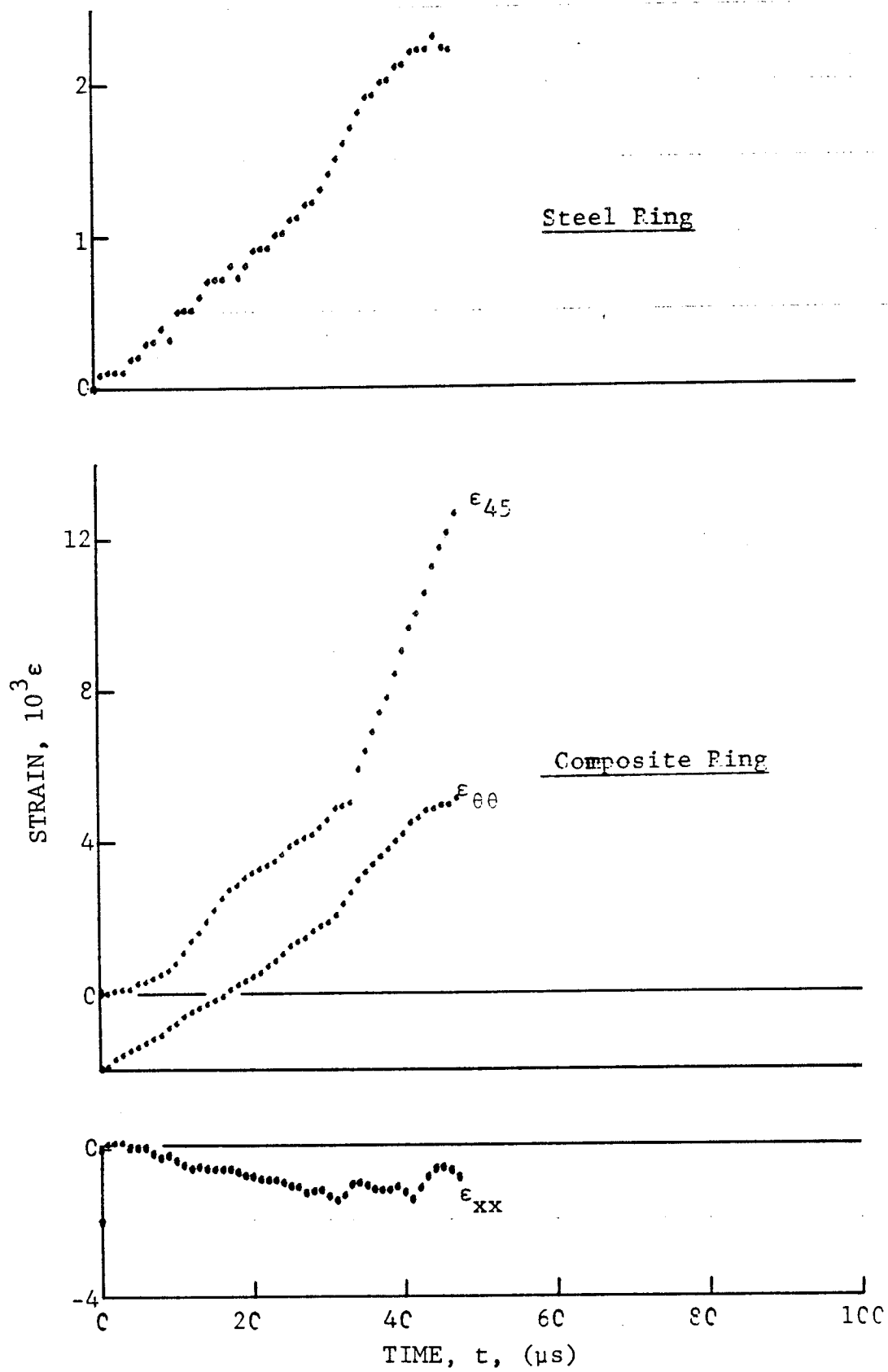


Figure 4-167. Strain records in steel ring and [10g] SP288/AS graphite/epoxy ring under dynamic loading for Specimen No. 15-5 (50 mg PETN detonator).

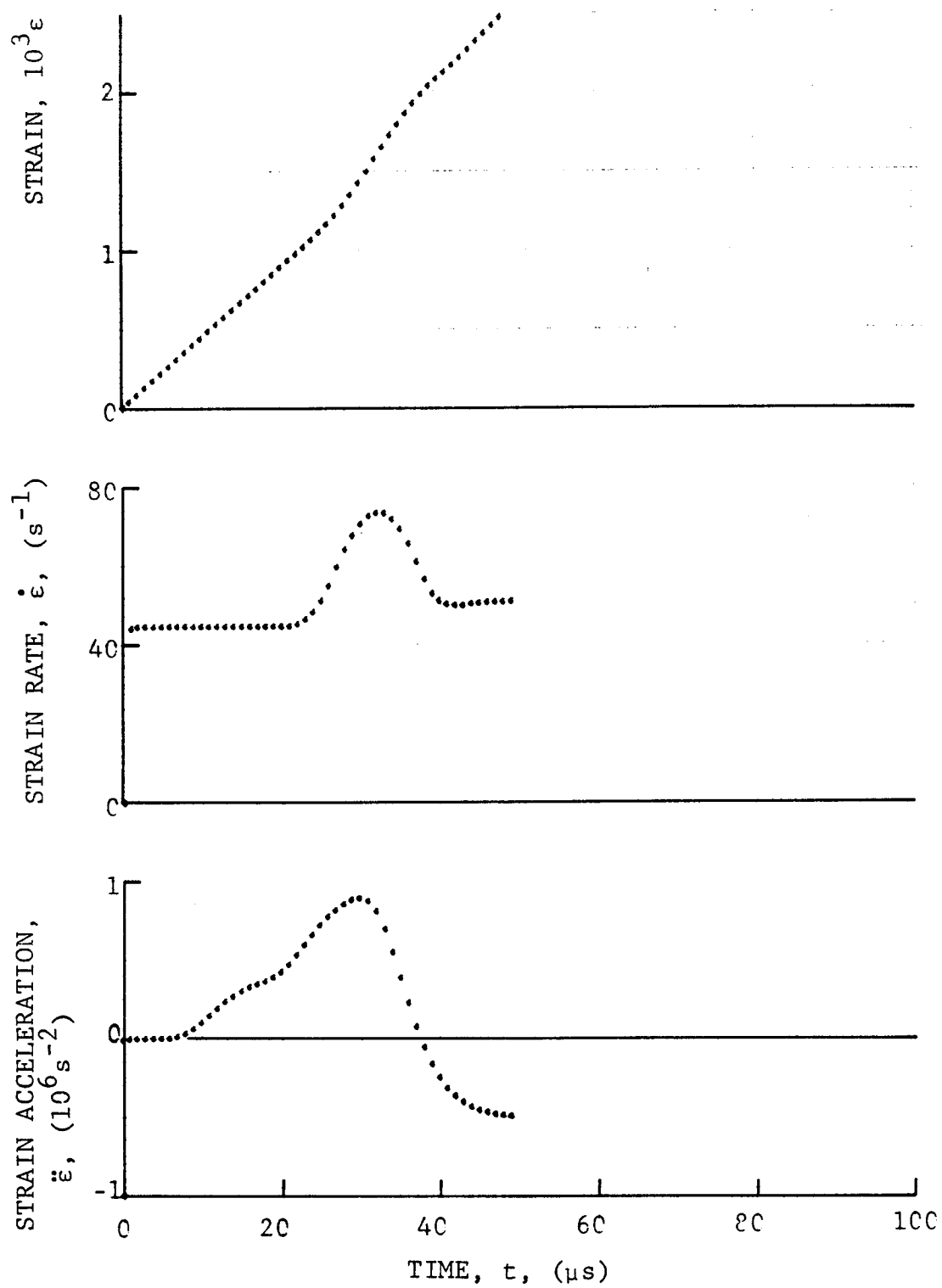


Figure 4-168. Strain and its derivatives in steel ring for Specimen No. 15-5.

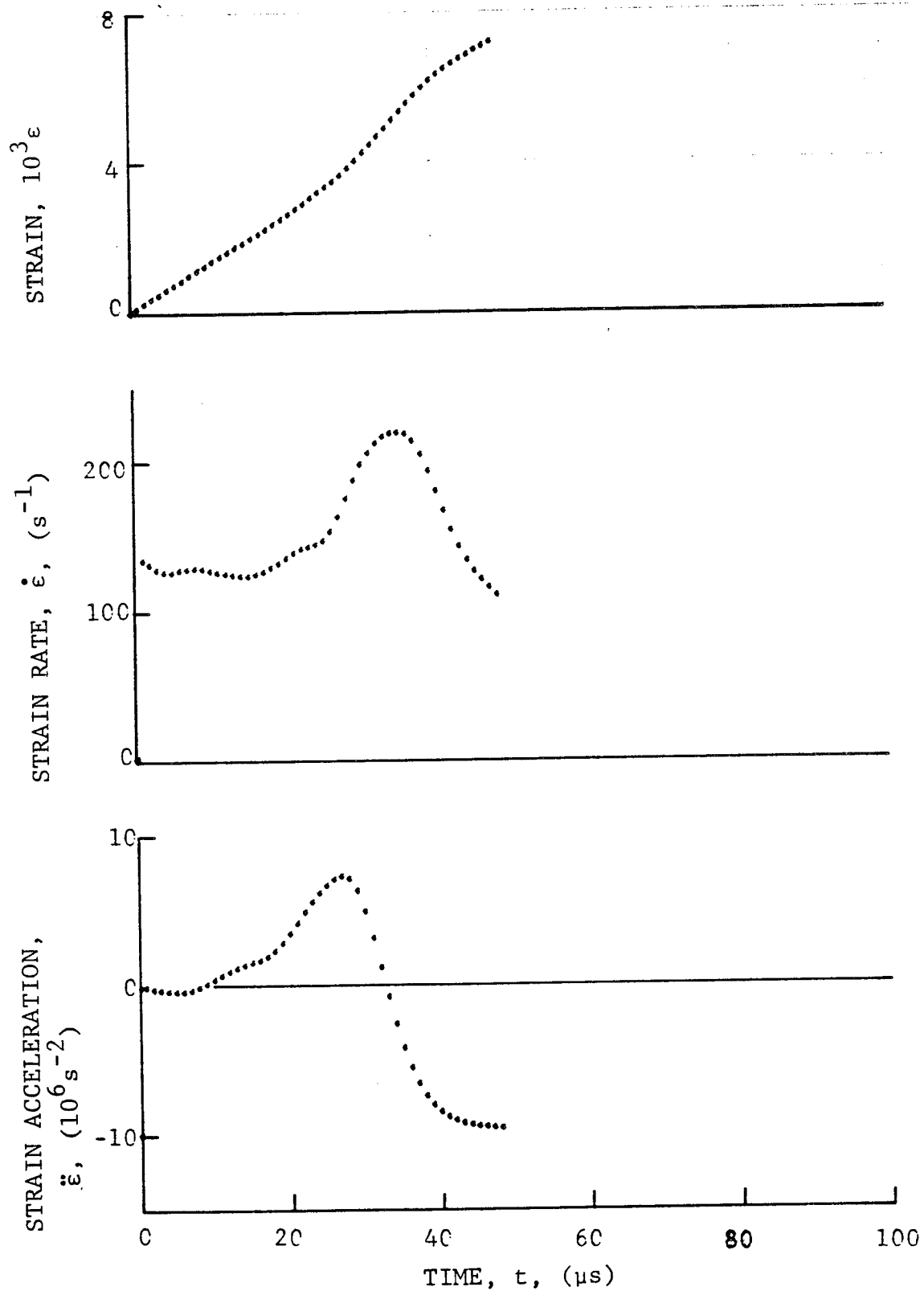


Figure 4-169. Circumferential strain and its derivatives in $[10_8]$ SP2R8/AS graphite/epoxy ring under dynamic loading for Specimen No. 15-5.

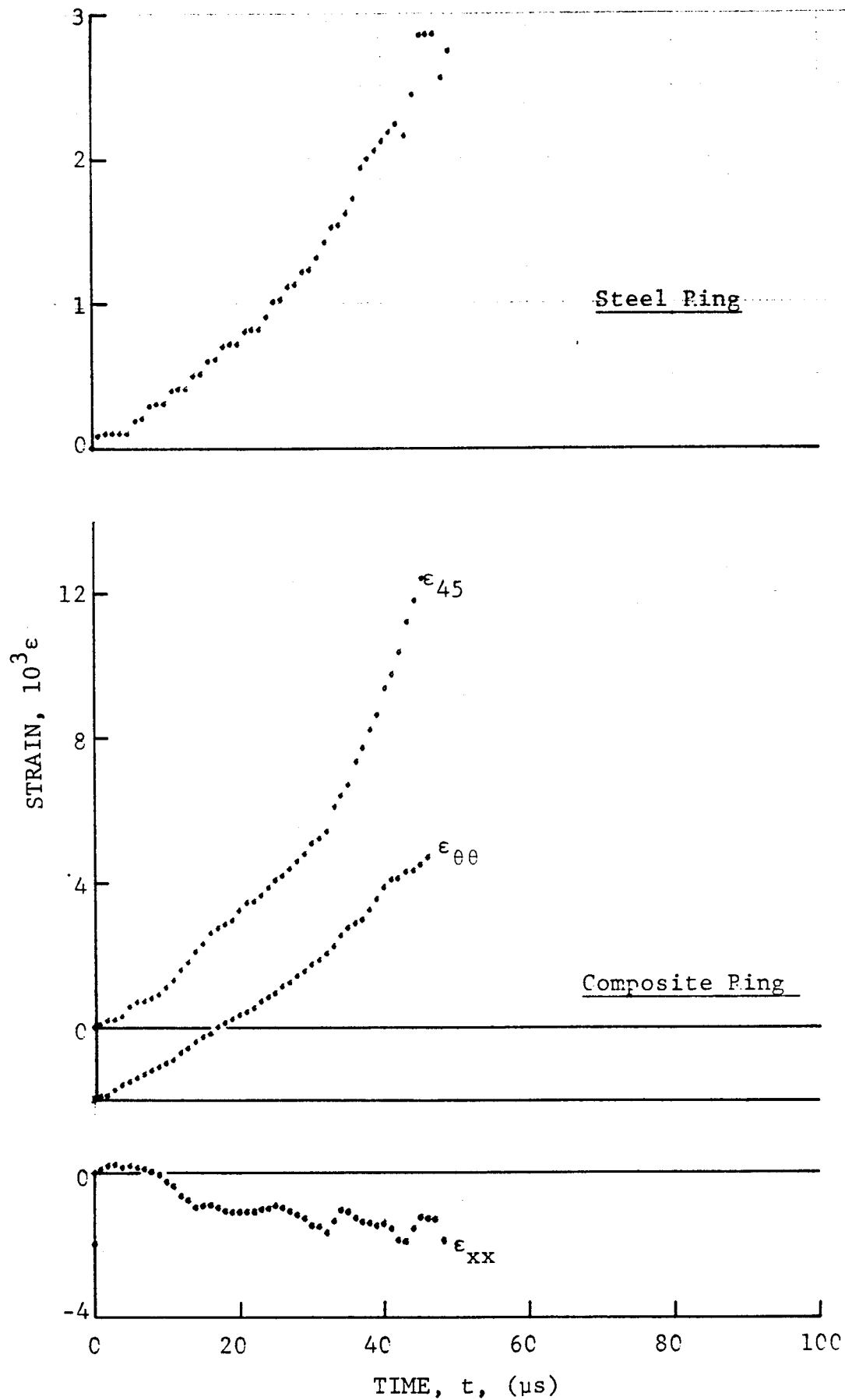


Figure 4-170. Strain records in steel ring and [10_g] SP288/AS graphite/epoxy ring under dynamic loading for Specimen No. 15-7 (50 mg PETN detonator).

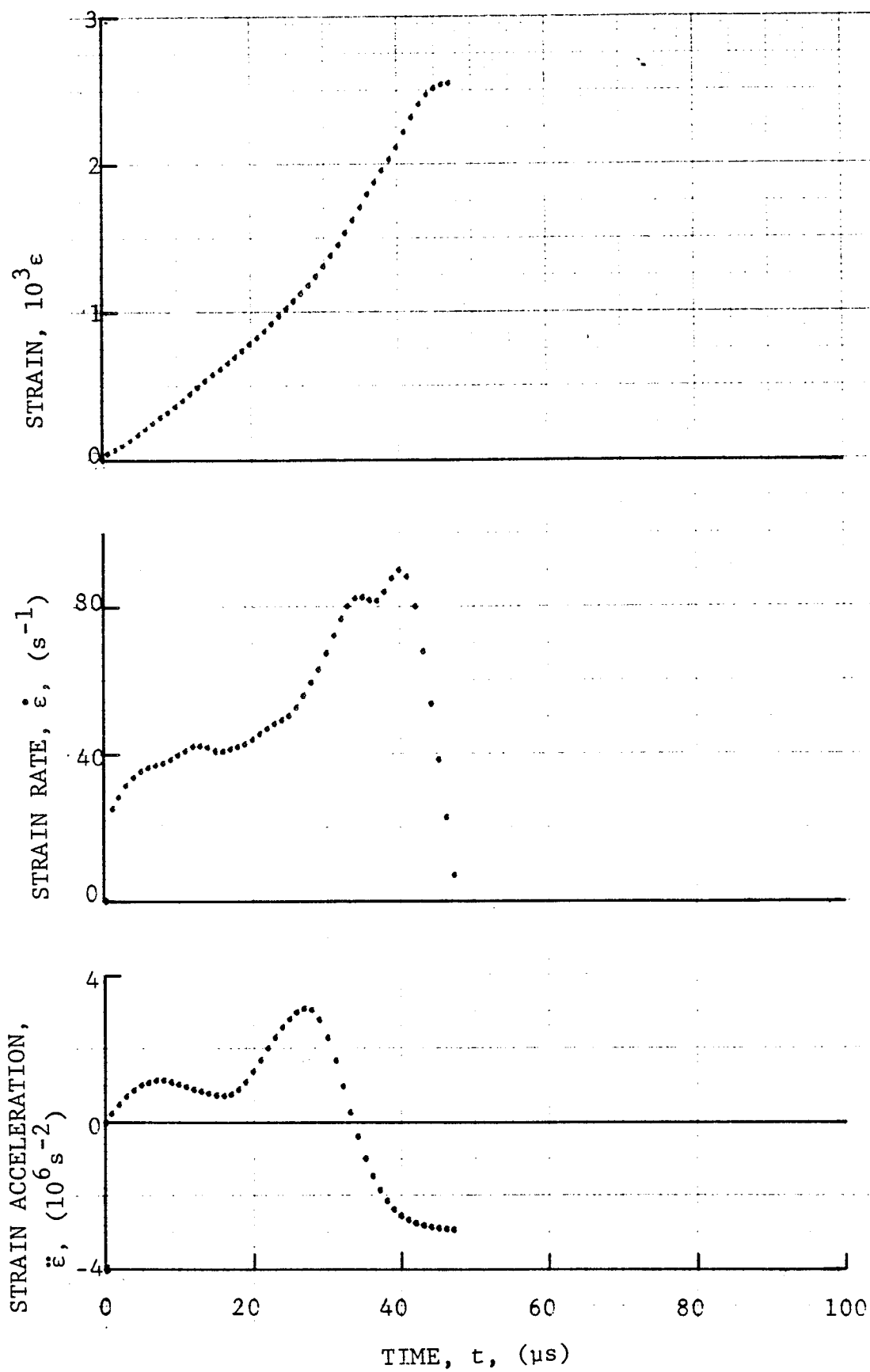


Figure 4-171. Strain and its derivatives in steel ring for Specimen No. 15-7.

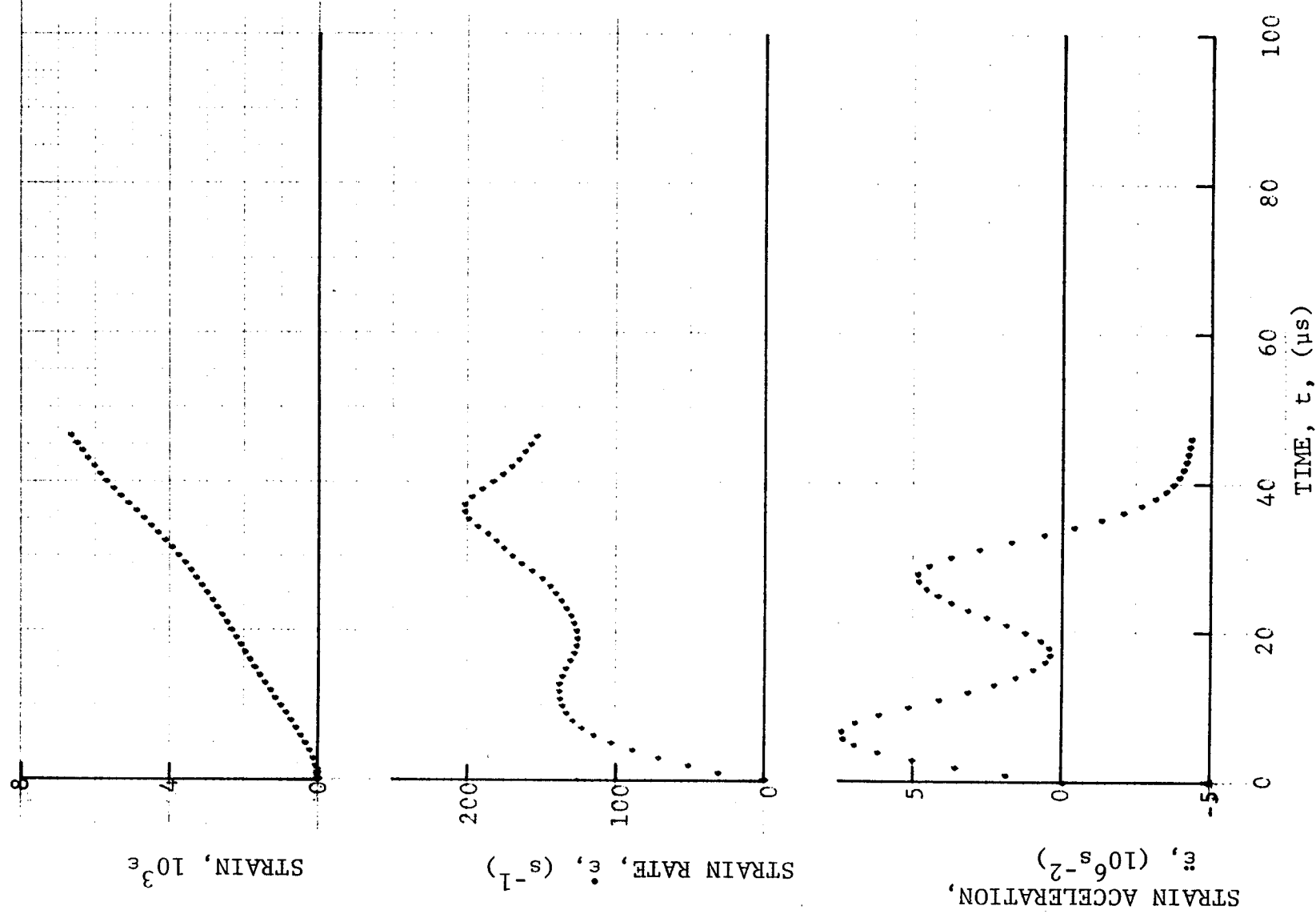


Figure 4-172. Circumferential strain and its derivatives in [10g] SP288/AS graphite/epoxy ring under dynamic loading for Specimen No. 15-7.

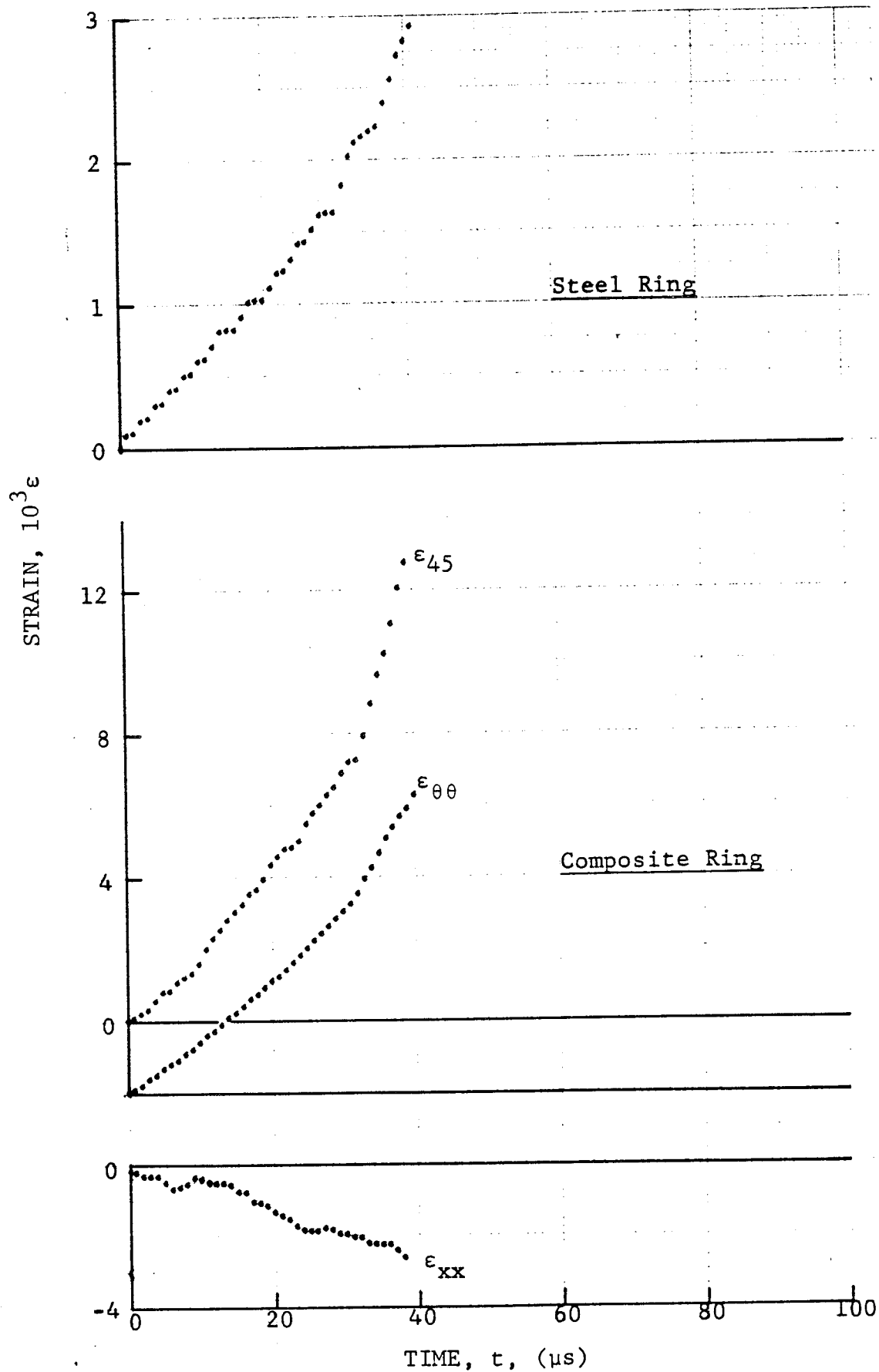


Figure 4-173. Strain records in steel ring and in [10g] SP288/AS graphite/epoxy ring under dynamic loading for Specimen No. 15-8 (100 mg PETN detonator).

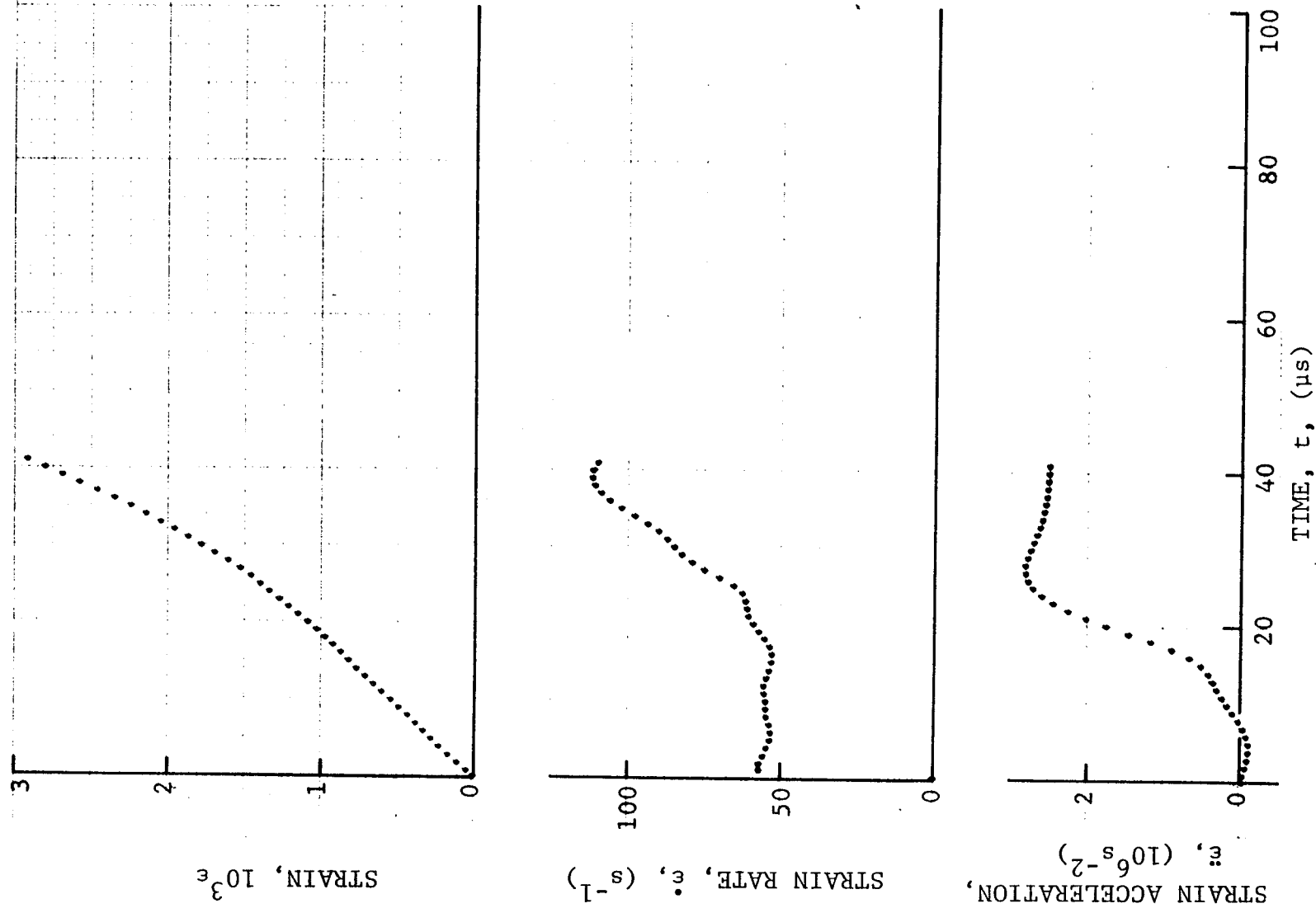


Figure 4-174. Strain and its derivatives in steel ring for Specimen No. 15-8.

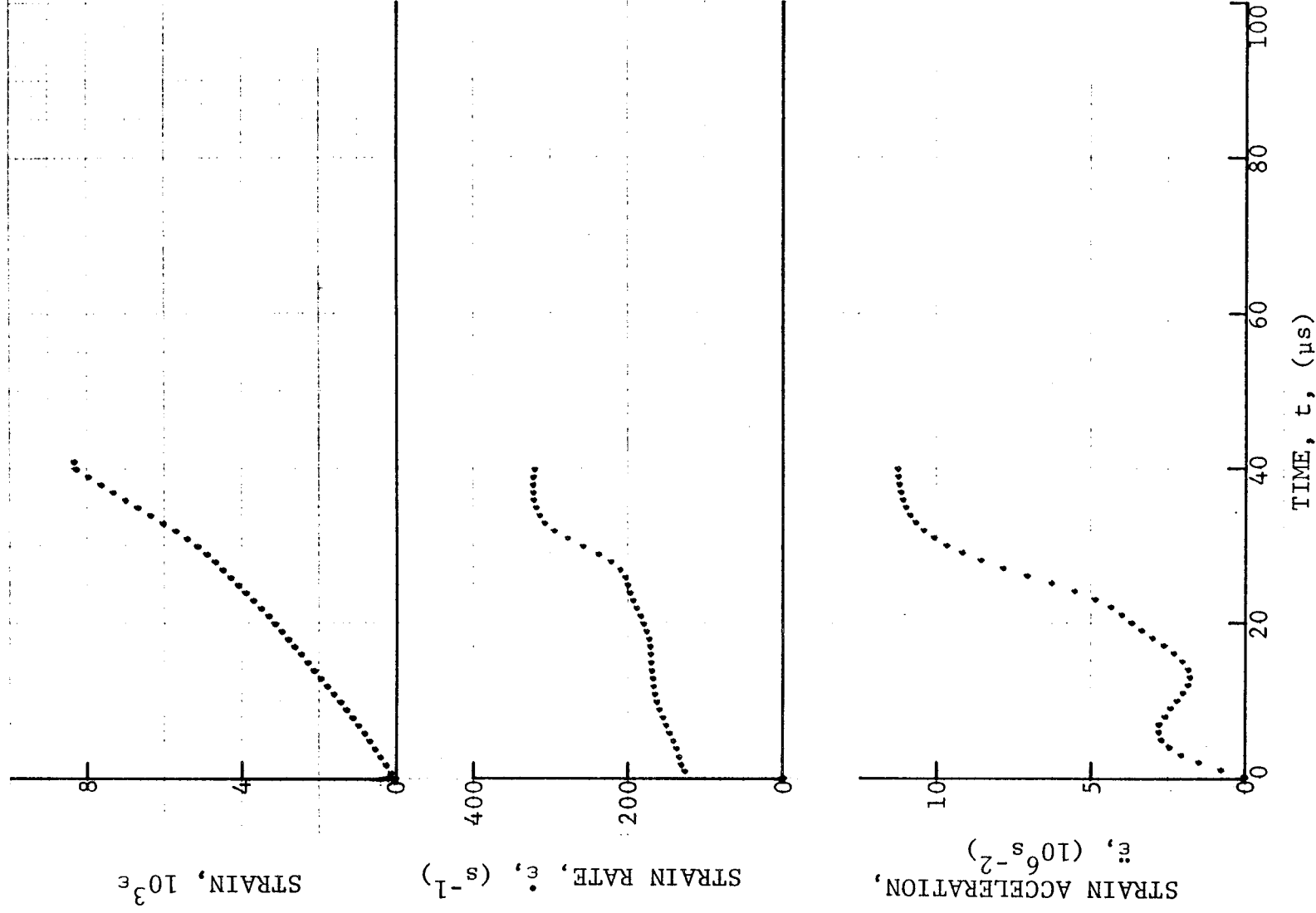


Figure 4-175. Circumferential strain and its derivatives in [10_g] SP288/AS graphite/epoxy ring under dynamic loading for Specimen No. 15-8.

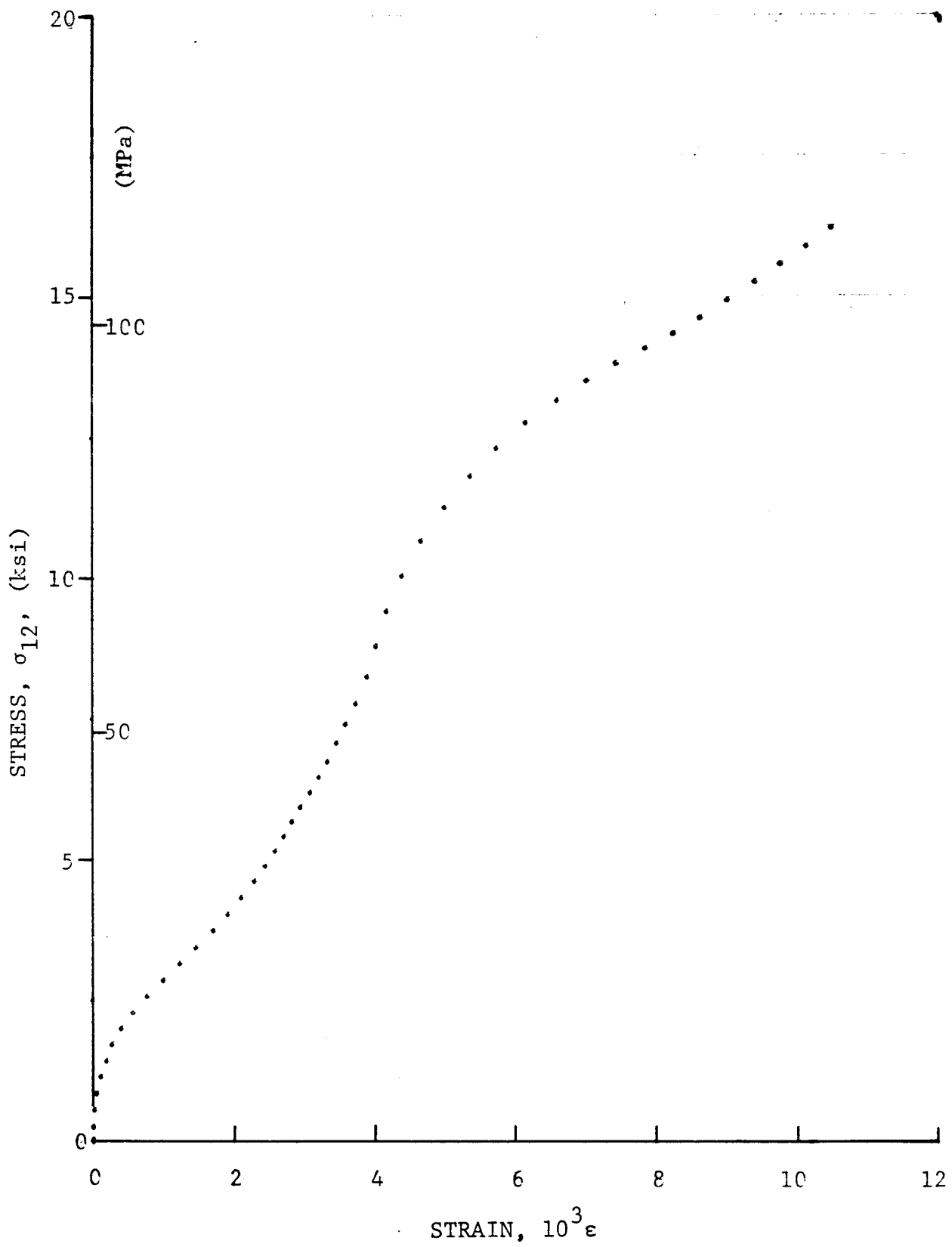


Figure 4-176. Shear stress versus shear strain curve for dynamically loaded [10₈] SP288/AS graphite/epoxy ring for Specimen No. 15-5 (50 mg PETN detonator).

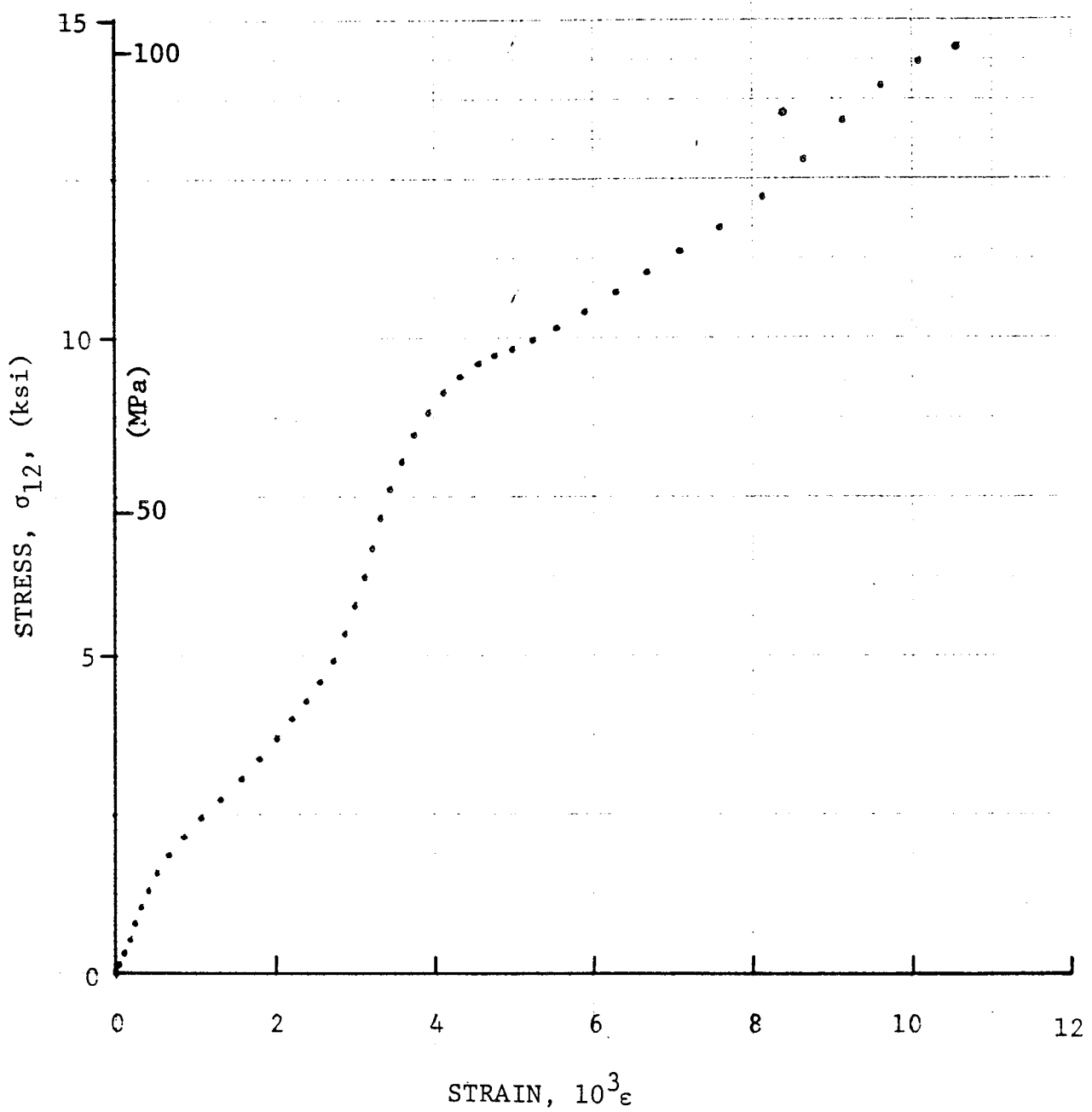


Figure 4-177. Stress-strain curve for dynamically loaded [10g] SP288/AS graphite/epoxy ring for Specimen No. 15-7 (50 mg PETN detonator).

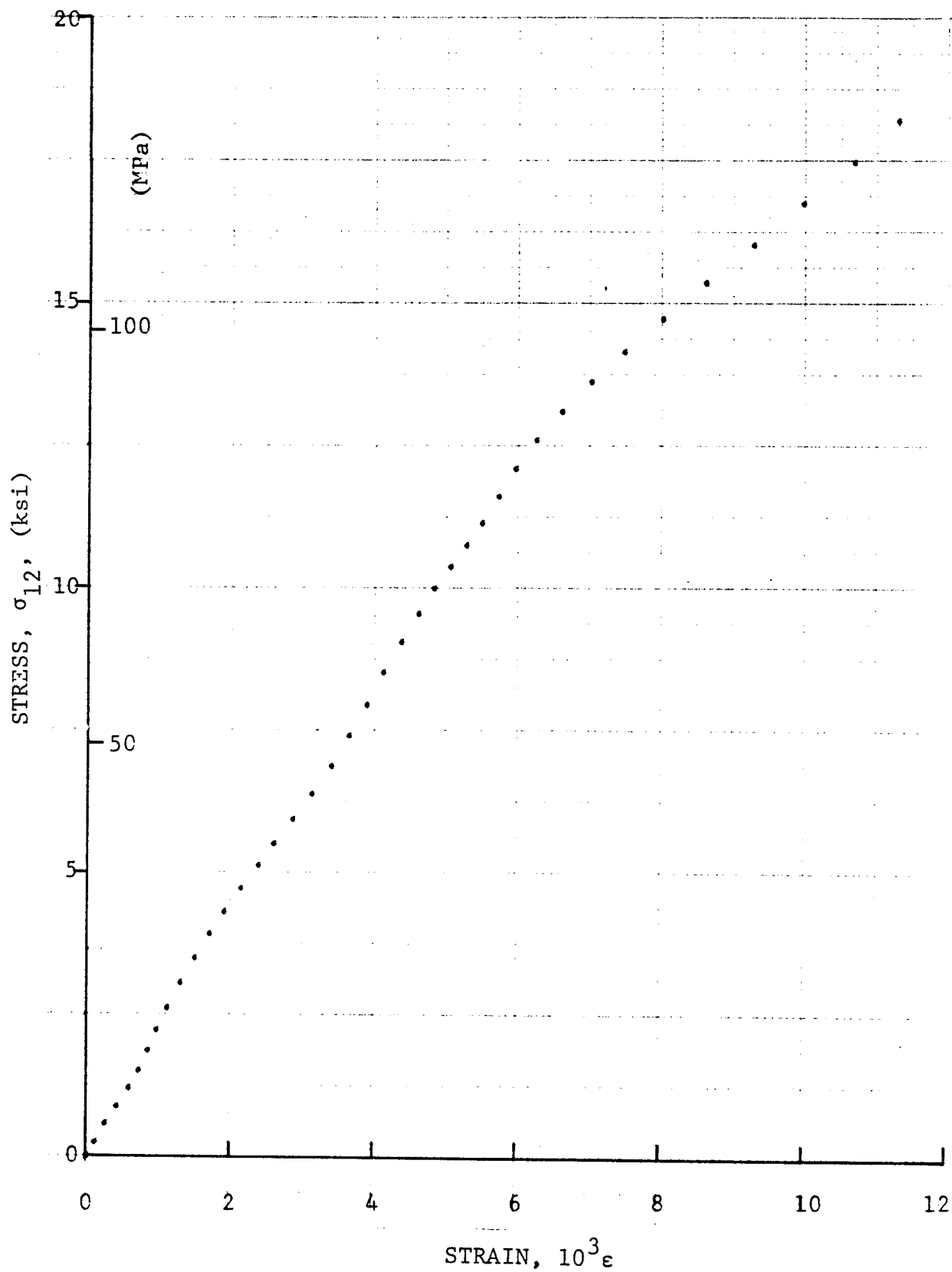


Figure 4-178. Shear stress versus shear strain curve for dynamically loaded $[10_8]$ SP288/AS graphite/epoxy ring for Specimen No. 15-8 (100 mg PETN detonator).

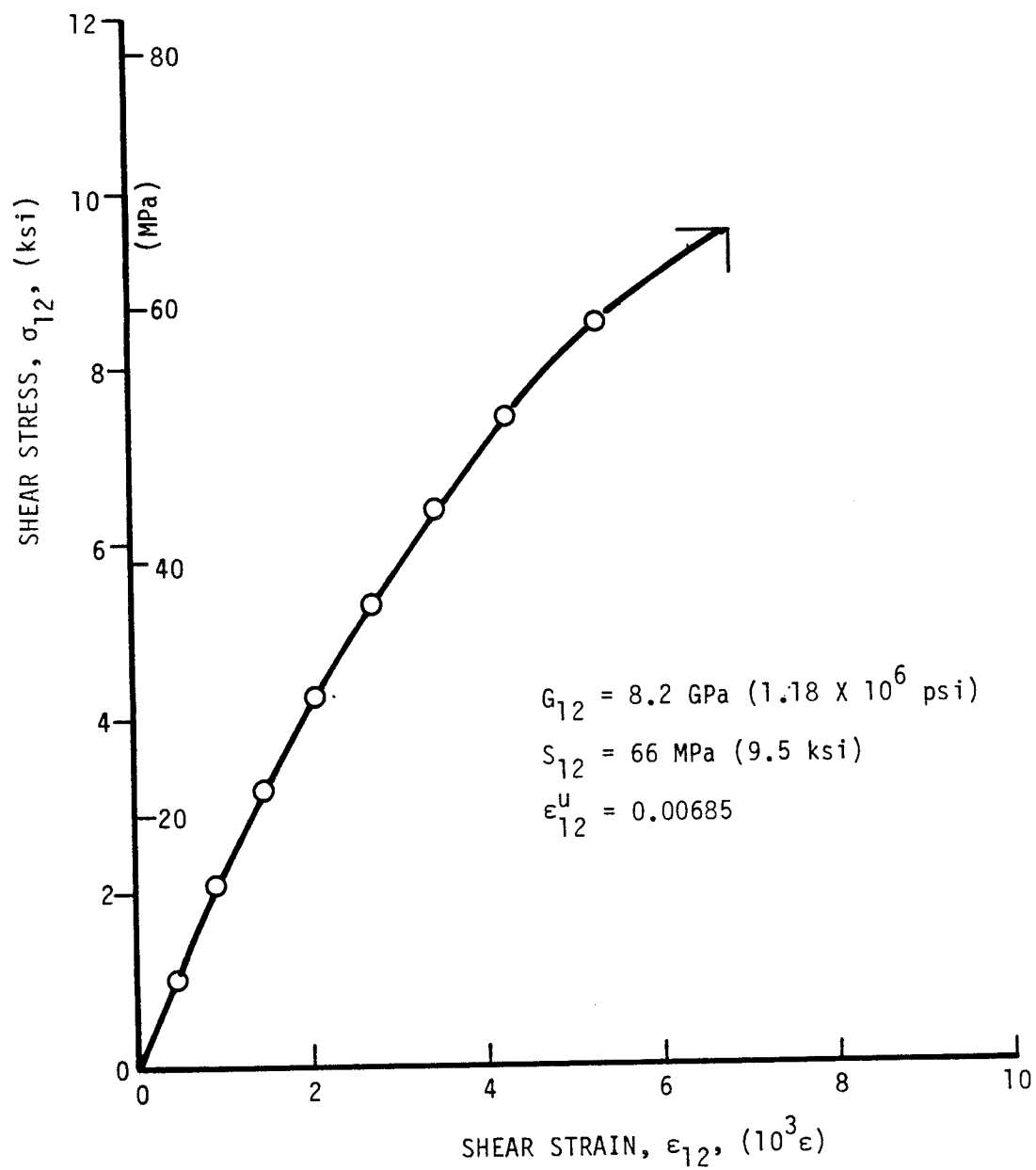


Figure 4-179. Shear stress versus shear strain for unidirectional 10-deg off-axis 80AS/20S/PR288 ring specimen (Specimen No. 18-2).

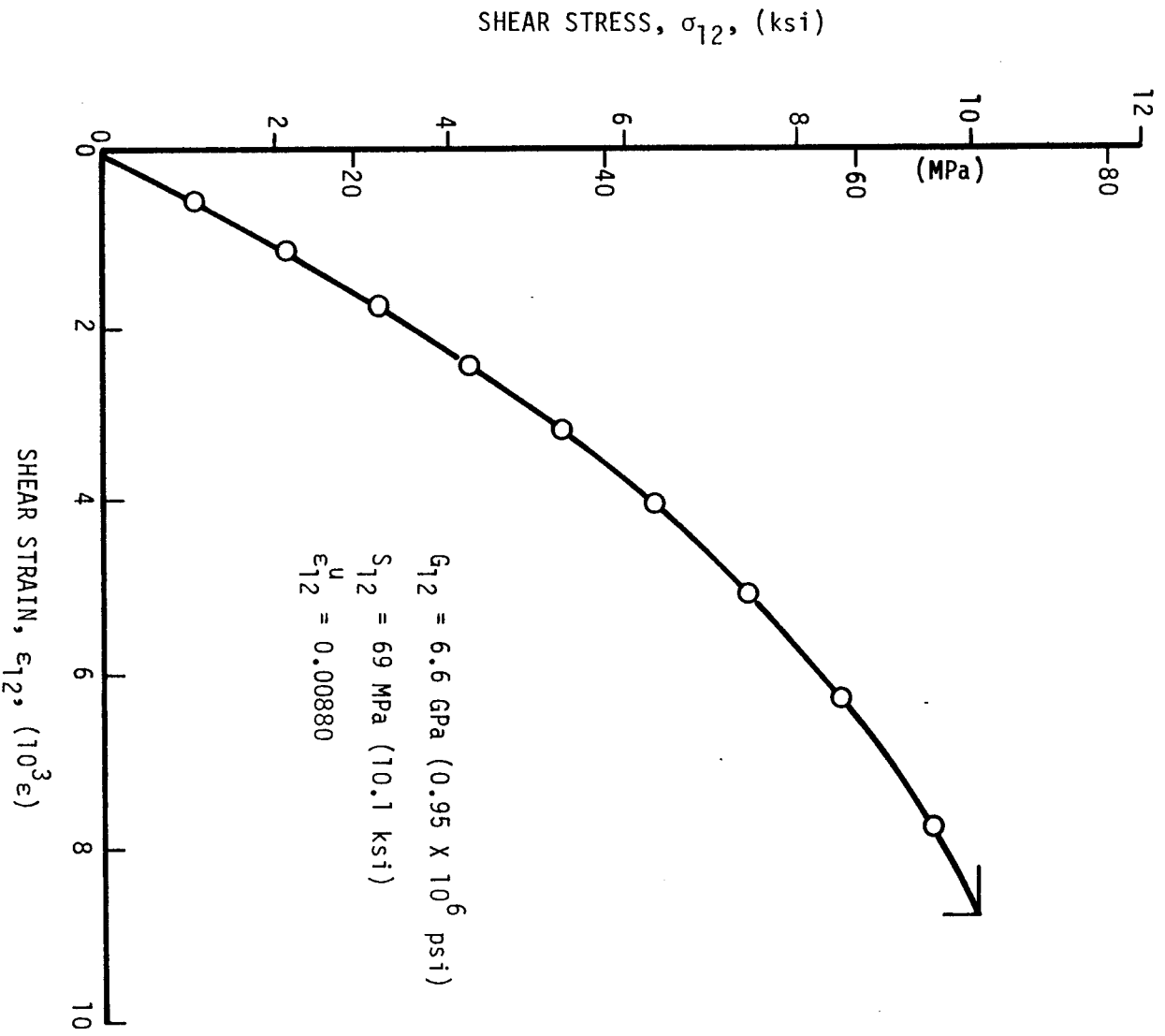
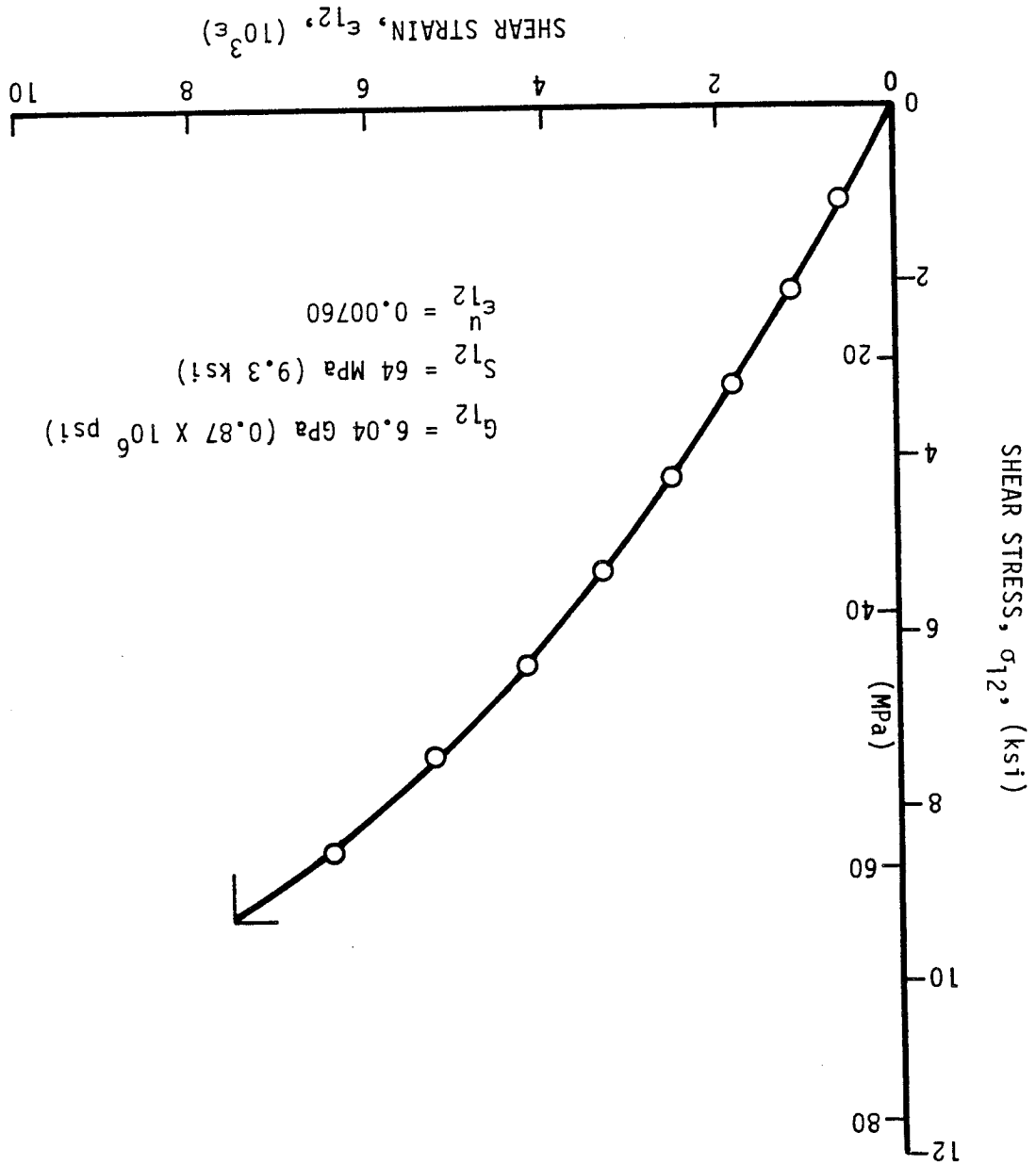


Figure 4-180. Shear stress versus shear strain for unidirectional 10-deg off-axis 80AS/20S/PR288 ring specimen (Specimen No. 18-3).

Figure 4-181. Shear stress versus shear strain for unidirectional 10-deg off-axis 80AS/20S/PR288 ring specimen (Specimen No. 18-4).



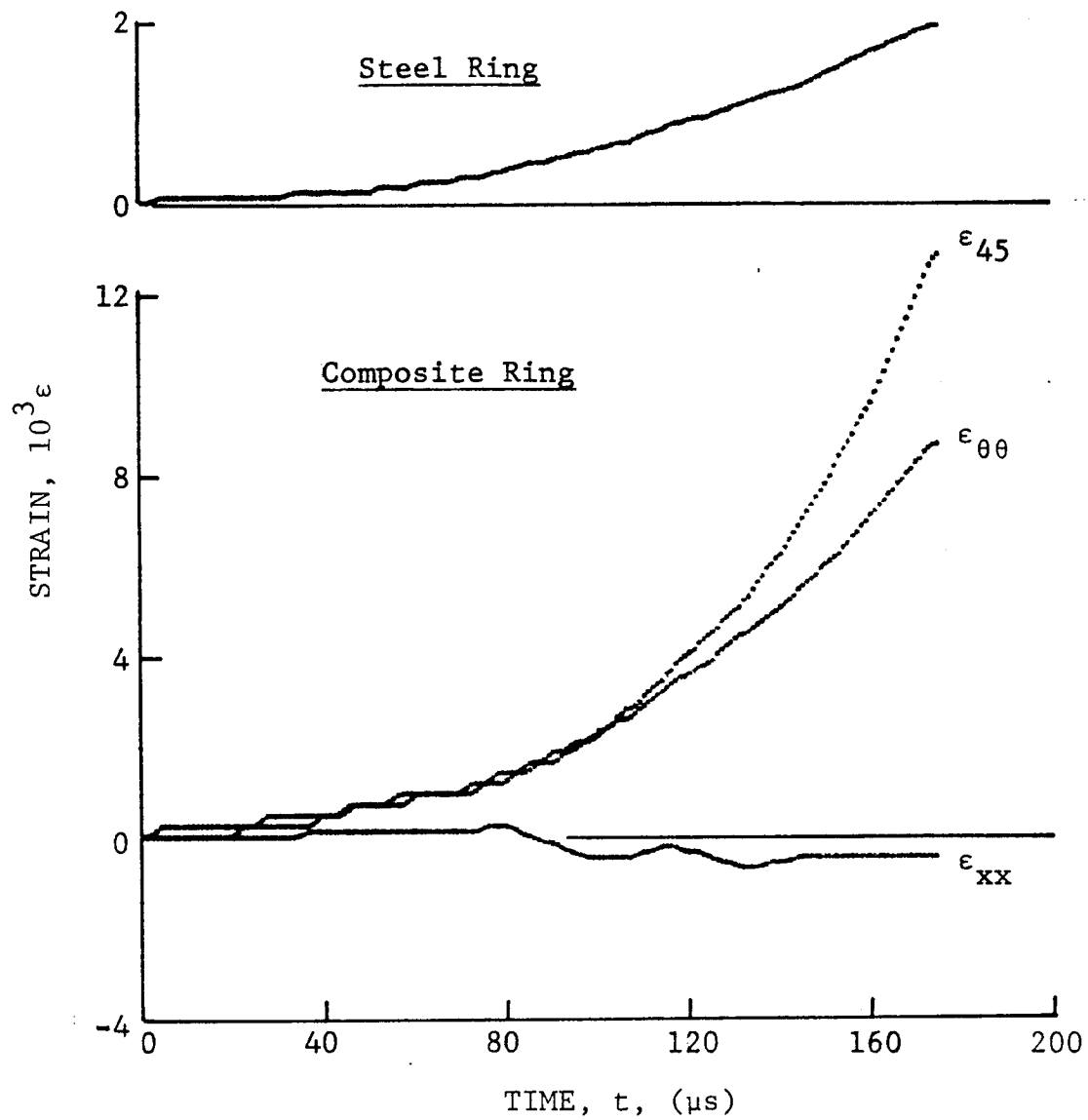


Figure 4-182. Strain records in steel ring and 80AS/20S/PR288 graphite/S-glass/epoxy ring under dynamic loading for Specimen No. 18-9 (650 mg pistol powder).

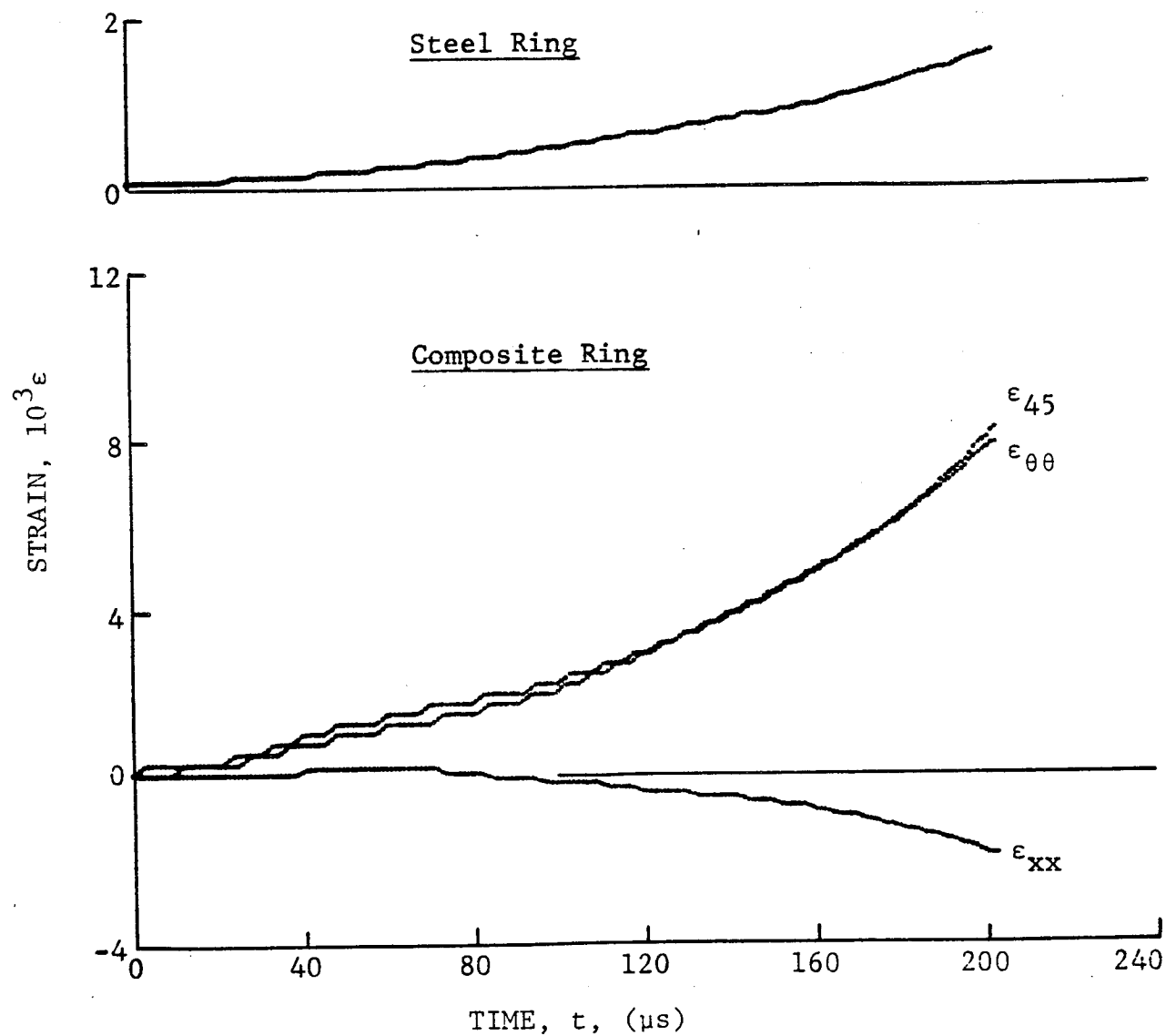


Figure 4-183. Strain records in steel ring and 80AS/20S/PR288 graphite/S-glass/epoxy ring under dynamic loading for Specimen No. 18-10 (650 mg pistol powder).

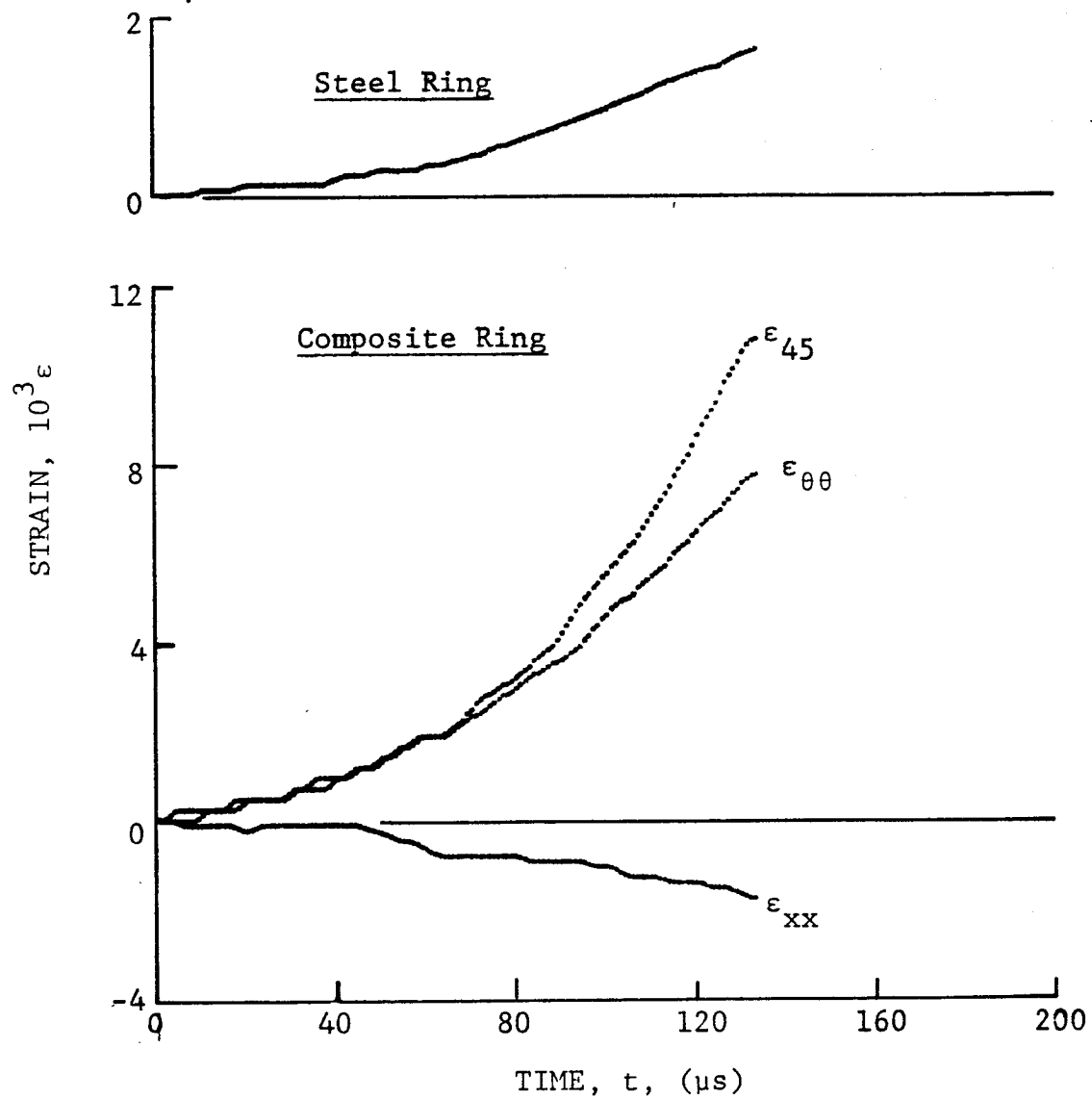


Figure 4-184. Strain records in steel ring and 80AS/20S/PR288 graphite/S-glass/epoxy ring under dynamic loading for Specimen No. 18-11 (650 mg pistol powder).

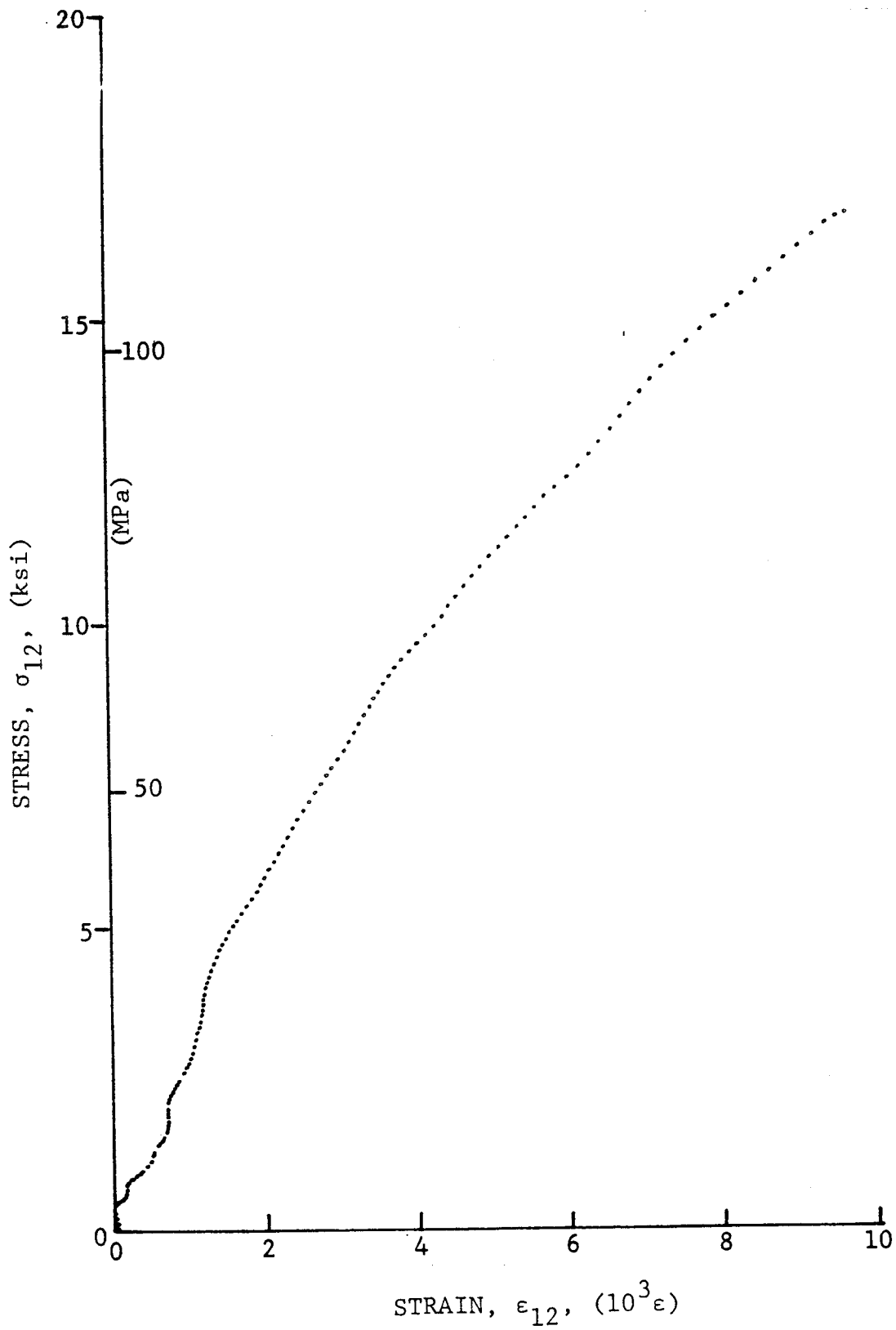


Figure 4-185. Shear stress versus shear strain curve for dynamically loaded $[10_6]$ 80AS/20S/PR288 graphite/S-glass/epoxy ring for Specimen No. 18-9 (650 mg pistol powder).

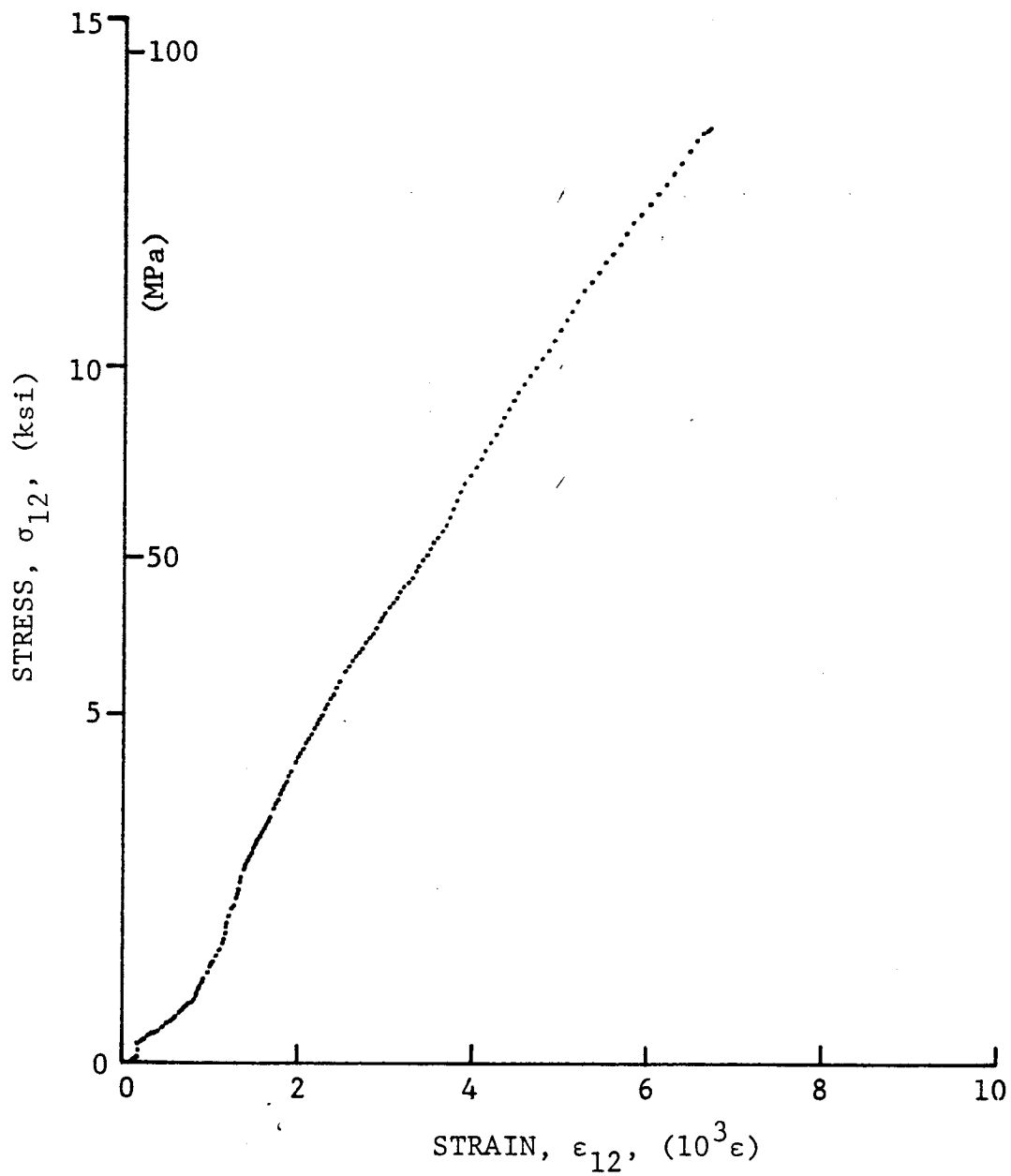


Figure 4-186. Shear stress versus shear strain curve for dynamically loaded $[10_6]$ 80AS/20S/PR288 graphite/S-glass/epoxy ring for Specimen No. 18-10 (650 mg pistol powder).

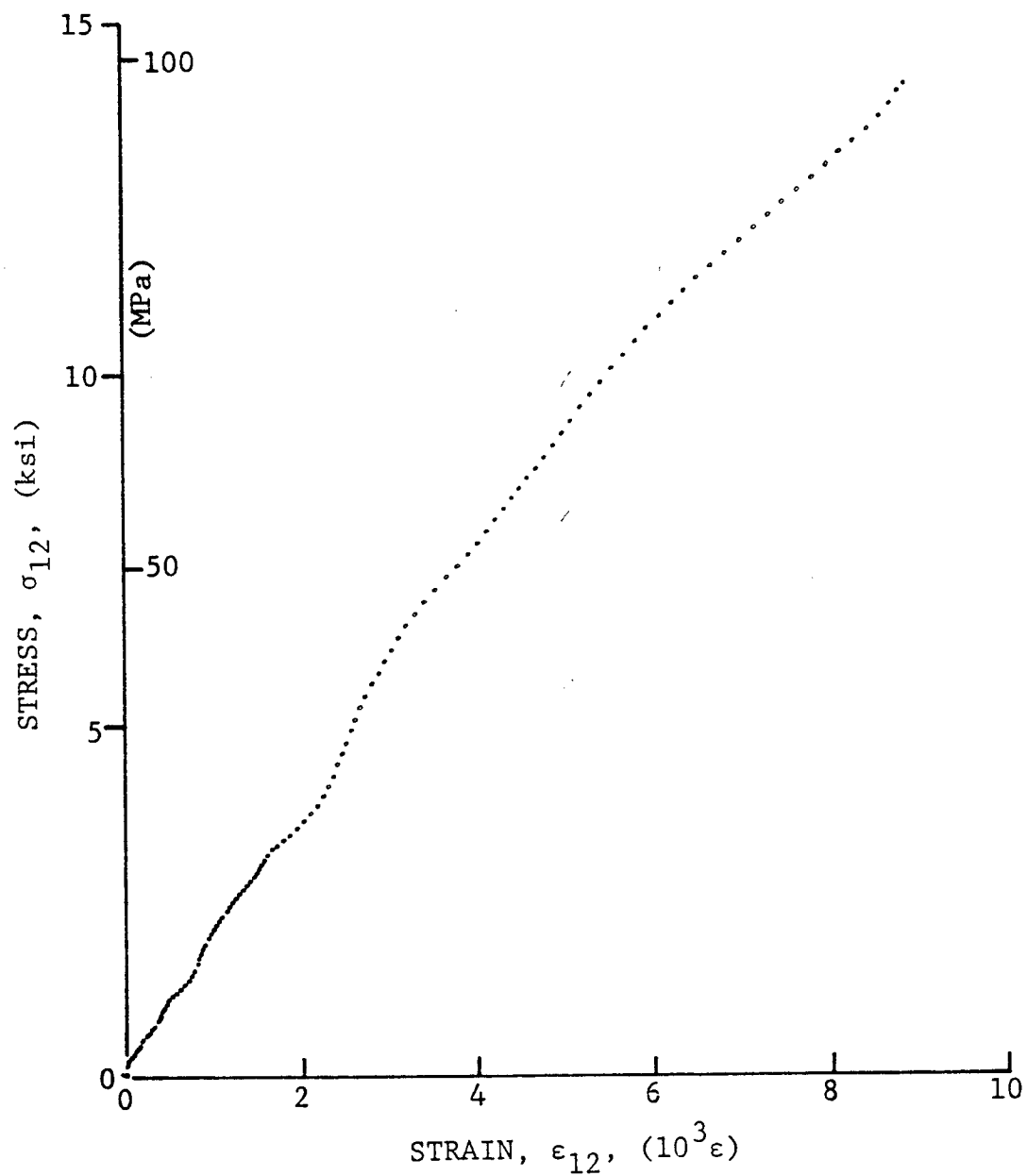


Figure 4-187. Shear stress versus shear strain curve for dynamically loaded $[10_6]$ 80AS/20S/PR288 graphite/S-glass/epoxy ring for Specimen No. 18-11 (650 mg pistol powder).

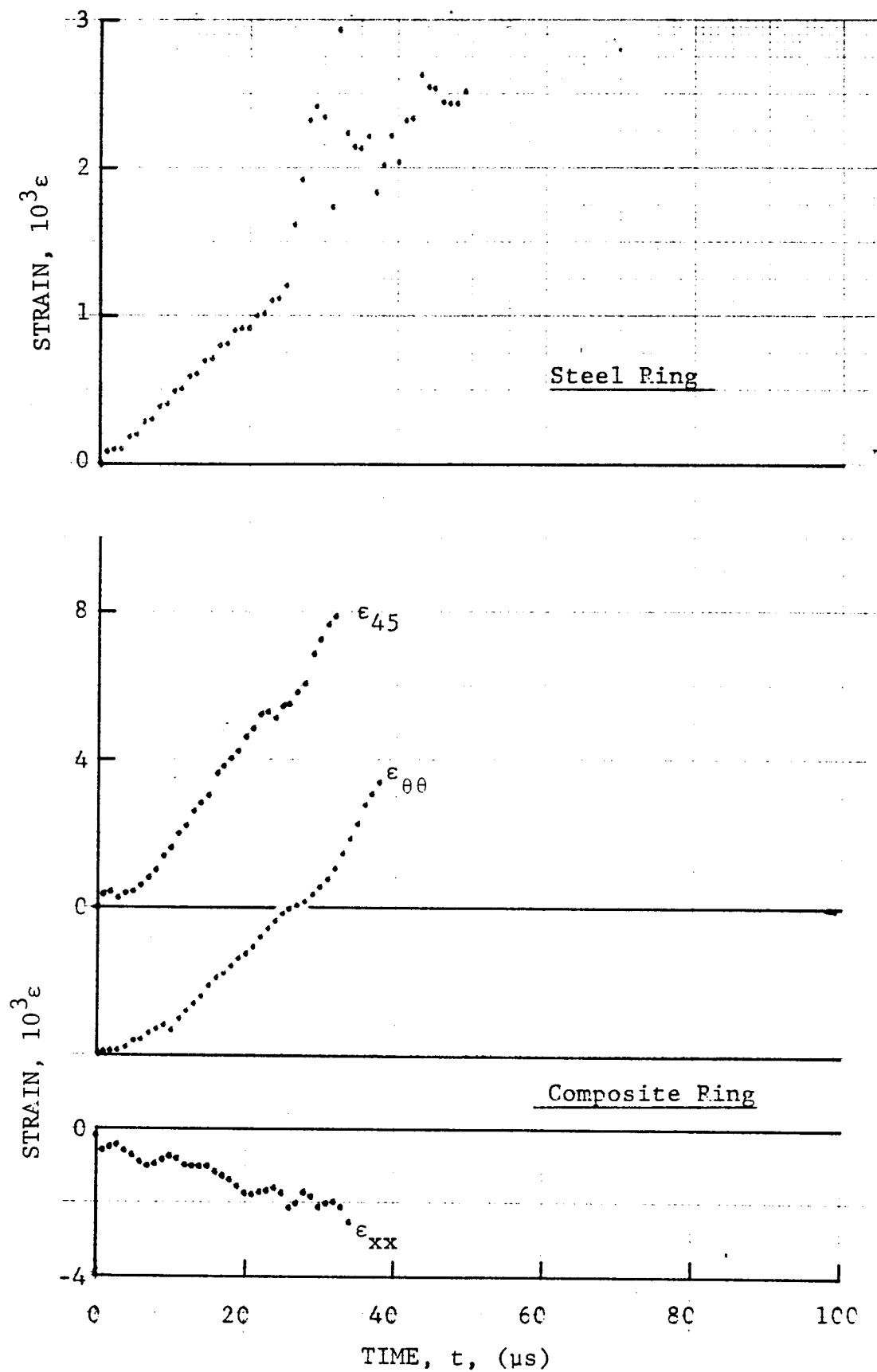


Figure 4-188. Strain records in steel ring and $[10_6]$ 80AS/20S/PR288 graphite/S-glass/epoxy ring under dynamic loading for Specimen No. 18-5 (100 mg PETN detonator).

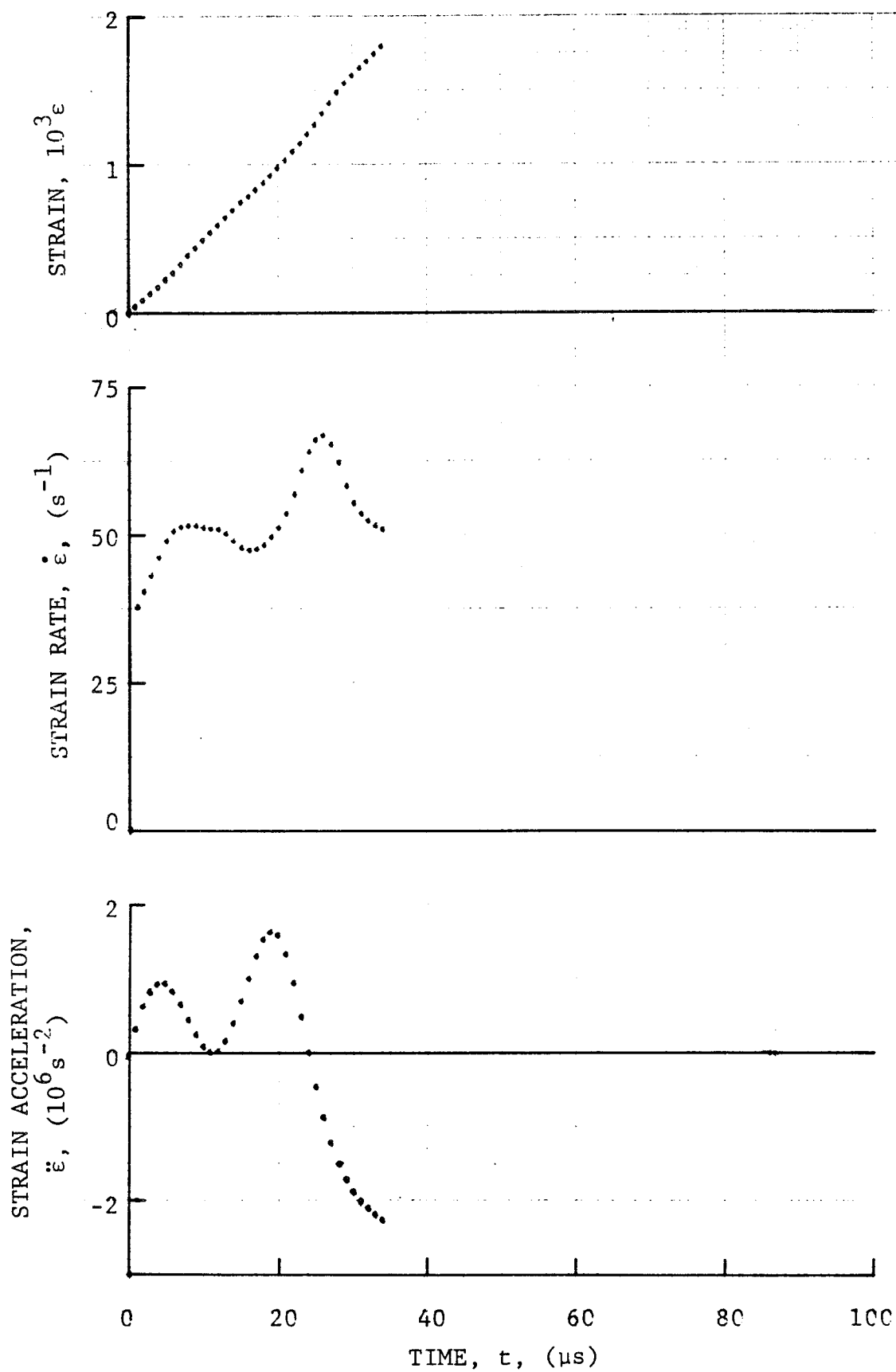


Figure 4-189. Strain and its derivatives in steel ring for Specimen No. 18-5.

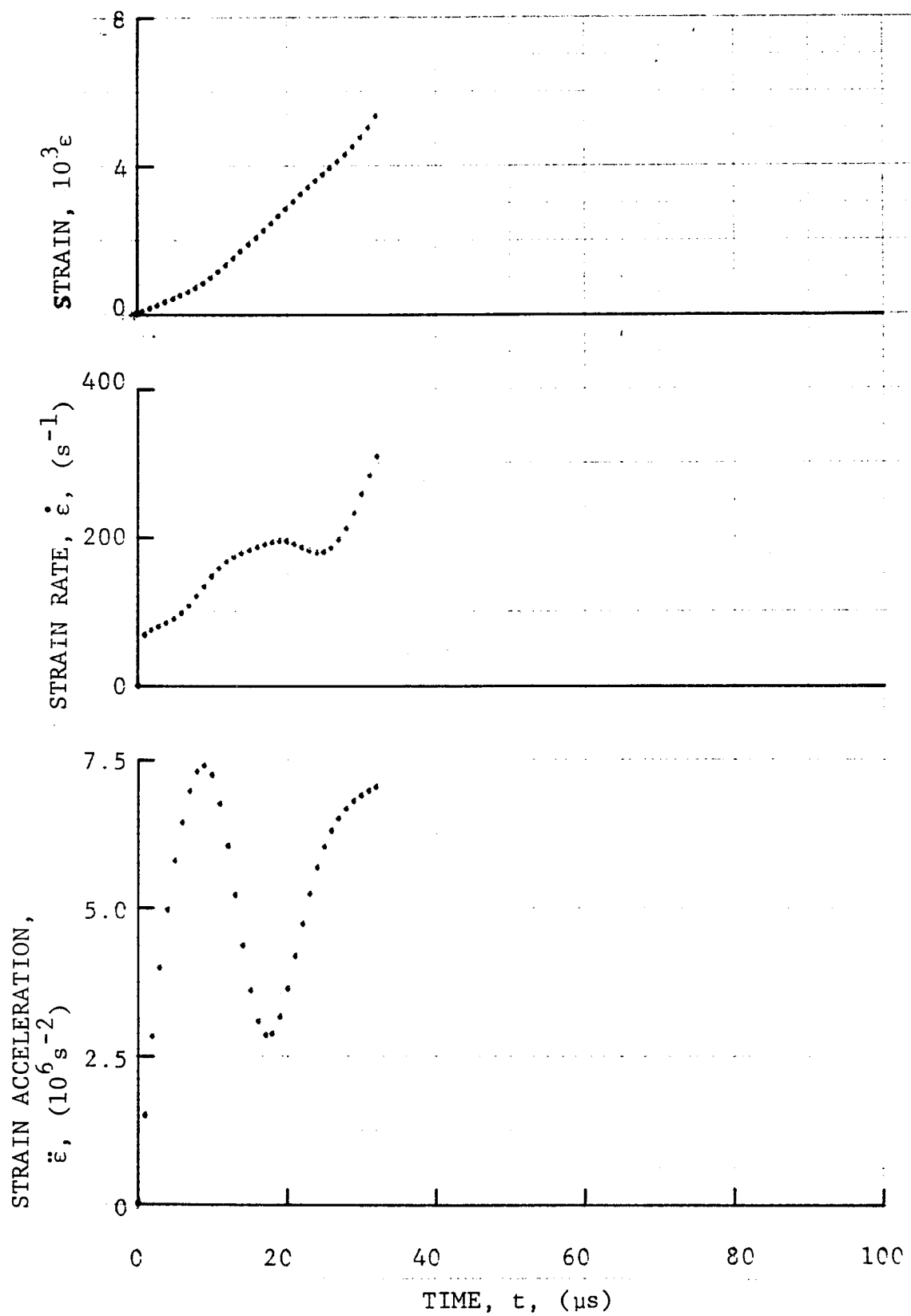


Figure 4-190. Circumferential strain and its derivatives in $[10_6]$ 80AS/20S/PR288 graphite/S-glass/epoxy ring under dynamic loading for Specimen No. 18-5 (100 mg PETN detonator).

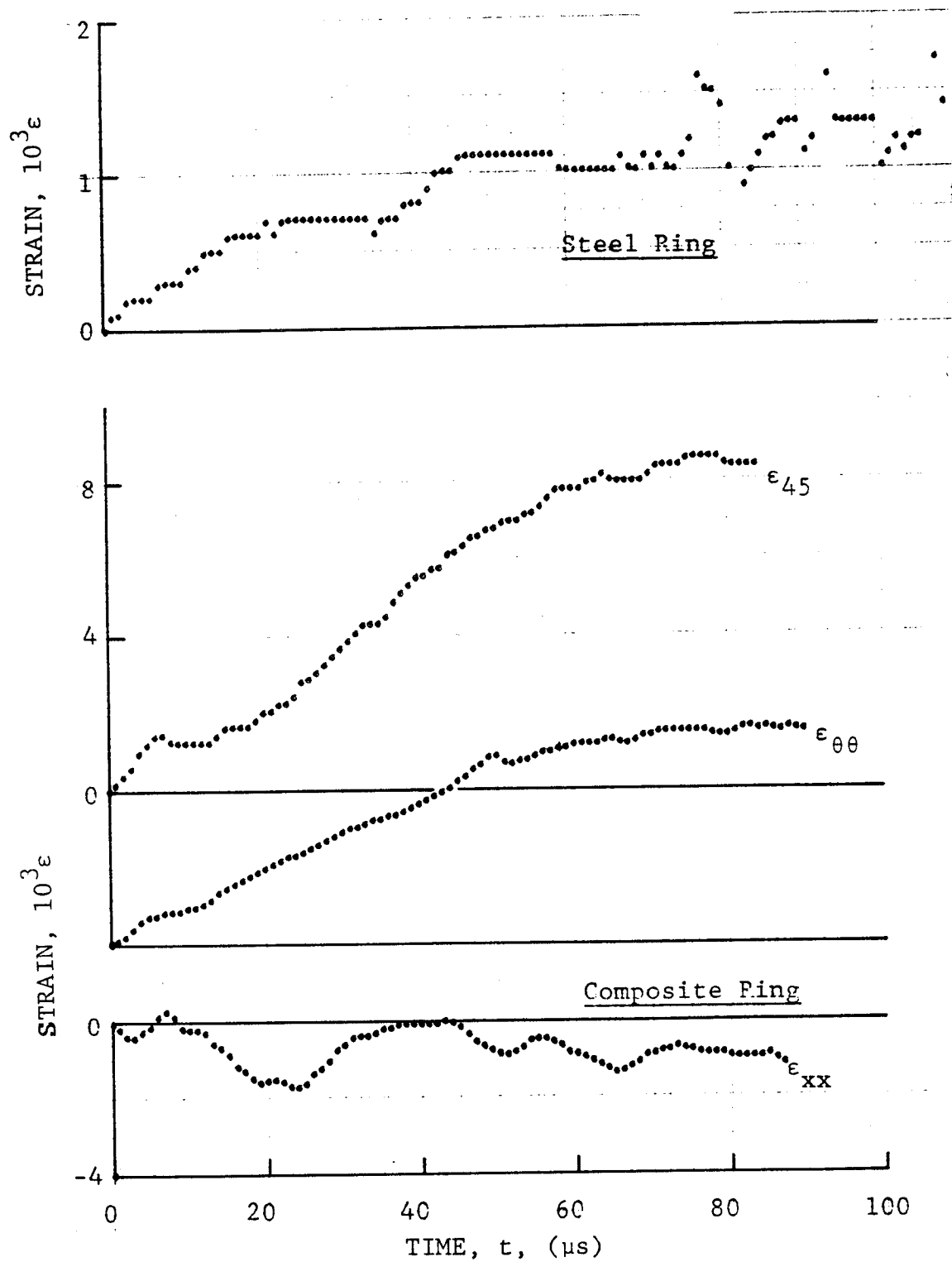


Figure 4-191. Strain records in steel ring and $[10_6]$ 80AS/20S/PR288 graphite/S-glass/epoxy ring under dynamic loading for Specimen No. 18-6 (455 mg pistol powder).

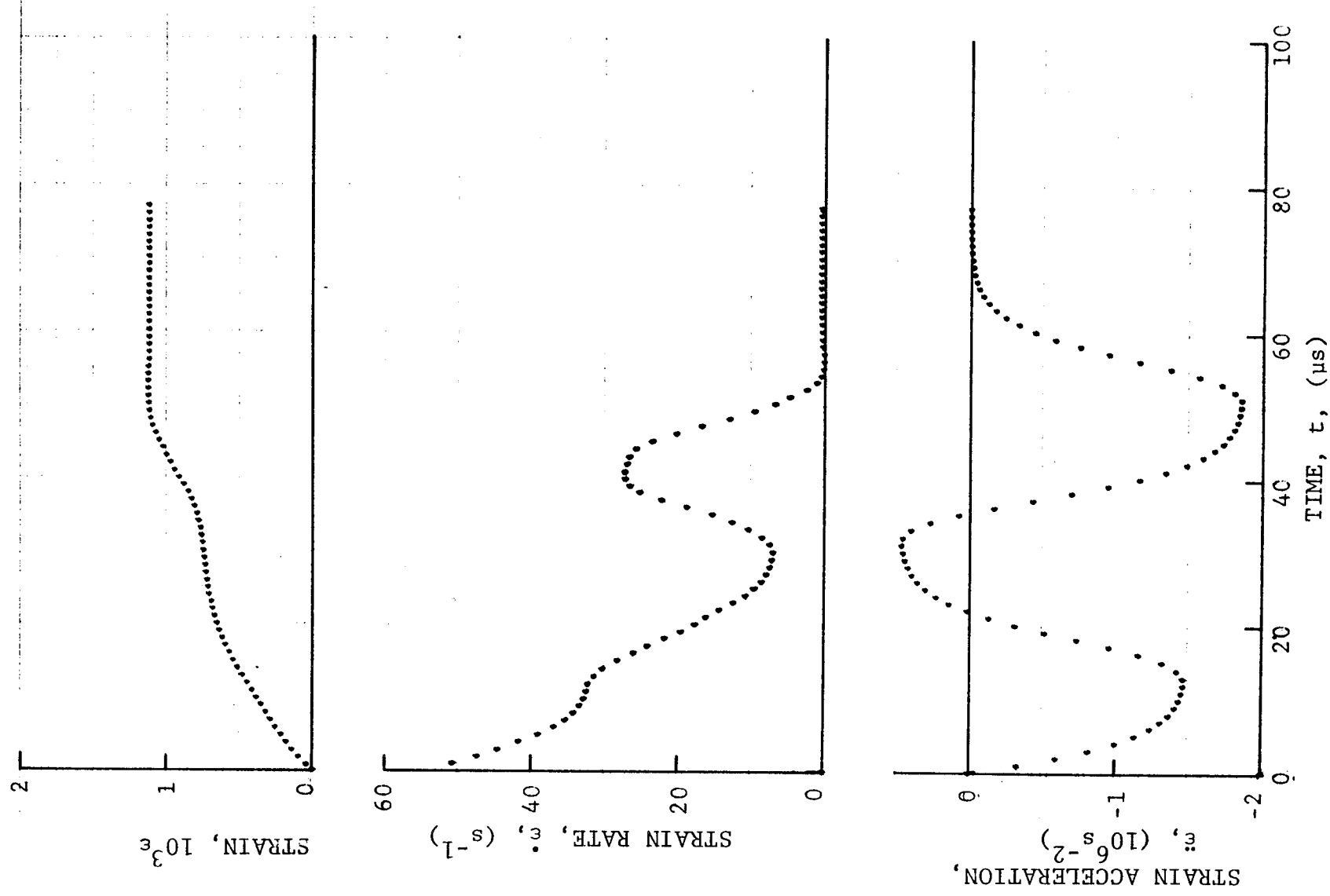


Figure 4-192. Strain and its derivatives in steel ring for Specimen No. 18-6.

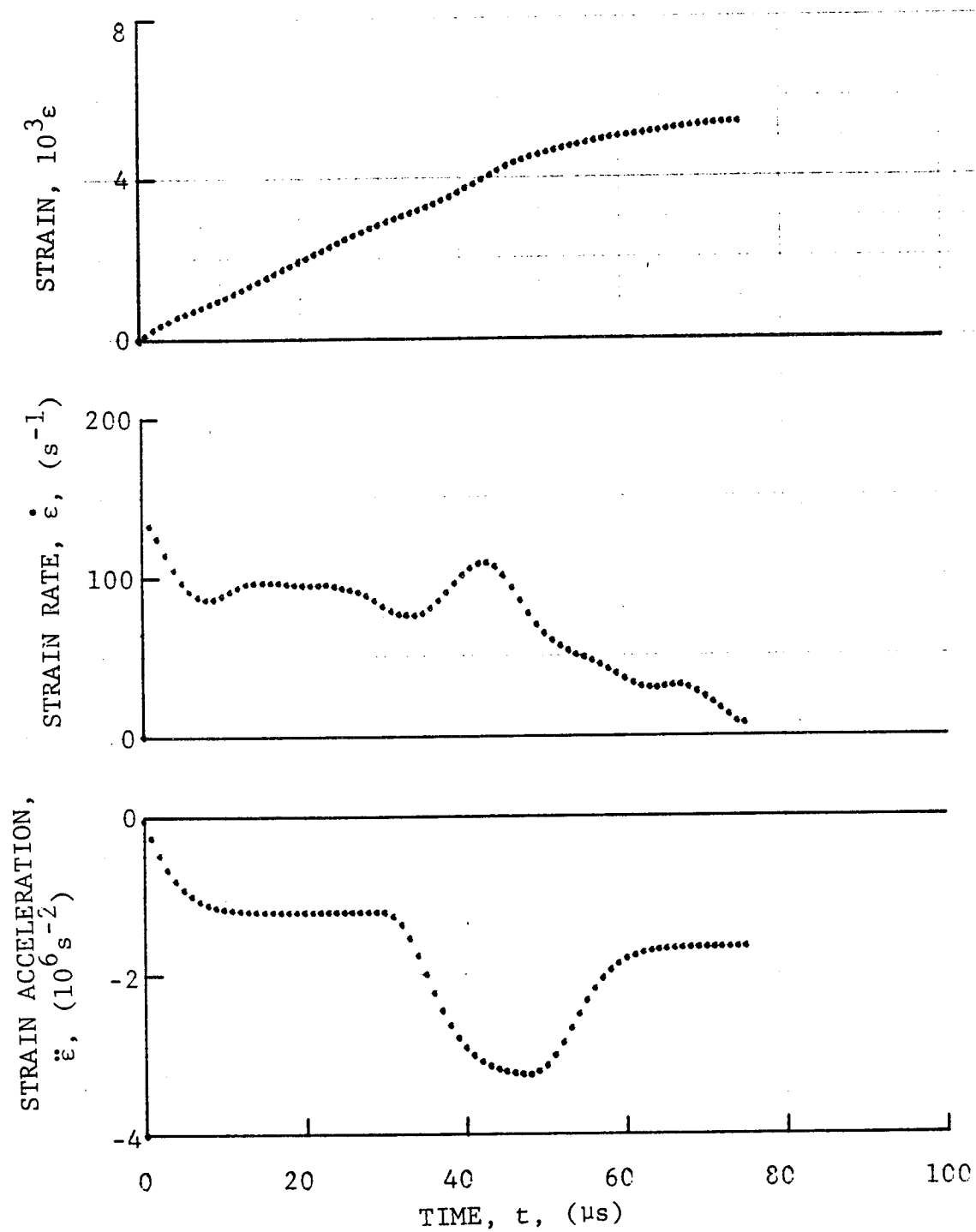


Figure 4-193. Circumferential strain and its derivatives in $[10_6]$ 80AS/20S/PR288 graphite/S-glass/epoxy ring under dynamic loading for Specimen No. 18-6 (455 mg pistol powder).

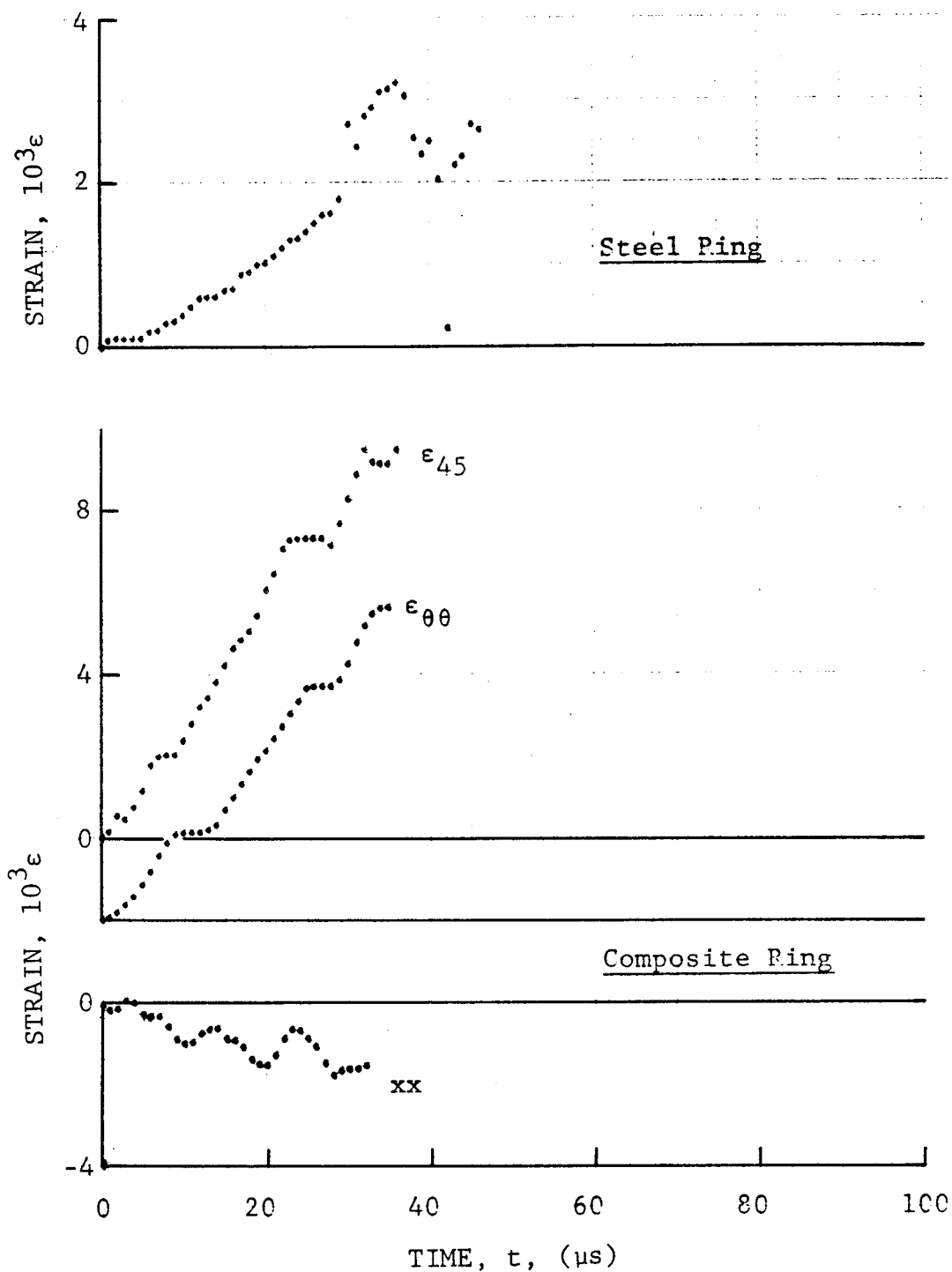


Figure 4-194. Strain records in steel ring and $[10_6]$ 80AS/20S/PR288 graphite/S-glass/epoxy ring under dynamic loading for Specimen No. 18-8 (100 mg PETN detonator).

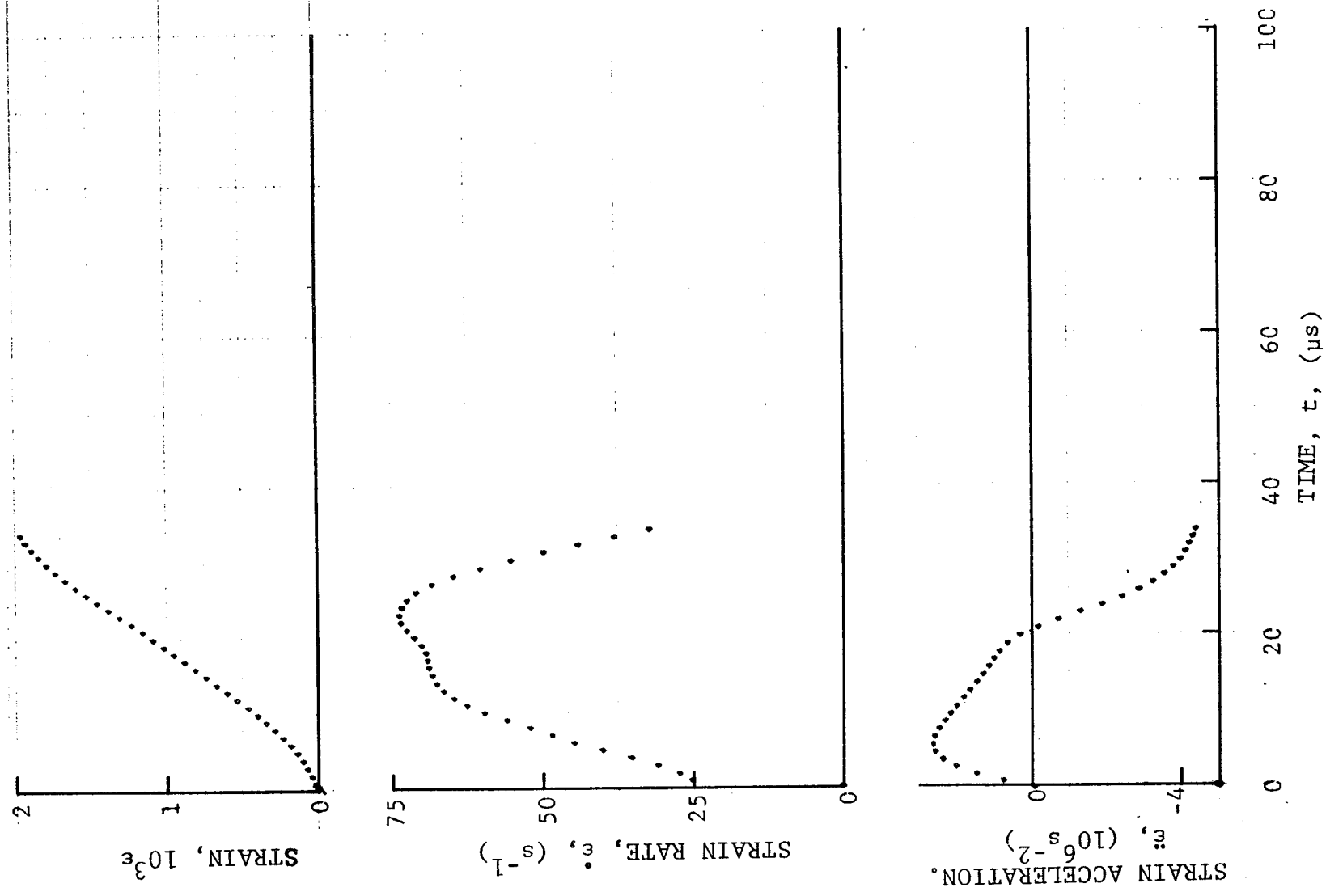


Figure 4-195. Strain and its derivatives for Specimen No. 18-8.

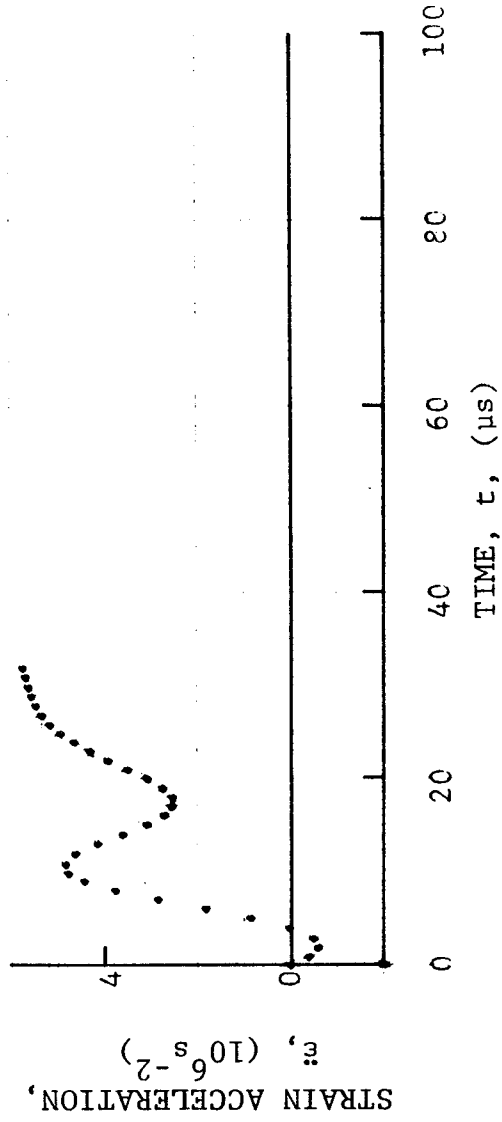
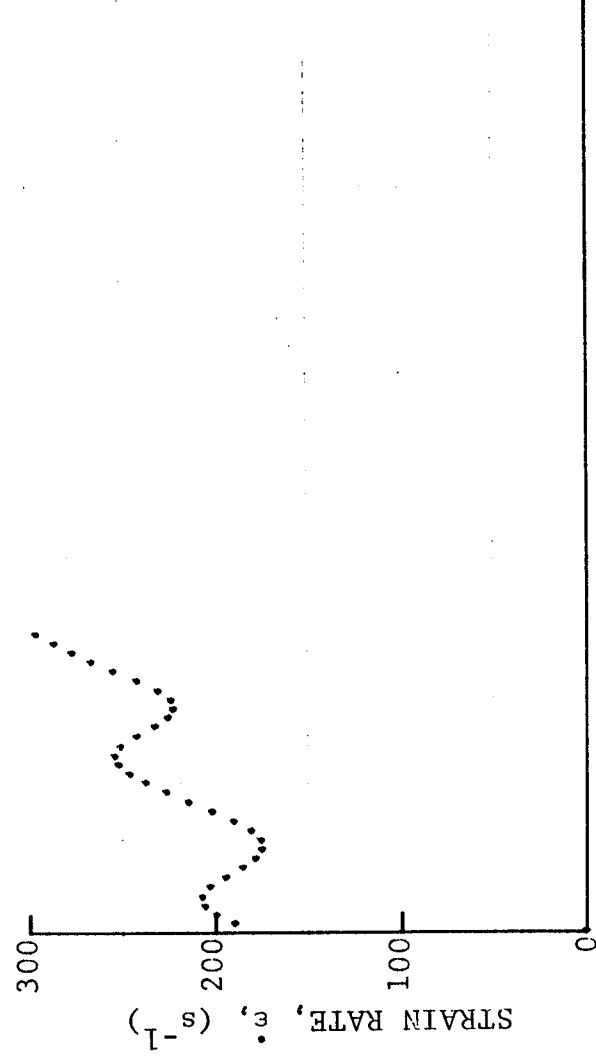
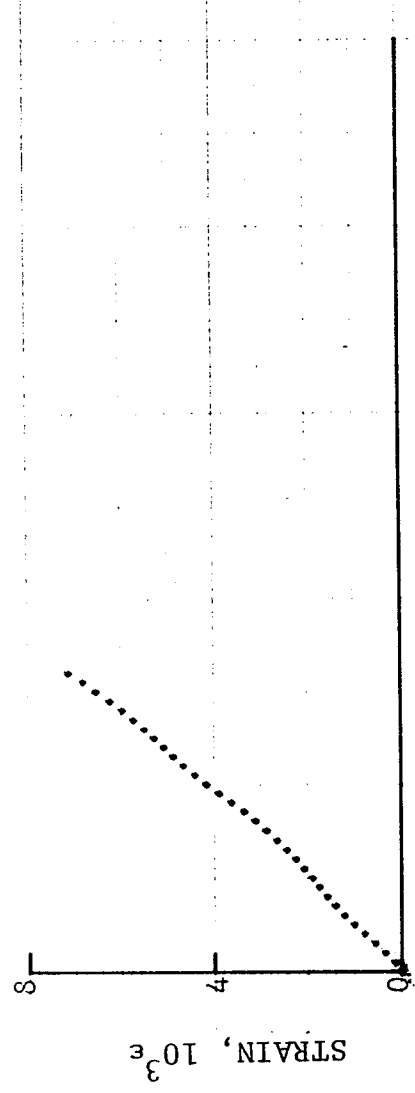


Figure 4-196. Circumferential strain and its derivatives in [10₆] 80AS/20S/PR288 graphite/S-glass/epoxy ring under dynamic loading for Specimen No. 18-8 (100 mg PETN detonator).

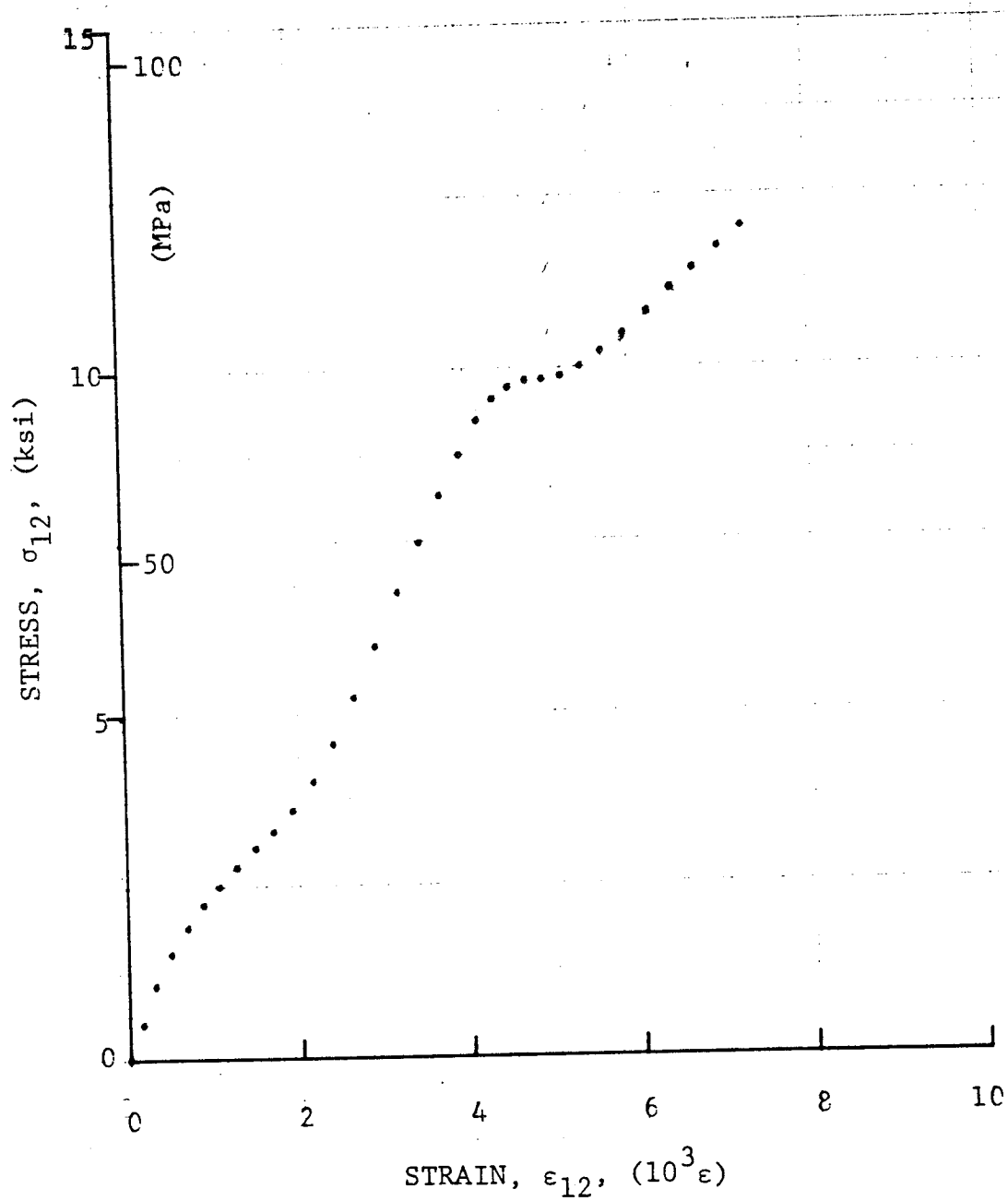


Figure 4-197. Shear stress versus shear strain curve for dynamically loaded $[10_6]$ 80AS/20S/PR288 graphite/S-glass/epoxy ring for Specimen No. 18-5 (100 mg PETN detonator).

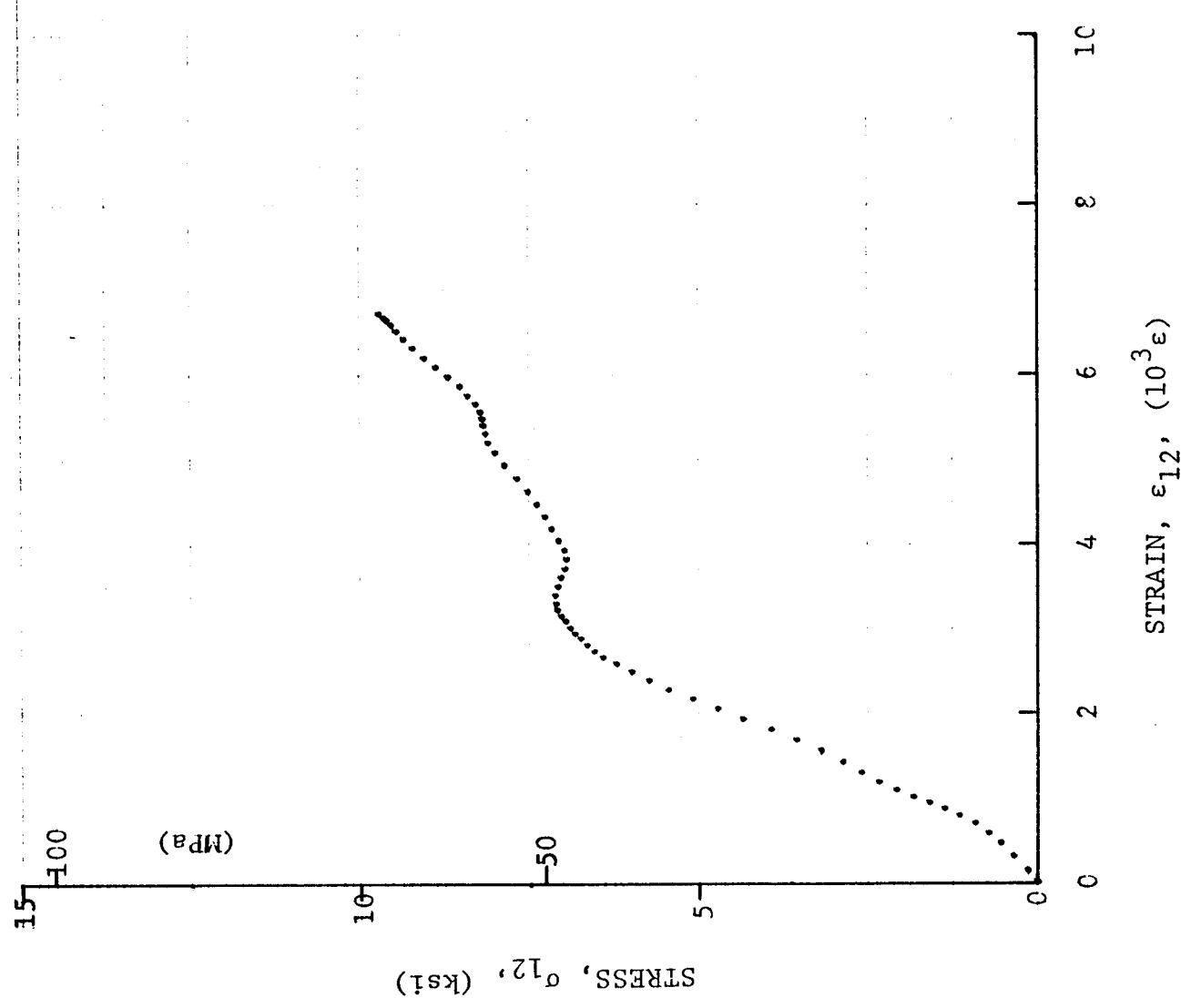


Figure 4-198. Shear stress versus shear strain curve for dynamically loaded [10₆] 80AS/20S/PR288 graphite/S-glass/epoxy ring for Specimen No. 18-6 (455 mg pistol powder).

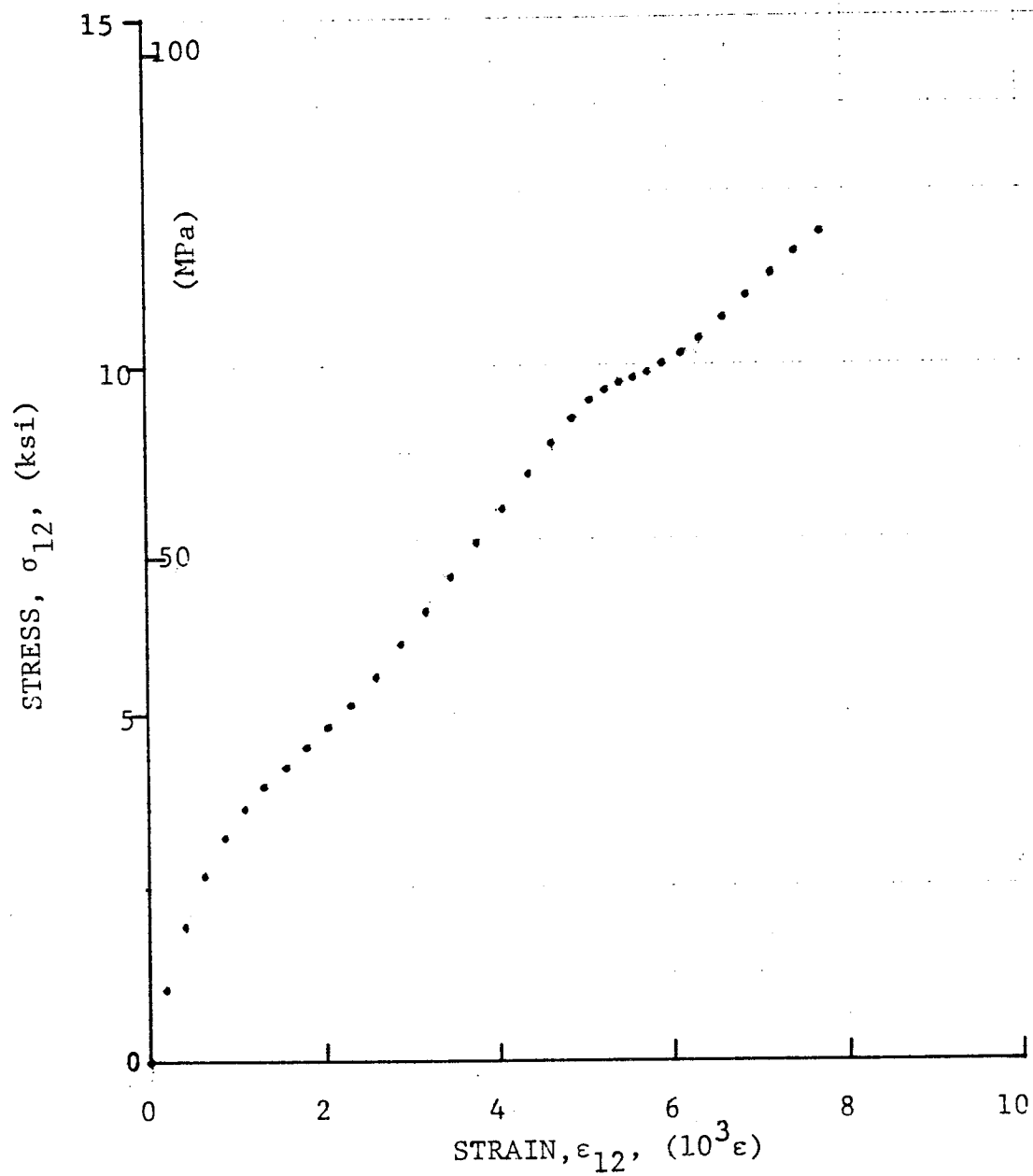
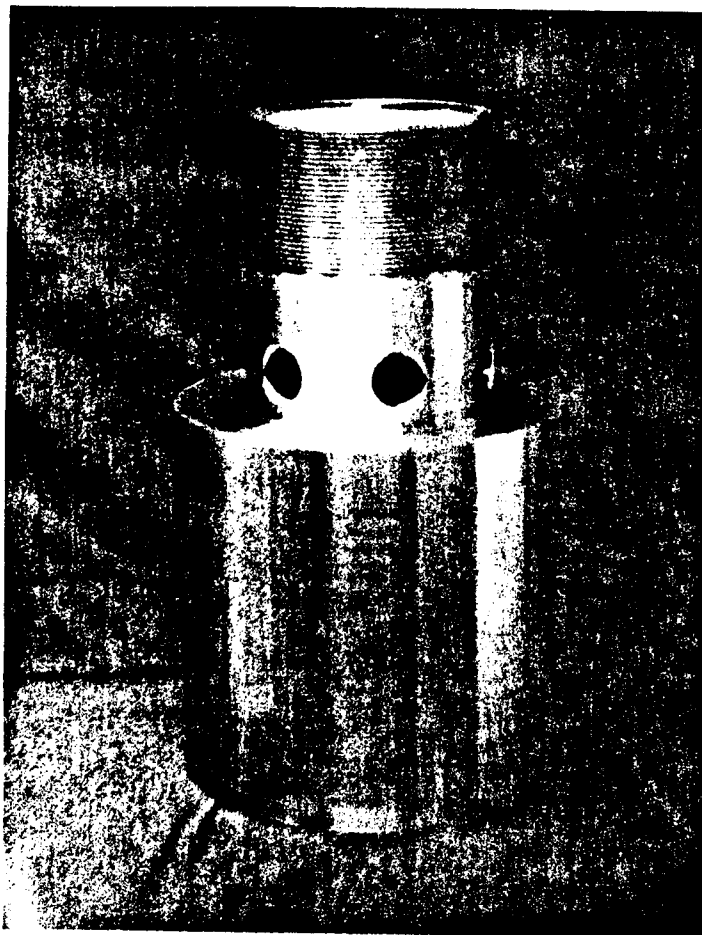
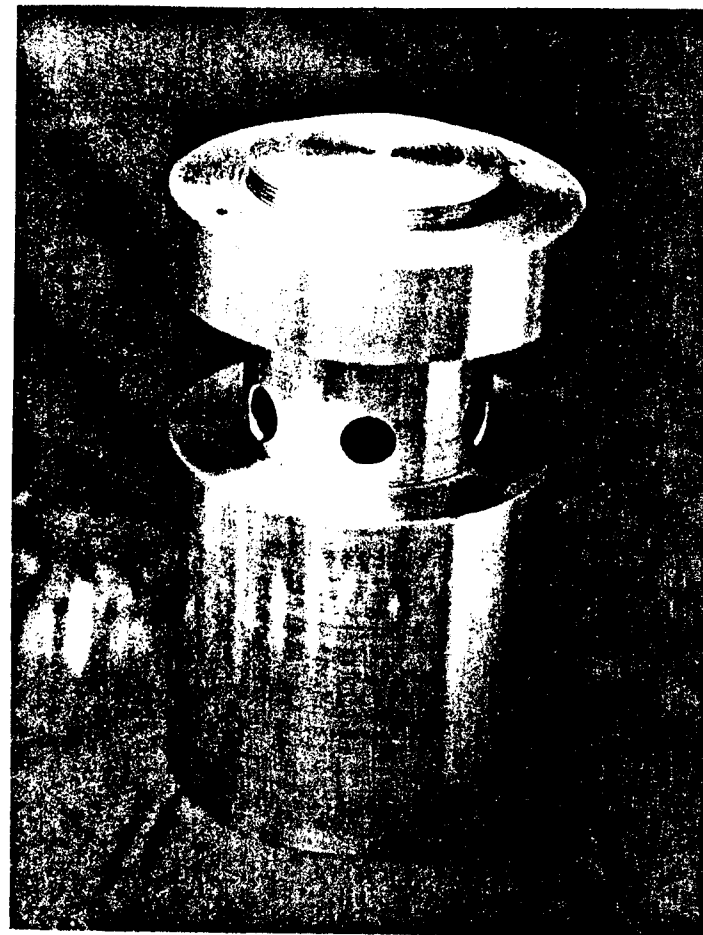


Figure 4-199. Shear stress versus shear strain curve for dynamically loaded $[10_6]$ 80AS/20S/PR288 graphite/S-glass epoxy ring for Specimen No. 18-8 (100 mg PETN detonator).

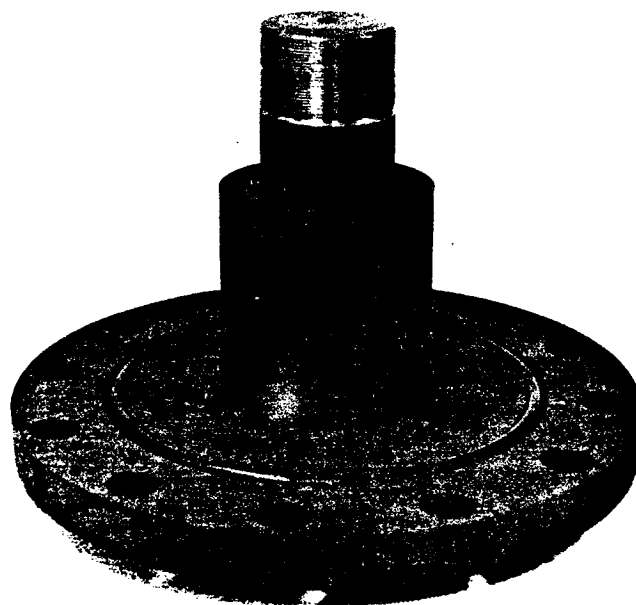


(a)



(b)

Figure 4-200. Arbor for holding test and calibration ring specimens in compression fixture.
(a) Arbor; (b) Arbor with retaining ring.



(a)



(b)

Figure 4-201. Specimen holding arbor attached to base plate.
(a) Without specimens; (b) With specimens and retaining ring.

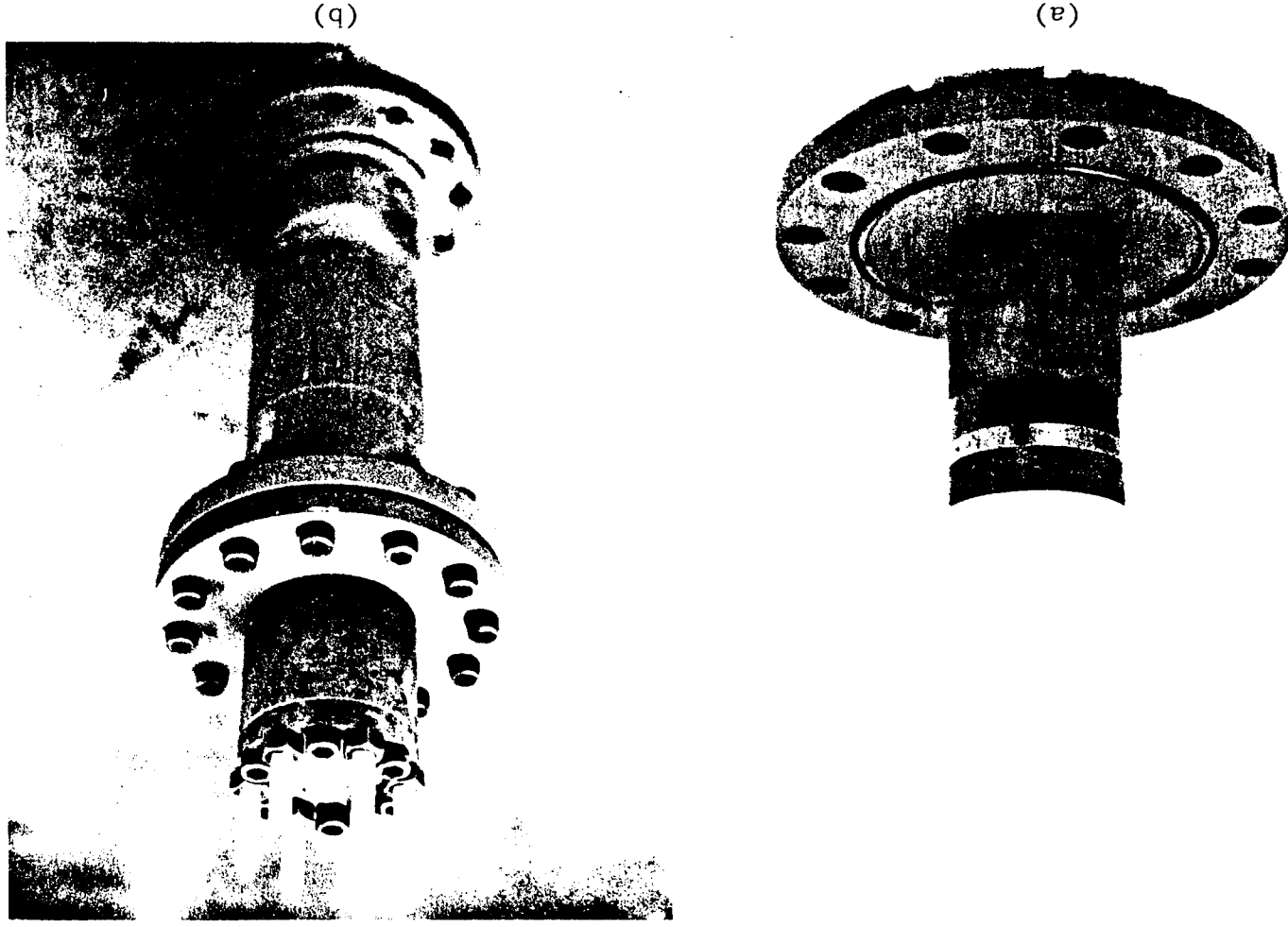


Figure 4-202. Dynamic compression fixture. (a) Arbor with specimens, retaining ring, and deflector cone; (b) Assembled fixture.

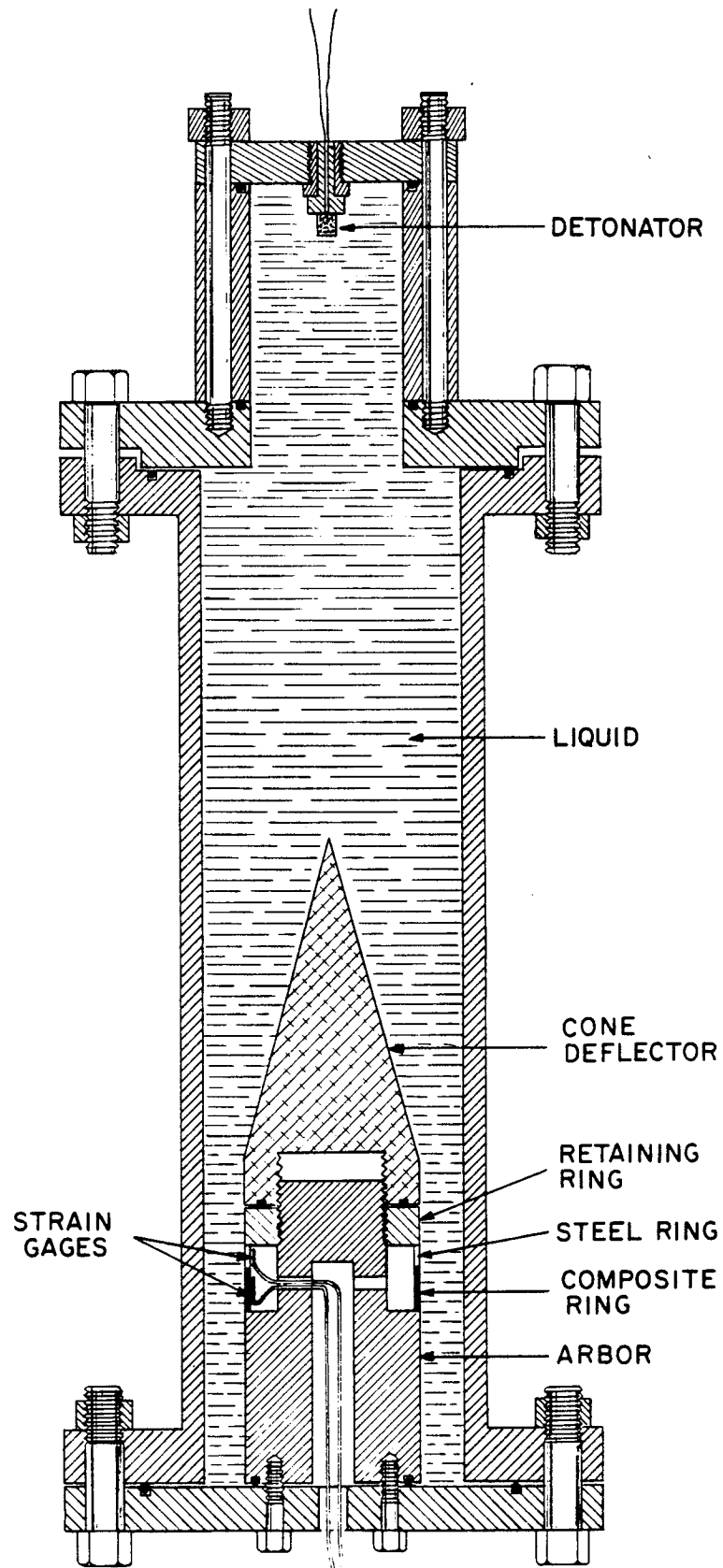


Figure 4-203. Fixture for dynamic compressive loading of composite ring specimens.

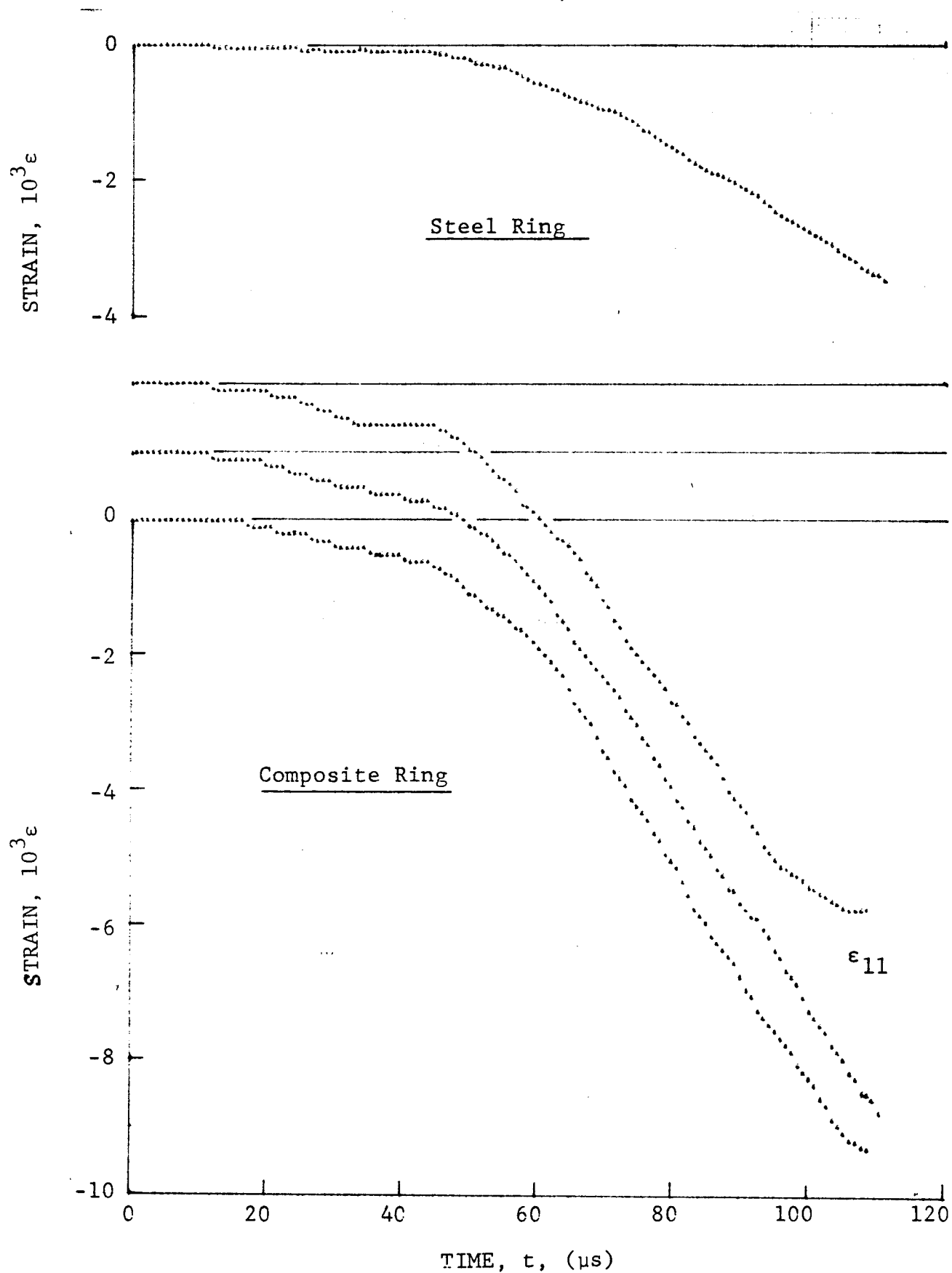


Figure 4-204. Strain records in steel ring and SP288/T300 $[O_6]$ graphite/epoxy ring under dynamic loading for Specimen No. 19-8 (1.56 g pistol powder, $KClO_4$, and aluminum dust).

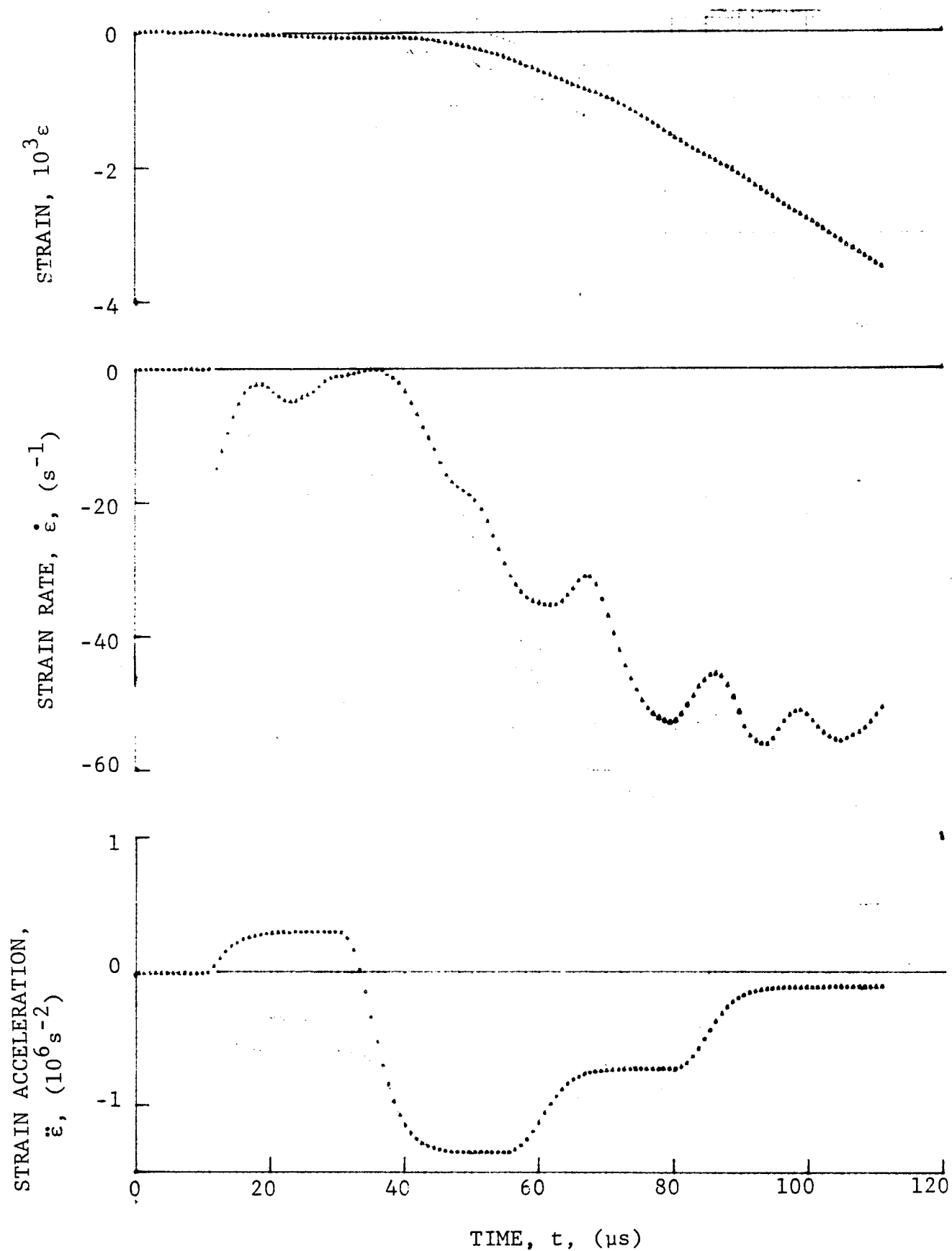
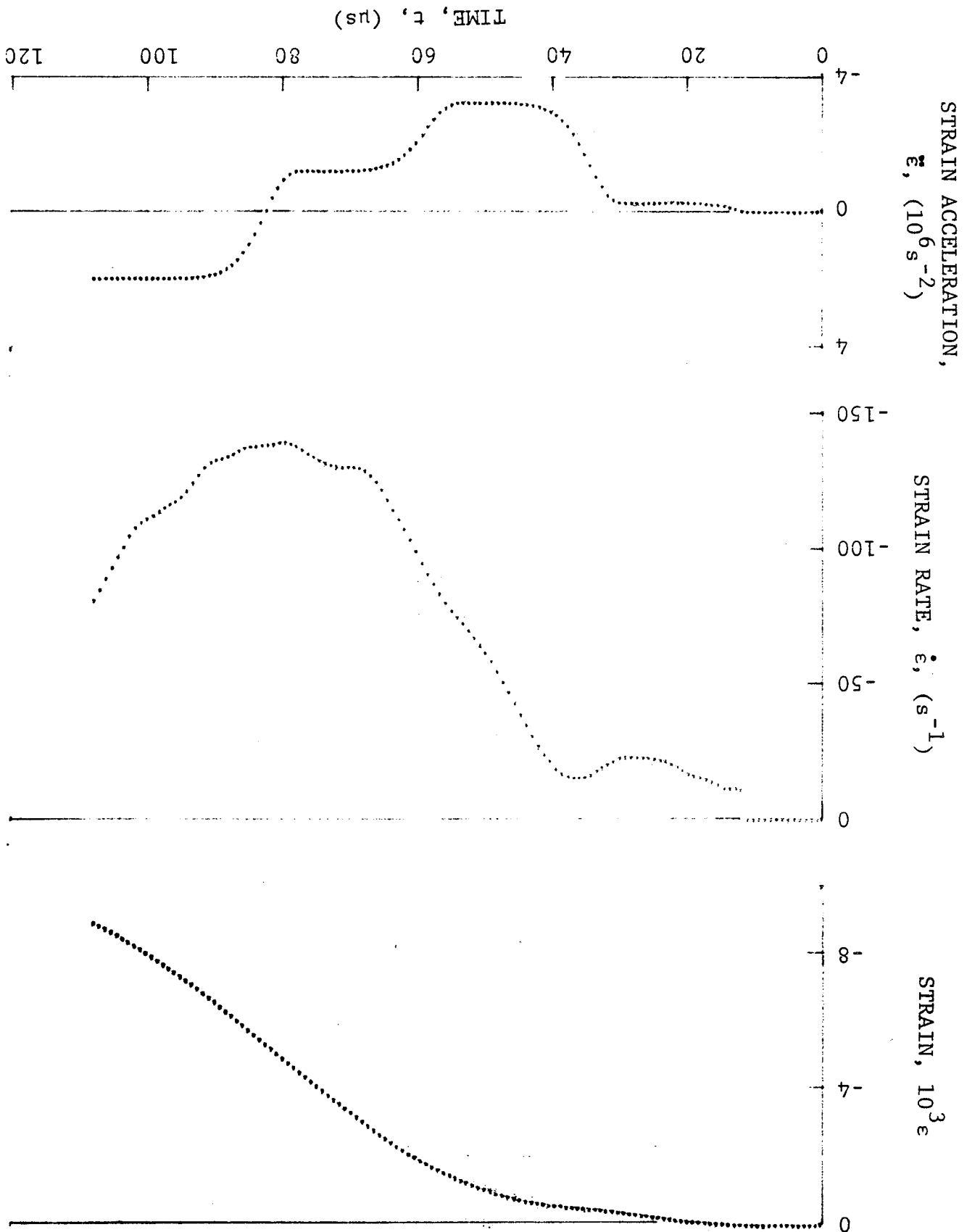


Figure 4-205. Strain and its derivatives in steel ring for Specimen No. 19-8.

Figure 4-206. Circumferential strain and its derivatives in SP288/T300 [06] graphite/epoxy ring under dynamic loading for Specimen No. 19-8 (1.56 g pistol powder, $KClO_4$, and aluminum dust).



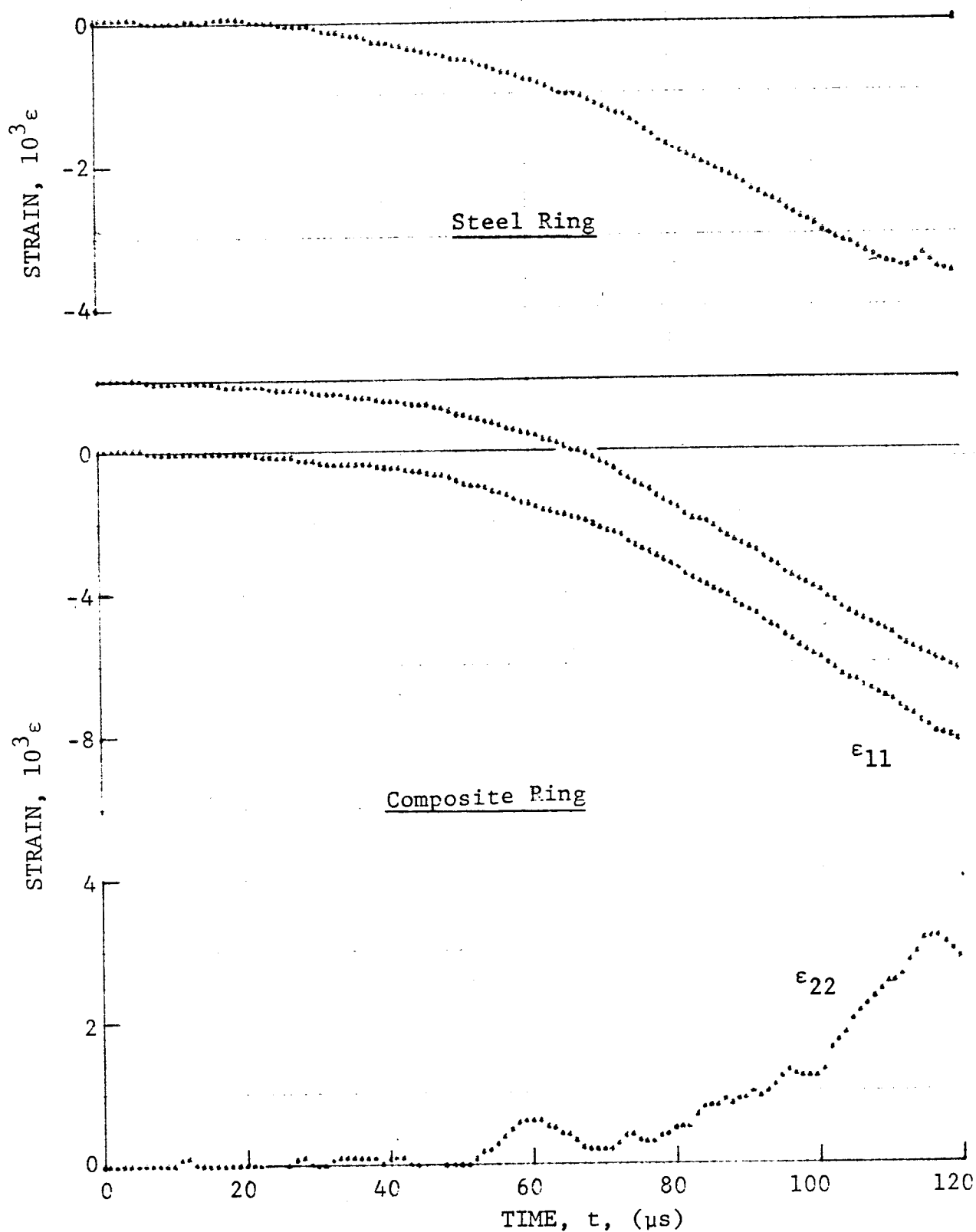


Figure 4-207. Strain records in steel ring and SP288/T300 $[0_6]$ graphite/epoxy ring under dynamic loading for Specimen No. 19-9 (1.56 g pistol powder, $KClO_4$, and aluminum dust).

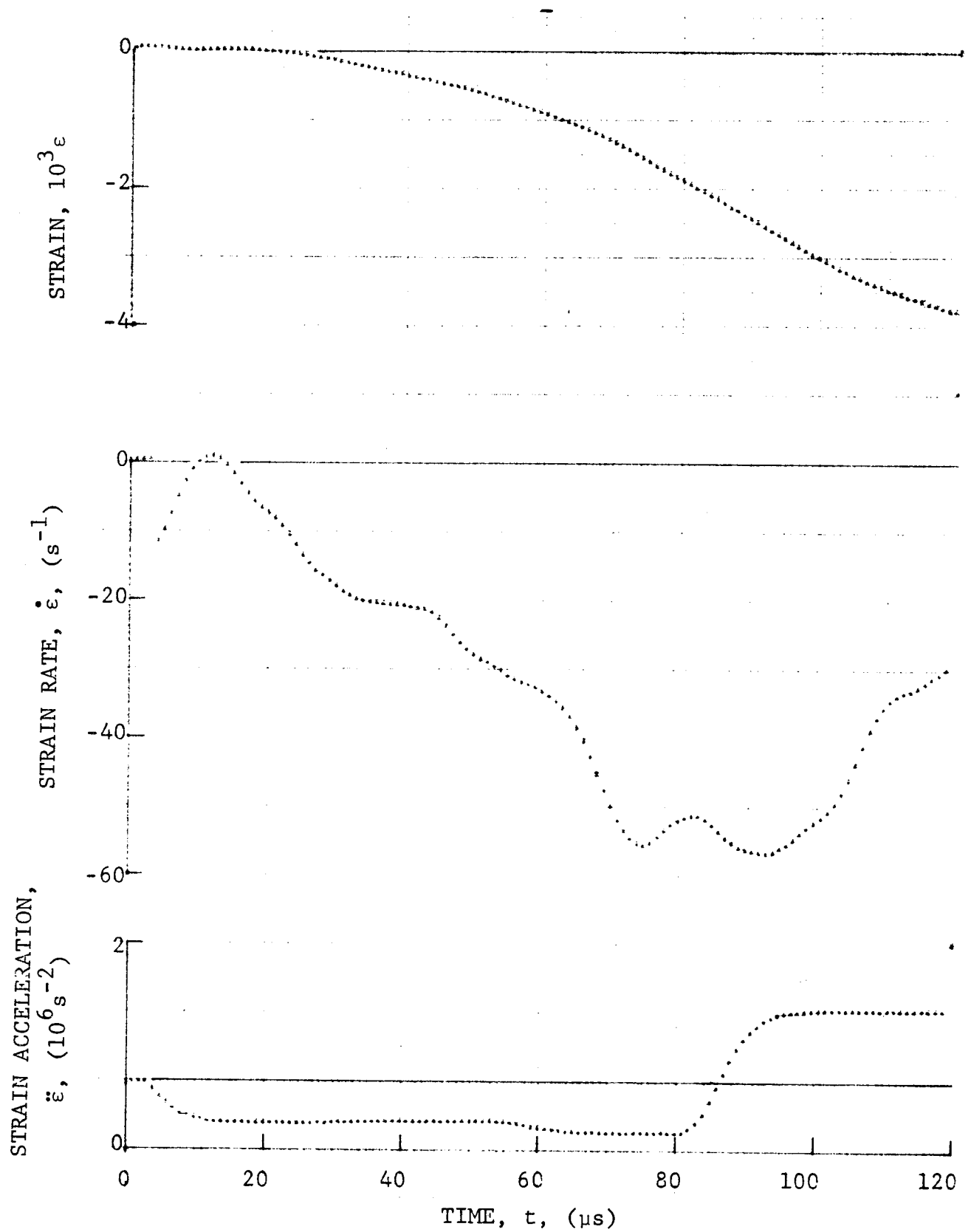


Figure 4-208. Strain and its derivatives in steel ring for Specimen No. 19-9.

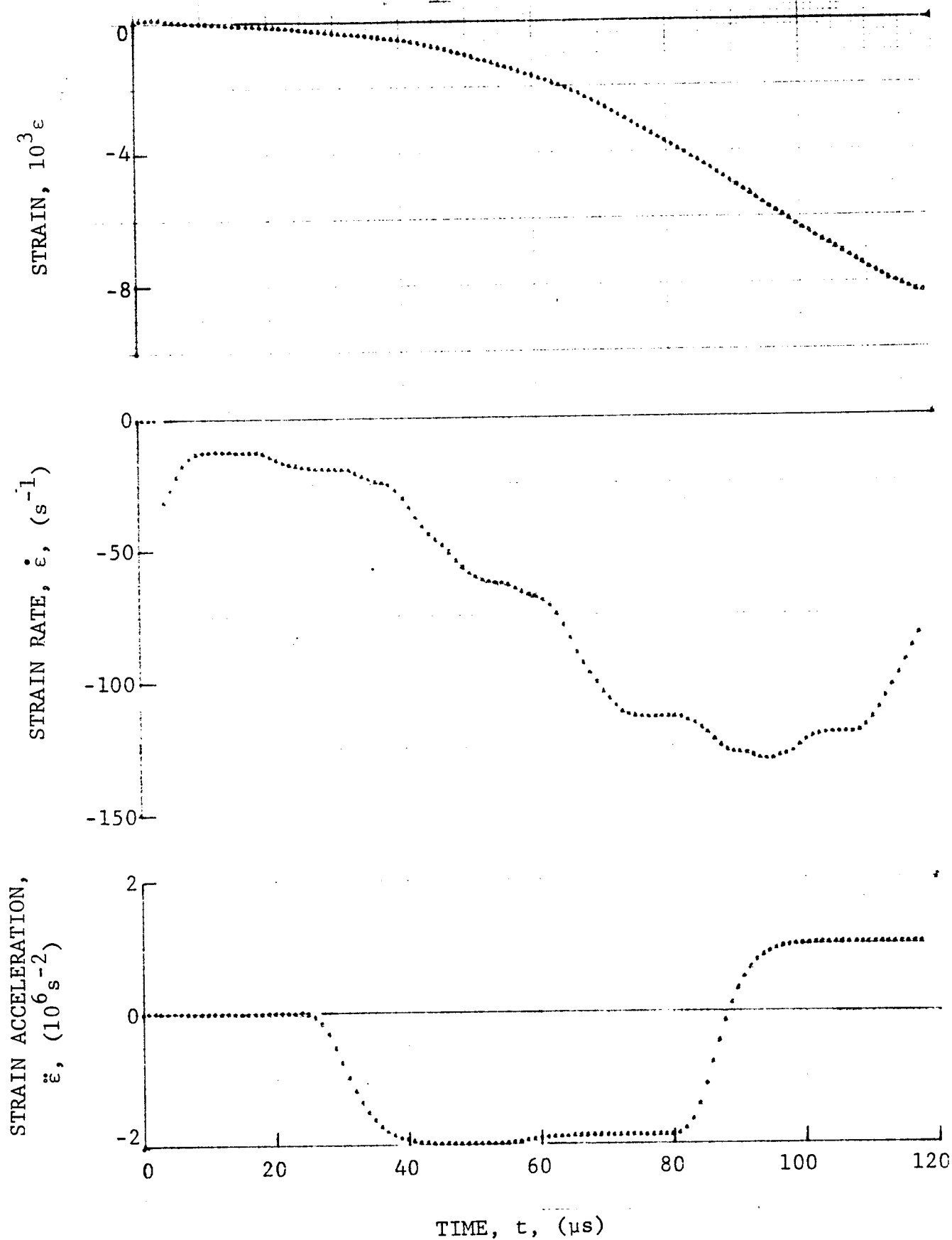


Figure 4-209. Circumferential strain and its derivatives in SP288/T300 $[O_6]$ graphite/epoxy ring under dynamic loading for Specimen No. 19-9 (1.56 g pistol powder, $KClO_4$, and aluminum dust).

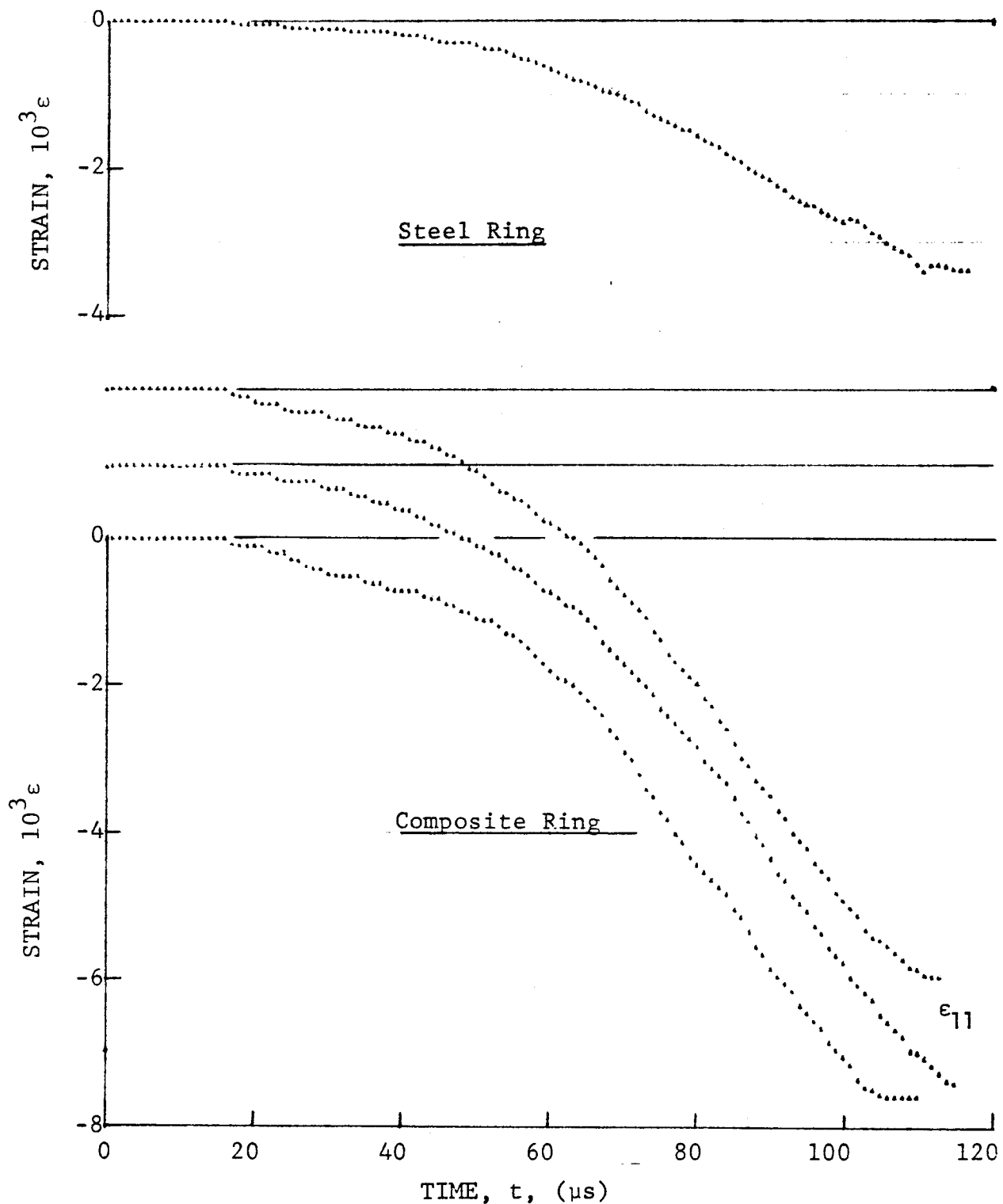


Figure 4-210. Strain records in steel ring and SP288/T300 $[0_6]$ graphite/epoxy ring under dynamic loading for Specimen No. 40-1 (1.56 pistol powder, $KClO_4$, and aluminum dust).

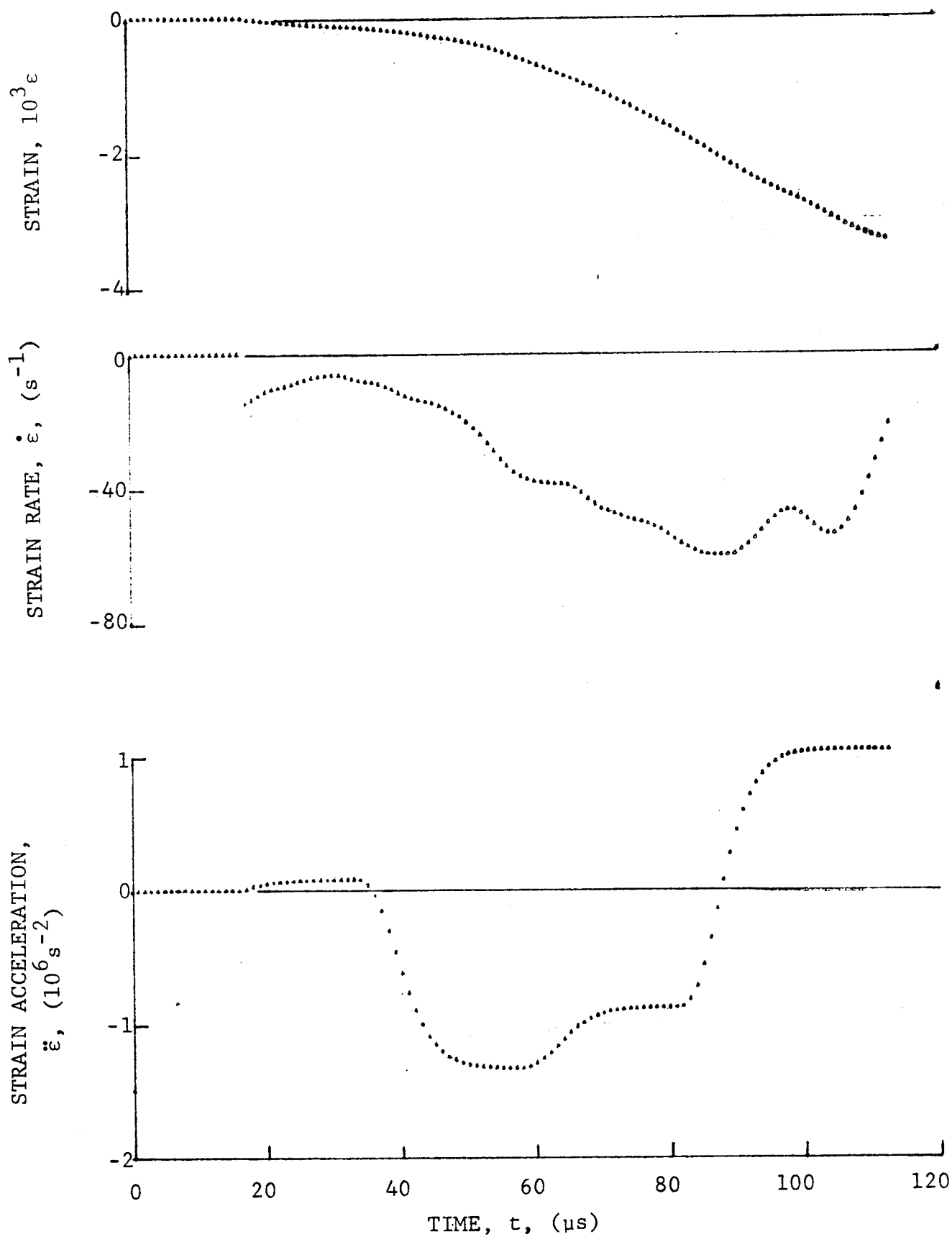


Figure 4-211. Strain and its derivatives in steel ring for Specimen No. 40-1.

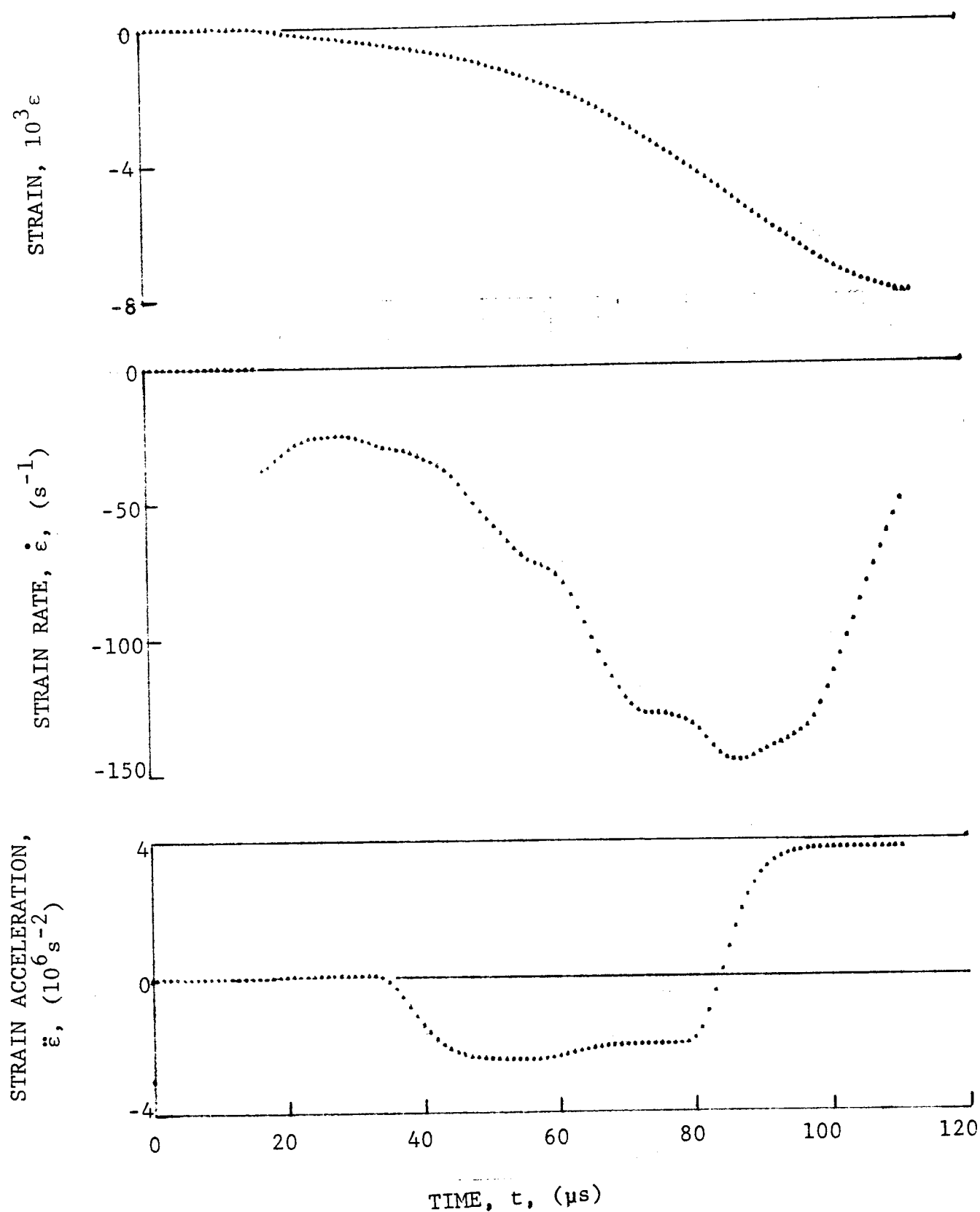
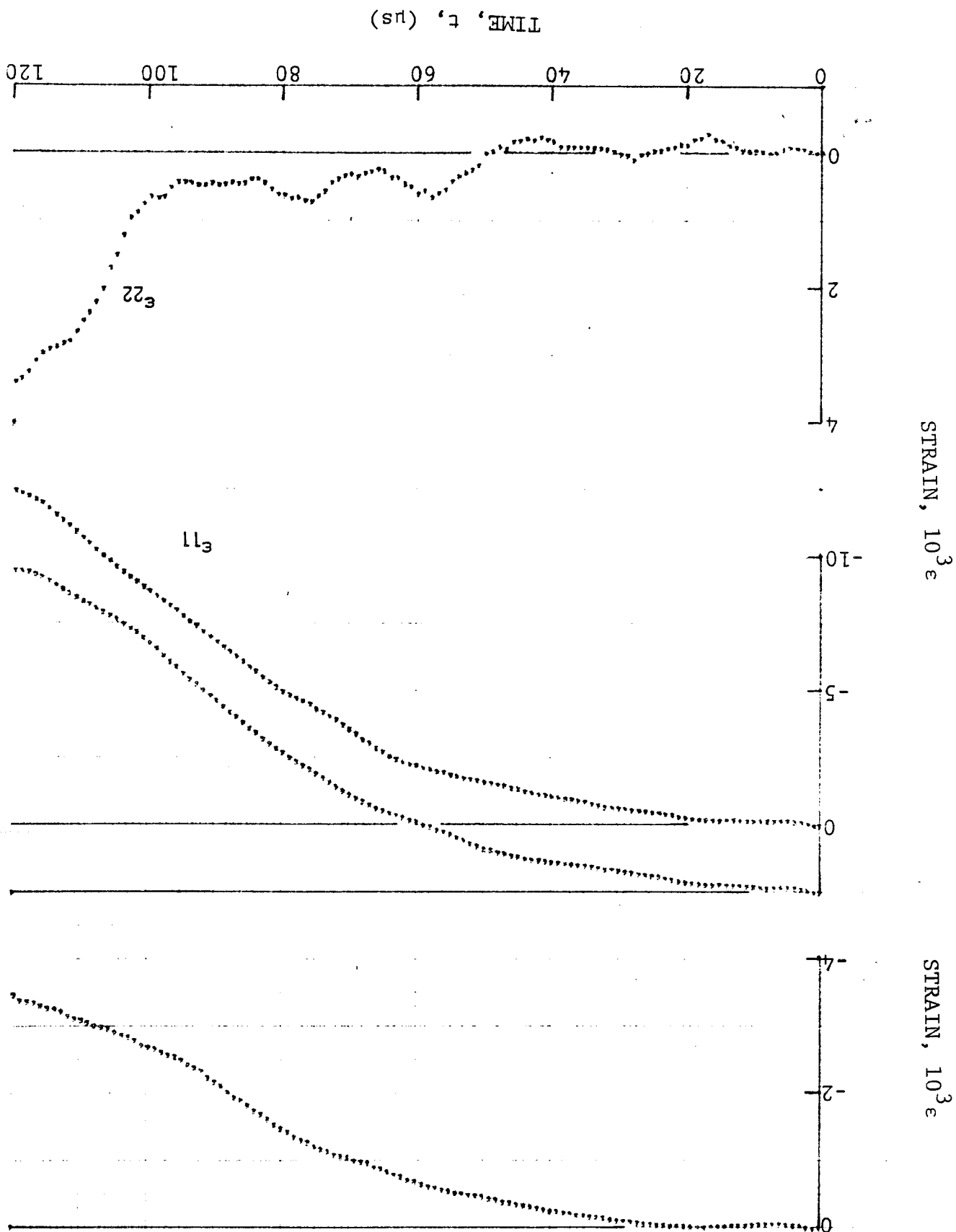


Figure 4-212. Circumferential strain and its derivatives in SP288/T300 $[0_6]$ graphite/epoxy ring under dynamic loading for Specimen No. 40-1 (1.56 g pistol powder, $KClO_4$, and aluminum dust).

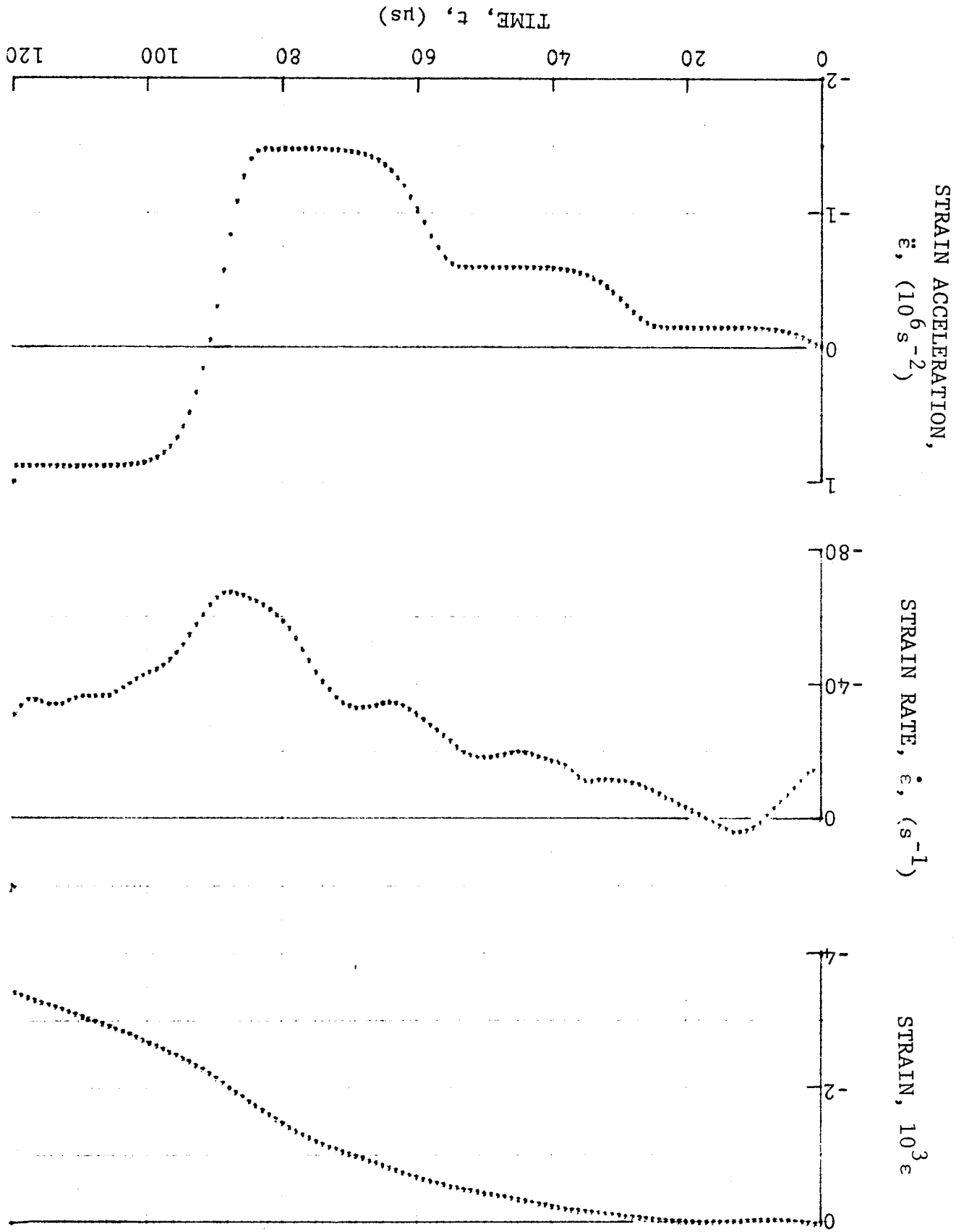
Figure 4-213. Strain records in steel ring and SP288/T300 [06] graphite/epoxy ring under dynamic loading for Specimen No. 40-2 (1.56 g pistol powder, $KClO_4$, and aluminum dust).

4-270



4-271

Figure 4-214. Strain and its derivatives in steel ring for Specimen No. 40-2.



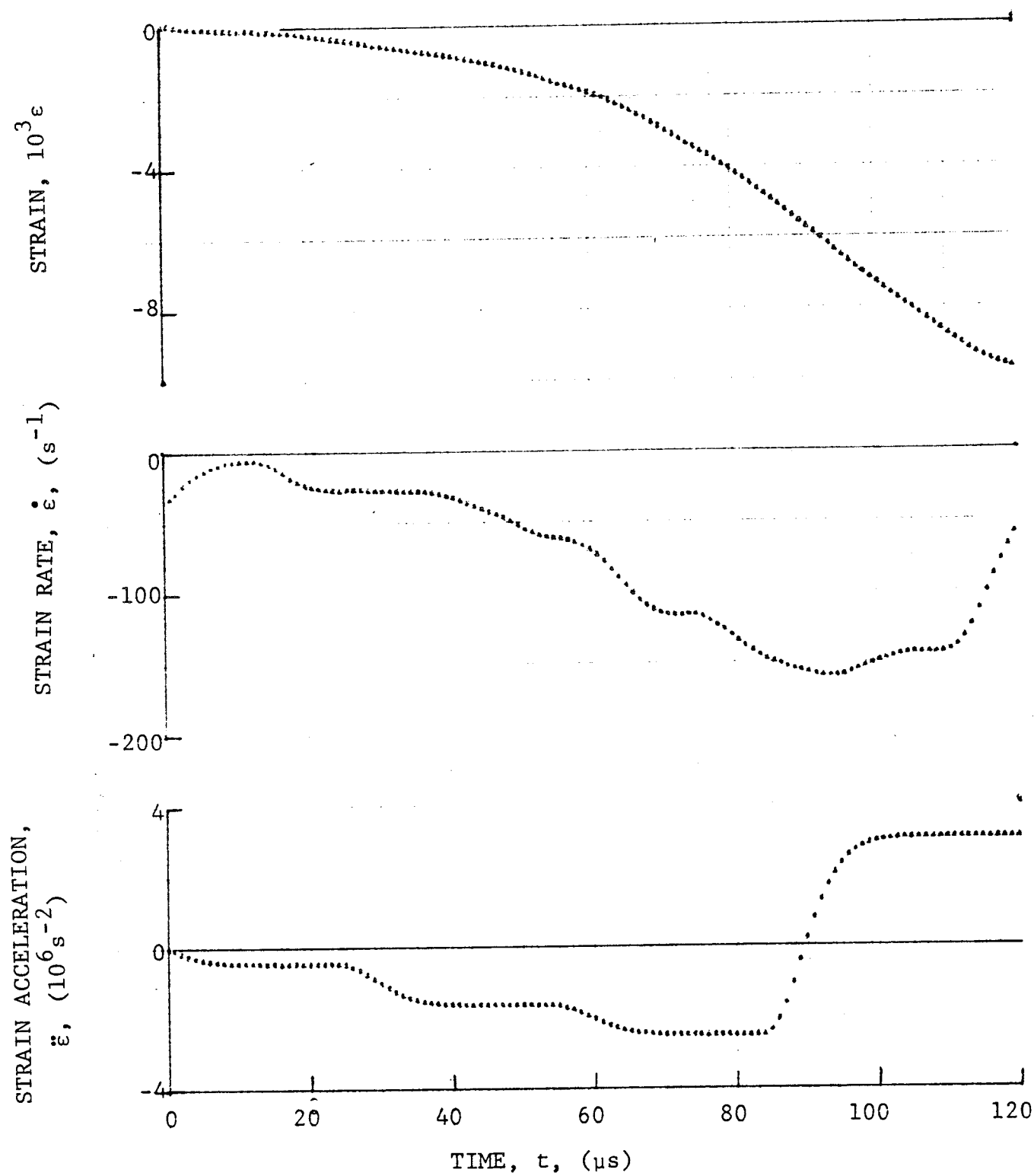


Figure 4-215. Circumferential strain and its derivatives in SP288/T300 $[0_6]$ graphite/epoxy ring under dynamic loading for Specimen No. 40-2 (1.56 g pistol powder, $KClO_4$, and aluminum dust).

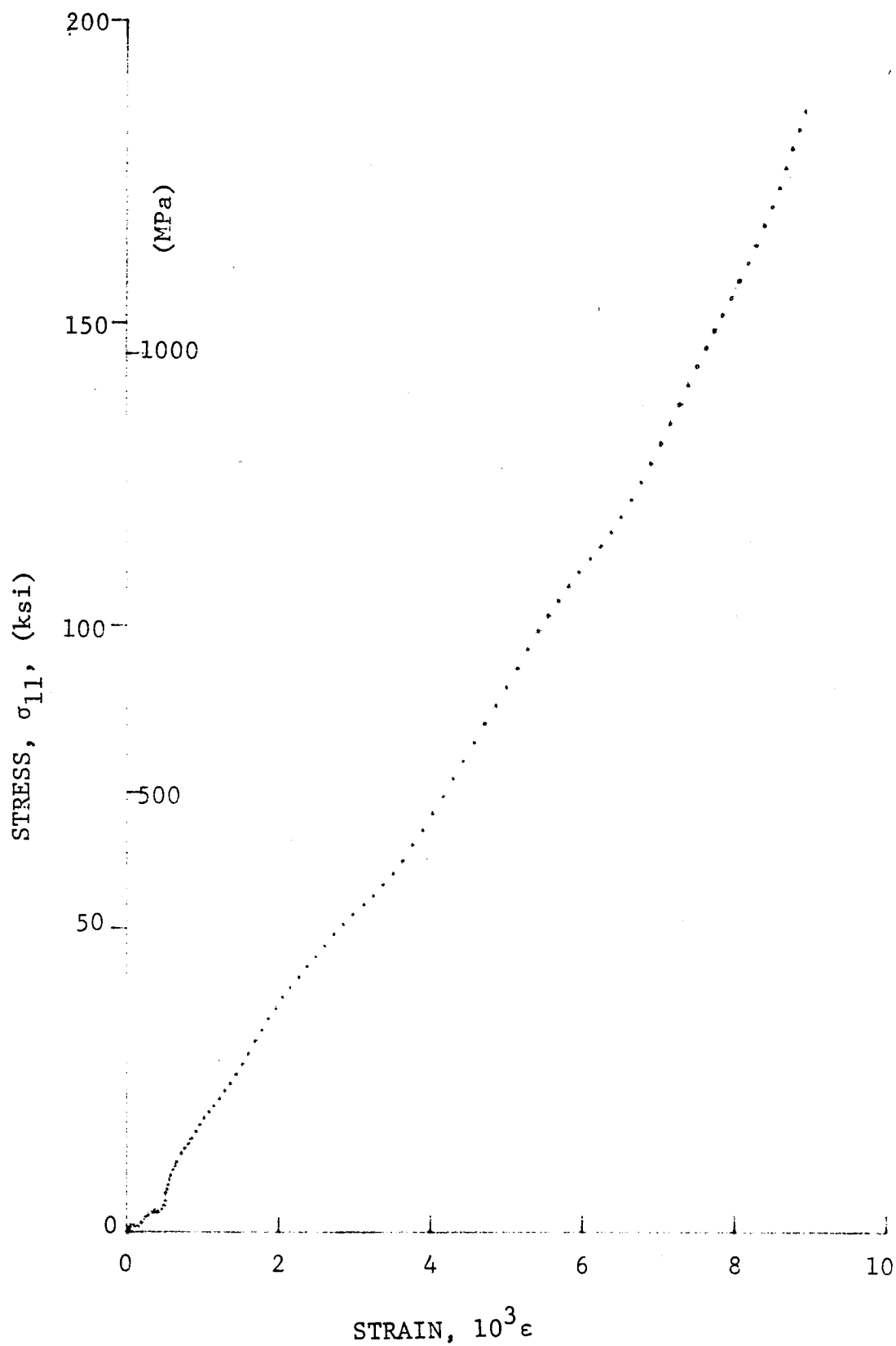


Figure 4-216. Stress-strain curve for SP288/T300 $[0_6]$ graphite/epoxy ring loaded in dynamic compression, Specimen No. 19-8 (1.56 g pistol powder, $KClO_4$, and aluminum dust).

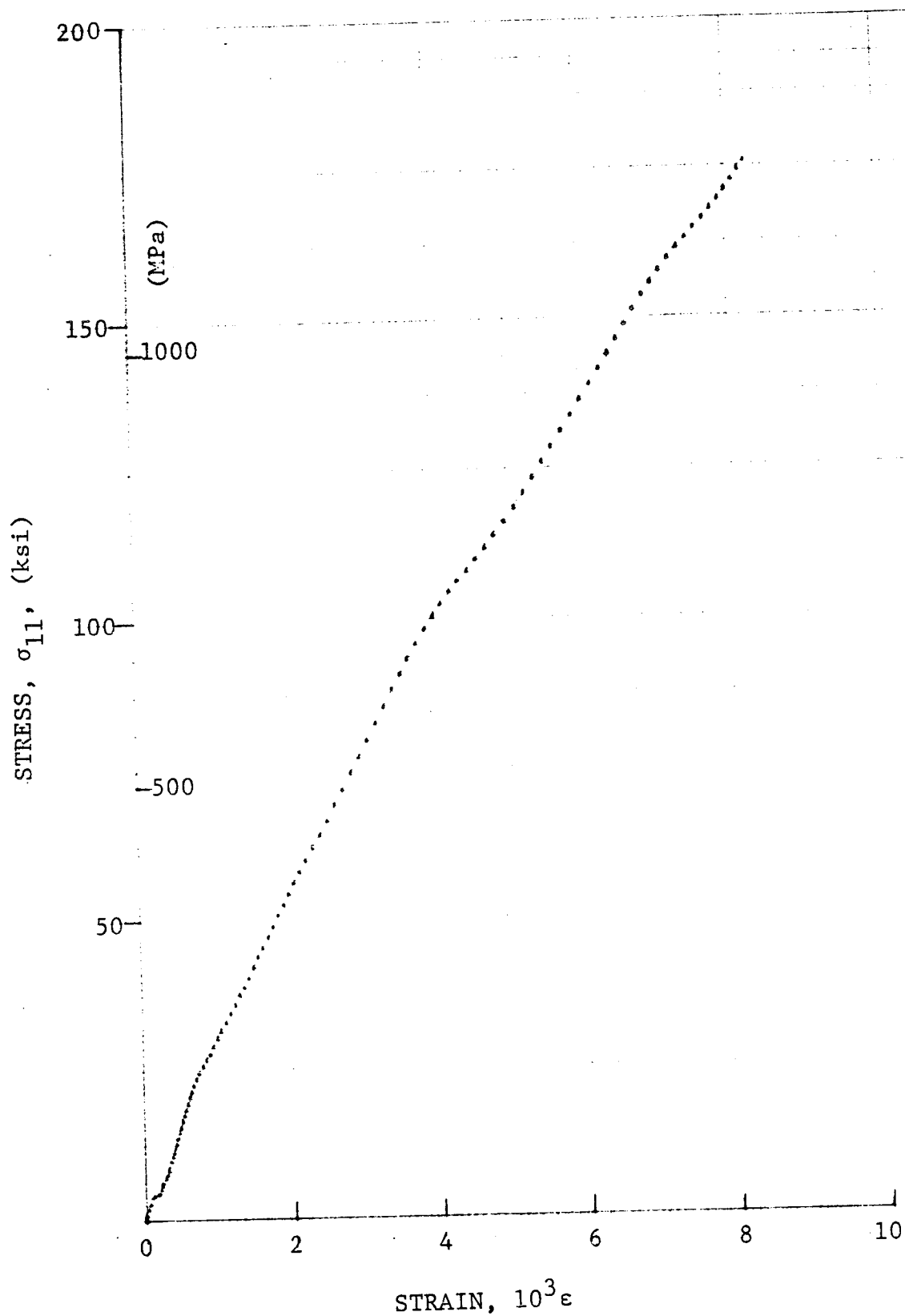


Figure 4-217. Stress-strain curve for SP288/T300 $[0_6]$ graphite/epoxy ring loaded in dynamic compression, Specimen No. 19-9 (1.56 g pistol powder, $KClO_4$, and aluminum dust).

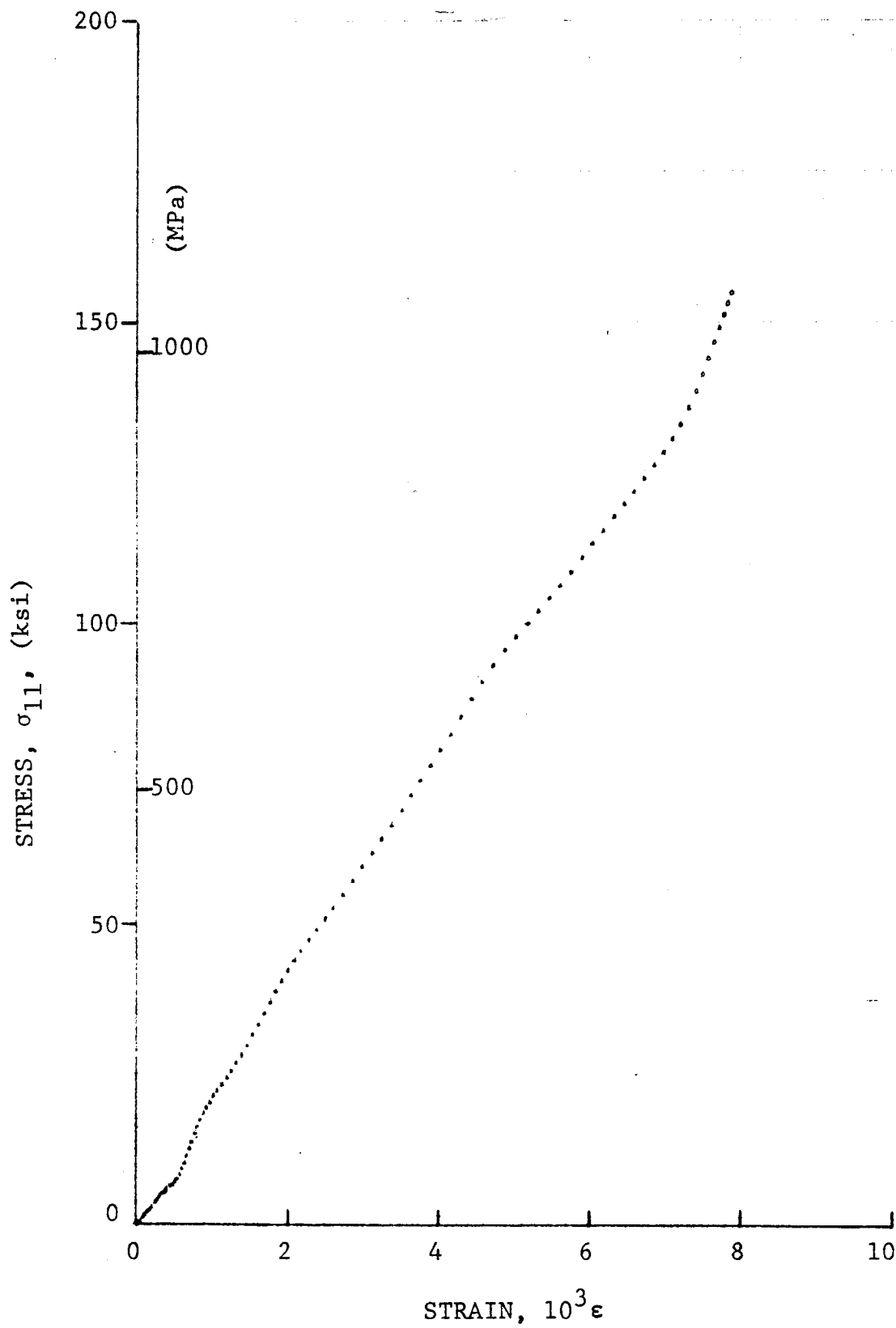


Figure 4-218. Stress-strain curve for SP288/T300 [0₆] graphite/epoxy ring loaded in dynamic compression, Specimen No. 40-1 (1.56 g pistol powder, KClO₄, and aluminum dust).

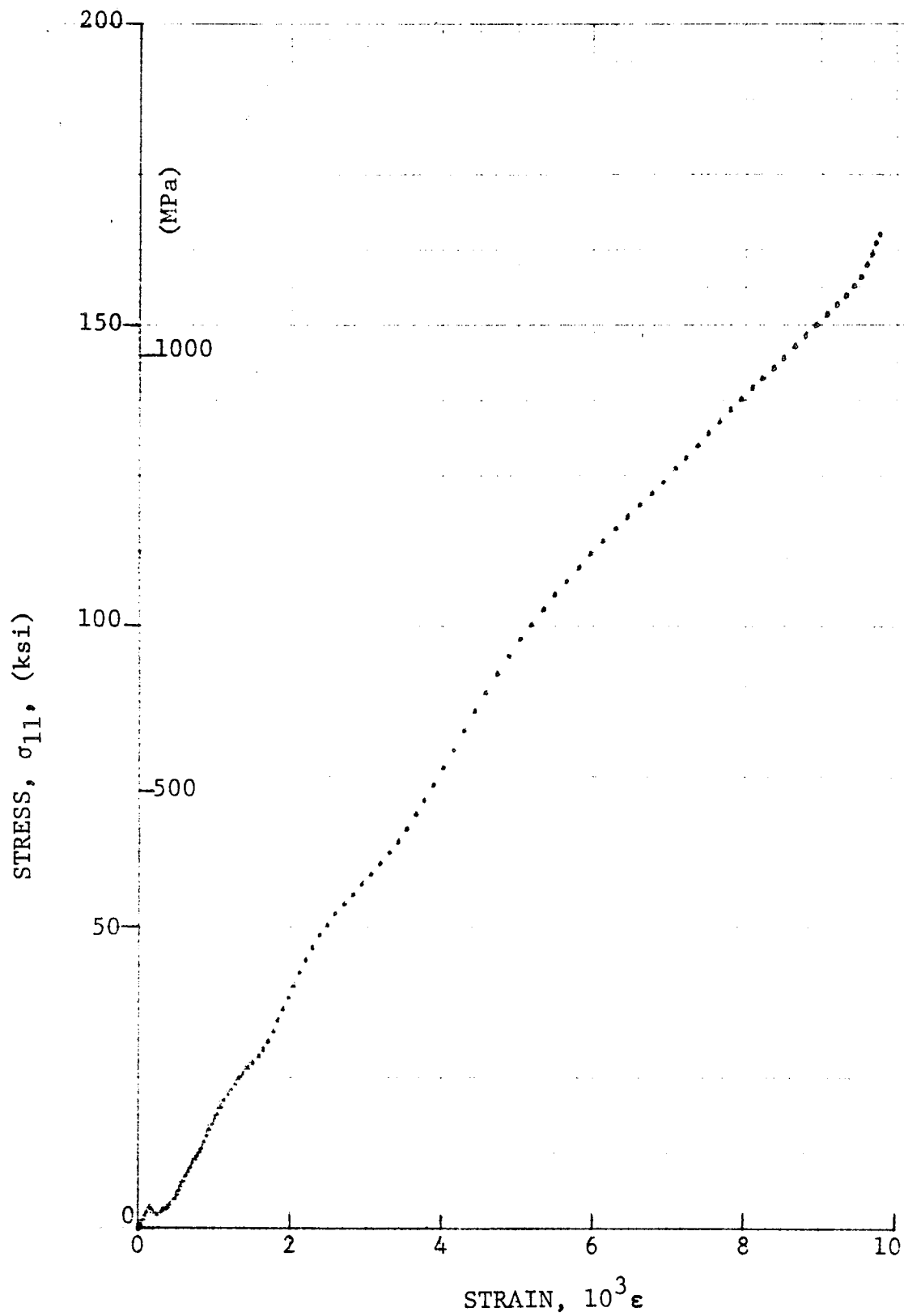


Figure 4-219. Stress-strain curve for SP288/T300 $[0_6]$ graphite/epoxy ring loaded in dynamic compression, Specimen No. 40-2 (1.56 g pistol powder, $KClO_4$, and aluminum dust).

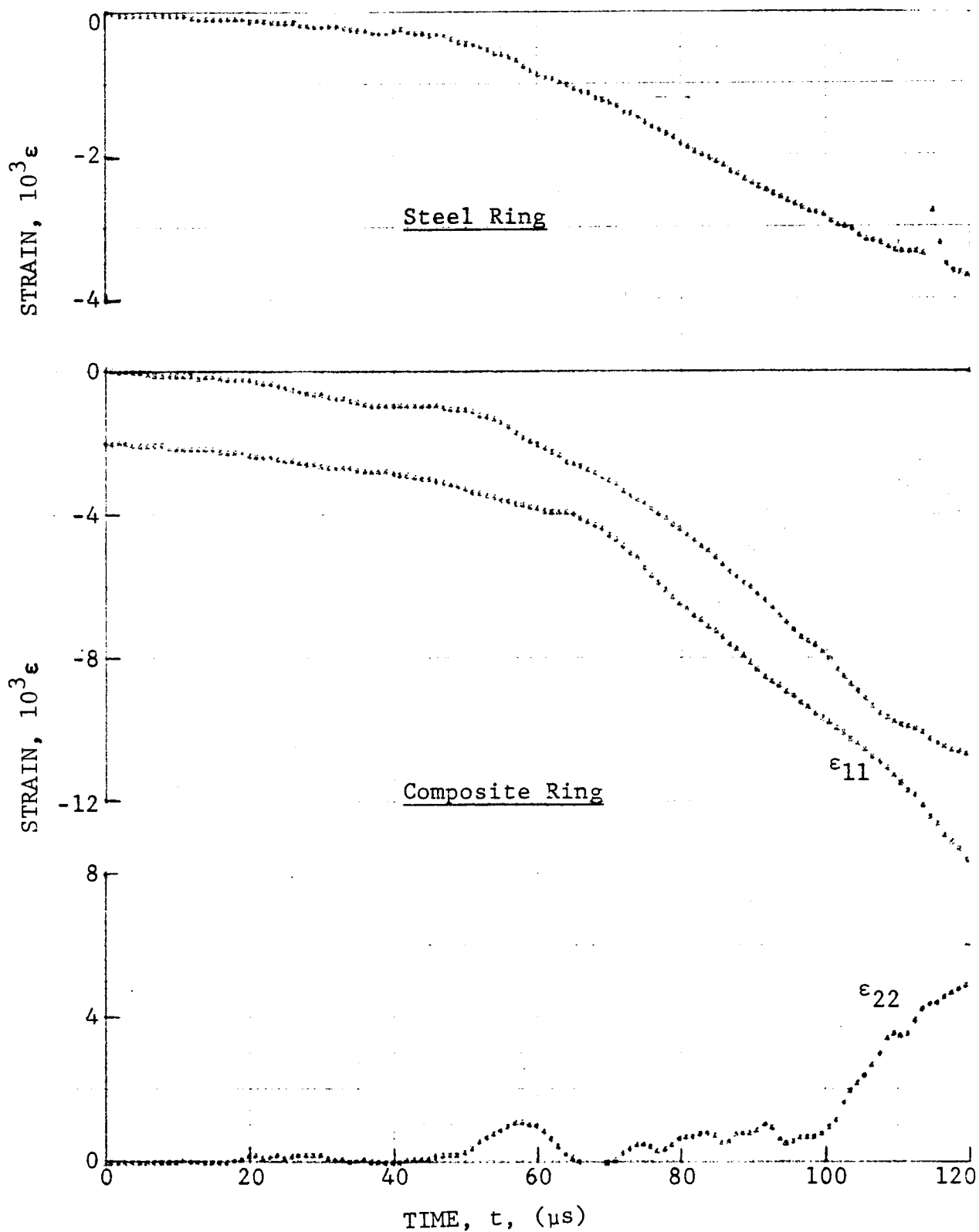


Figure 4-220. Strain records in steel ring and $[0_6]$ SP288/AS graphite/epoxy ring under dynamic loading for Specimen No. 45-2 (1.56 g pistol powder, $KClO_4$, and aluminum dust).

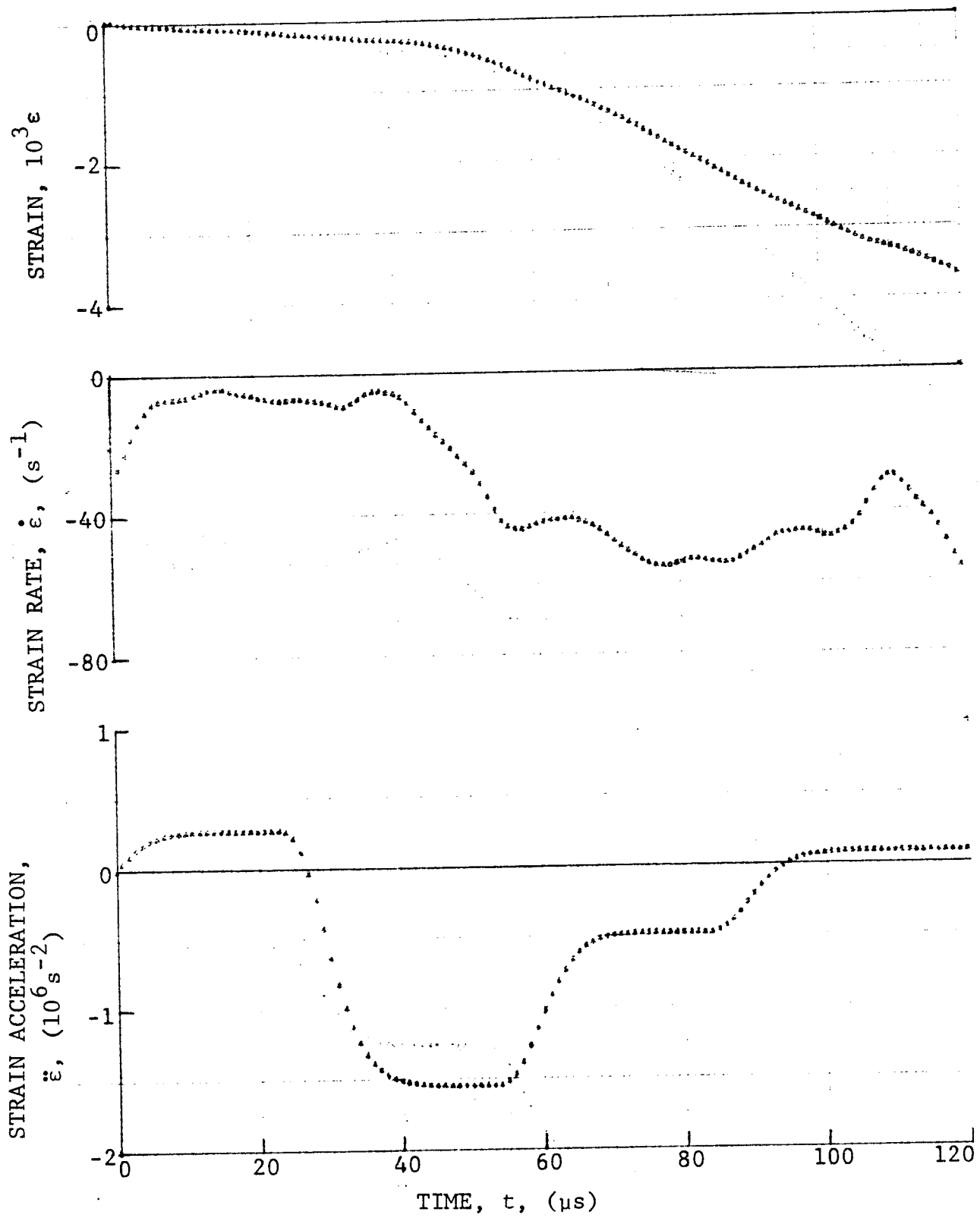


Figure 4-221. Strain and its derivatives in steel ring for Specimen No. 45-2.

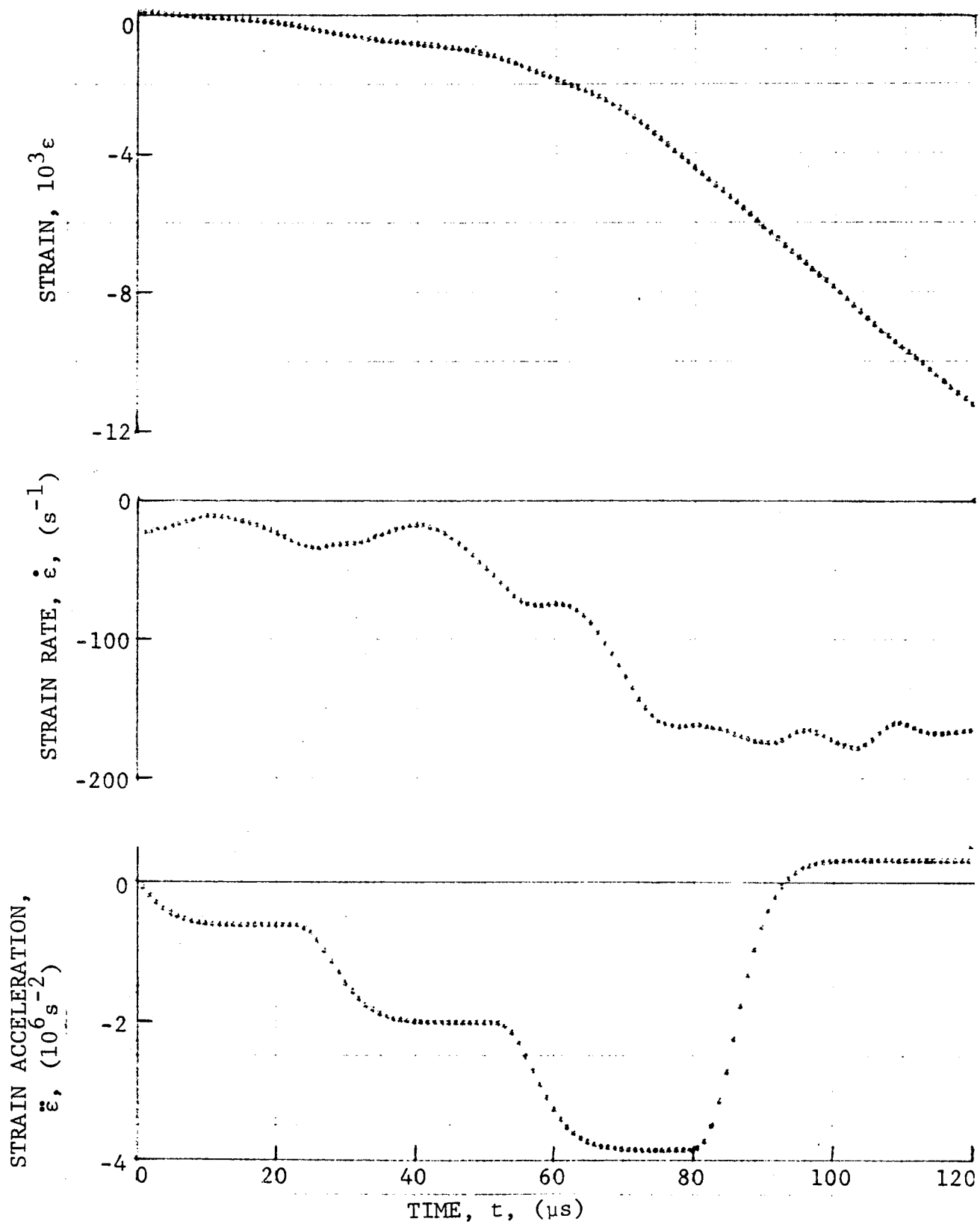
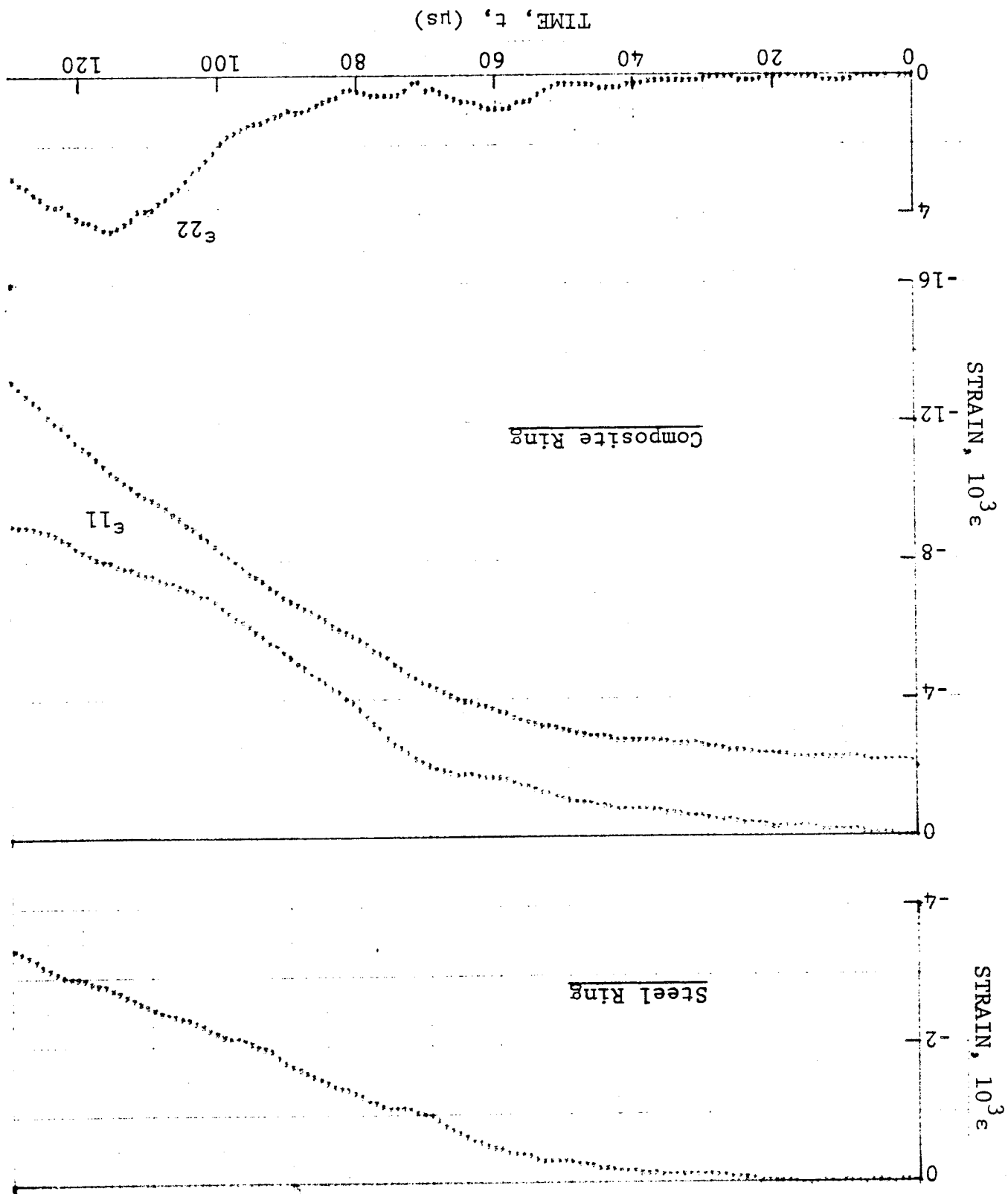


Figure 4-222. Circumferential strain and its derivatives in $[0_6]$ SP288/AS graphite/epoxy ring under dynamic loading for Specimen NO. 45-2 (1.56 g pistol powder, KClO_4 , and aluminum dust).

Figure 4-223. Strain records in steel ring and [0₆] SP288/AS graphite/epoxy ring under dynamic loading for Specimen No. 45-3 (1.56 g pistol powder, KClO₄, and aluminum dust).



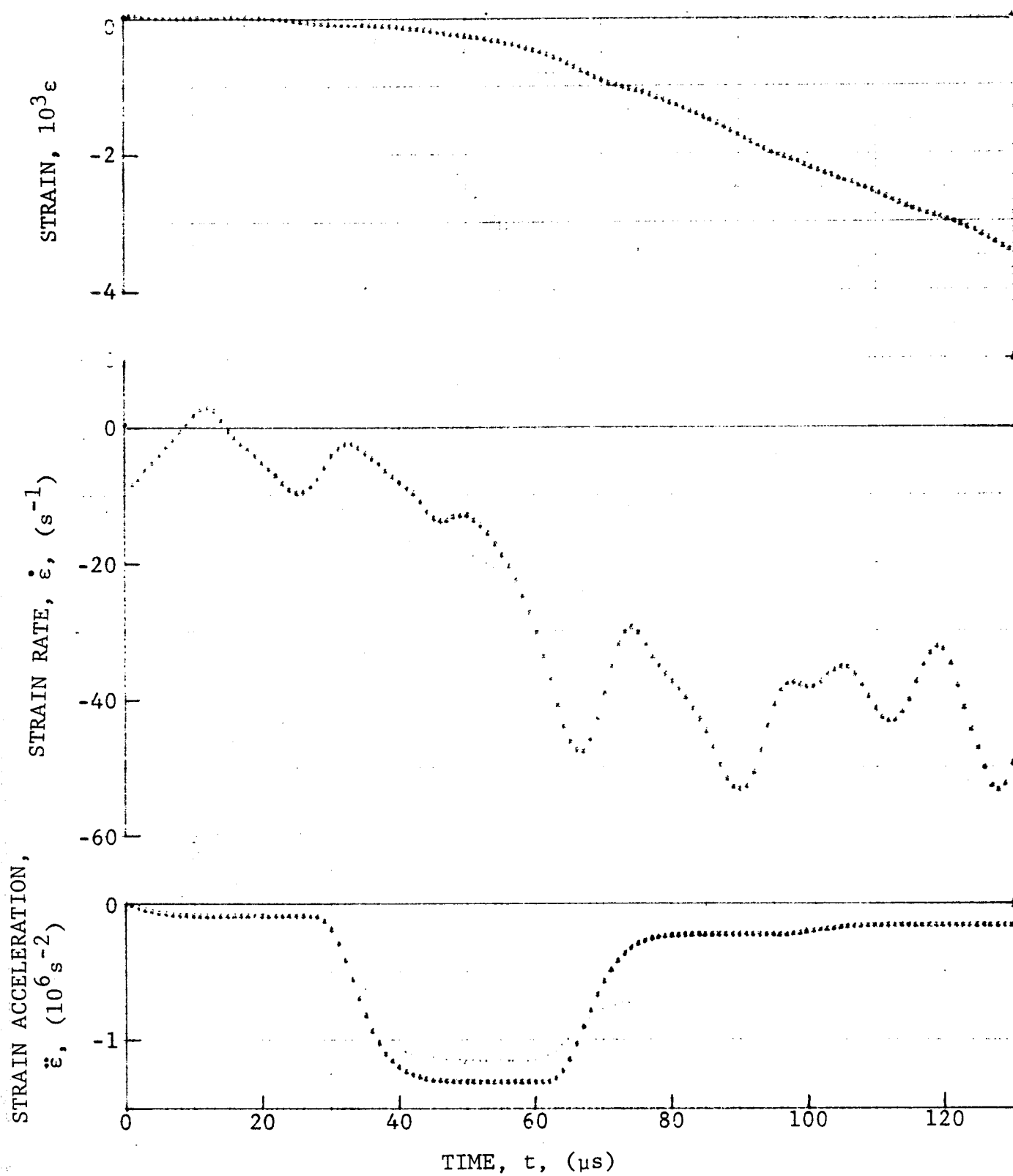


Figure 4-224. Strain and its derivatives in steel ring for Specimen No. 45-3.

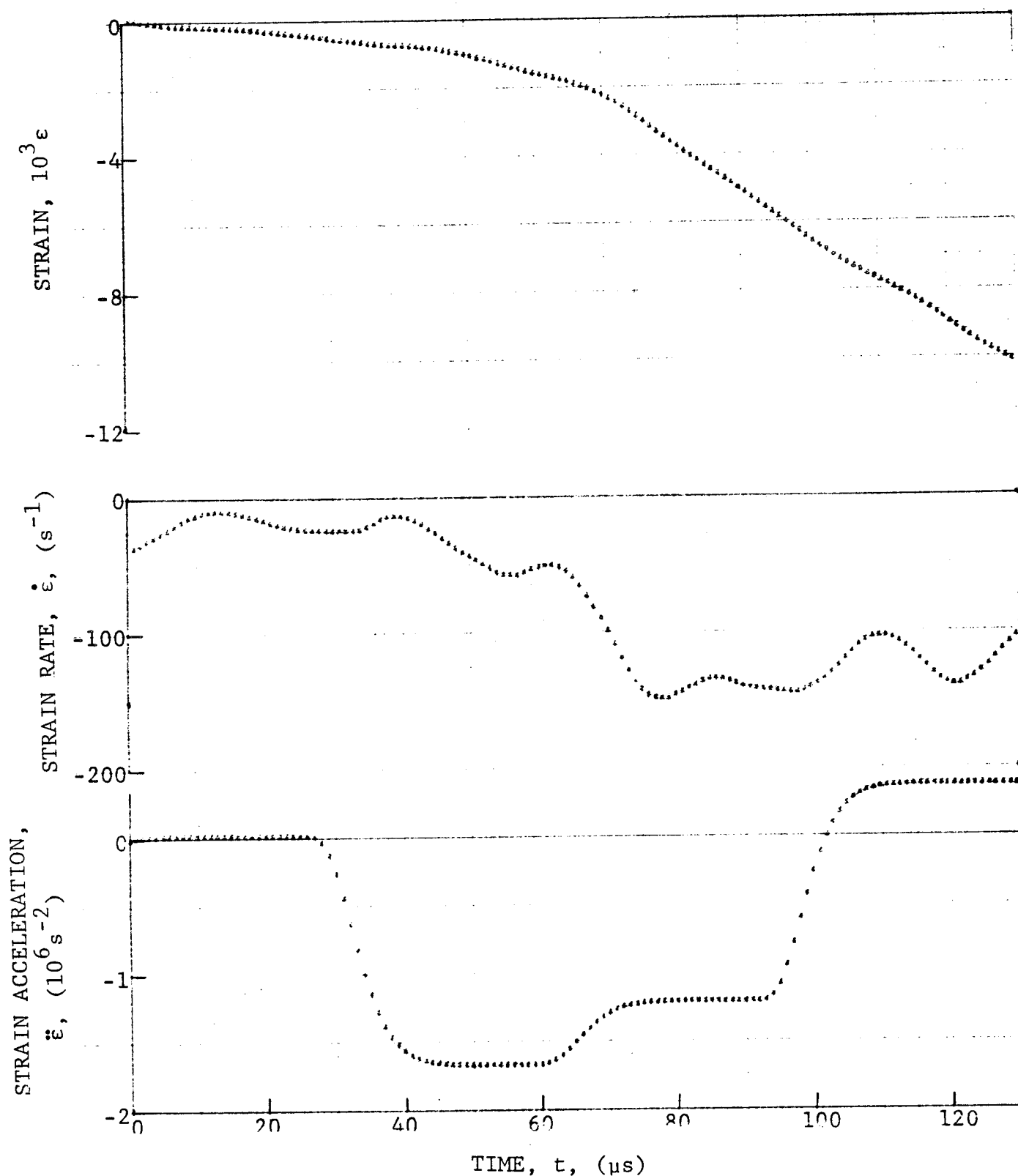


Figure 4-225. Circumferential strain and its derivatives in $[0_6]$ SP288/AS graphite/epoxy ring under dynamic loading for Specimen No. 45-3 (1.56 g pistol powder, KClO_4 , and aluminum dust).

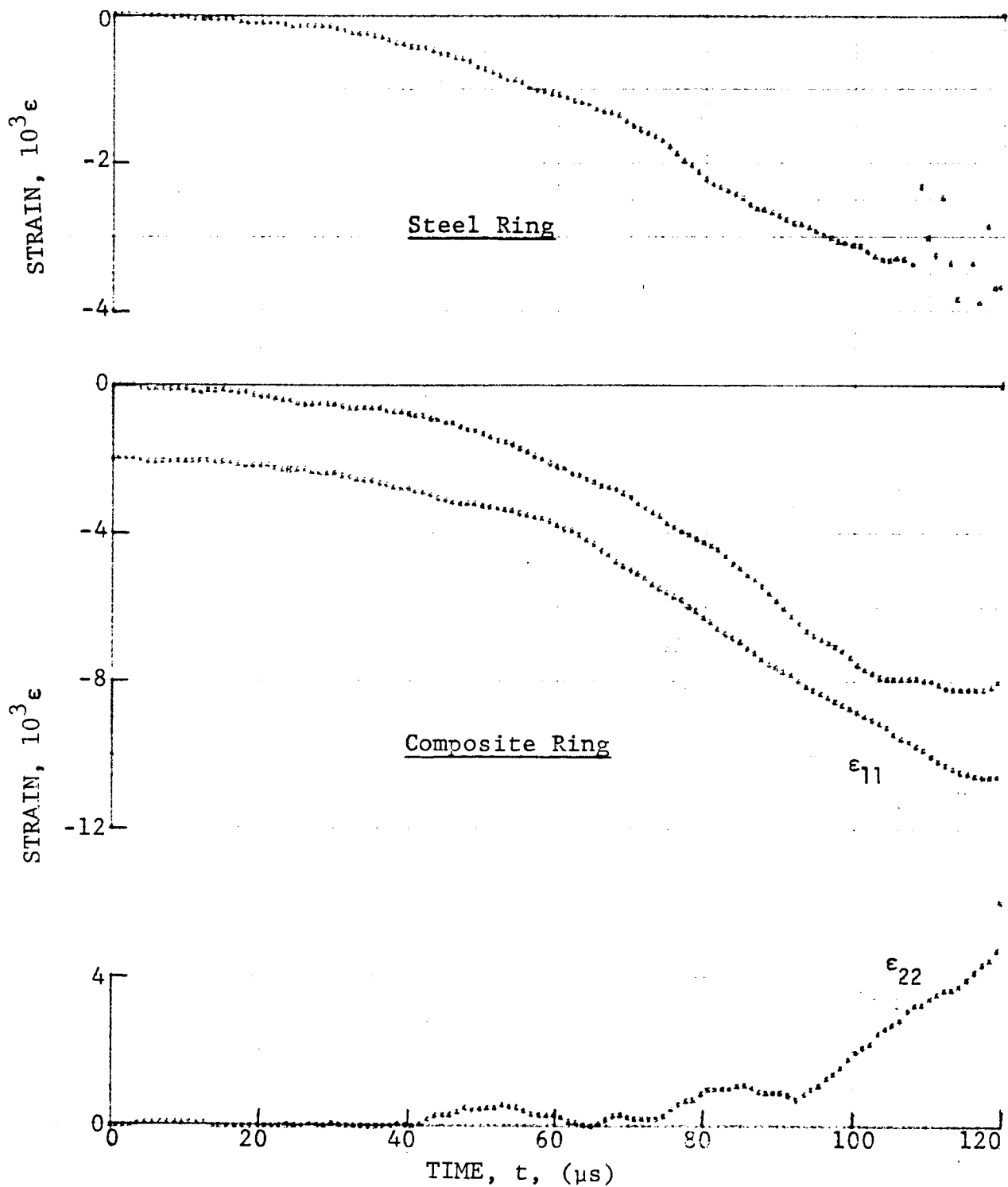


Figure 4-226. Strain records in steel ring and $[0_6]$ SP288/AS graphite/epoxy ring under dynamic loading for Specimen No. 45-4 (1.56 g pistol powder, $KClO_4$, and aluminum dust).

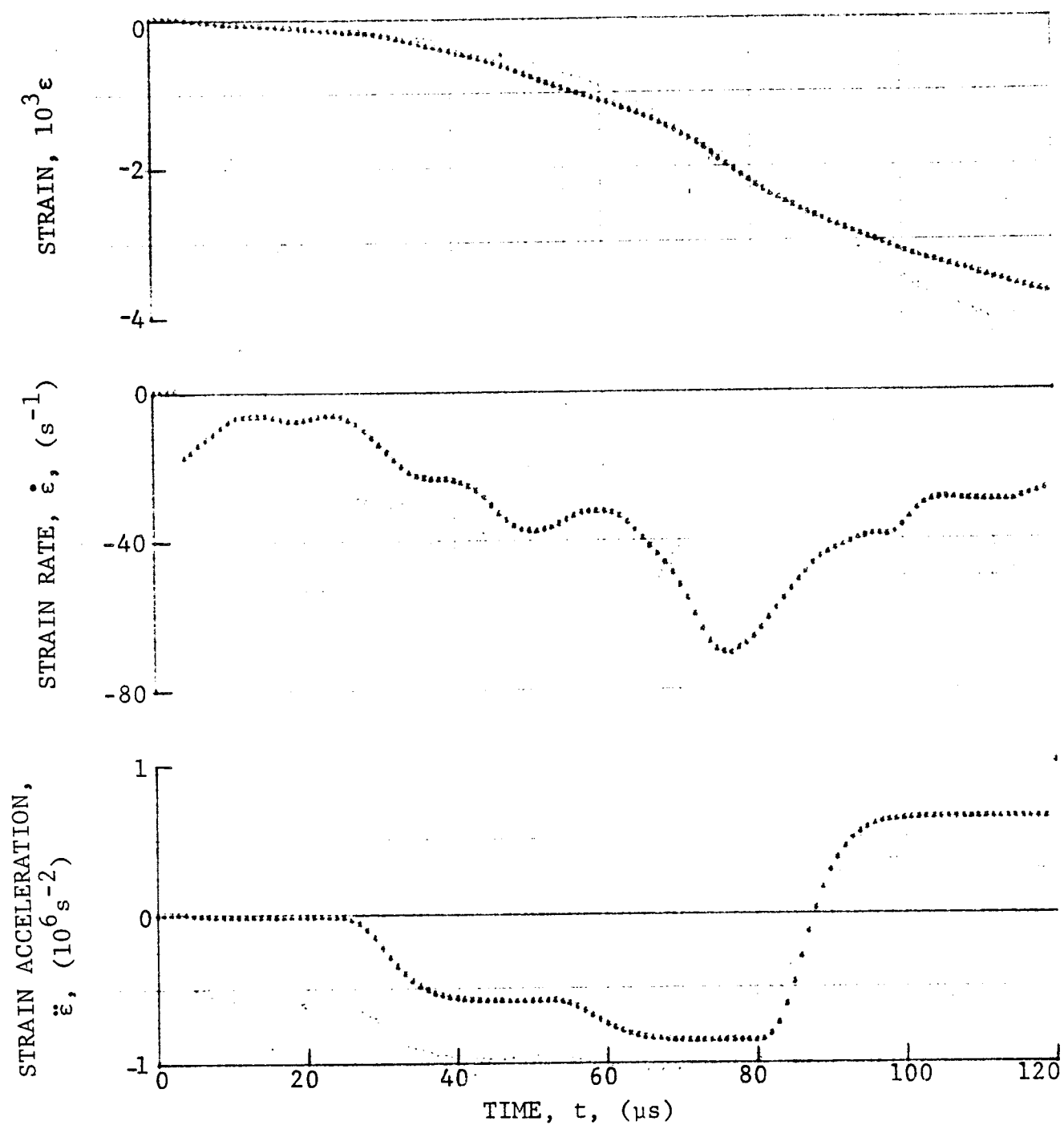


Figure 4-227. Strain and its derivatives in steel ring for Specimen No. 45-4.

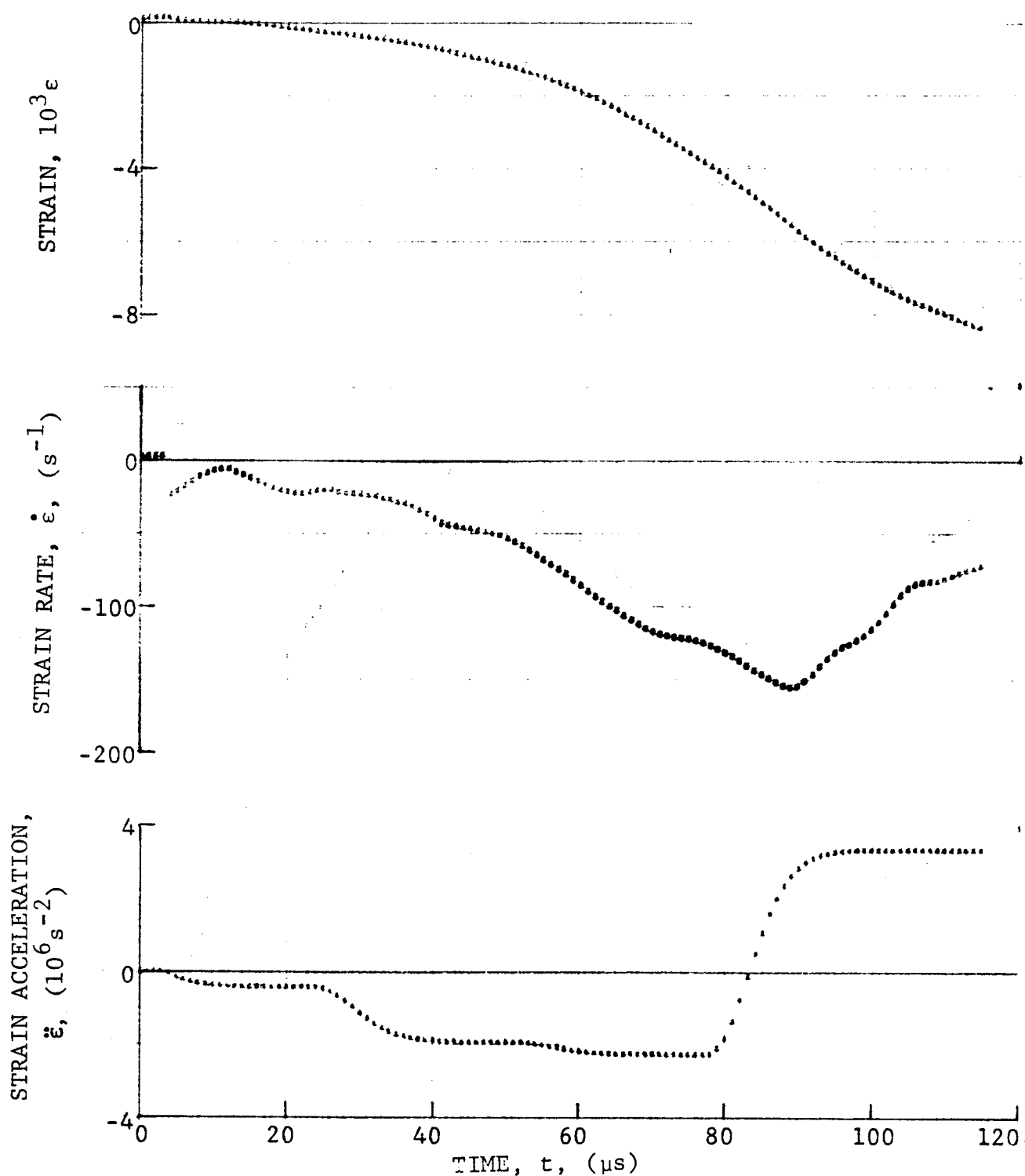


Figure 4-228. Circumferential strain and its derivatives in [06] SP288/AS graphite/epoxy ring under dynamic loading for Specimen No. 45-4 (1.56 g pistol powder, $KClO_4$, and aluminum dust).

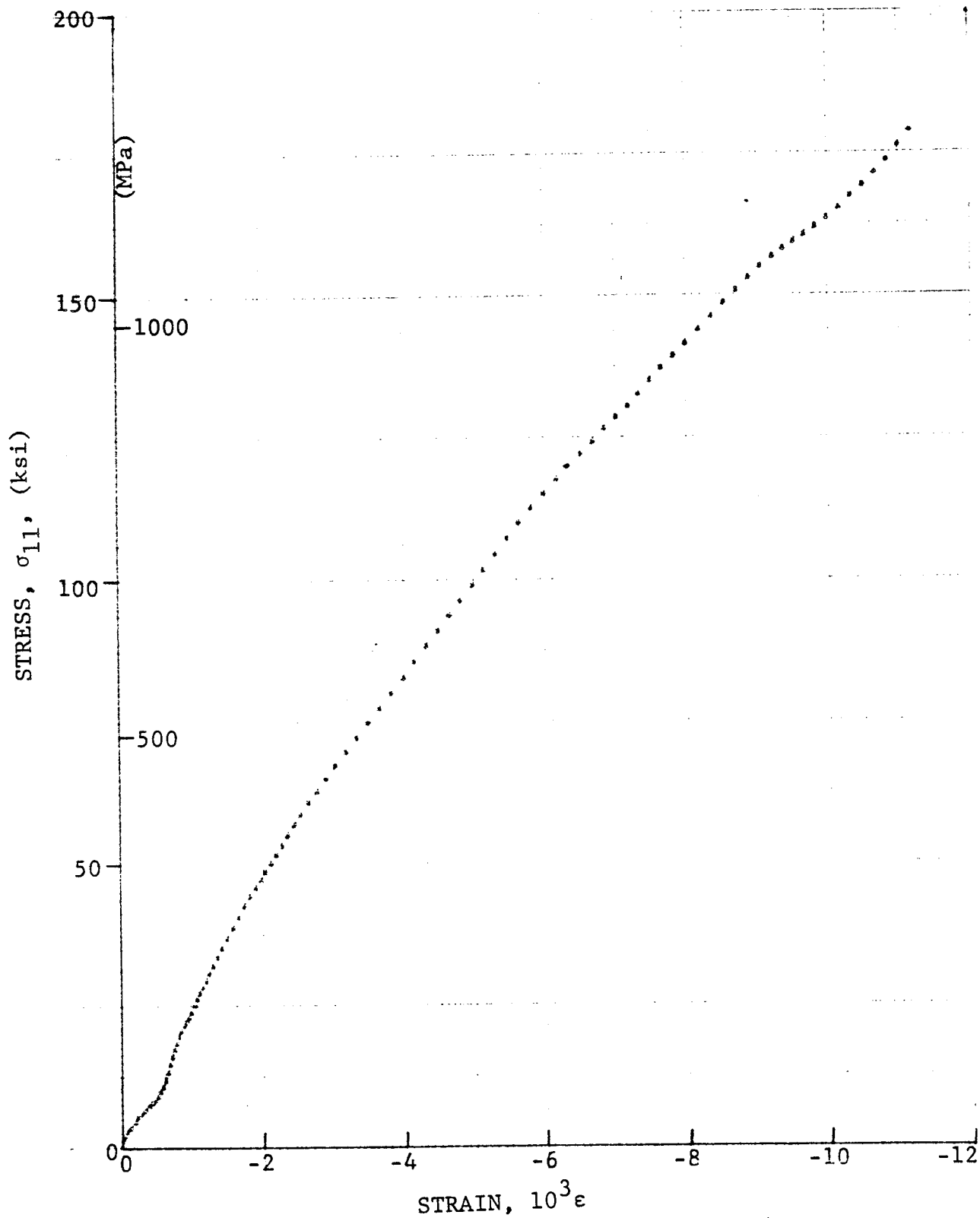


Figure 4-229. Stress-strain curve for $[0_6]$ SP288/AS graphite/epoxy ring loaded in dynamic compression, Specimen No. 45-2 (1.56 g pistol powder, $KClO_4$, and aluminum dust).

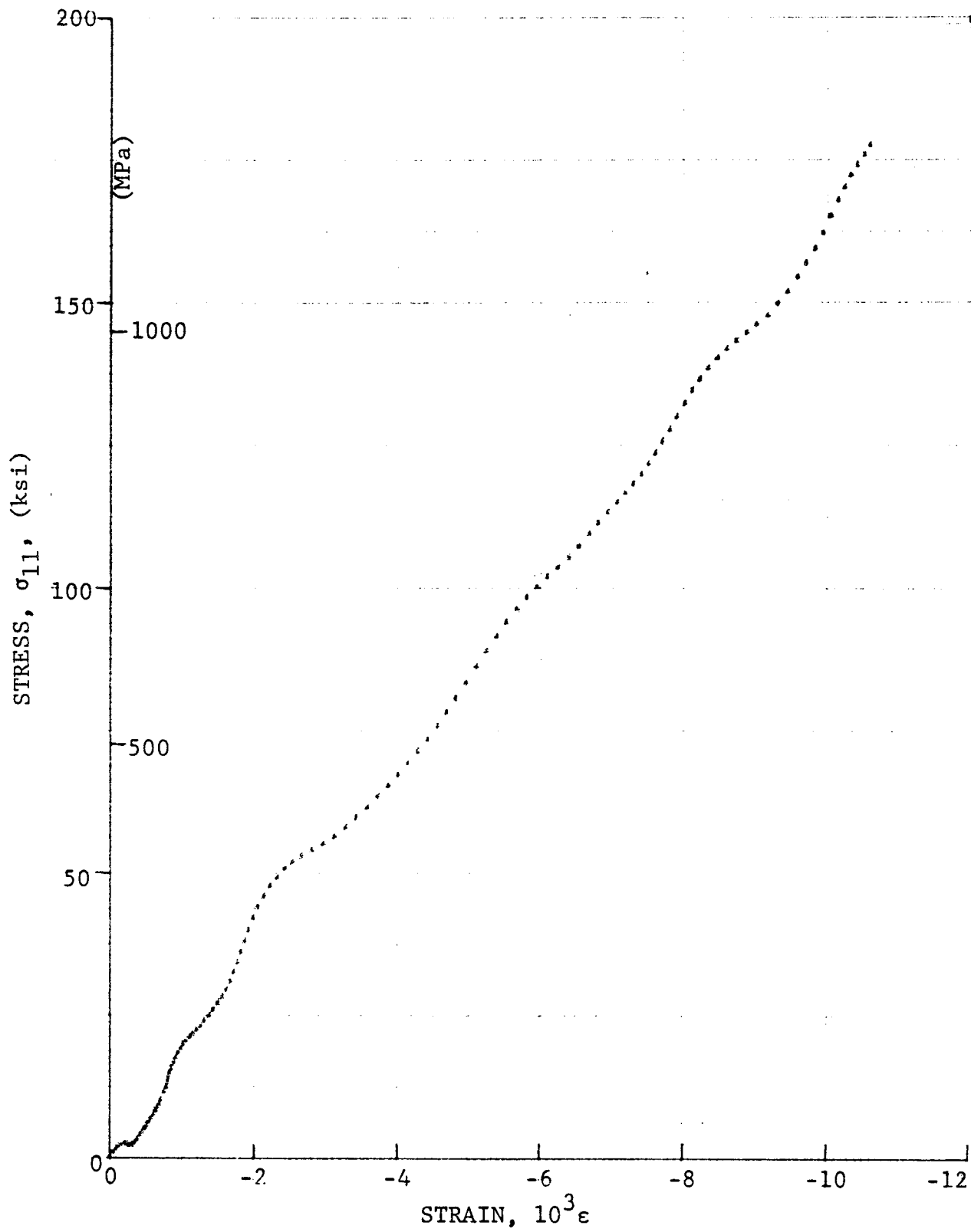


Figure 4-230. Stress-strain curve for [06] SP288/AS graphite/epoxy ring loaded in dynamic compression, Specimen No. 45-3 (1.56 g pistol powder, KC2O_4 , and aluminum dust).

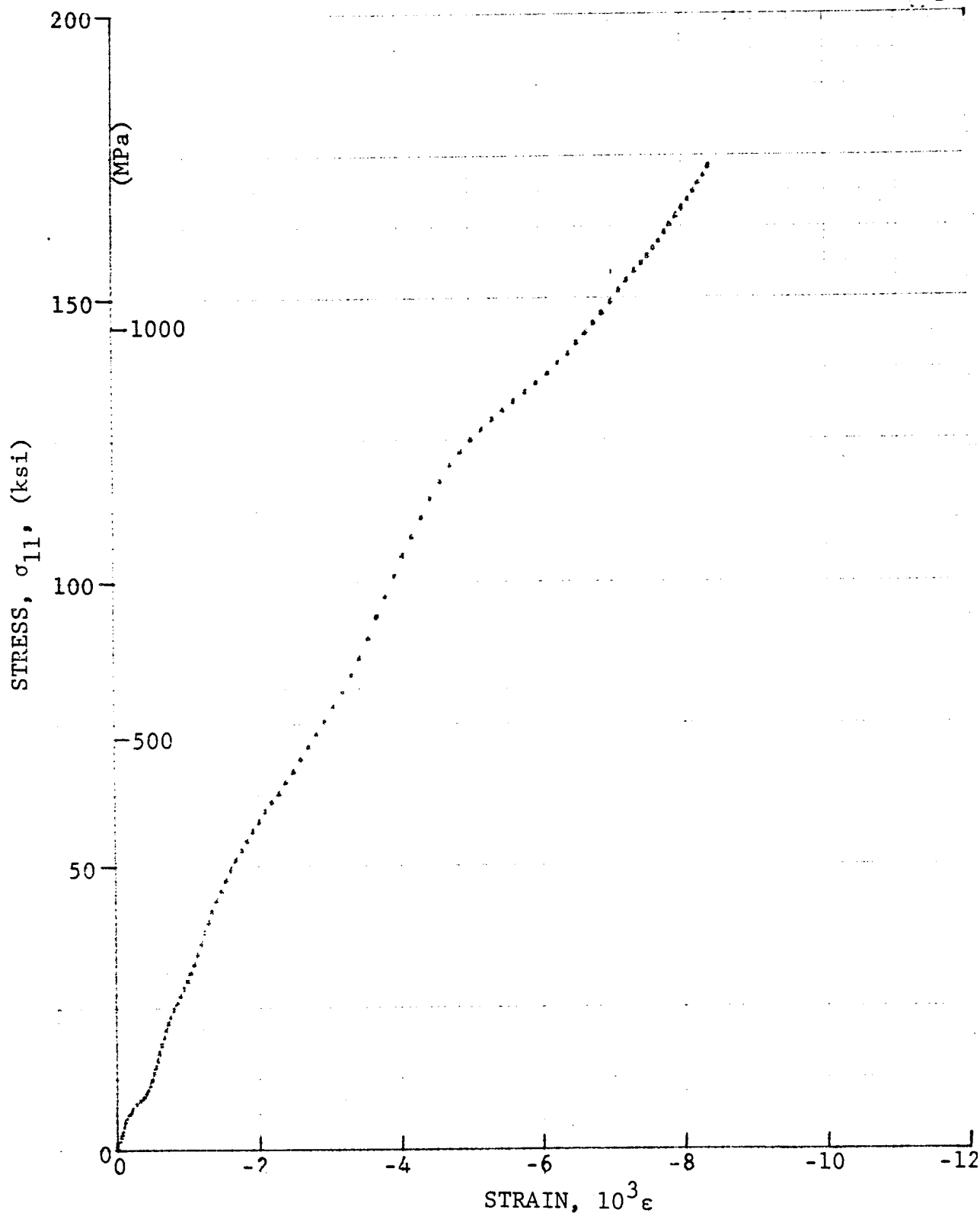
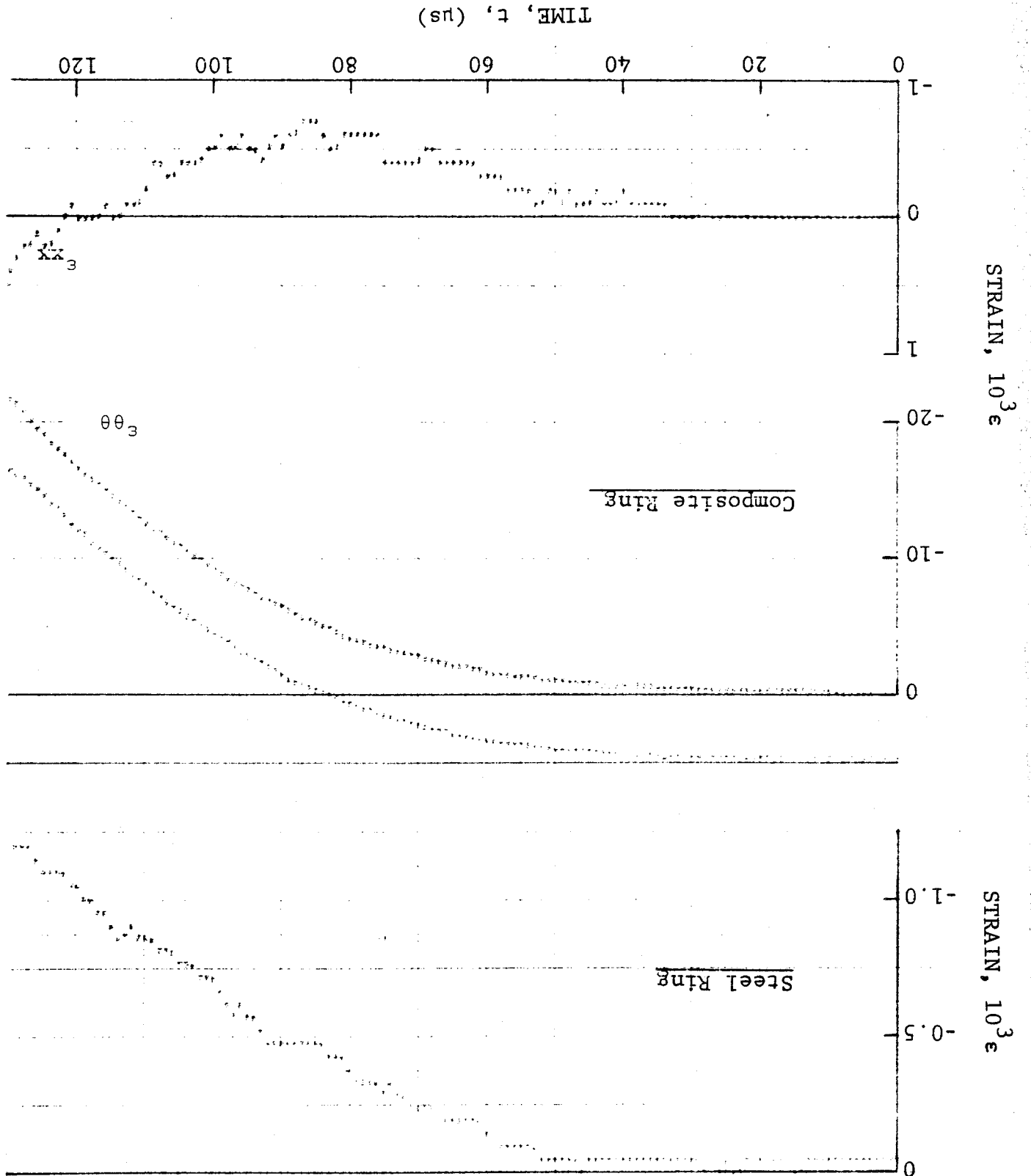


Figure 4-231. Stress-strain curve for $[0_6]$ SP288/AS graphite/epoxy ring loaded in dynamic compression, Specimen No. 45-4 (1.56 g pistol powder, $KClO_4$, and aluminum dust).

Figure 4-232. Strain records in steel ring and [90°] SP288/T300 graphite/epoxy ring under dynamic loading for Specimen No. 44-1 (1.56 g pistol powder, $KC\alpha_0^4$, and aluminum dust).



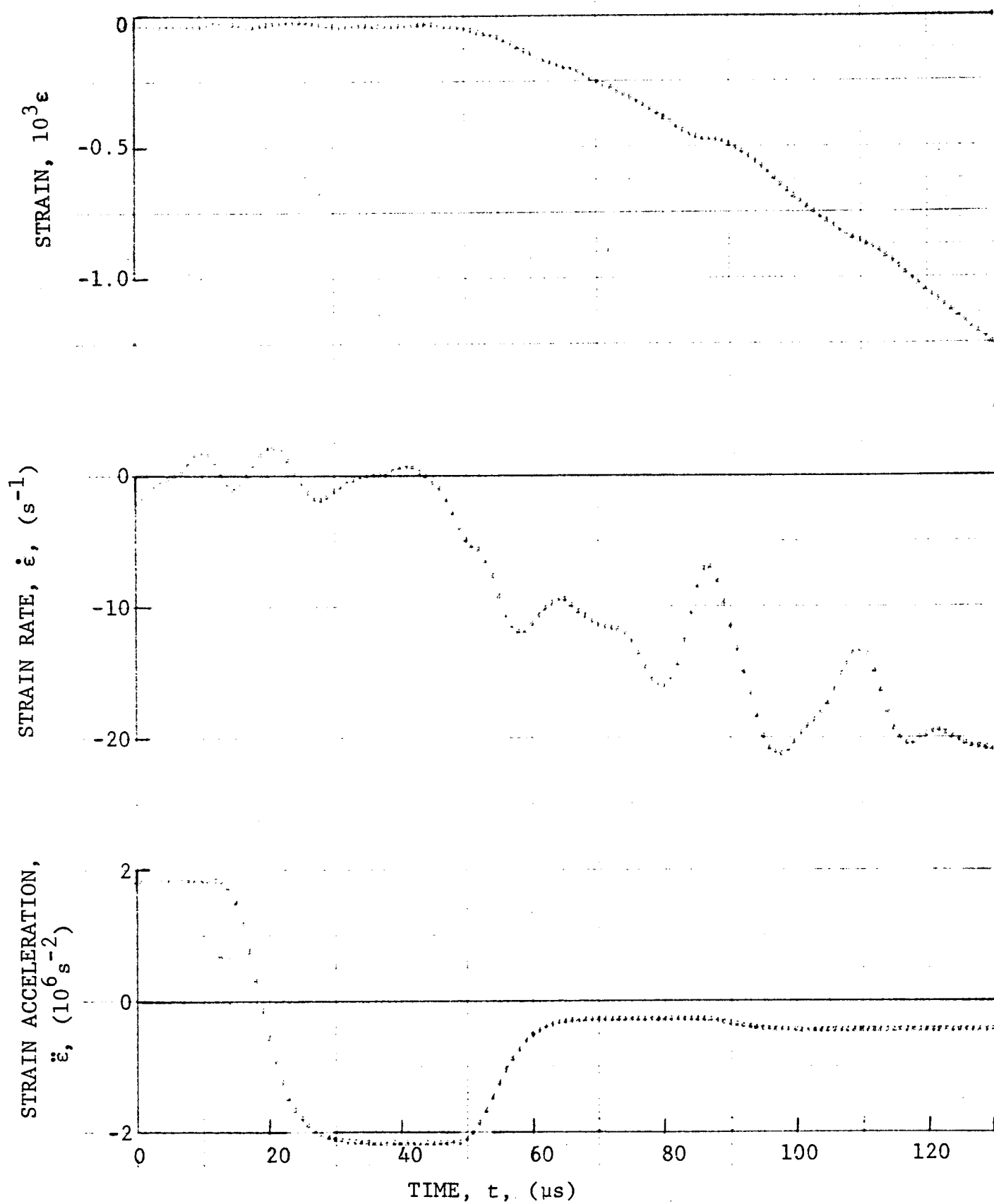
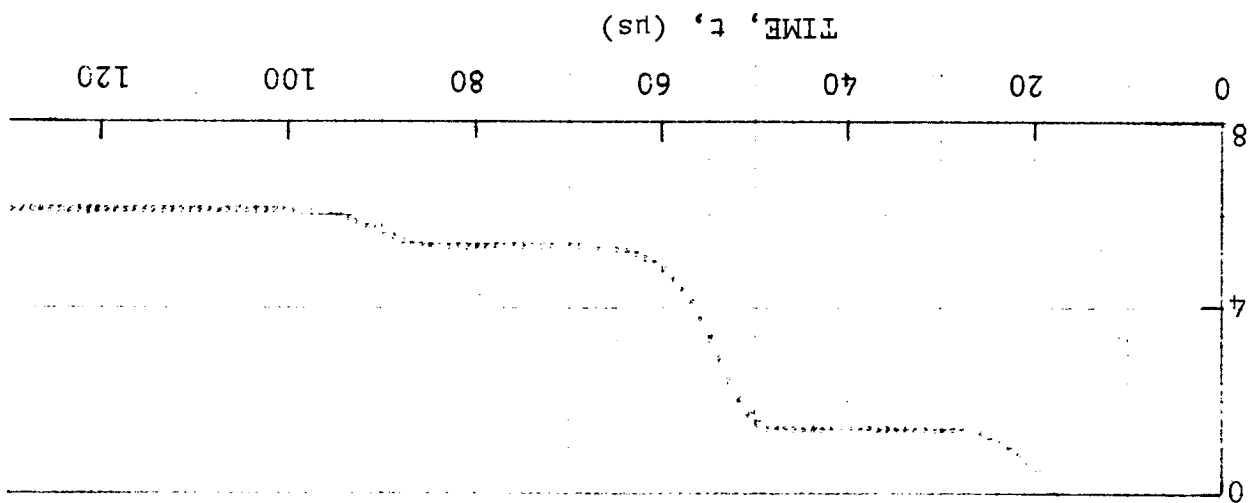
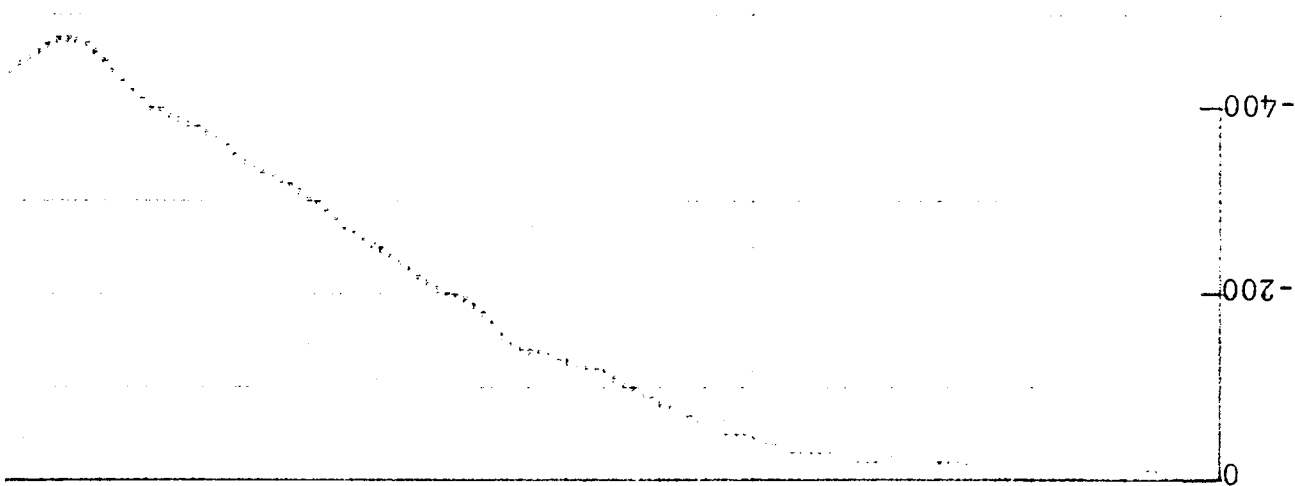


Figure 4-233. Strain and its derivatives in steel ring for Specimen No. 44-1.

STRAIN ACCELERATION,
 $\ddot{\epsilon}$, (10^6 s^{-2})



STRAIN RATE, $\dot{\epsilon}$, (s^{-1})



STRAIN, $10^3 \epsilon$

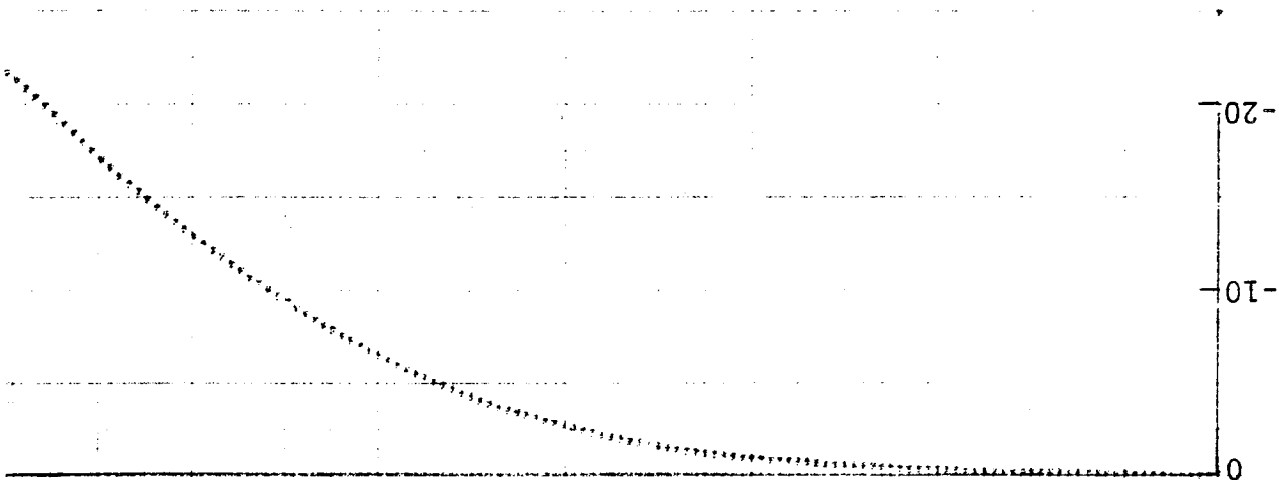


Figure 4-234. Circumferential strain and its derivatives in [90°] SP288/T300 graphite/epoxy ring under dynamic loading for Specimen No. 44-1 (1.56 g graphite powder, KClO_4 , and aluminum dust).

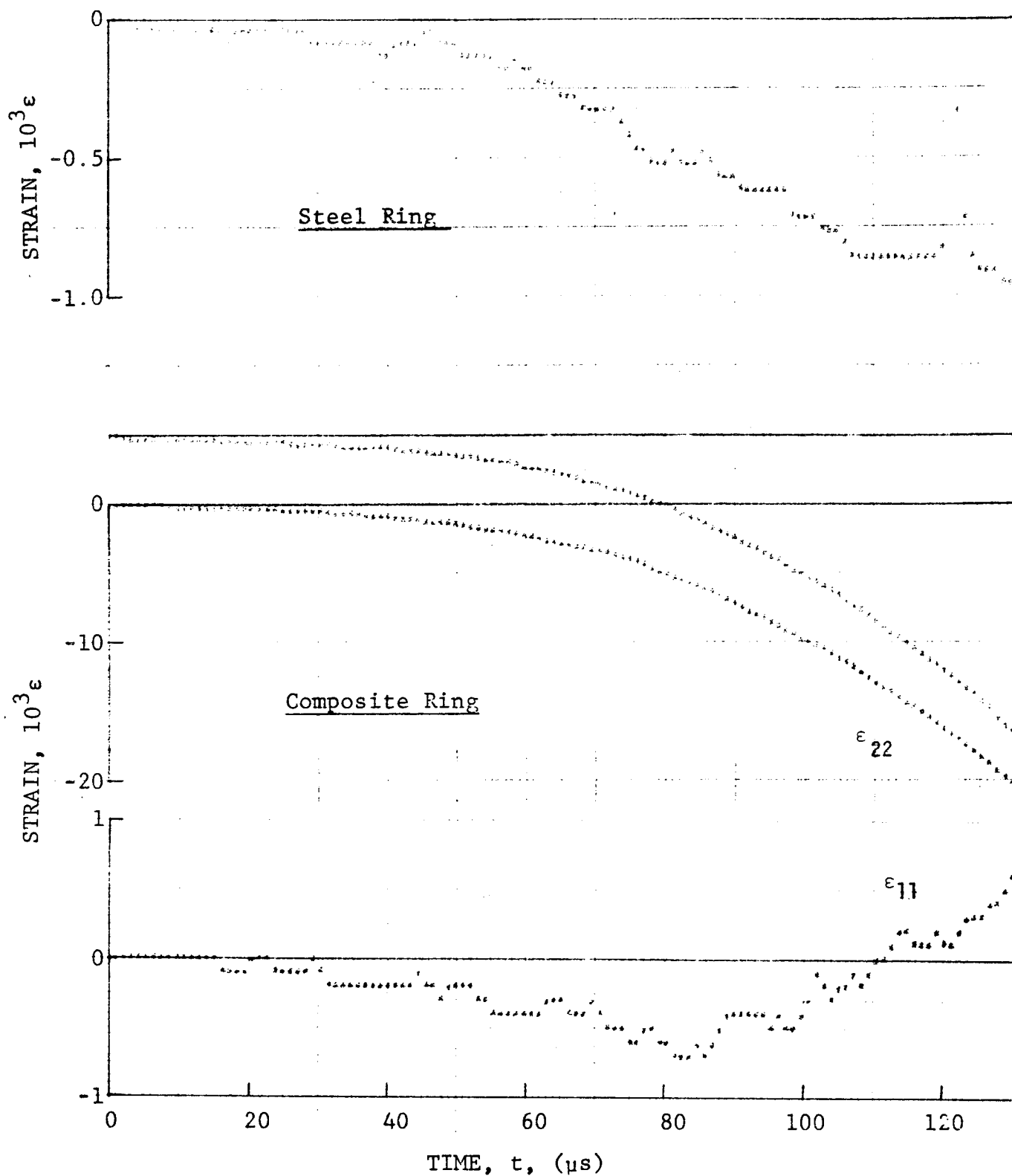


Figure 4-235. Strain records in steel ring and [90₈] SP288/T300 graphite/epoxy ring under dynamic loading for Specimen No. 44-3 (1.56 g pistol powder, $KClO_4$, and aluminum dust).

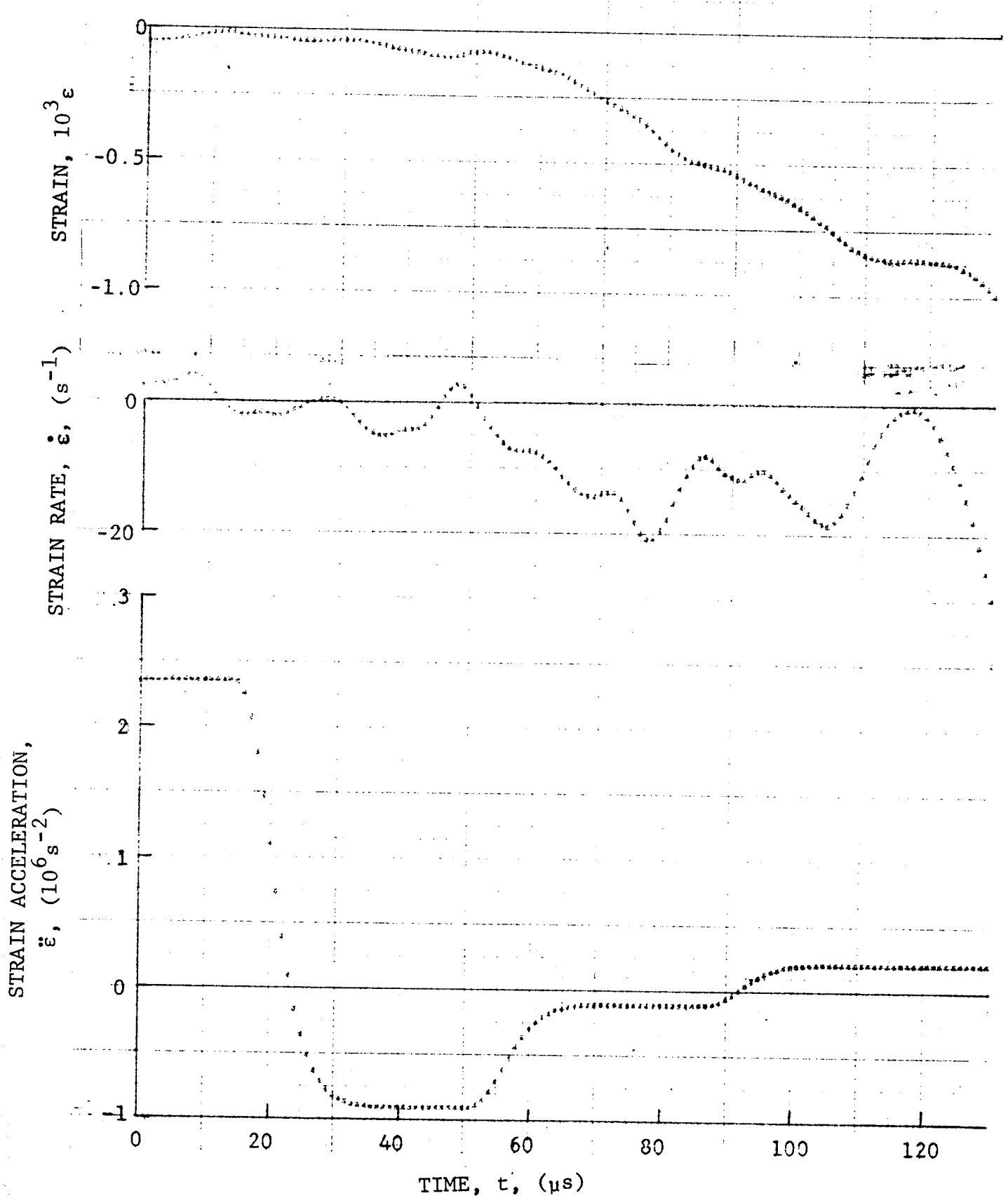
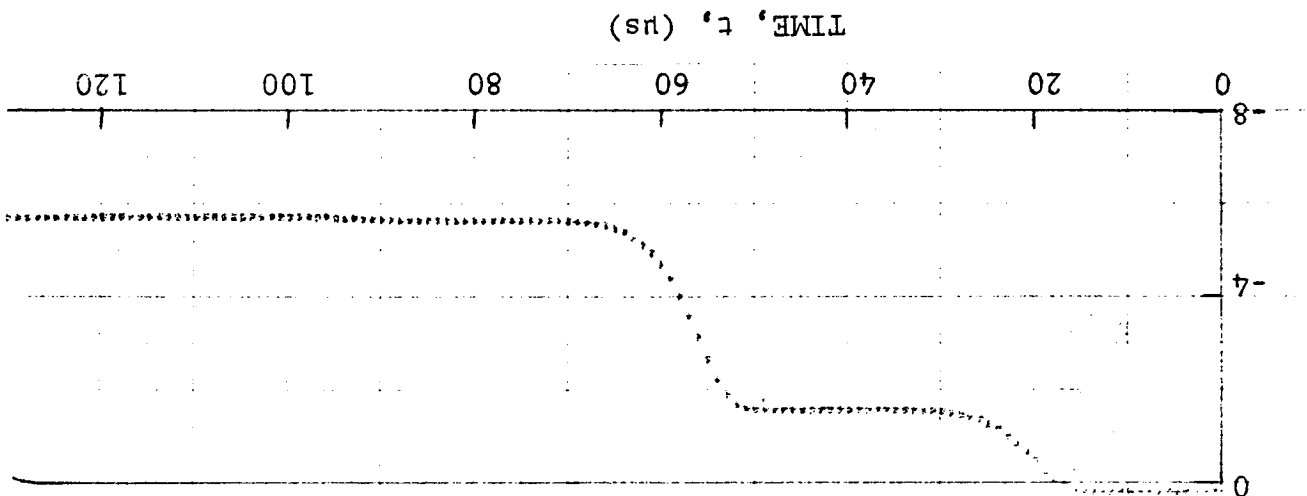
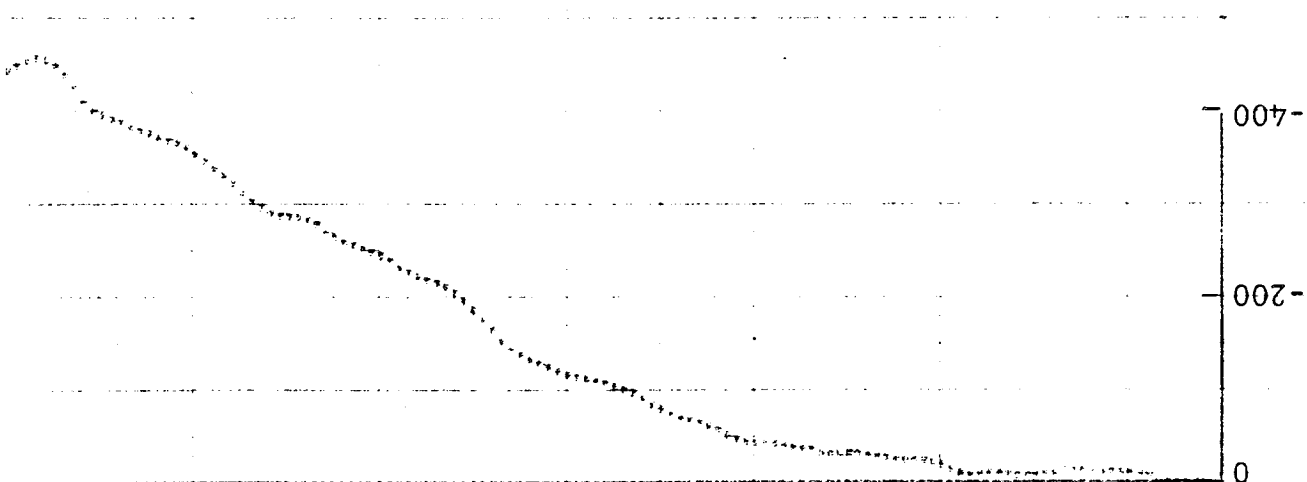


Figure 4-236. Strain and its derivatives in steel ring for Specimen No. 44-3.

STRAIN ACCELERATION,
 $\ddot{\epsilon}$, (10^6 s^{-2})



STRAIN RATE, $\dot{\epsilon}$, (s^{-1})



STRAIN, $10^3 \epsilon$

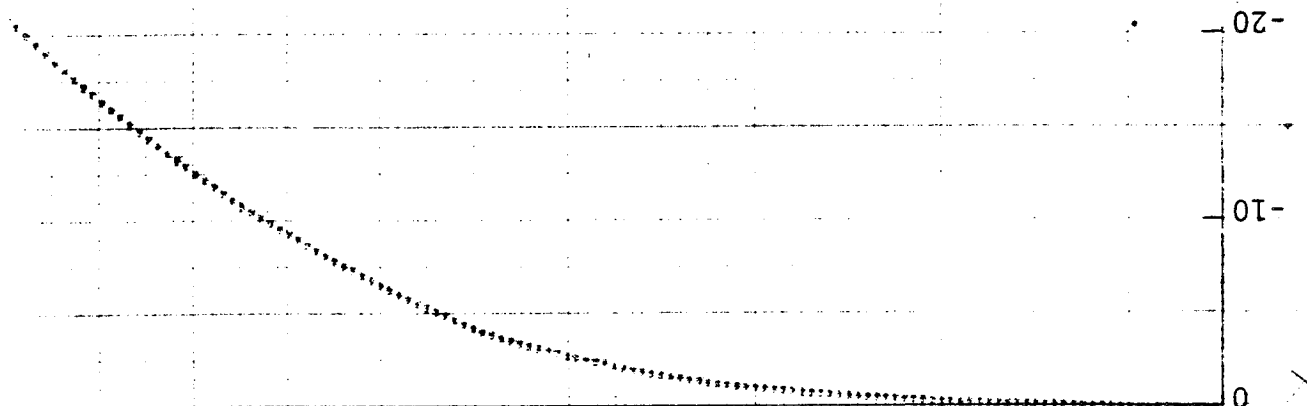


Figure 4-237. Circumferential strain and its derivatives in [90°] SP288/T300 graphite/epoxy ring under dynamic loading for Specimen No. 44-3 (1.56 g graphite powder, KClO_4 , and aluminum dust).

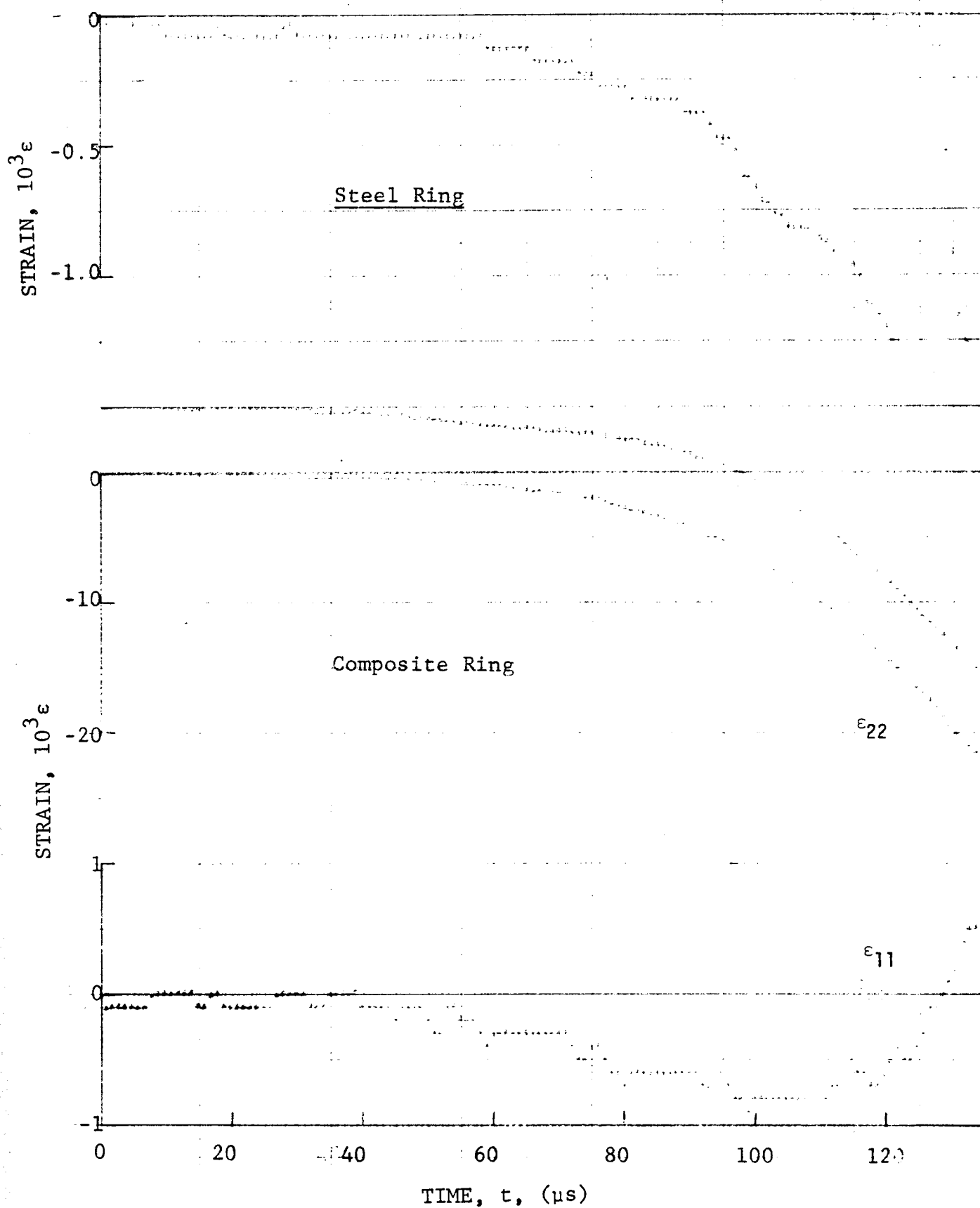


Figure 4-238. Strain records in steel ring and [90_g] SP288/T300 graphite/epoxy ring under dynamic loading for Specimen No. 44-4 (1.56 g pistol powder, $KClO_4$, and aluminum dust).

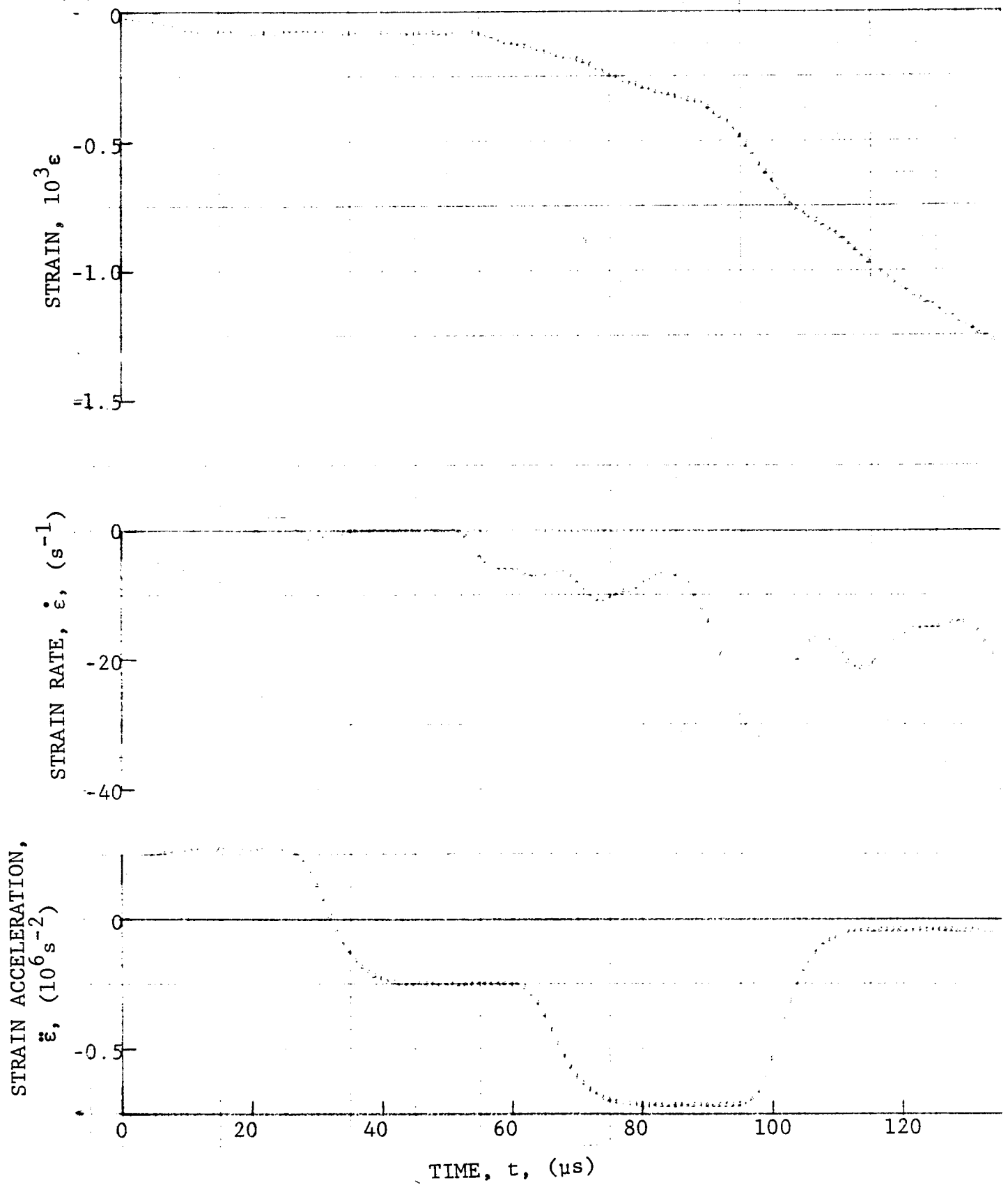


Figure 4-239. Strain and its derivatives in steel ring for Specimen No. 44-4.

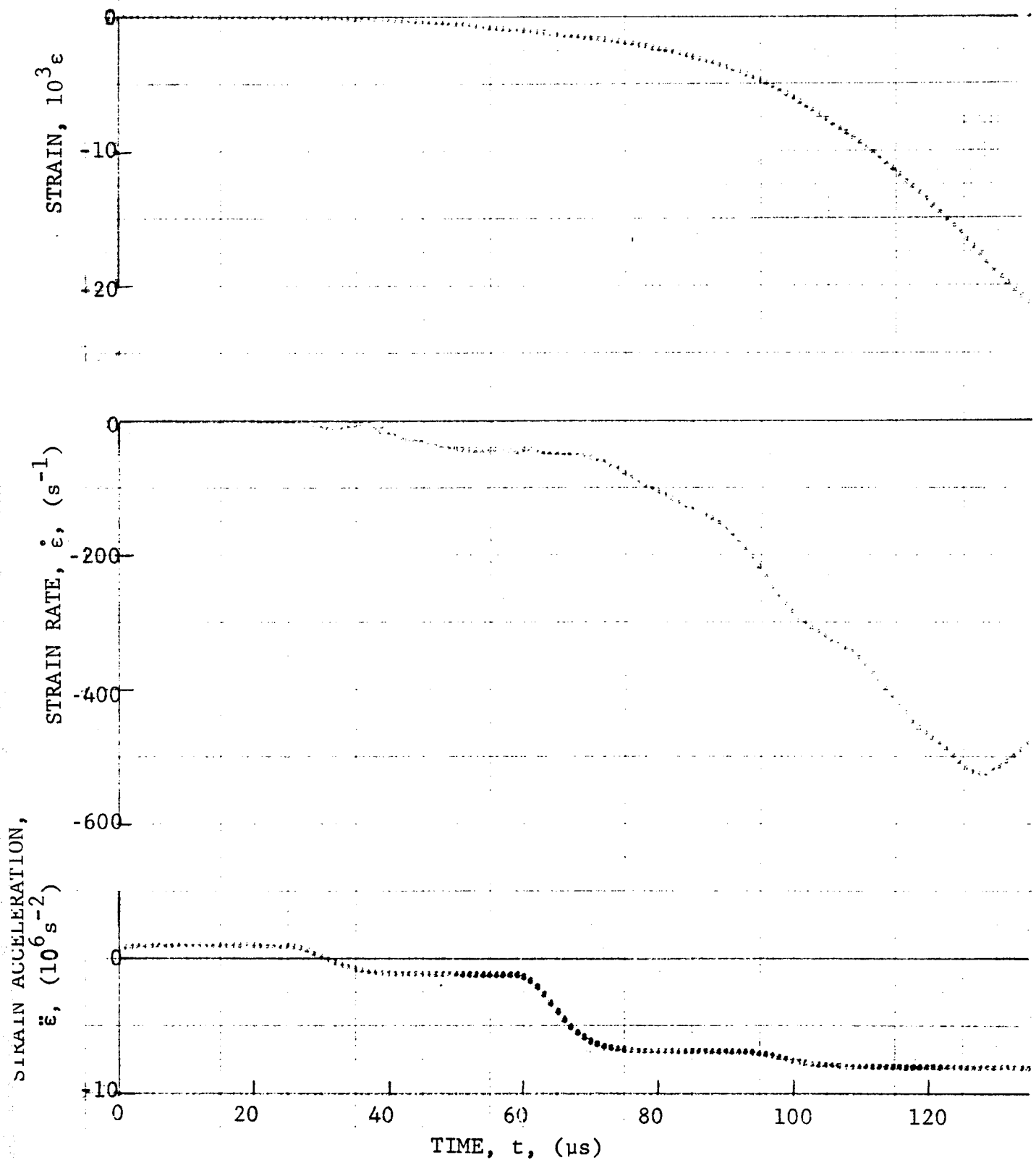


Figure 4-240. Circumferential strain and its derivatives in $[90_8]$ SP288/T300 graphite/epoxy ring under dynamic loading for Specimen No. 44-4 (1.56 g pistol powder, KCO_4 , and aluminum dust).

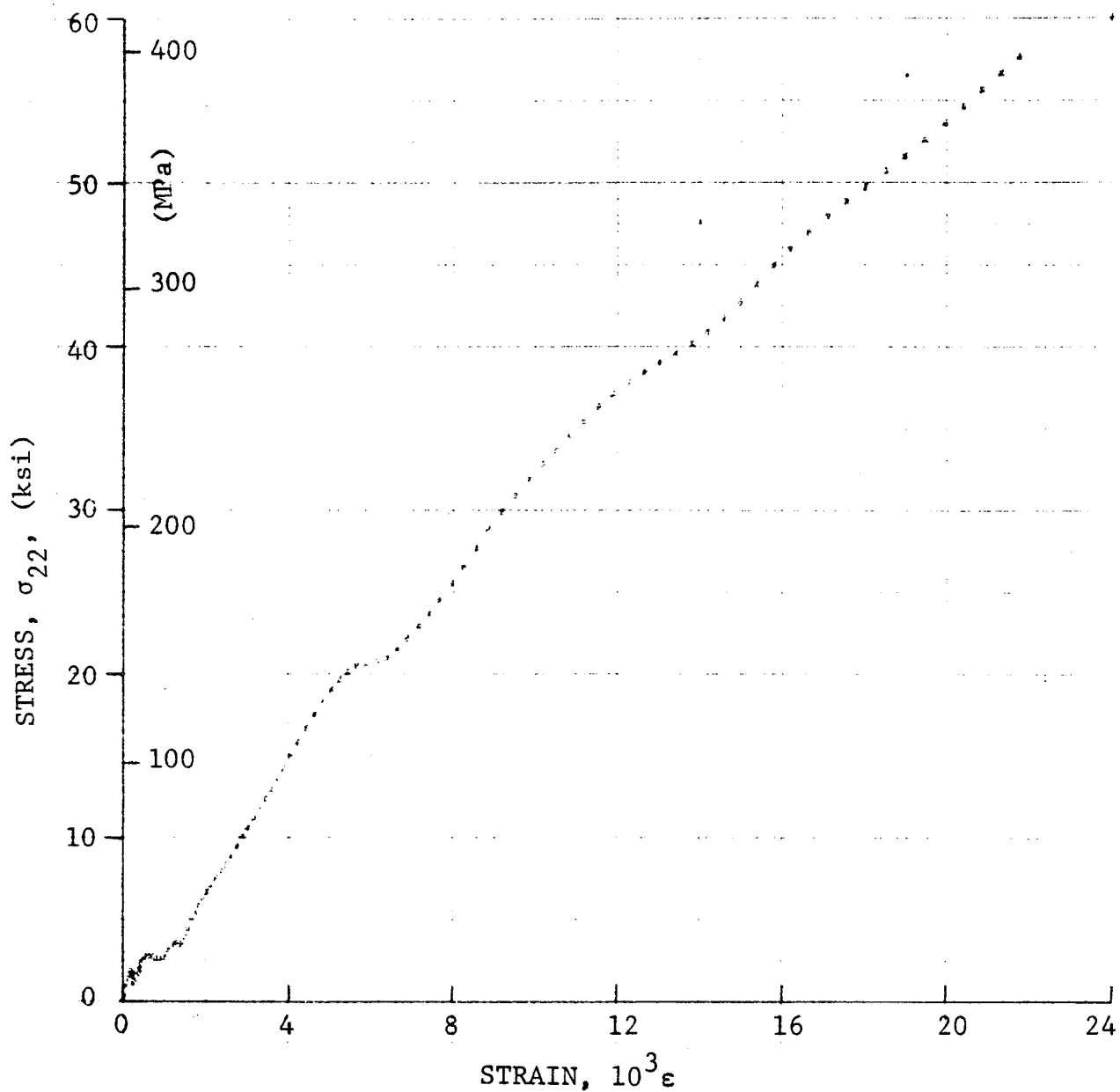


Figure 4-241. Stress-strain curve for dynamically loaded $[90_g]$ SP288/T300 graphite/epoxy ring, Specimen No. 44-1 (1.56 g pistol powder, $KClO_4$, and aluminum dust).

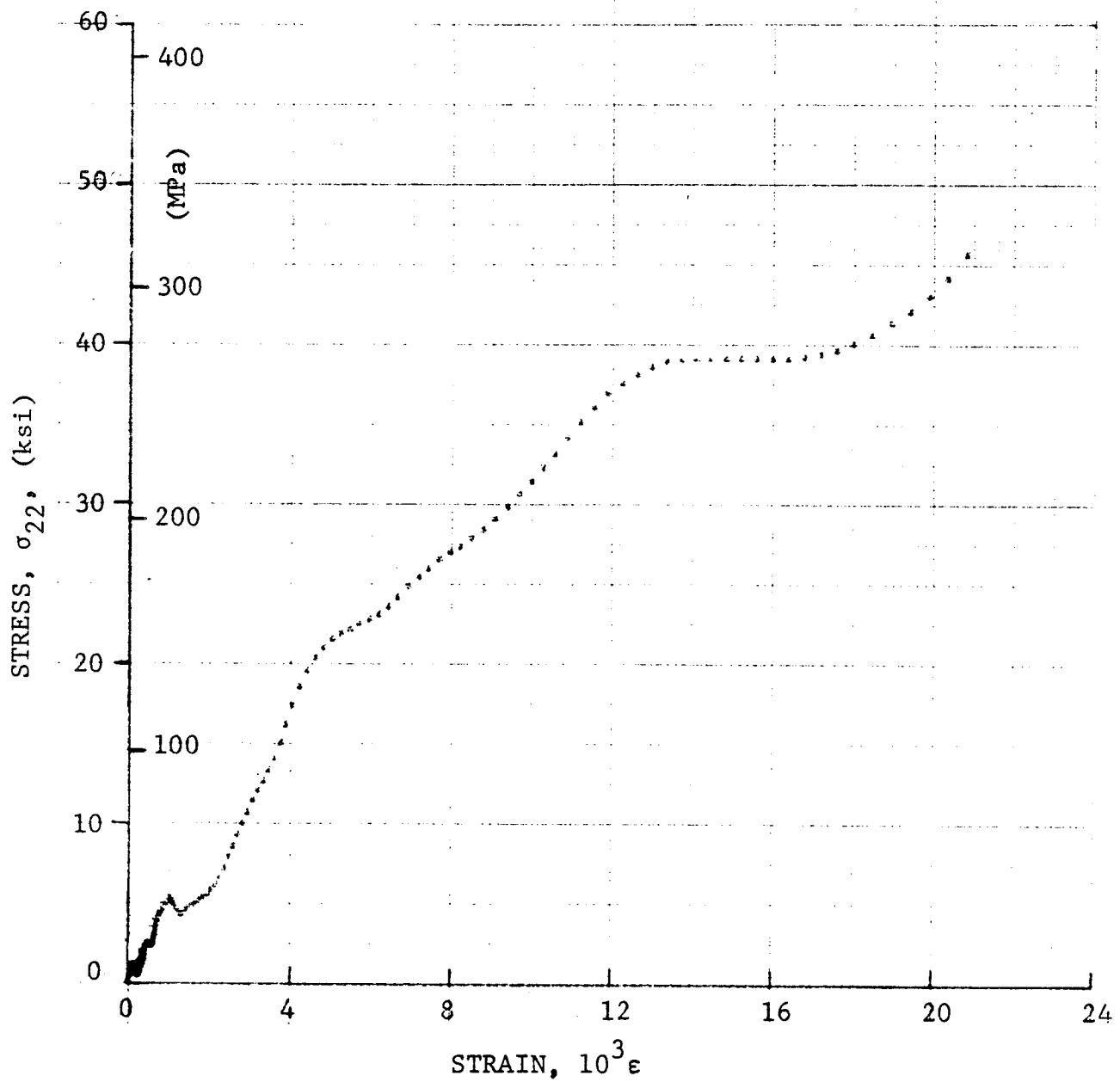


Figure 4-242. Stress-strain curve for dynamically loaded [90g] SP288/T300 graphite/epoxy ring, Specimen No. 44-3 (1.56 g pistol powder, $KClO_4$, and aluminum dust).

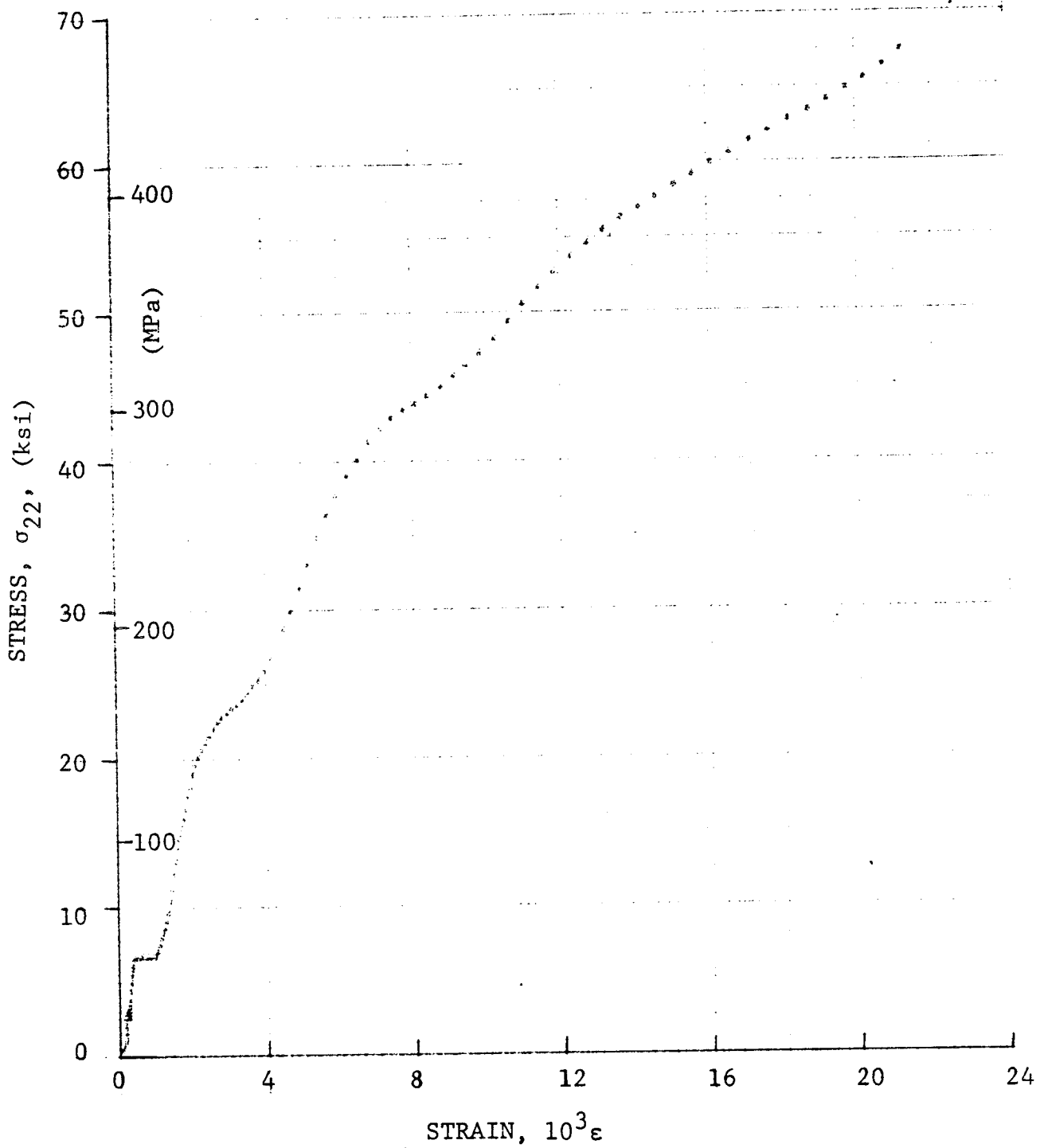
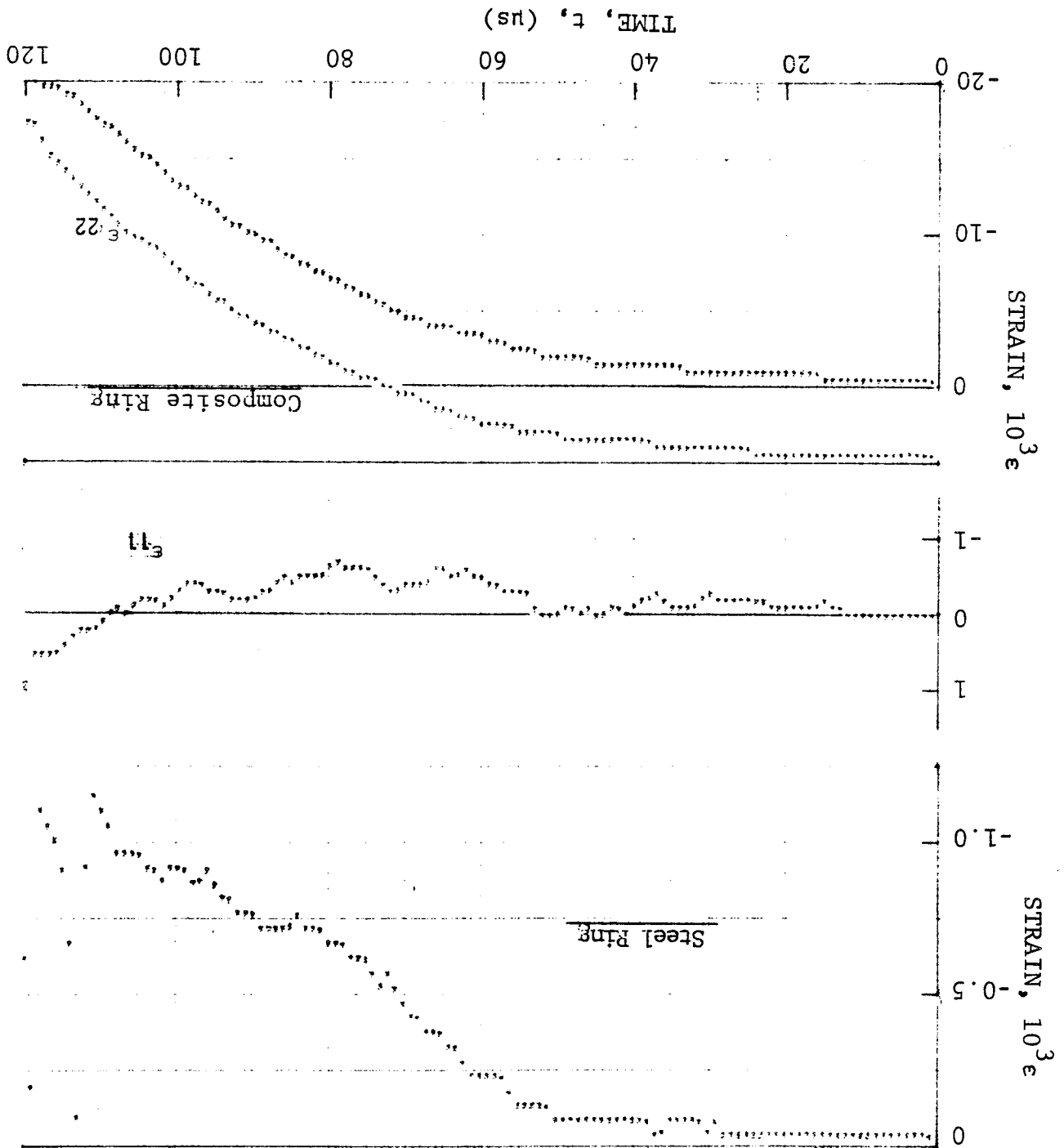


Figure 4-243. Stress-strain curve for dynamically loaded [90_g] SP288/T300 graphite/epoxy ring, Specimen No. 44-4 (1.56 g pistol powder, $KClO_4$, and aluminum dust).

Figure 4-244. Strain records in steel ring and [90°] SP288/AS graphite/epoxy ring under dynamic loading for Specimen No. 38-1 (1.56 g pistol powder, $KClO_4$, and aluminum dust).



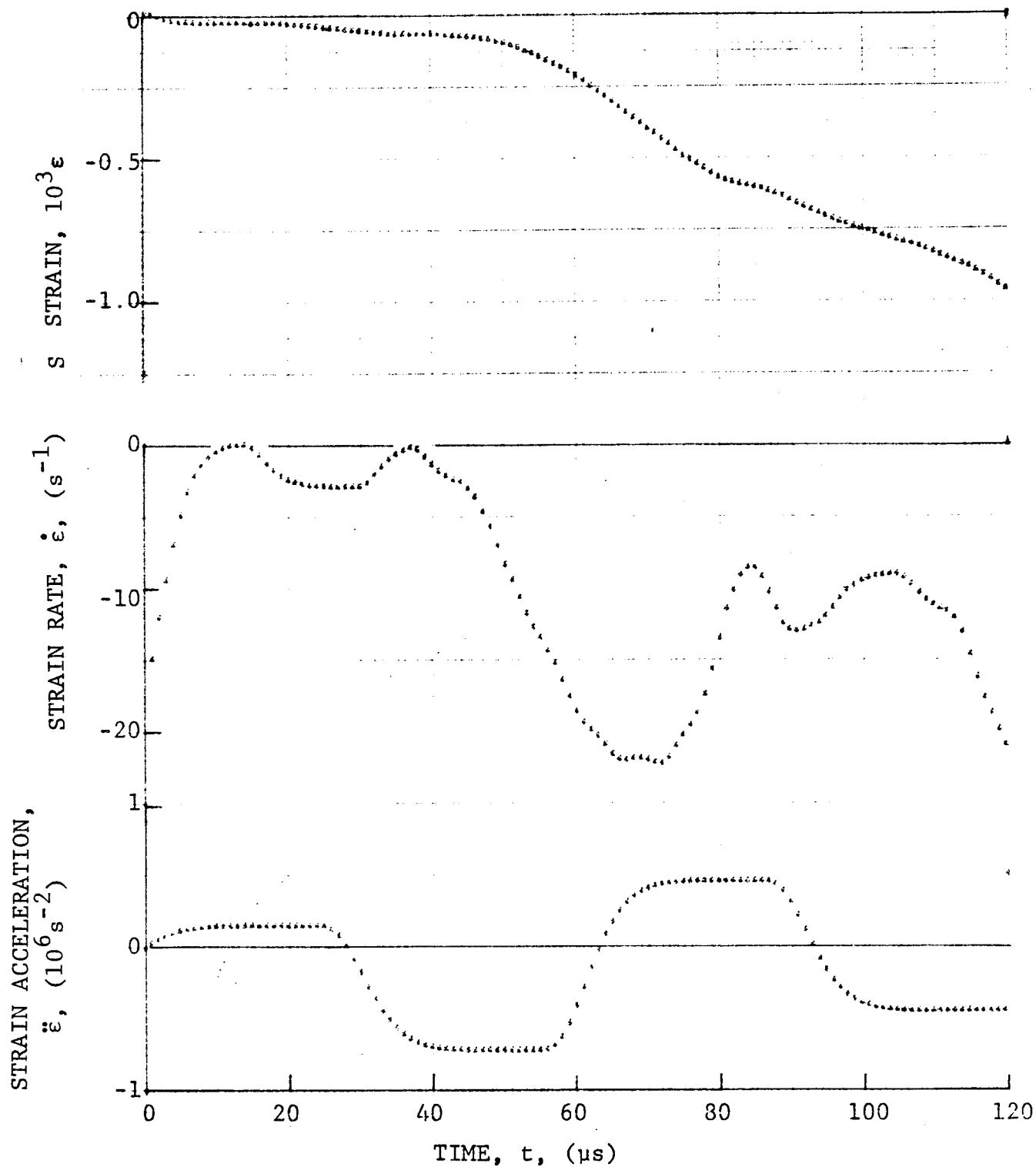
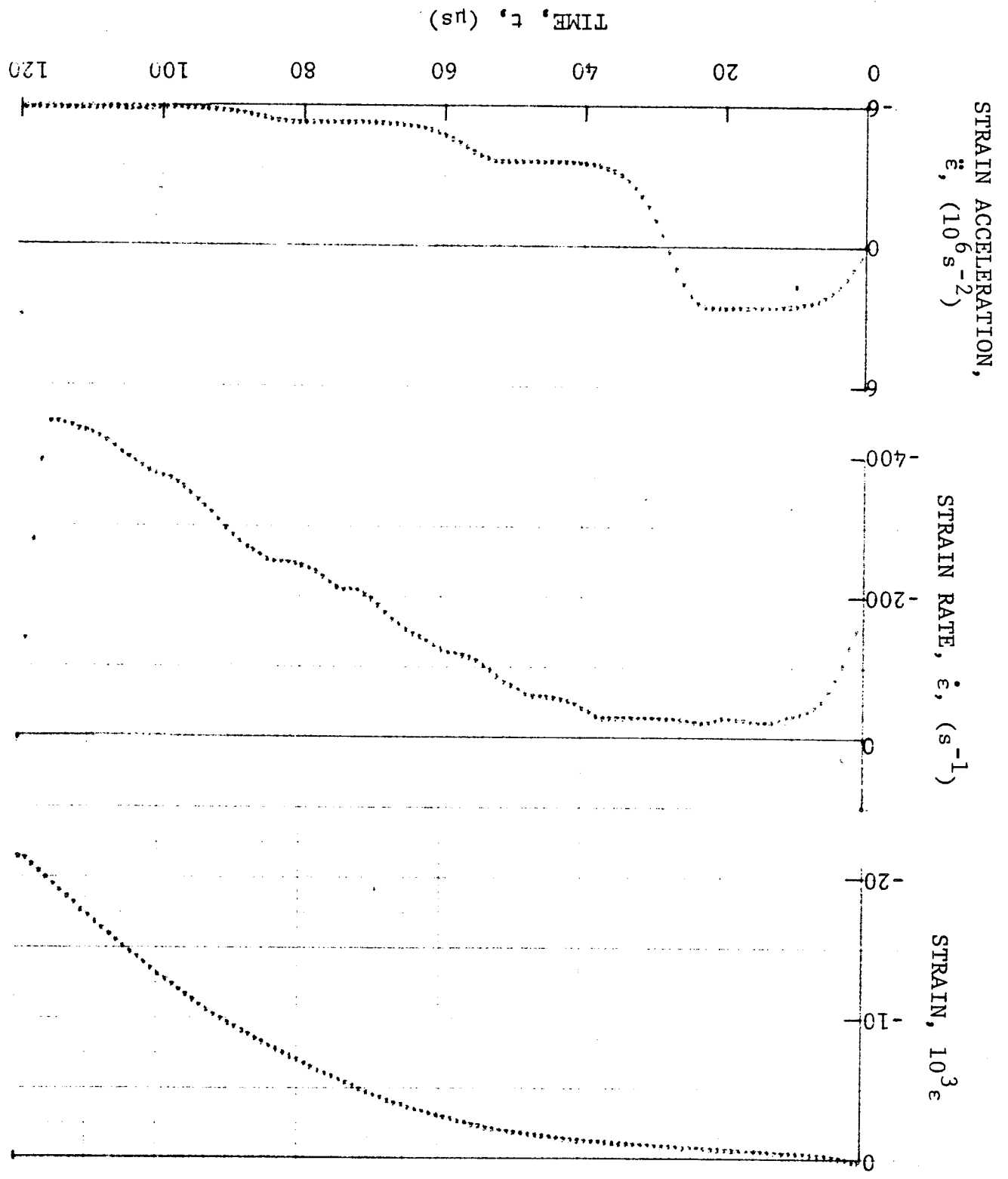


Figure 4-245. Strain and its derivatives in steel ring for Specimen No. 38-1.

Figure 4-246. Circumferential strain and its derivatives in [90°] SP288/AS graphite/epoxy ring under dynamic loading for Specimen No. 38-1 (1.56 g pistol powder, $KClO_4$, and aluminum dust).



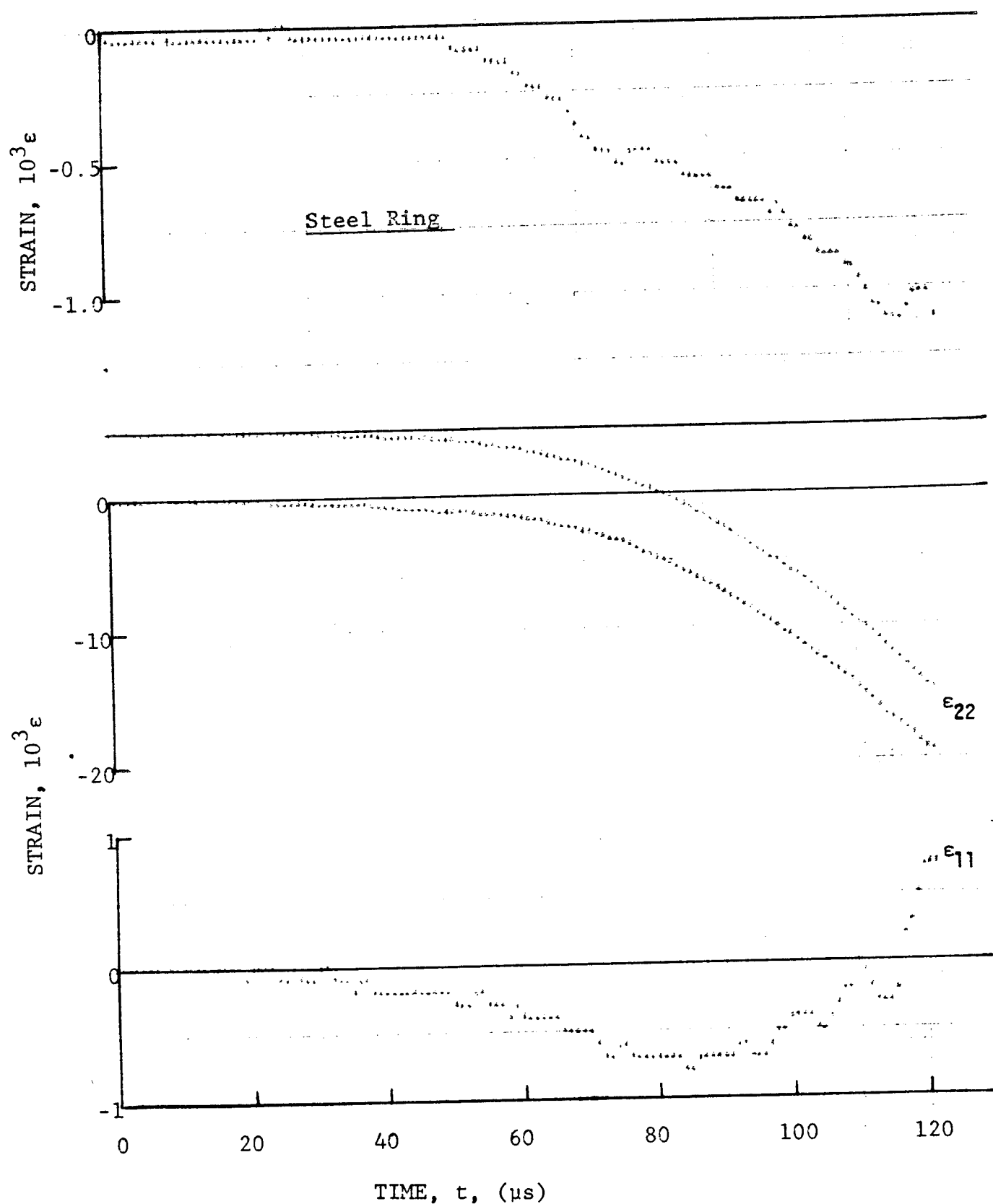


Figure 4-247. Strain records in steel ring and [90 $^\circ$] SP288/AS graphite/epoxy ring under dynamic loading for Specimen No. 38-2 (1.56 g pistol powder, $KClO_4$, aluminum dust).

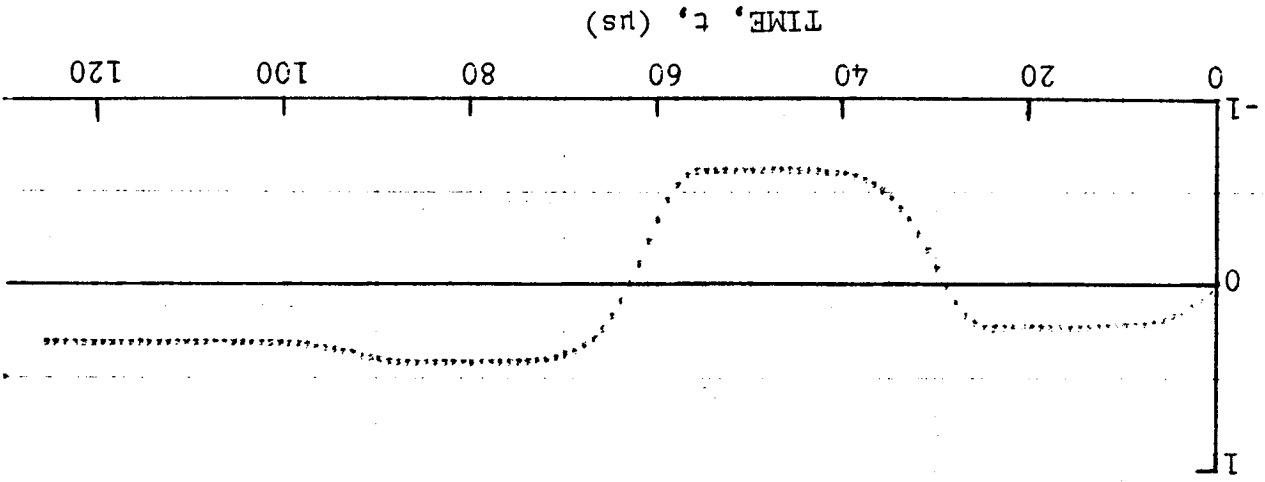
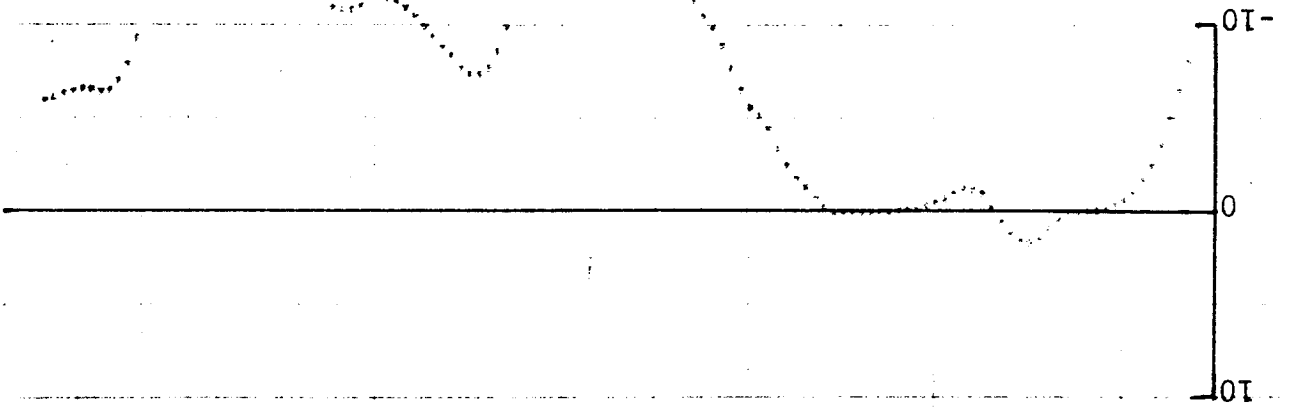
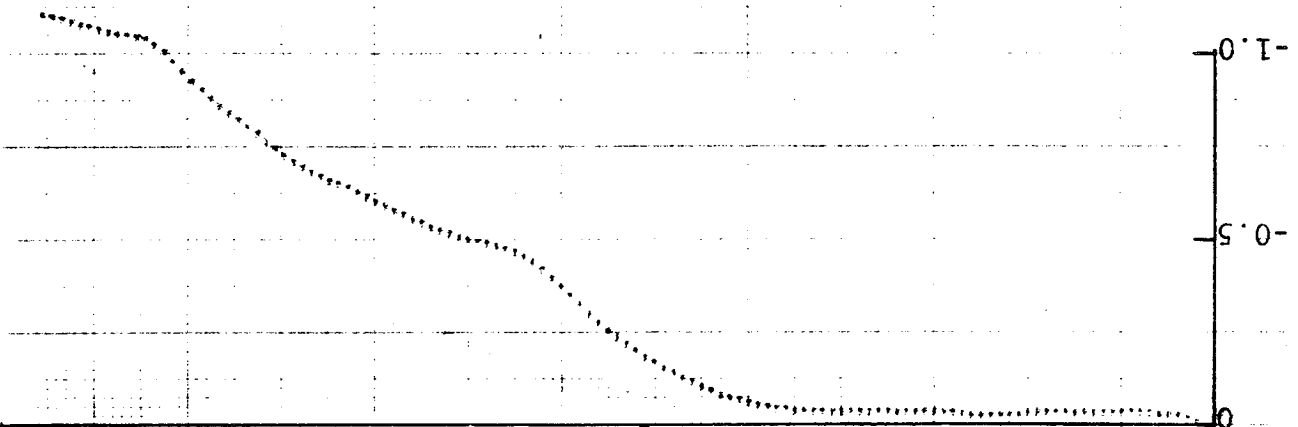
STRAIN ACCELERATION,
 $\ddot{\epsilon}$, (10^6 s^{-2})STRAIN RATE, $\dot{\epsilon}$, (s^{-1})STRAIN, $10^3 \epsilon$ 

Figure 4-248. Strain and its derivatives in steel ring for Specimen No. 38-2.

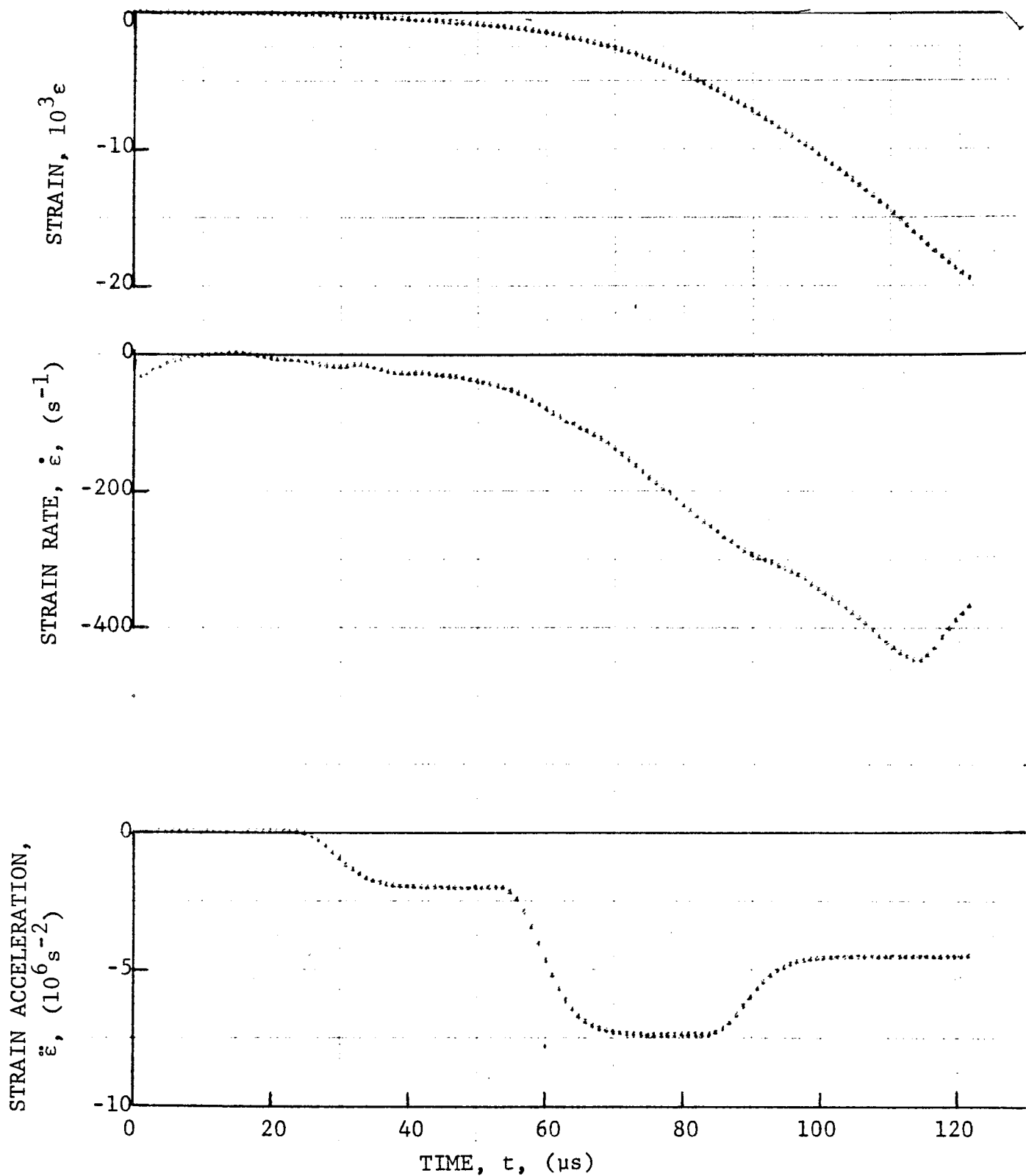


Figure 4-249. Circumferential strain and its derivatives in $[90_8]$ SP288/AS graphite/epoxy ring under dynamic loading for Specimen No. 38-2 (1.56 g pistol powder, $KClO_4$, and aluminum dust).

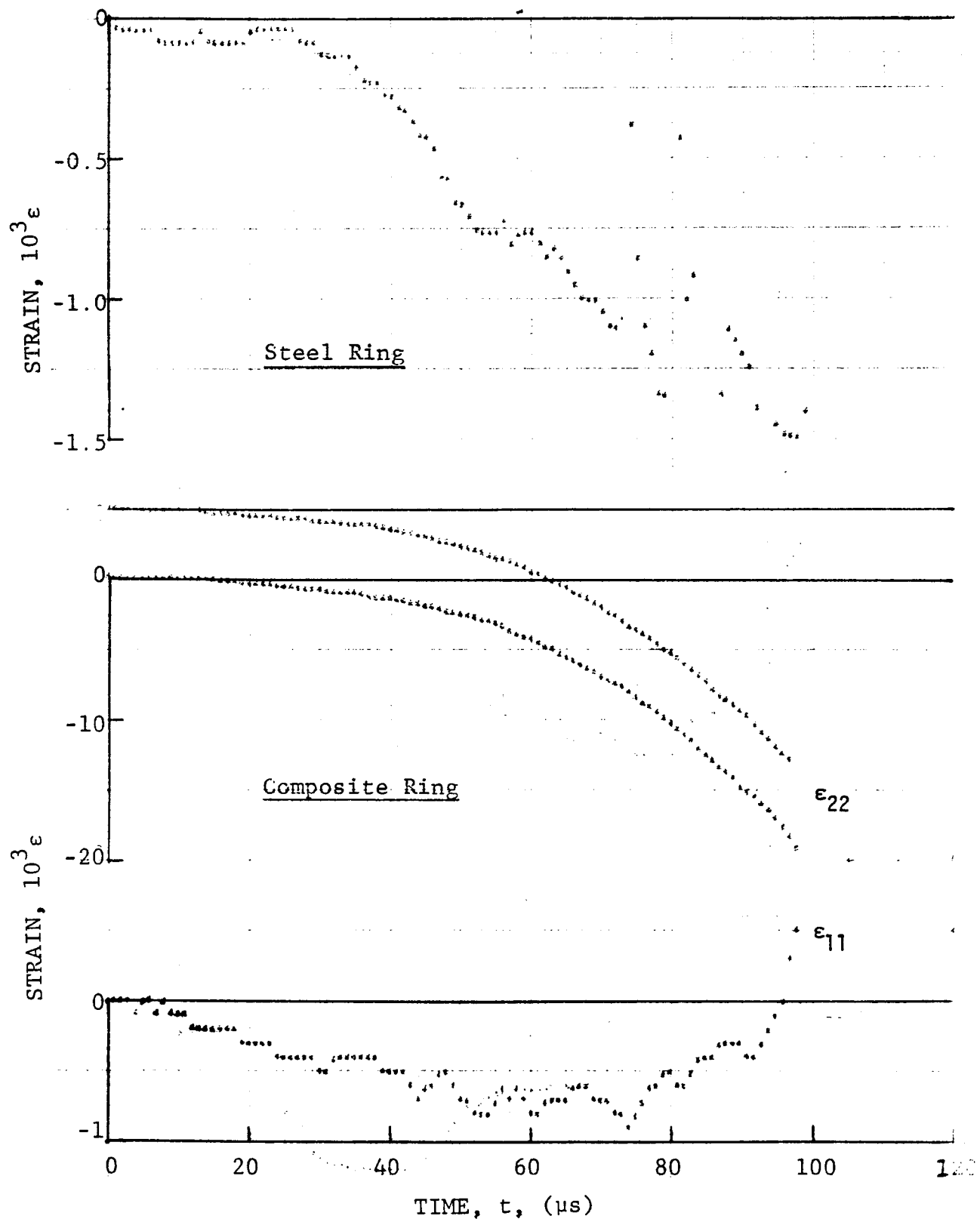


Figure 4-250. Strain records in steel ring and $[90_8]$ SP288/AS graphite/epoxy ring under dynamic loading for Specimen No. 38-3 (1.56 g pistol powder, $KClO_4$, and aluminum dust).

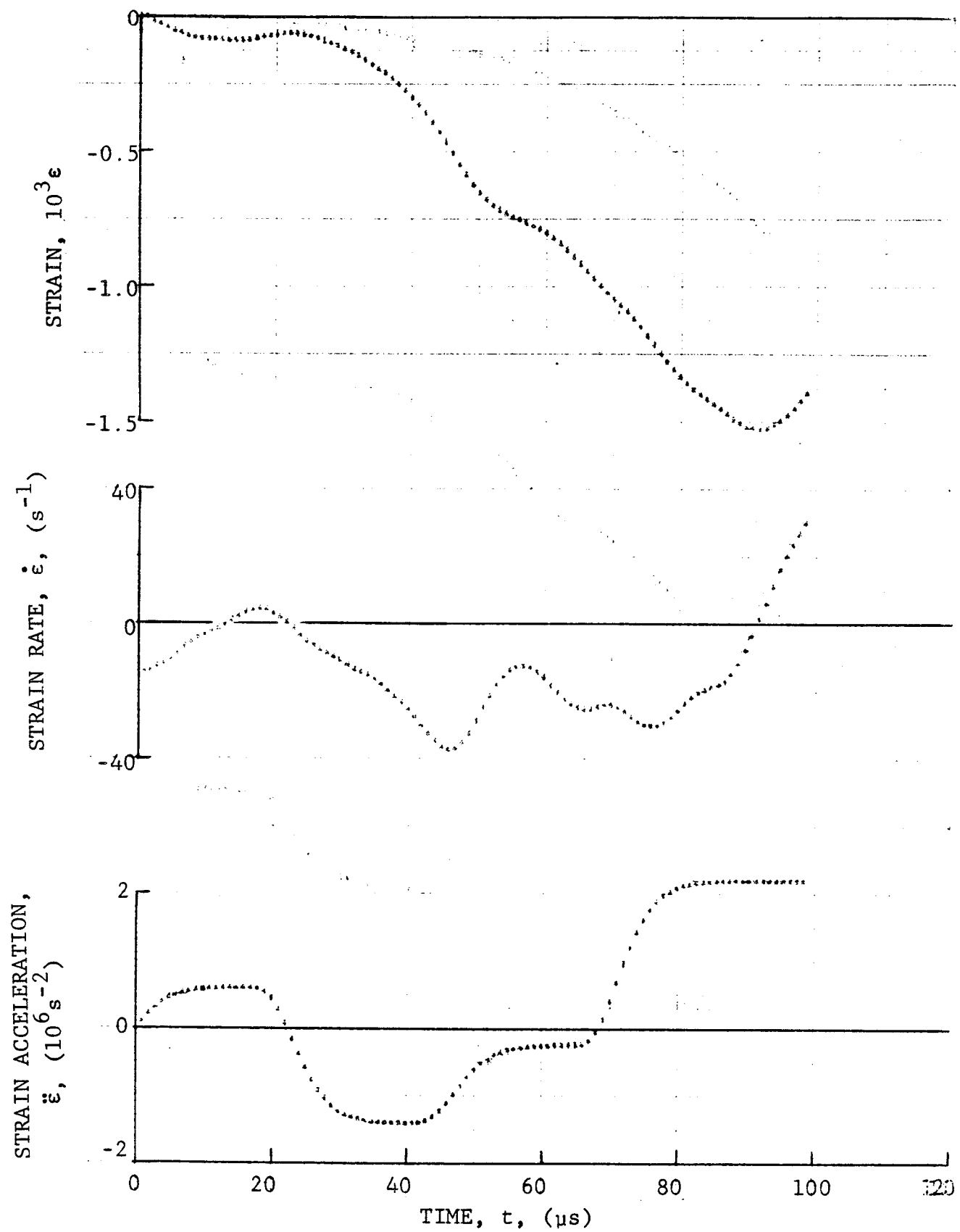
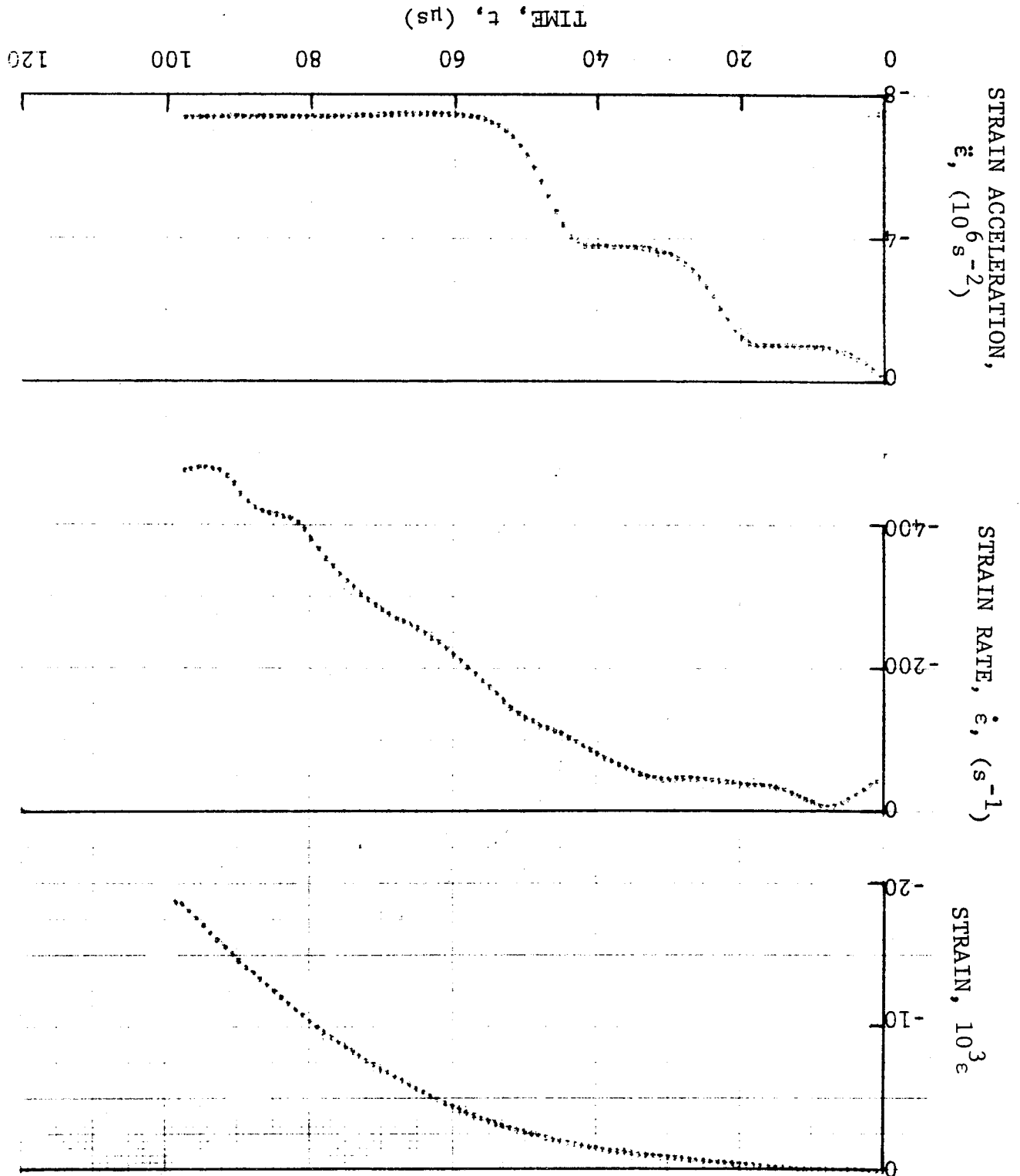


Figure 4-251. Strain and its derivatives in steel ring for Specimen No. 38-3.

Figure 4-252. Circumferential strain and its derivatives in [90°] SP288/AS graphite/epoxy ring under dynamic loading for Specimen No. 38-3 (1.56 g pistol powder, KClO_4 , and aluminum dust).



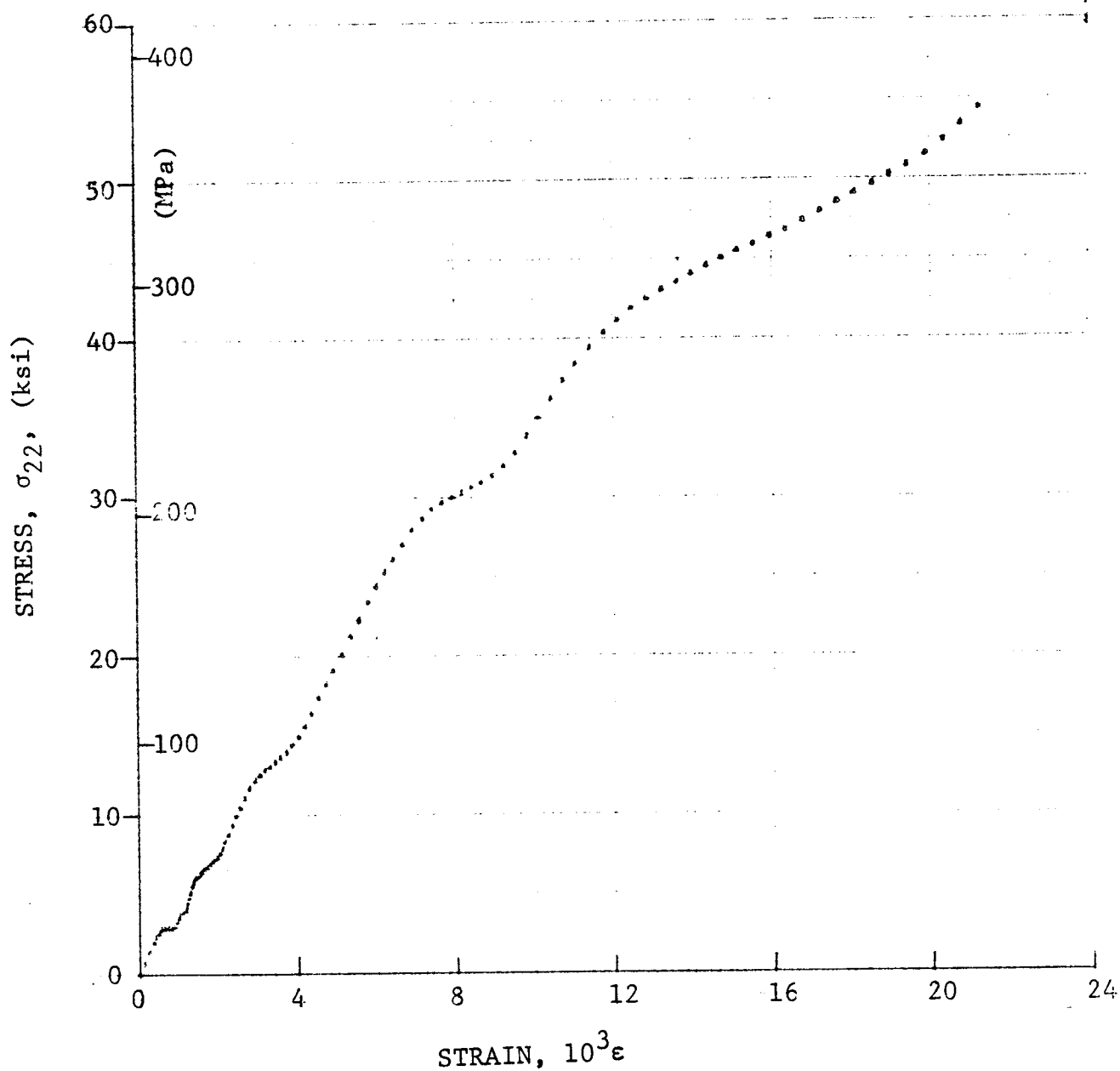


Figure 4-253. Stress-strain curve for dynamically loaded [90g] SP288/AS graphite/epoxy ring, Specimen No. 38-1 (1.56 pistol powder, $KClO_4$, and aluminum dust).

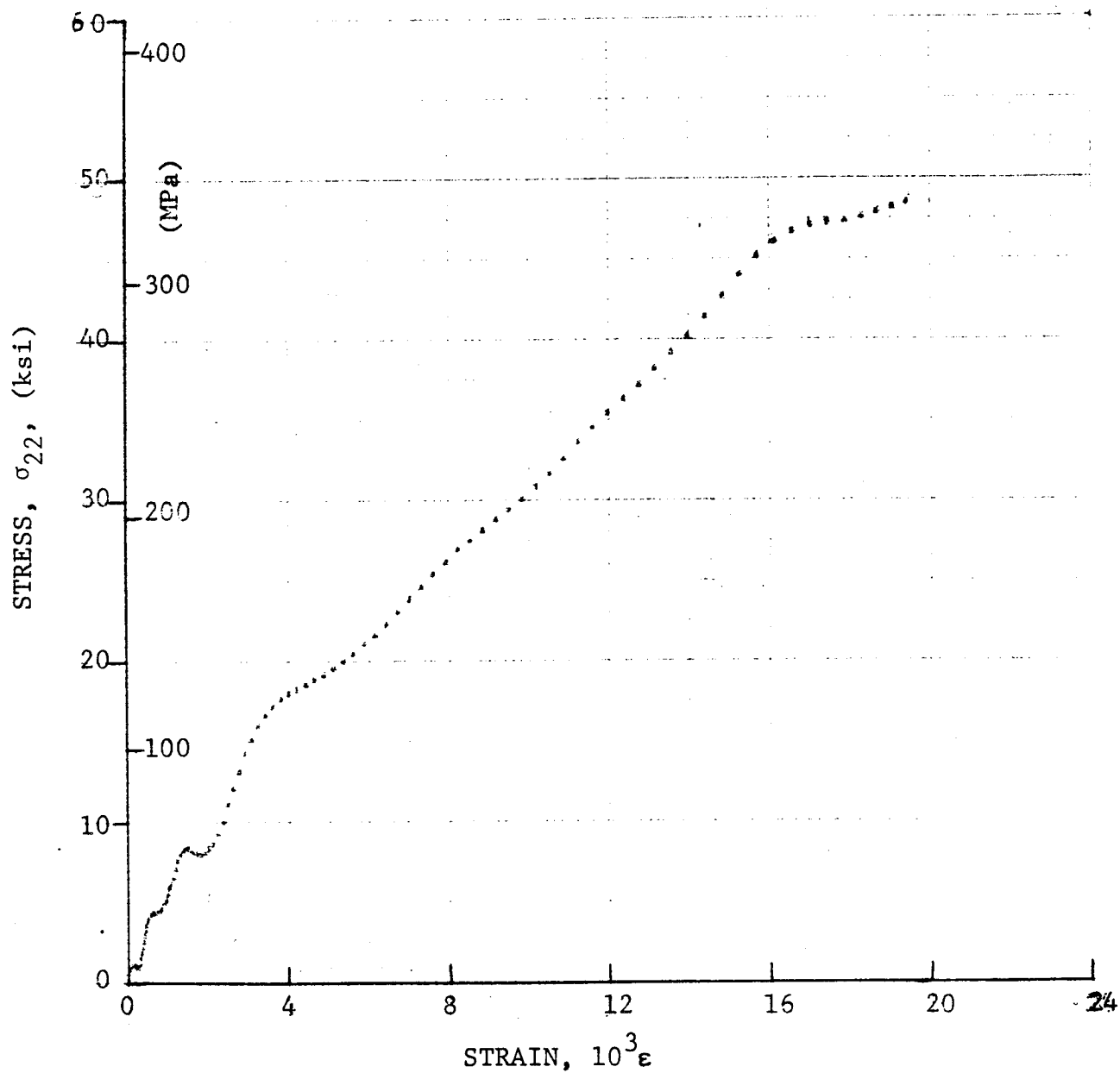


Figure 4-254. Stress-strain curve for dynamically loaded $[90_8]$ SP288/AS graphite/epoxy ring, Specimen No. 38-2 (1.56 g pistol powder, $KClO_4$, and aluminum dust).

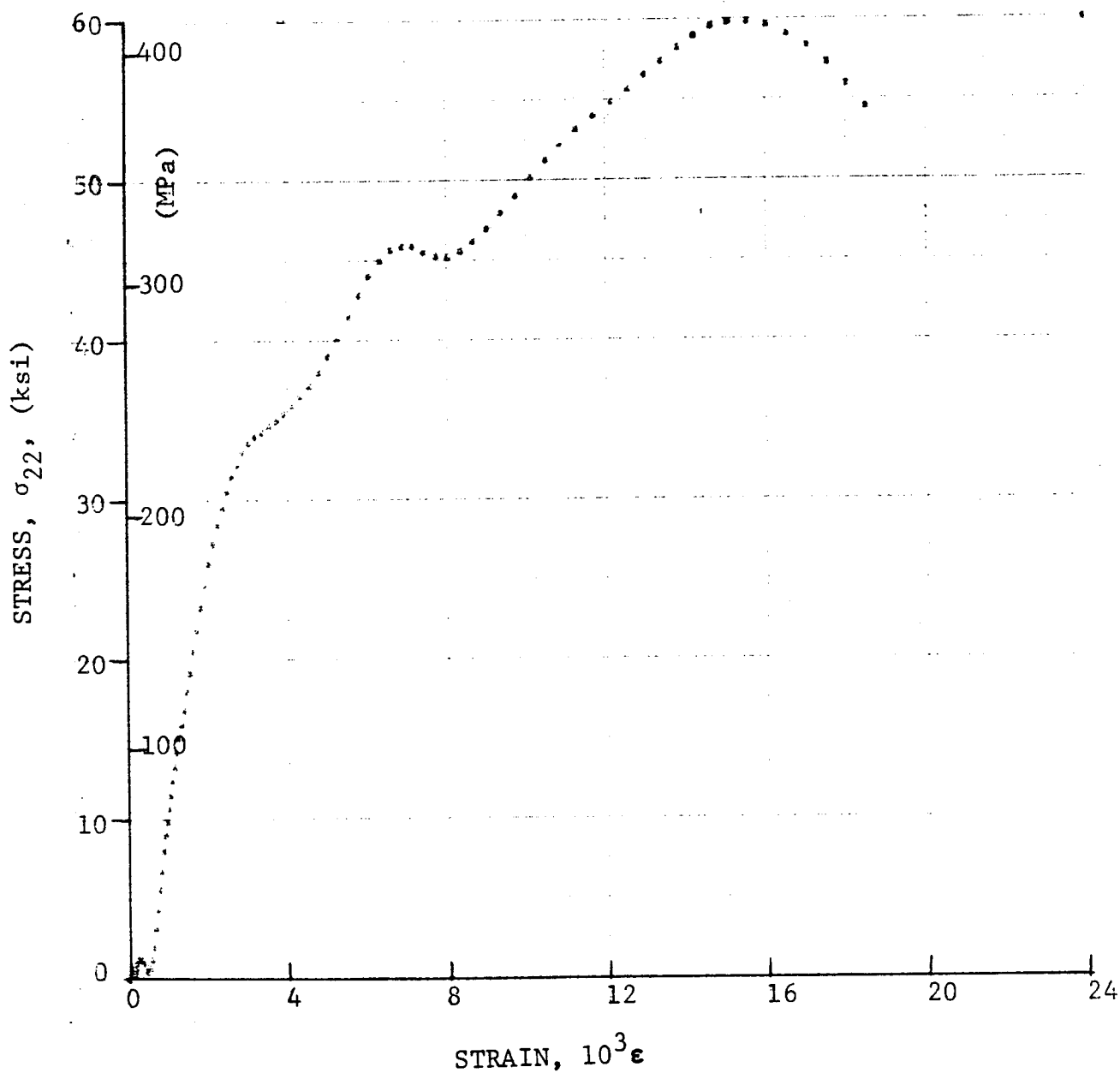
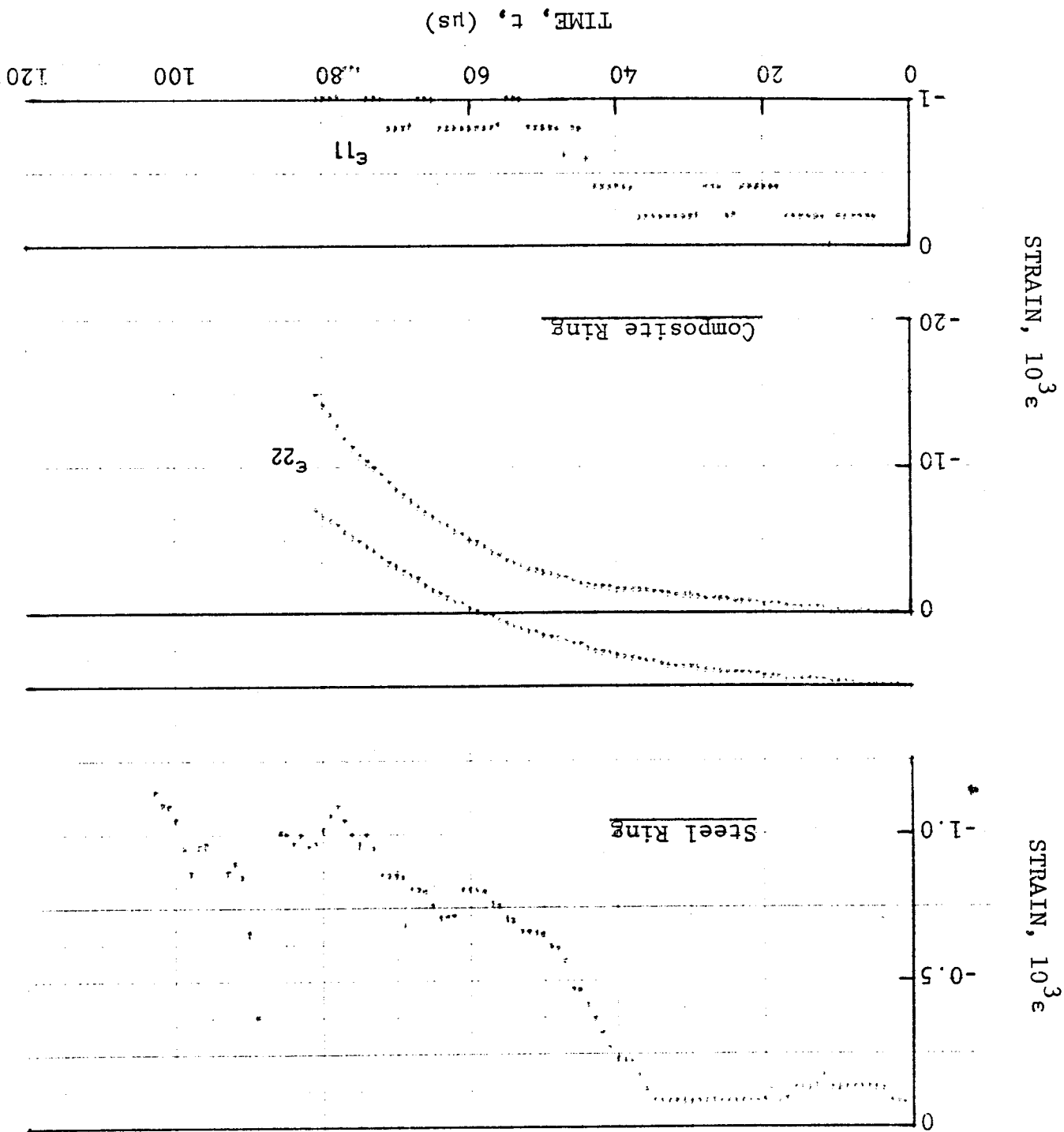


Figure 4-255. Stress-strain curve for dynamically loaded $[90_8]$ SP288/AS graphite/epoxy ring, Specimen No. 38-3 (1.56 g pistol powder, $KClO_4$, and aluminum dust).

Figure 4-256. Strain records in steel ring and [90°] 80AS/20S/PR288 graphite/S-glass/epoxy ring under dynamic loading for Specimen No. 39-1 (1.56 g pistol powder, $KClO_4$, and aluminum dust).



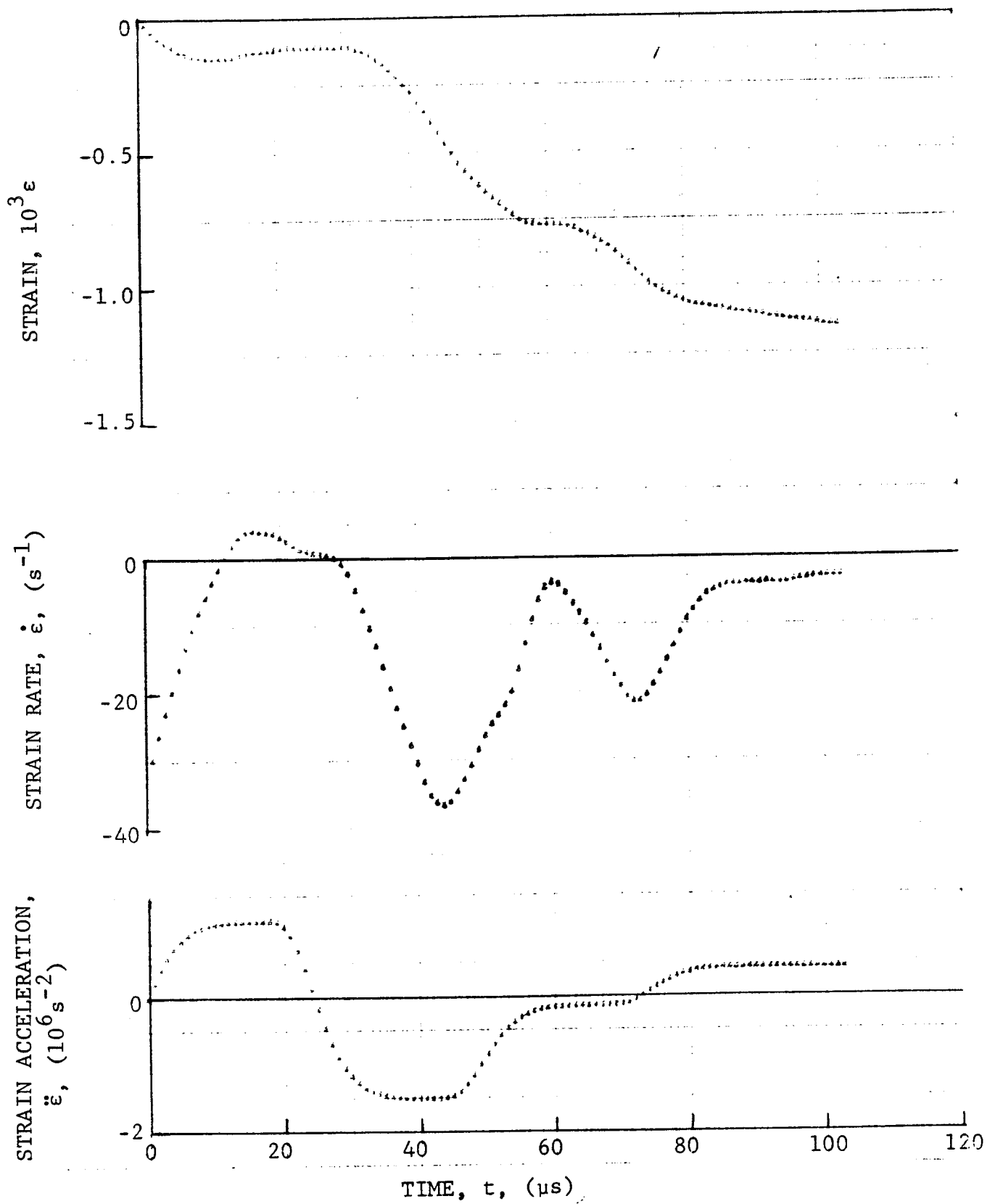


Figure 4-257. Strain and its derivatives in steel ring for Specimen No. 39-1.

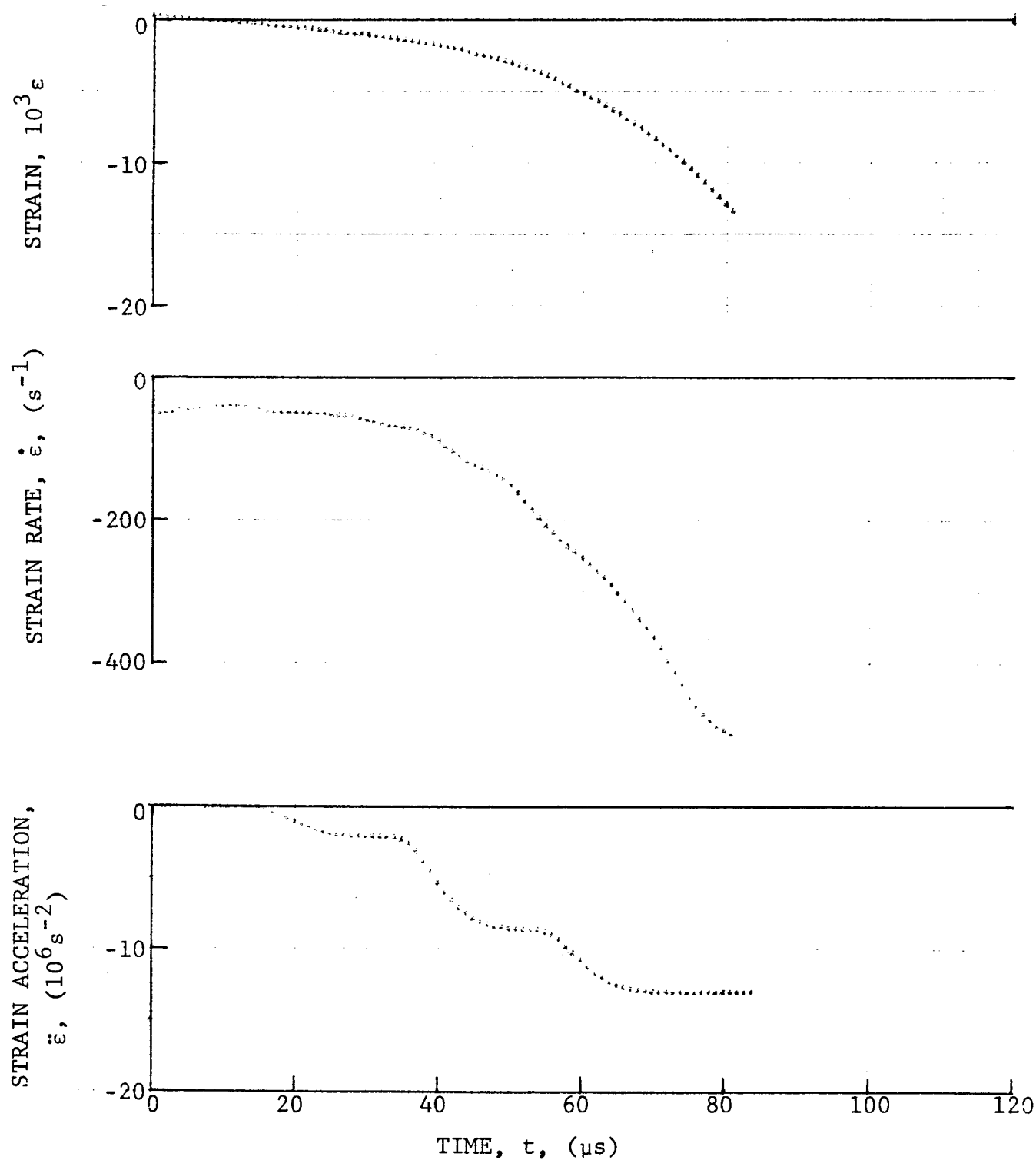


Figure 4-258. Circumferential strain and its derivatives in [90_g] 80AS/20S/PR288 graphite/S-glass/epoxy ring under dynamic loading for Specimen No. 39-1 (1.56 g pistol powder, KClO_4 , and aluminum dust).

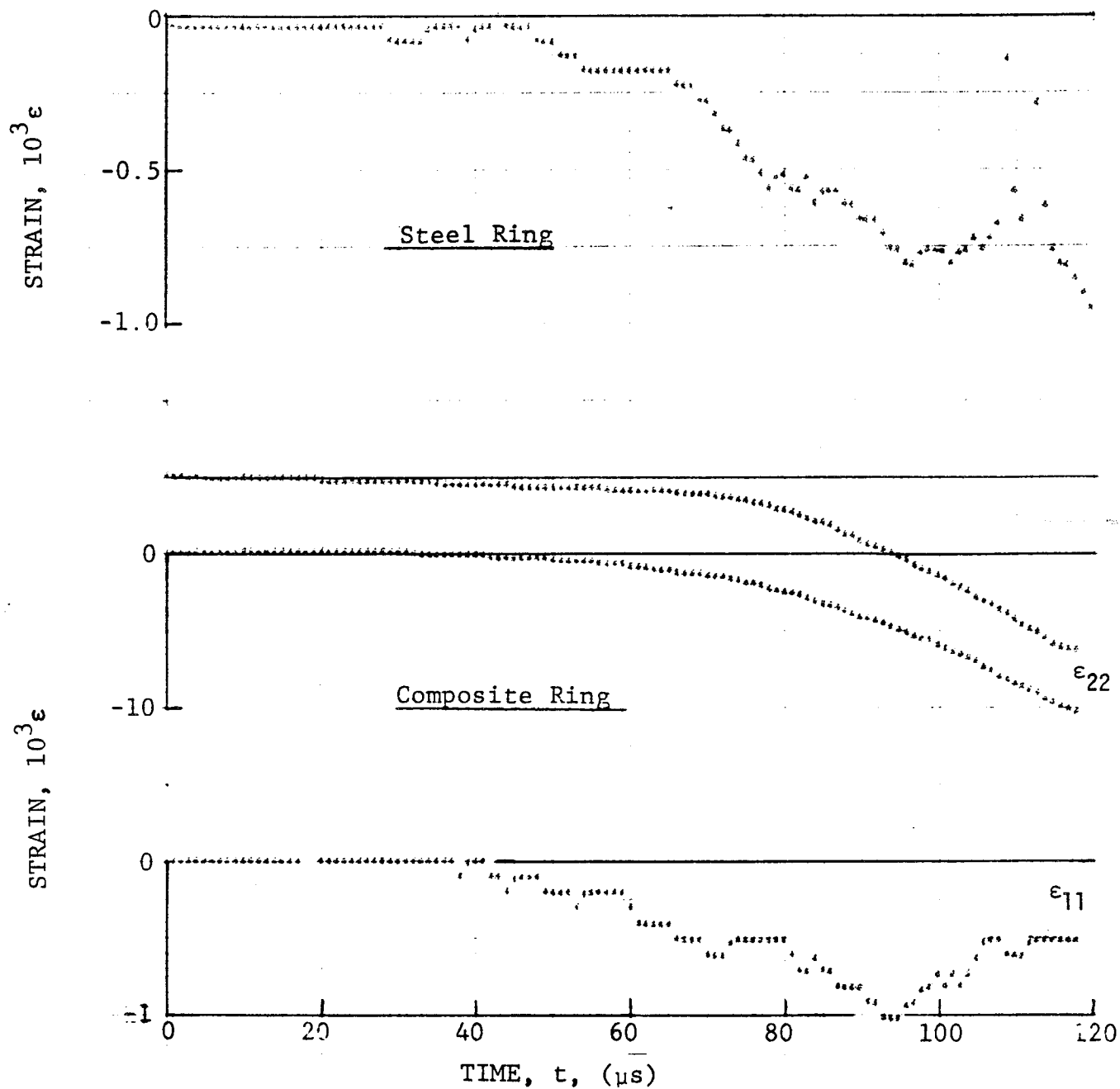


Figure 4-259. Strain records in steel ring and [90g] 80AS/20S/PR288 graphite/S-glass/epoxy ring under dynamic loading for Specimen No. 39-2 (1.56 g pistol powder, $KClO_4$, and aluminum dust).

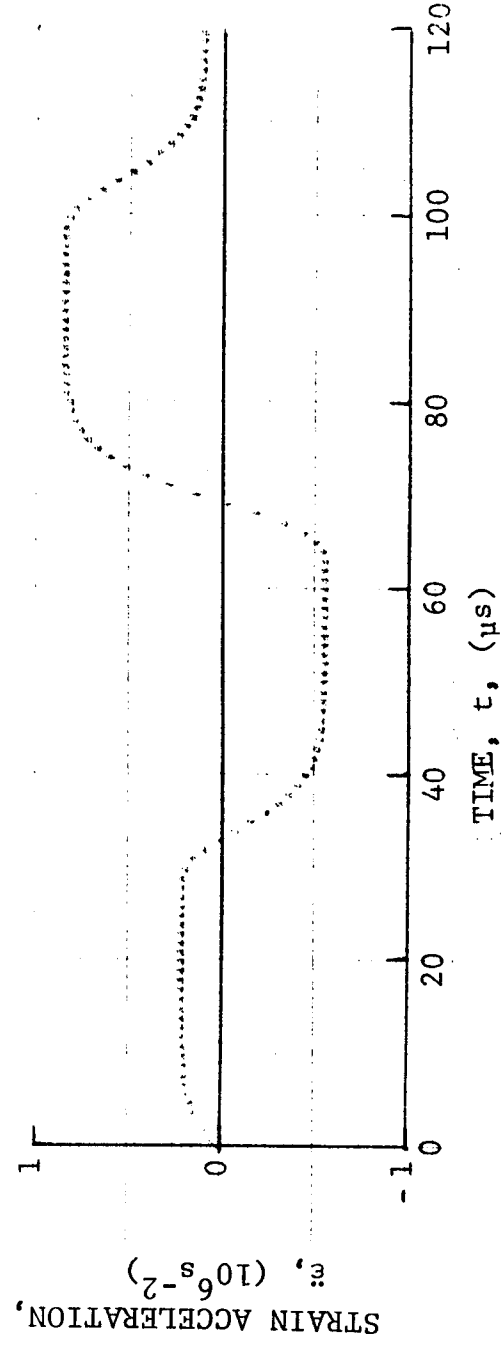
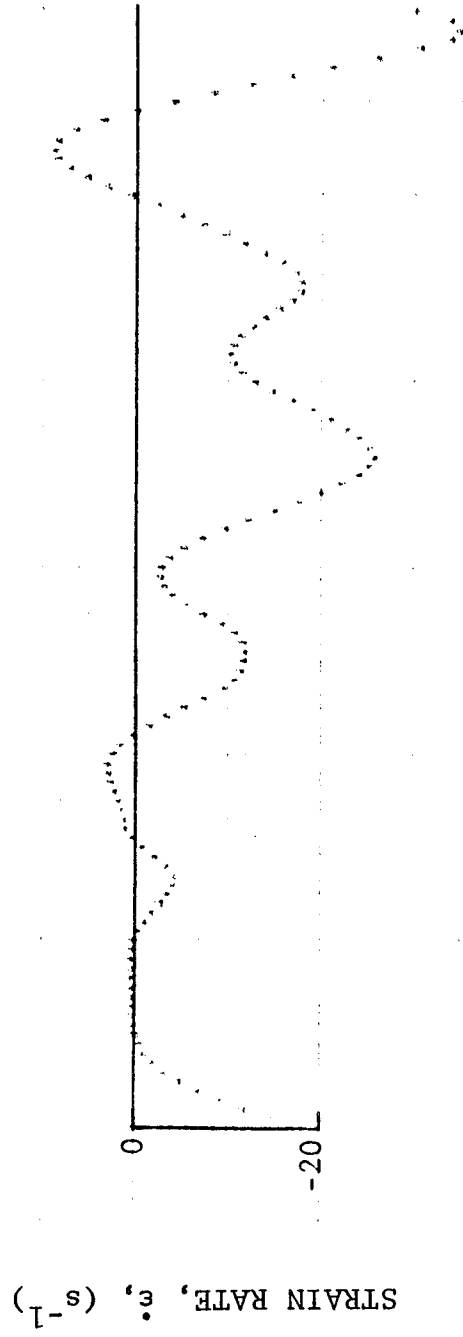
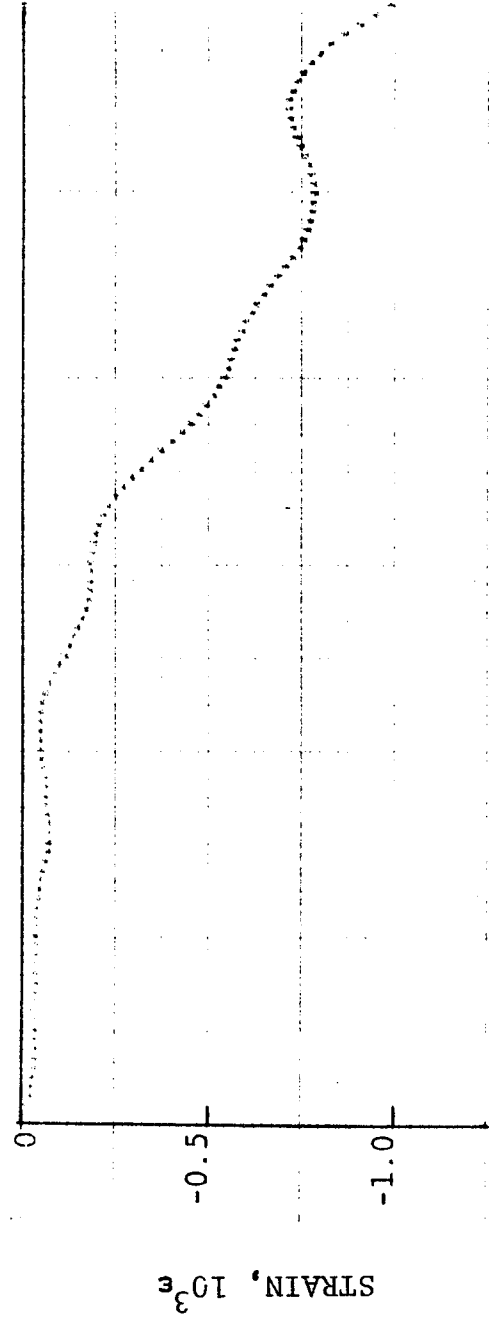


Figure 4-260. Strain and its derivatives in steel ring for Specimen No. 39-2.

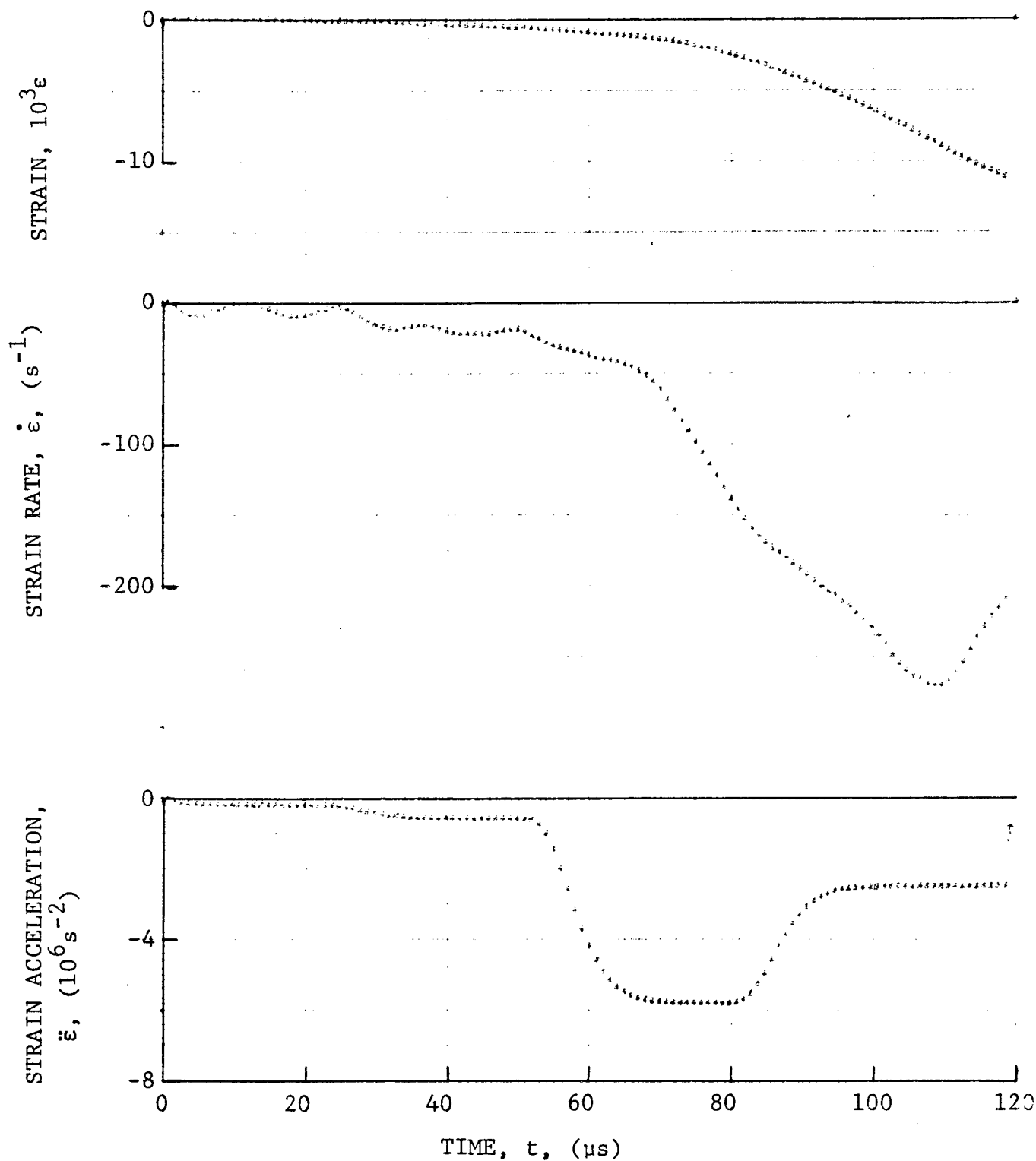


Figure 4-261. Circumferential strain and its derivatives in $[90_g]$ 80AS/20S/PR288 graphite/S-glass/epoxy ring under dynamic loading for Specimen No. 39-2 (1.56 g pistol powder, $KClO_4$, and aluminum dust).

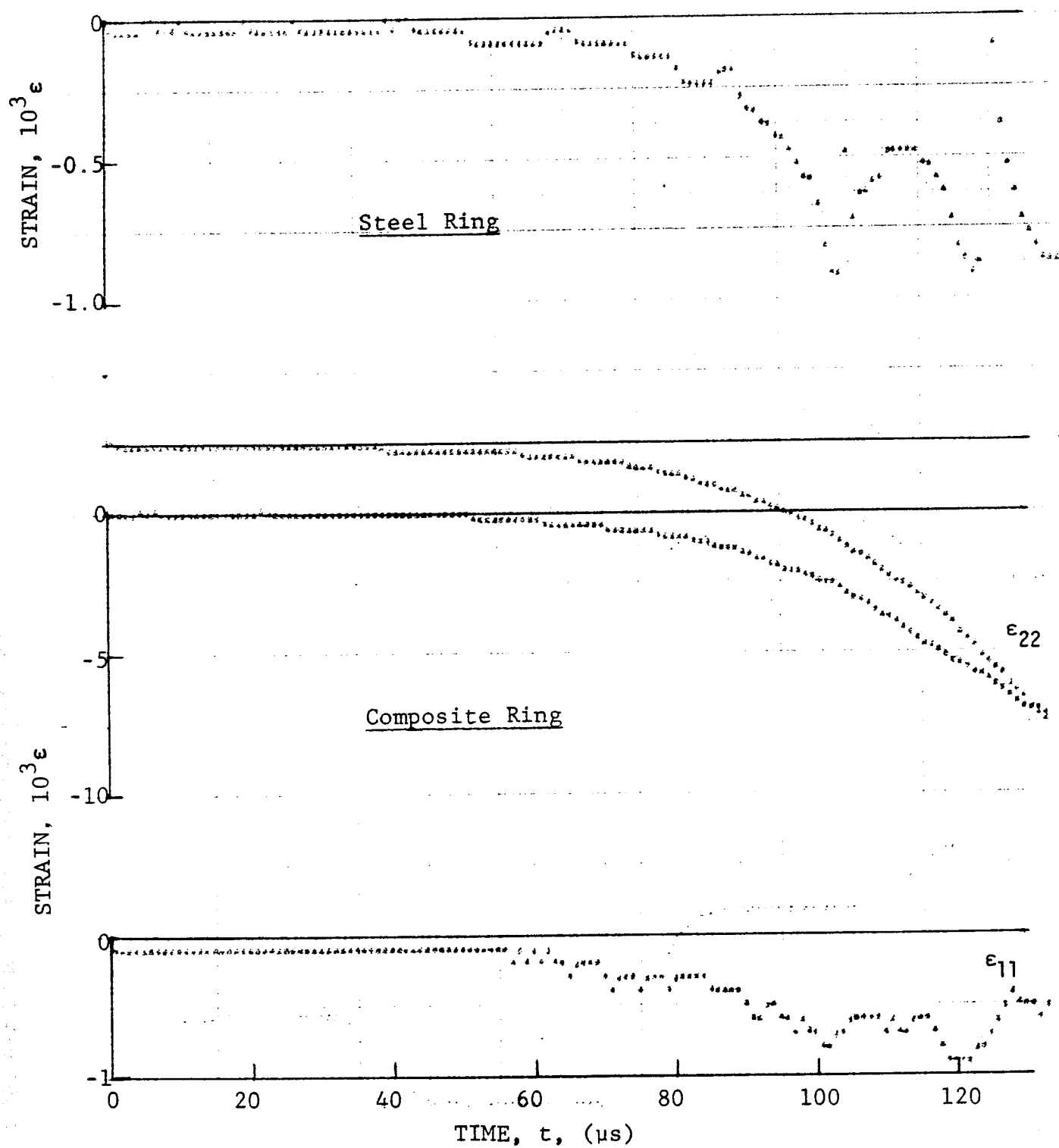


Figure 4-262. Strain records in steel ring and [90g] 80AS/20S/PR288 graphite/S-glass/epoxy ring under dynamic loading for Specimen No. 39-3 (1.56 g pistol powder, $KClO_4$, and aluminum dust).

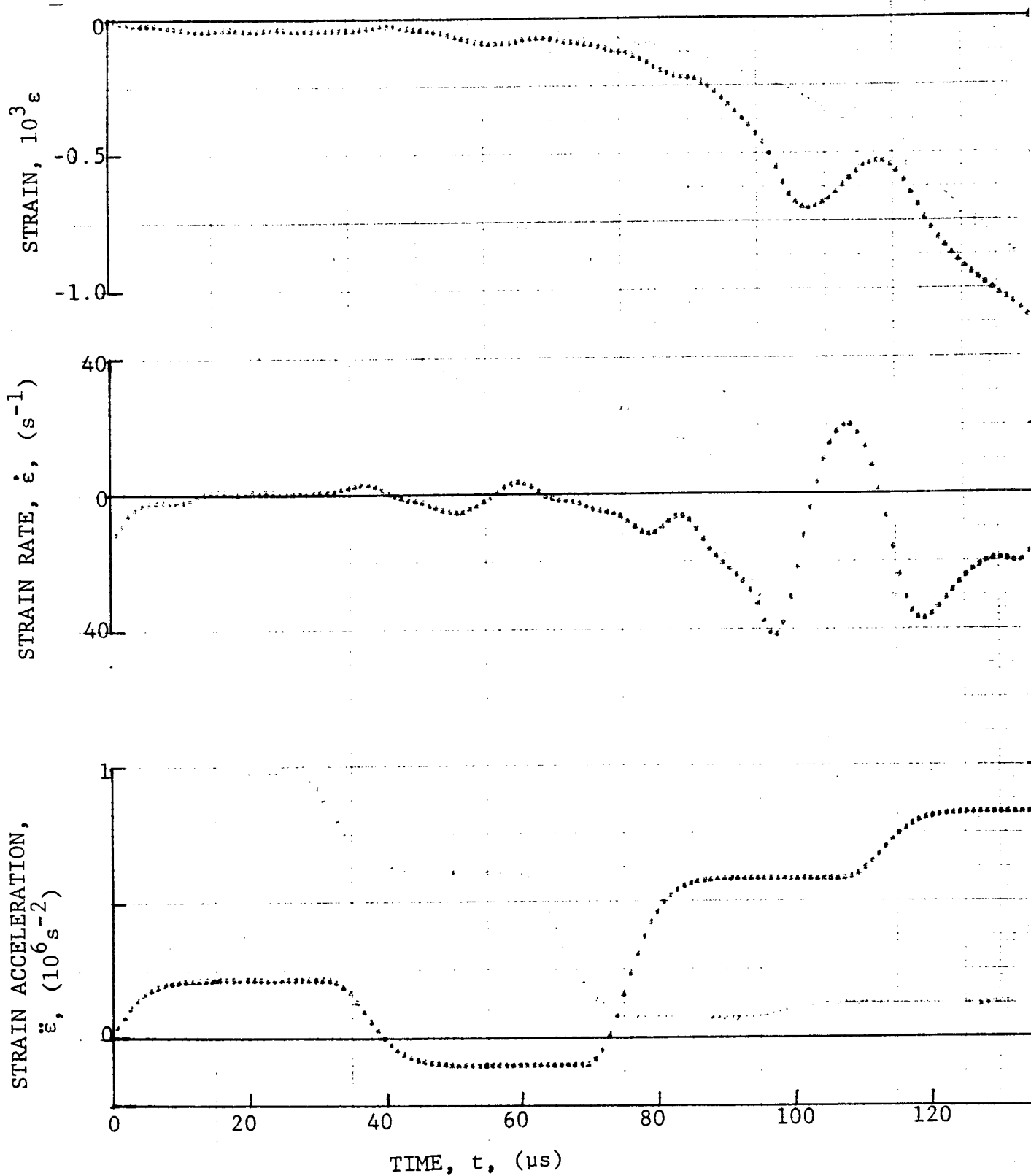


Figure 4-263. Strain and its derivatives in steel ring for Specimen No. 39-3.

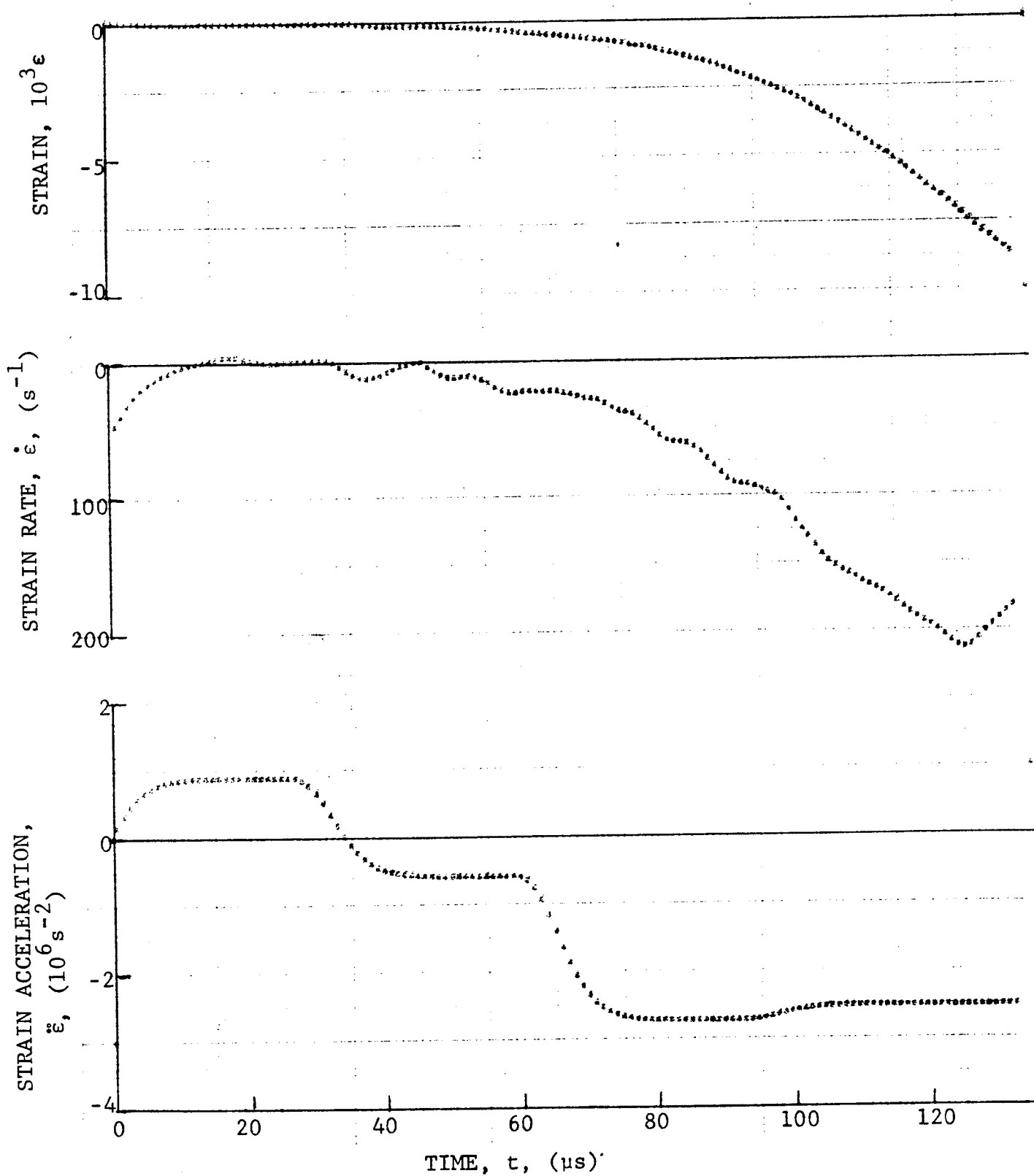


Figure 4-264. Circumferential strain and its derivatives in [90g] 80AS/20S/PR288 graphite/S-glass/epoxy ring under dynamic loading for Specimen No. 39-3 (1.56 g pistol powder, KClO_4 , and aluminum dust).

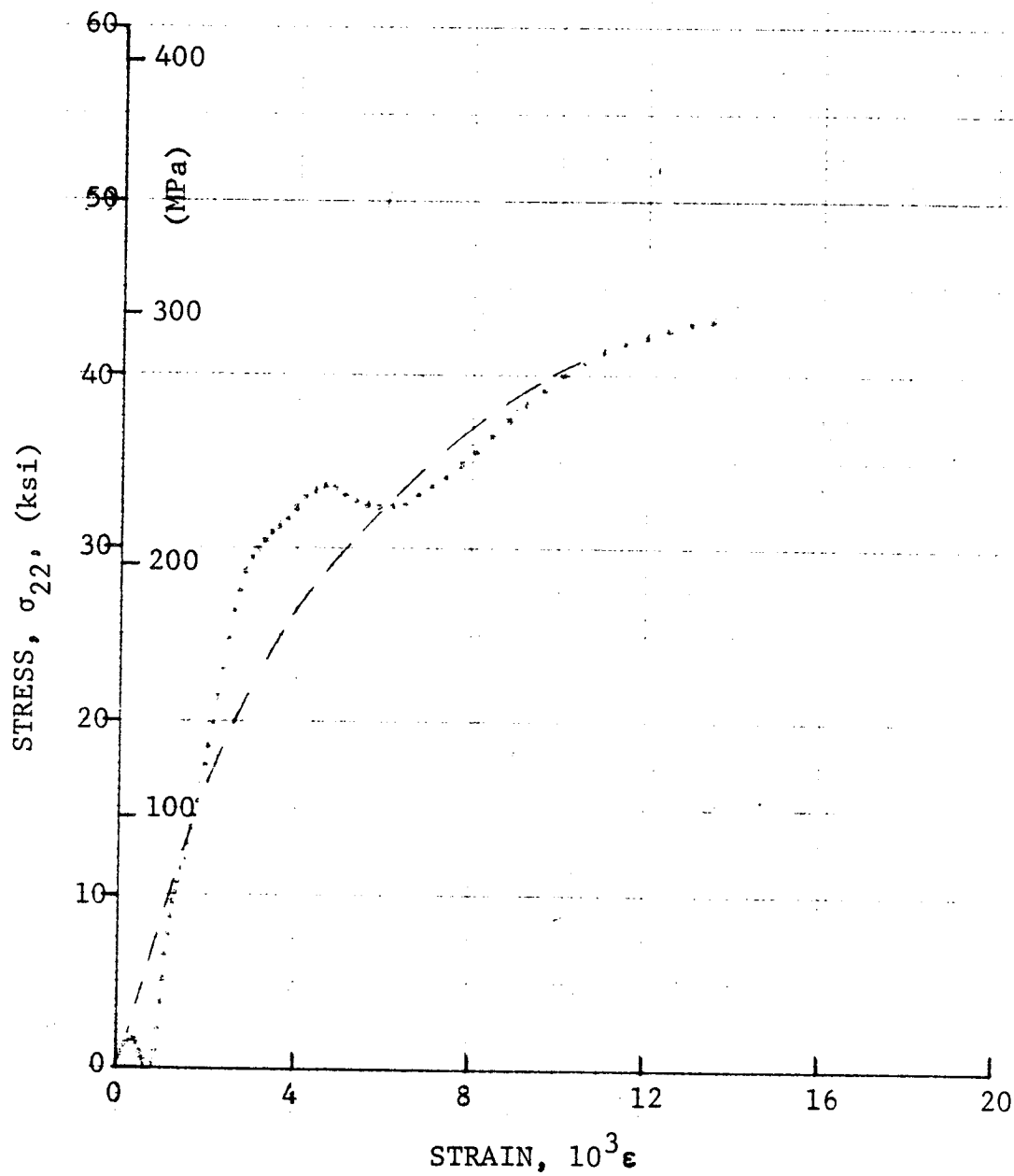


Figure 4-265. Stress-strain curve for dynamically loaded [90_g] 80AS/20S/PR288 graphite/S-glass/epoxy ring, Specimen No. 39-1 (1.56 g pistol powder, $KClO_4$, and aluminum dust).

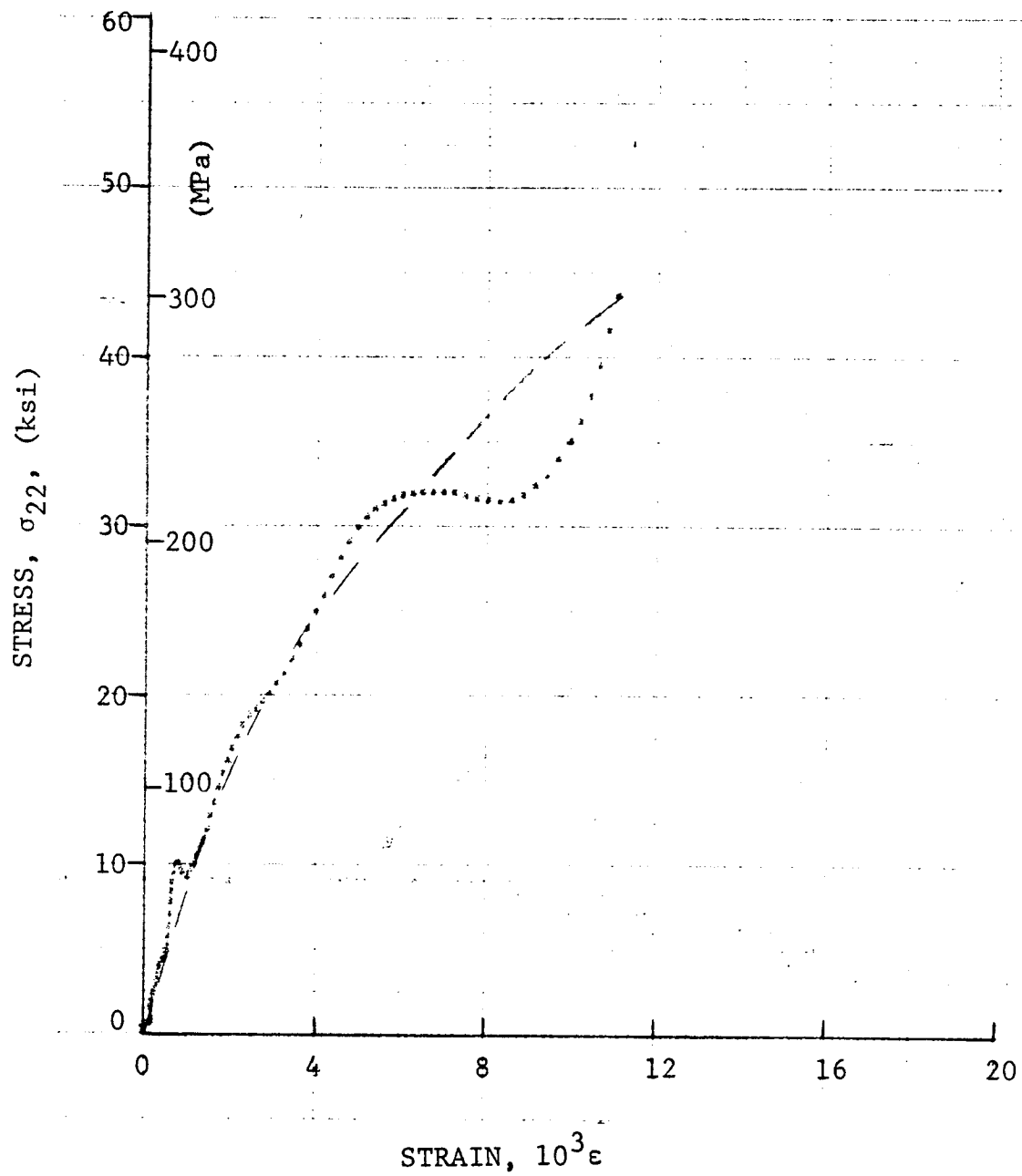


Figure 4-266. Stress-strain curve for dynamically loaded [90_g] 80AS/20S/PR288 graphite/S-glass/epoxy ring, Specimen No. 39-2 (1.56 g pistol powder, KClO₄, and aluminum dust).

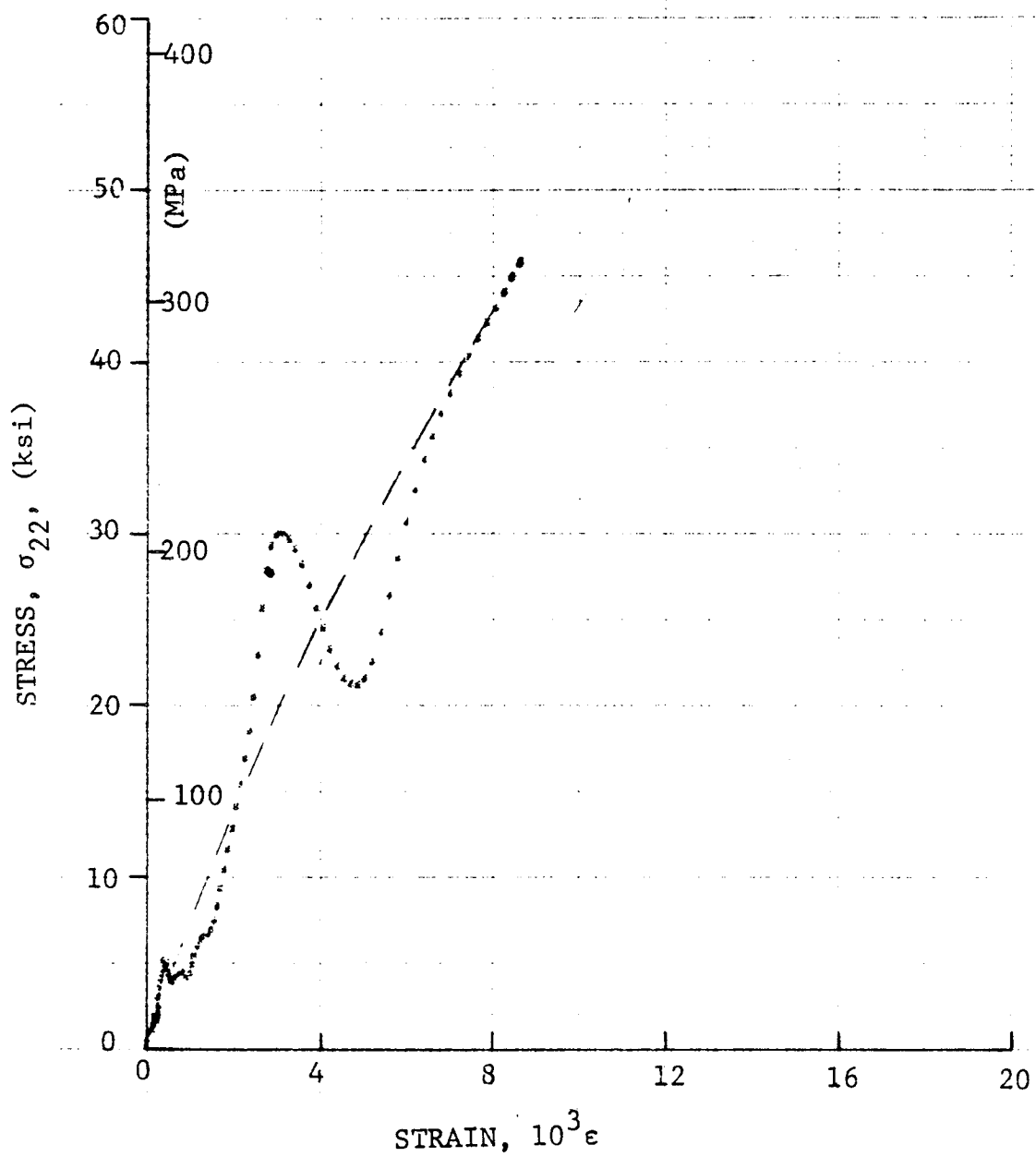


Figure 4-267. Stress-strain curve for dynamically loaded [90g] 80AS/20S/PR288 graphite/S-glass/epoxy ring, Specimen No. 39-3 (1.56 g pistol powder, $KClO_4$, and aluminum dust).

5. SUMMARY AND CONCLUSIONS

Experimental methods and procedures were developed for testing and characterization of unidirectional and angle-ply composite laminates over a wide range of strain rates.

The following three materials were selected for strain rate characterization:

- (1) SP288/T300 graphite/epoxy
- (2) SP288/AS graphite/epoxy
- (3) 80AS/20S/PR288 graphite/S-glass/epoxy.

These materials, in unidirectional form, were fully characterized under static conditions using standard coupon specimens and procedures.

The specimen geometry selected was a ring 10.16 cm (4 in.) in diameter, 2.54 cm (1 in.) wide, and 6 to 8 plies thick loaded under internal pressure. These specimens were cut from composite tubes fabricated in a manner producing a material of the same properties as those of flat laminates cured in an autoclave. Quality control procedures using thickness measurements, destructive testing, and ultrasonic inspection were employed.

A method was developed for testing thin ring specimens at strain rates up to approximately 500s^{-1} . Ring specimens were loaded by an internal or external pressure pulse applied explosively through a liquid in specially designed fixtures. The specimen forms part of a fluid-filled pressure chamber. The pressure pulse was produced by detonating an explosive in the pressure chamber. Strain rates were varied by varying the explosive charge. Strains from strain gages mounted on the composite specimen and a steel calibration ring were recorded with a digital processing oscilloscope. Data analysis was based on a numerical solution of the equation of motion. A computer program was written involving smoothing and approximations of the strain data, strain rate, and strain acceleration. In all cases results were presented in the form of stress-strain curves to failure and properties determined included initial,

secant, and terminal strain rates; initial, secant, and terminal modulus and Poisson's ratio; and strength and ultimate strain.

In the first phase of the program described in this volume unidirectional properties were determined of the three materials mentioned before at three strain rates. The strain rates investigated were quasi-static, intermediate, and high rates ranging from 10^{-4}s^{-1} to over 500s^{-1} . Longitudinal, transverse, and in-plane shear unidirectional properties were determined by testing ring specimens with their fibers oriented at 0-deg, 90-deg, and 10-deg with the circumferential direction. Stress-strain curves to failure were obtained in all cases.

Results for longitudinal tensile properties are tabulated in Tables 4-4, 4-8, and 4-12 of the preceding section. The modulus (initial and secant) increases with strain rate up to approximately 20% at the highest rate in the case of the SP288/AS material. The variation of the ratio of dynamic to static modulus with strain rate is illustrated graphically in Figure 5-1. All three materials follow the same trend. The only scatter is due to the uncertainty of determining accurately the initial modulus at the high strain rates. The tensile strength and ultimate tensile strain did not show any significant variations with strain rate.

Results for transverse tensile properties are tabulated in Tables 4-16, 4-20, and 4-24 of the preceding section. The secant modulus increases sharply with strain rate reaching values two to two and one-half times the static value. The initial modulus increases even more sharply but displays considerable scatter because of some uncertainty in its determination. The variation of the ratio of dynamic to static transverse secant modulus with strain rate is illustrated graphically in Figure 5-2. Each point on the curves represents the average of three tests. The three materials show different rates of modulus increase. The modulus of the hybrid material increases more than that of SP288/T300, which in turn shows a larger increase in modulus than the SP288/AS material. The strength increases with strain rate somewhat more sharply than the modulus reaching values of approximately three times the static values at the high strain rates. The ultimate transverse tensile strain does not vary significantly up to the intermediate strain rate, however, it

increases by 25 to 44% for all three materials. This result is related to the fact that the strength increases faster than the modulus with increasing strain rate.

Results for in-plane shear properties are tabulated in Tables 4-28, 4-32, and 4-36 of the preceding section. Both initial and secant moduli increase noticeably with strain rate for all three materials by up to approximately 65%. The variation with strain rate of the ratio of dynamic to static shear modulus is illustrated in Figure 5-3. Considerable scatter is evident. The shear strength increases with strain rate in approximately the same proportion as the modulus. No clearcut trend was evident with regard to the ultimate shear strain. A slight increase (10%) was noticed in the SP288/T300 material, and a noticeable decrease (26%) in the SP288/AS material at the high strain rate. The hybrid material showed increased ultimate strain at the intermediate rate and a reduced ultimate strain at the high rate.

Compressive, longitudinal properties were obtained for the two graphite/epoxy materials over a narrower range of strain rate, up to approximately 90s^{-1} . The initial longitudinal modulus was higher than the static value, and the secant modulus was approximately the same as the static modulus. The dynamic strength was equal or slightly lower than the static strength for the two graphite/epoxy materials. The dynamic ultimate strain was somewhat lower than the static value.

Compressive transverse properties were obtained for all three materials investigated at strain rates up to approximately 500s^{-1} . The dynamic initial and secant moduli for the two graphite/epoxy materials are approximately three and two times the static value, respectively. In the case of the hybrid material the dynamic moduli were even higher, 2.4 to 4.6 times the static. This may be attributed in part to the higher strain rate dependence of the glass/epoxy component of the hybrid material. The dynamic to static strength ratio for the two graphite/epoxy materials is approximately 1.5, whereas for the hybrid material it is 1.8. In all three materials the dynamic ultimate compressive strain is approximately two-thirds of the static ultimate strain.

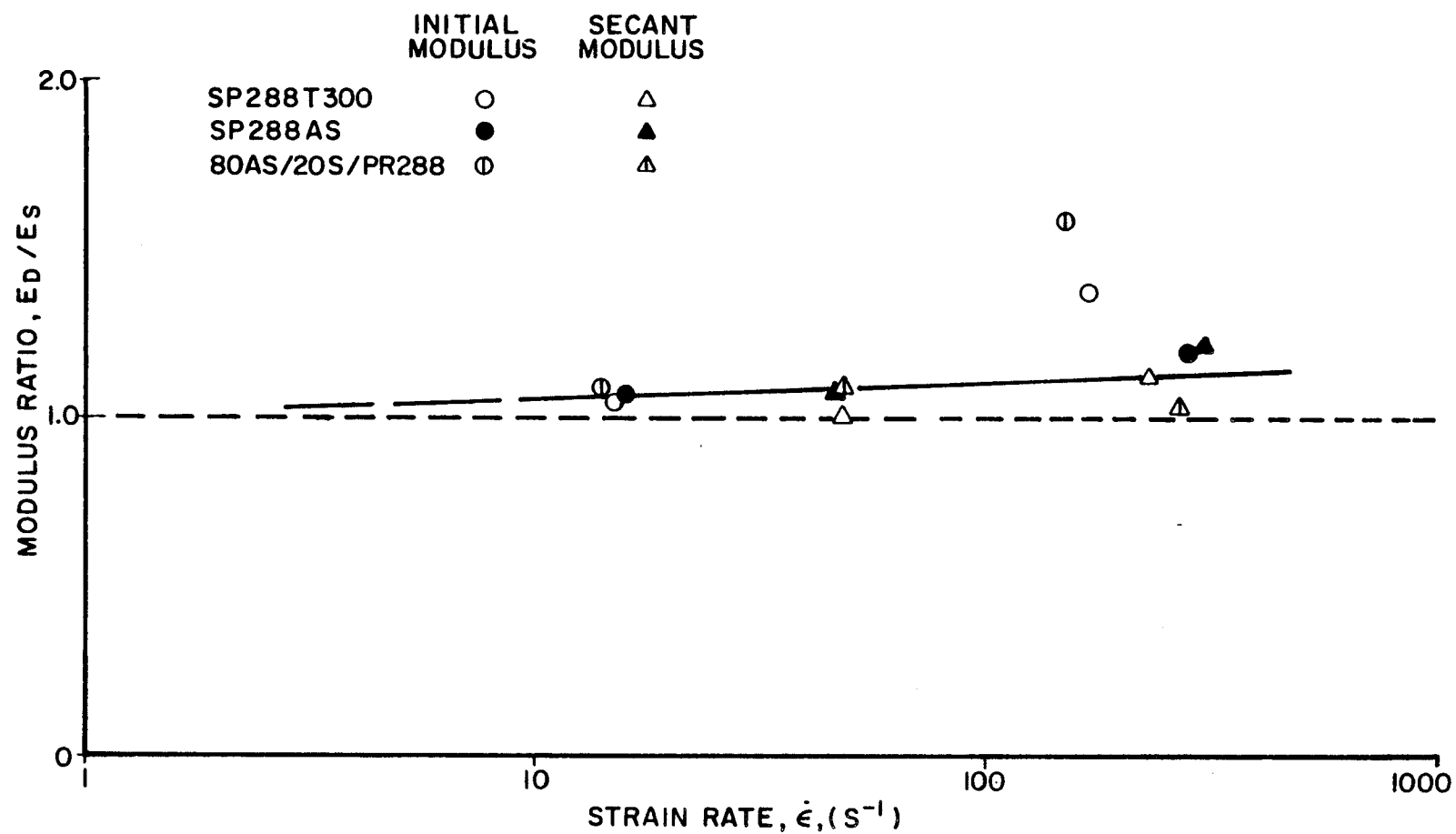


Figure 5-1. Ratio of dynamic to static longitudinal modulus for three materials as a function of strain rate.

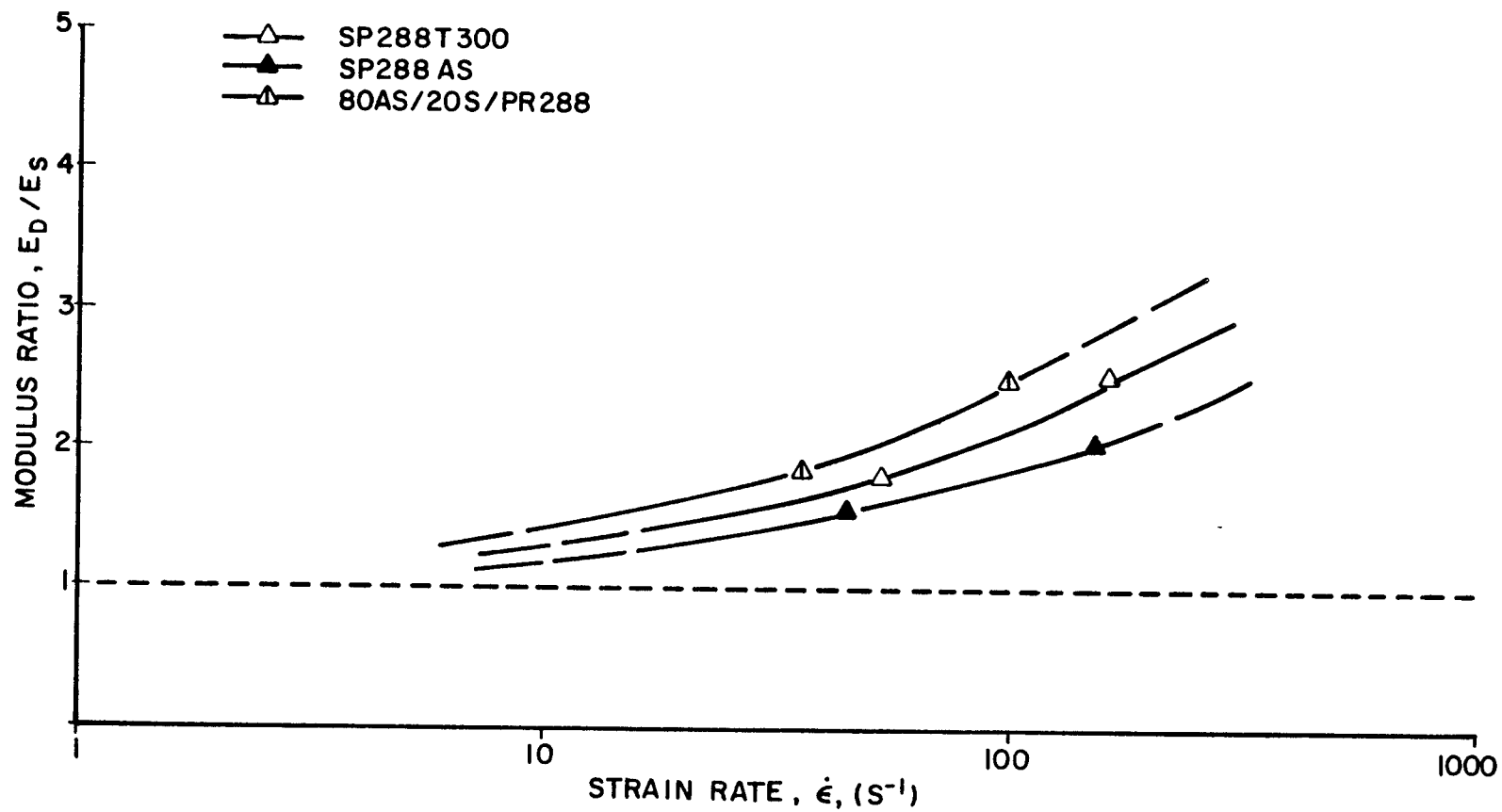


Figure 5-2. Ratio of dynamic to static transverse secant modulus for three materials as a function of strain rate.

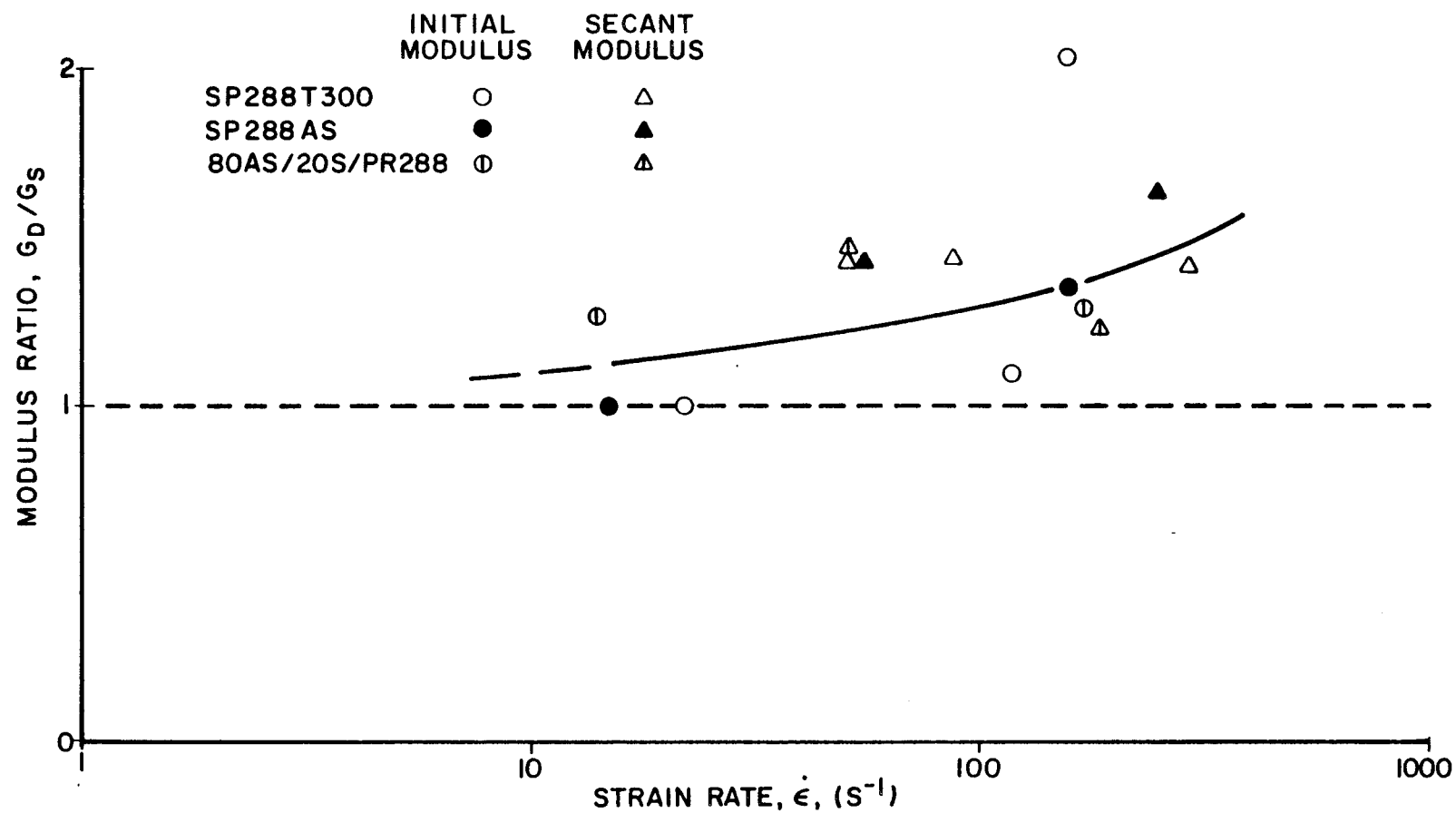


Figure 5-3. Ratio of dynamic to static in-plane shear modulus for three materials as a function of strain rate.

REFERENCES

1. Zimmer, J. E. and Cost, James R., "Determination of the Elastic Constants of a Unidirectional Fiber Composite Using Ultrasonic Velocity Measurements," J. Acoust. Soc. of America, Vol. 47, No. 3, 1970, pp. 795-803.
2. Gieske, J. H. and Allred, R. E., "Elastic Constants of B-Al Composites by Ultrasonic Velocity Measurements," Exper. Mechanics, Vol. 14, No. 4, April 1974, pp. 158-165.
3. Gibson, R. F. and Plunkett, R., "Dynamic Mechanical Behavior of Fiber-Reinforced Composites: Measurements and Analysis," J. Composite Materials, Vol. 10, October 1976, pp. 325-341.
4. Rotem, A. and Lifshitz, J., "Longitudinal Strength of Unidirectional Fibrous Composite Under High Rate of Loading," Proc. of 26th Annual Tech. Conf. 1971, Reinforced Plastics/Composites Division, The Soc. of Plastics Industry, Sect. 10-G, February 1971.
5. Lifshitz, J., "Impact Strength of Angle Ply Fiber Reinforced Materials," J. Composite Materials, Vol. 10, January 1976, pp. 92-101.
6. Armenakas, A. E. and Sciammarella, C. A., "Response of Glass-Fiber-Reinforced Epoxy Specimens to High Rates of Tensile Loading," Exper. Mechanics, Vol. 13, October 1973, pp. 433-440.
7. Daniel, I. M. and Liber, T., "Strain Rate Effects on Mechanical Properties of Fiber Composites," IITRI Report D6073-IV, for NASA-Lewis Research Center, NASA CR-135087, June 1976.
8. Daniel, I. M. and Liber, T., "Testing of Fibrous Composites at High Strain Rates," Proceedings of Second International Conference on Composite Materials, ICCM/2, Toronto, Canada, April 16-20, 1978, pp. 1003-1018.
9. Sierakowski, R. L., Nevill, G. E., Ross, C. A. and Jones, E. R., "Dynamic Compressive Strength and Failure of Steel Reinforced Epoxy Composites," J. Composite Materials, Vol. 5, July 1971, pp. 362-377.
10. Lindholm, U.S., "Dynamic Deformation of Metals," in Behavior of Materials Under Dynamic Loading, ed. by N. J. Huffington, Jr., American Society of Mechanical Engineers, 1965.
11. Daniel, I. M., LaBedz, R. H. and Liber, T., "New Method for Testing Composites at Very High Strain Rates," Exper. Mechanics, Vol. 21, No. 2, February 1981, pp. 71-77.
12. "Development of Composite Tube Fabrication and Testing," IIT Research Institute R&D Programs, 1970-1975, Reports No. D1039, D1049, D1055, D1061, D1075, and D1096.
13. Rowlands, R. E., "An Analytical-Experimental Correlation of the Biaxial State of Stress in Composite Laminates (T-300/5208)," AFFDL-TR-75-11, April 1975.

14. Liber, T., Daniel, I. M. and Senninger, M., "Failure Criterion for Kevlar 49/Epoxy Composites," IITRI Report No. D6101 for Hercules, Inc., July 1975.
15. Liber, T., Daniel, I. M., LaBedz, R. and Niro, T., "Fabrication and Testing of Composite Ring Specimens," Proc. of 34th Annual Technical Conference, 1979 Reinforced Plastics/Composites Institute, The Society of the Plastics Industry, Inc., Sect. 22-B.
16. Cole, B. W. and Pipes, R. B., "Filamentary Composite Laminates Subjected to Biaxial Stress Fields," AFFDL-TR-73-115, June 1974.
17. Weed, D. N. and Francis, P. H., "Process Development for the Fabrication of High Quality Composite Tubes," Fibre Science and Technology, Vol. 10, 1977, pp. 89-100.
18. Liber, T., Daniel, I. M. and Schramm, S., "Ultrasonic Techniques for Inspecting Flat and Cylindrical Composite Specimens," Nondestructive Evaluation and Flaw Criticality for Composite Materials, ASTM STP 696, American Society for Testing and Materials, 1979, pp. 5-25.

REPORT DOCUMENTATION PAGE			Form Approved OMB No. 0704-0188	
Public reporting burden for this collection of information is estimated to average 1 hour per response, including the time for reviewing instructions, searching existing data sources, gathering and maintaining the data needed, and completing and reviewing the collection of information. Send comments regarding this burden estimate or any other aspect of this collection of information, including suggestions for reducing this burden, to Washington Headquarters Services, Directorate for Information Operations and Reports, 1215 Jefferson Davis Highway, Suite 1204, Arlington, VA 22202-4302, and to the Office of Management and Budget, Paperwork Reduction Project (0704-0188), Washington, DC 20503.				
1. AGENCY USE ONLY (Leave blank)		2. REPORT DATE December 1991		3. REPORT TYPE AND DATES COVERED Final Contractor Report
4. TITLE AND SUBTITLE High Strain Rate Properties of Unidirectional Composites Final Report—Part I			5. FUNDING NUMBERS WU-505-63-5B C-NAS3-21016	
6. AUTHOR(S) I.M. Daniel				
7. PERFORMING ORGANIZATION NAME(S) AND ADDRESS(ES) IIT Research Institute 10 West 35th Street Chicago, Illinois 60616			8. PERFORMING ORGANIZATION REPORT NUMBER None	
9. SPONSORING/MONITORING AGENCY NAMES(S) AND ADDRESS(ES) National Aeronautics and Space Administration Lewis Research Center Cleveland, Ohio 44135-3191			10. SPONSORING/MONITORING AGENCY REPORT NUMBER NASA CR-198083	
11. SUPPLEMENTARY NOTES Project Manager, C.C. Chamis, Structures Division, NASA Lewis Research Center, (216) 433-3252.				
12a. DISTRIBUTION/AVAILABILITY STATEMENT Unclassified - Unlimited Subject Category 24			12b. DISTRIBUTION CODE	
13. ABSTRACT (Maximum 200 words) Experimental methods were developed for testing and characterization of composite materials at strain rates ranging from quasi-static to over 500s ⁻¹ . Three materials were characterized, two graphite/epoxies and a graphite/S-glass/epoxy. Properties were obtained by testing thin rings 10.16 cm (4 in.) in diameter, 2.54 cm (1 in.) wide, and 6 to 8 plies thick under internal pressure. Unidirectional 0-deg, 90-deg, and 10-deg off-axis rings were tested to obtain longitudinal, transverse, and in-plane shear properties. In the dynamic tests internal pressure was applied explosively through a liquid and the pressure was measured with a calibrated steel ring. Strains in the calibration and specimen rings were recorded with a digital processing oscilloscope. The data were processed and the equation of motion solved numerically by the mini-computer attached to the oscilloscope. Results were obtained and plotted in the form of dynamic stress-strain curves. Longitudinal properties which are governed by the fibers do not vary much with strain rate with only a moderate (up to 20%) increase in modulus. Transverse modulus and strength increase sharply with strain rate reaching values up to three times the static value. The in-plane shear modulus and shear strength increase noticeably with strain rate by up to approximately 65%. In all cases ultimate strains do not vary significantly with strain rate.				
14. SUBJECT TERMS Experimental methods; Unidirectional dynamic pressure; Test fixtures; Data acquisition; Data reduction; Equations of motions; Properties; Longitudinal transverse; In-plane shear; Tension; Compression; Strengths; Terminal			15. NUMBER OF PAGES 458	
			16. PRICE CODE A20	
17. SECURITY CLASSIFICATION OF REPORT Unclassified	18. SECURITY CLASSIFICATION OF THIS PAGE Unclassified	19. SECURITY CLASSIFICATION OF ABSTRACT Unclassified	20. LIMITATION OF ABSTRACT	